KIT SCIENTIFIC REPORTS 7592

Nuclear Fusion Programme

Annual Report of the Association Karlsruhe Institute of Technology/EURATOM

January 2010 - December 2010

KIT Scientific Publishing

I. Pleli (ed.)

Nuclear Fusion Programme

Annual Report of the Association Karlsruhe Institute of Technology/EURATOM

January 2010 - December 2010

Karlsruhe Institute of Technology
KIT SCIENTIFIC REPORTS 7592

Nuclear Fusion Programme

Annual Report of the Association
Karlsruhe Institute of Technology/EURATOM

January 2010 - December 2010

I. Pleli
(ed.)

KIT Scientific Publishing

Report-Nr. KIT-SR 7592

Impressum

Karlsruher Institut für Technologie (KIT)
KIT Scientific Publishing
Straße am Forum 2
D-76131 Karlsruhe
www.ksp.kit.edu

KIT – Universität des Landes Baden-Württemberg und nationales
Forschungszentrum in der Helmholtz-Gemeinschaft

KIT Scientific Publishing 2011
Print on Demand

ISSN 1869-9669

Overview

Preface

The KIT Fusion Programme is contributing to, and integrated in, the development of nuclear fusion worldwide and, in particular, in Europe via EURATOM. The goal of this coordinated effort is the development of fusion as a commercial source of energy, which is carbon-free and inherently safe, drawing from resources that are equally distributed around the world and unlimited on historical timescales.

This is a long-term goal, and important questions yet have to be addressed. Still, the general road map, i.e., what should be done when, and how, is clear, and researchers at KIT as well as in other labs in Europe and worldwide are determined to follow it and make fusion a success – a goal that is worth all efforts, as the need for it will persist, because there still will be a huge potential to replace fossil and, eventually, nuclear fission power generation for many decades from now.

The KIT Fusion Programme is focused on the development and the qualification of design approaches, technologies and materials for fusion. This is including structural materials for the severe requirements in terms of thermo-mechanical properties, neutron resistance and low activation, that will have to be met in a fusion power plant, the fusion-specific “in-vessel” components, i.e., breeder blanket and divertor, as well as the fusion (deuterium-tritium) fuel cycle. Moreover, technologies and components for microwave plasma heating & current drive are being developed at KIT, along with superconducting magnets and components. The spectrum of our activities is complemented by neutronics methodology development, simulations and validations, the simulation and validation of plasma-wall interactions, and fusion safety studies.

The current focus of the fusion work at KIT is on ITER, in many areas organized in a collaborative way together with other laboratories in “Consortia of (EURATOM) Associations” established to provide specific contributions to ITER via the European Joint Undertaking for ITER and the Development of Fusion Energy (F4E). With respect to this commitment, we have established a dedicated quality & project management team, which is now fully operational with all relevant processes in place. Furthermore, we are providing specific contributions for Wendelstein 7-X.

The KIT Fusion Programme has always been oriented towards fusion power, and hence, we have since long been working towards solutions that will be required beyond ITER only, but impose a long development time like materials development and qualification, and / or are needed as conceptual approaches already in an early phase of the design of a power plant, like, e.g., the in-vessel components or the power plant fuel cycle. In 2010, these activities have gained a new quality and momentum, in becoming part of a coordinated German activity to consider all – physics and technology – aspects of a fusion power plant and integrate them into a consolidated system approach. This activity will of course fertilise the DEMO-oriented work taking a new focus under EFDA from 2011 on.

2010 has been a “SOFT” year, and it is a pleasure for me to report that KIT has been present at this major event on fusion technologies, perfectly hosted by our Portuguese colleagues, with almost 60 participants and 50 papers, two of them invited plenary talks. – Along with the efforts being made by the Commission and EFDA to increase the number of qualified re-

searchers in the programme, KIT is giving more and more emphasis to training of young rearchers. In 2010, we were participating in 7 EFDA Goal Oriented Training networks, with a total of 11 trainees. The use of another European initiative, the High Performance Computer for Fusion, operated at the Forschungszentrum Jülich Supercomputer Centre, is also taking momentum at KIT: In 2010 we performed four dedicated applications requiring large computational resources in the areas of neutronics, vacuum, and breeder materials simulation. Hence, we have demonstrated that the HPC approach is useful in fusion also outside the classical, plasma physics approaches.

KIT Fusion cooperation with industry has seen a new peak in 2010. We have been involved in more than 40 collaborative projects, ranging from the delivery of specific equipment (e.g., diamond windows of extreme purity for microwave transmission) to the joint development of specialised systems (e.g., a test facility for Test Blanket Module mock-ups), materials (e.g., low activation ferritic steels) and processes (e.g., optimised production route for lithium compound pebbles to be used in the breeder blanket). Most of these collaborations are within Germany (i.e., more than 30). Still, we have more than 10 important industrial partners outside Germany, in Europe and worldwide – i.e., fusion is really a global business.

Klaus Hesch
July 2011

Plasma Wall Interaction

In ITER and DEMO transient events like disruptions and edge localised modes (ELMs) can result in brittle destruction (BD), melt motion and vaporization of the tungsten (W), CFC and beryllium (Be) wall surfaces of the plasma facing components (PFCs). To clarify tolerable transients and also for disruption mitigation by massive gas injection (MGI), computer codes are being developed at KIT. The damages to the wall as well as the impact of eroded and injected atoms on the plasma are modelled.

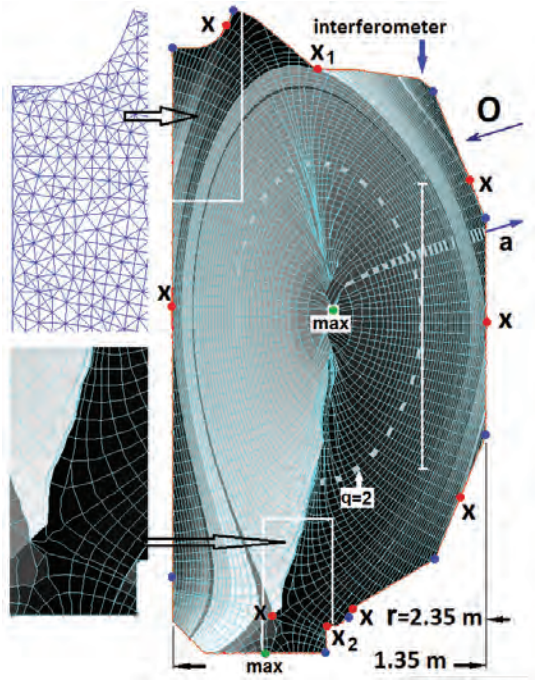

Magnetic field configuration of TOKES for the tokamak DIII-D. Triangle meshes are an underground for magnetic flux coordinates

The magneto-hydrodynamics and radiation tokamak code TOKES calculates plasma contamination, plasma and radiation fluxes onto the wall, and MGI atoms in the vessel, in a toroidally symmetric approach. The fluid dynamics code MEMOS simulates the melt motions on W and Be surfaces and bulk heat transport. The thermo-mechanic code PEGASUS is used to simulate the brittle destruction of CFC and W. The wall damage by the runaway electrons is modelled with the Monte-Carlo code ENDEP. Main models for BD and melt motion have been validated against experiments on plasma guns, electron beams and tokamaks.

A significant issue for ITER operation is the occurrence of disruptions, which can limit the lifetime of PFCs. For **disruption mitigation**, MGI is necessary. Tokamak experiments demonstrated effective ionization of the injected Ne, Ar and He atoms during MGI, which causes thermal quenching (TQ) of the plasma within a few ms. Modeling with TOKES has been focused upon further development of the code aiming at MGI simulations for ITER. A two-dimensional description of the plasma in the whole vessel was achieved applying magnetic flux coordinates (MFC). TOKES was successfully validated against a DIII-D experiment on argon MGI. A good agreement of experimental and simulated parameters indicates that TOKES adequately describes the main processes of TQ. The first consequence of the instabilities appears to be some small deteriorations of the toroidal symmetry and thus a slight overlapping of the nested magnetic surfaces, which drastically increases the electron cross-transport by the thermal conductivity along the entangled magnetic field lines.

The validation of MEMOS by experiments at the plasma gun QSPA-T and two-dimensional simulations taking into account the macrobrush structure of the targets have been continued for numerical modeling in support of experiments at TEXTOR simulating the **melt damage to W targets** in ITER. New calculations with MEMOS are performed to determine the magnitudes and the thresholds of melt splashing of W, Be and Li under pulsed heat loads. For TEXTOR relevant calculations, the energy deposition function was obtained by comparison of the experimental and the calculated surface temperature at the most heated place (hot spot). A good agreement between the calculations and the experimental data on heat load and surface temperature evolution is obtained. Furthermore, new MEMOS simulations have been performed to obtain the effective thermal conductivity of CFC deteriorated after multi-pulsed loads. The result is that degradation appears after heating CFC above a threshold of 3600 K, which results in a sub-surface layer of a few tens of microns.

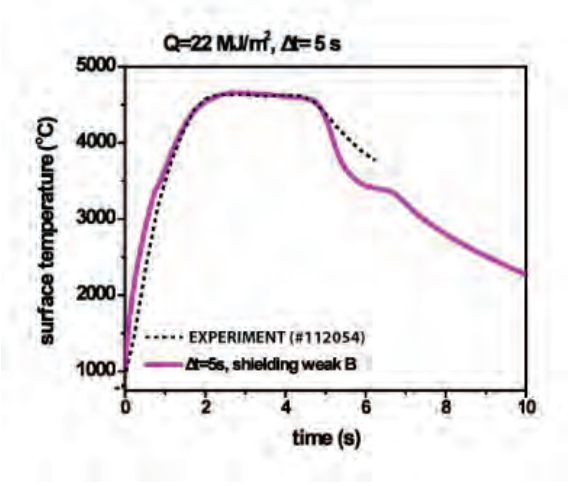

Time dependence of TEXTOR experimental and simulated surface temperature

A dedicated series of experiments have been performed with the plasma gun QSPA Kh–50 (Kharkov, Ukraine) for pulsed repetitive ELM-like plasma impacts on W targets of ITER grade. Measurements of residual tensile stress below and above the melting threshold were done and compared with the corresponding results obtained with the PEGASUS code. The stress was measured after a few shots with energy depositions up to the melting threshold. Further validation and improvements of PEGASUS models is continued. In addition, analytical calculations have been performed aiming at the interpretation of the experimental observation of residual stress dependence on the number of pulses and the threshold of BD cracking. The analytical solution obtained was fitted to the experimental data. The estimations predict that at large numbers of load pulses, the BD threshold should decrease from Q_{thr} = 0.3 down to Q ~ 0.1 MJ/m^2.

Disruption mitigations by MGI can result in the generation of **runaway electrons (RE)** which can damage the First Wall. Numerical simulations for the consequences of RE impact on the PFCs were carried out for JET and ITER conditions. For JET, the work was focused on the benchmarking of the codes ENDEP and MEMOS against experimental observations of RE beams. Reasonable qualitative and quantitative agreement between the numerical simulations and the JET experiments was obtained. Then, predictive modeling on melt damage to the ITER beryllium First Wall was performed. For the CFC target in a magnetic field of 3.5 T (JET case), the RE energy equals 5, 8 and 10 MeV. For the Be target (ITER) and the sandwich target with 1 cm Be PFC and 1 cm copper substrate, E_0 = 12.5 MeV is assumed. The main incident angle was varied from 1 up to 10 degrees. The transversal energy of the RE was varied up to 5% of the total energy. A typical penetration depth of RE of 1 mm is obtained. The Be melt layer exists for about 0.5 s. It is to note that during this time, the Rayleigh-Taylor instability caused by eddy currents can develop in the molten surface, resulting in significant splashing.

The energy depositions calculated by ENDEP are used in MEMOS to examine melting in ITER, starting heating from a wall temperature of 800 K, and in JET (starting heating from room temperature). For instance, at an RE heat load Q of 25 MJ/m^2, the surface temperature of the W target exceeds the melting temperature 1540 K after 10 ms. The melting depth and the evaporation erosion as a function of Q is shown in the figure.

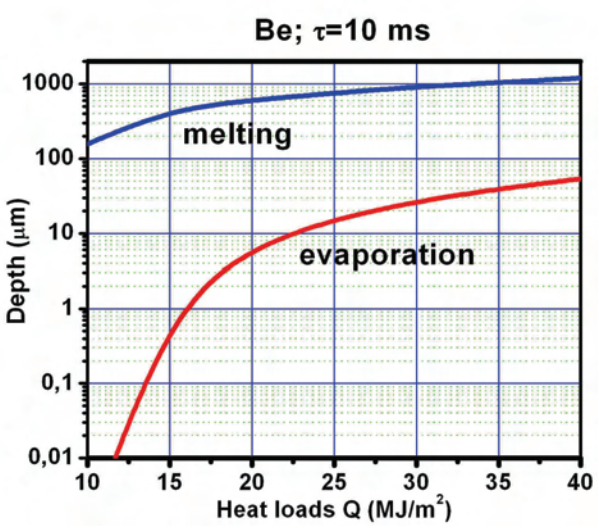

Melting pool depth and evaporation erosion thickness as function of RE heat load

Further numerical modeling using MEMOS for Li PFCs was performed. This work was motivated by the Li activity on the tokamak FTU. The melt motion and the evaporation at Li surfaces under a heat load of 0.1 MJ/m^2 during a rectangular pulse of 0.5 ms was considered assuming a Li film of 10-50 μm

thickness on an impermeable W substrate. It seems that the model of a porous substrate will not be effective as a compensator for melt layer evaporation or mechanical removal during transients.

Physics: Heating and Current Drive - ECRH

In recent years, electron cyclotron resonance heating and current drive (ECRH and ECCD) have successfully been established as powerful instruments in magnetically confined fusion plasmas. Gyrotrons are the unique devices meeting the extraordinary requirements of those applications: output power in the MW range, 100 – 200 GHz output frequency, pulse length of several seconds up to continuous wave. Due to its excellent coupling to the plasma and the very good localization of the absorbed RF power, ECRH is being applied in present day machines and is also foreseen in large forthcoming fusion projects: it will be the main heating system for the stellarator W7-X, which is currently under construction, and it will play a major role in the ITER tokamak.

Microwave Heating for Wendelstein 7-X

The complete ECRH system of W7-X (10 MW, 140 GHz, CW) will be provided under the leadership of KIT together with EU partners (IPF, University of Stuttgart; IPP Greifswald; CRPP Lausanne; CEA Cadarache; TED Vélizy). The acceptance tests of the series gyrotrons have been continued with the successful site acceptance test (SAT) of the gyrotron SN3a. SN4R, the first W7-X gyrotron equipped with an improved beam tunnel, was delivered and tested at KIT successfully without parasitic oscillations, full power operation of that gyrotron with 1 MW is expected. The manufacturing and installation of the components of the basic transmission system are finished now. Remaining work includes diagnostics and power measurement of the gyrotron beams.

Development of the European 170 GHz Gyrotron for ITER

The development of a 2 MW, CW, 170 GHz coaxial cavity gyrotron for ITER is pursued within the European Gyrotron Consortium (EGYC: CRPP, Switzerland; KIT, Germany; HELLAS, Greece; CNR, Italy), which acts as scientific partner for F4E, and in cooperation with ISSP, Latvia. The goal of this development is the supply of sources for 170 GHz ECH & CD at ITER providing 8 MW CW power, to cover the EU contingent on ECH & CD sources in ITER. The pre-prototype experiments were particularly successful in 2009, demonstrating 2.2 MW power at high beam quality and efficiency in short pulse operation.

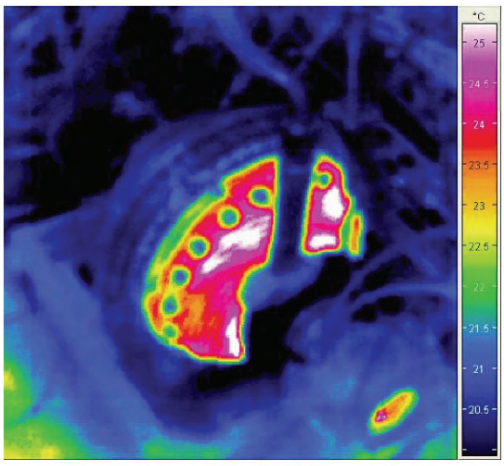

Thermal image of the spherical 1 MW CNR load (half coated, as model for the fully coated 2 MW load) at 700 kW / 140 GHz input power

Since the refurbishment of both the first industrial prototype and the pre-prototype gyrotron could not be completed in 2010, no high power experiments were done, and the next experimental campaigns are planned for 2011. In preparation of these experiments, a project for renewing the pre-prototype gyrotron and increasing its pulse length was started. In addition, a new normal conducting coil for upgrading the magnetic system at KIT and a new high power rf load were successfully tested. On the theoretical side, the design methods for quasi-optical systems were further improved, leading to rf mode converters with improved performance (Gaussian content of the rf beam increased from 96 % to 99 % and stray radiation reduced) and a first matching optics unit design. A backup 1 MW gyrotron design was finalized. For realisation, the next step would be the technical layout, to be

done by the manufacturer. This gyrotron will only be realised if the 2 MW tube development has to be replaced by a less ambitious project.

Activities in support of the gyrotron installation at ITER were conducted in parallel, aiming at improved definitions of interfaces, auxiliary devices and processes. In particular, the mutual influences of magnetic fields were thoroughly investigated.

Advanced Studies: 4 MW Gyrotron, New Emitters and Beam Diagnostic Systems

The design studies towards a 170 GHz 4 MW coaxial-cavity gyrotron were finalized and summarized in a dedicated dissertation. The result is that such a gyrotron would be feasible according to best current knowledge, regarding interaction and electron optics simulations as well as thermal limitations and technical feasibility. In parallel, the efforts on testing a new emitter concept were carried on, as well as the collaboration with the St. Petersburg State Polytechnical University (SPbSPU), on new electron beam diagnostic systems. The new emitter concept will be tested in a low power gyrotron, within the frame of another dissertation. For both topics, basic feasibility was validated by advanced simulations, aiming at first experiments towards the end of 2011.

ITER ECRH Upper Port Plug Development

The ITER ECH Upper Launcher consortium ECHUL-CA, including the EURATOM Associations CNR, CRPP, FOM, IPP and KIT was established to develop the ECH upper launcher design for ITER from preliminary to the final design level. In this last design phase, the new Extended Physics Launcher (EPL) design with its enhanced physics performance, as compared to the earlier ITER baseline, shall be consolidated into a robust system. In preparation of this step manufacturing routes have been further checked and the models for design validation by simulation have been improved.

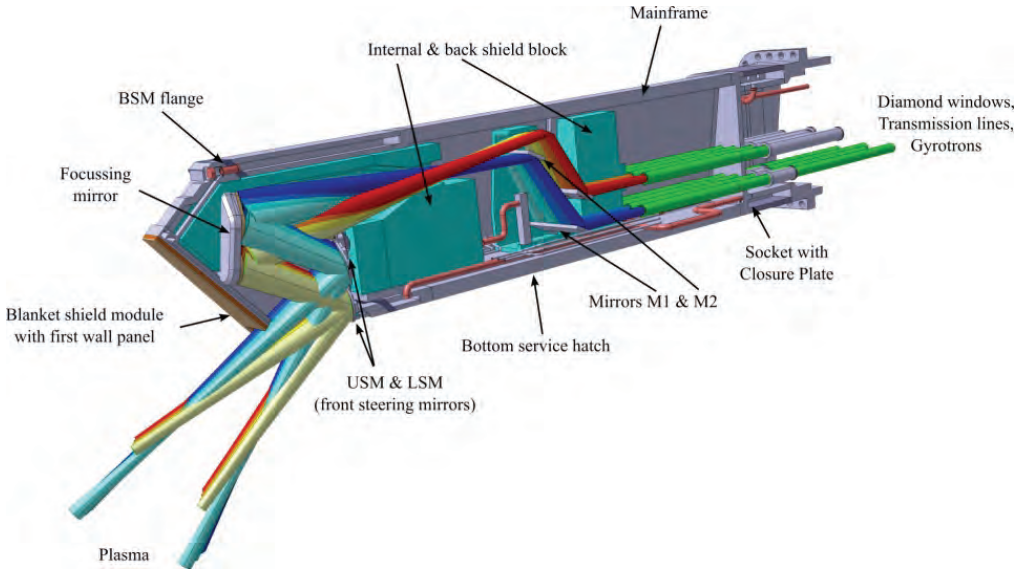

Preliminary design of the ITER ECH Upper Launcher

To allow fast procurement for ITER, the **diamond window development** has been accelerated in a separate contract with F4E. High power tests have lead to an improved design, suppressing coupling of higher order modes and resulting in a more robust behaviour w.r.t. non-ideal mm-wave beam properties.

Several upgrades for JET have been recently in discussion, one of those is an ECH system operating as 170 GHz. A pre-conceptual design of a **JET ECH launcher** has been developed to demonstrate possible capabilities in the specific JET port geometry.

Magnets and Affiliated Components

Highlight in 2010 was the successful test of the W7-X current lead prototypes. Based on rich experience from the test of the ITER TF model coil and the design, construction and testing of the ITER current lead demonstrator, KIT took responsibility for the procurement of high temperature superconducting (HTS) current leads for Wendelstein 7-X as well as for JT-60 SA. With respect to future fusion power stations, the application of high temperature superconducting coils is a promising target and KIT is preparing the use of novel High Tc Superconductors for fusion magnets.

For W7-X in total 14 **HTS current leads** are required with a maximum design current of 18.2 kA. By successfully testing two prototypes an important milestone has been reached on the way to the procurement of the current leads. The prototypes were manufactured by KIT and a special cryostat was connected to the TOSKA facility for testing. Both prototypes fully

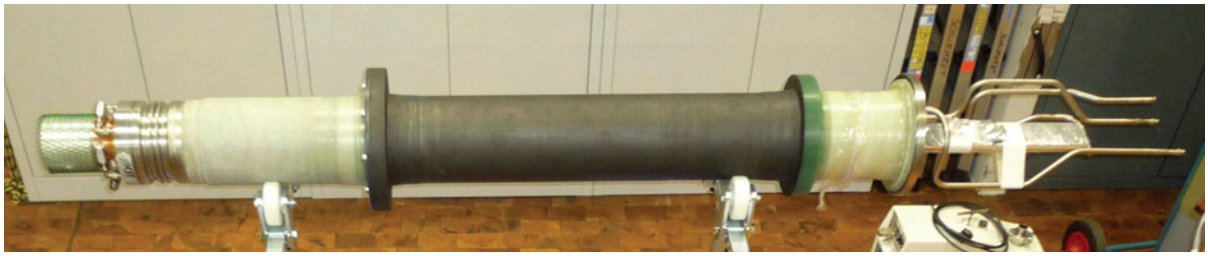

W7-X current lead prototype

complied with the expectations: The temperature margins measured are high enough and the time until quench under LOFA (Loss of Flow Accident) conditions is long enough to give sufficient safety margins under W7-X conditions. The tests demonstrate that the unconventional upside-down orientation of the W7-X heat exchangers does not affect optimal operation of the current leads, but opens new opportunities for spatially favourable design configurations.

For the TF and CS magnets of JT-60SA, 6 leads for a maximum current of 26 kA and 20 leads with a maximum current of 20 kA are required. To come to a fast and economic testing sequence, the Current Lead Test Facility Karlsruhe (CuLTKa) is under construction. The present planning expects the assembly of CuLTKa being finished until end of 2011. With the availability of this facility, the series testing of W7-X and JT-60SA current leads will be moved from TOSKA to CuLTKa.

Prototype of KIT quench detector UNIQD TYPE 3420

The development of a quench detection system for the magnets of ITER is based on the successfully completed production of ~ 600 quench detection units for W7-X. In contrast to W7-X the special requirements for use of the quench detectors at ITER are higher voltage capability (detectors input / potential separation) preserving reliable measurements of small differential signals. A first prototype of the new detector has recently been manufactured by KIT and the general function of the new design could be verified. First measurements confirm all improvements in consideration of offset-drifts, linearity and detectors internal power distribution.

Roebel-cables Assembled from Coated Conductors (RACC) are developed as high current low AC loss conductors for application in windings and magnets. Reduction of AC losses can be expected when a coated conductor is split into multifilamentary striations. A Roebel meander-shaped strand was successfully striated with a picosecond-infrared laser system. The measured magnetization loss of striated single strands is 3 to 5 times lower than that of the non-striated one. The development of a cabling concept for HTS conductors with I > 10 kA, B > 10 T and T > 50 K was continued by using Roebel cables as strands for a Rutherford type cable.

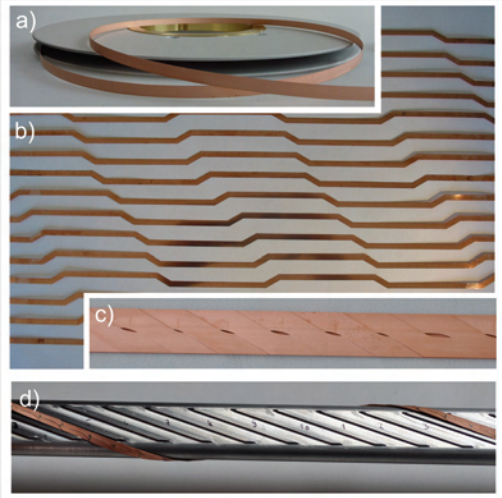

a) Commercial coated conductor tape;
b) punched tapes;
c) Roebel cable;
d) Rutherford cable former with one Roebel subcable

Breeding Blanket and Divertor

The development of breeding blankets and divertors, their integration in the core of a fusion reactor and their testing programme in ITER are central elements of KIT´s long term programme towards a fusion power plant. In particular, KIT is developing Helium cooled concepts for these systems, namely the Helium Cooled Pebble Bed (HCPB) blanket and the High Temperature Helium Cooled divertor. Several activities are also in support of the Helium Cooled Lithium Lead (HCLL) blanket concept developed by CEA. In addition tasks have been performed for the improvement (in fabrication, characterization and modeling) of functional materials like Li-orthosilicate and Beryllium.

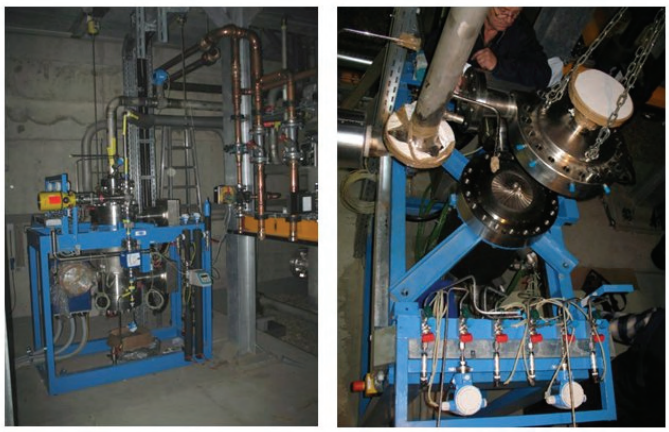

HELOKA circulator installed into the loop (left); tuning of the circulator during the commissioning in November 2010 (right)

The out-of-pile qualification of large blanket mock-ups up to 1:1 scale under high pressure He cooling is one of the major challenges in the breeder blanket development programme. To this end, the **HELOKA-High Pressure/TBM** loop is being set up at KIT. In 2010 the construction of the piping system has been finalized with the integration of the helium circulator. The work on the HELOKA DACS was continued with the definition of the technical specifications of the loop control and the integration of various subsystems. The contract has been awarded in October 2010 to Siemens. Currently, the detailed design of the system has been finalized and the cabling work is almost finished.

The institutions working on the European TBM programme have organised themselves in the **European Test Blanket Module Consortium of Associates** (TBM-CA, with the participation of KIT, CEA, ENEA, CIEMAT, RMKI and NRI) with KIT providing the project leader and hosting the central support team. A major activity for the design of the EU Test Blanket Systems in ITER was performed in the framework of the **F4E Grant F4E-2008-GRT-09(PNS-TBM)-01**. Main activities performed in KIT were: (1) Definition of an experimental & simula-

tion programme for reliable HCPB TBS test programme in ITER, (2) conceptual design of the HCPB TBM, including performance analysis and development plan, (3) preliminary plan for the manufacturing of a HCPB TBM, (4) conceptual design of the HCLL- and HCPB-Helium Cooling System and their integration in ITER. In addition, contributions for the definition of MHD Experiments for the HCLL TBM, for non-destructive testing in TBM manufacturing and for the development of the Tritium Technology for the TBM auxiliary systems have been performed in 2010, resulting in the compilation of more than 50 reports.

Another important work in 2010 was performed in grant **F4E-2009-GRT-030(PNS-TBM)**. The grant is divided in three actions and KIT is among the beneficiaries in all of them. The first action was accomplished in the frame of the TBM-CA for the “Elaboration of the Development/Qualification/Procurement Plan for Functional Materials”. KIT worked for the part related to the ceramic breeders and for the Be development in collaboration with NRG (Petten) for the irradiation of ceramics. The conclusion of the grant is foreseen at the beginning of the 2011 with the delivery of two important reports. KIT has taken a role of coordinator also for the Action 2 “Screening of an alternative production route/capacity for Be pebbles” in collaboration with the Institute of Nuclear Technology (ITN, Portugal). Within the Action 3, a series of Post Irradiation Examinations (PIE) is foreseen on a selection of beryllium grades with maximal resistance to the radiation damage. The irradiated Beryllium comes from a two years irradiation experiment (HIDOBE-01) in the Petten Reactor of different Be batches from EU, Japan and RF with an estimated He production in the reactor of ~3000 appm. Within the contract, several PIEs are planned in KIT on the irradiated beryllium materials: tritium release measurements, microscopy (OM and SEM), TEM and creep measurements. The main part of the PIE will be performed in 2011.

A further F4E grant **(F4E-2009-GRT-037 (PNS-TBM))** was awarded and completed in 2010, a “Study of the Impact Caused by the Implementation of Mitigation Means for ITER TF TBM-induced Ripple on TBMs Design”. The objective of this F4E Grant was to evaluate in the EU TBM Project (and in the other TBMs of the international Test Blanket Programme in ITER) the impact of some proposed counter measurements (e.g. reduction of TBM dimension or increase of recession from the plasma) on the design feasibility and on the testing programme of the ongoing design of the TBM. The contract was done in the framework of TBM-CA, with the participation of KIT and CEA.

In the framework of “Components and Instrumentation Development for TBM (**TW2-TTBB-007b**)” a “Preliminary Study of the Tritium Accountancy System and Conceptual Study for Alternative Processes based on Membrane and Membrane Reactor” has been completed in 2010, closing the EFDA task. The 3rd and last deliverable of this task discussed possible materials and separation techniques with membranes, reporting the state of the art for newly developed zeolite membranes, detailing different process options and expected performances using zeolite membranes, and discussing the use of water in the system. Another EFDA task, “Support of the EU/RF Collaborative Task on Fabrication of Be Pebbles for Fusion Application and Beryllium Recycling (EFDA/06-1394 - **TW6-TTB-RFMON2**) has been completed in 2010. The objective of this activity was the exploration of the possibilities to identify the properties of Be pebbles defined as a base material for application in the Solid Breeder Blanket; to this end, different aspects of the fabrication and utilization of the beryllium pebbles with different morphology were investigated. In addition, the particular features of beryllium recycling after operation has been considered and analyzed.

The development of the High Temperature Helium Cooled Divertor using W/W-alloy as a structural material continued in 2010 with 3 EFDA tasks: two on fabrication processes for W structures and one on testing of optimised finger Module mock-up's. In **WP10-MAT-WWALLOY-01-02** the deep drawing technology was investigated for the production of W-alloy thimble. This method promises a strength increase in the structure using a forming process orientating the grains of the material uniformly along the contour. Further development for the W-WL10 brazing joint was performed in **WP10-MAT-WWALLOY-01-13**. A new brazing technology was proposed based on 60Pd40Ni filler, new specimens were manufactured and investigated. The new series of experiments in Efremov **(WP10-MAT-WWALLOY-01-14)** achieved a first breakthrough in the qualification programme for the divertor target: one finger was able to survive 1000 cycles at 10 MW/m^2. From this result, further improvements are planned with the use of high temperature brazing filler metal such as Ti-alloy in the finger manufacturing.

First W deep draw attempt with a new developed tool (left), thimble cap from 1 mm W sheet (right)

Structural Materials - Steels

High performance structural materials for in-vessel components are indispensable for economical operation of fusion power reactors. Low activation is an additional prerequisite for sustainability. Outcome of intense R&D work of many years is the ferritic martensitic steel EUROFER which is the European reference structural steel for ITER-TBM and DEMO in-vessel components. One of the most crucial items for the application of EUROFER in a fusion power plant is its performance under intense neutron irradiation. This question – which can be ultimately only answered by IFMIF – was tackled in 2010 activities of KIT.

Recent knowledge on the irradiation behaviour of EUROFER is mainly based on two irradiation campaigns: the SPICE experiment in the HFR/Petten up to 15 dpa damage at temperatures between 250 and 450 ^{o}C and ARBOR 1+2 in BOR 60 with damage up to 70 dpa and a sole irradiation temperature of ~330 ^{o}C.

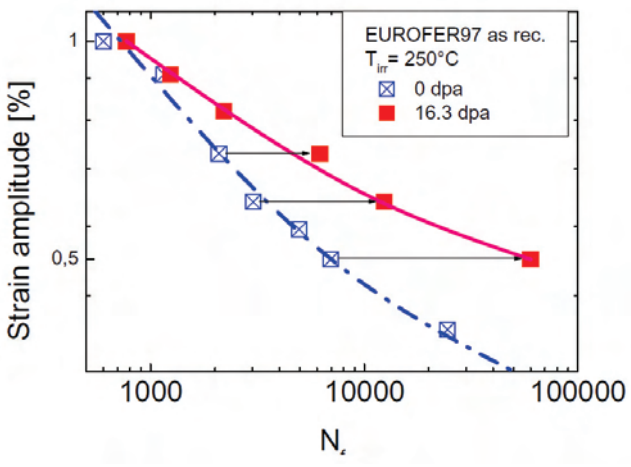

Effect of low temperature irradiation on fatigue lifetime N_f at $T_{test}=T_{irr}=250$ °C

Fatigue and creep-fatigue tests including crack monitoring were performed on SPICE irradiated EUROFER samples. It is a novel and major result of this work that specimens irradiated at the low irradiation temperature of 250 °C show a remarkable fatigue life increase that progressively steps up with decreasing strain amplitude. These results confirm the similar trend shown by the low cycle fatigue test results in ARBOR 1+2 and predicted by the coupled deformation damage model recently developed for RAFM steels under low cycle fatigue and high dose irradiation conditions.

One of the shortcomings of fission reactor irradiations compared to irradiation under real fusion neutrons is the inadequate formation of He. This lack was tried to be compensated by bringing artificially He into the material matrix by doping the material with boron which is transformed into He under neutron bombardment. **TEM characterizations** of boron doped specimens irradiated in SPICE confirmed the validity of this method. In contrast to some pessimistic claims regarding the general validity of boron doping, it can be stated that there is no obvious discrepancy compared to low dose rate based implantation techniques, neither in the helium bubble nucleation nor in the bubble size distribution.

The same general fatigue behaviour as found in the SPICE irradiation was found for the **boron doped versions of EUROFER** (ADS variants) in ARBOR irradiation up to 70 dpa. In most cases the neutron irradiation leads to a lifetime enhancement which is more pronounced for the low total strain ranges. In contrast to these findings for fatigue behaviour, the impact toughness of boron doped EUROFER at lower temperatures is heavily affected by the synergy of dpa-damage and He-damage.

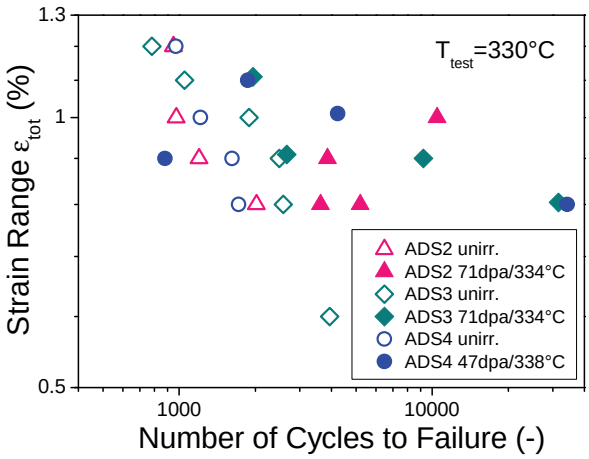

Fatigue lifetime vs. total strain range of unirradiated and irradiated boron doped EUROFER

An Oxide Dispersion Strengthened (ODS) version of EUROFER is being developed with the objective of increasing the temperature window up to the maximum operating temperature of 650 °C. ODS-EUROFER may be used to replace EUROFER parts at positions with high thermal loads. The level of development for ODS-EUROFER is by far not comparable to that of EUROFER. The fabrication, based on powder metallurgy, is in itself a significant and challenging issue, since there is presently no industrial capacity in the EU for fabricating this type of steel.

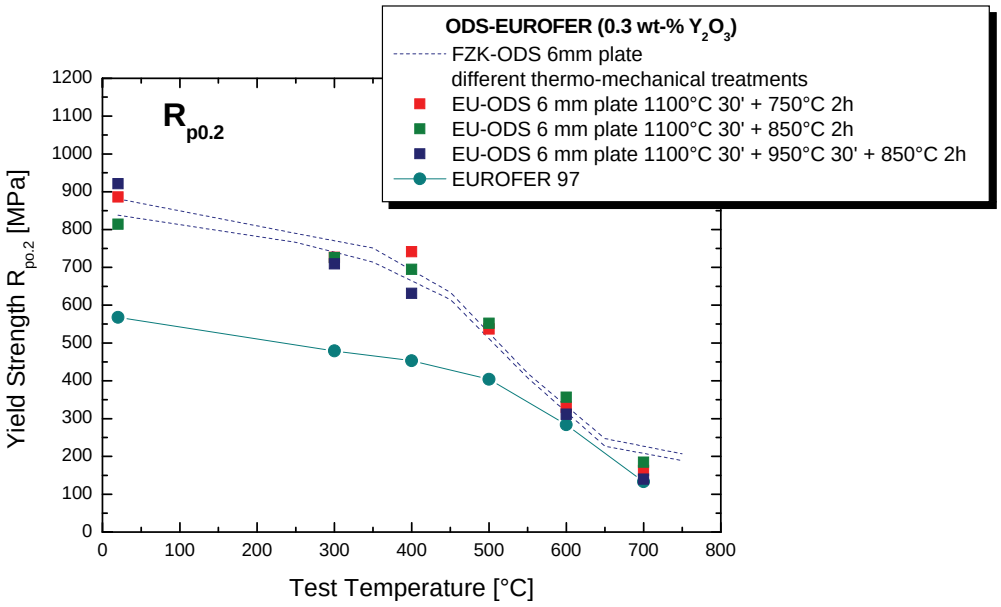

Yield strength $R_{p0.2}$ of ODS-EUROFER compared to EUROFER

A 50 kg batch of so-called EU-**ODS-EUROFER** was characterised by tensile and impact tests taking into account the effect of different heat treatments. It was shown that a double normalisation treatment followed by a tempering treatment marginally afflicts the tensile

properties but on the other hand improves the impact properties with respect to upper shelf energy and ductile to brittle transition temperature.

The development of technologies for **joining** of parts made of ODS material is also an important issue. It has been proven that EB-welding is not suitable since the mechanical properties of the weld seam are heavily affected. The deterioration of the mechanical properties can be related to the change in microstructure in the welding zone. The strengthening nano-dispersoids agglomerate to larger particles thus weakening the weld seam. Diffusion bonding provides a suitable alternative and is currently under development.

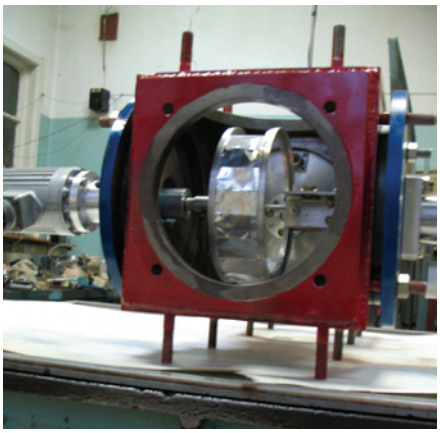

Target chamber for He implantation

The helium implantation facility based on the RRC KI cyclotron was used to study the effect of **helium atom implantation in ODS-EUROFER** samples on microstructure changes and mechanical properties. Helium embrittlement in irradiated ODS material has been observed. Microstructure investigations (TEM) before and after irradiation at T=300 °C and T=500 °C have revealed the formation of helium bubbles. At both temperatures ODS particles act as effective trapping centres for helium bubbles. With increasing irradiation temperature the number and size of trapped bubbles increase. Large bubbles observed in the bulk of the material are presumably located on dislocation lines providing additional obstacles for dislocation motion.

Structural Materials – Refractory Alloys

The helium cooled divertor concept envisaged to remove heat loads of up to 10-15 MW/m² is based on a modular arrangement of cooling fingers, which use refractory materials as tile at the plasma facing side and refractory materials as structural material forming the cap of the cooling fingers. Tungsten and tungsten alloys are presently considered for both applications mainly because of their high temperature strength, good thermal conductivity, and low sputter rates. For armour materials, high crack resistance under extreme thermal operation condition is required, while for structural materials, sufficient ductility within the operation temperature range is mandatory. Both material types also have to be stable with respect to high neutron irradiation and transmutation rates.

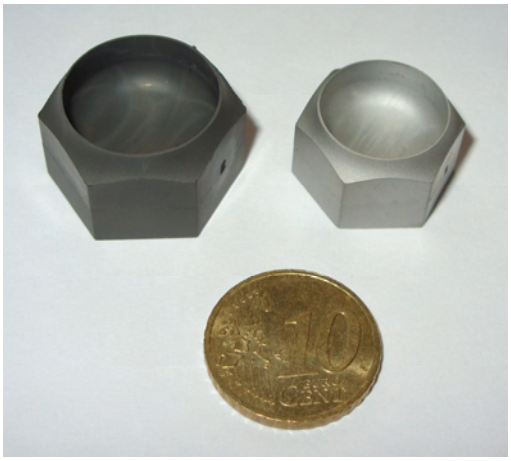

Green part (left) and finished W tile after pre-sintering and HIP treatment (right)

Powder Injection Moulding (PIM) offers a large potential for mass production of near-net-shape parts with high precision. Based on pre-tests a new tungsten feedstock with a binary W powder system was developed and a PIM tool to produce the divertor part W tile was designed. Also a filling simulation to define the gating system and to detect possible air traps was performed. The manufacturing of the W tiles with the new PIM tool was successful. After heat-treatment (pre-sintering and HIP), the finished parts were characterized and the results of density, hardness and microstructure were very satisfying.

Characterisation of W-alloys includes tensile, impact toughness (Charpy) tests as well as microstructural investigations. In Charpy tests pure tungsten rod materials show distinct temperature ranges for brittle (transcrystalline) fast fracture and for ductile fracture (upper shelf). The brittle to ductile transition shows broad scattering and is dominated by inter-granular delamination fracture. The WL10 (tungsten, dispersion strengthened with 1 wt.% La_2O_3 particles) results show a transition from brittle to delamination fracture, but no transition to ductile fracture. The delamination regime exceeds even 1100 °C. Fracture toughness investigations on W and W-Y endorsed the values generated by impact toughness tests.

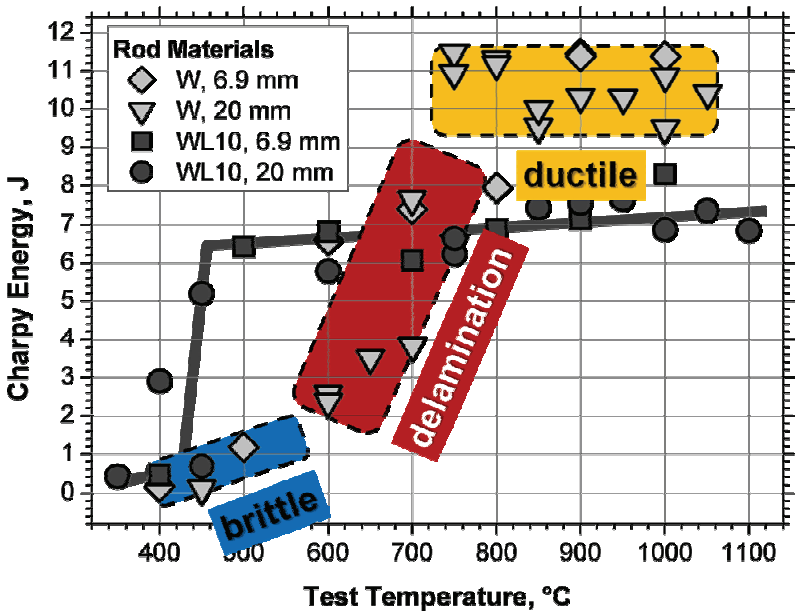

Results of Charpy tests on pure tungsten and WL10

State-of-the-art methods for machining and shaping of tungsten like milling and spark erosion have considerable drawbacks which could be overcome by the application of innovative ECM (Electro Chemical Machining) technologies. Defect-free surfaces and high precision parts at low costs could be produced by an etching process which is controlled by electrochemical dissolution. However, up to now such an electrochemical application in W-alloy processing was missing due to irreversible passivation effects at the tungsten surface. The development of the two component electrolytes (TCEE) for the first time opened the path for large area processing and shaping of tungsten. Meanwhile three different branches in ECM processing were selected and developed. Due to the different main application fields (surface finishing,

Effect of pulsed currents. From left to right increasing pulse frequency 0 Hz; 10 Hz; 100 Hz; 500 Hz; 1000 Hz

mask assisted surface structuring and 3D shaping by cathode tool dissolution) the processing parameters have to be adapted individually to each processing line The use of HF pulse currents lead to a drastic advancement in processing time and in the accuracy of shaping.

The reference concept for the helium cooled divertor implies joints between tungsten and tungsten as well as dissimilar joints between tungsten and ODS-EUROFER. For the latter one of the main problem consists in compensating for secondary thermal stresses caused by the different thermal expansion coefficients of the joining materials. Since no experience on such joining is available a basic screening of different joining methods had to be done. Three methods are currently being investigated in depth. (I) W-EUROFER brazing: To get suitable and long term stable joints the need for interlayers to suppress inacceptable diffusion reactions and for homogenous coating and complete wetting of surfaces to be joined is evident. High temperature fillers require combinations of, or with, refractory metals (e.g. W, Ta or Ti type).

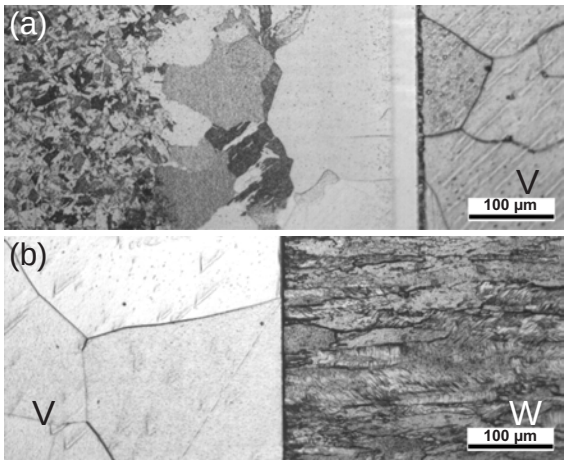

Diffusion bonding: microstructure at the interfaces between a) EUROFER and V interlayer, b) V interlayer and W

However these elements can not be deposited from aqueous electrolytes due to e.g. oxide formation. Thus an alternative and innovative development line in electro chemical deposition technology based on the use of novel ionic liquids (IL) as electrolytes was started. For first evaluation of the applicability of IL as electrolytes the aprotic component EMIM-Cl was selected. Deposition from liquid electrolytes near room temperature could be performed for the first time. (II) Diffusion bonded tungsten / EUROFER joints: A V interlayer was inserted to mitigate thermally induced residual stresses at the interface caused by different values of the thermal expansion. An improvement in strength and toughness was reached by decreasing the post weld treatment temperature. (III) Functionally graded tungsten/EUROFER97 joints: Layers with different tungsten/EUROFER compositions will be deposited on tungsten substrates.

Nuclear Data

Theoretical and experimental activities have been conducted in the frame of F4E grants, to provide a qualified nuclear data base and validated computational tools for neutronics calculations of fusion systems. The KIT contribution to the theoretical activities is on the evaluation of general purpose nuclear cross section data, the qualification of new and updated data evaluations and the development of advanced computational schemes for sensitivity calculations. The experimental activities aim at providing the experimental data base required for the validation analyses and the development of experimental techniques needed for the nuclear TBM test programme in ITER. The focus of the KIT contribution is on measurements of nuclear responses in TBM mock-up experiments and on advanced measurement techniques.

A release version of the **Monte Carlo sensitivity code MCSen** has been prepared and submitted to the NEA Data Bank of the OECD for dissemination among member countries. This will allow the users to create an MCsen executable using a patch to the standard MCNP code package. The MCsen based sensitivity and uncertainty analysis performed for the Helium Cooled Lithium Lead (HCLL) Test Blanket Module (TBM) in ITER showed comparatively low sensitivities and small uncertainties with a resulting computational uncertainty margin for the tritium production rates between 2 % and 4 %, based on available covariance data.

As part of the evaluation effort for **general purpose neutron cross-section data** of the stable chromium isotopes, **co-variance data** based on experimental and nuclear model uncertainties have been generated and utilized to update the evaluations in a consistent manner. The figures show examples of cross-sections and their uncertainties obtained from nuclear model calculations, and the evaluated final cross-sections and uncertainties. The co-variance data were processed for general use with uncertainty calculations.

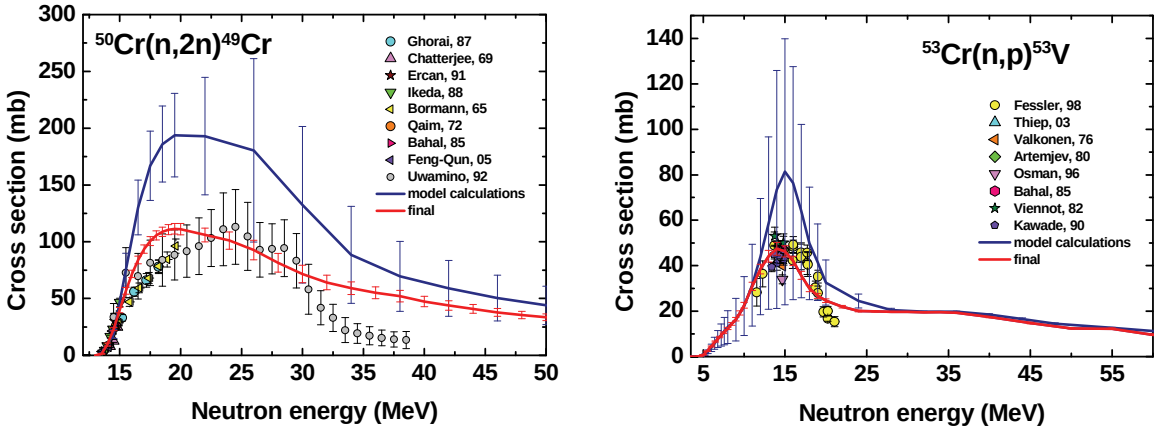

Calculated (blue lines) and evaluated (red lines) n + Cr cross-section data and uncertainties

Experimental tests have been performed for **measurement techniques for radiation doses** deposited in blanket structures in a mixed neutron-photon field, employing optically stimulated luminescence detectors (OSLD) made of beryllia (BeO) and utilizing higher order peaks in the glow curve of LiF thermoluminescense detectors (TLD). The tests conducted using the 14 MeV neutron generator at the neutron lab of the Technical University of Dresden (TUD) showed promising results in view of tritium production measurements in the ITER TBMs.

Validation experiments were done for the **activation of Ti/Li_2TiO_3 samples** upon irradiation in the DT fusion peak neutron field of the TUD neutron generator. While not all the produced radio-nuclides could be investigated due to the limited neutron fluence and some very low gamma line intensities, good agreement was found for the measured activities as compared to the predictions by the FISPACT inventory code with EAF-2007 activation cross-sections.

International Fusion Materials Irradiation Facility (IFMIF)

In the **Engineering Validation and Engineering Design Activities (EVEDA)** for the International Fusion Material Irradiation Facility IFMIF, the German contribution includes engineering tasks for the IFMIF Test Cell and the IFMIF High Flux Test Module, as well as development and application of dedicated neutronic simulation methods.

The **IFMIF facility** is dedicated to fusion-relevant irradiation of structural and functional material specimens, with the objective to create an experimentally validated material properties database suitable for design and licensing of future fusion power plants. The work performed at KIT is focused on the Test Facilities. In this part of the IFMIF plant, several irradiation experiments (“Test Modules”) will be installed inside a protective test cell, and radiation protected handling cells are provided to allow the installation/dismantling of the irradiation experiments and the examination of the specimen. The arrangement of the irradiation experiments inside the test cell is shown in the following figure.

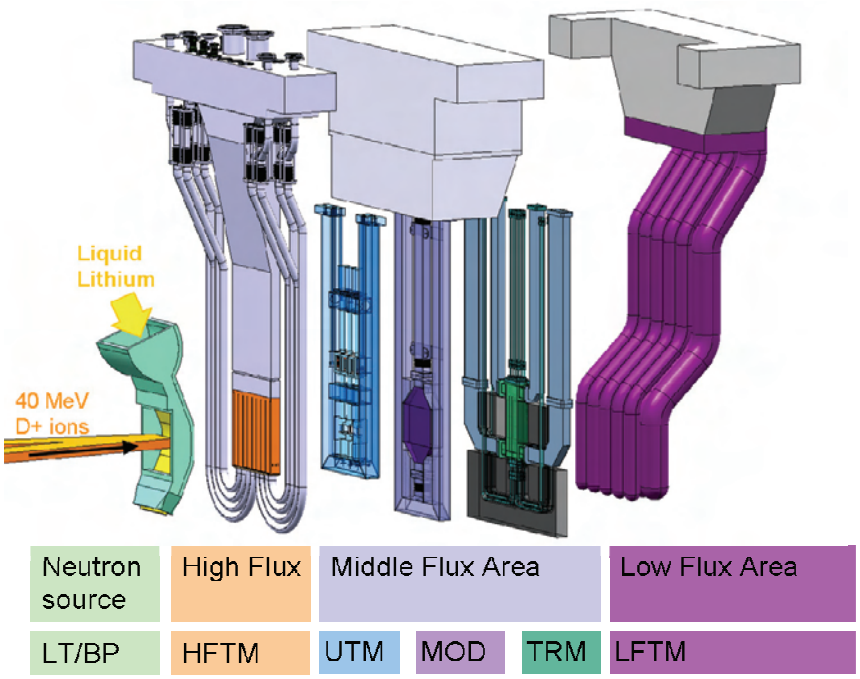

Overview on the irradiation experiments inside the IFMIF Target- and Test Cell (TTC)

The **design of the IFMIF** test cell has been advanced with emphasis on the following aspects:

- Performing functional analysis on the test cell to identify the detailed technical requirements on the test cell design;
- Optimizing the inner enclosure of the test cell and the means of attachment between the vessel and the concrete;
- Performing engineering designs on key elements, including Test Module Interface Heads, the pipe and cable connections, the supporting and transferring system for the TMs, in the TTC;
- Introducing additional shielding materials based on neutronic calculations in the TTC.

From the analyses, two new concepts have emerged for the test cell: The MTC-V concept features a cylindrical vessel with a gas tight cover, directly embedded in heavy concrete for radiation shielding. The MTC-L concept is a cuboid cavity in the concrete, completely covered with a thin steel liner. In the MTC-L case, the top radiation shielding is placed within the hermetic sealing. The MTC-L concept has a potential to arrange the necessary electrical connectors in a way, that they are shielded much more from the intense radiation than in all previous concepts. Neutronic studies have yielded that the lifetime of electrical connectors in the IFMIF test cell environment can be a severe limiting factor for lifetime and reliability.

The **design activities for the high flux test module (HFTM)** are being supported by an extensive experimental program. An experiment to test a single irradiation rig has been prepared to be taken into service. This experiment features measurements of pressure drop in the cooling gas streams, mass flow distribution, local temperatures and deformation of the structures. It serves to qualify the rig design as well as the engineering tools used, by providing experimental benchmark data.

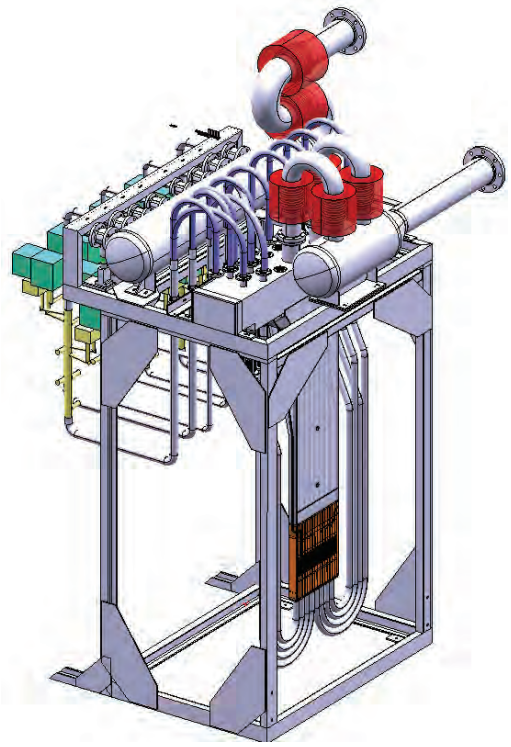

3D CAD design of the HELOKA TS-Port integrating the IFMIF High Flux Test Module prototype

The follow-up experiment, where three rigs in a 1:1 HFTM compartment will be studied, has been CAD-designed. This experiment will be integrated in the HELOKA-LP helium loop. The HELOKA-LP facility has been successfully operated in a test mode and optimized. Additionally, measurements on the cooling gas impurity chemistry were done.

Furthermore, the components for **six irradiation capsules have been prepared**. Three such capsules will be used to be irradiated in the BR2 test reactor. The purpose of this irradiation campaign is to verify the functionality of the employed heaters under irradiation and elevated temperatures. Also, the unloading of the specimen from the capsule will be studied after irradiation under hot-cell conditions, to validate the logistic procedures in the IFMIF plant.

A very important outcome of the HFTM design activities was proving the fitness of the concept for the very demanding temperature management requirements. It was proven by CFD analyses, that the system of heaters, insulation gaps and cooling channels can be used to adjust all irradiation temperatures in the required range of 250-550°C. Furthermore, it was shown in these analyses, that the non-uniformity of the specimen temperature field inside the capsules is limited to the allowed range of ±3%. Additionally, the transient behaviour of the HFTM was investigated.

The ability to model the steady state and the transient cases by CFD has been validated against experimental data from the ITHEX experiments.

Fuel Cycle – Vacuum Pumping

Since two decades, KIT has been developing vacuum pumping systems for fusion reactors. The concept of cryogenic pumping based on cryosorption at activated charcoal has been successfully demonstrated at KIT, and is now the common technology used for all primary vacuum pumping systems at ITER. As these cryopumps are part of the European procurement package for ITER, KIT has been charged with the elaboration of the detailed design of the large cryogenic pumping systems of ITER. This was organised via various F4E Grants.

The **detailed design work for the cryopumps** of ITER was started in 2009 and made excellent progress in 2010. The Preliminary Design Review held at ITER IO in March 2010 passed with only minor recommendations for changes. KIT will provide the complete build-to-print package of the torus cryopumps and the Heating-NBI cryopump. Both cryopump designs are unique and will be validated by a prototype each. The HNB prototype pump will be manufactured and tested in the NBI test facility MITICA which is under construction at Consorzio RFX, Padova, Italy.

To prepare the tests of the prototype of the torus cryopump at KIT, the **test facility TIMO-2** was upgraded in order to be able to replicate two novel ITER operational requirements, namely the direct supply with cryogenic helium gas at 100 K and the supply with supercritical helium at 4.35 K (instead of 4.5 K). Both operation modes could be successfully demonstrated in a final cryogenic acceptance test campaign. TIMO-2 will replicate ITER operation conditions for the large-scale ITER pumps in the same way as TIMO did in the past for the 50% model pump.

TIMO-2 facility: New 100 K supply facility

The detailed design of the **pre-production torus cryopump** evolved in an excellent manner. The main challenge of this activity is to design this prototypical pump in such a way that it can be optionally used at ITER as a spare pump. This requires elaborating a design in compliance with design codes and standards which are all still emerging at ITER. Along this process, off-normal event cases have been studied. It could also be demonstrated by theoretical analysis that permeation of tritium into the cryogenic circuits (especially during the high temperature regeneration at 470 K) is not a problem during the prospected lifetime of ITER.

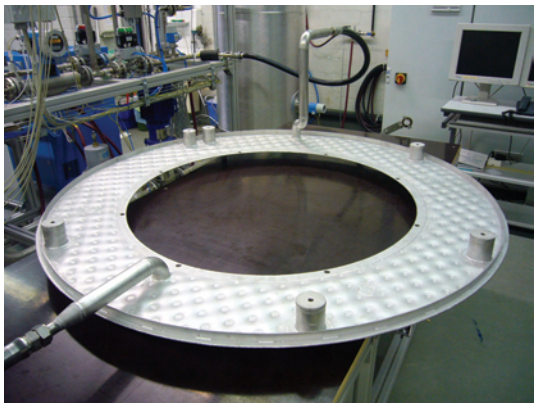

Thermohydraulic measurement of the torus cryopump front shield

In support of the design work, experiments were performed in two critical areas in which reliable predictive calculation tools are missing. One activity was the characterisation of the metal seal which is used to close the integral inlet valve during pump regeneration. Various designs of this seal ring were compared and the force needed to achieve a given leak rate was measured. Following from this number (which was fixed to 125 kN) the complete actuator system could be designed. The second critical area, especially regarding the cryogenic supply, are the pressure drops in the thermal shield and cryopanel circuits of the pump. To support the calculations, the front shield of the thermal shield system, which is assumed to be the most resistant component, was manufactured at 1:1 scale and tested in the THEA facility at KIT. The internal pressure drops at ITER relevant Reynolds numbers were measured and it could be verified that the requirements can be fulfilled with the current design.

The **HNB/MITICA prototype cryopump** design was continued and the conceptual design was further elaborated to a high level of detail. A milestone that has been reached was the detailed analysis of cryogen flow distributions and determination of the cryogenic mass flows needed to take up the heat loads. It could be shown that, after some optimisation and rearrangement of the circuit flowpaths, the achievable pressure losses are only half of what has been anticipated previously. This allowed significant relaxation of the cryoplant requirements at ITER.

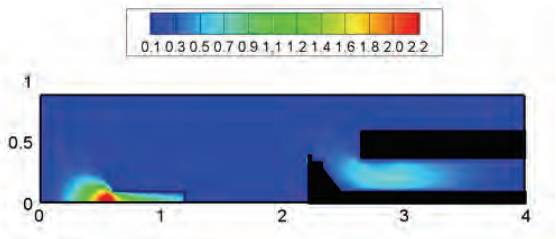

Typical plot of the Mach number contours for the pump installed in TIMO. The left side shows the gas injection pipe, the right side the pump with fully opened inlet valve

A special highlight was the progress in **modelling of vacuum flows** throughout the whole range of the Knudsen number. Here, for the first time, a complete ITER torus cryopump with all its internal complexity could be modelled in the full operational regime, which includes the transitional flow range. This was achieved by proper coupling of collisional and collisionless Monte Carlo simulations. Furthermore, the use of the existing codes could be simplified much by integrating proper graphical user interfaces. The ProVac3D code was successfully validated further and applied for the modelling of the ITER gas injection systems and the theoretical description of the gas density profiles for the ITER Neutral Beam. The various Monte Carlo codes which have been developed over the last years were parallelized, wherever possible, and implemented at the HPC-FF Supercomputer so that the calculation times could be drastically reduced.

Finally, first activities to **develop the fuel cycle of DEMO** were initiated under the EFDA Coordinated Committee on Fuelling and Pumping. They were devoted to a study of potential improvements and simplifications of the ITER inner fuel cycle in view of a variety of DEMO concepts with different requirements. It is anticipated that this work will be further detailed and extended in the next years under the EFDA Power Plant Physics and Technology Department.

Fuel Cycle – Tritium Plant

The Water Detritiation System (WDS) and the hydrogen Isotopic Separation System (ISS) are European contributions to the ITER tritium plant. Both systems have been set up at technical scale in the Tritium Laboratory of KIT in order to investigate the behaviour under various operating conditions. Specific data derived from the experiments are currently being incorporated into the design of the respective systems for ITER.

Further fusion research activities at TLK are related to the outer tritium fuel cycle, i.e. the processing of gas streams from breeding blankets. The aim is to establish for the test blanket modules (TBM) of ITER reliable systems for coolant processing and tritium extraction. As the solution favoured for the TBM is not the best choice when much larger flow rates, characteristic for a fusion power plant, are to be processed, innovative solutions are looked for.

The set-up of the experimental facility TRENTA based on the **combination of the WDS and the ISS** is almost completed. In 2010 the heat exchanger was optimized in terms of pressure drop and flow rate capability. The hardware of the glove box and valve box required as interface systems for the combined operation of the WDS and the ISS were installed. The schedule of the experimental programme has been set up in a way to simulate the dynamic interaction of WDS and ISS under different ITER operation scenarios.

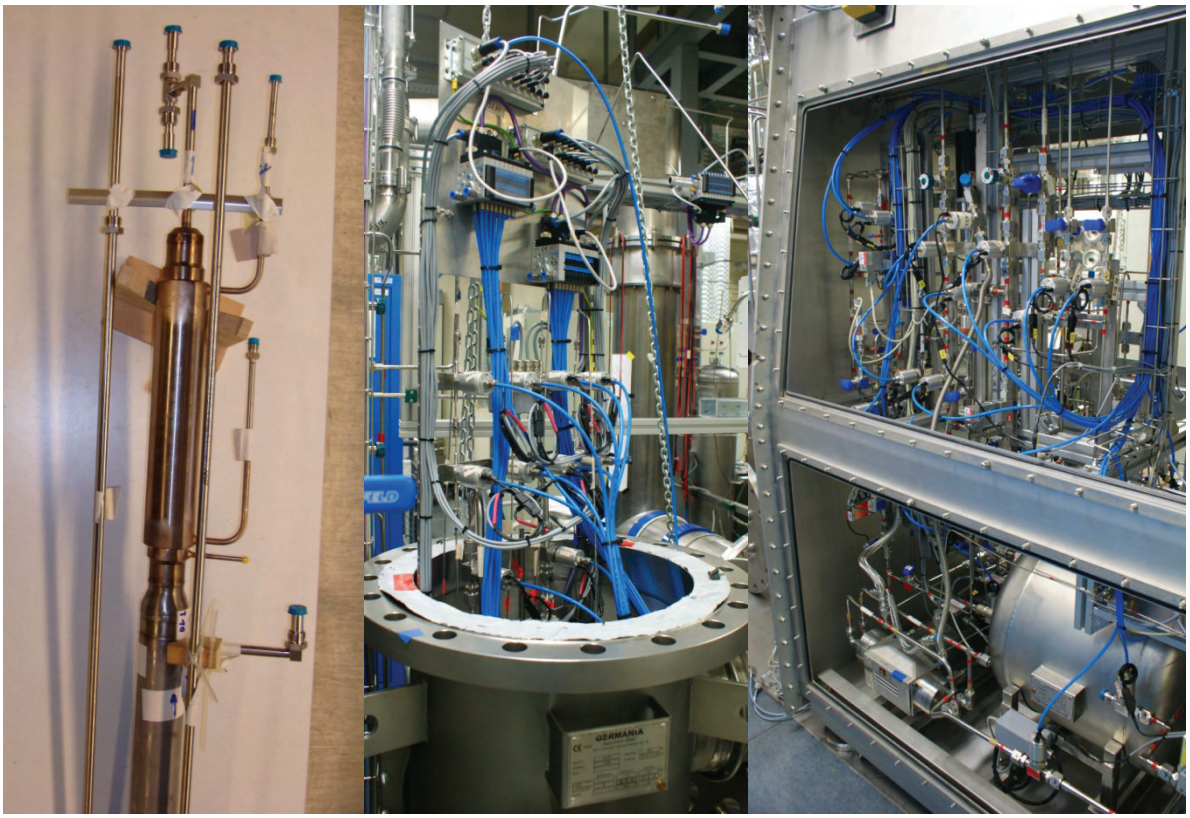

Modified heat exchanger to be installed inside the cold box of the CD (left); valve box (middle); glove box (right)

A **critical assessment of the ITER 2001 baseline design of the ISS** in the light of recent ITER requirements was performed. Tritium inventory and controlling strategies of the ISS were evaluated using different compositions of feed and product streams. The simulation codes employed were the TLK TRIMO code and the commercial code FLOSHEET.

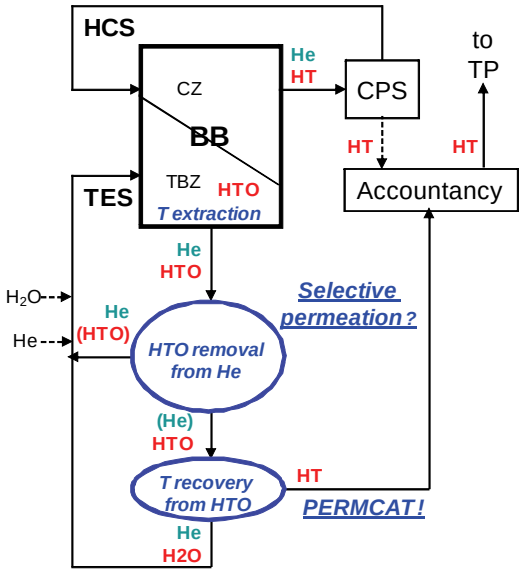

Alternative concept for TES based on permeation reactors

The preliminary design of the **Tritium Extraction System (TES) and Coolant Purification System (CPS)** for both HCPB and HCLL TBMs is nearing completion. The process options have been chosen to ensure a high reliability and to minimise the load on the future accountancy stage. A PERMCAT reactor (instead of the reducing bed) and a heated getter (replacing the cryogenic adsorption bed) are now considered in the baseline for TES and CPS.

For a **fusion power plant design studies** have been started, taking into account much higher flow rates in TES and CPS compared to ITER-TBM and looking for economic and robust solutions. Membrane reactors were found to be options worthwhile to be pursued in depth. Newly developed membranes could be competitive for tritium processes in the blanket. Different promising materials and process options have been identified. Combining PERMCAT with zeolite membranes as pre-concentration stage could offer a flexible, simple, and continuous process for the blanket. Significant benefits could also be expected by a very low tritium inventory by avoiding the need for cryogenic temperatures. Moreover, such an approach should greatly simplify and optimise the accuracy in view of an online and real-time tritium accountancy system.

Fusion Programme Management Staff

Head of the Research Unit	Dr. K. Hesch	ext. 25460 e-mail: klaus.hesch@kit.edu
Secretariat:	Mrs. A. Knoll	ext. 25461 e-mail: anja.knoll@kit.edu
	Mrs. M.-E. Tuzia	ext. 22435 e-mail: maria-elena.tuzia@kit.edu
Program Budget, Administration, Reports, EU-Affairs	BW. M. Henn	ext. 25547 e-mail: michael.henn@kit.edu
	Mrs. I. Pleli	ext. 28292 e-mail: ingrid.pleli@kit.edu
Blanket and Divertor Development, HELOKA, IFMIF, Public Relations	Dr. D. Radloff	ext. 28750 e-mail: dirk.radloff@kit.edu
Fuel Cycle, Structural Materials, Superconducting Magnets, CAD-Office	DI. S. Gross	ext. 25468 e-mail: sigurd.gross@kit.edu
Plasma Heating Technology, Safety Studies, Neutronics, Physics	Dr. K. Hesch	ext. 25460 e-mail: klaus.hesch@kit.edu
Quality Management, Resource Loaded Planning, Document Management	Dr. J. Gafert	ext. 22923 e-mail: juergen.gafert@kit.edu
	Dr. I. Ignatiadis	ext. 85465 e-mail: Ioannis.ignatiadis@kit.edu
	Dr. M. Ionescu-Bujor	ext. 28325 e-mail: mihaela.ionescu-bujor@kit.edu
	Mrs. DI. B. Keim	ext. 24194 e-mail: birgit.keim@kit.edu
	Mrs. DI. Ch. Schweier	ext. 28325 e-mail: christine.schweier@kit.edu

Address: **Karlsruhe Institute of Technology**
Nuclear Fusion Programme Management

Post Office Box 3640, D - 76021 Karlsruhe / Germany

Telephone No: **0721-608-Extensions .....**

Telefax No: **0721-608-25467**

world wide web: **http://www.fusion.kit.edu/**

Contents

Page

Page

Page

Page

Plasma Wall Interaction

Validation of KIT Numerical Modelling against Experimental Data obtained at Experimental Facilities in EU, RF and Ukraine (WP10-PWI-05-02)

Introduction

In the future tokamak ITER plasma edge localized modes (ELMs) and disruptions of the plasma confinement may produce vaporization and melting of the divertor and first wall surfaces made of reference ITER materials, beryllium and tungsten. For transient heat loads below the melting threshold the surface cracking should be accounted for in ITER design. In addition, thermoconductivity of carbon fibre composite (CFC) near the surface remains an issue in lifetime estimations.

For modelling of tungsten melt motion damage including bulk heat transport, the incompressible fluid dynamics code MEMOS was applied. The validation of MEMOS by experiments at the plasma gun QSPA-T and the applications of the code for supportive numerical modelling of the melt damage to the W targets in the ITER simulation experiments at the tokamak TEXTOR have been continued. Furthermore, new calculations with MEMOS have been performed to determine the magnitudes and the thresholds of melt splashing of Be and W under pulsed heat loads.

Brittle destruction (cracking) of the tungsten armour under action of ELMs is considered a serious problem for ITER divertor. The cracking can produce W dust with characteristic sizes of particles ranged from 1 to 10 μm. The particles can leave the surface with the velocities up to 10 m/s, they cross the scrape-off layer (SOL) and evaporate in the confined plasma.

The thermo-mechanics code PEGASUS was earlier applied for W surface cracking under the loads below the melting threshold. PEGASUS code describes processes as crack formation in W and CFC, thermal conduction and dust production. Analytical calculations have been performed aiming the interpretation of experimental observation at the plasma gun QSPA-Kh-50. In 2010 further validation and improvements of PEGASUS models have been developed.

Validation of MEMOS and simulations of melt motion damages for ITER

The code MEMOS describes the fluid motion on molten surfaces taking into account such material properties as the surface tension and the viscosity. In the code the plasma pressure variations along the surface, as well as the gradient of surface tension and the **JxB** force caused by the currents crossing the melt layer immersed in strong magnetic field as well as by the eddy current generated due to the poloidal field evolution, produce the melt acceleration.

In order to validate MEMOS against experimental data, two-dimensional simulations with account of the macrobrush structure of the targets were performed. The W macrobrush structure can effectively prevent gross melt layer displacement, thus decreasing the erosion both for single and multiple transient loads.

For TEXTOR relevant calculations, the energy deposition function of time t was obtained by comparison between experimental surface temperature Texp(t) and calculated T(t) at the most heated place (hot spot). The Child-Langmuir law was assumed (i.e. the thermoelectric current limited by the space charge in front of the target) for calculating the melt motion driven by the **JxB** force for the current density **J**. The simulations of the surface damage were performed for heat load duration τ = 5 c, plasma pressure 10-3 bar, the magnetic field B = 2.5 T, brush size D = 1 cm and gap width a = 0.5 cm. A good agreement between the calculations and the experimental data on heat load and surface temperature is obtained (Fig. 1 and Fig. 2). The calculated melt layer depth ~ 1.5 mm per one pulse of load is in some agreement with the TEXTOR experiments. However, the experimental mountains of resolidi-

fied tungsten of ~2 mm per shot were overestimated by a factor of 2 in the corresponding MEMOS simulations.

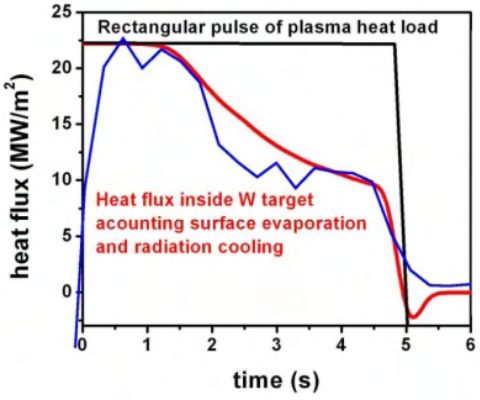

Fig. 1: Time dependence of experimental (blue) and simulated heat flux at the target surface.

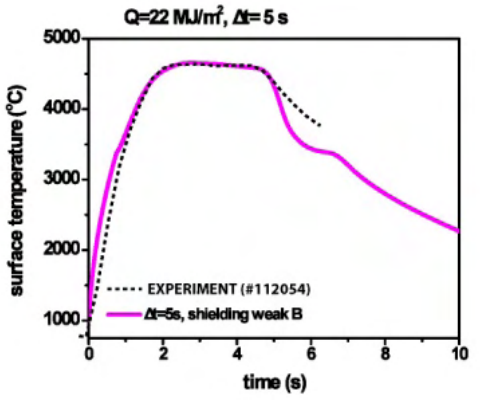

Fig. 2: Time dependence of experimental and simulated surface temperature.

Furthermore, new MEMOS simulations have been performed to obtain the effective thermoconductivity of CFC material deteriorated after multi-pulsed loads. The conclusion is that the degradation threshold appears by heating CFC above 3600 K. Those high temperatures can be reached at rather low deposited energies Q ~0.5 MJ/m^2, which is usually considered as still tolerable ELM size of ITER design. Thus we assume that the complex structure of CFC degenerates above the threshold, resulting in a carbon sub-surface layer of a few tens of microns. The effective heat conductivity of degenerated layer has been validated against experiments at the plasma gun QSPA-T (TRINITI, Troitsk, Russia) and it can be used for further numerical simulations for tokamaks (see Fig. 3). The obtained thermal conductivity in the degenerated layer correlates well with that of fine grain graphite.

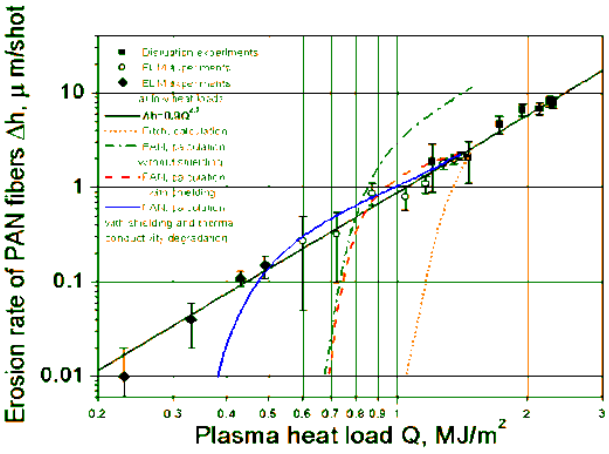

Fig. 3: Dependence of CFC erosion rate on Q. MEMOS simulations agree better with the experimental points if assuming decreased thermal conductivity in a sub-surface layer.

Simulation of tungsten armour cracking after repetitive ELM-like heat loads using the code PEGASUS

Numerical investigations with PEGASUS code of tungsten behaviour under the transient heat loads expected in ITER need experimental verifications. For this purpose, a dedicated series of experiments have been performed with the quasi-stationary plasma accelerator QSPA Kh–50 (Kharkov, Ukraine) for pulsed repetitive ELM-like plasma impacts on tungsten targets of ITER grade. Measurements of residual stress below and above the melting threshold were done and compared with the corresponding results of PEGASUS code.

The main plasma parameters of QSPA Kh-50 are the following: ion energy about 0.4 keV, averaged pressure during the pulse ~2 bar, pulse duration τ ~0.25 ms (triangular shape). The heat load *Q* was varied from 0.2, 0.3, 0.45 (no melting) to 0.75 MJ/m^2 (slightly above the melting threshold). W target initial temperature T_{init} was varied as well in the range 200600 C. The samples were exposed to a perpendicular plasma stream. The X-ray diffraction technique (XRD) was used in order to study the micro-structural evolution of the exposed targets.

The lattice parameter 0.3164 nm measured in a stress-free state is close to the reference value 0.3165 nm, which is an indication of a negligible number of vacancies in the W lattice.

If the surface melts, residual tensile stress appears after the pulse due to fast resolidification of the melt. If there was no melting during the pulse, the stress is due to plastic deformations of the heated material. After a number of pulses, if the tensile stress exceeds some maximum value, cracks appear in a thin sub-surface layer. Cracking should significantly reduce initial resolidification stress, and only the residual stress is practically measurable. The minimum pulse number necessary for cracking depends on Q.

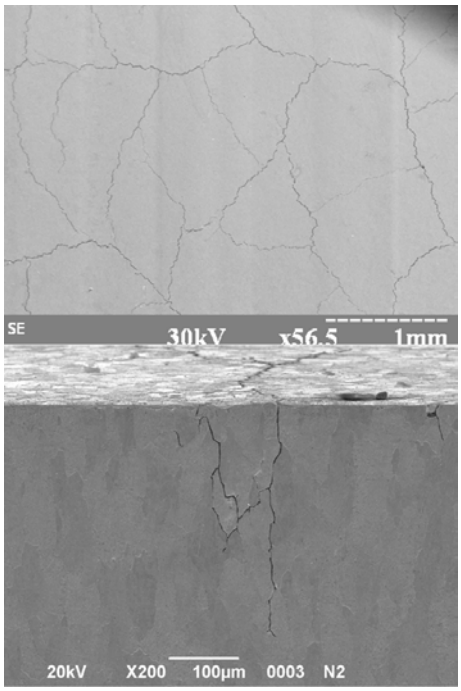

Fig. 4: Cracking at W surface after 5 pulses at Q = 0.45 MJ/m^2 (upper panel) and a normal cut showing crack depth ~ 0.3 mm.

In the experiments the cracks can appear after a small number of pulses. For instance, after 5 shots the cracks appear at Q > 0.3 MJ/m^2. The stress of 0.3-0.4 GPa was measured by tungsten cracking. Macroscopically, the damaged target becomes covered with a net of random cells formed by the cracks (see Fig. 4). Typical depth of the cracks is 0.2-0.3 mm, and cell sizes are of order of 1 mm. The crack width depends on T_{init} and Q varying in a wide range 0.3 to 8 μm.

The obtained experimental results are going to be used for validation of PEGASUS. In 2010 we performed analytical estimations which allowed the prediction that the threshold for tungsten cracking of $Q_{thr} \approx$ 0.3 MJ/m^2, which was measured after 5-10 shots, is not an universal value. The analysis leads to the conclusion that increasing pulse number results eventually in appearance of cracks even at $Q << 0.3$ MJ/m^2, i.e. the value of Q_{thr} substantially decreases (material fatigue) going down to Q_{thr} ~ 0.1 MJ/m^2 for τ = 0.25 ms. The fatigue is the reason for increasing plastic deformations. Thus, the residual stress should also increase from shot to shot until the mentioned maximum value necessary for cracking.

Presently it is not possible to perform a more detailed analysis of the cracking threshold, because the analytical solution for the dynamics of residual stress showed that the maximum pulse number of cracking onset depends also on the viscosity coefficient ν at the mean temperature of target during the pulse. The data on ν at the high temperatures in question (~ 3×10^3 K) is absent. The missing information could be eventually obtained from the dependence of the cracks width from the number of shots.

Conclusions

The model assuming thermo-electric current limited by space charge has to be improved. The 3D modeling of the TEXTOR experiments by MEMOS code has to be performed.

A series of dedicated experiments with the plasma gun QSPA Kh-50 has been performed for verification of the tungsten brittle destruction model used in the PEGASUS code in order to predict ITER divertor damage by ELMs of various powers and time durations. The residual tensile stress at the W target was measured after a few shots with energy depositions up to the melting threshold. The measurements are complemented with an analytical model for residual stress dependence on the number of pulses. The obtained analytical solution was fitted to the experimental data. The estimations predict that at large number of load pulses the threshold value should decrease from Q_{thr} = 0.3 down to Q ~ 0.1 MJ/m^2.

Further modelling of the W erosion for transient heat loads at varying surface geometries, benchmarking the codes against available plasma gun and tokamak data is necessary.

Staff:

B.N. Bazylev
I.S. Landman
S.E. Pestchanyi

Literature:

[1] B. Bazylev, et al., J. Nucl. Mater. 386-388 (2009) 919-921

[2] B. Bazylev, et al., J. Nucl. Mat. 390-391, (2009) 810

[3] B. Bazylev, et al., Fusion Eng. Des. 84 Iss 2 (2009) 441

[4] B. Bazylev, et al., Physica Scripta N138 (2009), 014061

[5] B. Bazylev, et al., 2009 ICFRM-14 Sapporo, Japan, Paper O3, to be published

[6] B. Bazylev, et al., The 19th PSI Conference, San Diego, USA, 2010, to be published

[7] S. Pestchanyi, Fusion Eng. Des. 83 (2009) 1054

[8] S. Pestchanyi, et al., Fus. Eng. Des (2010). doi:10.1016/j.fusengdes.2010.05. 005

[9] I.E. Garkusha, et al., J. Nucl. Mat. 386-388, (2009) 127

[10] I.E. Garkusha, et al., Performance of Deformed Tungsten under ELM-like Plasma Exposures in QSPA Kh-50. Paper submitted to the journal J. Nucl. Matter

[11] V.A. Makhlaj, et al., Phys. Scr. T138 (2009) 014060 (5pp)

[12] V.M. Safronov, et al., J. Nucl. Mat. 386-388, (2009) 744

[13] N. Klimov, et al., J. Nucl. Mat. 390-391, (2009) 721

[14] G. Arnoux, et al., The 19th PSI Conference, San Diego, USA, 2010

Acknowledgement

This work, supported by the European Communities under the contract of Association between EURATOM and Karlsruhe Institute of Technology, was carried out within the framework of the European Fusion Development Agreement. The views and opinions expressed herein do not necessarily reflect those of the European Commission.

Numerical Modelling for Lithium PFC (WP10-PWI-05-04-01)

The behaviour of Li as a plasma facing material is now under investigation at different tokamaks. For instance, FTU experiments are in progress, with a liquid lithium limiter and a capillary porous system through tungsten porous substrate. On NSTX, the installation of liquid lithium divertor based on molybdenum porous substrate is planned. Experiments demonstrated that the 'lithization' of the vessel surface leads to a strong reduction of the heavy impurities in the plasma and a longer wall lifetime for high power heat loads. Typical thickness of liquid Li layer can be from several microns up to several tens microns.

Further developments of the numerical modelling with the incompressible fluid dynamics code MEMOS for lithium plasma facing components (PFC) have been performed. This work was motivated by the Li activity on the tokamak FTU, where a liquid lithium limiter (LLL) with a capillary porous system (CPS) has been installed. A heating system increases the Li temperature above the melting point 450 C. As a result, a thin lithium film forms on the chamber wall coating. The impact of the hot confined plasma on the limiter surface produces Li ions in the vessel by physical sputtering and by evaporation.

The investigations carried out so far at tokamaks and plasma gun facilities demonstrated that the steady stationary heat loads expected in ITER do not fully destroy the Li liquid layer. However, ITER is anticipated to operate in the H-mode of plasma confinement, where the plasma edge localized modes (ELMs) may result in melting and vaporization erosion of the divertor and first wall surfaces even in case of tungsten PFCs (W melting point is 3600 K). Those transient events could lead to a significant damage of the liquid Li layer, and thus significant damages of the high Z material substrate.

In 2010, new numerical simulations with the melt motion code MEMOS have been performed for the following conditions: the melt motion and the evaporation at Li surface assume a Li film on the impermeable tungsten substrate, the Li coating of 10-50 μm thickness on W bulk material, the reference heat load Q = 0.1 MJ/m^2 during the pulse load time τ = 0.5 ms, the magnetic field B = 5 T, the tangential pressure varied in the range 2×10^{-4} to $.2\times10^{-3}$ bar, the electric current component normal to the target surface varied in the range 5 - 50 A/cm^2, the initial surface temperature T_0 = 30 C (thus Li melts during the transient). The applied force and the energy flux correspond to the rectangular pulse.

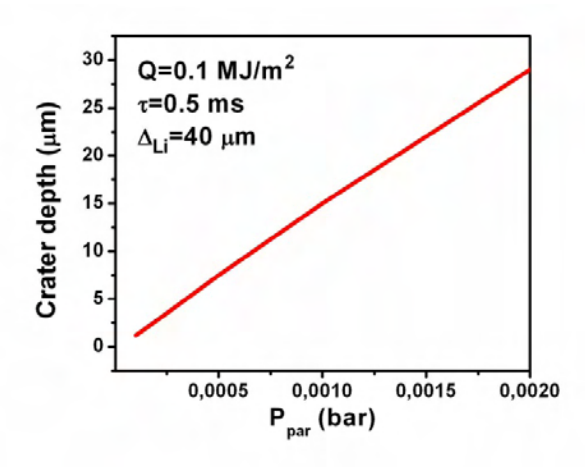

Fig. 1: Crater depth vs. tangential pressure. Thickness of Li layer Δ = 40 μm, No current.

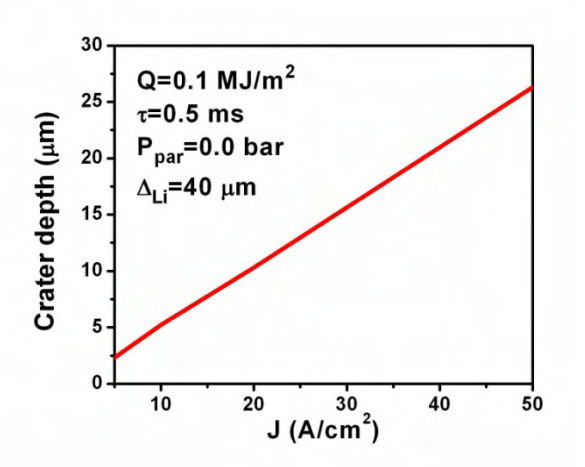

Fig. 2: Crater depth vs. crossing current. Thickness of Li layer Δ = 40 μm, No pressure.

The influences of the tangential pressure of the impacting plasma and of **J**x**B** force on liquid Li were investigated. For the reference heat load, the vaporization is negligible and the melt motion only causes the melt layer damage. Previous MEMOS simulations demonstrated that the melt layer damage, which means the amplitude of the melt altitude over the resolidified

surface, linearly increases with the tangential pressure and the current density (see Fig. 1 and 2).

The results also show that in the case of volumetric force (the **J**x**B** force) the thickness of the molten Li significantly influences the melt layer damage. It is obtained that the thinner the melt layer the larger the crater depth and the magnitude of mountains (see Fig. 3).

In the case of the surface driving force (tangential pressure) the thickness of melt layer weakly influences the magnitude of the crater depth and the mountains (see Fig. 4). Even small ELMs can completely remove Li away from the W substrate.

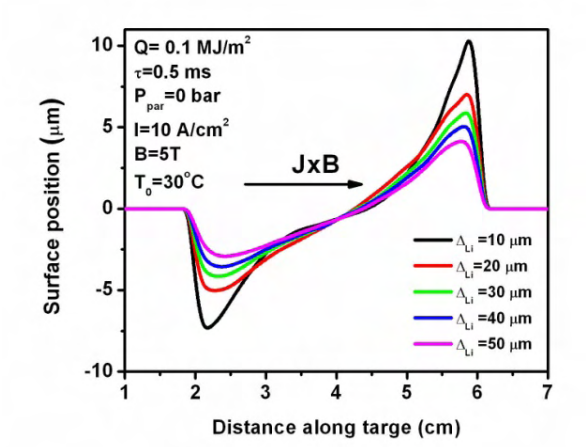

Fig. 3: Crater shape caused by the **J**x**B** force for different layer thickness after 3 ms from pulse trail.

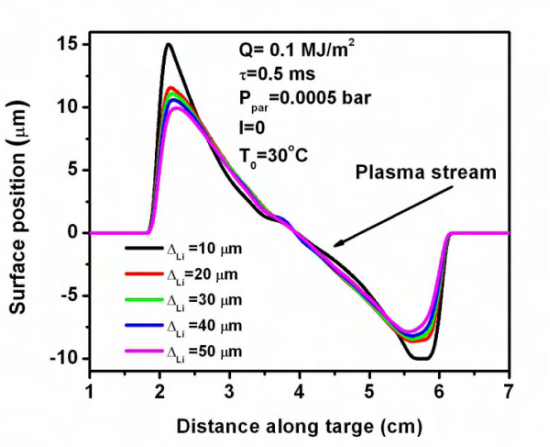

Fig. 4: Crater shape caused by the tangential pressure for different thickness of Li layer after 3 ms from pulse trail.

Conclusions

In the future, a model of porous substrate has to be implemented in MEMOS code. However, it seems that for the transients the CPS will not be effective as a compensator of the melt layer evaporation or the melt removal. Nevertheless, the influence of porous substrate on the melt motion damage should be also analyzed for low heat loads in dependence on melt layer thickness, and for the loads that account for the effect of Li vapour shielding. Finally, MEMOS simulations should be validated against experiments on FTU.

Staff:

B.N. Bazylev

Acknowledgement

This work, supported by the European Communities under the contract of Association between EURATOM and Karlsruhe Institute of Technology, was carried out within the framework of the European Fusion Development Agreement. The views and opinions expressed herein do not necessarily reflect those of the European Commission.

Numerical Modelling of ITER Runaway Deposition and MGI Optimization Simulations (WP10-PWI-07-02-01)

Introduction

A significant issue for the ITER operation with high fusion gain is the occurrence of disruptions, which can limit the lifetime of plasma facing components (PFCs). Disruption mitigations can result in generation of runaway electrons (RE) which can also damage the first wall. Numerical simulations for the consequences of RE impact on the PFCs are carried out in 2010 for JET and ITER conditions. For JET the work was focused on the benchmarking of the codes ENDEP and MEMOS by experimental observations of the RE beams. Reasonable qualitative and quantitative agreement between the numerical simulations and the experiments at JET was obtained. The predictive modelling on the melt damage of ITER beryllium first wall was performed.

Another activity consisted in the modelling of the massive gas injection (MGI) with the radiative MHD code TOKES. In the simulations, the injected noble gas gets ionized in the core and then the contamination results in the fast loss of plasma energy by radiation emission. For MGI modelling, TOKES was upgraded with a toroidally symmetric two-dimensional plasma model and the magnetic flux coordinates covering the whole volume of tokamak vessel. The new model has been successfully compared with an argon experiment on tokamak DIII-D.

Modelling of runaway electrons impact for ITER and JET

Relativistic runaway electrons can appear during the thermal quench of disruption and a massive gas injection. RE will be mainly generated by avalanches in ITER. RE density can be estimated as 10^{16} m^{-3}, their kinetic energy as 10-20 MeV and the associated magnetic energy can be of order of the thermal energy of plasma (in ITER ~ 1 GJ).

To estimate the RE damage to ITER first wall and to support JET experiments, dedicated numerical simulations have been done with the energy deposition Monte-Carlo code ENDEP for CFC, Be and W targets. The heating with melting of ITER Be target and the heating of JET CFC target were performed using the melt motion code MEMOS. Beam parameters used in the calculations were agreed with the teams of both tokamaks.

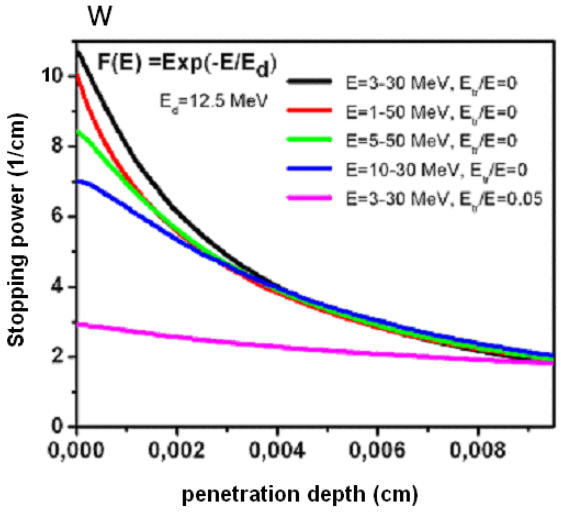

Fig. 1

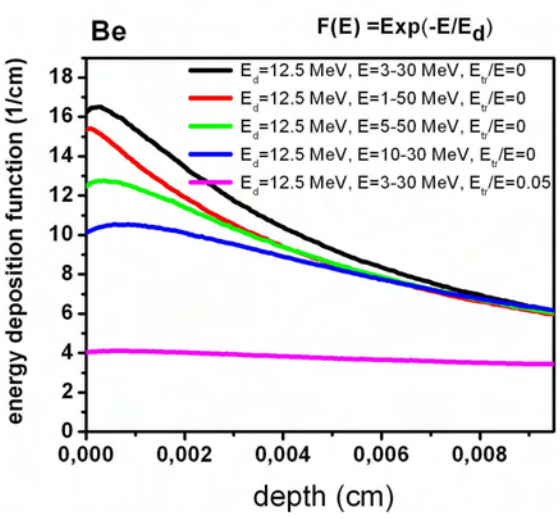

Fig. 2

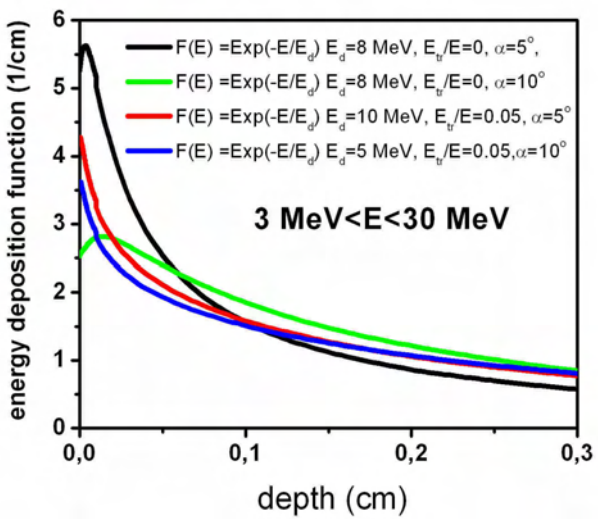

Fig. 3: CFC

For these tasks the code ENDEP was upgraded in order to take into account the effect of electron gyration in the magnetic field on incident angle and the effect of the polarization of bound electrons of target material by RE, which has as a result a slightly smaller stopping power. The energy distribution of RE is assumed to be exponential as $\exp(-E/E_0)$. For the CFC target in a magnetic field of 3.5 T (JET case) the characteristic energy E_0 equals 5, 8 and 10 MeV. For the Be target (ITER) and the sandwich target with 1 cm Be PFC and 1 cm copper substrate $E_0 = 12.5$ MeV is assumed. The main incident angle was varied from 1 up to 10 grad. The transversal energy of RE was varied up to 5% of the total energy.

Figs. 1, 2 and 3 show examples of obtained energy deposition profiles for the different targets.

A typical penetration depth of RE into CFC target of 1 mm is obtained. At large inclination angles α of JET case, the influence of transversal energy E_{tr} is small (CFC target), in contrast to the ITER case (Be target) where α is small, which decreases also the penetration depth of RE (~0.5 mm). The Be melt layer exists for about 0.5 s. It is to note that during this time the Rayleigh-Taylor instability caused by eddy currents can develop on molten surface, resulting in significant splashing.

Despite the larger RE stopping power, the RE energy deposition function in case of the W target has not increased compared to that obtained in case of the Be target, because RE energy is reradiated from W more effectively (~50%) than from Be (20%). The reflected energy can be attributed mainly to the secondary electrons (~40%) and the X-ray radiation (~10%).

The energy depositions calculated in ENDEP are used in MEMOS to get melting in ITER starting heating from wall temperature of 800 K and heating in JET (room temperature). For ITER the Gaussian profile of the spatial energy distribution with the characteristic width 10 cm was assumed. For instance, at RE heat load of 25 MJ/m^2, the surface temperature of the W target exceeds the melting temperature 1540 K after 10 ms.

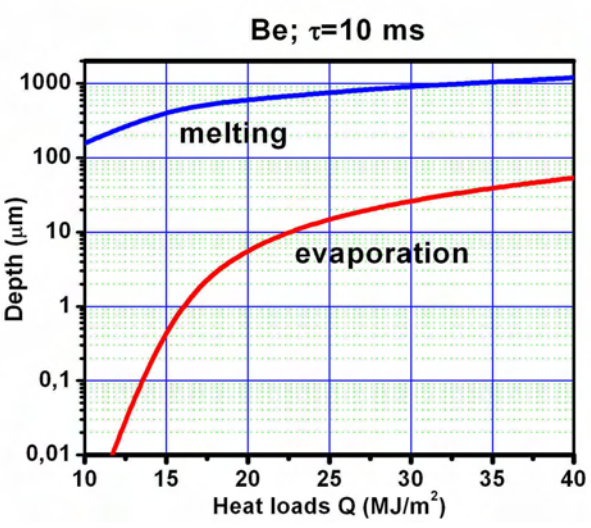

Fig. 4

In MEMOS simulations the melting thresholds in case of RE heating at large pulse durations of 10 ms are obtained: Be melts above 5 MJ/m^2 and W melts above 65 MJ/m^2. This ratio (W/Be = 13) is much larger than that of the plasma impact (~ 3) after ELMs with surface heating only. The simulations showed that the evaporation at beryllium surface significantly (by several times) decreases the melting threshold, which is favourable for ITER first wall armour.

At the regime with beryllium melting, the final depth of melt pool exceeds 1 mm at a heat load Q > 35 MJ/m^2 (Fig. 4). Noticeable evaporation starts for heat loads Q > 12 MJ/m^2. At Q = 40 MJ/m^2 evaporation depth reaches about ~50 μm. The melting continues for a long while (~0.2 s), which could cause splashing away of the whole melt layer by the **J**×**B** force.

For JET, simulations of the impact of the runaway electrons generated during MGI experiments are performed in order to apply and, if possible, validate using available experimental data, the codes ENDEP and MEMOS. The code MEMOS was applied for the calculations of temperature distributions inside the target, however without the melting. Detailed temperature evolution and spatial distributions over CFC tiles installed in JET during the RE impact were calculated as functions of the heat load density and compared with the experimental data, which are available as functions of the runaway current. The dependence of the surface temperature on heat loads was transformed to the dependence of the surface temperature on RE current using a dedicated model that is based on the Ohm law and some assumptions of contributions from as magnetic as kinetic energies of RE. Varying the heat load the simulated dependence of surface temperature T_w was fitted to direct measurements of T_w. By this way the RE energy density in JET was estimated as 3-4 MJ/m^2.

Simulation of massive gas injection (MGI) with tokamak code TOKES

Tokamak experiments demonstrated effective ionizations of the injected atoms G (G = Ne, Ar, He) during MGI, which causes the thermal quench (TQ) within a few ms, when the ionization front reached the magnetic surface of safety factor $q = 2$, and the toroidally well symmetric radiation flush. On the short time scale the ionization of G-atoms localized near the jet entry can result in a strong variation of the plasma parameters with poloidal coordinate y. For example, the electron temperature T_e decreases drastically near the jet. This can significantly decrease the ionization rate resulting in deep jet penetration.

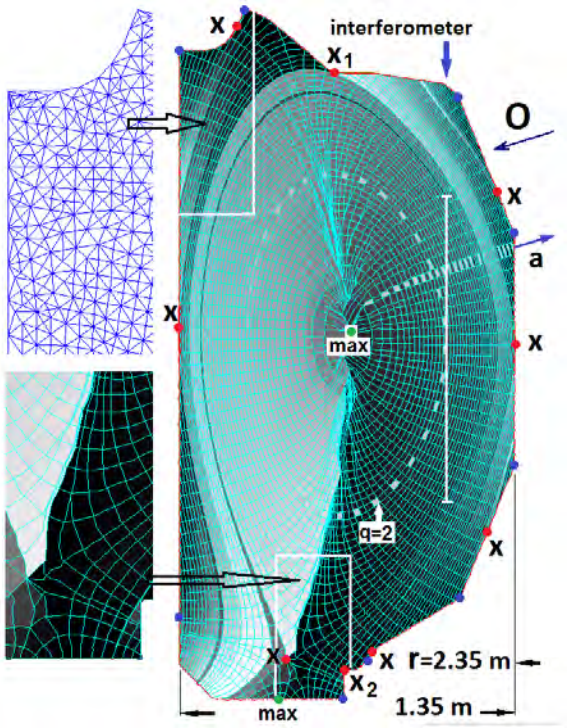

Fig. 5

In 2010 the modelling with the tokamak code TOKES has been focused upon further development of the code aiming MGI simulations. After significant elaborations of the generator of the magnetic flux coordinates two-dimensional description of the plasma in the whole vessel was achieved (Fig. 5). The model of 2D toroidally symmetric multi-fluid plasma includes fast cross-diffusion and non-equilibrium expansion of plasma along magnetic field lines.

TOKES was successfully validated against DIII-D experiment on argon MGI. Fig. 6 shows the comparison between the simulated and the experimental centre temperature $T_{e0}(t)$. The fitting is achieved tuning up a few parameters, which are not precisely known in the experiment but strongly influence $T_{e0}(t)$: 1) the position of $q = 2$ magnetic surface, 2) The electron thermal conductivities of the hot plasma before (k_{eini}) and after (k_{efin}) reaching the surface of q = 2 by the cooling front, which happened at $t = t_{q2} \approx 2$ ms after starting the gas injection.

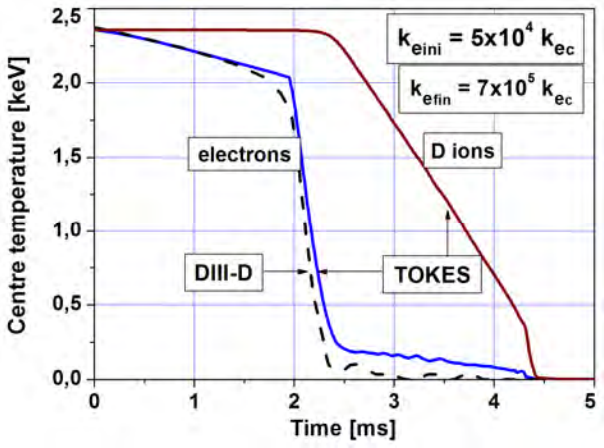

Fig. 6: Validation of TOKES by DIII-D electron temperature T_{e0}. k_{ec} is the electron classical thermal conductivity.

The good fitting indicates that the simulation reproduces the main processes of TQ. The first consequence of the core instabilities appears to be some small deteriorations of the toroidal symmetry and thus a slight overlapping of the nested magnetic surfaces, which drastically increases the electron cross-transport by the thermal conductivity along the entangled magnetic field lines. After starting the plasma periphery cooling, the instabilities can develop at many rational values of q in the core, but we assume they remain moderate until $t > t_{q2}$, due to which $k_{eini} << k_{efin}$ follows. The long tail of T_{e0} on Fig. 6 is due to a long electron-ion thermal energy exchange time. Therefore, centre ion temperature remains high until t = 4 ms (see Fig. 6).

Conclusions

Numerical simulations of Be and W armour damage under the runaway electron heat loads are carried out using the ENDEP and MEMOS codes and are validated against JET experiments. The melting thresholds for Be and W armour were determined. The numerical simulation estimated typical parameters and demonstrated that the mechanism of the surface evaporation significantly influences on the melt layer thickness of the metallic PFCs.

The obtained results provide useful benchmarks of MGI simulations, but more work is needed for further development of the code in order to reach reliable integrated modelling including plasma and surface aspects and the injector gas dynamics in the vessel.

Staff:

B.N. Bazylev
I.S. Landman
S.E. Pestchanyi

Literature:

[1] I.S. Landman, G. Janeschitz, J. Nucl. Mater., 390-391 (2009) 384-387.

[2] I.S. Landman, et al., Fusion Eng. Des. (2010), doi:10.1016/j.fusengdes.2010.03.044

[3] I.S. Landman, et al., Two-dimensional Modelling of Disruption Mitigation by Gas Injection. Presented at the Conference SOFT-2010, Porto, Portugal, Sep 2010.

[4] Yu. Igitkhanov, B. Bazylev, Presented at the 19th PSI Conference, San Diego, USA, 2010.

[5] B. Bazylev, et al., Proc. 19th PSI Conference, San Diego, USA, 2010, to be published

[6] Arnoux, et al., Proc. 19th PSI Conference, San Diego, USA, 2010, to be published.

Acknowledgement

This work, supported by the European Communities under the contract of Association between EURATOM and Karlsruhe Institute of Technology, was carried out within the framework of the European Fusion Development Agreement. The views and opinions expressed herein do not necessarily reflect those of the European Commission.

Physics: Heating and Current Drive – ECRH

Microwave Heating for Wendelstein 7-X (CoA)

Introduction

In recent years, electron cyclotron resonance systems have been established as standard means for localised heating (ECRH) or current drive (ECCD) in fusion relevant plasmas. Thus, ECRH will provide the basic day-one heating system for the stellarator W7-X, which is currently under construction at IPP Greifswald. In the first stage, W7-X will be equipped with a 10 MW ECRH system operating at 140 GHz in continuous wave (CW). The complete ECRH system will be provided by KIT, which established, together with EU partners, the 'Projekt Mikrowellenheizung für W7-X' (PMW) in 1998, covering the design, development, construction, installation and integrated tests of all components required for stationary plasma heating on site at IPP Greifswald. PMW also coordinates the contributions from the Institut für Plasmaforschung (IPF) of the University of Stuttgart (IPF), which is responsible for the microwave transmission system and part of the HV-system, and from the team at IPP Greifswald, which is responsible for the in-vessel components and for the in-house auxiliary systems. PMW benefits also from the collaboration with Centre de Recherche de Physique des Plasmas (CRPP) Lausanne, Commissariat à l´Energie Atomique (CEA) in Cadarache and Thales Electron Devices (TED) in Vélizy.

A contract between CRPP Lausanne, KIT and TED, Vélizy, had been settled to develop and build the continuously operating series gyrotrons. The first step of this collaboration was the development of a prototype gyrotron for W7-X with an output power of 1 MW for CW operation at 140 GHz. This step has been finished successfully.

Seven series gyrotrons have been ordered from the industrial company TED. First operation and long pulse conditioning of these gyrotrons will take place at the teststand at KIT, where pulses up to 180 s at full power are possible (factory acceptance test, FAT), 30 minutes shots at full power are possible at IPP (site acceptance test, SAT). Ten gyrotrons will be available for W7-X, including the pre-prototype tube, the prototype tube and the 140 GHz CPI-tube. To operate these gyrotrons, eight superconducting magnetic systems have been ordered at Cryomagnetics Inc., Oak Ridge, USA, in addition to the Oxford Instruments and Accel magnets.

Further progress was made in 2010 towards the completion of the project. Most of the components of the transmission system, HV-systems and in-vessel-components have been ordered, manufactured, delivered and are ready for operation at IPP Greifswald. A part of the existing ECRH system is already used to test new concepts and components for ECRH. Some delay arose in the project during the last 2 years due to unexpected difficulties in the production of the series gyrotrons.

Series Gyrotrons

The first TED series gyrotron SN1 has been tested successfully at KIT and IPP in 2005 (920 kW/1800 s). It fulfilled all the specifications; no specific limitations were observed during the acceptance test. this gyrotron has been sealed in order to keep the warranty; the two prototype gyrotrons are routinely used for experiments.

The next series gyrotrons showed a somewhat different behavior with respect to parasitic oscillations excited in the beam tunnel region. These oscillations induce excessive heating of the beam tunnel components, particularly in the absorbing ceramic rings. The gyrotrons reopened after operation showed significant damages due to overheating and brazing of the ceramic rings. This limited the pulse length in high-power operation to a few ms.

To avoid this problem, it was decided to test the series gyrotron SN3a at a lower output power, well below the threshold for excitation of the parasitic oscillations. The experiments

showed that it is possible to operate the tube at a maximum output power of about 700 kW without oscillations in the beam tunnel. Higher output power could not be achieved in long pulse operation due to the occurrence of parasitic oscillations in the beam tunnel region. The gyrotron was optimized in the short pulse regime having a typical pulse length of a few ms.

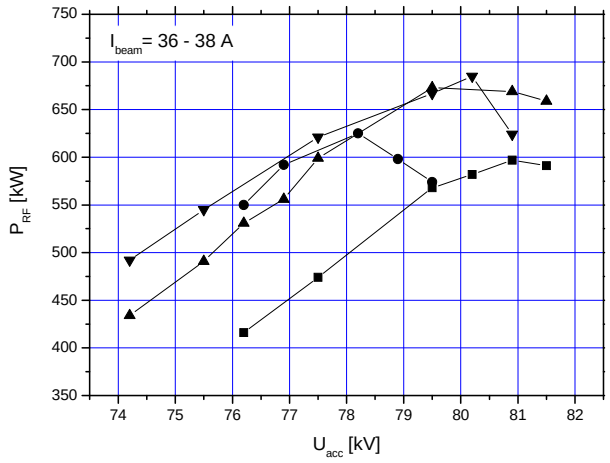

Fig. 1: Output power of series gyrotron SN3a, measured in short pulse operation at a beam current of about 36 – 38 A, the different curves correspond to different magnetic settings. The flattening of the curves at the maximum indicates the occurrence of parasitic oscillations.

The operation and the dependence of the output power and stable oscillating region of the design mode (TE28,8) on different parameters was investigated, by performing, in particular, scans of the output power versus the accelerating voltage for different magnetic field values in the cavity and the electron gun region (see figure 1). The maximum achievable output power is limited since this gyrotron is still equipped with a beam tunnel which tends to support parasitic oscillations. The operation of the gyrotron beyond this limit is usually associated with a strong reduction of output power, enhanced stray radiation, and an increased amount of absorbed RF power in the beam tunnel region (which may result in a thermal overload). It has been found that about 700 kW RF power can be produced at a beam current of about 40 A very reliably, avoiding any evidence of spurious oscillations.

Thermographic measurement and analysis of the output beam indicated a TEM00 content of 97%, thus, verifying the high quality of the internal converter and mirror system.

Long pulses up to 3 minutes were attained with a CW load at full power (700 kW) at an efficiency of 37 % in depressed collector mode for energy recovery. The temperature increase in several cooling channels is depicted in figure 2 for a shot with constant parameters. Note that the beam current is decreasing at the beginning of the pulse due to the cooling effect of the extracted electrons and that the control system needs about 60 s to attain a constant current. It can be seen that the calorimetric measurement shows a constant output power at the end of the pulse, after some regulation oscillations in the first 90 s.

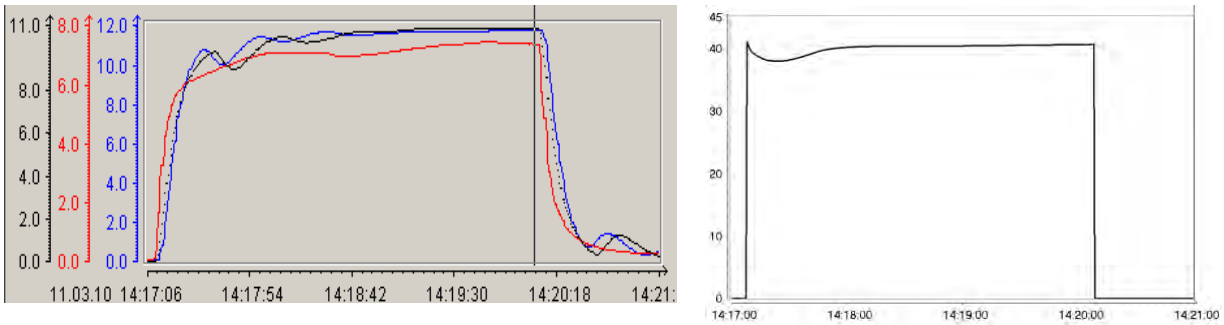

Fig. 2: Left: Temperature increase in cooling channels for 3 minutes operation at 700 kW (black: collector, red: cavity and body, blue: absorber load). The oscillations during the first 90 s are due to the secondary cooling system.
Right: Beam current behaviour.

The increasing temperature of the cavity is associated with an expansion of the cavity diameter and therefore influences the oscillation frequency. The typical frequency drop during the first second of the pulse is about 260 MHz (as compared to 140.33 GHz at the start).

During the acceptance tests it is standard for the W7-X gyrotrons to pass a reliability test to show a reproducible and stable operation within a pulse sequence. Figure 3 shows the beam current during this reliability study. The gyrotron has been operated in 3 min pulses at a power level of around 700 kW and a duty cycle of 10%. Repetitive and very reliable operation of the gyrotron was possible with a pulse length of 3 min. During this sequence all parameters were kept constant, except for the average beam current, which was increased slightly from 38.7 A (in the morning) to 40.2 A (in the evening), the measured power remained in a narrow range of 690 – 714 kW. All pulses were successful; one pulse was pre-terminated due to an arc in the pre-load.

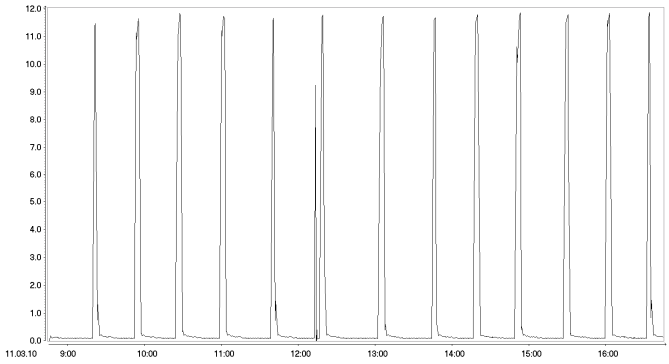

Fig. 3: Beam current variations for 13 pulses with 3 min length each (duty cycle 10%). One short pulse was due to an arc in the pre-load.

Due to the limitation of the power supply at KIT, a pulse length of up to 30 min (and even longer) is possible only at a beam current of less than 30 A. Tests at full power were performed at IPP Greifswald after transferring the gyrotron. Figure 4 shows a very stable behaviour of the total RF power during a 28 min pulse; , the variation of the output power after 16 min was caused by adjusting the body voltage and optimizing the boosting procedure to stabilize the beam current. The gyrotron passed both FAT and SAT, and is currently in regular operation at IPP Greifswald for testing transmission line components.

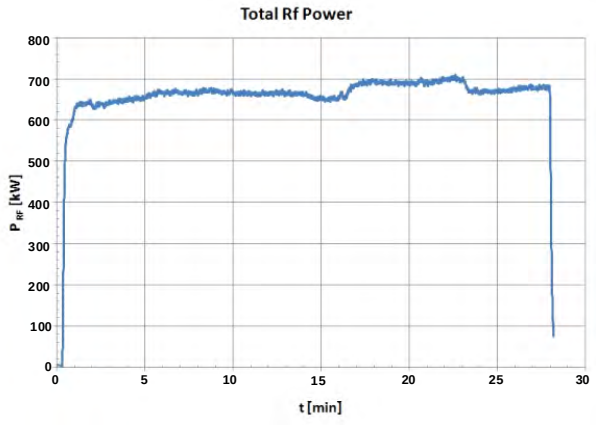

Fig. 4: Total RF power at 28 min pulse. Variation of the power after 16 min is due to adjustment of body voltage and beam current.

During the experiments, it was observed that the stainless steel housing of the gyrotron in the beam tunnel/cavity/uptaper area becomes hot. This is most probably due to stray radiation (inside the vacuum tube) which is absorbed at the non-cooled surfaces of the housing, so that operation with high duty over a long time is inconvenient. To reduce the absorption to tolerable values, the inner side of the tube will be covered with a high reflective copper layer.

Water was replaced by inert silicone oil to avoid any possible problems with corrosion in the window cooling circuit. A numerical study showed that the additional temperature increase of the diamond disk is not critical [4]. The high power experiments with the gyrotron showed that the increase of the oil temperature in regular operation is about 3°C and saturates after approximately 3 min.

The first W7-X gyrotron, which is equipped with an improved beam tunnel, was delivered and tested at KIT in the middle of 2010. In contrast to the usual beam tunnel, this design features corrugations in the copper rings which handicap the excitation of parasitic modes (as shown in an experimental campaign with two modular test gyrotrons in 2009). No parasitic oscillations originating from the beam tunnel region were observed during the tests at KIT. However, it has been observed that the dependence of the output power on beam current shows a saturation level, well below the currents observed in previous tubes. It was not possible to obtain more than 960 kW even for a beam current of 48 A. Possible reasons for this behavior (e.g. poor e-beam properties, misalignment of the magnet-gyrotron system and interaction in

the after cavity region) are under investigation. Although long pulses up to 180 s around 800 kW have been performed, the stable and reproducible operation of the tube needs to be improved.

The measurement and analysis of the output beam gave a Gaussian content as high as 97%.

Design, Construction and First Tests of a High-Power Stainless Steel Load

The load is a critical, required component of the test stand for high-power CW gyrotrons. It has to absorb and also to measure the microwave power in an accurate and reliable way. Cylindrical, ceramic-coated loads have been used at IHM until now. Although these types of loads show good absorption, the ceramic layer may degrade and even flake off due to local overheating. To avoid this problem, a load has been designed and constructed entirely of stainless steel. To enlarge the absorbing surface, the load is filled with an additional structure made of stainless steel pipes.

In 2010, measurements with a preliminary load without active cooling showed that 700 kW of microwave radiation with a pulse length of two seconds could be absorbed. During the measurement sequence, the load heated up to temperatures of 100°C at the outer surface and up to 250°C (which is a critical value in terms of arcing) at the inner structure. In these experiments, a water-cooled pre-load showed that the back-reflected power is approximately 2%, which is a very good value.

At the moment, the load is equipped with an assembly that allows water-cooling of the inner structure. This will help to increase both the pulse length and the power level.

Transmission Line

The transmission line consists of single-beam waveguide (SBWG) and multi-beam waveguide (MBWG) elements. For each gyrotron, a beam conditioning assembly of five single-beam mirrors is used. Two of these mirrors match the gyrotron output to a Gaussian beam with the correct beam parameters, two others are used to set the appropriate polarization needed for optimum absorption of the radiation in the plasma. A fifth mirror directs the beam to a plane mirror array, the beam combining optics, which is situated at the input plane of a multi-beam wave guide. This MBWG is designed to transmit up to seven beams (five 140 GHz beams, one 70 GHz beam plus an additional spare channel) from the gyrotron area (entrance plane) to the stellarator hall (exit plane). To transmit the power of all gyrotrons, two symmetrically arranged MBWGs are used. At the output planes of the MBWGs, two mirror arrays (beam distribution optic, BDO) separate the beams again and distribute them via two other mirrors and CVD-diamond vacuum barrier windows to individually movable antennas (launchers) in the torus. The BDOs and the successive mirrors are mounted in so-called towers with "pinnacles" on top.

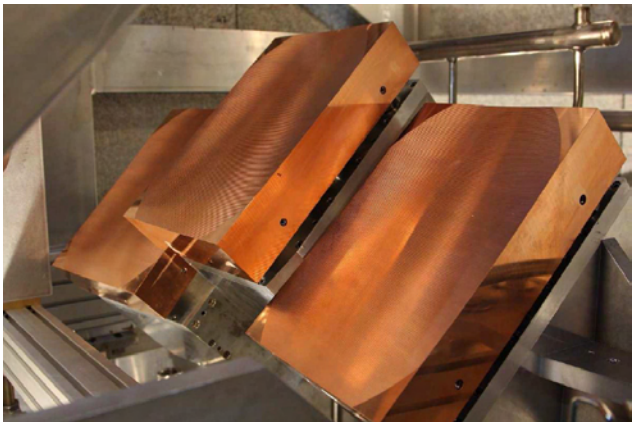

Fig. 5: Assembly of 3 mirrors type M13 installed in an ECRH antenna tower.

The manufacturing and installation of the components of the basic transmission system are finished now. Figure 5 shows an assembly of 3 mirrors of type M13 installed in an ECRH antenna tower. In 2010, gyrotron SNo. 3 was installed in Greifswald, and beam characteriza-

tion and the subsequent design and manufacturing of the surfaces of the two matching mirrors for this tube have been performed. SNo.4 is presently under test at KIT Karlsruhe, where the beam parameters have been measured.

Remaining work includes diagnostics and power measurement of the gyrotron beams. The receivers attributed to the directional couplers on the mirrors M14 have been designed, and are under fabrication; related alignment control is in development. Owing to the aging of the available absorber loads from CCR, which led to increased arcing problems at higher power, a replacement of these loads was pursued. For module 1, a water-cooled version of the "'long load"', which consists of a 24 m long absorbing stainless-steel waveguide, was designed and ordered in industry; delivery is scheduled for end of this year. In module 5, a cylindrical stainless-steel load from GYCOM was installed, and the system of coupling mirrors was upgraded to allow routing of the beam either to the old CCR load or to the new GYCOM load. Within the parameters used up to now (700 kW, 15 min), the GYCOM load performs well.

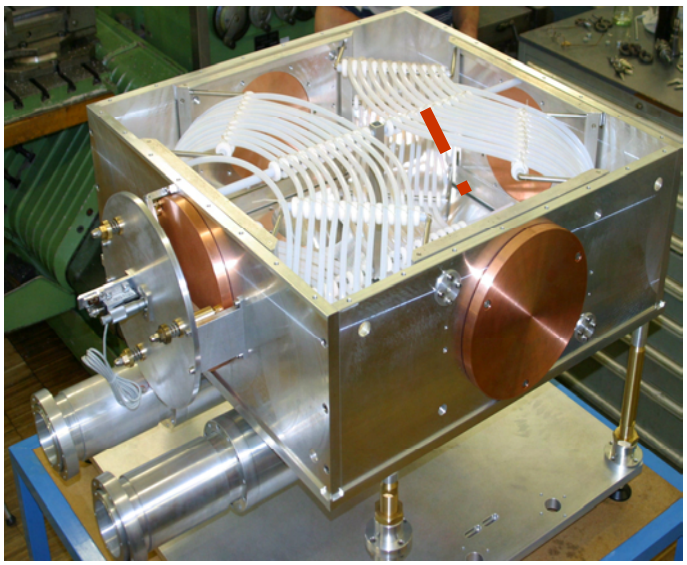

Fig. 6: Diplexer which has been investigated in the ECRH system for W7-X. At the bottom, one can see the two HE11-waveguide outputs. The top plate is removed to reveal the resonator geometry and the stray radiation absorbing hoses.

As in the past years, the ECRH system could be used for test of special components. Among others, the high-power tests of the compact long-pulse diplexer "Mk II" continued. This device (see Figure 6) is equipped with HE11 interfaces, and thus is compatible with waveguide transmission systems. It is developed for use as a combiner for the power of two gyrotrons as well as a fast directional switch (FADIS) between two outputs, and it is therefore of potential interest for ITER.

The output power diagnostics as well as the drive (developed by TNO in Delft) for the resonator mirror was optimized; as a result, tracking of the slope or the peak of the diplexer resonance to the gyrotron frequency now works on a 20-ms time scale. With this system, demonstration of several diplexer applications was possible, including "'slow"' switching between two output channels by controlled mirror movement, fast switching by frequency-shift keying of the gyrotron (using few kV voltage modulation of the body) with optimum contrast, and tracking the notch of the diplexer to the gyrotron as is needed for in-line ECE experiments. When feeding two gyrotrons to the diplexer, stable power combination with an output contrast of 90% could be reached. A power combination experiment is shown in Figure 7.

For two of the N-ports of W7-X, "remote-steering" (RS) launchers are foreseen. This is due to the fact that front steering launchers as used in the A and E ports (see chapter on launchers) will not fit into these narrow ports. The remote-steering properties are based on multi-mode interference in a square waveguide leading to imaging effects. For a proper length of the waveguide, a microwave beam at the input of the waveguide (with a defined direction set by a mirror system outside of the plasma vacuum) will exit the waveguide (near the plasma) in the same direction. For W7-X, the vacuum window, a vacuum valve as well as a mitre bend must be incorporated into the 4.6 m long waveguide.

A conceptual design for the two RS-launchers in Module 1 and Module 5 was performed. The waveguide will be fabricated by an electroforming process, thereby integrating the water-cooling channels. To enlarge the steering range, systematic investigations of small deformations for the basically square corrugated waveguide were started to find an optimised cross-section. In parallel, further calculations of the losses in the gap needed for installation of the vacuum valve continued. In conjunction with the optimised waveguide cross-section, a significant reduction of the gap losses especially for larger scanning angles is expected.

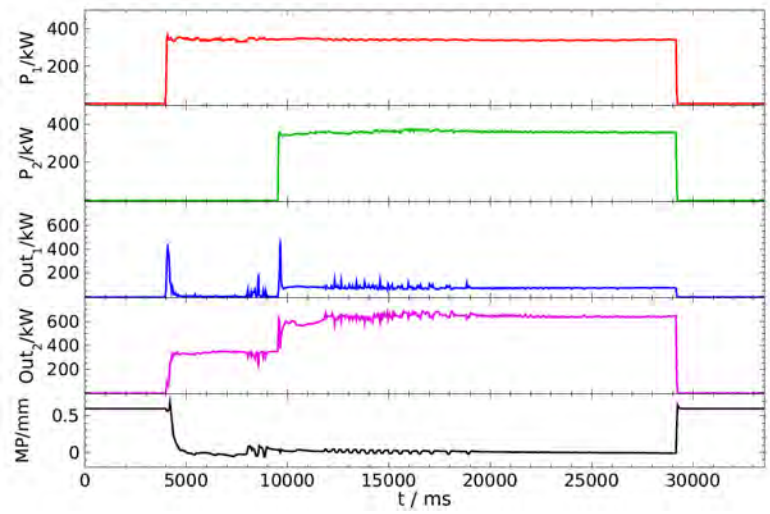

Fig. 7: Beam combination of two gyrotrons operating at slightly different frequencies with diplexer frequency tracking to dip. The RF power of gyrotron 1 (P1, top) at input 1 and gyrotron 2 (P2, 2nd from top) at input 2, respectively, are displayed together with the output power in channel OUT1 (3rd from top) and OUT2 (4th from top) as a function of time. The feedback controlled diplexer mirror position MP is shown at the bottom.

Low-power experimental investigations on a prototype waveguide have been started to benchmark the calculations.

HV-systems

For the operation of gyrotrons with depressed collector, a precisely controlled beam acceleration voltage is necessary, which is supplied by the body-voltage modulator. The beam current of the gyrotrons is controlled by the cathode heater supply, which is on cathode potential (about -55 kV). In case of arcing inside the gyrotron, a thyratron crowbar protects the tubes from being damaged.

All ten body-voltage modulators and the protection units are now ready for operation. With growing experience with the complete system, some final optimization issues concerning the system diagnostics in case of a gyrotron fault are implemented.

In-vessel-components

The first refurbished ECRH-plug-in launcher was successfully tested for vacuum tightness in the large MISTRAL vacuum chamber. In addition, extensive mechanical tests of the mirror drive mechanism were performed successfully. Thus the refurbishment of the remaining three launchers can go-on on track.

The N-Port-launcher design was refined. Production drawing could now be provided, if the decision for manufacture is done.

The electron cyclotron absorption (ECA) diagnostics, which measures the transmitted ECRH power and the beam position and polarization, was partially completed. The four B-port plug-in parts were fabricated and are currently tested for vacuum tightness. The design of the in-vessel parts, which consist of 4 waveguide bundles, could not be terminated, since the assembly test of a prototype bundle is pending. In addition a waveguide re-routing became necessary, since the piping of the KIP-components was changed.

A new small material test chamber was build-up, which enables to estimate the microwave stray radiation absorption properties of different materials at 140 GHz. Even though the chamber is feed with a power of 14 W only, it helps to select the materials for W7-X in-vessel components prior to the extensive high power tests at the MISTRAL chamber.

Staff:

IHM / KIT	IPF (University of Stuttgart)	IPP(Greifswald/Garching)
K. Baumann	P. Brand	B. Berndt
G. Dammertz	H. Höhnle	H. Braune
G. Gantenbein	W. Kasparek	V. Erckmann (PMW)
H. Hunger	H. Kumric	F. Hollmann
S. Illy	C. Lechte	L. Jonitz
S. Kern	R. Munk	H. Laqua
M. Kupper	F. Müller	G. Michel
R. Lang	B. Plaum	F. Noke
W. Leonhardt	S. Prets	F. Purps
M. Losert	P. Salzmann	T. Schulz
D. Mellein	K.H. Schlüter	P. Uhren
S. Miksch	U. Stroth	M. Weißgerber
A. Papenfuß	A. Zeitler	
B. Piosczyk	+ M. Bohner, H. Dadgostar,	
A. Samartsev	E. Filipovic, M. Saliba, and	
M. Schmid	D. Hermann (Diploma/Master students)	
W. Spiess		
D. Strauss		
J. Szczesny		
M. Thumm		
J. Weggen		

Literature:

[1] Braune, H.; Erckmann, V.; Illy, S.; Michel, G.; Noke, F.; Purps, F., W7-X ECRH teams at IPP, IPF and KIT, Collector loading during high frequency power modulation. 35th Internat. Conf. on Infrared, Millimeter and Terahertz Waves (IRMMW-THz 2010), Roma, I, September 5-10, 2010

[2] Bongers, W.A., Graswinckel, M.F., Goede, A.P.H., Kasparek, W., Danilov, I., Curto, A.F., de Baar, M.R., van den Berg, M.A., Donné, A.J.H., Elzendoorn, B.S.Q., Heidinger, R., Ivanov, P., Kruijt, O.G., Lamers, B., Meier, A., Piosczyk, B., Plaum, B., Ronden, D.M.S., Thoen, D.J., Schmid, M., Verhoeven, A.G.A., A remotely steered millimetre wave launcher for electron cyclotron heating and current drive on ITER. Fusion Eng. Design 85 (2010), pp. 69 - 86

[3] Bruschi, A.; Erckmann, V.; Kasparek, W.; Petelin, M.I.; Thumm, M.; Bin, W.; Cirant, S.; D'Arcangelo, O.; Hollmann, F.; Lubyako, L.; Noke, F.; Plaum, B.; Purps, F.; Zohm, H., ECRH Team at IPP Greifswald, Diplexers for power combination and switching in high power ECRH systems. IEEE Transactions on Plasma Science, 38(2010) S.1427-38, DOI:10.1109/TPS.2010.2047658

[4] Bruschi, A.; Bin, W.; Cirant, S.; Dell'Era, F.; Gantenbein, G.; Leonhardt, W.; Muzzini, V.; Samartsev, A.; Schmid, M., Progress and test of the spherical matched load designed for 2 MW-CW. Workshop on RF Heating Technology of Fusion Plasmas, Como, I, September 13-15, 2010

[5] Gantenbein, G.; Dammertz, G.; Kern, S.; Latsas, G.; Piosczyk, B.; Rzesnicki, T.; Samartsev, A.; Schlaich, A.; Thumm, M.; Tigelis, I., Progress in stable operation of high power gyrotrons. 16th Joint Workshop on Electron Cyclotron Emission and Electron Cyclotron Resonance Heating, Sanya, China, April 12-15, 2010, Book of Abstracts

[6] Gantenbein, G.; Erckmann, V.; Illy, S.; Kern, S.; Kasparek, W.; Lechte, C.; Leonhardt, W.; Lievin, C.; Samartsev, A.; Schlaich, A.; Schmid, M.; Thumm, M., 140 GHz, 1 MW CW gyrotron development for the ECH system of the stellarator W7-X. 35th Internat. Conf. on Infrared, Millimeter and Terahertz Waves (IRMMW-THz 2010), Roma, I, September 5-10, 2010, Proc.on USB-Stick

[7] Gantenbein, G.; Erckmann, V.; Illy, S.; Kern, S.; Kasparek, W.; Lechte, C.; Leonhardt, W.; Lievin, C.; Samartsev, A.; Schlaich, A.; Schmid, M.; Thumm, M., Status and recent results of the 140 GHz, 1 MW CW gyrotron

development for the stellarator W7-X. Workshop on RF Heating Technology of Fusion Plasmas, Como, I, September 13-15, 2010

[8] Gantenbein, G.; Dammertz, G.; Erckmann, V.; Kasparek, W.; Kern, S.; Latsas, G.; Lechte, C.; Piosczyk, B.; Rzesnicki, T.; Samartsev, A.; Schlaich, A.; Thumm, M.; Tigelis, I.; Vaccaro, A., Progress in stable operation of high power gyrotrons for ECRH. 22nd Joint Russian-German Meeting on ECRH and Gyrotrons, Nizhny Novgorod, Russia, June 29 - July 5, 2010

[9] Kasparek, W.; Erckmann, V.; Petelin, M.; Bruschi, A., Research Groups at IPF, IPP, IAP, IFP, KIT, TNO and FOM, High-power diplexers for plasma heating and diagnostic systems: developments, experiments, and prospects. 3rd Internat. Workshop on Far-Infrared Technologies (IW-FIRT 2010), Fukui, J, March 15-17, 2010, Abstracts S.20-21. Proc.on CD-ROM, University of Fukui

[10] Kasparek, W.; Erckmann, V.; Hollmann, F.; Michel, G.; Noke, F.; Purps, F.; Plaum, B.; Brand, P.; Lechte, C.; Filipovic, E.; Saliba, M.; Doelman, N.; van den Braber, R.; Bongers, W.; Krijger, B.; Petelin, M.; Koposova, E.; Lubyako, L.; Bruschi, A.; Stober, J.; Wagner, D.; Groups at IPF Stuttgart, IPP Greifswald, IAP N.Novgorod, IFP Milano, KIT Karlsruhe, TNO Delft, and FOM Rijnhuisen, Compact resonant diplexers for advanced ECRH: design, low- and high-power tests, and plans. Workshop on RF Heating Technology of Fusion Plasmas, Como, I, September 13-15, 2010

[11] Schmid, M.; Erckmann, V.; Gantenbein, G.; Illy, S.; Kern, S.; Lievin, Ch.; Samartsev, A.; Schlaich, A.; Rzesnicki, T.; Thumm, M., Technical developments at the KIT gyrotron test facility. 26th Symp. on Fusion Technology (SOFT 2010), Porto, P, September 27 - October 1, 2010

[12] Thumm, M.; Brand, P.; Braune, H.; Dammertz, G.; Erckmann, V.; Gantenbein, G.; Illy, S.; Kasparek, W.; Kern, S.; Laqua, H.P.; Lechte, C.; Leonhardt, W.; Marushchenko, N.B.; Michel, G.; Pisoczyk, B.; Schmid, M.; Turkin, Y.; Weissgerber, M., Status and high power performance of the 10-MW 140-GHz ECH system for the stellarator Wendelstein 7-X. Plasma and Fusion Research, 5(2010) S.1006/1-8

[13] Vaccaro, A.; Aiello, G.; Gantenbein, G.; Meier, A.; Scherer, T.; Schreck, S.; Spaeh, P.; Strauss, D., Silicon oil DC200(R)5cSt as an alternative coolant for CVD diamond windows. 16th Joint Workshop on Electron Cyclotron Emission and Electron Cyclotron Resonance Heating, Sanya, China, April 12-15, 2010, Book of Abstracts

Development of the European Gyrotron ("CCGDS6") F4E-2008-GRT-08(PMS-H.CD)-01)

Analysis of Design Issues, Interfaces and Preparation of the Procurement Arrangement for the ITER Gyrotron (F4E-2009-GRT-034-01)

Design and Development of the European Gyrotron (F4E-2009-GRT-049-01)

Introduction

The development of a 2 MW, CW, 170 GHz coaxial cavity gyrotron for ITER is pursued within the European Gyrotron Consortium (EGYC, consisting of CRPP, Switzerland; KIT, Germany; HELLAS, Greece; CNR and, within GRT-08, ENEA; Italy), which acts as scientific partner for F4E, and in cooperation with ISSP, Latvia. The goal of this development is the supply of sources for 170 GHz ECH & CD at ITER providing 8 MW CW power, to cover the EU contingent on ECH & CD sources in ITER. In contrast to other contributors to ECH & CD on ITER, the EU plans to provide sources with 2 MW RF power per unit (ITER minimum specification: 1 MW) for reduced cost and space requirements, to be able to double the system power if requested and to establish the - essentially more powerful - coaxial technology.

While the industrial gyrotron prototype, built by Thales Electron Devices (TED, France), is tested at CRPP, KIT provides support to the development and the tests through component design, scientific investigations and collaboration as well as low and high power tests. The latter are done with the modular short-pulse pre-prototype gyrotron at KIT (see figure 1). In particular, KIT is solely responsible for the design of cavity, uptaper and mode converter system, and is involved in gun, beam tunnel and collector design.

In parallel to the coaxial 2 MW gyrotron activities, a 1 MW conventional cavity design is in preparation as a fallback solution. This backup design intends to support the strategic decision about keeping the 2 MW design or switching to a conventional 1 MW design, which will be taken in mid 2011 after the next prototype experiments.

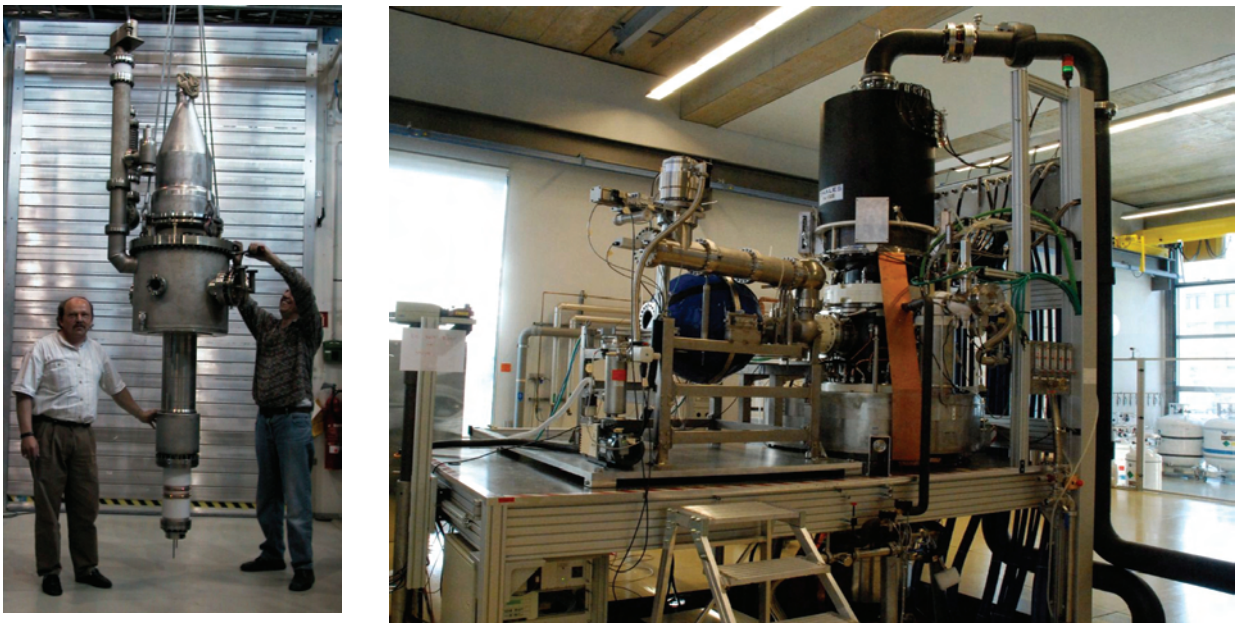

Fig. 1: Coaxial 2.2 MW 170 GHz short pulse pre-prototype gyrotron at KIT (left) and the industrial long pulse prototype, installed at the CRPP test stand (right). The blue sphere is the CNR 2 MW RF load (see fig. 4).

Status of work at the beginning of 2010

After the experiments with the first coaxial 2 MW prototype at CRPP were stopped without major success in autumn 2008, the efforts in 2009 concentrated on the demonstration of efficient high power operation with the pre-prototype at KIT, on the improvement of critical components and on a deeper understanding of the various problems. After the KIT Oxford Instruments magnet was enhanced using an additional normal conducting coil, it could finally operate (in pulses of tens of seconds) at the nominal field strength of 6.87 T. In combination with an adapted design of the electron gun and improved designs for beam tunnel and launcher antenna, the KIT pre-prototype finally reached a world record power of 2.2 MW at 170 GHz, at an efficiency of 30% (without energy recovery). This short-pulse experiment (1 ms) proved the feasibility of a stable and highly efficient single-mode gyrotron interaction at the chosen high order mode, the $TE_{34,19}$. At the same time, the new structure of the corrugated beam tunnel was verified (see the report on gyrotrons for W7-X), and the launcher antenna with arbitrary wall perturbations was also successfully tested with an RF output beam with 96% fundamental Gaussian beam content. The goal of this experiment, to demonstrate gyrotron operation at ITER parameters in short pulse, was fully reached. In particular, the output power and the RF beam quality exceeded ITER specifications (2 MW and 95% Gaussian content), while the efficiency without energy recovery matched the expectations – the ITER gyrotron specification calls for 50% efficiency with energy recovery, which appears reasonable with 30% non-recovered efficiency, but was not demonstrated.

The gyrotron was equipped with a broadband Brewster window which permitted experiments at different operation modes and the corresponding different frequencies. These experiments could not be finalized in the available time, but supported the theoretical prediction that with such a window, the 2 MW gyrotron could well be used as a step-tunable millimetre wave source over a wide frequency range (140 – 210 GHz). Unfortunately, it was not possible to go on with these experiments due to a crack in a ceramic insulator at the electron gun.

On theoretical side, the three important achievements of 2009 were the finalisation of a new launcher synthesis code which permits the design of a launcher with arbitrary wall perturbations, as well as an improved understanding of parasitic oscillations and of the relevance of particle traps for long pulse gun designs. The new launcher replaced the former launcher antenna with harmonic wall distortions, which turned out to be not suitable for a typical coaxial gyrotron mode (this is perfectly suitable for modes with caustic radius at the half cavity radius, but coaxial modes typically have smaller caustic radii). The launcher was successfully tested in low and finally high power, as reported above. The activities on parasitic oscillations and electron gun design were carried further in 2010 and will be described subsequently.

Achievements in 2010

<u>High power tests and redesigns of the pre-prototype</u>

Several attempts were made during 2010 to operate the short-pulse pre-prototype gyrotron at KIT. Initially, the crack in the gun insulator was repaired using a liquid sealant,but subsequently the sealant was dissolved by the insulating oil surrounding the gun contacts. Next, a similar electron gun from the former 165 GHz gyrotron experiment was employed, after a damage at the filament heater contact of this gun was diagnosed and repaired. Again, the conditioning of the gyrotron equipped with the old gun proceeded well, but unfortunately a sealing ring melted and the old gun got polluted by oil. Towards the end of 2010, the pre-prototype was re-assembled with the old gun and successfully conditioned, so a next experimental campaign will probably be possible (see figure 2 and 3). Since no high power experiments during 2010 could be done, the plans for these experiments were shifted to 2011 and beyond, as described in the next paragraph.

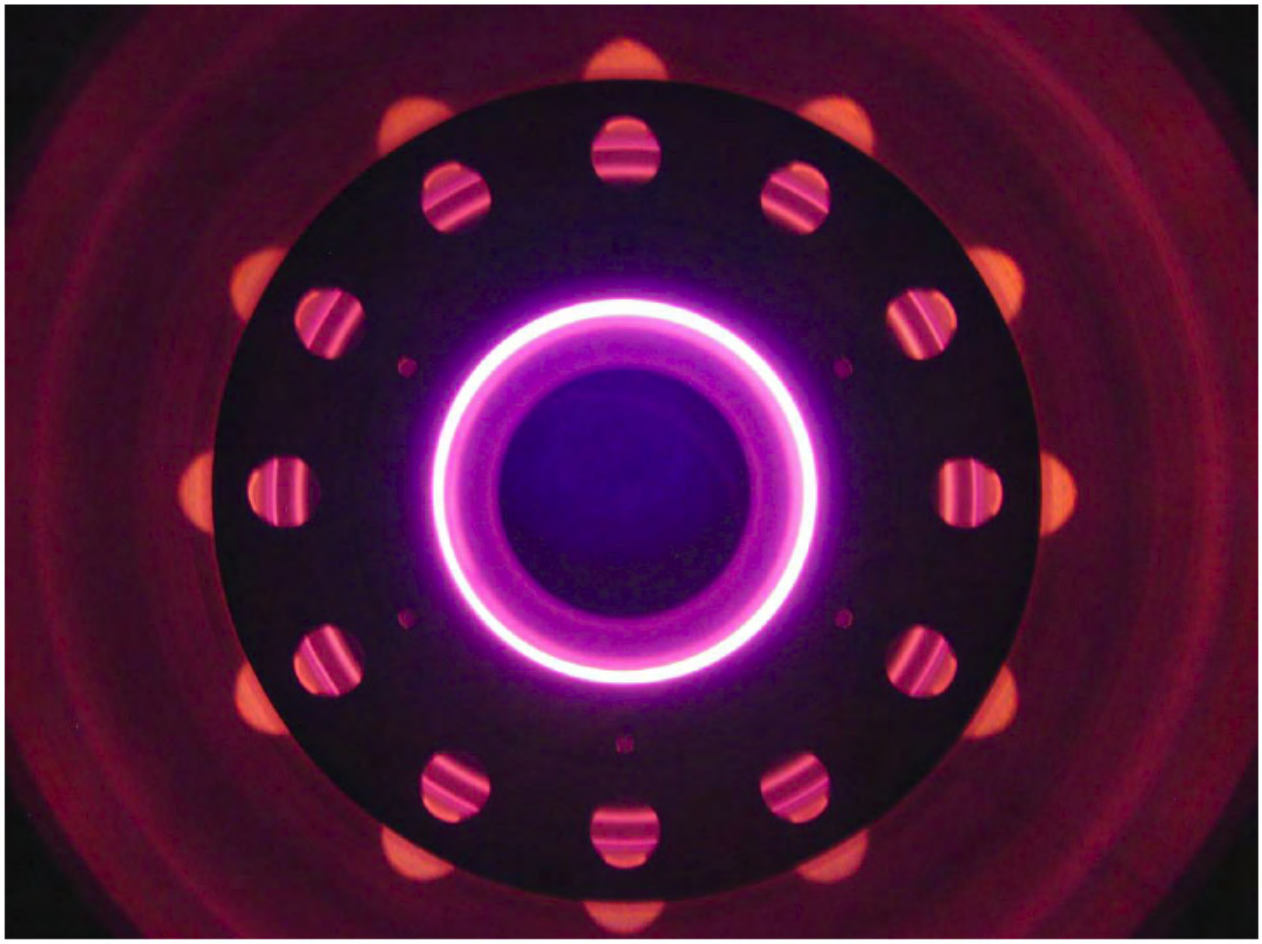

Fig. 2: View inside the 165 GHz electron gun test assembly with heated emitter ring.

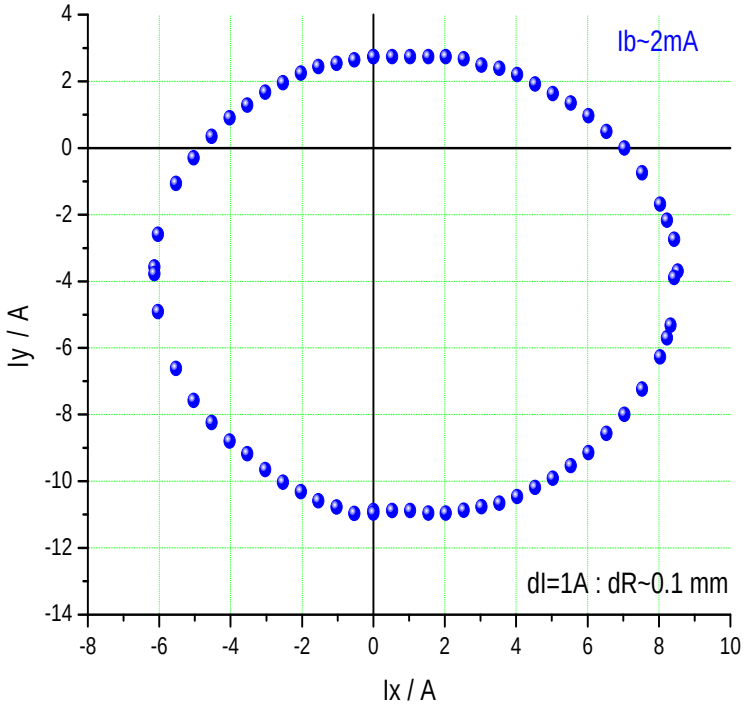

Fig. 3: Current measurement using controlled beam displacement. The round structure of the beam positions with 2 mA current to the coaxial inner rod indicates homogeneous emission of the re-conditioned 165 GHz gun emitter. The rod itself is not aligned in these measurements.

Since it was already obvious at the beginning of 2010 that the electron gun of the pre-prototype needed to be replaced, several activities for refurbishment and redesigns were started in parallel to the experiments. The aim was not just a replacement of worn-out components, it was also intended to gain flexibility and improve the relevance of the experiments for the long-pulse tests with the prototype at CRPP. Two basic decisions were made: The KIT Oxford Instruments magnet shall be directly equipped with a cooled normal conducting coil, suitable for CW operation. This reduces the warm bore hole of the magnet to a diameter of 220 mm, which in turn calls for a redesign of the pre-prototype tube to make it fit into this smaller hole. The other decision was to build a more modular electron gun, for easier design changes and also for easier repair. A condition for all those redesigns was to gain more similarity to the prototype, for easier comparisons and more relevant test cases. Under consideration of all these conditions, the redesigns were done, the corresponding hardware will in subsequent steps be purchased and build into the pre-prototype and the magnet. The changes were projected in a way that the tube can be operated at intermediate steps of redesign, so the first purchases aim at replacing the emitter, to be able to operate the gyrotron again as soon as possible.

Activities in support of the prototype refurbishment, future tests and for the gyrotron installation at ITER

The refurbishment of the industrial prototype for the ITER gyrotron was started in 2009 and aimed at delivery to CRPP Lausanne in summer 2010. Due to various delays, the delivery date now shifted to end March 2011. The biggest problem was a cracking ceramic isolator during the final bake-out of the tube.

Through these delays, the activities in direct support of experiments with the refurbished prototype had to be postponed to 2011. Only one directly related measurement could be done, the new launcher of the refurbished gyrotron was measured with an RF beam quality slightly worse than expected: 94.2 % Gaussian mode content at the RF window instead of 95.5 %, which was reached by the KIT system. The reason for this decline could not be determined; more information will be gained with the high power experiments. Another preparation for high power measurements was the test of a high power RF load, designed by CNR Milano. This load, a cooled absorbing sphere, was designed for 2 MW CW operation. The concept was tested with a sphere that was covered by attenuating material only in half, so it would be suitable for 1 MW only and could be tested with the W7-X SN3 gyrotron (see figure 4). The test validated the design as far as possible with this gyrotron. Apart from that, work was done on simulating particle traps and understanding their relevance for electron gun designs. The results of these investigations were considered in the gun redesign. Finally, the design for a new magnet for the second industrial prototype was investigated through different design models and corresponding electron gun calculations, and intensively discussed among the contributing parties, which resulted in a design proposal which will be used in a call for tender by F4E.

Independent of the delayed gyrotron test, a variety of activities was performed within the collaboration with CRPP to prepare the gyrotron procurement and installation at ITER. These activities range from investigations on the influence of stray magnetic fields and neighbouring gyrotrons over interface specifications to first estimations and observations on operation reliability. As an example, calculations on the influence of the Tokamak field on the magnetic fields at the gyrotron collectors are shown in figure 5. Another example is the work on advanced collector sweeping schemes, as described in the section about the 1 MW backup design below. The goal of these different efforts is to define specifications and recommendations for the gyrotron installation at ITER for reliable nominal operation.

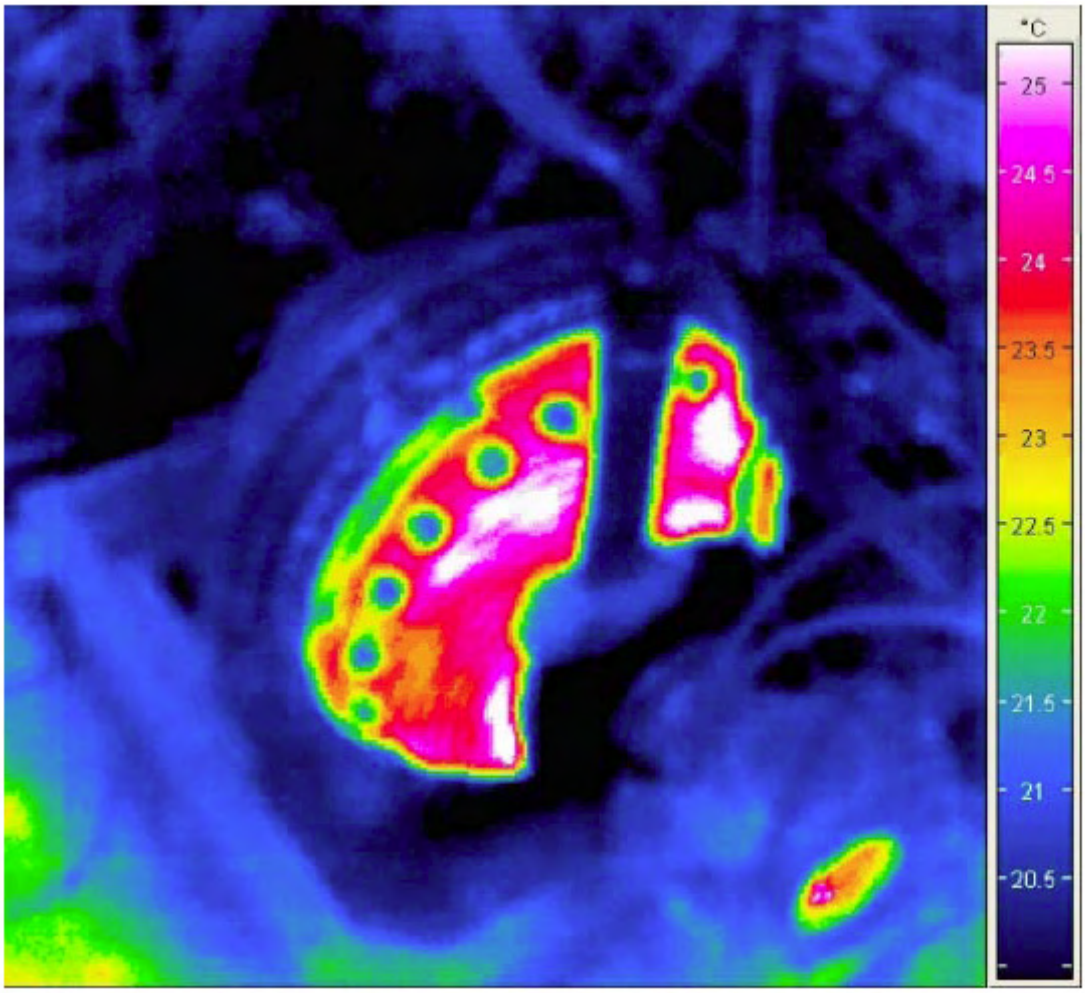

Fig. 4: Thermal image of the spherical 1 MW CNR load (half coated, as model for the fully coated 2 MW load) at 700 kW / 140 GHz input power.

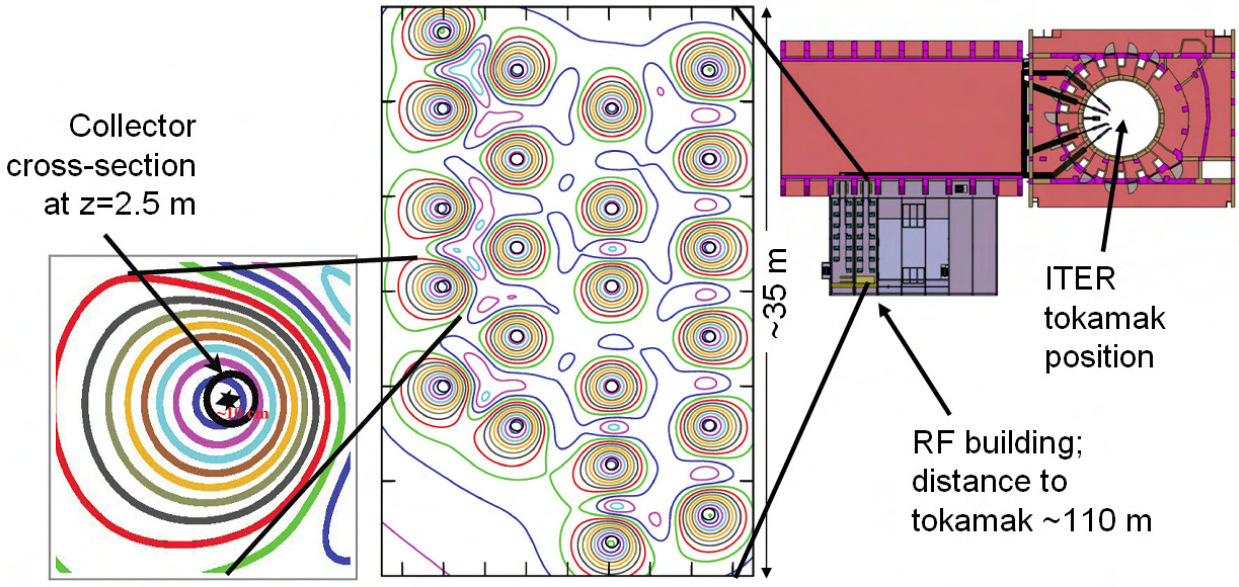

Fig. 5: Magnetic field lines at the gyrotron collectors under influence of neighbouring gyrotrons and the ITER tokamak field. The misplacement of the circular collector fields indicates that compensation of stray fields will be required.

Simulation codes and designs for quasi-optical systems

The new TWL_DO code for launcher synthesis was further improved by a better optimisation routine, by inclusion of ohmic losses, transmission and reflection calculation, and by the calculation of the cross-polarized part of the output power. In addition, the launcher designs for the prototype refurbishment were further enhanced by adding phase correcting mirrors and optimizing them for improved transformation through a matching optics unit (MOU) into a HE_{11}- waveguide. The most relevant of these alternative designs will be ordered and characterized by low- and high power measurements.

In addition, a complete mirror design for the MOU for the ITER gyrotron was accomplished. The purpose of this device is to match the gyrotron output beam to the transmission lines of the ITER ECRH system, and in particular compensate tolerances (see figures 6 and 7). It turned out that the mirrors had to be designed by a new method for an optimal tolerance compensation without unacceptable coupling losses at high input beam misplacements.

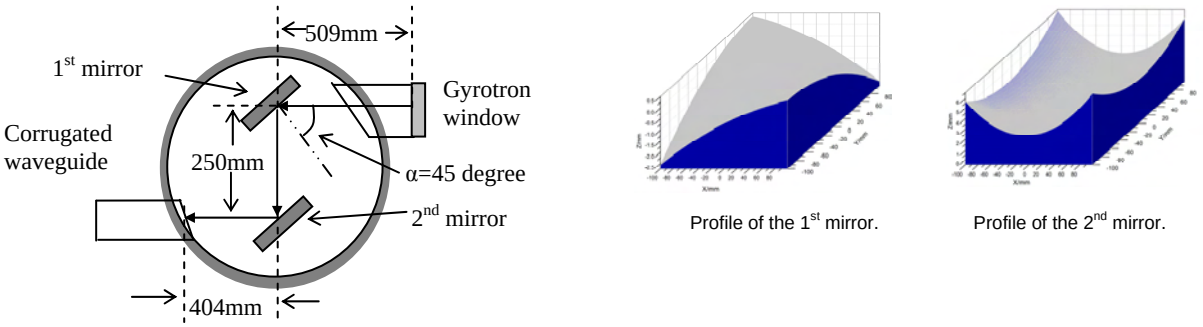

Fig. 6: Sketch of the MOU box and the newly designed matching mirrors.

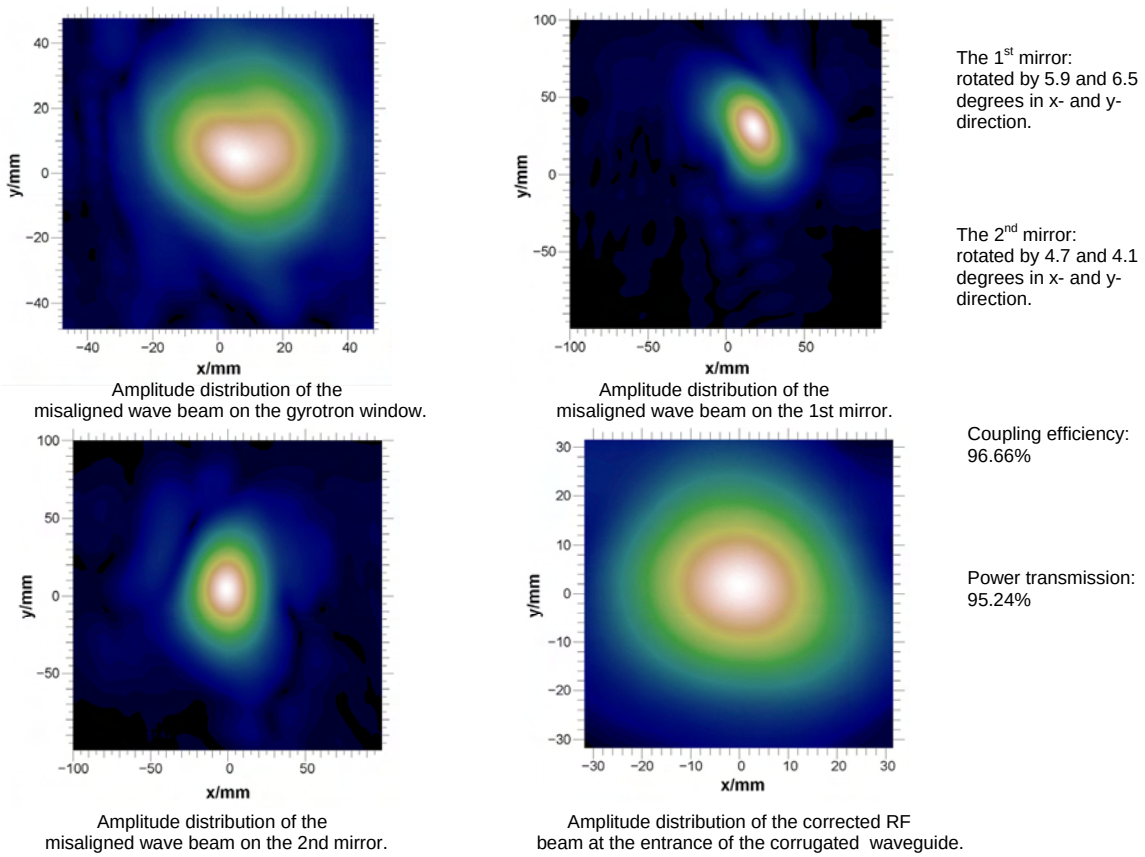

Fig. 7: Example for the calculation of a misaligned RF input beam. The misalignment of 10 mm in both x and y direction is compensated by rotating the MOU mirrors.

In addition to the TWL_DO code, a new, faster analysis code LAUNCHER was successfully tested. Based on accelerated convolution techniques, this code calculates the wave propagation inside the launcher essentially faster than TWL_DO and can furthermore be extended for modelling tapered launchers.

Progress with the 1 MW backup design

The 1 MW backup design, projected as an alternative to the 2 MW coaxial ITER gyrotron, was finalized. In detail, an electron gun, a cavity with the appropriate uptaper, and a conventional launcher with the appropriate mirror system were designed. Other components like the collector, RF window and beam tunnel were merely copied from existing designs for the W7-X gyrotron or the 2 MW tube. All components were successfully tested for stability of operation and for fulfilling the ITER specification. In particular, the suitability of the W7-X collector for power modulated gyrotron operation was investigated, with the result that the conventional longitudinal beam sweeping would need to be replaced by a transversal sweeping system for a 50 % power modulation – the way of modulation requested by ITER, using only the collector depression voltage for power modulation, increases the power load on the collector at lower RF output powers and requires a more efficient power distribution method over the collector surface.

For an actual realisation, the next step would be the technical layout, to be done by the manufacturer. This gyrotron will only be realised when the 2 MW tube development has to be replaced by a less ambitious project.

Conclusions and prospects

After the essential delays for all high power experiments during 2010, it remains the main goal to start again with long pulse prototype experiments at CRPP as well as with short pulse experiments with the pre-prototype at KIT. The central objective of the prototype experiments is, of course, the demonstration of a stable operation, which fulfils the criteria for ITER gyrotrons. With this 1st prototype, the aim is to operate in pulses of 1 s, which is an important step towards CW operation. The main purpose of the pre-prototype is to support these experiments. This means that the plans for pre-prototype experiments will in case be aligned with the investigation needs of the prototype. Apart from that, there is a range of topics that will be investigated with varying priority. These are measurements of different launchers and quasi-optical systems (currently, an alternative launcher antenna provided by IAP is installed and will be tested for RF beam quality and stray radiation), in order to determine sources of stray radiation and to test the different concepts of further improved launchers that were proposed and designed during 2010. Then, different versions of beam tunnels will be employed for comparison. The experiments at different frequencies will be completed, and operation with depressed collector for energy recovery is foreseen, to demonstrate high efficiency operation and as first step towards longer pulses with the pre-prototype. It should be clear that not all of these tests can be done in 2011, so these works will be carried on over the next years.

In parallel to the experiments, the purchase of modular components for the pre-prototype will be continued. It is foreseen to operate a new modular electron gun at the end of 2011. In a later step, the body of the gyrotron will be replaced, in order to operate the pre-prototype inside the small bore hole which is left by the normal conducting CW coil – this coil must also be finally purchased. Furthermore, in preparation of a possible operation of the industrial prototype at KIT, this normal conducting coil needs to be amended by two smaller coils at the gun region (see figure 8) After all these changes, a flexible modular pre-prototype gyrotron as a model for supporting the long pulse prototype will be available, suitable for better comparability of experiments and for easier design changes.

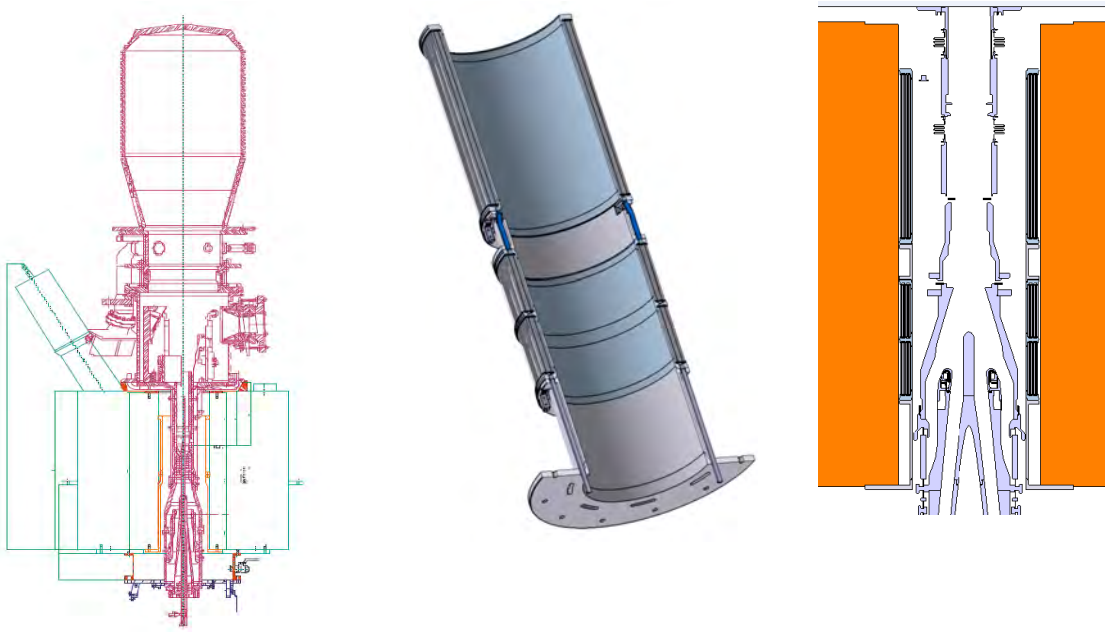

(a) (b) (c)

Fig. 8: Cross section of the industrial prototype, installed in the KIT OI magnet (a). To adapt the OI magnet for operating this gyrotron, an additional normal conducting coil (b) has to be installed into the warm bore hole of the magnet, as detailed in (c).

The activities for the design and procurement of a second long pulse prototype and a corresponding new magnet (the existing magnet at CRPP has a too high helium consumption) have to be continued in parallel. The need for compatibility with ITER requirements has to be taken into account in the specifications of the envisaged 10 MW test stand at KIT as well.

On the theoretical and simulative side, a clear need remains for improved modelling of non-idealized geometries. This will be approached on the one hand through removing some of the assumptions of the existing simulation codes, for example by extending the numerical models towards non-uniform magnetic fields, lossy materials and deviations from the azimuthal symmetry. With regard to quasi-optical systems, the efforts on faster simulations and inclusion of tapered launchers will be continued. On the other hand, the activities for using full-wave codes at least as verification tools will be intensified. In particular, the in-house full wave code PicLas will be equipped with suitable interfaces for gyrotron applications, and will be tested as complementary verification tool for all components of the gyrotron.

Staff:

K. Baumann
E. Borie
G. Dammertz
D. D'Andrea
J. Flamm
G. Gantenbein
H. Hunger
S. Illy
J. Jin
S. Kern
R. Lang
W. Leonhardt
M. Losert
D. Mellein
I. Pagonakis
B. Piosczyk
T. Rzesnicki
A. Samartsev
A. Schlaich
M. Schmid
R. Schneider
W. Spieß
J. Szczesny
M. Thumm
J. Weggen

Literature:

[1] Albajar, F.; Alberti, S.; Avramides, K.A.; Benin, P.; Bonicelli, T.; Cirant, S.; Darbos, C.; Gantenbein, G.; Gassmann, T.; Goodman, T.P.; Henderson, M.; Illy, S.; Ionnidis, Z.; Hogge, J.P.; Jin, J.; Kern, S.; Latsas, G.; Lievin, C.; Pagonakis, I.G.; Piosczyk, B.; Rzesnicki, T.; Thumm, M.; Tigelis, I.; Tran, M.Q.; Vomvoridis, J., „The European 2 MW gyrotron for ITER", 16th Joint Workshop on Electron Cyclotron Emission and Electron Cyclotron Resonance Heating, Sanya, China, April 12-15, 2010 Book of Abstracts

[2] Avramides, K.A.; Dumbrajs, O.; Vomvoridis, J.L.; Kern, S., "Gyrotron interaction simulations with tapered magnetostatic field", 35th Internat. Conf. on Infrared, Millimeter and Terahertz Waves (IRMMW-THz 2010), Roma, I, September 5-10, 2010 Proc.on USB-Stick

[3] Braune, H.; Erckmann, V.; Illy, S.; Michel, G.; Noke, F.; Purps, F. W7-X ECRH teams at IPP, IPF and KIT, "Collector loading during high frequency power modulation", 35th Internat. Conf. on Infrared, Millimeter and Terahertz Waves (IRMMW-THz 2010), Roma, I, September 5-10, 2010

[4] Bruschi, A.; Bin, W.; Cirant, S.; Dell'Era, F.; Gantenbein, G.; Leonhardt, W.; Muzzini, V.; Samartsev, A.; Schmid, M., "Progress and test of the spherical matched load designed for 2 MW-CW", Workshop on RF Heating Technology of Fusion Plasmas, Como, I, September 13-15, 2010

[5] Darbos, C. ITER EC International Design Team, "Status of the ITER electron cyclotron H&CD system", 35th Internat. Conf. on Infrared, Millimeter and Terahertz Waves (IRMMW-THz 2010), Roma, I, September 5-10, 2010

[6] Flamm, J.; Jin, J.; Neudorfer, J.; Roller, S.; Thumm, M., "Investigations on wave propagation in launchers of advanced gyrotron output couplers", 35th Internat. Conf. on Infrared, Millimeter and Terahertz Waves (IRMMW-THz 2010), Roma, I, September 5-10, 2010 Proc.on USB-Stick

[7] Flamm, J.; Jin, J.; Thumm, M., "An FFT based spectral method for analysis of launchers in advanced gyrotron output couplers", ITG Vacuum Electronics Workshop, Bad Honnef, November 15-16, 2010

[8] Flamm, J., "Analysis of cylindrical waveguides with specifically perturbed inner wall using an FFTF based spectral method", KIT PhD Symp., Karlsruhe, 30. September 2010

[9] Gantenbein, G.; Dammertz, G.; Kern, S.; Latsas, G.; Piosczyk, B.; Rzesnicki, T.; Samartsev, A.; Schlaich, A.; Thumm, M.; Tigelis, I., "Progress in stable operation of high power gyrotrons", 16th Joint Workshop on Electron Cyclotron Emission and Electron Cyclotron Resonance Heating, Sanya, China, April 12-15, 2010 Book of Abstracts

[10] Gantenbein, G.; Dammertz, G.; Flamm, J.; Illy, S.; Kern, S.; Latsas, G.; Piosczyk, B.; Rzesnicki, R.; Samartsev, A.; Schlaich, A.; Thumm, M., "Experimental investigations and analysis of parasitic RF oscillations in high-power gyrotrons", IEEE Transactions on Plasma Science, 38(2010) S.1168-77 DOI:10.1109/TPS.2010.2041366

[11] Gantenbein, G.; Dammertz, G.; Erckmann, V.; Kasparek, W.; Kern, S.; Latsas, G.; Lechte, C.; Piosczyk, B.; Rzesnicki, T.; Samartsev, A.; Schlaich, A.; Thumm, M.; Tigelis, I.; Vaccaro, A., "Progress in stable operation of high power gyrotrons for ECRH", 22nd Joint Russian-German Meeting on ECRH and Gyrotrons, Nizhny Novgorod, Russia, June 29 - July 5, 2010

[12] Gantenbein, G.; Rzesnicki, T.; Piosczyk, B.; Kern, S.; Illy, S.; Jin, J.; Samartsev, A.; Schlaich, A.; Thumm, M., "2.2 MW operation of the European coaxial-cavity pre-prototype gyrotron for ITER", 23rd IAEA Fusion Energy Conference, Daejeon, Korea, October 11-16, 2010

[13] Henderson, M.; Albajar, F.; Alberti, S.; Baruah, U.; Bigelow, T.; Becker, B.; Bertizzolo, R.; Bonicelli, T.; Bruschi, A.; Caughman, J.; Chavan, R.; Cirant, S.; Collazos, A.; Cox, C.; Darbos, C.; deBaar, M.; Denisov, G.; Farina, D.; Gandini, F.; Gassman, T.; Goodman, T.P.; Heidinger, R.; Hogge, J.P.; Illy, S.; Jean, O.; Jin, J.; Kajiwara, K.; Kasparek, W.; Kasugai, A.; Kern, S.; Kobayashi, N.; Kumric, H.; Landis, J.D.; Moro, A.; Nazare, C.; Oda, J.; Omori, T.; Paganakis, I.; Piosczyk, B.; Platania, P.; Plaum, B.; Poli, E.; Porte, L.; Purohit, D.; Ramponi, G.; Rzesnicki, T.; Rao, S.L.; Rasmussen, D.; Ronden, D.; Saibene, G.; Sakamoto, K.; Sanchez, F.; Scherer, T.; Shapiro, M.; Sozzi, C.; Spaeh, P.; Strauss, D.; Sauter, O.; Takahashi, K.; Tanga, A.; Temkin, R.; Thumm, M.; Tran, M.Q.; Udintsev, V.; Zohm, H.; Zucca, C., "EC H&CD system for ITER", 16th Joint Workshop on Electron Cyclotron Emission and Electron Cyclotron Resonance Heating, Sanya, China, April 12-15, 2010 Book of Abstracts

[14] Henderson, M.; Albajar, F.; Alberti, S.; Baruah, U.; Bigelow, T.; Becket, B.; Bertizzolo, R.; Bonicelli, T.; Bruschi, A.; Caughman, J.; Chavan, R.; Cirant, S.; Collazos, A.; Cox, C.; Darbos, C.; deBaar, M.; Denisov, G.; Farina, D.; Gandini, F.; Gassman, T.; Goodman, T.P.; Heidinger, R.; Hogge, J.P.; Illy, S.; Jean, O.; Jin, J.; Kajiwara, K.; Kasparek, W.; Kasugai, A.; Kern, S.; Kobayashi, N.; Kumric, H.; Landis, J.D.; Moro, A.; Nazare, C.; Oda, J.; Omori, T.; Pagonakis, I.; Piosczyk, B.; Platania, P.; Plaum, B.; Poli, E.; Porte, L.; Purohit, D.; Ramponi, G.; Rzesnicki, T.; Rao, S.L.; Rasmussen, D.; Ronden, D.; Saibene, G.; Sakamoto, K.; Sanchez, F.; Scherer, T.; Shapiro, M.; Sozzi, C.; Spaeh, P.; Strauss, D.; Sauter, O.; Takahashi, K.; Tanga, A.; Temkin, R.; Thumm, M.; Tran, M.Q.; Udintsev, V.; Zohm, H.; Zucca, C., “An overview of the ITER EC H&CD system and funtional capabilities”, 23rd IAEA Fusion Energy Conference, Daejeon, Korea, October 11-16, 2010

[15] Illy, S.; Beringer, M.; Kern, S.; Thumm, M., “Collector design studies for a 1 MW cylindrical-cavity and a 4 MW coaxial-cavity gyrotron”, 35th Internat. Conf. on Infrared, Millimeter and Terahertz Waves (IRMMW-THz 2010), Roma, I, September 5-10, 2010 Proc.on USB-Stick

[16] Illy, S.; Flamm, J.; Gantenbein, G.; Jin, J.; Kern, S.; Piosczyk, B.; Rzesnicki, T.; Samartsev, A.; Schlaich, A.; Thumm, M., “Recent experimental results of the 2 MW, 170 GHz European pre-prototype coaxial-cavity gyrotron for ITER”, 37th IEEE Internat. Conf. on Plasma Science (ICOPS 2010), Norfolk, Va., June 20- 24, 2010

[17] Ioannidis, Z.C.; Kern, S.; Avramides, K.A.; Latsas, G.P.; Tigelis, I.G., “The contribution of higher-order spatial harmonics in eigenvalues and ohmic losses calculations in coaxial corrugated cavities”, 35th Internat. Conf. on Infrared, Millimeter and Terahertz Waves (IRMMW-THz 2010), Roma, I, September 5-10, 2010 Proc. on USB-Stick

[18] Jin, J.; Flamm, J.; Kern, S.; Rzesnicki, T.; Thumm, M., “Design of phase correcting mirror system for coaxial-cavity ITER gyrotron”, 11th Internat. Vacuum Electronics Conf.(IVEC 2010), Monterey, Calif., May 18-20, 2010 Proc.S.29-30 Piscataway, N.J. : IEEE, 2010 ISBN 978-1-422-7099-0

[19] Jin, J.; Kern, S.; Rzesnicki, T.; Thumm, M., “Improved design of a quasi-optical mode converter for the coaxial-cavity ITER gyrotron”; 16th Joint Workshop on Electron Cyclotron Emission and Electron Cyclotron Resonance Heating, Sanya, China, April 12-15, 2010 Book of Abstracts

[20] Jin, J.; Flamm, J.; Kern, S.; Rzesnicki, T.; Thumm, M., “Theoretical and experimental investigation of a quasi-optical mode converter for a coaxial-cavity gyrotron”, ITG Vacuum Electronics Workshop, Bad Honnef, November 15-16, 2010

[21] Kern, S.; Avramides, K.A.; Ray Choudhury, A.; Dumbrajs, O.; Gantenbein, G.; Illy, S.; Samartsev, A.; Schlaich, A.; Thumm, M., “Simulation and experimental investigations on dynamic after cacity interaction (ACI)”, 35th Internat. Conf. on Infrared, Millimeter and Terahertz Waves (IRMMW-THz 2010), Roma, I, September 5-10, 2010 Proc.on USB-Stick

[22] Kern, S.; Avramides, K.A.; Roy Choudhury, A.; Borie, E.; Gantenbein, G.; Illy, S.; Samartsev, A.; Schlaich, A.; Thumm, M. Different types of after cavity interaction in gyrotrons. Workshop on RF Heating Technology of Fusion Plasmas, Como, I, September 13-15, 2010

[23] Latsas, G.P.; Tigelis, I.G.; Moraitou, M.D.; Kern, S.; Vomvoridis, J.L.; Ioannidis, Z.C., “Parametric study on the effect of the dielectric and geometric properties on the parasitics in gyrotron beam tunnels”, 35th Internat. Conf. on Infrared, Millimeter and Terahertz Waves (IRMMW-THz 2010), Roma, I, September 5-10, 2010 Proc.on USB-Stick

[24] Li, G.; Jin, J.; Rzesnicki, T.; Kern, S.; Thumm, M., “Analysis of a quasi-optical launcher toward a step-tunable 2-MW coaxial-cavity gyrotron”, IEEE Transactions on Plasma Science, 38(2010) S.1361-68 DOI:10.1109/TPS.2010.2043267

[25] Omori, T.; Albajar, F.; Alberti, S.; Baruah, U.; Beckett, B.; Bigelow, T.; Bonicelli, T.; Bruschi, A.; Caughman, J.; Chavan, R.; Cox, D.; Darbos, C.; deBaar, M.; Denisov, G.; Gandini, F.; Gassman, T.; Goodman, T.P.; Henderson, M.; Hogge, J.P.; Jean, O.; Kajiwara, K.; Kasparek, W.; Kasugai, A.; Kern, S.; Kobayashi, N.; Kushwah, M.; Moro, A.; Nazare, C.; Oda, J.; Purohit, D.; Ramponi, G.; Rao, S.L.; Rasmussen, D.; Ronden, D.; Saibene, G.; Sakamoto, K.; Scherer, T.; Shapiro, M.; Singh, N.P.; Strauss, D.; Takahashi, K.; Temkin, R., “Status of the ITER EC H&CD system”, Workshop on RF Heating Technology of Fusion Plasmas, Como, I, September 13-15, 2010

[26] Pagonakis, I.G.; Hogge, J.P.; Alberti, S.; Illy, S.; Piosczyk, B.; Kern, S.; Lievin, C.; Tran, M.Q., “Status of the EU 170 GHz/2 MW/CW coaxial cavity gyrotron for ITER: the dummy gun experiment”, 35th Internat. Conf. on Infrared, Millimeter and Terahertz Waves (IRMMW-THz 2010), Roma, I, September 5-10, 2010 Proc. on USB-Stick

[27] Rzesnicki, T.; Piosczyk, B.; Roy Choudhury, A.; Illy, S.; Jin, J.; Kern, S.; Samartsev, A.; Schlaich, A.; Thumm, M., “Recent results with the European 2 MW coaxial-cavity pre-prototype gyrotron for ITER”, 35th Internat. Conf. on Infrared, Millimeter and Terahertz Waves (IRMMW-THz 2010), Roma, I, September 5-10, 2010 Proc. on USB-Stick

[28] Rzesnicki, T.; Piosczyk, B.; Kern, S.; Illy, S.; Jin, J.; Samartsev, A.; Schlaich, A.; Thumm, M., “Experiments with the European 2 MW coaxial-cavity pre-prototype gyrotron for ITER”, 11th Internat. Vacuum Electronics Conf.(IVEC 2010), Monterey, Calif., May 18-20, 2010 Proc.S.27-28 Piscataway, N.J. : IEEE, 2010 ISBN 978-1-422-7099-0

[29] Rzesnicki, T.; Piosczyk, B.; Kern, S.; Illy, S.; Jin, J.; Samartsev, A.; Schlaich, A.; Thumm, M., “2.2-MW record power of the 170-GHz European preprototype coaxial-cavity gyrotron for ITER”, IEEE Transactions on Plasma Science, 38(2010) S.1141-49 DOI:10.1109/TPS.2010.2040842

[30] Rzesnicki, T.; Piosczyk, B.; Choudhury, A.R.; Illy, S.; Jin, J.; Kern, S.; Samartsev, A.; Schlaich, A.; Thumm, M., “Recent improvements on the 2 MW, 170 GHz coaxial-cavity pre-prototype gyrotron”, ITG Vacuum Electronics Workshop, Bad Honnef, November 15-16, 2010

[31] Schlaich, A.; Flamm, J.; Gantenbein, G.; Kern, S.; Latsas, G.; Rzesnicki, T.; Samartsev, A.; Thumm, M.; Tigelis, I., “Investigations on parasitic oscillations in megawatt gyrotrons”, 11th Internat. Vacuum Electronics Conf.(IVEC 2010), Monterey, Calif., May 18-20, 2010 Proc.S.33-34 Piscataway, N.J. : IEEE, 2010 ISBN 978-1-422-7099-0

[32] Schlaich, A.; Flamm, J.; Gantenbein, G.; Kern, S.; Latsas, G.; Rzesnicki, T.; Samartsev, A.; Thumm, M.; Tigelis, I.; Zwick, T., „Erweiterung der Gyrotron-Frequenzmesstechnik“ Treffen des Kompetenzbereichs Systeme und Prozess, KIT, Karlsruhe, 24.-25.März 2010

[33] Schlaich, A., „Aufbau und Anwendung eines Systems zur Spektralanalyse von Gyorotronpulsen im Millimeterwellenbereich“, Diplomarbeit, Karlsruher Institut für Technologie 2009 KIT Scientific Reports, KIT-SR 7541 (Juli 2010)

[34] Schlaich, A.; Flamm, J.; Gantenbein, G.; Kern, S.; Samartsev, A.; Thumm, M., „Characterization of undesired RF oscillations in megawatt gyrotrons“, ITG Vacuum Electronics Workshop, Bad Honnef, November 15-16, 2010

[35] Schlaich, A., „Investigations on parasitic oscillations in megawatt gyrotrons“, KIT PhD Symp., Karlsruhe, 30.September 2010

[36] Schmid, M.; Erckmann, V.; Gantenbein, G.; Illy, S.; Kern, S.; Lievin, Ch.; Samartsev, A.; Schlaich, A.; Rzesnicki, T.; Thumm, M., “Technical developments at the KIT gyrotron test facility“, 26th Symp. on Fusion Technology (SOFT 2010), Porto, P, September 27 - October 1, 2010

[37] Thumm, M.; Rzesnicki, T.; Piosczyk, B.; Flamm, J.; Gantenbein, G.; Illy, S.; Jin, J.; Kern, S.; Samartsev, A.; Schlaich, A., „2.2 MW record power of the 0.17 THz European pre-prototype coaxial-cavity gyrotron for ITER“, Terahertz Science and Technology, 3(2010) Nr. 1, S.1-20

[38] Thumm, M.; Rzesnicki, T.; Piosczyk, B.; Flamm, J.; Gantenbein, G.; Illy, S.; Jin, J.; Kern, S.; Samartsev, A.; Schlaich, A., „Recent results of the 2 MW-0.17 THz European pre-prototype coaxial-cavity gyrotron for ITER“, 3rd Internat. Workshop on Far-Infrared Technologies (IW-FIRT 2010), Fukui, J, March 15-17, 2010 Abstracts S.12-13 Proc. on CD-ROM University of Fukui

[39] Thumm, M.; Rzesnicki, T.; Piosczyk, B.; Flamm, J.; Gantenbein, G.; Illy, S.; Jin, J.; Kern, S.; Samartsev, A.; Schlaich, A., „Status of the European 2 MW, 170 GHz pre-prototype coaxial-cavity gyrotron for ITER“, Workshop on RF Heating Technology of Fusion Plasmas, Como, I, September 13-15, 2010

[40] Thumm, M., “Progress on gyrotrons for ITER and future thermonuclear fusion reactors”, 37th IEEE Internat. Conf. on Plasma Science (ICOPS 2010), Norfolk, Va., June 20- 24, 2010

[41] Thumm, M.; Rzesnicki, T.; Piosczyk, B.; Flamm, J.; Gantenbein, G.; Illy, S.; Jin, J.; Kern, S.; Samartsev, A.; Schlaich, A., “Status of the 2 MW, 170 GHz pre-prototype coaxial-cavity gyrotron for ITER”, 22nd Joint Russian-German Meeting on ECRH and Gyrotrons, Nizhny Novgorod, Russia, June 29 - July 5, 2010

[42] Zaginaylov, G.I.; Kern, S., “Simplified analytic model for improved field calculation inside the coaxial gyrotron cavity”, European Microwave Week, Paris, F, September 26 - October 1, 2010

Intellectual Property Rights (IPR)

In the frame of this work a new element of know-how has been generated.

Acknowledgement

This work was supported by Fusion for Energy under the grant contracts No. F4E-2008-GRT-08(PMS-H.CD)-01, No. F4E-2009-GRT-034-01 and No. F4E-2009-GRT-049-01 with collaboration by EPFL, Switzerland; HELLAS, Greece; CNR, Italy and ENEA, Italy. The views and opinions expressed herein reflect only the author's views. Fusion for Energy is not liable for any use that may be made of the information contained therein.

Studies on Advanced Emitter and Electron Beam Diagnostic Systems (CoA)

Introduction

Today, the capability of high power gyrotron oscillators for ECRH & CD, to deliver high millimetre wave power in fusion devices (for example 10 x 1 MW CW power at the W7-X ECRH system) has been proven in principle. Consequently, the focus now shifts towards improved reliability and efficiency of gyrotron devices. While gyrotrons today reach efficiencies of typically 50 % (up to 70 % at best) using a single stage depressed collector, an improved efficiency calls for multi-stage depressed collectors combined with optimized electron guns providing well controlled electron beam parameters, suitable for efficient millimetre wave generation. It can be expected that such advanced gyrotrons will reach efficiencies in excess of 80 % typically. This will in return also improve reliability through reduced thermal loading of the collector of the device, which today is the most critical component of a gyrotron. A second critical component is the emitter in the electron gun, which has a limited life time by design and which can deteriorate the millimetre wave generation through inhomogeneous emission. New emitter materials, developed by the company Calabazas Creek Research (CCR; see R.L. Ives et al., “Controlled Porosity Cathodes From Sintered Tungsten Wires”, IEEE Trans. on Electron Devices, Vol. 52, No. 12, 2005), promise higher emission current densities and a better controlled and extended life time.

Status of work at the beginning of 2010 and achievements in 2010

The works were initiated at the beginning of 2010 by setting up a project and by building up the appropriate collaborations. The main part of the work in 2010 – 2012 will be within a dedicated dissertation for advanced concepts. It is foreseen to build a new low power gyrotron equipped with the new CCR emitter material, arranged as small and separated emitter ring segments. For comparison, a conventional emitter will also be ordered for the new gyrotron. With this device, the new emitter material will be qualified. Since such emitters must be segmented by design, the device also opens large fields for investigations on the influence of emission inhomogeneities on the gyrotron interaction and possibly related effects on parasitic oscillations.

These experiments are complemented by the development of new electron beam diagnostic systems that allow measurements during full operation of the gyrotron, in contrast to current electron beam testers which can only characterize the separated electron gun at scaled low power parameters. In a first approach, it is envisaged to calculate electron energy distributions from measurements of the electron’s bremsstrahlung at the collector. Such measurements will give valuable insights into interaction mechanisms and electron beam parameters. In combination with the segmented emitter test gyrotron, it will be possible to qualify the measurement system, and on the other hand to use it both to investigate the properties of the new emitters as well as to support experiments on inhomogeneous emission.

The X-ray electron beam diagnostic is currently developed within a collaboration among KIT and the St. Petersburg State Polytechnical University (SPbSPU), Russia. In 2010, an extensive theoretical study on the calculation of electron energy distributions from bremsstrahlung was accomplished. The result is that a very good reconstruction of energy distributions is possible if the radiation is measured through materials and walls which don’t absorb strongly, like the ceramic isolators on the gyrotron or additional windows, for example at the collector top (see figure 1).

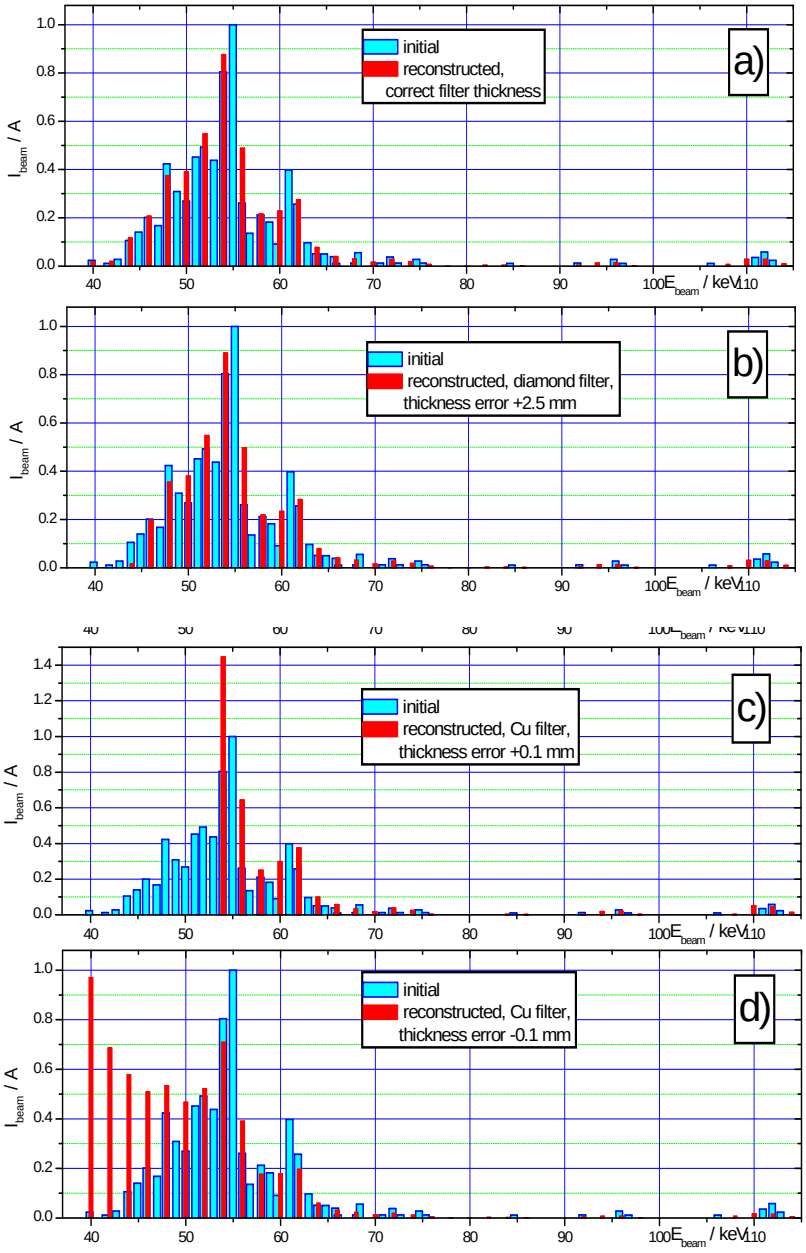

Fig.1: Influence of material parameter deviations on the reconstruction of electron beam energy spectra from X-ray measurements through different materials.

The construction of the test gyrotron was started. In order to start the work quickly and at low costs, the first attempt was to re-use one of the available electron guns from earlier projects as conventional comparison test case. An old $TE_{10,4}$-gyrotron appeared suitable, but it was not possible to achieve any electron emission from it. It was therefore decided to order both a new emitter and a newly designed conventional emitter with the same overall shape from CCR. A first contract was given to CCR about investigations on the segmented emitter construction.

To determine the beam parameters for the design of the new gun, it was necessary to first design the cavity of the low power test gyrotron. In addition, an available 0.5 T normal conducting magnet was checked and characterized for this project, to become independent from the highly loaded fusion test stands. The $TE_{3,1}$ mode was chosen as operating mode at the following parameters: frequency f = 28 GHz (second harmonic), cavity radius R_{cav} = 7.15mm, optimum radius of the electron beam R_e=3.13 mm and magnetic field in the cavity 0.516 T.

Table 1 gives some of the most important parameters of the optimized triode-gun design. Figure 2 shows beam parameter simulations with different mod-anode voltages.

Table 1: Nominal triode-gun parameters.

Beam current	2.2 A
Accelerating voltage	20 kV
Mod-anode voltage	15.6kV
Compression ratio	2.4
Beam radius (interaction)	3.13 mm
Cathode radius	7.15 mm
Cathode angle	32.2 °
Axial width of the emitter	1.7 mm
Emitter current density	2.5 A/cm^2
Velocity ratio	1.56

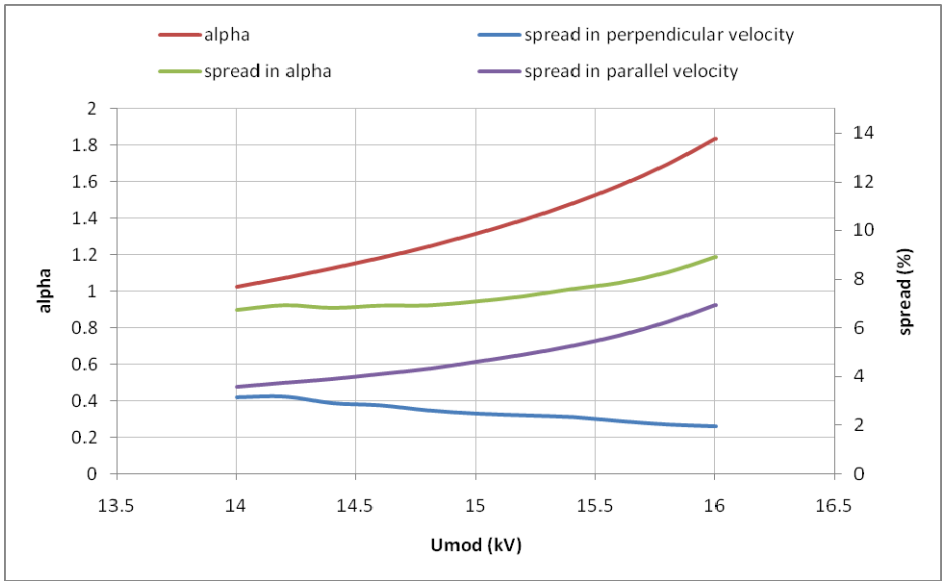

Fig. 2: Velocity ratio (alpha), spread in alpha, as well as spread in parallel and perpendicular velocity components as a function of U_{mod}.

Conclusions and prospects

The first steps towards advanced gyrotron emitter materials, beam diagnostics and, in consequence, higher efficiency and reliability through better physical understanding and through the employment of multi-stage depressed collectors, were done by projecting and designing a test gyrotron with a novel, segmented emitter, and by starting investigations on an X-ray based beam diagnostic system. Within the next year, a first version of the new gyrotron should be assembled and tested. The X-ray diagnostic will also be tested in principle, to get the necessary experimental experience to build up a dedicated beam diagnostic system in subsequent steps during 2012.

Staff:

S. Illy
S. Kern
G. Link
A. Malygin
I. Pagonakis
B. Piosczyk
M. Thumm

ECR Heating and Current Drive – Step-Tunable Gyrotron Development (CoA)

Introduction

In recent years electron cyclotron resonance heating and current drive (ECRH and ECCD) have been established as successful instruments in magnetically confined fusion plasmas. Gyrotrons are the unique devices which meet the extraordinary requirements of those applications: output power in the MW range, 100 – 200 GHz output frequency, pulse length of several seconds up to continuous wave. Due to its excellent coupling to the plasma and the very good localization of the absorbed RF power, ECRH is applied in present day machines and is also foreseen in large forthcoming fusion projects: it will be the main heating system for the stellarator W7-X, which is currently under construction, and it will play a major role in the ITER tokamak. In particular, advanced tokamaks are operated in a plasma regime where MHD instabilities which may limit the performance are present. To a large extent, the stability in a tokamak is influenced by the distribution of the internal plasma currents which can be manipulated by the injection of RF waves. The location of the absorption of RF waves with the angular frequency ω is dependent on the resonance condition $\omega - k_z v_z = \omega_c$ (k_z: z-component of the wave number, v_z: electron velocity along z-axis). Thus, by changing the wave frequency ω the absorption can be moved to any radial position where the local cyclotron frequency of the electrons ω_c holds for the expression above.

Industrial gyrotrons in the relevant frequency range with an output power of about 1 MW are usually designed for a fixed frequency. Thus, frequency tunable gyrotrons are not a standard product since these broadband tubes require additional optimization of major components like the electron beam forming optics, cavity, quasi-optical mode converter and output window.

For experiments on plasma stabilisation at ASDEX Upgrade (IPP Garching) with advanced ECRH and ECCD, multi-frequency tunable (105 – 143 GHz) 1-MW long-pulse gyrotrons are highly needed.

Investigations on frequency spectrum and output power characteristics of the step-tunable gyrotron.

Short pulse measurements (few milliseconds) performed at KIT in 2008-2009 with a step-tunable gyrotron, have shown an unexpectedly low efficiency of the device. The output power at 140 GHz with $TE_{22,8}$ mode was limited to 650 kW power at nominal operating parameters of cathode voltage and current. In addition, the appearance of parasitic oscillations having a frequency 4 GHz lower than the main mode was oserved with increase of the power.

Spectrometric measurements revealed a broad spectrum of these unwanted oscillations, shown in Fig.1. These measurements provide valuable information for theoretical investigation of this phenomenon. The suggestion was that the low efficiency of the gyrotron at working mode and parasitic oscillations are related to the so-called After Cavity Interaction (ACI) of the electron beam passing through the up-taper region with the propagating electromagnetic wave.

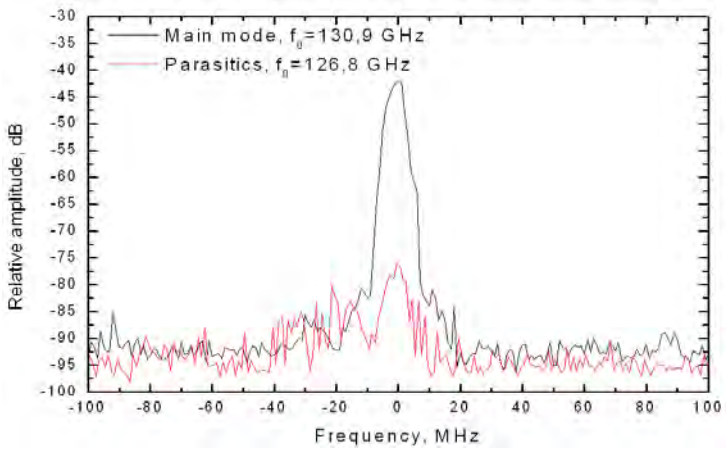

Fig. 1: Spectra of parasitic and main mode $TE_{22,7}$ oscillations.

Several computer simulations with a multimode self consistent time domain model of the gyrotron interaction were performed. The simulations confirmed that combinations of the installed up-taper geometry and magnetic field in the up-taper may lead to a significant effect of coupling between the electrons with transversal rest energy and the RF wave. The interaction may initiate the complicated effects resulting in RF power reduction and absorption by electrons in the region of the up-taper, in auto modulation and instabilities of the output power.

As an example, the simulated start up scenario for the $TE_{22.8}$ mode is shown in Fig. 2. In the simulation, the geometry of the up-taper is included. As can be seen, the produced power does not reach more than 600 kW in average, which is in agreement in with experimental measurements. In addition, Fig. 3 shows the axial structure of the field at 1500 ns. The field profile is not stable and varies very rapidly with time. The instantaneous efficiency deviates strongly from the time averaged efficiency demonstrating maximal value of the field in the up-taper region.

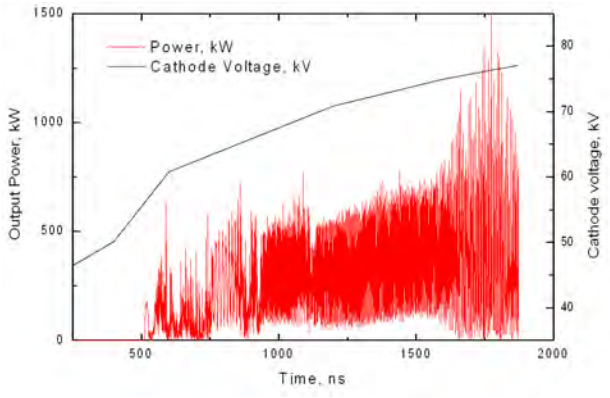

Fig. 2: Start up scenario for $TE_{22.8}$ mode.

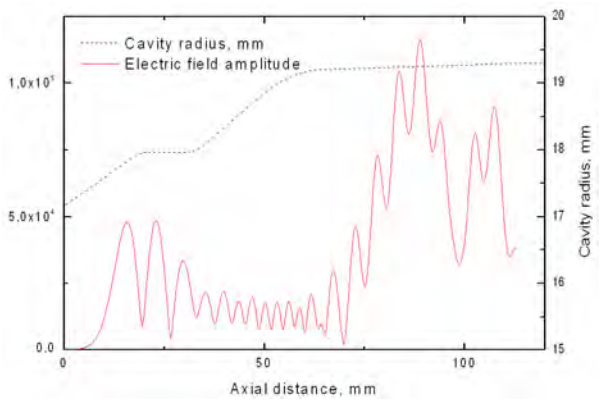

Fig. 3: Field profile of $TE_{22,8}$ mode at t=1500 ns.

In order to avoid gyro-resonance matching in the structure of the uptaper, a stronger gradient of the magnetic field would improve the stability of the cavity oscillations. The magnetic field profile is determined by the arrangement of the super-conducting coils and is fixed. Since the axial gradient of the field is increasing with the distance from its maximum, it is possible to affect the field amplitude of the electric field in the uptaper without significant influence on the field in cavity by moving the arrangement of cavity and up-taper in axial direction. Numerical simulations have yielded that a shift of 20 mm would be an optimal value. The layout of the axial magnetic field distribution and cavity profile before and after shifting are shown in the Fig. 4. Simulations with the cavity shifted by 20 mm, with respect to the maximum of the axial component of the magnetic field distribution, were performed. All the other parameters in the simulations remained the same. Simulated power and field profile are shown in Fig. 5 and Fig. 6. As one can see from Fig. 5, the generated power is exceeding 1 MW at the same parameters, though it still demonstrates an unstable behavior with fluctuations of about 10 % around the average value.

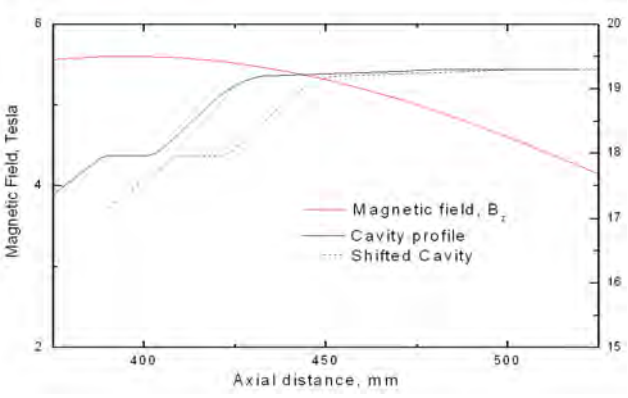

Fig. 4: Magnetic field distribution and the cavity profiles.

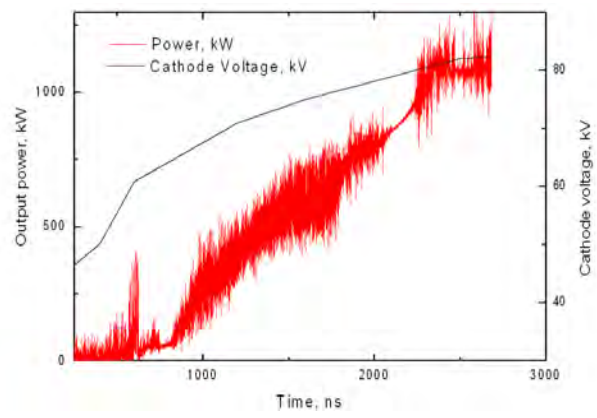

Fig. 5: Start-up scenario for $TE_{22.8}$ mode with 20 mm shift of the cavity.

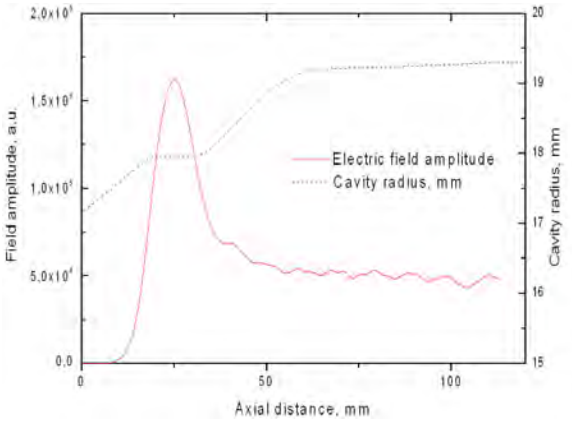

Fig. 6: Field profile at t=2400 ns with 20 mm shift of the cavity.

The field profile in this case has one maximum located at the cavity's center; the distribution is close to the expected one, having the Gaussian shape. At the position of the up-taper starting from 60 mm, the field distribution still has instabilities (ripples) varying rapidly in time, but with lower amplitude compared to the one illustrated in Fig.3. In all simulations, an energy spread of the electrons of 5 % was assumed to realize the simulation close to realistic conditions.

ESRAY calculations of the electron beam parameters for the case when the gyrotron is shifted by 20 mm have shown that the pitch factor and beam radius are very sensitive to the position of the emitter in the inhomogeneous field of the gun coil and deviate from nominal values significantly, so that no optimal operation is possible. Results of calculations are shown in Fig 7. and Fig. 8. A strong increase of the pitch factor reaching the value of 2 with very high variance can be clearly observed.

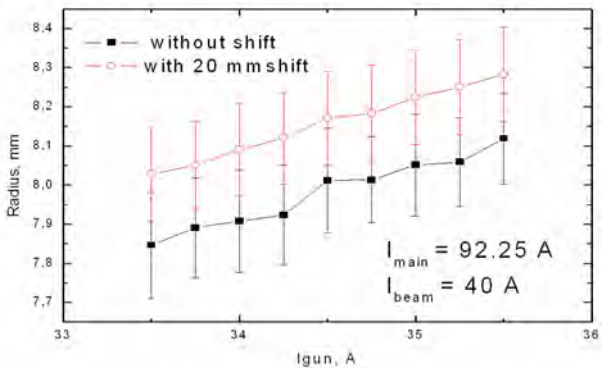

Fig. 7: Radius of the electron beam in dependence of I_{gun}.

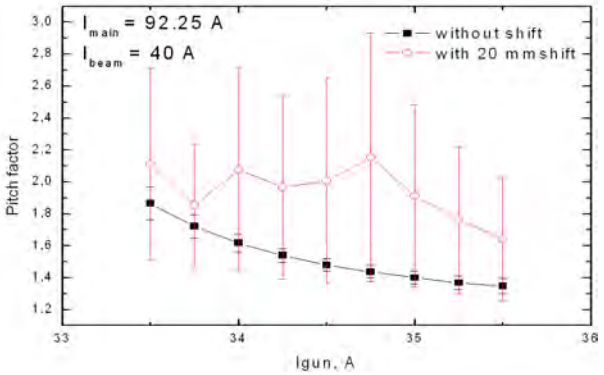

Fig. 8: Pitch factor of the electron beam in dependence of I_{gun}.

Therefore, it was necessary to change the construction of the gyrotron in a way that the cathode remains at the same position. After modification of the experimental setup, the measurements for a series of working modes were performed. In Fig.9 the curves for the $TE_{22.8}$ mode are shown. The beam currents are 43 and 45 A, for a measurement without shift and with 20 mm shift, respectively. After modification it was possible to obtain higher power and better efficiency by the $TE_{22,8}$ mode at 140 GHz. The efficiency is calculated without the effect of voltage depression which takes place in the regime of short pulses.

The highest efficiency up to 30% and output power of up to 950 kW was achieved for the modes $TE_{23,8}$ and $TE_{24,8}$ at reduced cathode voltage. As an example, Fig. 10 shows the dependencies of power and efficiency as a function of cathode voltage. The RF efficiency of the $TE_{22,8}$ mode is lower in comparison with the modes $TE_{23,8}$ and $TE_{24,8}$, which both have larger

caustic radii. The optimization for modes with lower value of caustic radii may be performed by implementation of a triode type MIG. This performance needs further investigations.

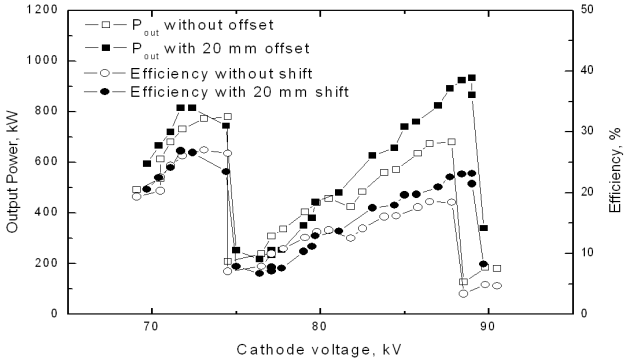

Fig. 9: Power and efficiency of $TE_{22,8}$ mode.

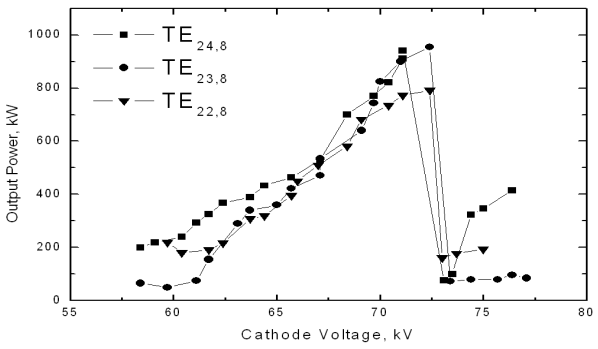

Fig. 10: Generated power by the modes $TE_{24,8}$, $TE_{23,8}$ and $TE_{22,8}$ at reduced cathode voltage.

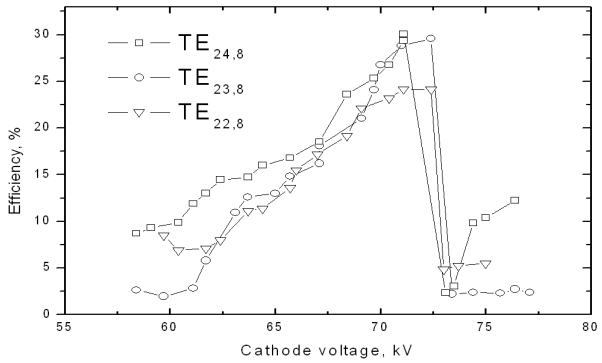

Fig. 11: Efficiency for the modes TE24,8, TE23,8 and TE22,8 at reduced cathode voltage.

In summary, Table 1 shows the generated RF power and efficiencies for all measured modes in the frequency range from 130 to 146 GHz. In the last column, the efficiency of modes corrected for the voltage depression effect calculated by ESRAY at working parameters of the electron beam is shown.

Table 1: Operating parameters, output power and efficiency of investigated cavity modes.

Mode	Frequency [GHz]]	U_{cath} [kV]	Power [kW]	Efficiency [%]	Efficiency Corrected [%]
$TE_{24,8}$	146.5	72.4	960	29.2	31.8
$TE_{23,8}$	143.5	88.4	1060	26.6	28.7
$TE_{23,8}$	143.5	72.4	960	29.5	32.3
$TE_{22,8}$	140.3	89	934	23.2	25
$TE_{22,8}$	140.3	71	773	24.2	26.5
$TE_{21,8}$	137	75	665	20.3	22.2
$TE_{22,7}$	130.9	89	1085	26.5	28.3
$TE_{22,7}$	130.9	73	820	25	26.7

Gyrotron interaction codes: Investigations on dynamic After-Cavity Interaction (ACI)

On the theoretical side, the investigations on dynamic ACI were carried further. The hypothesis that the spent electron beam undergoes active interactions after leaving the cavity, in the so-called uptaper section, is still under discussion. Investigations with different KIT cavity designs indicate that this ACI actually manifests itself as an oscillation driven by the electron beam through its bunched structure that is created by the cavity interaction before. Such behaviour, labelled dynamic ACI, could be demonstrated in several simulations, which seem to be supported by measurements of parasitic oscillations in the W7-X tube experiments and, in

particular, in experiments with the step-tuneable tube (see previous section). These investigations are ongoing.

Since such observations indicate that dynamic ACI may be an important factor for gyrotron operation, a new method for a fast and simple prediction of dynamic ACI in an early design phase is under development. This method relies on an estimation of possible interaction frequencies along the gyrotron cavity and uptaper, to identify regions prone to dynamic ACI. The preliminary result is that extended regions with nearly constant interaction frequency have to be avoided. The easiest way to do that is to employ a steeply declining magnetic field in the region after the cavity.

Progress on measurement devices

Through the implementation of a highly sensitive low noise amplifier, the high power millimetre source of the vector network analyzer could be replaced by a solid state multiplier source. This change was one important step in the process of modernizing this instrument for the measurement of quasi-optical components, since the high power source, based on a phase-locked backward wave oscillator tube, rapidly lost power and reliability.

The equipment for spectral measurement of the gyrotron output signal was further automated and prepared for integration into the test stand system. Now, a highly dynamic measurement system for finding parasitic oscillations and measuring their spectrum as well as the spectrum of the main frequency line is available, which will be routinely employed for investigations on undesired oscillations and on spectral purity in general. This system removes the ambiguity of harmonic mixer measurements through a multipath frequency measurement using different harmonics and a highly sensitive spectral analyzer. The measurement of a complete output spectrum over ranges of more than 40 GHz is now possible automatically, but needs of course long pulse lengths or repeated pulses.

New quasi-optical mode converter

In 2010, measurements on the output beam pattern have been performed for several modes. The Gaussian content of the output beam is less than expected. It is assumed that ACI is the main reason for the poor beam quality.

A new type of quasi-optical mode converter for the step-tunable gyrotron was developed using an advanced code for the launcher and mirrors synthesis. The launcher is optimized for nine modes, the Fundamental Gaussian Mode Content of the field calculated at the position of the output window (250 mm from gyrotron axis) for 9 Modes is presented in Table 2.

Table 2: Calculated Fundamental Gaussian Mode Content at the position of the output window for 9 modes.

Mode	Frequency [GHz]	FGMC [%]
$TE_{17,6}$	104.9	96.4
$TE_{18,6}$	108.2	93.8
$TE_{19.6}$	111.5	90.3
$TE_{19.7}$	120.8	96.1
$TE_{20.7}$	124.1	97.0
$TE_{21.7}$	127.4	94.6
$TE_{21.8}$	136.7	91.0
$TE_{22.8}$	140.0	93.4
$TE_{23.8}$	143.3	94.3

The launcher will be used with a quasi-elliptical mirror and new toroidal mirrors. The field propagation in the complete system consisting of launcher and mirrors is being verified with the commercial code Surf3D for the $TE_{22.8}$ mode. The field pattern and phase distribution calculated at the position of the Brewster window are presented in Figures 12 and 13. The Gaussian fundamental mode content for $TE_{22.8}$ mode at the window is 93.5 %.

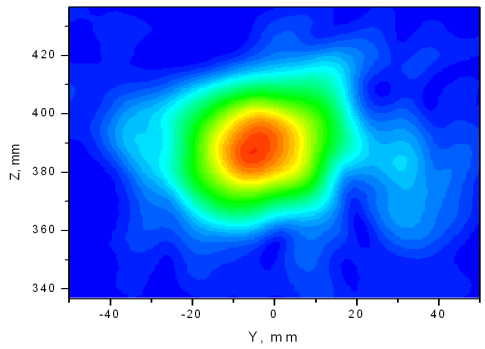

Fig. 12: Amplitude distribution of the RF field in the window plane for $TE_{22,8}$.cavity mode.

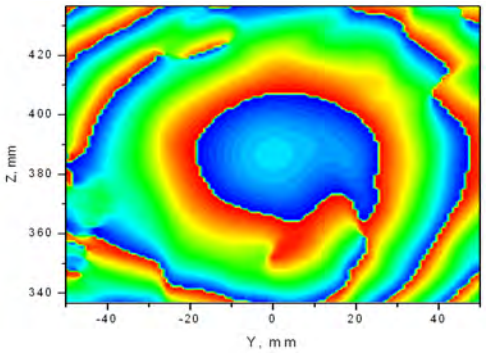

Fig. 13: Phase distribution of the RF field in the window plane for the $TE_{22,8}$.cavity mode.

CVD-diamond Brewster window

Efficient operation for the large number of operating modes at different frequencies is only possible using a broadband synthetic diamond Brewster window fabricated by chemical vapor deposition (CVD). Due to the large Brewster angle of 67.2° deg, the diameter of the disk has also to be rather large in order to have a sufficiently large aperture for the RF beam. One disk with a thickness of 1.7 mm and a diameter of 140 mm was developed by Element Six and has already been delivered. This disk can be used for the elliptic shape of a Brewster window with an effective aperture of 50 mm.

Because of the ellipticity, the stresses occurring during the brazing procedure are different from that for circular disks. An increase by a factor of 1.3 was calculated for these stresses in the elliptical case. After successful preliminary brazing tests at TED with a quartz disk and a small diamond disk, the brazing of the 140 mm diamond disk was ordered from TED.

Fast step-tunable magnet

A fast step tunable magnet which offers the possibility to change the magnetic field in the range 4.15 – 5.67 T has been ordered. With this magnet there shall be the unique possibility to change the gyrotron frequency from 105 GHz to 143 GHz in steps of approximately 3 GHz within 0.5 s every 10 s. The maximum field will be 7.2 T, suitable also for the investigation of 170 GHz gyrotrons for the ITER ECRH system.

In 2010, the complete magnet has been tested at the factory (Cryomagnetics, USA). It has been shown that the magnet fulfills important specifications, e.g. fast tunability, maximum magnetic field, Helium hold time and others. However, the required alignment of the mechanical and magnetic axis could not be realized. There is a large deviation of one axis from the other. Possible improvements and solutions are currently under discussion with the manufacturer.

Staff:

G. Dammertz
J. Flamm (Uni Karlsruhe)
G. Gantenbein
S. Illy
S. Kern
W. Leonhardt
M. Losert
J. Jin
D. Mellein
A. Papenfuss
B. Piosczyk
A. Samartsev
T. Scherer
A. Schlaich (Uni Karlsruhe)
M. Schmid
R. Schneider
W. Spieß
D. Strauss
J. Szczesny
M. Thumm

Literature:

[1] Flamm, J.; Jin, J.; Neudorfer, J.; Roller, S.; Thumm, M., Investigations on wave propagation in launchers of advanced gyrotron output couplers. 35th Internat. Conf. on Infrared, Millimeter and Terahertz Waves (IRMMW-THz 2010), Roma, I, September 5-10, 2010, Proc. on USB-Stick

[2] Flamm, J.; Jin, J.; Thumm, M., An FFT based spectral method for analysis of launchers in advanced gyrotron output couplers. ITG Vacuum Electronics Workshop, Bad Honnef, November 15-16, 2010

[3] Flamm, J., Analysis of cylindrical waveguides with specifically perturbed inner wall using an FFTF based spectral method. KIT PhD Symp., Karlsruhe, 30.September 2010

[4] Gantenbein, G.; Dammertz, G.; Flamm, J.; Illy, S.; Kern, S.; Latsas, G.; Piosczyk, B.; Rzesnicki, R.; Samartsev, A.; Schlaich, A.; Thumm, M., Experimental investigations and analysis of parasitic RF oscillations in high-power gyrotrons. IEEE Transactions on Plasma Science, 38(2010) S.1168-77, DOI:10.1109/TPS.2010.2041366

[5] Schlaich, A.; Flamm, J.; Gantenbein, G.; Kern, S.; Latsas, G.; Rzesnicki, T.; Samartsev, A.; Thumm, M.; Tigelis, I., Investigations on parasitic oscillations in megawatt gyrotrons. 11th Internat. Vacuum Electronics Conf.(IVEC 2010), Monterey, Calif., May 18-20, 2010, Proc.S.33-34, Piscataway, N.J. : IEEE, 2010, ISBN 978-1-422-7099-0

[6] Schlaich, A.; Flamm, J.; Gantenbein, G.; Kern, S.; Latsas, G.; Rzesnicki, T.; Samartsev, A.; Thumm, M.; Tigelis, I.; Zwick, T., Erweiterung der Gyrotron-Frequenzmesstechnik. Treffen des Kompetenzbereichs Systeme und Prozess, KIT, Karlsruhe, 24.-25.März 2010

[7] Schlaich, A., Aufbau und Anwendung eines Systems zur Spektralanalyse von Gyrotronpulsen im Millimeterwellenbereich. Diplomarbeit, Karlsruher Institut für Technologie 2009, KIT Scientific Reports, KIT-SR 7541 (Juli 2010)

[8] Schlaich, A.; Flamm, J.; Gantenbein, G.; Kern, S.; Samartsev, A.; Thumm, M., Characterization of undesired RF oscillations in megawatt gyrotrons. ITG Vacuum Electronics Workshop, Bad Honnef, November 15-16, 2010

[9] Schlaich, A., Investigations on parasitic oscillations in megawatt gyrotrons. KIT PhD Symp., Karlsruhe, 30.September 2010

[10] Stober, J.; Wagner, D.; Gianone, L.; Leuterer, F.; Monaco, F.; Maraschek, M.; Mlynek, A.; Mszanowski, U.; Münich, M.; Poli, E.; Reich, M.; Schmid-Lorch, D.; Schütz, H.; SChwinzer, J.; Treutterer, W.; Zohm, H.; ASDEX Upgrade Team; Meier, A.; Scherer, T.; Flamm, J.; Thumm, M.; Höhnle, H.; Kasparek, W.; Stroth, U.; Litvak, A.; Denisov, G.G.; Chirkov, A.V.; Tai, E.M.; Popov, I.G.; Nichiporenko, V.O.; Myasnikov, V.E.; Soluyanova, E.A.; Malygin, S.A., ECRH on ASDEX upgrade. System extension, new modes of operation, plasma physics results. 16th Joint Workshop on Electron Cyclotron Emission and Electron Cyclotron Resonance Heating, Sanya, China, April 12-15, 2010, Book of Abstracts

[11] Wagner, D.; Stober, J.; Leuterer, F.; Monaco, F.; Münich, M.; Reich, M.; Schmid-Lorch, D.; Schütz, H.; Zohm, H.; Thumm, M.; Scherer, T.; Meier, A.; Gantenbein, G.; Flamm, J.; Kasparek, W.; Höhnle, H.; Lechte, C.; Litvak, A.G.; Denisov, G.G.; Chirkov, A.; Popov, L.G.; Nichiporenko, V.O.; Myasnikov, V.E.; Tai, E.M.; Solyanova, E.A.; Malygin, S.A., Status of the multi-frequency ECRH system at ASDEX upgrade. Workshop on RF Heating Technology of Fusion Plasmas, Como, I, September 13-15, 2010

[12] Wagner, D.; Stober, J.; Leuterer, F.; Monaco, F.; Münich, M.; Schmid-Lorch, D.; Schütz, H.; Zohm, H.; Thumm, M.; Scherer, T.; Meier, A.; Gantenbein, G.; Flamm, J.; Kasparek, W.; Höhnle, H.; Lechte, C.; Litvak, A.G.; Denisov, G.G.; Chirkov, A.; Popov, L.G.; Nichiporenko, V.O.; Myasnikov, V.E.; Tai, E.M.; Solyanova, E.A.; Malygin, S.A., Multi-frequency ECRH at ASDEX upgrade, status and plans. 35th Internat. Conf. on Infrared, Millimeter and Terahertz Waves (IRMMW-THz 2010), Roma, I, September 5-10, 2010

Design Studies towards a 170 GHz 4 MW Coaxial-Cavity Gyrotron (EFTS EC-Tech – Contract No. 042636 (FU06))

For future fusion devices it is desirable to make available gyrotrons with highest possible unit power to reduce the costs and space requirements for new ECRH systems. Currently, the 2 MW coaxial-cavity gyrotron has reached prototype status, so consequently a detailed design study for a 170 GHz 4 MW coaxial-cavity gyrotron was started in 2008. Within the EURATOM Fusion Training Scheme EC-TECH No. 042636 (FU06), this work is done as the main topic of a Ph.D. thesis. After physical and technical feasibility studies, the designs for the major gyrotron components (electron gun, coaxial cavity, quasi-optical system for a two beams output and collector) are being developed. In addition, several thermo-mechanical studies are being performed to identify long-pulse operation effects. Tab. 1 summarizes the major design parameters and goals.

Tab.1: Design requirements for a 170 GHz 4 MW CW coaxial-cavity gyrotron.

Operating frequency f_0	170 GHz
RF output power P_{out}	4 MW
Total interaction efficiency η_{tot}	> 35 % (without depressed collector)
Peak ohmic wall loading (realistic) ρ_{wall}	< 2.0 kW/cm²
Loading coaxial insert (realistic) ρ_{coax}	< 0.2 kW/cm²
Emitter current density j_{beam}	< 5.0 A/cm²

In a mode selection process, one well qualified mode, namely $TE_{-52,31}$, was found to deliver the desired output power and frequency. Extensive optimization on the geometry of the interaction cavity has been performed to achieve highest efficiencies and acceptable low wall losses. All calculations have been done using self-consistent and instationary slow-variables code packages, which are available at KIT. In addition, the tapers of the cavity have been designed using scattering matrix codes to guarantee lowest mode conversion towards the quasi-optical output launcher and lowest backward power transmission towards the electron gun. Overall mode conversion of less than 0.3% of the total power from the main mode is possible. A typical start-up simulation with linear voltage rise considering realistic gun parameters can be seen in Fig. 1.

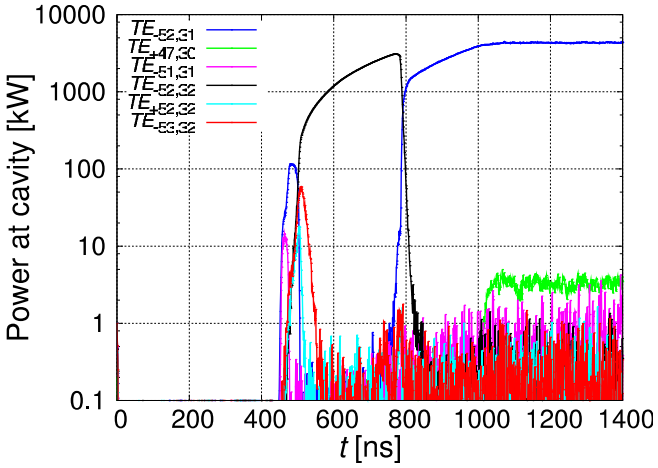

Fig. 1: Self-consistent start-up simulation for the $TE_{-52,31}$ mode.

In a next step, diode and triode-type magnetron injection gun designs have been developed. It was possible to find suitable designs using well-known script-based optimization algorithms. Automated optimization is necessary to determine results within a huge solution space of the electrical and geometrical parameters. Extensive parameter studies have been carried out to specify the adjustability and sensibility of the electron beam quality to the electrical and geometrical parameters. Within a triode-type magnetron injection gun, the ratio α between perpendicular and axial velocity components of the electron can be smoothly tuned using the voltage applied to the modulation anode. This can be seen in Fig. 2. In addition, considering the limitation imposed by the maximum allowable electric field, the required ra-

dial dimension of a triode-type gun at the axial position of its cathode is small, compared to the diode-type gun, due to the lower modulation voltage. The triode's additional modulation anode compensates the high electric field along the electrons' trajectories in the emitter region.

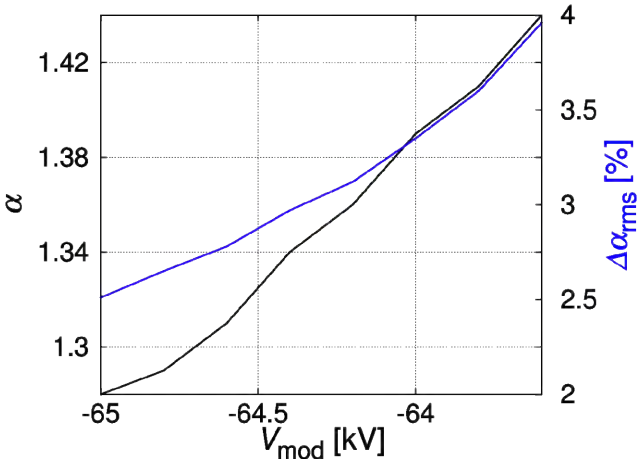

Fig. 2: Velocity ratio α and its spread over voltage applied to modulation anode.

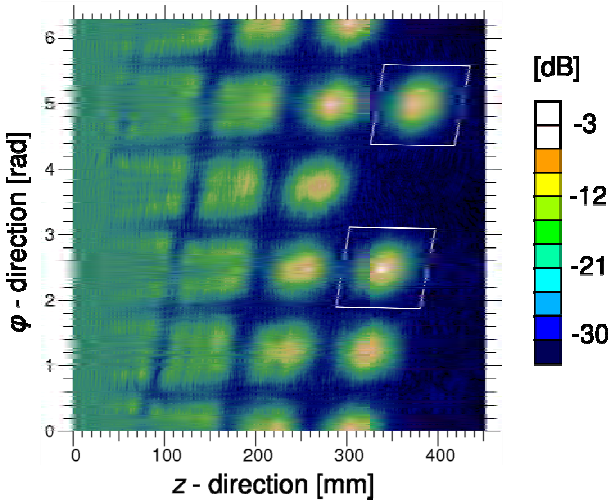

Fig. 3: Field distribution on optimized launcher (irradiated beams in the white parallelograms).

Synthetic diamond discs, which are suitable for microwave beams of up to 2 MW, are used as output windows for gyrotrons. Consequently, a gyrotron with an output power of 4 MW needs two windows, and its quasi-optical system should convert the high order volume mode into two Gaussian-like output beams. For this conversion, a launcher antenna with two cuts was designed, using a newly developed KIT in-house code. The beams are radiated with a very high Gaussian-content of 97% and 98% (vector correlation coefficient) and have an azimuthal separation of 144°. The field on the optimized launcher surface is shown in Fig. 3. In addition, two-dimensional filter techniques are introduced to simplify the launcher's surface perturbations without lowering the beam quality. Reducing the perturbation depths allows a simplified fabrication process of the launcher and consequently reduces its overall costs.

Two collector layouts are being optimized employing normal and dispersion strengthened copper as wall material which absorbs the electron beam. The designs are being optimized using longitudinal magnetic sweeping systems with wobbled coil currents and optimized collector surface shapes. The admissible limit for the overall wall loading in the collector is only achievable with a high depression voltage, which requires in turn a high quality of the electron beam. The copper collector layout with an average wall loading of < 500 W/cm^2 has an inner radius of 400 mm and an absorbing length of approximately 1.0 m along the gyrotron axis. The higher admissible limit for dispersion strengthened copper of < 1000 W/cm^2 allows a more compact collector design with 300 mm in radius and 0.8 m in length.

For the characterization of several long-pulse operation effects, various computing scripts have been introduced to allow the data exchange between commercial finite-element approaches and the corresponding KIT in-house codes. The expected surface temperature of the optimized coaxial 4 MW cavity is strongly sensitive to its surface roughness, and the efficiency of the applied cooling technique. Fig. 4 shows the deformed cavity in thermal steady state.

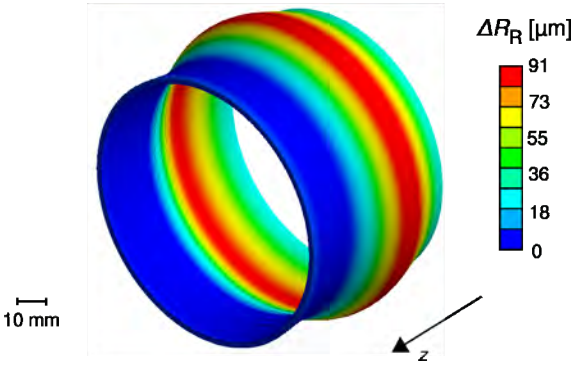

Fig. 4: Deformed 4 MW cavity at thermal steady state.

The frequency shift due to thermal expansion of the cavity at nominal operating conditions with a peak wall loading of 1.7 kW/cm^2 for realistic dispersion strengthened copper is determined to be approximately -130 MHz. In addition, the resonator shows a strongly increasing quality factor for a reduced heat exchange coefficient at the cylindrical cavity section. In order to guarantee stable operation, the efficiency of the cavity cooling and the inner wall's surface roughness have to be controlled carefully. The utilized calculation techniques are being verified with experimental data available for the 1 MW 140 GHz series tube #1 for the stellarator Wendelstein 7-X and show satisfactory correlation.

During CW gyrotron operation, the coaxial insert and its impedance corrugation for advanced mode competition are heated and deformed. Based on two different models for the loading on the insert, the surface temperature was calculated and shows a strong dependence on the velocity of the cooling liquid in the insert's cooling channel. At nominal parameters, the surface temperature reaches 120 °C, and the corresponding deformation of the several grooves of the impedance corrugation is not critical.

The optimized inner surface structure of the quasi-optical output launcher consists of fine perturbations in the scale of several tens of millimeters. Towards the end of the launcher, both beams are highly focused, resulting in high local wall loading and a corresponding deformation of the optimized profile. The cooling channels with a rectangular cross-section are aligned in the shape of a double helix structure around the output coupler. The surface temperature at the launcher's focus points reaches 410 °C for nominal operating conditions. The vector correlation coefficient in relation to the ideal Gaussian distribution, and therefore the quality of both beams, decreases strongly with reduced efficiency of the cooling structure. As a consequence, adequate launcher cooling is necessary in order to guarantee efficient conversion of the high-order cavity mode into two Gaussian beams and to minimize the generated stray radiation. After application of the newly developed two-dimensional filter techniques, the simplified launcher surface can operate more reliably at higher temperatures and smaller corresponding thermal deformations.

Staff:

M.H. Beringer
S. Illy
J. Jin
S. Kern
J.C. Rode
M. Thumm

Literature:

[1] M.H. Beringer, S. Illy, J. Jin, S. Kern, M. Thumm, *4 MW 170/204 GHz Coaxial-Cavity Gyrotron*, EFDA Technical Meeting - Heating and Current Drive, February 2010, Cadarache, France

[2] M.H. Beringer, S. Illy, J. Jin, S. Kern, C. Lievin, M. Thumm, *Design of Major Components for a 4 MW 170 GHz Coaxial-Cavity Gyrotron*, 11th IEEE International Vacuum Electronics Conference, May 2010, Monterey, CA, USA

[3] M.H. Beringer, S. Illy, J. Jin, S. Kern und M. Thumm, *A 4 MW 170 GHz Coaxial-Cavity Gyrotron - Design of the Major Components*, 22nd Joint Russian-German Meeting on ECRH and Gyrotrons, June 2010, Nizhny-Novgorod and Moskow, Russia

[4] M.H. Beringer, S. Illy, J. Jin, S. Kern, M. Thumm, *Physical Component Designs and Thermo-Mechanical Studies towards a 4 MW 170 GHz Coaxial-Cavity Gyrotron*, 2nd International VDE ITG Workshop an Vacuum Electronics, November 2010, Bad Honnef, Germany

Acknowledgement

This work was supported by the European Communities under the Contract of Association between EURATOM and Karlsruhe Institute of Technology. The views and opinions expressed herein do not necessarily reflect those of the European Commission.

Manufacturing of ITER ECRH Upper Port Plug Structural System Prototypes (BMBF Reference No. 03FUS0010)

The outer structure of the ITER ECRH Upper Port Plug consists of two separate units, i.e., the Blanket Shield Module (BSM) and the Launcher Mainframe, providing mechanical support for all internal components. The Mainframe is bolted at the launcher back end as a cantilever to the port extension of the vacuum vessel. Both units are connected with a bolted joint, which allows dismantling of the plug. In the present concept, both the BSM and the Mainframe are designed as a welded assembly with a double-wall structure in particular areas of enhanced heat loads (Figure 1). The Mainframe has to fulfil three functions. First, it has to house the mm-wave components. Second, it should assure that a physical gap is maintained between itself and the neighbouring components, even during severe load conditions in case of plasma disruptions. Third, it has to house the shielding blocks that provide the necessary radiation shielding for the port plug parts and also for the surrounding components. To validate the conceptual design of the ITER ECH Upper Port Plug, feasibility studies on manufacturing processes including prototype testing are mandatory.

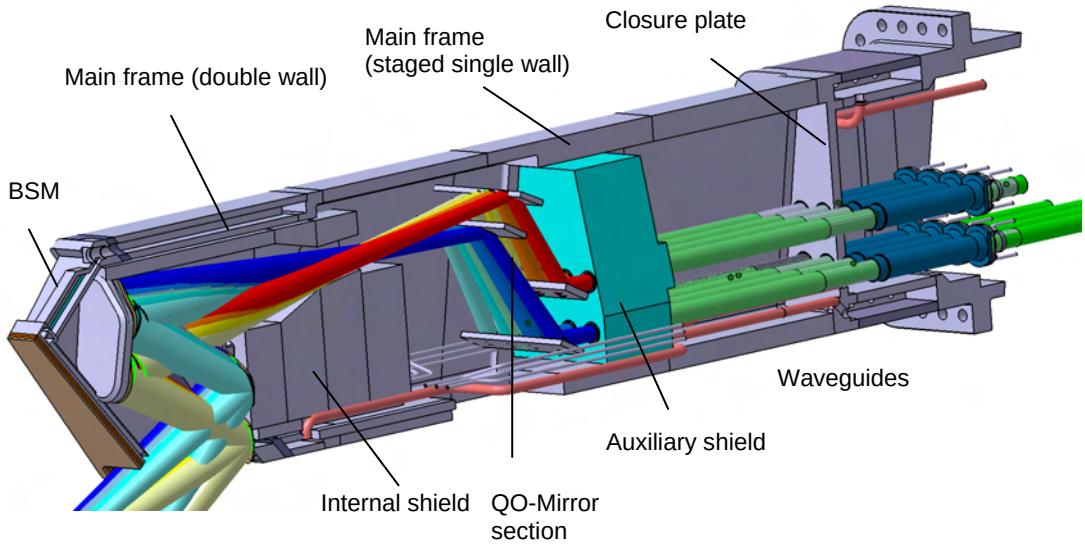

Fig. 1: Schematic representation of the ITER ECRH Upper Port Plug.

For investigating the manufacturing process of the main frame, both a section of the uncooled and a section of the cooled structure were selected to be manufactured as prototypical components. In 2009, the so-called single-wall prototype was designed, manufactured and the associated processes were described. This was followed in 2010 by investigating manufacturing routes for the cooled double wall front-section of the Upper Port Plug.

In this area of the plug, enhanced volumetric heat loads of up to 3 W/cm³ will occur. At a position 1.5m to the rear, the loads decay down to 0.005 W/cm³, where cooling is no longer needed. Thus, the front part of the ECRH Upper Port Plug is formed by two shells, connected with stiffening ribs, which also form a meandering rectangular cooling channel, ensuring homogenous cooling and proper removal of the heat loads. Figure 2 shows a CAD-model of the double wall prototype.

The wall thickness of each shell was calculated to be 30mm, the cooling channels have a width of 20mm and the coolant is routed symmetrically on both sides of the component. For entrance and exit of the coolant, standard flanges will be used. The number of stiffening ribs depends on cooling requirements, mechanical properties, and on the manufacturing route chosen, and will be determined during the investigation process. To avoid “dead flow” zones, leakage gaps between the face sided walls and the stiffening ribs are envisaged.

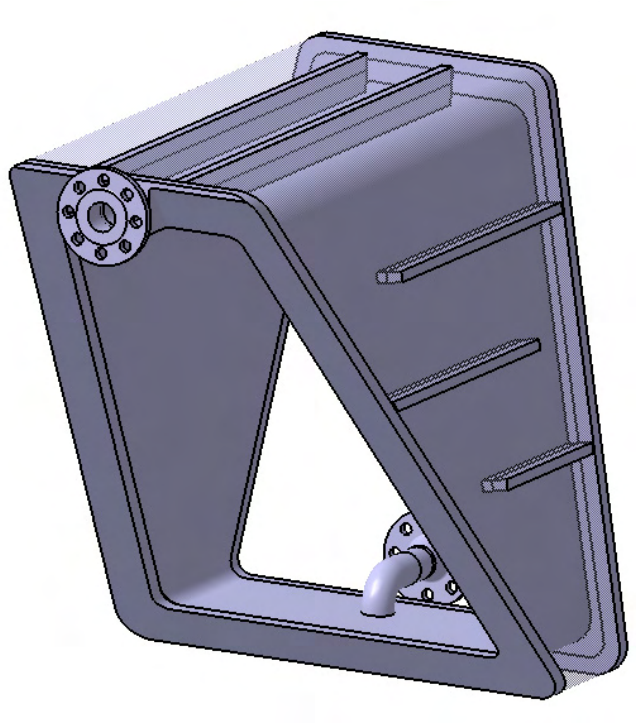

Fig. 2: ITER ECRH Upper Port Plug double wall prototype.

The prototype is designed at 1:1 scale, and its typical dimensions are 1250x1100x850 mm³. Its total mass is about 1100 kg. Preliminary calculations indicate a pressure loss of 0.002 MPa and an average coolant velocity of 0.6 m/s. The mechanical system must withstand an inner pressure of 4.4 MPa at 240°C or 6.3 MPa at 20°C. The maximum coolant mass flow will be 6.0 kg/s. The double wall prototype will be made from stainless steel 1.4404.

In close collaboration with the industrial partner MAN Diesel&Turbo, three design variants have been developed:

D1: Rib design, whith massive ribs providing both the guiding of the coolant and the mechanical joint between the shells.

D2: Bolt design, where the cooling channels are formed by ribs, but the mechanical stiffness is provided by additional bolts.

D3: Full metal design, where the inner cooling structure will be formed by mechanical processing like deep drilling, milling or wire-eroding. The face sided plates will seal this structure.

Further analysis has been performed on these design variants, and two of them were chosen to be preferable. To choose the optimum manufacturing route of the double wall prototype, two smaller sized specimens with all relevant features of the particular designs will be built. After analysing these test components, the decision on the optimum manufacturing process will be made and the manufacturing of the double wall prototype will be initiated.

Staff:

A. Meier
T. Scherer
P. Späh

Acknowledgement

This work was financially supported by the Ministry of Research and Education (BMBF) under the grant No. 03FUS0010. The views and opinions expressed herein do not reflect necessarily those of the BMBF or the European Commission.

Electron Cyclotron System Technology for ITER (EFTS EC-Tech-Contract No. 042636 (FU06))

Overview

High mechanical loads (Lorentz forces) will act on the structure of the Electron Cyclotron Resonance Heating (ECRH) Upper Launcher in ITER as a consequence of the interaction between the static magnetic field and the eddy currents generated during plasma disruptions. A new 20degree-sector electromagnetic (EM) model of ITER has been developed to assess the EM loads acting on the structure of the Upper Launcher and, by means of sub-modelling techniques, on the front steering mirrors.

The cooling system of the front steering mirrors has been studied by Computational Fluid Dynamics (CFD) analysis, the load being given by the mm-wave power absorption resulting from the resistivity of the mirror surface.

Modal analyses and a comparison between static and transient simulations have provided information about the dynamic amplification factors (DAF) for the structure of the Upper Launcher.

Electromagnetic models

Coarse model

The 20degree-sector model (see Fig. 1) features the vacuum vessel's shells, blanket modules with Be-Cu first walls, the equatorial and the upper ports and plugs. This model is used for analysis of an upward Vertical Displacement Event (VDE) scenario (15MA current quench in 36ms with upward displacement), thus the divertor has a minor influence and is not included. The calculations have shown a good agreement with the results of previous similar analyses.

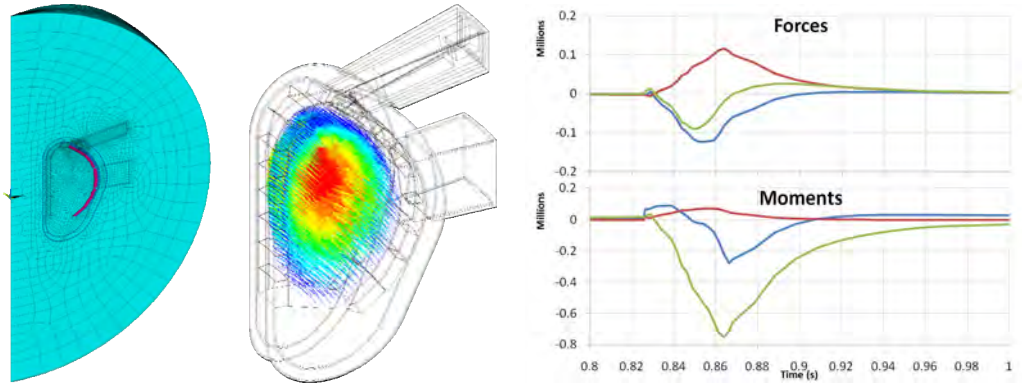

Fig. 1: Snapshots and results of the EM 20 degree sector model under development at KIT: entire model (left); conducting region and plasma current (middle); loads acting on the BSM (right), *x*-direction blue, *y*-direction red, *z*-direction green.

Submodel

A submodel of the front section of the Upper Launcher has been developed for detailed EM simulation of the front steering mirrors. The boundary condition is provided by the coarse model.

A parametric study has been carried out by changing the position (angle) of the mirror. The maximum total forces/moments corresponding to each position have been calculated (Fig. 2).

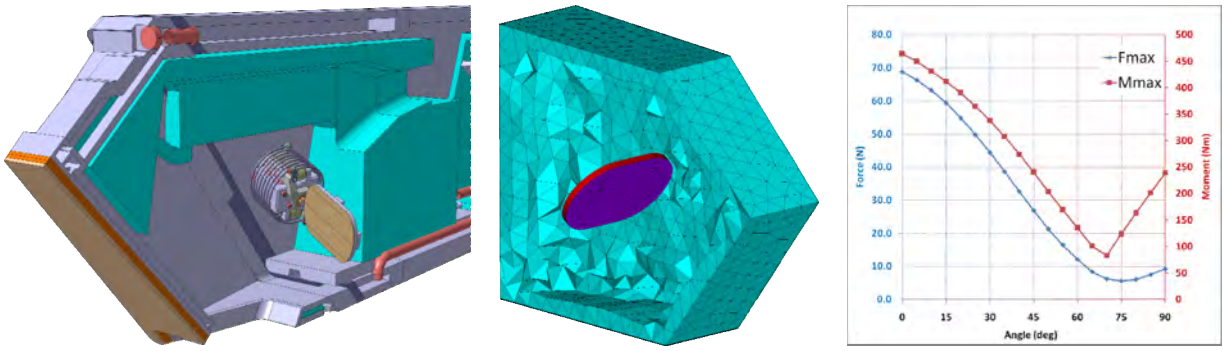

Fig. 2: Left: front section of the Upper Launcher containing the steering mirrors; middle: section of electromagnetic submodel showing the entire mirror plate; right: maximum force and momentum at different angles with respect to the vertical axis.

Front steering mirror cooling

The cooling circuit of the front steering mirror's plate (Fig. 3) of the ITER Upper Launcher has been simulated to assess the temperature distribution on the mirror plate. The surface heat flux is due to the resistive losses on the copper plate. Beryllium may deposit on the copper surface during normal operation of ITER, thus resulting in higher loads due to the higher resistivity. The temperature distribution on the mirror plate for both cases is shown in Fig. 4.

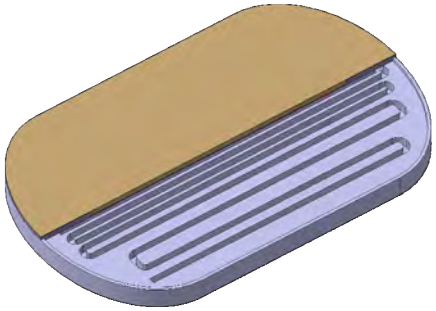

Fig. 3: CATIA model of the front steering mirror's plate. The cooling channels are shown.

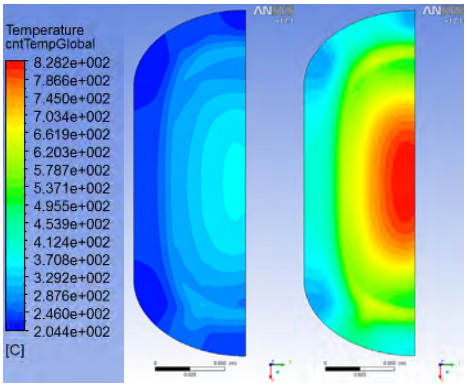

Fig. 4: Temperature distribution on the mirror plate. Copper (left) and beryllium-covered (right) surfaces.

Modal and transient mechanical analysis of the Upper Launcher

Modal and transient analyses of the structure of the quasi-optical design (Preliminary Design Review status) of the Upper Launcher have been studied [1], [2].

The modal analysis yielded the natural oscillation frequencies of the structure, which have compared with the duration of the transient load function (typically, the duration of the disruption) to get first information about dynamic effects. The results of the modal analysis are shown in Fig. 5.

The results of transient and static analyses then were compared together to obtain more detailed information, summarized by the dynamic amplification factor (DAF), calculated as the ratio between one result (e.g. the maximum displacement or a reaction force) of transient and static analyses (see Fig. 6).

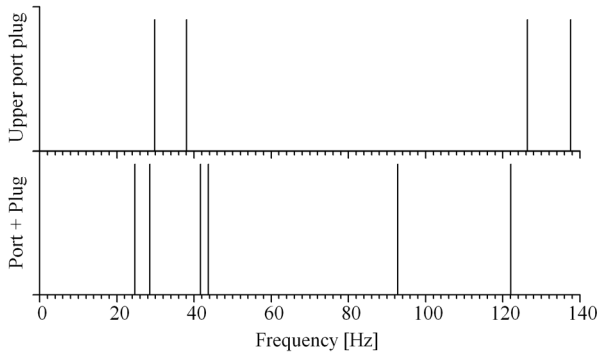

Fig. 5: Natural oscillation frequencies of the upper launcher (top) and the assembly launcher+port (bottom).

Load	Toroidal Displacement (mm)		DAF
	Static	Dynamic	
F_y	3.355	3.727	1.11
M_x	0.197	0.390	1.98
M_z	7.851	8.320	1.06
Sum	11.402	12.436	1.09

Load	Reaction Force/Moment (MN/MNm)		DAF
	Static	Dynamic	
F_y	0.243	0.298	1.22
M_x	1.53	1.85	1.22
M_z	1.58	2.03	1.29

Fig. 6: Dynamic amplification factors for displacements and reaction forces of the assembly plug+port.

Staff:

G. Aiello
A. Meier
T. Scherer
S. Schreck
P. Spaeh
D. Strauß
A. Vaccaro

Literature:

[1] “Launching the Launcher”, Robert Arnoux, ITER newsline #109, http://www.iter.org/newsline/Pages/109/1509.aspx

[2] "The ITER ECH&CD Upper Launcher: Transient mechanical analysis", A. Vaccaro *et al.*, 26th SOFT Conference, Porto, Portugal, 2010.

Acknowledgement

This work was supported by the European Communities under the Contract of Association between EURATOM and Karlsruhe Institute of Technology. The views and opinions expressed herein do not necessarily reflect those of the European Commission.

Testing at Low and High Power of a Window for the EC Upper Launcher (Concept Testing) (F4E-2010-OPE-140-01 (PMS-H.CD)

Overview

The Electron Cyclotron Resonance Heating system (ECRH) for ITER is designed to provide localized heating and current drive (H&CD) to the plasma (four EC launchers are located at 4 ITER Upper ports). EC power is transmitted from the generators to the plasma via evacuated waveguides equipped with diamond windows (CVD diamond disk + structure). These high power diamond window assemblies composed of metallic and nonmetallic components are part of the primary vacuum boundary and thus act as primary tritium barrier.

On the basis of an existing window prototype (prototype I, developed within EFDA task TW6-TPHE-ECHULA on “FS Torus window design, optimisation and test”; EFDA Contract No. 06-1406), a new design will be developed and a prototype II will be manufactured in collaboration with industry (Reuter/Alzenau, Germany) and characterized in low and high power tests at KIT and at the 1 MW / 170 GHz gyrotron facility at JAEA, Naka, Japan.

Status of Activities

The 170 GHz high-power mm-wave experiments with the prototype I performed at JAEA in 2009 (~1MW EC power, <1minute) showed localized spot heating of the window structure. This localized heating has been attributed to the interaction of higher order modes in the EC beam interacting with small features in the window structure. The scope of the current F4E grant is to design and fabricate an improved window assembly with low coupling to higher order modes, by including a waveguide insert into the window housing, including reports describing the new design of the EC Upper Launcher diamond window and the results of low and high power tests.

At the end of the current reporting period, the design work was finished and the CAD drawings have been transferred to the manufacturer. A first report (Definition of window test programme) was delivered and accepted by F4E. The CVD diamond disk (FhG Freiburg, Germany) for the window assembly which was made available by KIT, was characterized at low power level at the measurement facility (Fabry-Perot-resonator)at the IAM-AWP and showed low losses tan $\delta < 10^{-5}$. The multi-step manufacturing process (manufacturing of cuffs and waveguides, brazing of the diamond disk to the housing) is ongoing, and the low power tests of the whole assembly will take place after the window assembly will be finished. As agreed with F4E, high power testing at JAEA is planned for end of January 2011.

Staff:

A. Meier
T. Scherer
S. Schreck

Acknowledgement

This work was supported by Fusion for Energy under the service contract No. F4E-OPE-140-01 (PMS-H.CD). The views and opinions expressed herein reflect only the author’s views. Fusion for Energy is not liable for any use that may be made of the information contained therein.

Goal Oriented Training Programme “ITER Port Plug Engineering” (WP08-GOT-ITER-PPE (FU07-CT-2008-00047))

Design, Manufacturing and Integration of ITER relevant Structural Components

In the frame of the ITER European training network on Port Plug Engineering six work packages have been established. In the Karlsruhe Institute of Technology (KIT), Institute for Neutron Physics und Reactor Technology (INR), the WP 4: “Design, manufacturing and integration of ITER relevant structural components” is hosted. In the frame of this work package, structural components for the integration of test and diagnostic devices into the equatorial port plug dedicated to the European Helium Cooled Pebble Bed Test Blanket Module (EU-HCPB-TBM) are developed.

The temperature level of the plasma facing part of the Test Blanket (First Wall) has a maximum temperature of about 550°C, the rear part of the test device, the so called Back Plate, has a temperature of about 300°C. The in-homogeneous temperature distribution leads to a three dimensional thermal deformation between the plasma facing test device and the mechanical connection structure (Port Plug). The TBM is located inside the port plug and mechanically connected to the shield. The shield is water-cooled to a temperature of 120°C. The connection between shield and TBM is formed by a so-called attachment system. The three dimensional thermal deformation between the TBM and the port plug has to be compensated by the flexibility of the attachment system.

In addition to the thermal loads, mechanical loads act on the TBM as well. The mechanical loads are caused by electro-magnetic effects during different operating states and plasma scenarios as well as by the dead weight.

The attachment system has to transfer the mechanical loads to the shield and on the other hand it has to compensate the differing thermal expansions between shield and back plate of the TBM. This leads to two contradicting requirements. The attachment system has to be flexible to compensate the thermal expansion and it has to be rigid to resist the high mechanical loads.

In the past, different concepts have been developed and investigated at the INR and other research institutions. A promising concept developed at the INR has been further developed and optimized. The characteristic attribute of this concept is that the flexibility of the structure is formed by lamellas.

The design optimization is based on EM-analysis and thermo-mechanical analyses carried out with the engineering simulation software ANSYS. The input data for the analyses is taken from thermo-hydraulic and electro-magnetic analyses. As the design is still in a preliminary state, only static analyses under a worst-case scenario have been performed yet.

Figure 1 shows the TBM-box and the four attachment blocks connecting the TBM-box to the shield. The design in figure 1 was developed during different optimization steps. These steps include number and thickness of the lamellas, arrangement of the attachment blocks, dimensions of the attachment blocks and form optimization of high stress regions.

An evaluation of the stresses according to relevant design codes shows that the stresses are in an acceptable range in most of the regions. Only minor design optimization will be necessary to reach a final design.

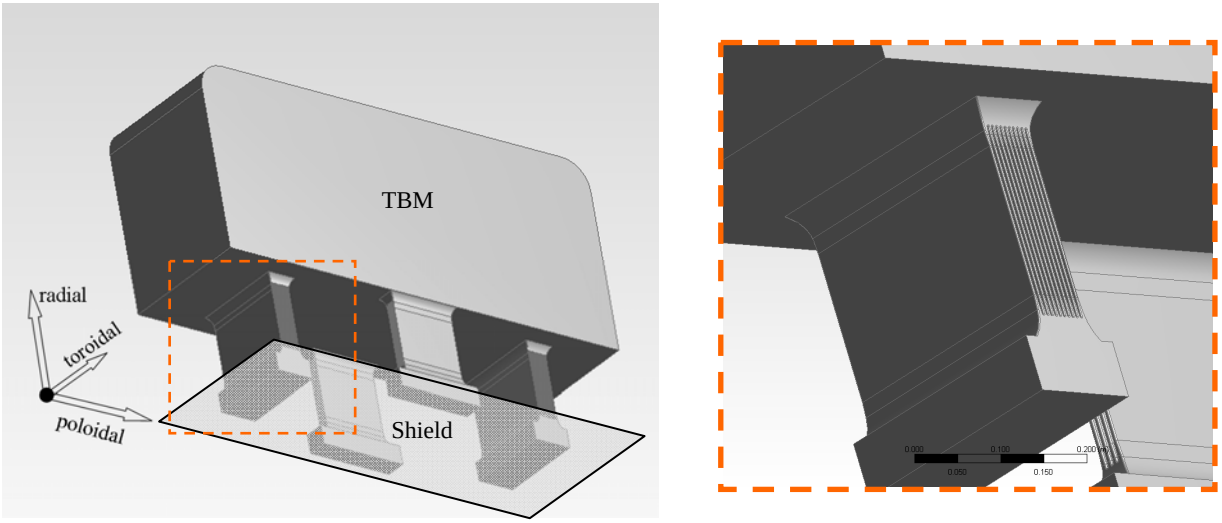

Fig. 1: TBM- box with four attachment blocks.

Staff.

H. Neuberger
C. Zeile

Literature:

[1] ITER Port Plug Engineering Trainee Program: Design, manufacturing and integration of structural components (Analysis of the attachment) presented at the SOFT 2010, to be published in Fusion Engineering and Design, Proceedings of the SOFT 26.

Acknowledgement

This work, supported by the European Communities under the contract of Association between EURATOM and Karlsruhe Institute of Technology, was carried out within the framework of the European Fusion Development Agreement. The views and opinions expressed herein do not necessarily reflect those of the European Commission.

Goal Oriented Training Programme “ITER Port Plug Engineering” (WP08-GOT-ITER-PPE (FU07-CT-2008-00047))

Materials, Manufacturing and Assembly of Upper Port Plug Structures

Overview

In the framework of the EFDA fusion training programme PPE (Port Plug Engineering) the trainee Gaetano Aiello fills the third position under the supervision of PD Dr. Theo Scherer. His activity is devoted to materials, manufacturing and assembly of upper port plug structures, with particular application on the ITER Electron Cyclotron Resonance Heating (ECRH) upper port plug. 2010 is the 2nd year of training. The trainee carried on his experimental activity related to the outgassing measurements for the ECRH Upper Launcher (UL) and he performed the first campaign of experimental measurements. In the framework of the programme some sharing periods are foreseen for the trainees among the involved associations. The trainee spent three months (May-July 2010) in the institute IRFM at CEA/Cadarache working at the CATIA model of the ITER diagnostic equatorial port plug 1 (EPP 1).

Outgassing measurements

In most applications involving both vacuum and high temperatures, outgassing of structural materials is a critical issue. As released gas contaminates the ITER plasma, outgassing rates must be very low for materials inside the vacuum system. Outgassing limits are specified in the ITER vacuum handbook for all components according to their position in the vacuum quality classification [1]. The UL is a torus primary vacuum component and the limits are very strict. The structural material foreseen for the UL is the 316L(N)-IG stainless steel. It has to withstand temperatures in the range 120-150°C during normal operation and 240°C during the baking process. One of the preferred manufacturing routes for UL components is Hot Isostatic Pressing (HIP) which is a method to manufacture powder metallurgical structural components of complex geometry with good mechanical properties. Outgassing data for HIPed stainless steel are not available in literature yet and so experimental measurements are necessary in order to verify the compliance with the limits.

An experimental setup was developed to investigate the partial outgassing rates of stainless steel prototype samples AISI 316LN (on which the 316L(N)-IG is based) and AISI 317LMN, obtained by rolling, rolling with additional solid HIPing and powder HIPing. The samples have cylindrical shape with 1cm diameter and 3cm length and different surface finish. A variant of the gas throughput method in vacuum systems was used for the measurements which were performed over periods larger than 8 hours and at different temperatures [2]. The surface finish of the samples and the experimental setup are shown in figure 1.

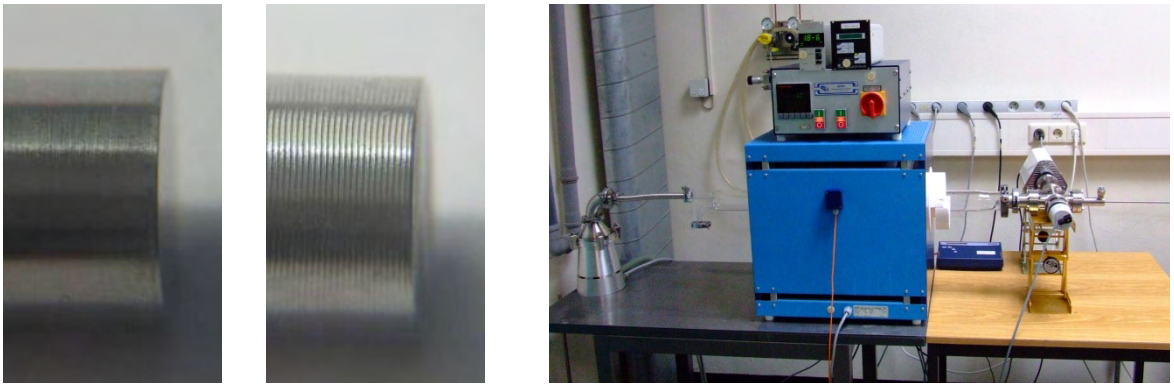

Fig. 1: Polished sample (left), sample with rills (middle) and experimental setup (right). A quartz tube installed in an oven forms the vacuum chamber. The left side of the chamber is connected to the pumping station while the right one to the vacuum gauges.

The gas species released from the samples were generally H_2, H_2O, CO/N_2, O_2, Ar, CO_2/N_2O. Figure 2 shows the typical mass spectrum obtained during the measurements and the typical behaviour of the outgassing rate of the gas species during the pump-down time for two investigated samples.

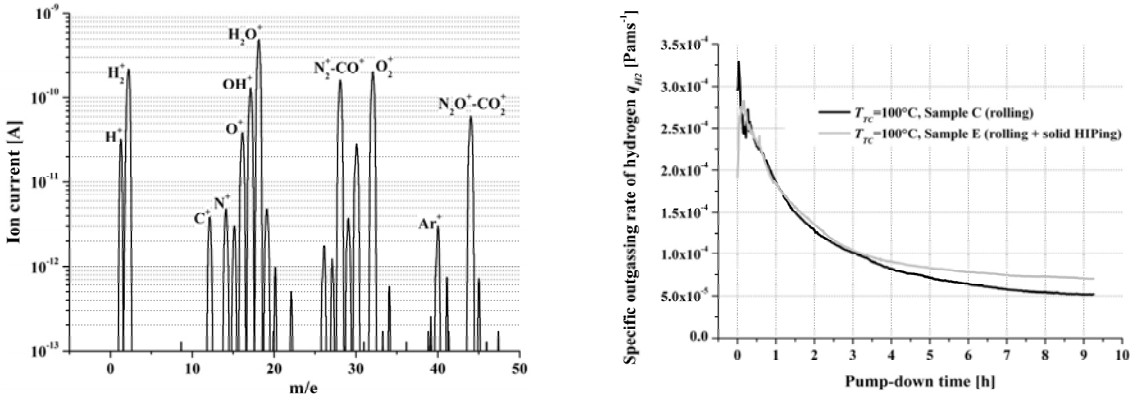

Fig. 2: Mass spectrum obtained during the tests (left) and effect of the solid HIPing method on the specific outgassing rate of hydrogen (right).

Comparing the outgassing rates among the samples, no significant difference due to the HIPing method was found. A possible reason might be that the samples were too small in order to see an effect of the different fabrication technique.

It was also observed that in the case of the rills the outgassing value is about four times greater than that of the polished sample. Since the outgassing values were calculated per unit of the real area (taking into account the surface roughness) of the samples, this increase cannot be explained with a bigger sample area exposed to the vacuum. The explanation for this increase would be the microstructural change close to the surface that the material undergoes when the rills are generated.

The obtained results are only preliminary and as a consequence cannot be compared to the outgassing limits given in the ITER vacuum handbook. Future work aims to further improve the experimental setup considering in particular higher dimensions of the samples and different cleaning methods of their surface.

EPP 1 neutronic CATIA model

Neutronic calculations for the equatorial port plug 1 have been started in the institute IRFM at CEA/Cadarache using the Monte Carlo transport code MCNP. On the one hand the modelling of complex geometries performed directly in MCNP is a very time consuming task, on the other hand the CATIA data cannot be put directly in MCNP because the geometry representation scheme is different. Currently, the development of appropriate CAD (Computer Aided Design)/MCNP interface programs is in progress and they are able to convert CAD data in a suitable model for the MCNP code. However the CAD design models are mainly created for manufacturing purposes and are usually over detailed for neutronic purposes. Generally a geometric simplification of the CATIA models is therefore necessary before using the interface programs like McCAD or MCAM. In this context, the creation of a simplified CATIA model of the plug has been started in order to carry out neutronic analyses using CAD/MCNP interface programs and the code MCNP.

The equatorial plug contains 9 different diagnostic systems in order to measure several plasma parameters. The requirement of the CATIA model was to create a “flexible” model, in a way that position and geometry of every internal component (the diagnostics) of the plug can be easily changed from the top of the catia tree. This flexibility would allow creating quickly different configurations of the plug for the neutronic analyses. Thus a “skeleton” part

has been created at the top of the tree and it contains all the geometric references for the diagnostics. Figure 3 shows the neutronic CATIA model of the plug together with the related CATIA tree. In general each diagnostics has been modelled as a box which follows the shape of the particular diagnostic system as much as possible. The planes which define the boundaries of each box have been created in the skeleton part and moving these planes, each box can change its shape and position with respect to the other boxes. The result is that different configurations of the plug can be quickly obtained by managing the skeleton part and therefore from the top of the CATIA tree.

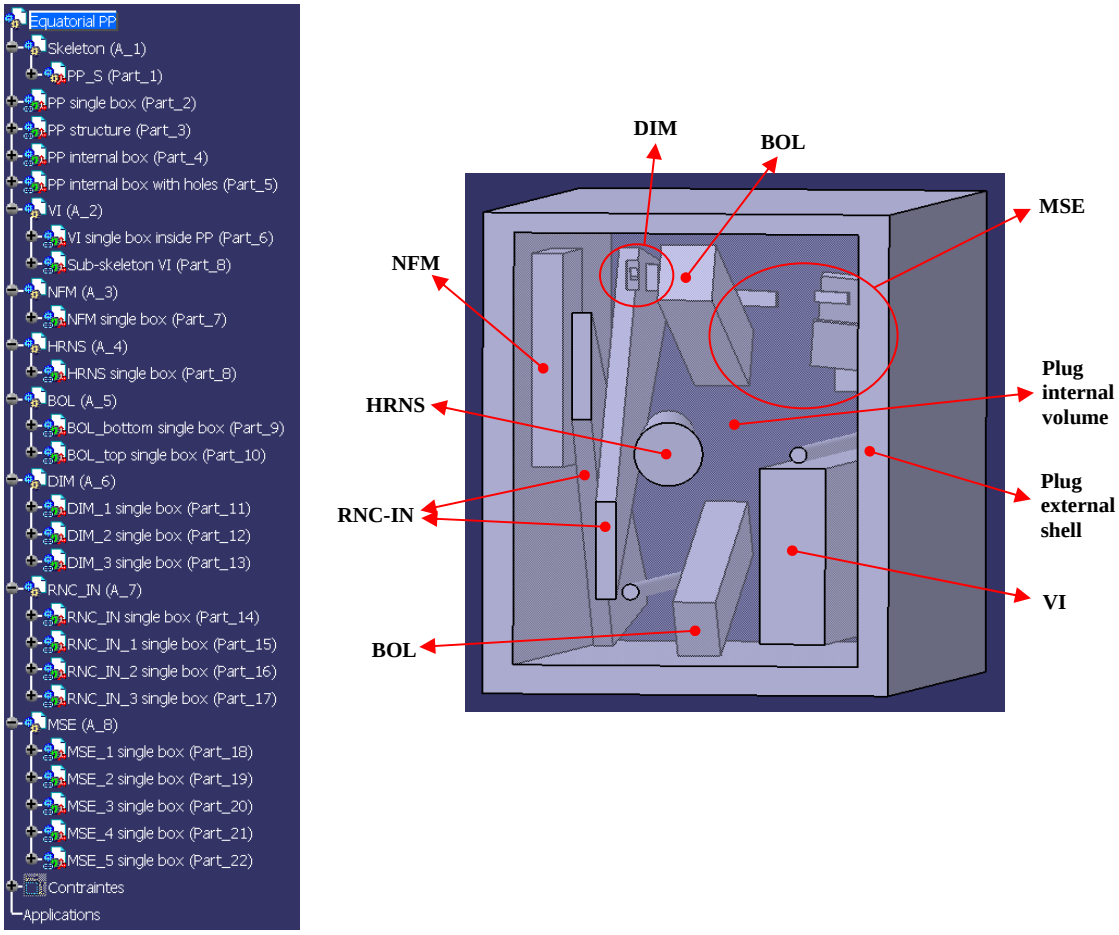

Fig. 3: CATIA tree (left) and neutronic model (right) of the ITER diagnostic equatorial plug 1. All the diagnostic boxes integrated in the model are indicated: visible/infrared wide angle viewing system (VI), radial neutron camera inside the port plug (RNC-IN), motional stark effect (MSE), divertor impurity monitor (DIM), neutron flux monitor (NFM), high resolution neutron spectrometer (HRNS) and bolometers (BOL).

Staff:

G. Aiello
A. Meier
T. Scherer
S. Schreck
P. Spaeh
D. Strauss
A. Vaccaro

Literature:

[1] ITER Vacuum Handbook, 12 June 2009

[2] ITER Vacuum Handbook Appendix 17, Guide to Outgassing Rates and their Measurements, 29 July 2009

[3] G. Aiello, A. Meier, T. Scherer, S. Schreck, P. Spaeh, D. Strauss, A. Vaccaro; Outgassing measurements for the ITER EC H&CD Upper Launcher; Proc. 26th Symposium on Fusion Technology, Porto, Portugal, September 27 – October 1, 2010.

[4] S. Schreck, G. Aiello, G. Gantenbein, A. Meier, T. Scherer, P. Spaeh, D. Strauss, A. Vaccaro; Prototype manufacturing and testing of components of the ECH upper launcher for ITER; Proc. 23rd IAEA Fusion Energy Conference, Daejeon, Korea, October 11-16, 2010.

Acknowledgement

This work, supported by the European Communities under the contract of Association between EURATOM and Karlsruhe Institute of Technology, was carried out within the framework of the European Fusion Development Agreement. The views and opinions expressed herein do not necessarily reflect those of the European Commission.

Goal Oriented Training Programme on Remote Handling (WP10-GOT-GOTRH (FU07-CT-2010-00065))

Overview

The aim of the EFDA European Goal Oriented Training programme on Remote Handling (RH) "GOT RH " is training engineers for activities to support the ITER project and the long-term fusion programme in European Associations, Fusion for Energy, in the ITER organization and in industry. The GOT RH shall establish coherent practical and theoretical training in the area of remote handling among 5 participating European Associations: TEKES - Finland; coordination, CEA - France, CIEMAT - Spain, FOM - Netherlands, KIT - Germany.

Planned activities and status

The work of GOT RH is organised in three work packages. WP1 covers case studies on the ITER RH system requirements, concepts and designs including virtual reality (VR) prototyping. WP2 includes case studies on the ITER RH control system requirements, architectures and designs including VR prototyping. In any case, there is mentoring support. WP 3 represents high level courses and workshops.

The KIT trainee will be involved in the topic *"Maintenance of components of the ECH Upper Port Plug",* which is part of WP1. The aim is to identify the main requirements and elaborate RH procedures for providing a high availability of the ECH Upper Port Plug system. The trainee will work on two basic aspects of remote handling: first on the optimization of the Upper Port Plug design (components and structure) towards remote handling procedures and second on the use of standardized tools or on the development of specialized tools, e.g., for the handling of optical components. He or she will also familiarize with F4E's quality management, including development of a work breakdown structure (WBS), time scheduling (using software PRIMAVERA), determination and observation of milestones and deliverables and preparing of reports. The training includes stays at the partner laboratories (30% of the time) and attendance of project meetings, the participation in relevant conferences (e.g. SOFT, SOFE) and the presentation of the work progress at the RH workshops of the GOT-program.

The start of the project with an overall duration of 4 years, including an individual training programme of 3 years, was on October 1st 2010. Currenty, KIT is in the phase of recruitment.

Staff:

S. Schreck
N.N. (trainee)

Acknowledgement

This work, supported by the European Communities under the contract of Association between EURATOM and Karlsruhe Institute of Technology, was carried out within the framework of the European Fusion Development Agreement. The views and opinions expressed herein do not necessarily reflect those of the European Commission.

Structural Design of an ECRH Launcher for JET (JW10-OEP-KIT-07 - JW9-TA-EP-E4J-03)

The future JET (Joint European Torus) programme, after the installation of the ITER-like wall, will be mainly focused on the consolidation of the physics basis of the main ITER scenarios. This gives a strong motivation for examining the feasibility of the construction and implementation of an ECRH (Electron Cyclotron Resonance Heating) system in JET for an intensive exploitation before the start of ITER operation. To advance this feasibility study towards the approval of the project, a collaborative approach among the E4J (ECRH for JET) project team and the KIT (Karlsruhe Institute of Technology) design team of the ITER ECH Port Plug was established. The aim of this collaboration was to determine the principal design requirements and to set up a rough model of the main components of an E4J system. The optimum position for an ECRH system inside the JET torus would be one of the equatorial ports, in order to provide sufficient space for the system. The JET equatorial ports have a very complex shape, caused by the available interspaces between the field coils. Its geometry features a rectangular cross-section, changing into trapezoidal shape both towards the plasma and to the rear side. Figure 1 shows CAD models and a photograph of the port.

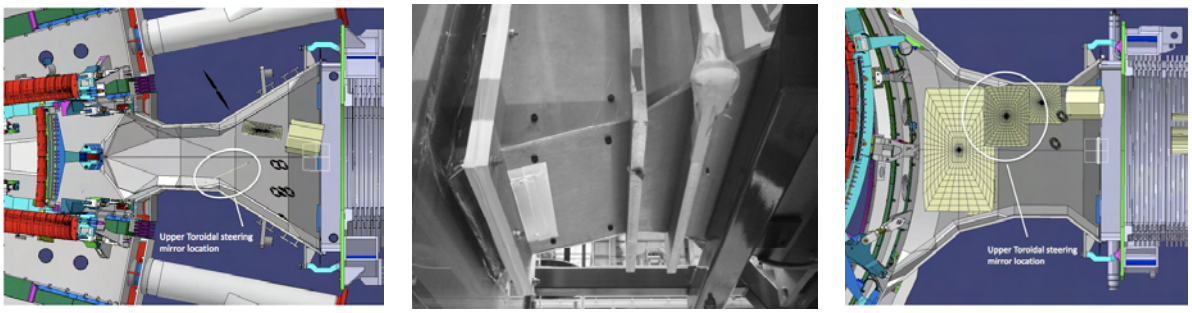

Fig. 1: JET Equatorial port: CAD models and photograph.

For elaborating a first concept of the structural design, an outline of the design issues needs to be compiled. The mechanical structure of the port plug is going to be designed as an integral system. It will be mounted into the port as a completely pre-assembled unit. EM-forces during operation will cause substantial deflection of the plug. In order to guarantee mechanical integrity and to avoid collisions with adjacent components, the maximum tolerable deflection must be defined and proven by structural design analysis.

The mirrors of the ECRH-system need to be cooled, however no cooling of the port plug structure is required. Thermal elongation w.r.t. to the cooled structures will be compensated by a bellow between the port and the port plug. The design goal of an integrated system requires a plug-geometry with a cross-section decreasing from the rear towards the plasma facing side. Thus, a combined structure, whose profile changes from a cylindrical shape at the rear end to a rectangular cross-section in the front area, was established (Figure 2).

The geometry of the plug mimics the inner contour of the port and the bellow in order to provide as much space as possible. With respect to manufacturing tolerances and deflections during plasma disruptions, a minimum gap of 10mm between port and plug structure is considered.

At the first stage of developing a conceptual design, no sustainable load cases were available. Due to that fact and because of complex shape and required stiffness, the wall thickness of the plug structure was specified to be 20mm as a safe assumption, which is equivalent to the wall thickness of the port. The port plug will be made either from Inconel 625® or

from stainless steel and shall be manufactured as a welded assembly. Figure 3 shows different perspectives of the plug with a selection of internal features.

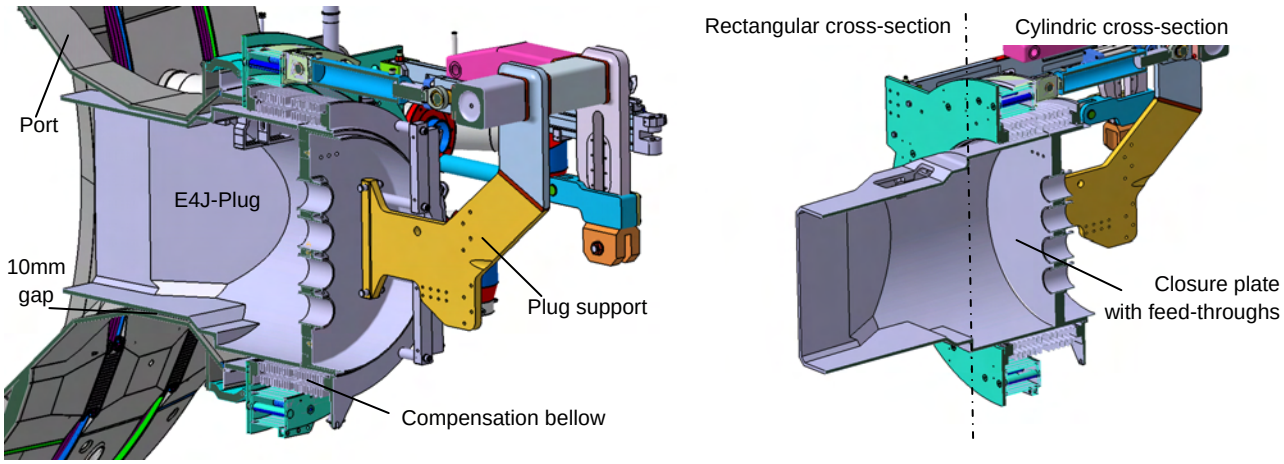

Fig. 2: Cutaways of equatorial port and E4J plug (1st Conceptual design).

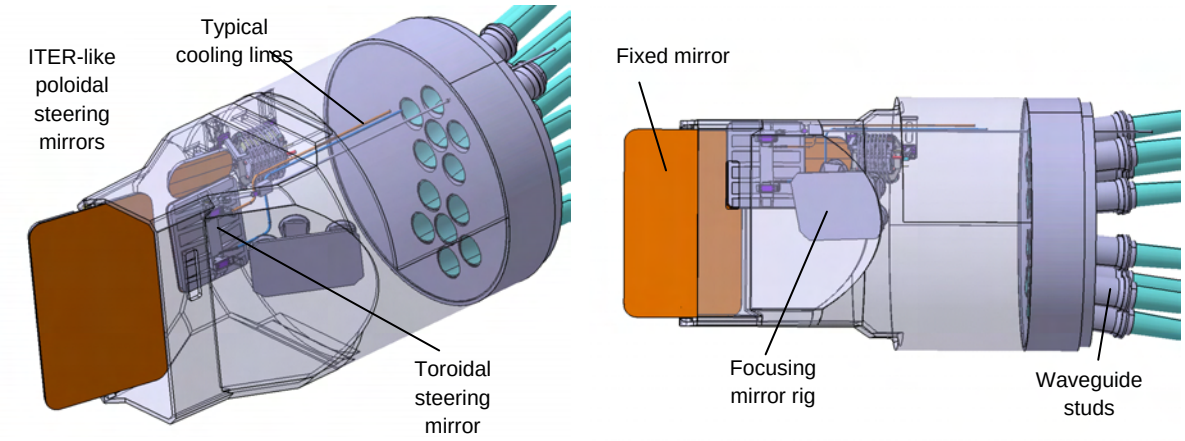

Fig. 3: Outer structure of the E4J plug.

The so-called “closure plate”, serving as mechanical support of the cantilevered port plug arrangement inside the port, will serve as the tritium barrier as well. To make sure that these purposes will be fulfilled, its thickness is chosen to be 70mm. The skewed position of the waveguides makes transition fits necessary, to be machined into the forged body of the closure plate. Individual studs for proper support of the waveguides will be attached (cf. Fig. 4).

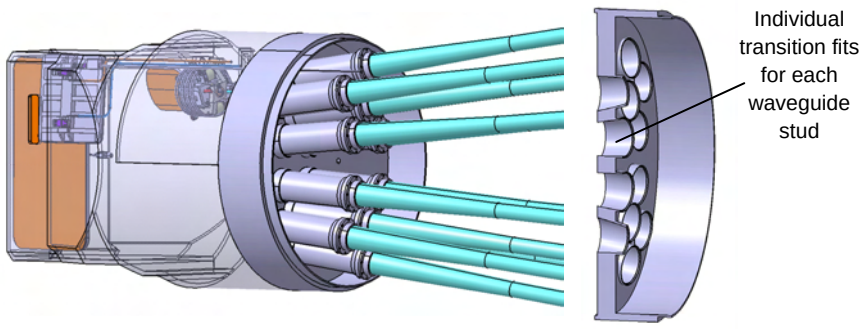

Fig. 4: Design concept of the E4J closure plate.

The studs consist of a turned part, welded into the particular fit of the closure plate. On its opposite end, a flange allows the integration of sealing rings and mechanical connection using individual clamps, welded to the waveguides. Opening that clamps allows individual removal of the waveguides for maintenance or replacement. Figure 5 shows a sectional view of a waveguide stud.

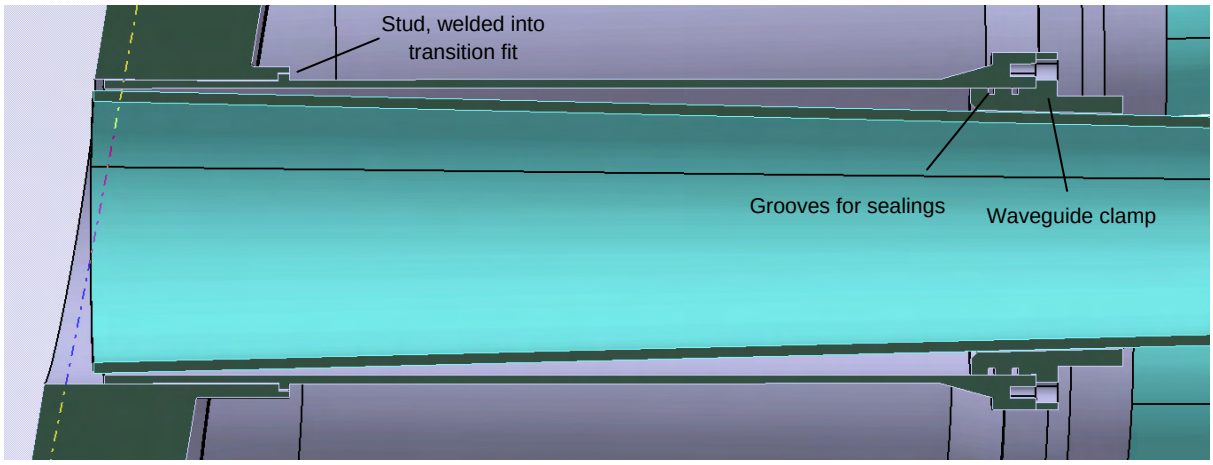

Fig. 5: Design concept of the waveguide stud (sectional view).

The mm-wave system inside the launcher features four sets of mirrors, namely the twelve focusing mirrors, two poloidal steering mirrors, two toroidal steering mirrors and one fixed mirror. All these mirrors must be mounted precisely and securely to the plug structure. With respect to different sizes and varying steering mechanisms, the mechanical support systems of the mirrors must be designed individually.

The design of the focusing mirrors and their position need further investigation in terms of design issues and geometrical arrangement, thus initially no action was taken on their structural integration. However, a concept of the physical mirror arrangement was outlined.

The fact that JET can be used as a test bed for EU launcher components gave rise to the idea to use for the poloidal steering mirrors the design made for ITER. Thus, a mechanical support structure is proposed for the conceptual design, consisting of three hollow beams, fixed to the stator of the steering mechanism. Bolts will be fed through these beams to connect the mirror with L-shaped fasteners, welded to the plug structure. To bring the mirror system into the oblique position required, and to compensate manufacturing tolerances and welding distortions, customized shims serve as interfaces between fasteners and mirrors (cf. Fig. 6, left hand side).

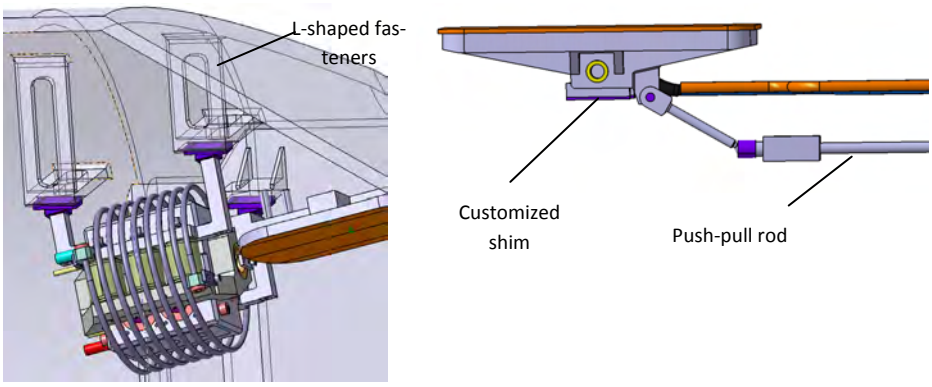

Fig. 6: Mechanical integration of E4J steering mirrors

The toroidal mirrors will be actuated by a push-pull rod and a hinged bracket., Two fasteners are welded to the plug structure to fix the mirror precisely. Two customized shims provide compensation for manufacturing tolerances and are connected to pivot joints. The joints consist of a bolted flange and two flexure pivots to allow friction-less and backlash-free rotation of the mirror. Fig. 6 (right hand side) shows the conceptual design. The push-pull rods are connected to the mirror by a hinged bracket. It is mounted in parallel to the poloidal position of one of the flexure pivots, in order to avoid moments perpendicular to the rotation axis of the mirror. The connections have the capacity to rotate freely and independently around their centre line, thus avoiding torque in the system. Since a universal joint would be too large and too complicated, it was decided use a spherical bearing.

For the integration of the fixed mirror, a preliminary concept has been outlined. The mirror consists of a cooled support structure and a bonded reflection surface. A mechanical support structure with two flexure pivots was designed.

A preliminary stress analysis has been performed using a slightly simplified geometrical model: a cylindrical section on the backside, a rectangular/trapezoidal section on the plasma side and a transition section in the middle. Conservative assumptions on the EM disruption forces have been adopted in absence of detailed information, close to the yield strength of Inconel 625. The following analyses have been performed on the structure of the plug:

S1: Structural analysis of the entire component, to show the overall displacements of the structure and the locations of the highest stresses. A maximum deflection of 3mm in the front opening and of 1.5mm in the rest of the launcher has been obtained, assuming a load applied to the front and to the transition segments and consisting of a 1MN force in toroidal direction plus a 1MNm moment in radial direction (cf. Figure 7).

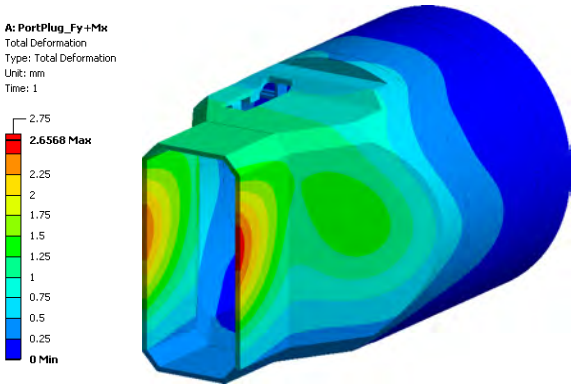

Fig. 7: Total deformation of the plug due to a 1MN force in toroidal direction and a 1MNm moment in radial direction.

S2: Two structural analyses with different temperature conditions, to show how the component expands when heated up. When heated up to 150°C, the plug elongates by 2.8mm, the distance being measured between the backside of the closure plate and the front face of the opening. The elongation rises to 6.8mm when the plug is heated to 350°C. As the mm-wave beams are reflected several times inside the plug, some compensation might be required to correct the relative displacement between the different mirrors. The result of this simulation has to be considered in the context of the entire system, that is, the thermal expansion of the entire vessel is to be taken into account.

S3: Two structural analyses of three-points fixation for the ITER-like poloidal steering mirror. The highest stress (443MPa) is obtained when the load (60kN) acts in vertical direction. This high stress value is mostly due to the geometrical singularity of its location; the rest of the structure is affected by much lower values. The situation is much more relaxed when loads are acting in toroidal direction. The deformation of the supports is lower than 0.2 millimetres.

At this design stage, the simulations have shown that the structure is capable to respect the geometrical constraint of the system, as long as the stresses in the material are lower than the yield strength. Such limit has been reached assuming values for the loads not likely to be reached during a disruption.

Staff:

P. Späh
A. Vaccaro

Acknowledgement

This work, supported by the European Communities under the contract of Association between EURATOM and Karlsruhe Institute of Technology, was carried out within the framework of the European Fusion Development Agreement. The views and opinions expressed herein do not necessarily reflect those of the European Commission.

Magnets and
Affiliated Components

Materials Cryogenic Testing (EFDA/07-1704-1604 (TW6-TMSM-CRYOGT))

Background and objectives

The mechanical testing of materials for magnet components at cryogenic temperatures is an activity carried out for many years at KIT. Different tests were performed investigating tensile properties, fatigue properties, and thermal contraction for selected magnet component materials at cryogenic temperatures (4-77 K). Materials tested include metals, metal composites, and glass/resin composites. The tests are carried out at the facilities and with the equipment available at the cryogenic laboratory of KIT, CryoMaK.

The work was partly covered by the task EFDA/07-1704-1604 and the service contract ITER/CT/09/4300000115. New contracts with ITER and F4E are under preparation.

Scope of contracts

The scope of the contracts is described as follows:

- Fatigue life tests on the chosen structural materials
- Cryogenic mechanical characterization of structural materials and welds according to the task progress
- Tensile strength and fatigue properties tests for the selected candidate structural materials at cryogenic temperature (4-7 K)
- If required thermal expansion and thermal conductivity measurements of the structural and non-structural materials in the cryogenic temperature range.

Preparation for future contracts

ITER has specified a so called standardized tensile test procedure using ½ inch width specimens. Therefore, new grips for testing of such specimens and appropriate 50 mm gauge length extensometers were manufactured.

To test prototype insulation breakers for ITER a special test rig combining torsion and axial loads was commissioned. This test rig allows axial loads up to 160 kN and torsion moments of 1000 Nm.

Butt welds of jackets from TF materials

TF tube material from SMST (Salzgitter Mannesmann Steel Tubes) was provided by ITER in different treatment stages: virgin, compacted and compacted and aged (see table 1). To investigate the influence of these stages 4 flat specimens were machined by EDM from each of these tubes. Tensile tests according to ASTM E 1450 at 4 K were performed and are summarized in tables 2-3. As the compacted and aged material revealed very low elongation values, additional SEM pictures of the fracture surface were taken and compared with pictures of Japanese TF tube material tested in 2009 (figures 2 and 3). This compacted and aged material did comply with the ITER specification of an elongation $\varepsilon > 30\%$.

Table 1: Sequence (1 to 9) of tests.

Dimension (OD)	47 mm	47.5 mm	48 mm
Virgin tube (reference)	5	9	4
Compacted	7	8	6
Compacted & Aged	1	3	2

Heat Number RG698

C is below 0.01% (below target),

N is near 0.18% (high end of spec).

Fig. 1: Picture of TF tubes.

Table 2: Results of tensile tests.

Filename	Tempera-ture	Young's Modulus	Yield Strength	Ultimate Tensile Strength	Uniform Elongation	Total Elongation
-	K	GPa	MPa	MPa	%	%
SMST OD 47, virgin						
CR47V-1	4	204.1	1087	1628	46.8	46.8
CR47V-2	4	214.4	983	1586	34.6	35.2
CR47V-3	4	198.5	1077	1644	42.9	47.3
CR47V-4	4	182.4	1048	1596	40.6	41.8
SMST/ENEA initial OD 47, compacted						
EN47C-1	4	198.3	1265	1694	32.3	36.0
EN47C-2	4	198.9	1322	1791	38.5	38.5
EN47C-3	4	173.0	1258	1676	41.3	44.9
EN47C-4	4	207.4	1327	1743	36.1	36.1
SMST/ENEA initial OD 47, compacted & aged						
EN47CA-1	4	202.3	1195	1539	13.2	13.3
EN47CA-2	4	194.6	1172	1470	14.5	15.5
EN47CA-3	4	213.0	1168	1446	10.4	10.5
EN47CA-4	4	212.6	1173	1486	14.2	14.9
SMST/ENEA initial OD 47.5, compacted & aged						
E475CA-1	4	206.6	1245	1571	16.0	16.0
E475CA-2	4	185.2	852*	1576	13.0	13.6
E475CA-3	4	194.2	1272	1585	14.2	16.2
E475CA-4	4	215.3	1332	1658	17.3	17.8

* unexpected behaviour of elastic plastic transition leading to low YS.
Note:
- All "virgin" and "compacted" samples exhibit a clear "45 degree", slant fracture
- All "compacted and aged" samples exhibit a clear "90 degree", flat facture

Table 3: Results of tensile tests.

Filename	Tempera-ture	Young's Modulus	Yield Strength	Ultimate Tensile Strength	Uniform Elongation	Total Elongation
-	K	GPa	MPa	MPa	%	%
SMST OD 48 mm, virgin						
CR48V-1	4	208.1	1075	1601	43.4	43.8
CR48V-2	4	199.0	1122	1621	36.9	37.0
CR48V-3	4	194.8	1107	1632	42.5	42.5
CR48V-4	4	211.6	1119	1650	38.8	39.8
SMST/ENEA initial OD 48, compacted						
EN48C-1	4	206.4	1313	1704	32.3	33.0
EN48C-2	4	196.0	1297	1708	34.5	46.1
EN48C-3	4	208.2	1278	1681	44.1	44.2
EN48C-4	4	210.6	1279	1695	41.0	42.5
SMST/ENEA initial OD 48, compacted & aged						
EN48CA-1	4	201.7	1269	1565	10.9	12.2
EN48CA-2	4	217.4	1253	1549	12.4	13.8
EN48CA-3	4	188.1	1220	1556	14.1	15.6
EN48CA-4	4	198.2	1209	1494	10.4	11.0

Note:
- All "virgin" and "compacted" samples exhibit a clear "45 degree", slant fracture
- All "compacted and aged" samples exhibit a clear "90 degree", flat facture

SEM pictures

The compacted & aged SMST/ENEA samples exhibit a significant brittle fracture component as shown by the morphology of the intergranular fracture surfaces. As a comparison, the compacted & aged" JAEA samples exhibit a clear "dimple" pattern, representative for a ductile fracture. These results point to the fact, that the mechanical behaviour is very sensitive to the chemical composition (see tables 4 and 5).

Table 4:: Typical chemical composition of SMST specimen.

COMPOSITION CHIMIQUE (% poids) CHEMICAL COMPOSITION (% weight) CHEMISCHE ZUSAMMENSETZUNG (% Gewicht)					Coulée N° Heat Nr : RG698 Schmelze Nr				
C	Mn	Si	S	P	Ni	Cr	Mo	Cu	Co
0,007	1,50	0,61	0,001	0,017	12	18	2,9	0,073	0,05
Nb	Ti	N2	Ta	B	Fe				
0,009	0,007	0,18	< 0,003	0,0011	64,5				

Table 5: Chemical composition of TFb Japanese specimen.

Heat No.		Chemical Composition (%) C ×100	Si ×100	Mn ×100	P ×1000	S ×1000	Ni ×100	Cr ×100	Mo ×100	CO X100	N X100
Specification	Min.						1100	1600	200		14
	Max.	2.0	75	200	35	30	1400	1800	300	10	18
HA2647		0.6	27	103	5	3	1314	1672	244	1	14
		0.6	27	103	6	3	1317	1660	243	1	14

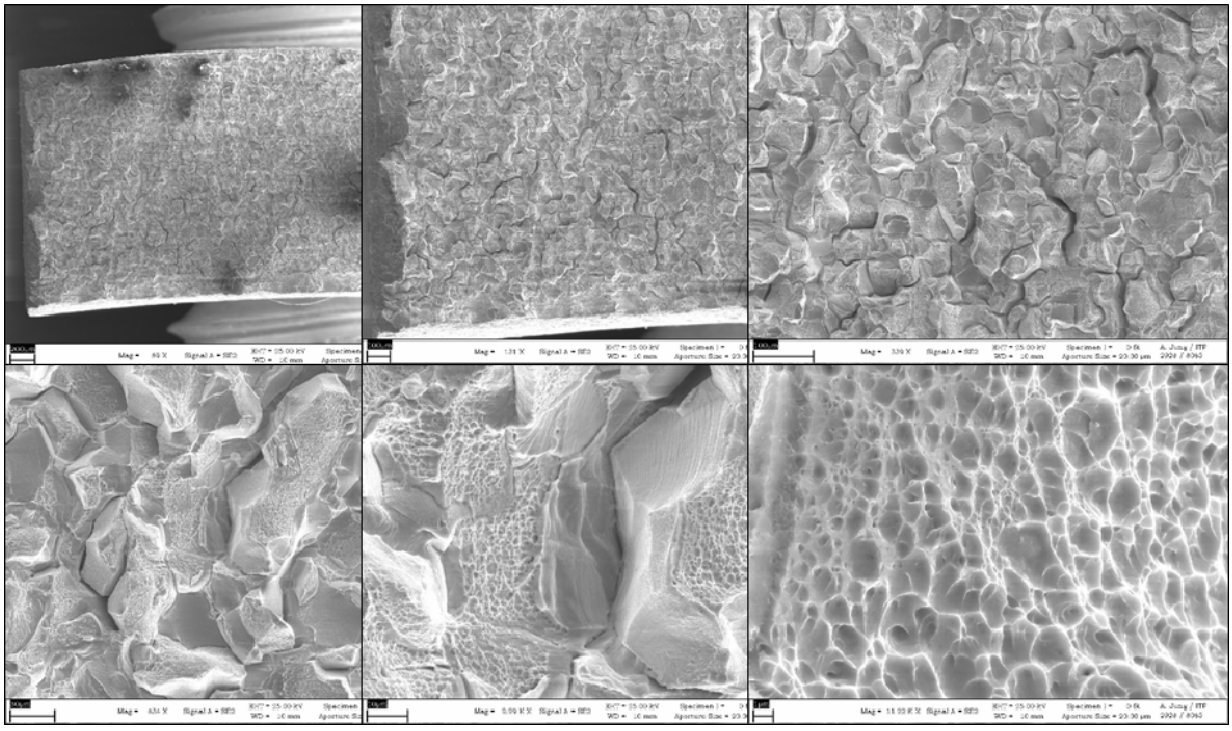

Fig. 2: SEM of specimen EN48CA-1 (magnification factors 70x, 140x, 340x, 800x, 2800x, 12000x), max. elongation < 20%.

Staff:

A. Jung,
K.-P. Weiss,
S. Westenfelder

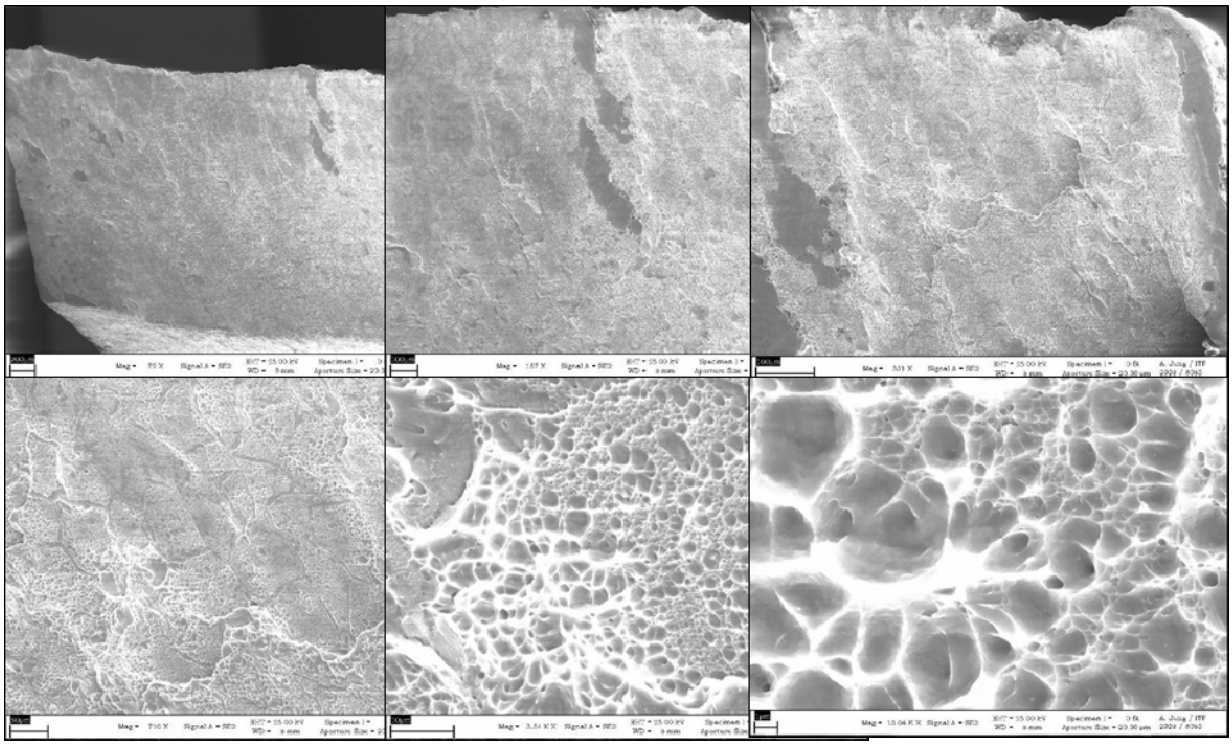

Fig. 3: SEM of specimen TFb4-Japan (magnification factors 70x, 140x, 340x, 800x, 2800x, 12000x), max. elongation > 30%.

Acknowledgement

This work, supported by the European Communities under the contract of Association between EURATOM and Karlsruhe Institute of Technology, was carried out within the framework of the European Fusion Development Agreement. The views and opinions expressed herein do not necessarily reflect those of the European Commission.

Current Leads for Wendelstein 7-X and JT-60SA (CoA; BMBF Reference No. 03FUS0013)

Current Leads for Wendelstein 7-X

KIT will deliver the current leads for the magnet system of the stellarator W7-X which is presently under construction at the Greifswald branch of the Max-Planck-Institute for Plasma Physics. W7-X includes 50 non-planar and 20 planar coils with a maximum conductor current of 17.6 kA. In total 14 current leads are required (maximum design current I_{max} = 18.2 kA, nominal current I_{nom} = 14 kA).

Prototype current lead test

After completion of the assembly of the two prototype current leads (Fig. 1) and the mounting into the test cryostat the connection to the superconducting short circuit bus bar provided by IPP was performed. After completion of the test set up a Paschen test was conducted and a weak insulation was found. Since the detection of the failure had been a very lengthy task and moreover, the insulation failure would cause no problems for the test it was decided to continue the installation of the test cryostat at TOSKA (Fig. 2) and perform the prototype test as planned.

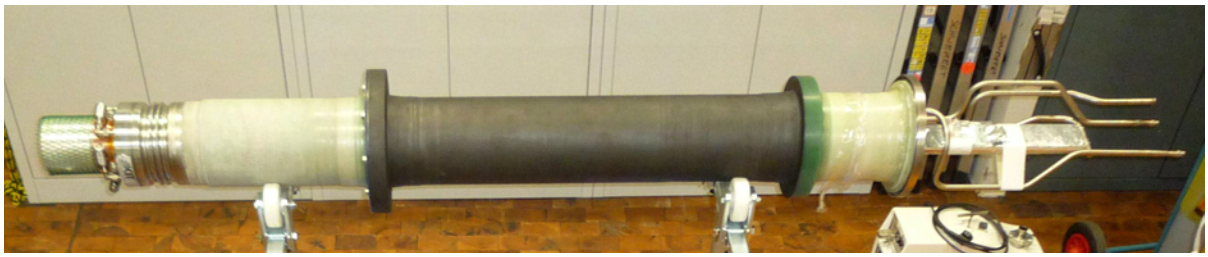

Fig. 1: Prototype of the HTS current lead.

Fig. 2: Test cryostat mounted at TOSKA main vacuum vessel.

After final installation and check-out the cool down of the test set up started on June 2 and the prototype test started on June 5. Tests at zero current, steady state operation up to 20 kA, ramp tests, temperature margin and quench tests, loss-of-helium-flow simulation tests and long time tests were carried out successfully.

Table 1 summarizes the main test results of the prototype current leads. It could be demonstrated that the prototype HTS current leads for W7-X behave as expected. The design is validated. The long time stability is excellent and mainly determined by the stability of the cryogenic supply system. The heat load at the 4.5 K end in nominal conditions is (2.4±1) W and the He mass flow rate at 18.2 kA is 1.38 g/s. The temperature margin has been measured to be >26 K which gives enough safety margin under W7-X conditions, i.e. >14 K including magnetic stray field from the torus. Under LOFA conditions at 18.2 kA, the time until quench is approximately 18 min. The stable and optimal operation of the current leads is not affected by the up-side-down orientation. Figure 3 to 6 show examples of the main results.

Table 1: Main Results of W7-X Prototype Current Leads.

Parameter	Result
Nominal/maximum current	14/18.2 kA
Helium inlet temperature	50 K
Nom. temperature at warm end of HTS-module	60 K
Cold end resistance incl. clamp to bus bar	(11.5±0.6) nΩ
Warm end resistance of HTS-module	10 nΩ
Voltage drop along HEX[a] at 14/18.2 kA	51.9/80.8 mV
He mass flow rate at 0 kA	0.55 g/s
4.5 K heat load at 0 kA and nominal conditions	(2.4±1) W
He mass flow rate at 14 kA	1.04 g/s
4.5 K heat load at 14 kA and nominal conditions	(4.8±1) W
He mass flow rate at 18.2 kA	1.38 g/s
Pressure drop at 18.2 kA	(250±50) mbar
4.5 K heat load at 18.2 kA and nominal conditions	(6.3±1) W

[a] HEX = heat exchanger

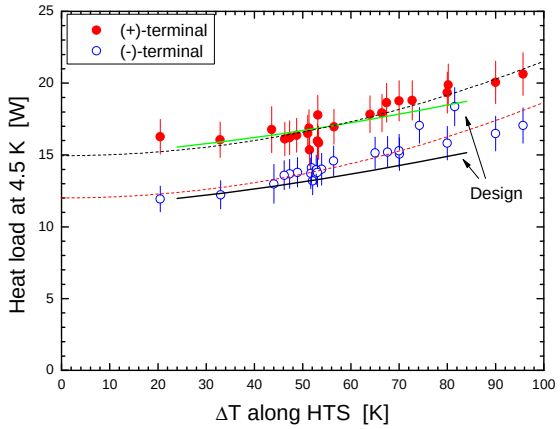

Fig. 3: 4.5 K heat load at 0 kA vs temperature gradient along HTS-module.

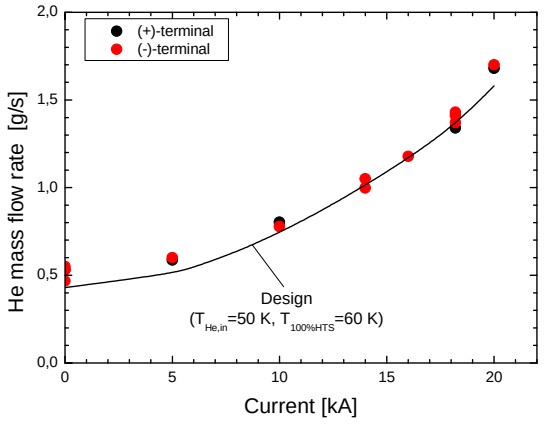

Fig. 4: 50 K helium mass flow rate vs. current.

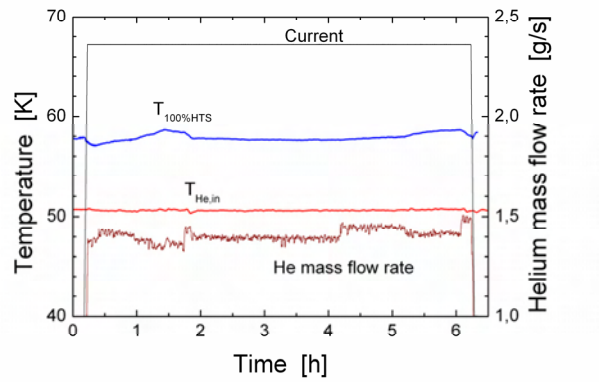

Fig. 5: Temperatures and He mass flow rates of both prototype current leads during 6 hours operation.

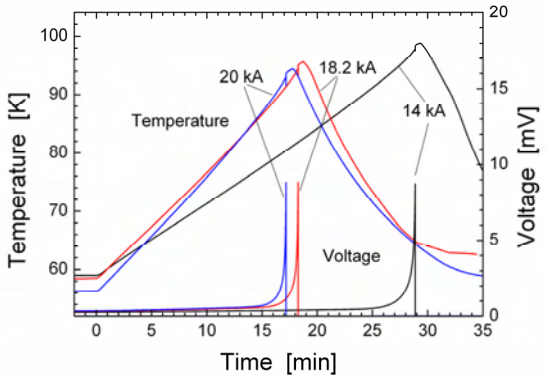

Fig. 6: Temperature at 100% HTS and voltage along HTS-module vs. time during loss of flow simulation.

After warm-up which was completed on July 2 the 2nd HV-failure which was observed after cool-down was located and repaired. The investigations for locating the Paschen-problem took some time but at the end the connection piece between the QD cables of the bus bar and the cryostat feed through was found to be the weak component. After elimination of the

whole test setup, i.e. two prototype current leads and sc bus bar, the Paschen test was successful.

The actual status is that the test set up is prepared for a second cold test. If this test is successful the test setup will be dismantled and the test facility will be prepared for the first series test.

Series current lead manufacturing

Due to the tight schedule it was decided to manufacture and assemble the series current leads for W7-X in KIT. A large fraction of the components have been prefabricated. The assembly of the first series current lead pair is underway.

Preparation of test facility

Because the main goal in 2010 was to test the prototype current leads in the TOSKA facility, the preparation of the dedicated facility CuLTKa was not given full focus. Currently the construction of cryo parts for CuLTKa is ready. First cryostats are already under construction at the KIT workshop. The specification for the control cryostat has been finalized and the tendering will be started soon. During 2011 CuLTKa will be assembled, reaching full functionality in 2012. With this dedicated test facility the testing of W7-X and JT-60SA current leads can be simplified, saving operation costs and testing time in comparison to the prototype test at TOSKA.

Current Leads for JT-60SA

In the frame of the Broader Approach Agreement between Japan and the EU and concomitantly to the ITER project, a satellite tokamak project called JT-60SA has been agreed. The magnet system of JT-60SA consists of 18 toroidal field (TF) coils (25.7 kA), 4 central solenoid (CS) modules (20 kA) and 7 poloidal field coils (20 kA). Following the commitment of the German Government to the EU, FZK shall design, construct and test the current leads. In total 6 leads for a maximum current of 26 kA and 20 leads with a maximum current of 20 kA, mounted in vertical, upright position are required.

Status

The status is as follows:

- The Procurement Arrangement for the HTS current leads for JT-60SA was signed by F4E and Japan. The Agreement of Collaboration was signed between F4E and KIT as well.
- The Procurement Plan and the Project Schedule were approved, the Risk Management Plan has been prepared.
- The first batch of HTS stacks for the CS/EF current leads has been manufactured and delivered by Bruker HTS.
- The design of the HTS current lead for TF and CS/EF coils of JT-60SA has been updated. The interfaces have been discussed and proposals for the room temperature termination as well as for the cold clamp contact have been made by KIT and distributed to JAEA and F4E. The design will be finalized in 2011 depending on the progress in the agreement phase between JAEA and KIT.
- During the prototype test of the W7-X current leads, specific tests, i.e., pulse tests, which are relevant for the operation of the CS/EF current leads in JT-60SA have been performed. The test results demonstrate the applicability of the current leads in pulsed operation.

Staff:

W7-X CL:	JT-60SA:
W.H. Fietz	W.H. Fietz
R. Heller	R. Heller
M.S. Darweschsad	B. Ganninger,
G. Dittrich	M. Gehrlein
S. Eckerle	R. Heger
S. Fink	C. Lange
U. Fuhrmann	T. Möhring
M. Gehrlein	U. Saller
F. Gröner	A. Opitz
R. Heger	
M. Heiduk	
S. Heuser	
C. Lange	
R. Lietzow	
I. Meyer	
T. Möhring	
R. Müller	
R. Rotondo	
U. Saller	
E. Specht	
V. Zwecker	
A. Kienzler	
C. Molnar	
T. Vogel	
P. Wagner-Nagy	

Literature:

[1] R. Heller, A. Class, A. Batta, R. Lietzow, H. Neumann, M. Tischmacher, “Modelling of the fin type heat exchanger for the HTS current leads of W7-X and JT-60SA”, Cryogenics 50 (2010) 222-230

[2] L. Savoldi Richard, A. Class, W.H. Fietz, R. Heller, E. Rizzo, R. Zanino, “CtFD Analysis of HTS Current Lead Fin-Type Heat Exchanger for Fusion Applications”, IEEE Trans. on Appl. Supercond. 20(3) (2010), 1733-1736

[3] R. Heller, W. H. Fietz, S. Fink, M. Heiduk, A. Kienzler, C. Lange, R. Lietzow, T. Möhring, P. Rohr, T. Rummel, T. Mönnich, K. Buscher, “Test results of the high temperature superconductor prototype current leads for Wendelstein 7-X”, presented at 2010 Appl. Supercond. Conf., Washington, USA, Aug. 1 – 6, 2010, submitted to IEEE Trans. on Appl. Supercond.

[4] H. Fietz, S. Fink, M. Heiduk, R. Heller, C. Lange, R. Lietzow, T. Möhring, P. Rohr, M. Süßer, T. Rummel, “Test arrangement for the W7-X HTS-current lead prototype testing”, presented at 2010 Appl. Supercond. Conf., Washington, USA, Aug. 1 – 6, 2010, submitted to IEEE Trans. on Appl. Supercond.

[5] R. Heller, W.H. Fietz, A. Kienzler, R. Lietzow, “High Temperature Superconductor Current Leads for Fusion Machines”, presented at 2010 Symposium on Fusion Technology, Porto, Portugal, Sep 27 – Oct 1, 2010, submitted to Fus. Eng. & Design

Acknowledgement

This work was financially supported by the Ministry of Research and Education (BMBF) under the grant No. 03FUS0013 and is done in the Project JT-60SA under the Broader Approach Agreement between Europe and Japan. The views and opinions expressed herein do not reflect necessarily those of the BMBF or the European Commission.

Quench Detection System for Fusion Magnets (HGF)

Introduction

After determination of the basic technical specifications of quench detector units (QDU) for operation at ITER, a redesign phase was started at KIT in spring 2009. The new detectors should be based on the existing KIT´s quench detection technology with several extensions mainly concerning high voltage capability (detectors input / potential separation) and reliable measurement of small differential signals.

Basic intended properties of new quench detector units are:

- 30 KV potential separation to ground,
- 1 KV input range (2 KV input to input),
- 100 seconds record buffer of differential quench signals,
- Reliable detection of small signals in the range of 5 to 20 mV.

The new detectors should be arranged with fixed input cable (pull relief instead of plug at detectors frame). The final wiring to the coils will be provided by separate patch panel.

Redesign of IPE's quench detector electronics to new type UNIQD 3420

To achieve the above-mentioned requirements while keeping detectors external dimensions (3 RU standard euroboard module) a major redesign of the printed circuit board was necessary. In addition to this redesign the schematic of the electronic circuit was enhanced to lower internal offset drifts for proper setting of very small thresholds

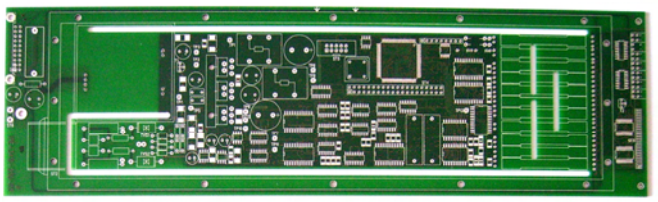

Fig. 1: Printed Circuit Board (PCB) of detector UNIQD TYPE 3410

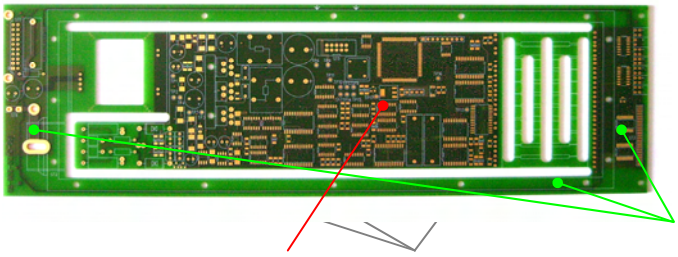

Fig. 2: Printed Circuit Board (PCB) of HV-detector UNIQD TYPE 3420 (new design)

Effective potential separation in the spacers is accomplished by sealing of the PCB by a special silicon gel with an electric field strength of minimum E = 20 KV / mm (from Wacker chemicals Germany). Critical points of 30 KV high voltage separation are the DC/DC converter (left side of detectors PCB) and the optical couplers for communication and signal links (right side of detectors PCB). A first version of 30 KV prototypes of optical couplers are presently manufactured at Elmic GmbH / Germany.

Enhancement of measurement and detection accuracy is accomplished by revising and extending of the electronic circuit.

Signal conditioning inside the detector UNIQD Type 3420 is improved by:

- Lower drifts by use of internally pairwise matched components,
- New active clipping and clamping circuit for ADC signal path with improved linearity,
- Stringent differential design of the electronic circuit and layout of board,
- Additional digital noise reduction.

New internal power processing and sequencing circuits permit the use of inexpensive power supply devices.

Manufacturing of first prototype of detector UNIQD 3420 at IPE

A first prototype of the new detector with standard assembly (input range and potential separation limited to type UNIQD 3410 by use of standard DC/DC-converter and 20 KV optical couplers) has presently been manufactured by KIT at the Institute for data processing and electronics - IPE.

Fig. 3: Prototype of new KIT quench detector UNIQD TYPE 3420

With this prototype the general function of the new design could be verified. First measurements confirm all improvements in consideration of offset-drifts, linearity and detectors internal power distribution.

A second prototype with 30 KV high voltage assembly will be completed when the 30 KV high voltage optical couplers will be available (estimated date is January 2011). This manufacturing of prototypes will be followed by several internal test procedures at KIT (e.g. temperature and vibration tests, check-up of accuracy, high voltage tests).

Further objectives in 2011

Manufacturing of 8 prototypes for test purposes at ITER current leads

After successfully internal testing at IPE the manufacturing of 8 HV quench detectors (= 1 rack) is planned for test measurements at ITER current leads. The potential drop at current leads is very small. The required very low thresholds of detection in the range of only few millivolts are challenging, because built-in series-resistors (for safety) in the quench signal path of each superconducting devise result in an extra voltage divider with the detectors input impedance. This voltage divider additionally lowers the wanted signal.

Completing software package QVision

Approx. 80% of the software is now available in English language. The software also was upgraded for use with latest operation systems. An integrated operational supervision mode was extended to a full logging of all events activated by quench detection or system operator.

The new version QVision 3.0 will also include a differential auto-balancing feature (automatic balancing of two superconducting coils or balancing of the coil with its co-wound wire). An extended parameter management and additional safety options will complete the new version. Release of version 3.0 is planned in the second quarter of 2011.

Staff:

A. Ebersoldt
K. Petry
S. Stricker
D. Tcherniakhovski

Development of HTS Conductors (BMBF Reference No. 03FUS0008)

The ITER fusion reactor to be built in Cadarache, France, will use LTS (i.e., Nb_3Sn and NbTi) coils cooled at 4.5 K for plasma confinement. Due to the low Carnot efficiency the required cooling power consumption is very high for the large magnet systems. With HTS magnets operated at temperatures around 65 K the efficiency of future fusion reactors like DEMO could be significantly increased. Furthermore, the higher operating temperature would allow omitting the complex radiation shield that is inevitable using LTS magnets with an operating temperature of 4.5 K.

The work that has been done on HTS cables in 2010 concentrated on two main topics: reduction of ac losses of single tapes by application of striations and development of a cabling concept for HTS conductors with I > 10 kA, B > 10 T and T > 50 K.

Reduction of ac losses of single tapes by application of striations

The Roebel cable geometry allows the transposition of the current path, which is important to achieve a uniform repartition of the current between the strands and to reduce the ac losses. Further ac loss reduction can be obtained by modifying the strands or by improving the cable structure:

(1) Reduction of the width of the meander shaped strands to lower the hysteretic ac losses.

(2) Decrease of aspect ratio (width/thickness) of the cable by assembling stacks of strands instead of individual strands.

(3) Introduction of striations in the individual strands to reduce the effective width of the superconducting layer, based on the well known fact that the hysteresis losses of a superconducting tape are proportional to the width of the conductor when the tape is fully penetrated by the magnetic field.
The efforts in 2010 concentrated on the latter option for further ac loss reduction in Roebel cables: application of longitudinal striations to coated conductor Roebel strands.

The multifilamentary modification of coated conductors in Roebel meander-shaped strands was successfully performed with a picosecond-infrared laser system (Fig. 1). The grooving process turned out to be very reliable: no significant degradation of the critical current on single strands, measured after the striation process, was observed.

Effective ac loss reduction due to the striation process was confirmed. The measured magnetization loss of a 125 mm long striated single strand is 5 times lower than that of the non-striated one. In case of a cable sample shown in Fig. 1c the loss reduced by factor of 3 at high field amplitudes: at field amplitudes lower than 10 mT the loss of the cable with striated strands is higher than that of the cable with non-striated strands.

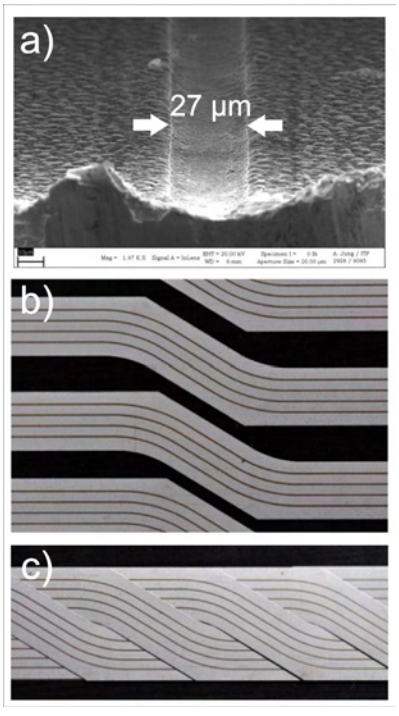

Fig. 1: a) SEM image showing a 27 µm wide groove made by a pico second-infrared laser; b) striated Roebel strand; c) Roebel cable with striated strands. Figure adapted from [2].

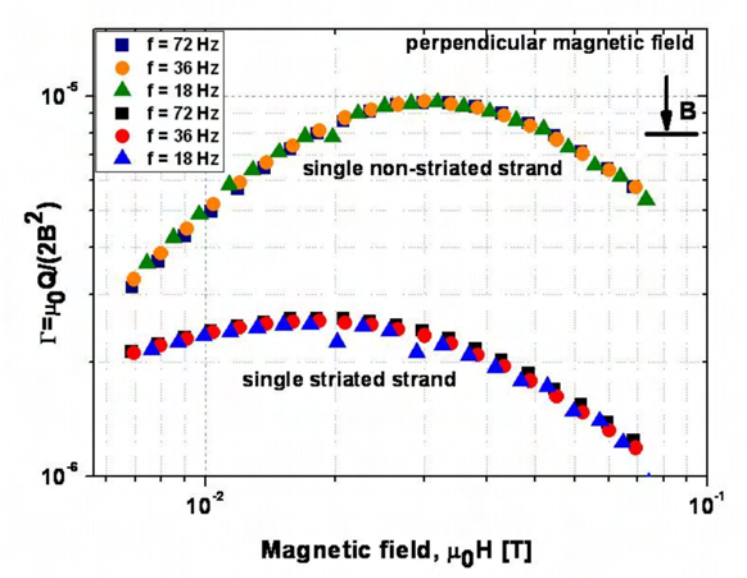

Fig. 2: Magnetization ac losses for single non-striated and striated strands [2].

In general, the curves of the losses as a function of field measured at different frequencies do not perfectly overlap, which indicates the existence of coupling currents. The ac losses measured on a cable sample composed with insulated filamentarized strands are very similar to those measured on the cable with non-insulated strands: this seems to indicate that the coupling currents occur mostly between the filaments not between the strands, but needs confirmation.

The ongoing investigation of the current distribution in the various strands and filaments by means of numerical models is expected to provide valuable information for a better understanding of the observed loss behavior.

Cabling concept for HTS conductors with I > 10 kA, B > 10 T and T > 50 K

While thin strands of round LTS conductors can easily be assembled to multi-stage cables with high current carrying capability, cabling of flat HTS tapes still remains a big challenge. The Roebel technique is one of few promising concepts for production of coated conductor cables (Fig. 3). In 2006 a first 12 mm wide Roebel cable assembled from 16 punched tapes was presented. The current carrying capability at 77 K and self field was 1020 A. By assembling stacks of tapes instead of single tapes, a current carrying capability of 1320 A for a 4 mm wide Roebel cable with 50 punched strands was achieved in 2009. However, transport currents of the order of > 10 kA are difficult to realize with a simple scale-up of the Roebel technique. Instead, the Roebel cables themselves could be used as strands to form a larger cable, e.g. a Rutherford cable (Fig. 3d). The transposition of strands helps to reduce coupling losses. ITEP presented this idea and started with the development of a subsize Coated Conductor Rutherford Cable (CCRC) demonstrator (Fig. 4).

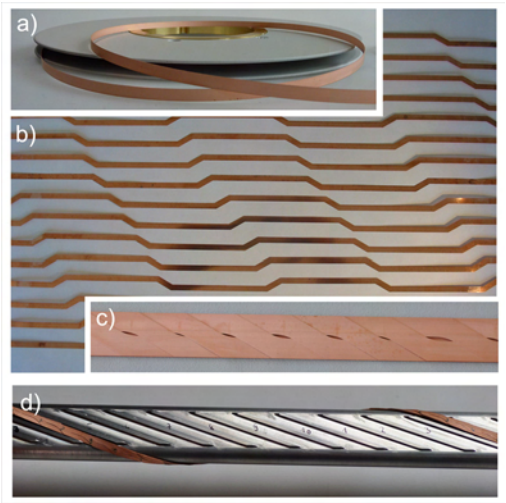

Fig. 3: a) Commercial coated conductor tape;
b) punched tapes;
c) Roebel cable; Rutherford cable former with one Roebel subcable.

In CCRCs all strands are fully transposed and experience similar fields and forces in a magnet winding. Maximum winding angle and minimum thickness of the former have to be adjusted according to the bending properties of the strands. In order to estimate the minimum thickness of a Rutherford cable that allows winding without degradation of the current carrying capability, a special setup to measure the critical current of tapes or Roebel subcables exposed to edge-bending has been developed (Fig. 5). The setup allows changing the angle β corresponding to the winding angle in CCRCs continuously while the thickness of the plate around which the tape or cable is wound remains fixed.

Fig. 4: CAD drawing of the subsize CCRC demonstrator cable **[3]**

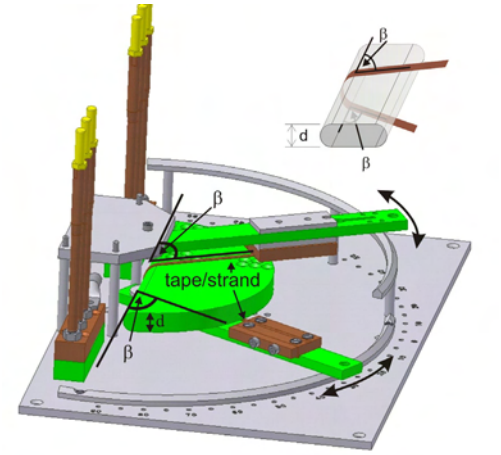

Fig. 5: Edge-bending device to simulate strain effects on tapes and cables in step-over region of CCRCs. The critical current is measured as function of the winding angle β for fixed former thickness d [**3**].

So far the $I_c(\beta)$ dependence for 4 mm wide tapes for simulated former thicknesses of 5 mm and 10 mm was measured with the superconductor side outwards. The results are shown in Fig. 6. For a simulated former thickness of 5 mm a strong decrease of Ic for winding angles > 10° is observed. With a simulated former thickness of 10 mm the degradation of current carrying capability was only 3.5%. According to these results it seems possible to wind single 4 mm wide tapes with a winding angle of 20° around a 10 mm thick former. Edge-bending experiments on Roebel subcables will be carried out in the near future to see if winding of the Roebel subcables around the 10 mm thick former of the CCRC demonstrator cable causes degradation of the current carrying capability.

Due to self-field effects the current carrying capability of a superconducting cable is lower than the sum of I_c values of the single strands before the cabling process, especially when no external field is applied. In order to judge if an I_c decrease in the final cable is due to defects caused by the punching and cabling process or by self field effects, the angular and field dependence of the original wires that are used for preparation of the subsize CCRC demonstrator was carefully analyzed. First Roebel subcables for the CCRC demonstrator cable were assembled and tested.

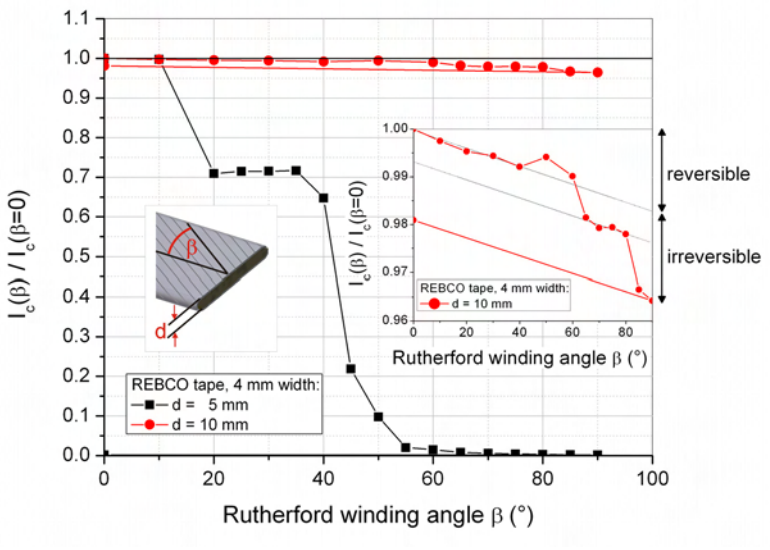

Fig. 6: Dependence of critical current I_c on winding angle β for 4 mm wide tapes at 77 K, self field (I_c-criterion 1 µV/cm). The measurements are performed with simulated former thickness of 5 mm (squares) and 10 mm (circles). The insert shows the results for the former thickness of 10 mm on a different scale [3].

Future Work

As next steps towards realization of a high-current low-ac-loss HTS cable for fusion magnets the construction of the CCRC demonstrator cable will be completed and the current distribu-

tion and self-field effects will be studied. Transport ac losses will be measured for striated tapes and cables and the results will be compared with results of modeling.

Staff:

A. Drechsler
H. Fillinger
W. Goldacker
F. Grilli
A. Kling
R. Nast
B. Ringsdorf
B. Runtsch
S. Schlachter
S. Terzieva
M. Vojenčiak

Literature:

[1] S. Terzieva , M. Vojenčiak, E. Pardo , F. Grilli , A. Drechsler, A. Kling, A. Kudymow , F. Gömöry and W. Goldacker; Transport and magnetization ac losses of ROEBEL assembled coated conductor cables: measurements and calculations; Supercond. Sci. Technol. 23 (2010) 014023

[2] S. Terzieva, R. Nast, F. Grilli, M. Vojenčiak, J. Souc, W. Goldacker, A. Jung, A. Kudymow, A. Kling; "Investigation of the effect of striated strands on the AC losses of 2G Roebel cables"; submitted to Superconductor Science and Technology

[3] S.I. Schlachter, W. Goldacker, F. Grilli, R. Heller and A. Kudymow; "Coated Conductor Rutherford Cables (CCRC) for High-Current Applications: Concept and Properties"; Accepted for Publication in IEEE Transactions on Applied Superconductivity

Cryogenic infrastructure (CoA)

Introduction

The cryogenic infrastructure of the Institute for Technical Physics (ITEP) supplies different experiments within the ITEP and other institutes of the Karlsruhe Institute of Technology (KIT), which are working for the Fusion Programme with refrigeration power or liquid helium. Such experiments in the ITEP are tests of superconductive components in the TOSKA facility, experiments for the ITER-cryopump in TIMO, and mechanical material tests in different cryostats equipped with traction engines.

For these experiments the cryogenic infrastructure comprises among other things:

- A 2 kW-refrigerator at 4.4 K with a liquefaction rate of 21 g/s (equivalent to 600 litres/h).
- A 300 W-refrigerator at 1.8 K with a liquefaction rate of 5 g/s (equivalent to 145 litres/h).
- A high pressure helium purifier working at 200 bars with a continuous purification mass flow of 14 g/s and a discontinuous purification mass flow of 28 g/s. The residual impurity content is lower than 1 ppm.
- Three recovery compressors with a pressure increase from one to 200 bars and a maximum mass flow of 26 g/s or 527 standard cubic meters respectively.
- A helium storage system consisting of:
  - stationary liquid helium vessels with a capacity of 15,000 litres or 1,875 kg respectively
  - storage tanks for impure helium with a capacity of 1,075 kg
  - storage tanks for pure helium with a capacity of 1,275 kg.

  The whole storage system has consequently a capacity of 4,225 kg or 23,985 standard cubic meters respectively, see Fig. 3.
- A liquid nitrogen storage vessel with a capacity of 32,650 litres for the supply of all experiments and a filling station to distribute liquid nitrogen in transport vessels.

Fig. 1: 2 kW-refrigerator with valve box and calorimeter.

Fig. 2: 8-ary vacuum pump station of the 300 W@1.8 K-refrigerator.

The cryogenic infrastructure is controlled by a state-of-the-art control system based on PCS7 and WinCC. The operation of the components can be done in two control rooms or via clients installed directly at the experiments.

Fig. 3: Helium storage system.

A team of five operators, three engineers and one academic staff member is responsible for maintenance, repair, upgrading and extension of the cryogenic infrastructure for new or changed experiments.

Additional tasks are the supervision of peripheral installations such as

- Energy distribution system
- Re-cooling water unit
- Compressed-air distribution system.

Also, maintenance, repair, upgrading and extension of the

- Vacuum systems
- Different safety devices like oxygen monitors

are tasks of this group.

Beyond these regularly routine works this report is focused on selected extension projects, as well as giving an overview of the cryogenic supply activities for fusion projects.

Selected maintenance and extension works

2 kW (4.4 K) refrigerator

The following selected maintenance and extension works at the 2 kW-refrigerator were done in 2010: Repair of a leakage at an oil-pump of one screw-compressor of the 2 kW-refrigerator,

- Filter change of
  - two coalescers
  - super fine filter
  - oil-removal system,
- Change of Teflon sealing's at two cold valves,
- Installation of new turbo molecular pumps including control system for the cold and valve box.

Fig. 4: Oil-pump for compressor V2 of the 2 kW-refrigerator.

He-recovery and purification system

The following selected maintenance and extension works at the He-recovery and purification system were done in 2010:

- Revision of three He-recovery compressors.

Miscellaneous

- Design and construction of the pressure transducer cabinets including leakage tests,
- Adaption and extension of the process control system.

Fig. 5: New turbo molecular pumps including control system for cold and valve box.

Cryogenic supply for the Fusion Programme

The different experiments for the Fusion programme in ITEP are supplied with circa 11,393 litres liquid Helium or 8,099 standard cubic meters. In addition, the refrigerators ran nearly 875 hours in 2010 for the supply of refrigeration power.

For comparison, the average consumption for such experiments in the period between 2001 and 2009 is about 24,350 litres liquid helium or 17,309 standard cubic meters respectively and 1,913 hours of refrigeration power. So in 2010 the consumption was significantly lower than the years before. This decreased consumption was caused by the time consuming structural reconstruction work for new experiments in TOSKA and TIMO which also resulted in modifications of the cryogenic infrastructure.

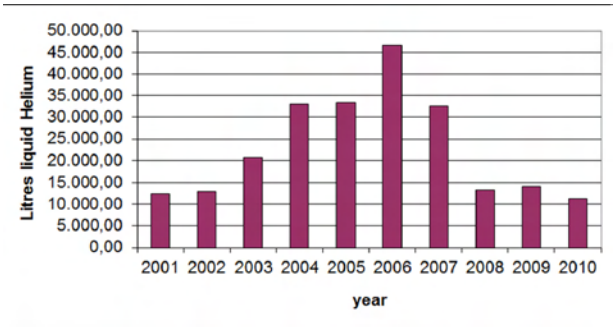

Fig. 7: Liquid helium supply between 2001 und 2010

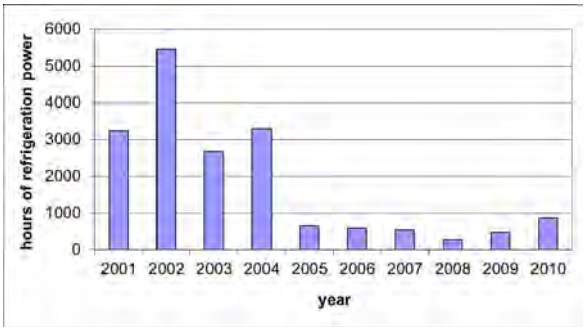

Fig. 8: Hours of refrigeration power between 2001 und 2010

Staff:

A. Baumgärtner
S. Bobien
M. Duelli
U. Fuhrmann
H. Neumann
B. König
K. Metzger
D. Wetzel
H. Zimmermann

Magnet Technology for Fusion
(EFTS MATEFU - Contract No. 042913 (FU06))

Objectives

In the framework of the ITER Project, Europe will have to procure in-kind components for the ITER machine. Among these components there are conductors and coils for the ITER superconducting magnets as well as parts of the cryogenic system. Due to retirements the available engineering manpower at the beginning of this training activity was rather small to carry out the large amount of tasks to be performed during ITER construction. The aim of the proposal is to train young engineers in the magnet and cryogenics field by involving them in the present R&D programme and in the preparation activities for the manufacture of the conductor lengths and coils.

Status

The two trainees of KIT Michael Schwarz and Thomas Richter have been employed since July and September 2007, respectively. Their contract ended in July and September 2010 as foreseen and the complete training program was performed in this time.

Especially the secondment to industry (Babcock Noell and Bruker HTS) and to CEA gave valuable stimulation, offering different views on the training aspects besides the training done within KIT. The additional lectures, schools and the participation to conferences helped to form both trainees to experts in fusion relevant engineering work as planned. In the case of Thomas we were lucky to offer him a 3 year position as a cryoengineer with the framework of the Broader Approach work, whereas Michael decided after the training to have additional lectures to open additional fields for his personal career.

Looking back, this training activity was perfectly suited to create experts which are needed for fusion - and it is obvious that such expertise is not available on the market.

We thank the EU for this possibility to create new staff that is perfectly prepared for fusion work.

Staff:

W.H. Fietz
T. Richter
M. Schwarz
K.P. Weiss

Acknowledgement

This work was supported by the European Communities under the contract of Association between EURATOM and Karlsruhe Institute of Technology. The views and opinions expressed herein do not necessarily reflect those of the European Commission.

Goal Oriented Training Programme "Cryogenic Training Program for Fusion" (WP10-GOT-GIRO (FU07-CT-2010-00065))

Objectives

In the frame of a structured training program, it is intended to train early-stage engineers during 3 years. This program will take place within a collaborative group to provide the technical know-how and the skills which are necessary for the engineering of components for ITER or fusion program and for the management of ITER relevant projects. The aim of the training is to reinforce the knowledge of the trainees thanks to their involvement in an engineering team constituted of experts in various domains.

Status

The contract was signed end of June 2010. A first coordination meeting was held in Porto end of September 2010 with attendees of the 3 involved associations KIT, CEA and JET.

The agenda included:

- The status of the trainee recruitment,
- Working program of each trainee,
- Organisation of the first schools,
- Presentation for the EFDA meeting during SOFT conference about GOT,
- Miscellaneous.

KIT was able to find a first trainee (B. Kuffner). He has a Master of engineer and will work for 3 years in cryogenic activity for the test of superconducting current leads.

Interviews were held for the second trainee position ("Design of measurement and control system for large cryogenic systems") and a candidate was selected. A contract is under preparation.

Staff:

W.H. Fietz
B. Kuffner
R. Lietzow
M. Süßer

Acknowledgement

This work, supported by the European Communities under the contract of Association between EURATOM and Karlsruhe Institute of Technology, was carried out within the framework of the European Fusion Development Agreement. The views and opinions expressed herein do not necessarily reflect those of the European Commission.

Breeding Blanket and Divertor

Construction of the High Pressure Helium Loop (HELOKA-HP/TBM) for Testing of TBMs (TW5-TTB-001)

The objective of this task is to construct the HELOKA-HP/TBM loop as presented and agreed in the “EFDA HELOKA Assessment Report” in KIT (former FZK) comprising the purchase of loop components and supply systems, acceptance tests at the manufacturer’s site, installation, commissioning and acceptance tests.

In 2010 the construction of the piping system has been finalized with the integration of the helium circulator. This last piece of equipment was delivered to the KIT on the 31st of March 2010; by the end of June 2010 the circulator was connected to the rest of the loop and all the corresponding piping has been verified.

On July 2010 the pressure test of the loop has been successfully performed. Following the pressure test the commissioning of the circulator has been performed. This commissioning had the objective of mapping the operational domain of the circulator and to demonstrate the capabilities of the machine to operate for longer periods of time (48h) under Test Blanket Module specific conditions: 8MPa, 1.3kg/s and a compression ratio of 1.13.

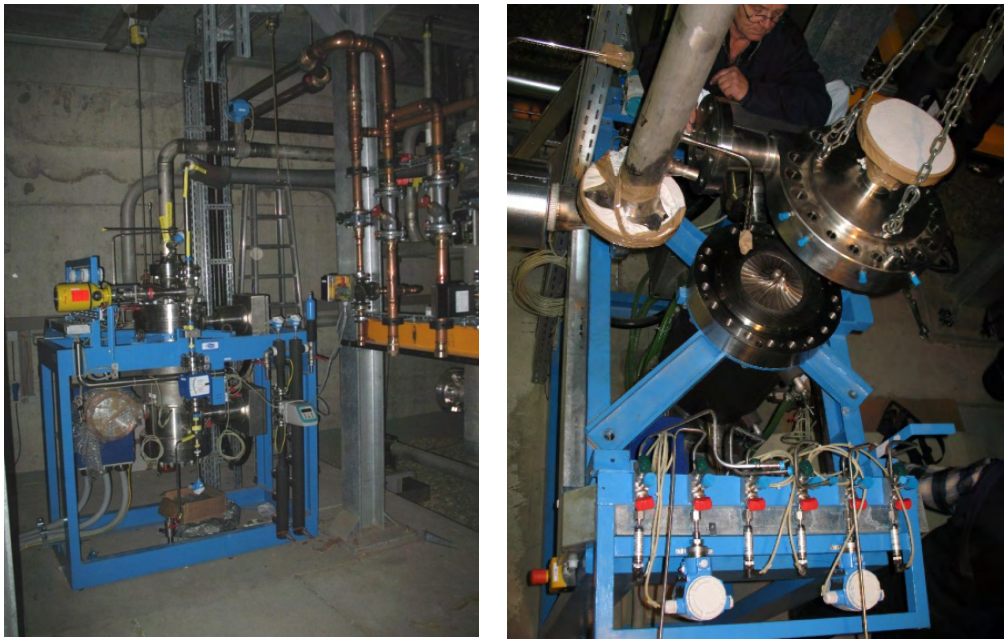

Fig. 1: Left: HELOKA circulator installed into the loop;
Right: Tuning of the circulator during the commissioning (November 2010)

The commissioning was done in two sessions: one in October 2010 when the operating domain was mapped and the tuning of the magnetic bearings has been performed, and a second one at the end of November were the clearings inside the circulator were adjusted and the endurance test was performed.

Due to the fact that the operation of the circulator requires cooling water with a temperature of 5 to 10°C, an additional chilled water system has been purchased and installed in the experimental hall.

On the power supply side, the auxiliary and mains power distribution system of the Helium loop, including the 750 kW electric heater and the 300 kVA turbo-circulator were finalized in the first month of the year. In addition, the control of the electric heaters, made with power thyristors, was delivered in the first half of 2010. Both electric loads are powered from new circuit breakers, available on the market, that incorporates analogue to digital converters for the three phase voltage and current measurements as well as calculations of power factors

and PROFIBUS interface with the HELOKA distributed Data Acquisition and Control System (DACS).

In 2010 the work on the HELOKA DACS has continued with the technical specifications of the loop control and the integration of various subsystems like Pressure Control, Chilled Water and Circulator control systems. The contract has been awarded in October 2010 to Siemens. Currently the detailed design of the system has been finalized and the cabling work is almost finished.

Staff:

B.E. Ghidersa
J. Freund
V. Marchese
G. Messemer
N. Prothmann

Acknowledgement

This work, supported by the European Communities under the contract of Association between EURATOM and Karlsruhe Institute of Technology, was carried out within the framework of the European Fusion Development Agreement. The views and opinions expressed herein do not necessarily reflect those of the European Commission.

Components and Instrumentation Development for TBM (TW2-TTBB-007b)

Preliminary Study of the Tritium Accountancy System and Conceptual Study for Alternative Processes based on Membrane and Membrane Reactor

Scope and objectives

Beyond ITER, the tritium self-sufficiency will be one of the main issues to be demonstrated in future fusion machines. Considering the Helium Cooled Pebble Bed (HCPB) concept, two adjacent helium gas loops containing tritium have to be considered:

- The Tritium Extraction System (TES) that purges the breeder zone and recovers the tritium to be re-injected in the machine,
- The He cooling loop containing tritium via permeation through the structural material, in which the tritium concentration has to be minimised using a Coolant Purification System (CPS).

Beside the efficiency of the processes in TES and CPS, accurate tritium accountancy is mandatory for the reliable operation of the plant.

Basic and major difficulties for processes and accountancy arise from the presence of tritium in different chemical forms only as traces in huge helium flow rates. Even if numerous concepts have been proposed in the past, the DEMO relevancy of the proposals including the present configuration adopted for ITER Test Blanket Modules (TBM) remains questionable.

This study tackles the main issues for tritium management in the solid breeder blanket and proposes alternative solutions for DEMO.

Previous results

In the previous period, the activities of this task focused on the two topics:

- The preliminary study of the tritium accountancy system as an interface between the tritium processing systems (TES and CPS) and the tritium plant,
- The study of the possible use of PERMCAT (catalytic membrane reactor) instead of a reducing bed to recover tritium from water in the TES and CPS.

Concerning the tritium accountancy system, it has been first recognised that the process options and corresponding operations for TES and CPS (i.e. dilution or pre-concentration, batch wise or continuous) have a fundamental and direct impact on the tritium accountancy stage. Considering the current baseline for tritium processes in the TBM, this study highlighted that the dynamic volumetric accountancy based on flow rates and activity measurements will not be accurate enough to ensure reliable and precise results mandatory for the validation of the neutronics predictions. Therefore, even if more demanding, a static approach based on the collection of all the gases at the TES and CPS outlets followed by pVT-c measurements (pressure, volume, temperature, concentration) has to be implemented in ITER to ensure accuracy better than 10%. As a consequence, the total gas load to the accountancy stage needs to be carefully studied.

In a first approach, it seems valuable to separate upstream of the accountancy stage, and to route to the accountancy only the tritium rich streams (to be sent afterwards to the Tokamak Exhaust Processing, cf. Fig. 1), while tritium depleted streams could be discharged without accountancy in the Detritiation Systems. For this purpose, the use of a catalytic membrane reactor such as PERMCAT for the recovery of tritium from the water vapour would be of advantage compared to a reducing bed. Besides minimising the waste production while ensuring high tritium recovery efficiency, it enables separating the tritiated stream into two different

products: on the one hand an enriched tritiated stream as pure molecular hydrogen isotopes sent to the accountancy, and a depleted one directly discharged in the detritiation systems without accountancy. The designs of TES and CPS for TBM have been recently reviewed accordingly.

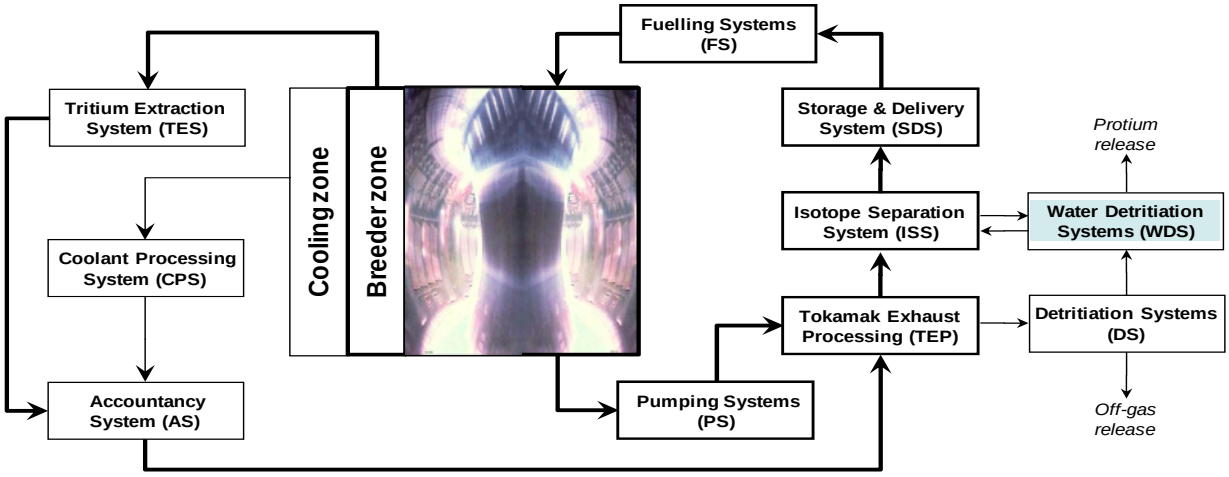

Fig. 1: Simplified view of the inner and outer tritium fuel cycles in a future fusion machine (bold lines reflect main tritium streams, thin lines mean tritium depleted streams; in yellow: main inner cycle, in blue: infrastructure for tritium handling; in green: breeder loop; in orange: accountancy as interface between blanket loops and inner cycle) (from [1]).

However, due to the rather large total flow rates and the low tritium concentrations in TES and CPS, the direct use of PERMCAT is not recommended, especially for DEMO. A pre-separation and pre-concentration stage should be of advantage to optimize the operation and the investment costs. Promising membranes have been identified, and preliminary design studies have been conducted. Such preliminary investigation has shown that newly developed zeolite membranes could be competitive for tritium processes in the blanket [2].

Table 1: Comparison between conventional (current options) and alternative (based on membranes) concepts for TES for DEMO (from [2]).

	conventional	Membrane
T inventory	> 30 g	< 10 g
T recovery	≈ 90%	> 97%
T enrichment	100 - 1000	≤ 200
energy use	>1 MW	≈ 2 MW
material	many tons	≈ 5700 m^2

Achievement in 2010 on the conceptual study for an alternative TES based on PERMCAT with a pre-concentration stage using membranes

In order to facilitate the separation process with membranes, it is proposed as shown on Fig. 2 to handle the tritium as water vapour. Indeed, zeolite membranes have proven to be highly hydrophilic, thus ensuring high performance for the membrane pre-concentration stage. However, the direct use of water vapour to dope the purge gas is presently not envisaged, mainly because of the presence of beryllium in the breeder zone. Helium with hydrogen addition has to be considered as the baseline.

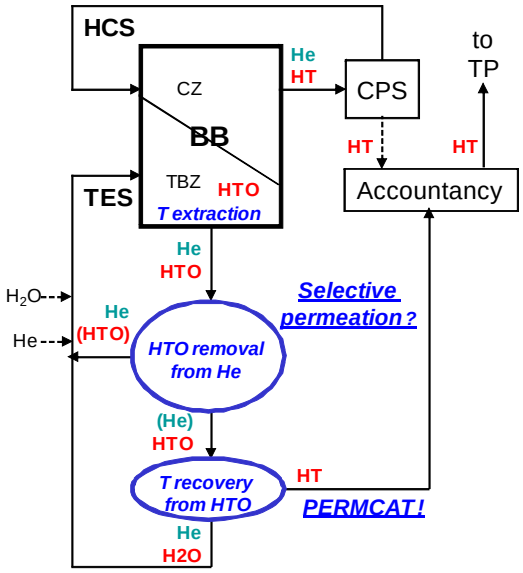

Fig. 2: Alternative concept for TES based on PERMCAT process for tritium recovery from water in combination with a pre-concentration stage using membrane for tritium removal from the He purge gas doped with water vapour (from [1]).

The purge gas could be oxidised downstream of the breeder zone, either using metal oxide or catalytic oxidation. Both options have been carefully compared. Even if the oxidation using a metal oxide bed is simple and easy to operate, the irreversible consumption of the bed would yield to unacceptable levels of waste for DEMO. Catalytic oxidation appears the only solution but a well controlled addition of oxygen in the system will be required. However, if water addition directly into the He purge would be workable, it could simultaneously facilitate the tritium release from the breeder zone and reduce significantly the tritium permeation into the coolant. Such approach and possible benefits need to be considered in more details.

Since the commercial availability of adequate zeolite membranes is still an issue (only few providers and limited type of materials), contact(s) with laboratory(ies) and company(ies) involved in zeolite membranes production has(ve) been engaged.

Due to the lack of experimental data on permeability and selectivity of such new membranes, a new dedicated experimental facility is being progressively set up. In addition, model and simulation of a multi-stage (cascade) permeator is under progress. Both experimental and model activities are being conducted under collaboration with the KIT Campus South (Institute for Thermal Process Engineering) and a PhD thesis has been started on this topic.

Concerning the tritium recovery from water using PERMCAT, an experimental campaign has been performed in the CAPER facility that has been especially upgraded to accommodate new components enabling the production and handling significant flow rates of highly tritiated water. Using a laboratory scale single-tube PERMCAT reactor, successful tritium recovery has been demonstrated with detritiation factor between 100 and 1000, corresponding to between 99 and 99.9% tritium recovery from the water [3]. At a bigger scale, using a technical PERMCAT reactor, experiments without tritium have been performed in support to the scale up of the process and to study the influence of the reactor geometry [4]. In parallel, the refinement of the PERMCAT simulation has been continued. Using the previously developed 1-D numerical code, the axial dispersion equation has been newly included. It has been shown that the numerical predictions tend to better reflect the experimental results. In addition, a big milestone has been achieved with the development of the 2-D model and the corresponding code that will enable in the future optimising the PERMCAT reactors [5].

Conclusion and perspectives

The 3rd and last deliverable of this task has been completed, discussing possible materials and separation techniques with membranes, reporting the state of the art for newly developed zeolite membranes, detailing different process options and expected performances using zeolite membranes, and discussing the use of water in the system.

These preliminary investigations have shown that newly developed membranes could be competitive for tritium processes in the blanket. Different promising materials and process options have been identified. Combining PERMCAT with zeolite membranes as pre-concentration stage could offer a flexible, simple, and continuous process for the blanket. Significant benefits could also be expected with respect to the very low tritium inventory and

while avoiding the need of cryogenic temperatures. Moreover, such approach should greatly simplify and optimise the accuracy in view of an online and real-time tritium accountancy system.

However, in any case huge membrane areas will be required even with operation at high pressure; and membrane performances have to be optimised and the availability has to be ensured to consider such options as a viable solution. Also the lack of experimental data asks for further efforts, and a dedicated program to gather experimental data and demonstrate the benefit of zeolite membranes for tritium process has started. Process simulation for the scale up of the components (membrane and membrane reactor) and optimisation of the operation need to be continued.

A new grant shall be launched for the next period to study more in detail the operation of the TBM processes and operation in order to design in more details the accountancy stage.

Staff:

D. Demange
O. Borisevich
E. Fanghänel
T.L. Le
K.H. Simon
R. Wagner
S. Welte
M. Kind from KIT Campus South

Literature:

[1] D. Demange, S. Stämmler, M. Kind “A new combination of membranes and membrane reactors for improved tritium management in breeder blanket of fusion machines” Poster presented at the 26th Symposium on Fusion Technology, Sept 27th – Oct 1st 2010, Porto, Portugal (to be published in Fusion Engineering and Design)

[2] S. Stämmler, D. Demange, M. Kind ”Potential use of zeolite membranes for separation and recovery of tritium produced in the breeder blanket of fusion machines” Oral presented at the 5th International Zeolite Membrane Meeting, May 23rd – 26th 2010, Loutraki, Greece (no peer review publication)

[3] D. Demange, E. Fanghänel, B. Kloppe, T.L. Le, F. Scheel, K.H. Simon, R. Wagner, S. Welte “CAPER modifications and first experimental results on highly tritiated water processing with PERMCAT at the tritium laboratory Karlsruhe” Invited oral presented at the 9th International Conference on Tritium Science and Technology, Oct. 24th – 29th 2010, Nara, Japan (to be published in Fusion Science and Technology)

[4] S. Welte, D. Demange, R. Wagner “Characterisation of a multitube PERMCAT reactor in view of a technical facility for highly tritiated water processing at the Tritium Laboratory Karlsruhe” Poster presented at the 26th Symposium on Fusion Technology, Sept 27th – Oct 1st 2010, Porto, Portugal (to be published in Fusion Engineering and Design)

[5] K. Munakata, D. Demange, “Development of numerical simulation code of membrane reactor for detritiation” Poster presented at the 26th Symposium on Fusion Technology, Sept 27th – Oct 1st 2010, Porto, Portugal (to be published in Fusion Engineering and Design)

Acknowledgement

This work, supported by the European Communities under the contract of Association between EURATOM and Karlsruhe Institute of Technology, was carried out within the framework of the European Fusion Development Agreement. The views and opinions expressed herein do not necessarily reflect those of the European Commission.

Manufacturing and Testing of a FW Channel Mock-up for Experimental Investigation of Heat Transfer with He at 80 bars and Reference Cooling Conditions. Comparison with Numerical Modelling (TW5-TTBB-001 D 10)

Introduction

Within the task TW5-TTBB-001 D 10 an experimental test section has been designed and built at the Institute for Neutron Physics and Reactor Technique in Karlsruhe Institute of Technology for investigations of heat removal from the first wall (FW) of the Helium-Cooled-Pebble-Bed Test Blanket Module (HCPB TBM). The purpose of planned investigations is to experimentally prove the numerically found decrease of heat transfer coefficient due to the asymmetry of heat loads at the first wall of HCPB TBM.

The test section named HETRA involves a single first wall channel of HCPB TBM Ver.1.1. The test section is attached to HEBLO facility which can provide Helium parameters relevant for HCPB TBM conditions – pressure of 8MPa and inlet temperature of 300°C. The surface heat load is represented by a set of electrical heaters. The verification of the 3D computational results is going to be done through the following two phases of the HETRA experimental campaign (i) measurements of pressure losses in the cooling HETRA channel in cold state (no heating) and (ii) detailed temperature measurements in the Eurofer structure of the test channel for prescribed power of heaters.

This report presents the work performed in 2010 within the task which mainly concerns (i) bringing the HETRA test section in conditions necessary for reliable measurements, (ii) development of corresponding numerical models, (iii) experimental and computational determination of pressure losses in HETRA cooling channel and (iv) current activities on measurement and computation of temperature distribution in heated components of HETRA test section. For an easy reference an outline of the design of HETRA test section is given first.

HETRA experimental test section: an outline of its design and construction

The main components of the HETRA experimental facility are presented in Figure 1. The facility involves one U sweep of the first wall channel. The connection to the HEBLO facility is made by two side channels. As the purpose of the side channels is to provide the developed flow conditions at the entrance of the heated section, their flow cross-section is identical to the one of the first wall - square 14.3x14.3mm with rounded corners (radius of 4mm). The side channels are not heated.

The heated HETRA section involves two channel bends and a long straight section which simulates the plasma adjacent part of the first wall. This section is heated only on the side which represents the plasma facing side. The heating of the back side is neglected due to its multiple lower magnitude. The heat flux of 270kW/m^2 at the plasma facing side of the first wall is simulated by a set of 8 flat ceramic heaters. To ensure uniform heat flux and to diminish effects of imperfect thermal contact, the gap between the heaters and the first wall has been bridged by two thin graphite layers (thickness of 0.5mm) between which a 10mm layer of copper is placed. At the exit of the outlet side channel a mixer is placed, which should provide a uniform helium temperature, i.e. avoid incorrect determination of fluid bulk temperature.

The heated channel section is connected to the side channels with flanges. Use of flanges enables replacement of the heated section, i.e. use of different heated sections in which different roughness heights/types can be examined. In the current experimental campaign two heated sections are considered: (i) a section with hydraulically smooth channel walls (surface roughness less than 4μm) which is taken to be a reference case and will primarily be used to verify numerical results and (ii) a section with artificially produced microscopic roughness which will be used to prove reliability of the numerically based conclusion that the surface

roughness of 20μm is sufficient to provide satisfactory cooling of the first wall. The heated HETRA section is thermally isolated by the use of a vacuum tube (see insert in Figure 1).

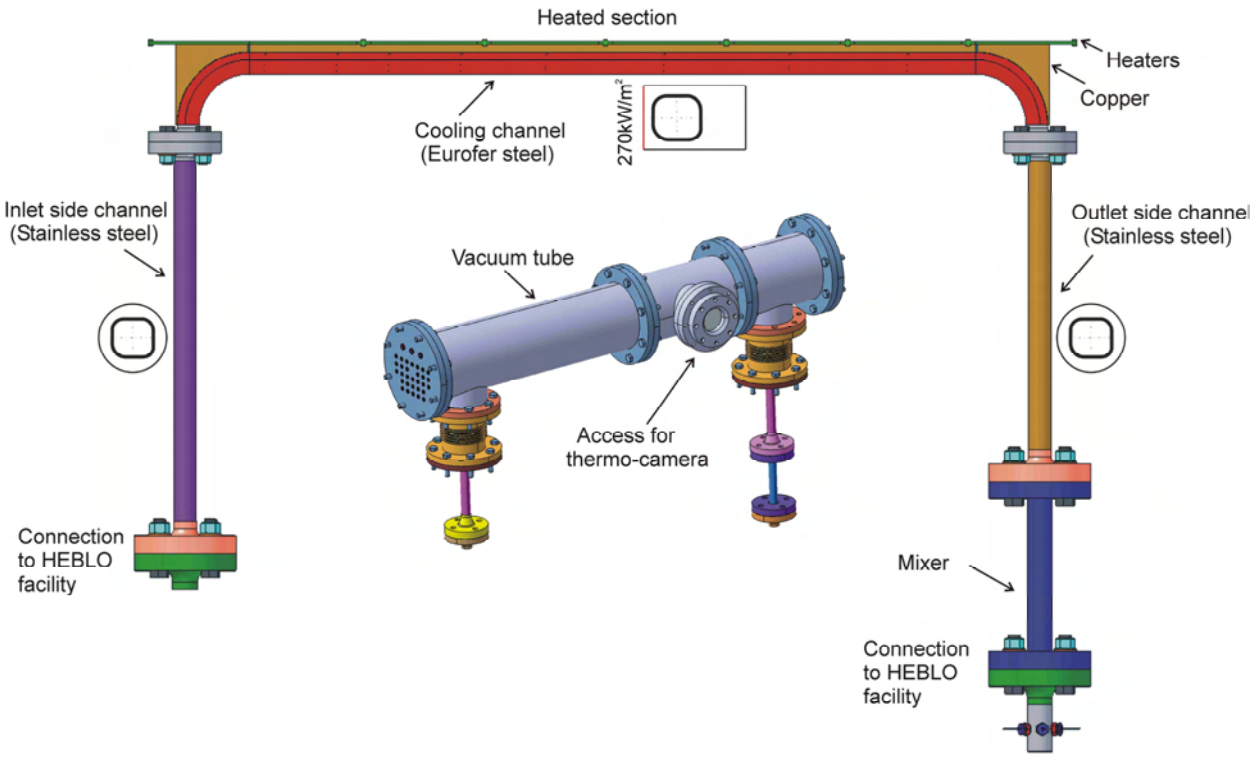

Fig. 1: Main parts of the HETRA test section. Insert presents the vacuum tube for thermal isolation of HETRA test section.

Achieving of satisfactory conditions for reliable measurements in HETRA test section

Although the HETRA section has been fully assembled and installed in HEBLO loop at the beginning of 2010, the measurements could not be started because a number of difficulties has been encountered when trying to bring it to the state which will ensure reliable measurements.

The first difficulty was that the sealing of the vacuum tube was not good enough to provide the required vacuum value. A detailed inspection has shown that the majority of the leak occurs at the plugs for thermocouple and heater cables. In order to overcome this problem, new plugs with better leakage parameters have been applied and the new flanges with improved plug holes have been manufactured. After this the pressure level of 10^{-2}Pa could be reached in the vacuum tube. Under such conditions there is no convection [1] and the thermal conductivity of the air residing in the vacuum tube is ~$4 \cdot 10^{-5}$W/mK (evaluated according to [2]), which is less than 1% of its value at atmospheric conditions. Therefore, this vacuum can be considered as satisfactory.

The next problem was connected with the thermal contacts between the different layers of materials placed on the heated side of the test section (heaters – graphite – copper – graphite – Eurofer). These contacts were not tight enough which caused inefficient cooling and overheating of the heaters. The original arrangement (see Figure 2a) where the tightness of heater-layer arrangement was provided by pressing a steel rail with ordinary screws was replaced by pressing the rail with numerous clamps equipped by spring screws (see Figure 2b). Careful fastening of spring clams provided uniform force acting on the steel rail, i.e. on heater-layer arrangement and ensured good thermal contacts along the whole heated section. The quality of the thermal contacts was checked by determining the temperature of indi-

vidual heaters with thermo camera. The test was done in the following way: the test section was heated with helium at 300°C and the heaters were kept off. For these conditions the expected result with almost the same heater temperatures was obtained.

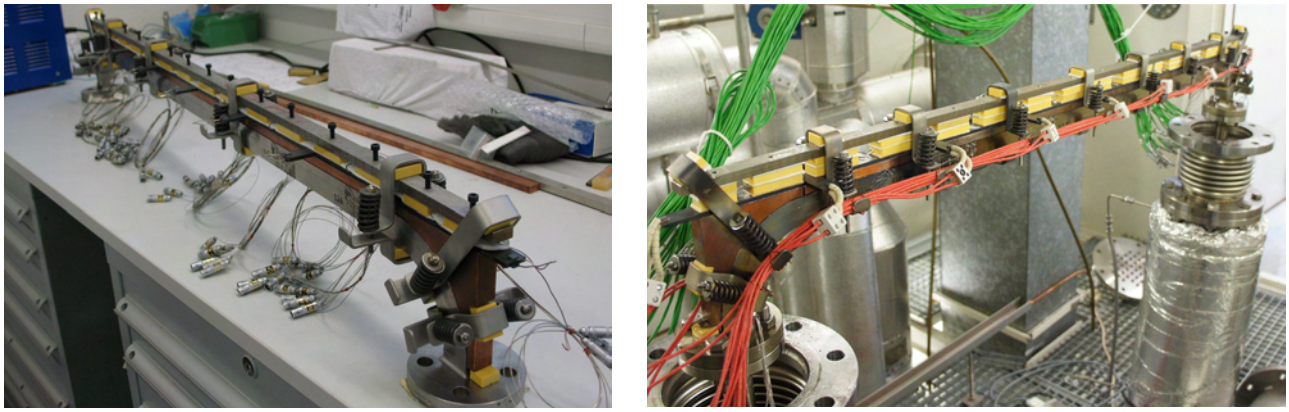

Fig. 2: Original arrangement of heated HETRA section (left) where the problems with heater overheating occurred and improved version (right) which gave satisfactory thermal contacts.

The problem of electrical supply of heaters had also to be solved. With the existing electrical arrangement in HEBLO facility (three sources) the supply of HETRA heaters had to be solved in the following way: side heaters (above the channel bends) were connected to one source, while the six heaters along the straight heated section were arranged in two groups and connected by the remaining two electrical sources. The power of the electrical sources could be adjusted at the control desk of the HEBLO facility. A careful analysis of the measuring results for temperature distribution showed that the power released by individual groups of heaters does not correspond to the one which was displayed at the control desk. For this reason, the following detailed measurements had to be done: voltage and electrical current have been measured at each individual heater, at the electrical source and at the positions shown at the control desk. The measurements have been done for the whole range of the heating power. Having these data a correlation between the actual power of heater groups and the power displayed at the control desk has been derived. Using these correlations the same heating power at individual heater groups could be set. The aforementioned measurements have also been used to prove that that the electrical resistance of individual heaters is the same.

Finally, the reliable positioning of thermocouples within the holes in Eurofer steel was a very diificult task. The diameter of the thermocouples is 0.5 mm, the diameter of the holes in Eurofer is 0.6 mm. The depth of the holes varies between 3 and 9.65mm. No brazing has been applied. The thermocouples are positioned from outside by a careful bending (which causes spring effect) and fastening by thin rail splices which were welded at Eurofer surface. It is noted that for experimental determination of Eurofer temperature 60 thermocouples are applied and that these are grouped at 6 measuring planes. Such a tight thermocouple distribution made their proper fastening especially difficult.

Determination of pressure losses in cooling channel of HETRA test section

In order to determine the hydraulic characteristics of HETRA cooling channel as well as to find out how good it can be retrieved by 3D computations and engineering 1D correlations for pressure losses, measurements have been performed using Helium at 8MPa and ambient temperature (20°C).

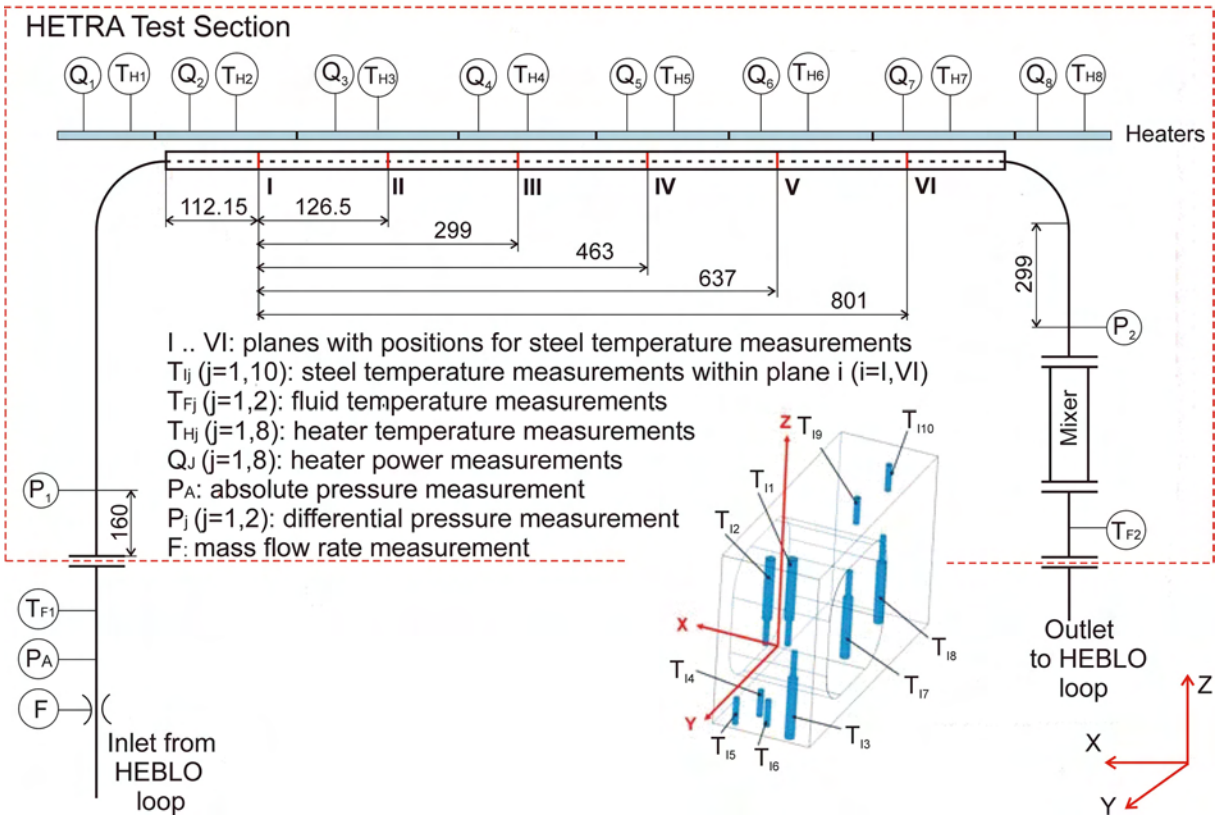

Fig. 3: HETRA measuring plan. Insert represents the pattern of thermocouples within one of the measuring planes I-VI.

Assuming that the pressure drop between the measuring points P1 and P2 (notation of measuring positions is given in Figure 3) is relevant for the hydraulics of the HETRA cooling channel, measurements are done for the flow rate range m=0.4-1.15m_n, where m_n=0.1kg/s is the nominal mass flow rate of Helium. The results presented in Figure 4 show that the dependence of the pressure drop on mass flow rate Δp=Δp(m) in the HETRA cooling channel is friction dominated.

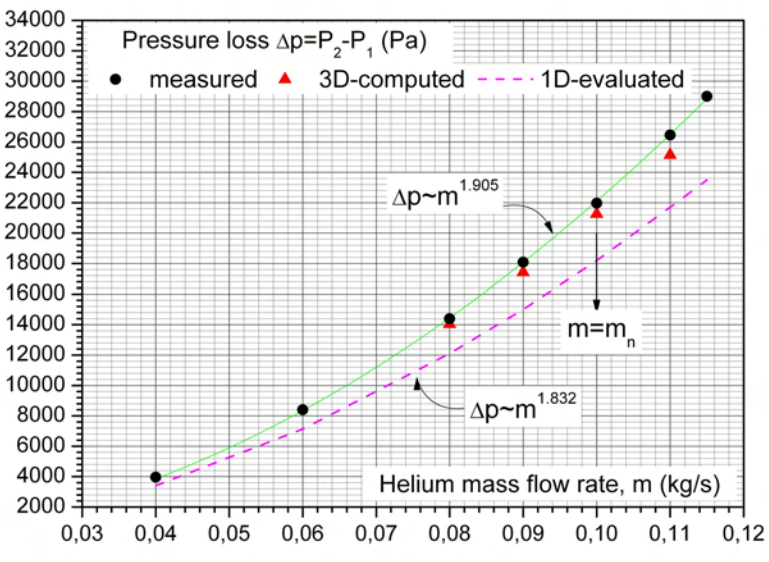

Fig. 4: Measured and computed pressure losses in HETRA cooling channel. For notation of pressure recording positions see Figure 3.

Taking into account the simple geometry of HETRA cooling channel it was expected that the results of measurements can easily be obtained by use of standard 1D correlations for pressure losses. However, the comparison between the measured pressure drops and the ones evaluated by use of 1D correlations revealed a discrepancy of ~15-20% (the discrepancy increases with an increase of mass flow rate). It is noted that this comparison concerns the evaluations by use of correlations for friction losses and losses in channel bends given in [3], but that other correlations gave similar results.

To find the reason for this surprising result, the flow in the HETRA cooling channel has been simulated by use of 3D code STAR-CD. These simulations have shown that the higher magnitudes of measured pressure losses then predicted by 1D correlations are caused by the strong disturbance of the flow at location where HETRA channel is connected to the HEBLO facility (connection of a 30mm HEBLO pipe with 14.3x14.3mm HETRA channel is done using flanges –see Figure 1).

Actually, the first 3D computations performed without accounting for flow disturbance due to the flanges retrieved the aforementioned results of 1D evaluation. But when the flow through the flanges is included into the simulated flow domain, a discrepancy of only 2-5% has been found between measured and 3D-computed results. These results of 3D computations have been considered as acceptable as they are in the range of experimental error.

Conclusions

The HETRA experimental test section has been built for the verification of numerically found effects of asymmetrical heating on the heat removal from the first wall of Helium-Cooled-Pebble-Bed Test Blanket Module (HCPB TBM).

In 2010 the following activities have been performed: (i) the experimental section has been brought to the conditions which ensure reliable measuring results; (ii) measurements at ambient (20°C) have been performed to determine pressure losses in HETRA cooling channel; (iii) a numerical model for 3D computations has been developed and verified with the aforementioned pressure measurements.

Currently the experimental tests which should mimic the FW conditions (with heating) are running. For these preliminary results on heat transfer and fluid flow in ‘hot’ HETRA conditions the CFD model is being developed and is under testing.

Staff:

M. Ilic
K. Zinn

Literature:

[1] Hablanian, M.H., High Vacuum Technology – A Practical Guide, Marcel Dekker, Inc., 1990.

[2] VDI Heat Atlas, 10th edition, Springer Verlag, 2006

[3] I.E.Idelchik, Handbook of Hydraulic Resistance, Jaico Publisching House, 2008.

Acknowledgement

This work supported by the European Communities under the contract of Association between EUROATOM and Karlsruhe Institute of Technology, was carried out within the framework of the European Fusion Development Agreement. The views and opinions expressed herein do not necessarily reflect those of European Commission.

Manufacturing and Testing of Mock-ups for Investigation of Coolant Flow in the Manifold System of HCPB TBM (GRICAMAN Experiments) (TW5-TTBB-003 D 1)

This report presents activities done on the development of a Gricaman experimental facility for the investigation of flow distribution in the coolant system of HCPB TBM.

The flow domain to be investigated in GRICAMAN experiments is defined to be the upper poloidal half of HCPB TBM Version 2.1. bounded at the outlets of the first wall channels, at the outlets of by-pass pipes and at the inlets of breeding units, i.e. involving one half of manifold 2, cooling channels in four horizontal and eight vertical stiffening grids, 8 cooling channels within two cap halves, half of manifold 3 and inlets of 8 breeding units. Significant simplifications of the experimental facility are achieved (i) assuming that the flow is adiabatic, (ii) replacing helium with air pressurised at 3bar and ambient temperature and (iii) representing complicated stiffening grid- and cap channels by simple pipes with the equivalent flow resistances. The facility is designed keeping real geometry of manifold 2 and manifold 3 and replacing complicated grid and cap cooling channels with simple pipes having the same flow resistance as the real channels.

The design and fabrication of two manifold chambers (denoted as Mf2 and Mf3 chamber in Figure 1) have been done in 2009. In 2010 the following activities have been performed.

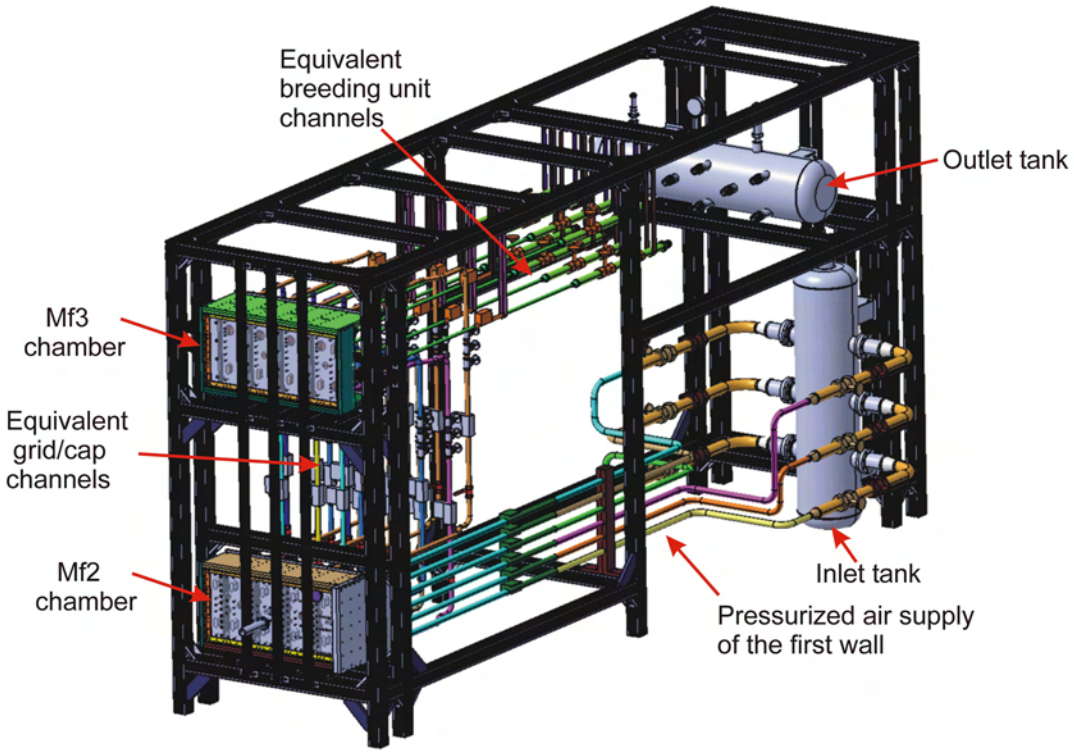

Fig. 1: CAD design of Gricaman facility and Gricaman frame.

The frame from aluminium profiles at which the components of Gricaman facility is going to be fixed has been constructed (see Figure 1). When designing the frame the safety conditions like preventing the falling down or overturning the manifold chambers were taken into account. The frame has been built and a part of the components of the Gricaman facility (like inlet tank, outlet tank) have already been mounted (see also Figure 4).

Equivalent grid/cap and breeding unit channels have been designed (see Figure 2). The design of these channels has been especially demanding due to their tight packing in limited space between two manifold chambers. The non-straight parts of the channels are manufactured by bending of stainless pipes DN ¾". The equivalent channels are currently being assembled. Their final attachment to the manifold chambers will be done after their hydraulic resistance is adjusted (by adjustment of corresponding slide valves) in the framework of Gricaman pre-experiments.

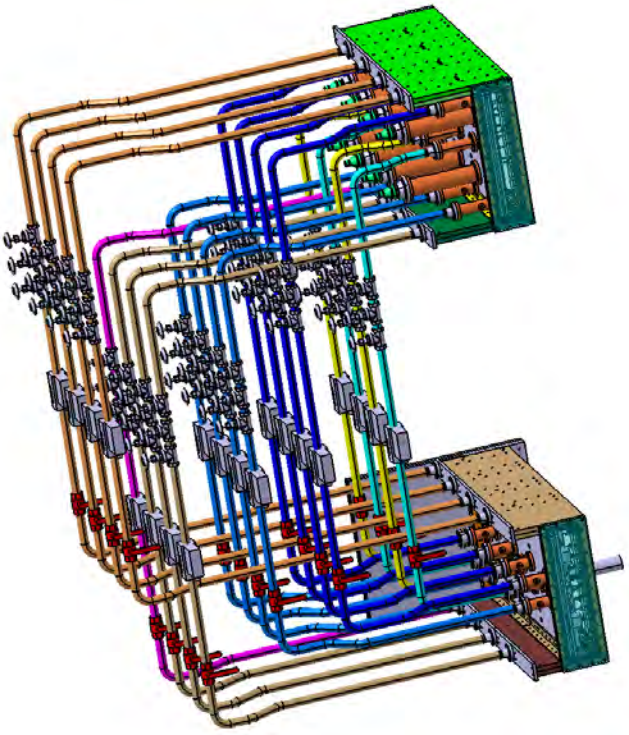

Fig. 2: CAD Design of equivalent grid/cap channels in the Gricaman facility.

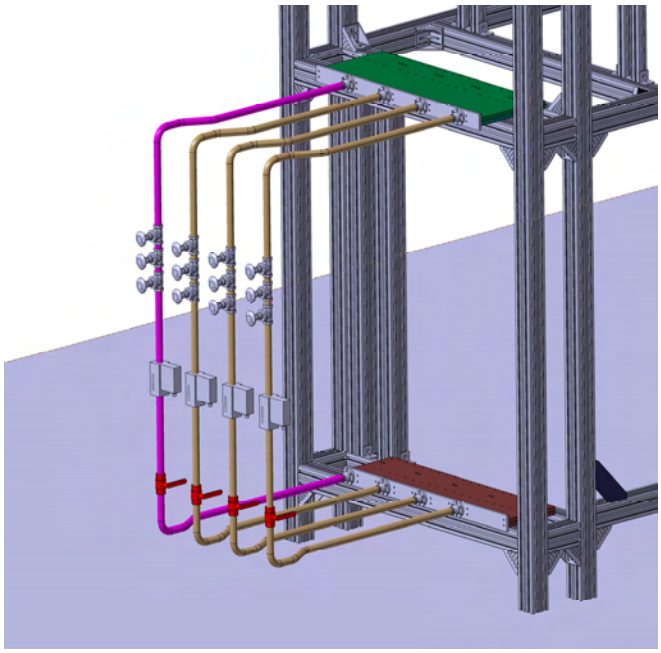

Fig. 3: Gricaman pre-experiment for adjustment of hydraulic resistance of cap channels.

The design of the Gricaman pre-experiments for adjustment of the hydraulic resistance of equivalent grid/cap channels has been completed. Currently the experimental section for cap channels is being assembled see Figure 3).

The flow scheme of the whole Gricaman facility has been defined. The first phase in the construction of the Gricaman facility according to this scheme - the building of the main supply line of pressurized air has been completed (see Figure 4).

It is expected that the building of Gricaman facility will be finished in the beginning of 2011. After this the instrumentation will be done. The first tests will be done in Spring 2011.

Fig. 4: Main supply line of pressurized air for Gricaman facility.

Staff:

O. Bitz
M. Ilic

Acknowledgement

This work supported by the European Communities under the contract of Association between EUROATOM and Karlsruhe Institute of Technology, was carried out within the framework of the European Fusion Development Agreement. The views and opinions expressed herein do not necessarily reflect those of European Commission.

KIT-Contribution to the Development of the European Test Blanket Modules (TBM) Systems

Design and Development of the European Test Blanket Modules (TBM) Systems (F4E-2008-GRT-09(PNS-TBM)-01)

In 2010 the Grant F4E-2008-GRT-09 (PNS-TBM) was in its second and conclusive year of work. The Grant was awarded by a Consortium of Associates (called TBM-CA). The partners in the TBM-CA, all of them EURATOM Associates or operating as Research Units under the umbrella of a EURATOM Associate, are CEA, CIEMAT, ENEA, KIT, NRI (Czech Republic) and RMKI (Hungary).

The TBM-CA has built a management structure with a Project Leader, four Deputy Project Leaders (that are leader of a TBM-CA Division), and a Management Support and Design Integration Team (MDIT). The latter is the main instrument to ensure the coherence of the work (system engineering coordination, design integration and Configuration Management) and to provide all the management support tools (Project Office, Documentation System, CAD Office, etc.) required to keep on track a project of this complex nature. I.e., the MDIT has both technical) and administrational (project management, control of planning, resources and funds, quality management) functions, as well as tasks towards the regulatory authorities (safety and licensing). The Project Leader and the MDIT are hosted by KIT, acting as coordinator in the grant agreement. Other main involvement of the KIT is the leadership of a TBM-CA Division (D1:“HCPB TBM Design and Specifications”) and the three related Engineering Groups: EG1.1 “HCPB TBM Design and System specification Group”, EG1.2 “HCPB TBM Manufacturing and Material Group”, EG1.3 “HCPB Predictive Tools”. KIT is leading also the EG3.1 (“Helium Cooling System Group”) under Division 3.

In the following the description of the activities done in KIT for the GRT-09 are reported.

1. PM and MDIT: Project Management and Design Integration

In addition to the Project Management function, the MDIT is involved in technical work in the field of System Engineering and Configuration Management. One important task accomplished in KIT was the set-up of the technical baseline of the TBS Project [1].

The first step to set up a baseline configuration was to subdivide the EU TBS systems in a set of Sub-Systems (SS); this allows the definition of specifications for the different SSs and of interface documentations among them. This work is described in further detail in [2]. The Figure 1 presents the result of this work, namely the proposed breakdown. The sub-systems of the EU TBSs (HCPB and HCLL concepts integrated in Equatorial Port #16) can be divided in three parts: 1) specific SSs for the HCPB, 2) specific SSs for the HCLL TBS and 3) common SSs.

The SSs grouped under “HCPB specific SSs” are: the HCPB TBM-Set, the HCPB Helium Coolant System (HCS), the HCPB Tritium Extraction System (TES), the HCPB Coolant Purification Systems (CPS) and the HCPB Data Acquisition and Control System (DACS). Under the “HCLL specific SSs” analogous systems are grouped, like the HCLL TBM-Set, the HCLL HCS, the HCLL CPS and the HCLL DACS. To this list few HCLL specific SSs are added, like the PbLi Loop and the Tritium Removal Systems (TRS), according to the different T extraction mechanism that is based on the external recirculation of the liquid PbLi. The equipment located in the Port Cell (PC)#16, namely the Auxiliary Equipment Unit (AEU) Structure, the Pipe Forest (PF) and the PC Equipment, has been grouped under “Common SSs”. Also the Equipment in the Hot Cell Facility (HCF), namely the Hot Cell Equipment (HCE), is part of this group. The definition of the SSs belonging to the EU TBSs is not complete: to this list has to be added the TBM Port Plug (PP), two Dummy (water cooled) TBMs and some spe-

cial diagnostic equipments to be allocated in the PC. These SSs are not included in Figure 1 as they are or under IO development or not yet included in the EU Project.

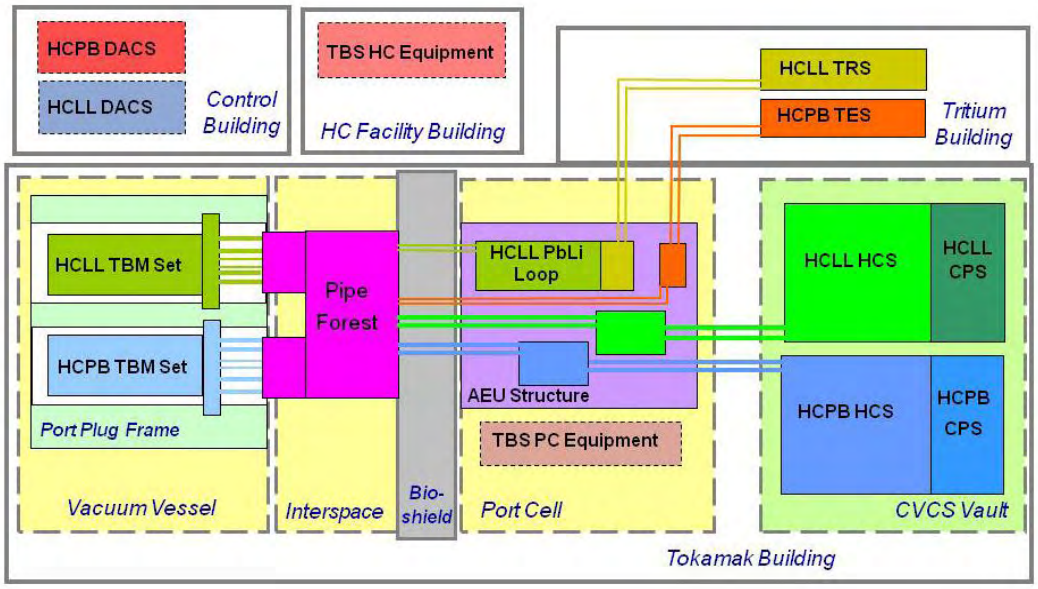

Fig. 1: Sub-System Breakdown for the EU TBSs.

Staff of Project Management and MDIT:

L. Bankos
L.V. Boccaccini
F. Cismondi
J. Gafert
D. Panayotov
P. Sardain (delegated by CEA)
S. Schreck

List of External Contributors:

A. Aiello (ENEA)
O. Bede (RMKI)
T. Ilkei (RMKI)
L. Jourd'heuil (CEA)
L. Kosek (NRI)
J-F. Salavy (CEA)
L. Sedano (CIEMAT)

2. HCPB TBM Design and System Specification Group: Conceptual Design of the HCPB TBM

The main activities on design and analyses of the HCPB TBM have been performed in this Group. These activities include the design and qualification plan of the HCPB TBM generic box (Task T-10), of the EM-TBM (T-11) and IN-TBM breeder zone (T-12). Analogous Tasks have been worked in 2010 by the Design Group of Saclay on the development of the HCLL TBM. A strong cooperation between the two design teams permits a very successful completion of the task under technical and management point of view. Detailed objectives and activities performed for each task are:

T10 - HCPB TBM generic box: The main structure of the HCPB TBM generic box will be common for all successive versions of TBMs to be tested in ITER. The design of the generic box has to fulfil functional requirements which rely mainly on the DEMO relevancy of the most important geometrical and functional parameters. In the design assessment phase, the box integrity under normal and accidental conditions has to be insured. A convergence effort has been made with the TBM foreseen for the HCLL concept in order to ensure a maximum similarity of the designs within the European TBM project, and sharing of the development effort.

During this year all the technical activities of the task T10 as detailed in the technical specifications of the Grant F4E-2008-GRT-09 have been completed. The preliminary generic box design has been completed by further analyses and the workplan presented under the documents ‘’Workplan for analyses and model development for the detailed design activities of the HCPB TBM box’’. The “Design Description document for the HCPB TBM generic box” has been completed. The following step has been preparing the “Status Report on the development and future needs of the HCPB TBM generic box” and the “Proposal for a design and technology qualification plan for the HCPB TBM generic box”. In particular, in the frame of the design and analyses activities for the DDD an important effort has been made for the assessment of the structural behaviour of the TBM box with respect the selected codes & standard (RCC-MR and SDC-IC). The outcomes of the structural analyses have been presented in the SOFT conference [3]. Furthermore, the results obtained by the joint effort of the EU HCPB & HCLL design teams have been presented in the TOFE conference [4]. In particular the transient behaviour of the TBM boxes has been investigated for the first time under typical ITER pulse (see Figure 2).

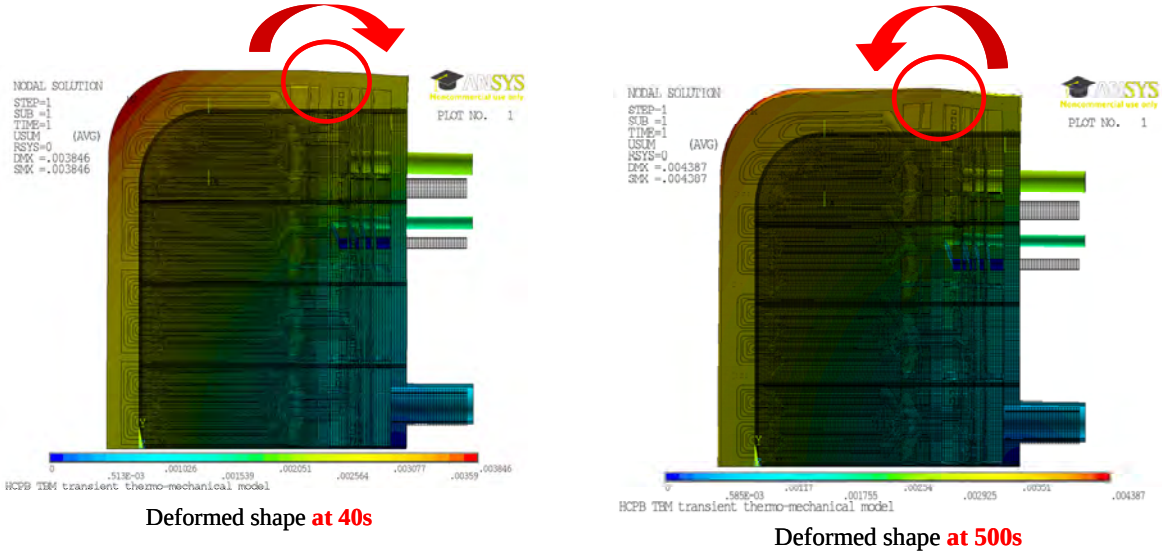

Deformed shape **at 40s** Deformed shape **at 500s**

Fig. 2: Transient thermo mechanical analyses of the HCPB TBM box under a typical ITER pulse: deformation pattern of the TBM box at 40s (left) and 500s (right) during the plasma pulse.

T11 - HCPB EM and T12 - IN-TBM breeder zones: the objective is to propose a preliminary design of the breeder zone of the HCPB TBM for the so-called “Electro-Magnetic” test phase in ITER and for the so-called “Integral” test phase in ITER. During this year the technical activities for Task T11 and T12 as detailed in the technical specifications of the Grant F4E-2008-GRT-09 have been completed. In particular a Design Description Document for the reference configuration of the HCPB EM and IN-TBM BUs has been proposed. Subsequently a “Status Report on the development plan and future needs for the HCPB EM and IN-TBM BUs” has been prepared and delivered. The next step consisted in proposing a “preliminary BU specific qualification plan” for both the EM and IN-TBM BUs reference configurations. The last work consisted in delivering a “Preliminary Design of an experiment for the qualification of the HCPB IN-TBM BU”. Structural thermo mechanical analyses have been performed for the HCPB IN-TBM BU: as for the TBM box the design assessment with respect the Codes and Standard has been performed.

The breeding zones development shares with TBM generic box development three fundamental points: (1) the space allocation defined by the internal orthogonal structure of Stiffening Grids defines the available space for the breeding zone, (2) the thermal coupling between breeding cells and box structure provides boundary conditions for both models and defines the helium mass flow rates distribution in the different TBM components, (3) feed-through solutions allow feeding breeder units with coolant and breeder, connecting instrumentation. A detailed CFD model of the BU, including the surrounding TBM components, has been devel-

oped for tuning the helium mass flow rate in the different components of the TBM and establishing the heat flux produced in the BU and deposed on the TBM components.

Preliminary studies have been conducted for the instrumentation choice (imposed by box geometry and technical choices). Instrumentation for specific experimental objectives has been addressed along with instruments for the acceptability to operate and control of the TBM box and BU. Detailed FE model of the TBM box have been produced optimizing the mesh strategy. Geometrical issues in the design will be addressed by means of the sub modelling technique, a sophisticated FE approach available in ANSYS. Detailed parametrical CAD model have been built and are under evolution following the feedback of the fabrication experts and the improvements dictated by the designers to cope with the structural design limits.

Staff:	List of External Contributors:
F. Cismondi	S. Kecskes (RMKI)
L. Bankos	B. Kiss (RMKI)
I. Maione	G. Legradi (RMKI)
	V. Szabo (RMKI)
	G. Aiello (CEA)

3. HCPB Predictive Tools Group (PTG): Experimental Programme & Simulation Capacity for reliable HCPB TBS Test Programme in ITER

The group of tasks under completion in EG1.2PTG have as final goal to develop an Experimental Programme & Simulation Capacity for the HCPB-TBS to be performed in ITER over the next ten years. Among these 7 tasks T31.3 is related to the coordination, assessment and integration of the Experimental programme, while the others (T23.2, T24.2, T26, T27.2, T28.2, T29.2) have been assigned to experts in charge to define this Programme in different fields (thermo-hydraulics, neutronics, electro-magnetic, tritium transfer and cycle, pebble bed mechanics and system/coupled phenomena). An analogous PTG has been established for the HCLL TBS, which includes also the field of the Magneto-Hydrodinamics and PbLi-steel Corrosion that are investigated in KIT. This Group is leaded in Saclay by our French Colleagues in the Consortium.

The main objectives for these tasks, achieved during this year, are:

1. The definition of a list of experiments/tests in each field to be performed in ITER with the aim to achieve a reliable TBMs testing programme. Each group released, in agreement with F4E, a technical report (D1) in which experiments/tests requirements in ITER and model/code validation and extrapolation for DEMO [5] has been defined.
2. On the basis of the proposed experiments the Milestone M2 of the sub-task T31-3 (“Assessment of the proposed TBM experiments for ITER experimental campaign. Main objectives and main issues”) has been accomplished. In the related deliverable (T31.3-D3), a ranking of the proposed experiments in increasing complexity order, and synthesis of the main issues and request for each modelling field in terms of models, software, control of the environmental variables and instrumentations have been provided.
3. Based on the needs concerning the development of HCPB TBS modeling tools, each expert has compared the proposed experiments to the state-of-the-art in order to identify a list of actions for the future research activities aiming at covering the gap between the present knowledge and the needs for EM experiments to be performed in ITER. The research work in each field has been reported in relative deliverable D2.
4. An overview of the status of the art and rationale for future developments for the fields involved in the HCPB TBM experimental program has been reported in deliverable T31.3-

D4. For each field, the state of the art of existing instrumentation, experimental facilities for out-of-pile experiments and modelling tools have been presented and needed developments discussed.

5. As last objective, on the basis of the outcome of deliverables D2 and T31.3-D4, a R&D programme/work plan is going to be proposed including the development of the HCPB TBS experimental programme and simulation capacity (T31.3-D5).

Staff:	List of External Contributors:
A. Abou-Sena	G. Aiello (CEA)
L. Bühler	M. Angelone (ENEA)
F. Cismondi	Ll. Batet (GREENENER-TF4, UPC)
D. Demange	M. Chiumentti (CIMNE)
U. Fischer	M. Eid (CEA)
Y. Gan	F. Gabriel (CEA)
M. Ilic	A. Li Puma (CEA)
A. Jianu	A. Lyoussi (CEA)
M. Kamlah	P. Martinez (CIEMAT)
A. Klix	E. Mas de les Valls (GREENENER-TF4, UPC)
W. Krauss	F. Moro (ENEA)
I. A. Maione	C. Moreno (CIEMAT)
E. Magnani	L. Petrizzi (ENEA)
C. Mistrangelo	M. Pillon (ENEA)
P. Perslavstev	L. Sedano (CIEMAT)
J. Reimann	R. Villari (ENEA)

4. Helium Cooling System Group: Preliminary Design of the HCLL- and HCPB-Helium Cooling System for ITER

One of the activities performed by KIT (FZK) as part of the F4E grant (F4E-2008-GRT-09) is the preliminary engineering design of the Helium Cooling systems for the two European TBM: HCLL and HCPB. During 2010 the work was focused mainly in compiling the work done in 2009 and documented it in the form of 12 Technical reports (6 for each system):

T04/13-D1	HCLL/HCPB HCS preliminary engineering design and analyses
T04/13-D2	Status of HCLL/HCPB HCS integration in ITER Plant
T04/13-D3	HCLL/HCPB HCS interfaces and requirement to ITER
T04/13-D4	Preliminary HCLL/HCPB HCS measurement and instrumentation plan
T04/13-D7	HCLL/HCPB HCS-related chapter of DDD
T04/13-D8	Status report on the HCLL/HCPB HCS future needs

Results coming from these tasks have been used for a paper presented at the SOFT-2010 in the framework of the TBM-CA activities on the Auxiliary systems of the EU TBSs [6].

Staff:	List of External Contributors:
B. E. Ghidersa	G. Porempovics (RMKI)
A. Jianu	A. Tincani (ENEA)
X. Jin	
V. Marchese	
V. Weber	

Literature:

[1] L.V. Boccaccini, A. Aiello, O. Bede, F. Cismondi, L. Kosek, T. Ilkei, J-F. Salavy, P. Sardain, L. Sedano, Study on the conceptual design of the EU Test Blanket Systems, Invited talk presented to the SOFT-2010 in Porto (September 2010).

[2] D. Panayotov, P. Sardain, L.V. Boccaccini, J.-F. Salavy, F. Cismondi, L. Jourd'Heuil, System engineering approach in the EU Test Blanket Systems Design Integration, Poster presented to the SOFT-2010 in Porto (September 2010).

[3] F. Cismondi, S. Kecskes, G. Aiello, HCPB TBM thermo mechanical design: assessment with respect codes and standards and DEMO relevancy, Poster presented to the SOFT-2010 in Porto (September 2010).

[4] F. Cismondi, G. Aiello, S. Kecskes, G. Rampal, Thermo mechanical performance of the EU TBMs under a typical ITER transient, presented to TOFE 2010, to be published in Fusion Science and Technology.

[5] E. Magnani, F. Gabriel, L.V. Boccaccini, A. Li-Puma, DEMO relevance of the test blanket modules in ITER - Application to the European test blanket modules, Fusion Engineering and Design 85 (2010)1271-1278.

[6] A. Aiello, A. Ciampichetti, F. Cismondi, B.E. Ghidersa, T. Ilkei, L. Kosek, J.F. Salavy, European Testing Blanket Modules auxiliaries design, Oral contribution presented to the SOFT-2010 in Porto (September 2010).

Contribution to Division 2 (CEA leadership):

5. Non-destructive Testing (NDT)

Objectives

Qualification of adequate NDT (non-destructive testing) techniques for detecting cracks particularly in the welded areas of TBM components built from EUROFER 97 and to realise it with an automated NDT testing procedure.

Task current status

Within the reporting time period the non-destructive testing procedures were further optimized. Thereby diffusion bonded specimens with artificial flaws of sizes down to 50 µm at the interface are produced and inspected by immersion ultrasonic testing. The small artificial flaws are realized by laser structuring of the surfaces to be bonded before diffusion bonding. With a new 20 MHz probe the flaws could be clearly detected. In addition, pre-cracked specimens were manufactured and subsequently loaded to obtain certain amount of crack extension. By immersion ultrasonic testing using the new probe the crack extensions could be quantified with an accuracy of 10 µm which was afterwards verified by computer tomography measurements and destructive inspection as well.

Currently a first wall mock-up fabricated by a new manufacturing technique for the realisation of curved inner cooling channels is investigated. The main focus lies on the relatively complicated geometry of the many diffusion bonded interfaces and their inspectability using the immersion ultrasonic technique established to date.

Staff:

T. Martin
S. Knaak
J. Aktaa

Contribution to Division 3 (ENEA leadership):

6. Breeder Blanket and Tritium Technology Group

Design Review for the Tritium Extraction and Coolant Purification Systems of the ITER Test Blanket Modules and Analysis of the Tritium Behaviour in the Solid Breeder Blanket Concept

Scope and objectives

One of the missions of ITER is to test breeder blanket concepts. It is mandatory to increase the confidence that the next reactor (i.e. DEMO) will demonstrate the required tritium self-sufficiency. Europe will operate two different Test Blanket Modules (TBM) in ITER: the Helium Cooled Pebble Bed (HCPB) and the Helium Cooled Lithium Lead (HCLL) concepts.

The objectives of this grant managed by the European Consortium of Associates for the TBM (CA-TBM) are the following:

- Fix the design and the integration in ITER of the TBM boxes and the ancillary units, i.e. the Helium Cooling System (HCS), the Coolant Purification System (CPS) and the Tritium Extraction System (TES),
- Define precisely the experiments to be performed in ITER along the different phases of the testing programme,
- Identify the remaining issues and consolidate the road map until the implementation in ITER.

Within this grant, the Tritium Laboratory Karlsruhe (TLK) is contributing:

- As contributing expert, support ENEA in the design review of the TES and CPS for both HCLL and HCPB TBMs, including the review and selection of appropriate processes, preliminary engineering design and ITER integration, preliminary measurement and instrumentation plan, and identification of future needs,
- As task coordinator, describe of the state of the art for tritium behaviour in the breeder zone of the HCPB concept (i.e. in Li-based ceramics and beryllium) and clarify the coupled phenomena occurring during operation in the machine, define dedicated experiments to be performed in ITER, and propose the future work plan.

Previous results

During the previous period, the review and selection of appropriate processes for CPS has been completed [7]. Based on the previous concepts proposed by TLK and ENEA, a review has been performed with emphasis on performances, operation, instrumentation, and interfaces, including the tritium accountancy stage. High requirements have been put on the reliability of the system, so that robust process options have been privileged.

A three stage process has been proposed as follows:

- First, an oxidiser (CuO) converts molecular tritium (Q_2) into tritiated water vapour (Q_2O); using an over-estimated reactor will facilitate operation, ensuring high efficiency and minimising maintenance.
- Then, an adsorption step removes tritiated water Q_2O using a molecular sieve bed (zeolite as adsorption material); 2 adsorption columns are working simultaneously, one in adsorption mode at room temperature, the second under regeneration at elevated temperature, with a reducing bed or a PERMCAT reactor placed downstream to convert Q_2O in Q_2.
- A final step removes residual impurities using a heated getter made of zirconium alloy working at about 400°C, in replacement to the previous process based on cryogenic adsorption onto molecular sieves or activated charcoals.

For the instrumentation, it has been shown that online tritium measurements using ionisation chambers fulfil the required measurement range for the control and operation of the processes. However, such measurements are sensible to memory effect [8] and not enough accurate to provide quantitative information needed to validate neutronics calculations and to accurately track tritium between the TBM tritium systems and the tritium plant. A dedicated accountancy stage shall be implemented to collect the gases and accurately measure tritium concentrations.

Concerning the tritium coupled phenomena in the solid breeder concept, a list of experiments in ITER has been proposed to study crucial issues related to the ageing effect, i.e. the material modifications resulting from the long term operation under severe operating conditions, including high lithium burn-up. In-line tritium measurements should enable highlighting eventual changes in the tritium release rate. Combined with post irradiation examinations, some material changes particularly important for the tritium behaviour (porosity, chemical composition…) might be revealed.

Achievement in 2010 for the design of the tritium processes for the ITER TBM

For the recovery of tritium from water vapour during the regeneration of the adsorption columns [9], a comparison between the nominal option using a reducing bed and the alternative use of PERMCAT based on counter-current isotope swamping in a palladium membrane reactor [10-12] has been performed. Even if water reduction over hot metals seems straightforward; it is unsatisfactory with regard to operation due to the strongly exothermic reaction, the limited conversion, and the irreversible consumption yielding to waste production and maintenance. Moreover, it does not help the tritium accountancy because of the batch-wise operation and the dilution with carrier gas. In contrast, tritium recovery from water using PERMCAT [13] is a simple continuous, intrinsically safe, and clean process. In addition, it facilitates the tritium accountancy since tritium is recovered in the pure molecular form [14], and it can be enriched by a factor of 10 or more. The main stream is detritiated (more than 99% of tritium removed) so that it can be directly routed without accountancy to the tritium plant, thus reducing drastically the load on the accountancy stage. Therefore, PERMCAT has been proposed as the reference solution; the reducing bed should be considered as a back up solution.

Another important step of the process review has been the adoption of a reversible hydrogen getter to replace the adsorption at cryogenic temperature for the recovery of tritium in the molecular form. From the thermodynamic point of view, ZrCo is a good candidate, but the kinetics might be the limiting factor so that dedicated tests will have to be performed before.

After having fixed the process options, and according to the requirement for operation, the next activities have focused on:

- The preliminary engineering design (sizing) of the main components of the processes such as the oxidation bed, the adsorption columns, the heated getters, the PERM-

CAT reactor, and the economiser/heat exchanger; 3D models of systems have been produced;

- The preliminary measurement and instrumentation plan with the selection and location of the appropriate tools for the on-line monitoring of relevant information such as pressures, temperatures, flow rates, tritium levels, together with the chemical composition including the tritium isotopic composition [15];
- The assessment of the industrial and technological state-of-the-art of the components, an identification of the needs for future developments, qualification and modelling activities.

The preliminary design of the TES and CPS for both HCPB and HCLL TBMs is now nearly completed.

Achievement in 2010 on Tritium behaviour in solid breeder considering coupled phenomena

In this period, the state of the art on the tritium behaviour in the breeder zone has been reported, and the work plan for the next years has been proposed. A comprehensive literature study throughout the abundant papers published over the last 20 years has been completed, focusing on both the modelling and experimental activities related to lithium-based ceramics and beryllium as well.

It has been highlighted that a huge database of experimental results has been accumulated worldwide for different materials:

- Either during in-pile experiments and on line tritium release measurements in a configuration close to the operation inside a machine; however this approach is limited to integrated bed size studies (if the bed is heterogeneous, it is impossible to draw conclusions on the specific materials) and face some issues for integration in the reactor; this method mainly produces interesting results from the engineering point of view;
- Or with out-of-pile studies (from materials previously irradiated) and tritium measurements during thermo-desorption experiments; these studies allow the relevant operating parameters (temperature, flow rate, purge gas composition, magnetic field…) to be varied with a better control and within a wider range, therefore of highest interests in view of the understanding on the scientific level the multiple phenomena affecting the tritium behaviour in the functional materials.

The modelling activities have reached different degrees of maturity. It is important to note that the mechanisms for tritium release from Li-ceramics or Be are totally different, so that simulation cannot be easily transposed. Despite the early work mainly performed in Europe and in US, Japan is now well in advance for the simulation of tritium in breeder materials; the last models tend to well reflect the tritium release for out-of-pile experiments, so that predictive capabilities for ITER and DEMO can be envisaged. For tritium in beryllium, Europe seems in advance.

However, from both experimental and modelling point of view, the ageing effect and the coupled phenomena have not been sufficiently studied yet. Important experimental results recently produced have highlighted new complex mechanisms for tritium release when magnetic field and/or irradiation are applied during the experiment. But the irradiation experiments and associated ageing effects performed so far are still very far from the operating conditions of a DEMO relevant blanket. The modelling activities have ignored so far the ageing effect and coupled phenomena, mainly because of the difficulty to apprehend such a complex system. However, such effects may have a major impact on the tritium behaviour so that severe deviations from the results (experimental and numerical results) obtained so far can be expected.

It has been concluded that a huge gap still exists between the present know-how on tritium behaviour in the solid breeder blanket and reliable predictive capabilities in view of DEMO. The experiments in ITER should be a major step to consolidate and validate predictive tools developed in the mean time. A road map towards this objective has been proposed as follows:

- Produce a wide range of new promising materials by varying chemical composition and microstructure,
- Perform wide-range irradiation programme varying purge gas composition and temperature,
- Carry out in-pile and out-of-pile tritium release measurement also under a wide range of conditions including coupled effect, accompanied with post irradiation examinations to reveal some correlation between the structure changes and the tritium behaviour,
- In parallel and in addition, develop model and simulation at the pebbles size including ageing effect and any coupled phenomena.

Conclusion and perspectives

The preliminary design of the TES and CPS for both HCPB and HCLL TBMs is now nearly completed. The process options have been chosen to ensure a high reliability and minimise the load on the future accountancy stage. A PERMCAT reactor (instead of the reducing bed) and a heated getter (in replacement to the cryogenic adsorption) are now considered in the baseline for TES and CPS. The instrumentation and tritium measurements have been defined. The work should be continued within a new grant in order to optimise and design the tritium accountancy system. A model and numerical simulation of the tritium migration along the TBM and ancillary units will be performed considering to different plasma scenarios, different sizes of the TBM, and taking into account the particular operation of TES and CPS. A main objective will be to assess the quantity of tritium actually collected and measured at the accountancy stage (compared to the amount produced in the breeder zone of the TBM) considering parasitic effects and tritium losses along the systems.

In parallel, R&D activities related to the final design of the TES and CPS systems for ITER TBM shall be launched. A preliminary work-plan of 5 years has been proposed, including the construction of new component testing facilities [16] at the laboratory scale or at the technical scale, with parallel activities on the development of computing tools for the interpretation of experimental results and the scale up of the components to the technical scale. Integrated experimental demonstration should be performed prior to the final procurement for ITER. Specific tests with tritium shall be performed when isotope effects are anticipated, e.g. for the combination of the adsorption column and the PERMCAT reactor, and for the heated getter bed for the adsorption of molecular tritium.

It will also be important to start as soon as possible an exhaustive program for experiments and simulation to develop reliable and advanced predictive tools required for the proper interpretation of the results produced in ITER as well as for the design of the DEMO machine.

Staff:

D. Demange
E. Fanghänel
R. Wagner
S. Welte

Literature:

[7] A. Ciampichetti, A. Aiello, G. Coccoluto, I. Ricapito, K. Liger, D. Demange, C. Moreno "The Coolant Purification System of the European Test Blanket Modules: preliminary design" Fusion Engineering and Design 85 (2010) 2033–2039

[8] R. Wagner, U. Besserer, D. Demange, H. Dittrich, T.L. Le, K.H. Simon, K. Guenther "Improvement and characterization of small cross-piece tritium ionization chambers at the Tritium Laboratory Karlsruhe" (presented at the 9th International Conference on Tritium Science and Technology, Oct. 24th – 29th 2010, Nara, Japan; to be published in Fusion Science and Technology)

[9] A.I.R.T. Parracho, P.D. Brennan, D. Demange, S. Knipe "Characterisation and optimisation of small molecular sieve beds in adsorption/desorption process of tritiated water" (presented at the 9th International Conference on Tritium Science and Technology, Oct. 24th – 29th 2010, Nara, Japan; to be published in Fusion Science and Technology)

[10] S. Welte, D. Demange, R. Wagner "Mechanical design and first experimental results of an upgraded technical PERMCAT reactor for tritium recovery in the fuel cycle of a fusion machine" Fusion Engineering and Design 85 (2010) 1320–1325

[11] F: Borgognoni, D: Demange, L: Dörr, S: Tosti, St: Welte "Processing test of an upgraded mechanical design for PERMCAT reactor" Fusion Engineering and Design 85 (2010) 2171–2175

[12] S. Welte, D. Demange, R. Wagner "Characterisation of a multitube PERMCAT reactor in view of a technical facility for highly tritiated water processing at the Tritium Laboratory Karlsruhe" (presented at the 26th Symposium on Fusion Technology, Sept 27th – Oct 1st 2010, Porto, Portugal; to be published in Fusion Engineering and Design)

[13] D. Demange, E. Fanghänel, B. Kloppe, T.L. Le, F. Scheel, K.H. Simon, R. Wagner, S. Welte "CAPER modifications and first experimental results on highly tritiated water processing with PERMCAT at the tritium laboratory Karlsruhe" (presented at the 9th International Conference on Tritium Science and Technology, Oct. 24th – 29th 2010, Nara, Japan; to be published in Fusion Science and Technology)

[14] D. Demange, S. Stämmler, M. Kind "A new combination of membranes and membrane reactors for improved tritium management in breeder blanket of fusion machines" (presented at the 26th Symposium on Fusion Technology, Sept 27th – Oct 1st 2010, Porto, Portugal; to be published in Fusion Engineering and Design)

[15] K. Liger, A. Ciampichetti, D. Demange "HCLL and HCPB Coolant Purification System: Preliminary measurement and instrumentation plan" (presented at the 9th International Conference on Tritium Science and Technology, Oct. 24th – 29th 2010, Nara, Japan; to be published in Fusion Science and Technology)

[16] A. Aiello, L. Bühler, A. Ciampichetti, D. Demange, L. Dörr, J.F. Freibergs, B. Ghidersa, M. Ilic, G. Laffont, G. Messemer, I. Platnieks, G. Rampal "Mockup testing facilities and qualification strategy for EU ITER TBMs" Fusion Engineering and Design 85 (2010) 2012–2021

Acknowledgement

This work was supported by Fusion for Energy under the grant contract No. F4E-2008-GRT-09(PNS-TBM)-01 with collaboration by CEA, France; ENEA, Italy; CIEMAT, Spain; KFKI-RMKI, Hungary and NRI Řež, Czech Republic. The views and opinions expressed herein reflect only the author's views. Fusion for Energy is not liable for any use that may be made of the information contained therein.

Elaboration of the Development/Qualification/Procurement Plan for Functional Materials (F4E-2009-GRT-030(PNS-TBM) - Action 1)

The Grant *F4E-2009-GRT-30 (PNS-TBM)* Action 1 was published on F4E web page on April 2009. The proposal of TBM-CA was presented in June 2009 and the Grant Agreement was signed in March 2010. KIT has the role of coordinator of this Action, leading a Group of Association (CEA, CIEMAT and ENEA) under the EU TBM Consortium Agreement of Associates.

The general objective of the Action 1 of this Grant is to elaborate the development/qualification/procurement plan for the three main functional materials used in the European TBM programme:

1. Ceramic breeders for the solid blanket in form of pebbles (Li_4SiO_4 and Li_2TiO_3).
2. Beryllium multiplier for the solid blanket in form of pebble (Be or/and Be-alloy).
3. Pb-Li alloy for the liquid blanket.

The development/qualification/procurement plans for the three functional materials constitute the goals of three distinct tasks, in which the Action 1 has been broken down. Task 1 and 2, for the ceramic breeders and Beryllium functional materials respectively, are under the responsibility of KIT. Task 3 deals with Pb-Li alloy and is under CIEMAT responsibility.

On this basis, detailed technical objectives for each task have been derived and described in detailed technical specifications that accompanied the Call for Proposal. For each one of the task one final deliverable has to be provided.

In addition as the ITER TBM Systems is classified as Quality Class 1 a complete set of Quality Management Provision has been applied. The Execution Quality Plan has been completed in KIT in 2010; task monitoring by means of Primavera Planning and monthly Progress Report are part of the Quality Procedure. The Kick-off Meeting for Action 1 tasks 1, 2 and 3 took place on May 26, 2010. The official starting date for the technical activities has been agreed on July 15, 2010.

For Task 1 and Task 2 the technical tasks have been broken down identifying the technical responsible within KIT, CEA and NRG. NRG participates as third party for KIT in the TBM CA structure for this Action. All the technical activities have started in time. A first draft of the final report has been scheduled at the end of December 2010.

For task 1 the following activities have started and are under completion:

- Review of the Functional Requirements of TBM/DEMO for Ceramic Breeder Pebbles.
- Review of the Development Status of Ceramic Breeder Pebbles (Fabrication of ceramic breeder pebbles, Fabrication related properties of ceramic breeder pebbles - see Figure 1 -, Modelling and simulation of pebbles and pebble beds, Patents related to pebble production processes, Irradiation Behaviour of ceramic breeder pebbles).
- Suitability of the Material Properties for the HCPB TBM Design.
- Missing Elements in the Material Assessment Report and in the Material Data Base Report (Fabrication related properties and Irradiation properties).
- Development Needs and Roadmap (Further development needs, Development roadmap).

- Qualification Plan for Ceramic Breeder Pebbles (Qualification plan concerning the fabrication related properties, Qualification plan concerning the irradiation behaviour).
- Survey of Li-6 Enrichment and Regulation Aspects (Li-6 enrichment and international regulations, Requirements of French authorities and ITER organization for Li-6 enrichment).
- Preliminary Procurement Plan of Ceramic Breeder Pebbles (Quantity of ceramic breeder pebbles, Quality of ceramic breeder pebbles).
- Evaluation of the Procurement Plan.

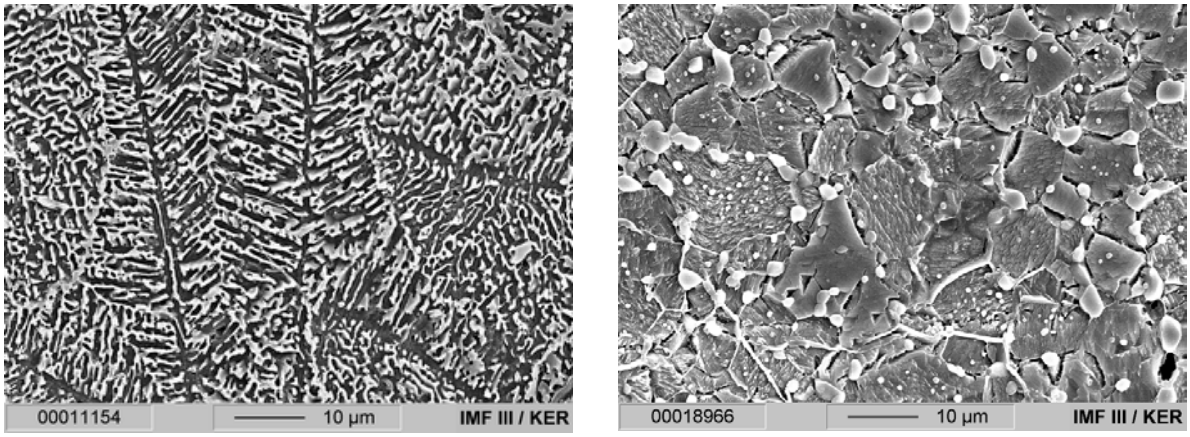

Fig. 1: Microstructure of lithium orthosilicate pebbles, (left) in the initial state and (right) after conditioning at 970 °C for 1 week.

For task 2 the following activities have started and are under completion:

- Review of the Functional Requirements of TBM/ITER & DEMO blanket for Be-based Pebble Materials.
- Review of the Development Status of Be-based Materials and Fabrication Routes of Pebbles (Fabrication of Be/Be-alloy pebbles, Fabrication routes of Be pebbles, Development of fabrication routes of pebbles from beryllides, Fabrication related properties of Be/Be-alloy pebbles, Fabrication related properties of Be pebbles, Fabrication related properties of beryllide pebbles, Modelling and simulation of pebbles and pebble beds, Patents related to pebble production processes, Irradiation behaviour of Be pebbles)
- Suitability of the Material Properties for the HCPB TBM Design.
- Missing Elements in the Material Assessment Report and in the Material Data Base Report (Fabrication related properties, Irradiation properties).
- Development Needs and Roadmap for TBM/ITER and DEMO blanket (Further development needs, Development roadmap).
- Qualification Plan for Be Pebbles (Qualification plan concerning the fabrication related properties, Qualification plan concerning the irradiation behaviour).
- Handling/Processing, Waste Management and Regulation Aspects (Handling/Processing, Waste Management, Requirements of French authorities and ITER organization for Be).
- Preliminary Procurement Plan for Be/Be-alloy Pebbles (Quantity of Be pebbles, Quality of Be pebbles, Commercial availability and development needs for fabrication).

The conclusion of the Grant is foreseen for the 28 February 2011.

Staff:

F. Cismondi
L.V. Boccaccini
R. Knitter
P. Vladimirov

List of External Contributors:

J.F. Salavy (CEA)
L. Magielsen (NRG)
J. Quinones (CIEMAT)

Acknowledgement

This work was supported by Fusion for Energy under the grant contract No. F4E-2009-GRT-030(PNS-TBM) - Action 1 - with collaboration by CEA France, CIEMAT Spain and ENEA Italy. The views and opinions expressed herein reflect only the author's views. Fusion for Energy is not liable for any use that may be made of the information contained therein.

Screening of an Alternative Production Route/Capacity for Be Pebbles (F4E-2009-GRT-030(PNS-TBM) - Action 2)

Introduction

The call for proposals (F4E reference number *F4E-2009-GRT-30 (PNS-TBM)*) was published on F4E web page in April 2009. KIT has taken a role of coordinator for the Action 2 “Screening of an alternative production route/capacity for Be pebbles” of this call. This grant is performed in collaboration with the Institute of Nuclear Technology (ITN, Portugal). The first version of the proposal was sent to F4E in June 2009. Long negotiations and six version of the grant proposal were required to come to an agreement with F4E on the scope and the content of the grant for this Action. The final version of the proposal was signed in September 2010 and the Kick off Meeting was held on November 19, 2010.

- The general objective of the Action 2 of this Grant is the screening of alternative Be pebble production routes and to qualify the pebbles produced by these routes with respect to their applicability for fusion reactor blankets.
- Presently several industrial production routes of beryllium pebbles are available and some are still under development. The main aim of the current activities is to check applicability of the existing beryllium pebbles production routes and their quality for fusion reactor blankets (ITER TBM and DEMO blankets).
- Until now only one industrial supplier (NGK Insulators Ltd., Japan) has shown the capability of producing several batches of Be pebbles with a scalable technology and based on regular purchase regulations. However, the purchase of Be pebbles based on “rotating electrode fabrication method” was quite expensive in the past. By this reason, production routes different from the patented rotating electrode method used by NGK will be screened for their capacity to be used for industrial production of Be pebbles with respect to the needs of ITER and DEMO TBMs.
- Three batches of Be pebbles with different characteristics of microstructure. (i.e.., sizes of grains) produced by Bochvar Institute, Russia are under investigation. Mechanical milling of beryllium hot-pressed blocks or ingots was used for the production of all three batches of Be pebbles.

The accepted proposal for the Action 2 includes the following Tasks:

Task 1: Screening of Alternative Routes for Be-pebble Production and Procurement of a Small Batch of Material for Characterization.

- Elicitation of alternative routes for Be pebble production
- Procurement of a small batch of Be pebbles produced by alternative route for preliminary characterization

Task 2: Preliminary Characterization of Be pebbles Produced in Task 1

Task 3: Characterization of Be pebbles produced by Bochvar Institute

Characterization methods

The characterization program includes the following measurements/methods:

1. Porosity, density, specific surface, pebble size distribution
2. Chemical composition of Be pebbles including the contents of highly-activated elements
3. Investigations of microstructure (optical and SEM)

4. Pebble bed characteristics (e.g. packing density)
5. Mechanical properties of Be pebbles: Microhardness tests
6. Tritium release from Be pebbles after thermal loading with tritium

Preliminary results

Execution of the grant was started by contacting the three largest beryllium producing companies: Brush Wellman Inc., USA, NGK Insulators Ltd., Japan and Ulba Metallurgical Plant, Kazakhstan. The following questions were addressed:

- availability of fabrications processes of Be pebbles different from the rotating electrode method and their annual production rates;
- characteristics of the pebbles produced by these processes;
- availability of a small batch of Be pebbles for characterization.

At the moment we got a preliminary reply from the Brush Wellman. More detailed information will follow.

At the same time characterization of Be pebbles produced by Bochvar Institute was started. The following steps were obtained by the end of November 2010:

- Grinding and polishing followed by the optical microscopy investigations in order to study grain sizes, texture and distribution of pores in the body of Be pebbles were performed. As an example, Fig, 1 shows the microstructure of Be pebble with the grain sizes ranging from 10 to 30 µm.

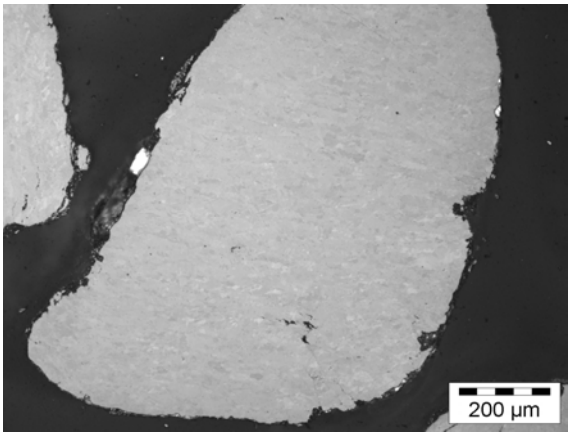

Fig. 1: Microstructure of Be pebble, grain sizes 10-30 µm (polarized light).

- The surface chemical composition of all three batches of Be pebbles was investigated by means Ion Beam Analysis (quantitative PIXE Technique) at ITN, Portugal. The contents of some elements which are present on the surface of Be pebbles is shown in Table 1. Table 2 shows the chemical content of Be pebbles after acid digestion what reflects the concentration of impurities in the bulk of material.

Table 1: Element contents (10^{-4} wt.%) obtained from the surface scan areas of three different batches of Be pebbles.

Grain sizes, µm	Si	P	Cl	Ca	Sc	Ti	Cr	Mn	Fe	Ni	Cu	Zn	Mo
10-30	83	-	5	11	2	75	196	13	504	62	25	8	-
30-60	48	44	-	8	-	7	79	14	151	11	14	-	29
>100	44		-	2	5	69	175	26	941	133	27	-	-

Table 2: Element contents (10^{-4} wt.%) after sample acid digestion for different charges of Be pebbles.

Grain sizes, μm	Ca	Ti	Cr	Mn	Fe	Ni	Cu	Zn	Mo
10-30	48	37	132	20	443	58	25	7	-
30-60	5	-	43	15	132	9	14	6	44
>100	20	140	218	40	854	112	29	6	15

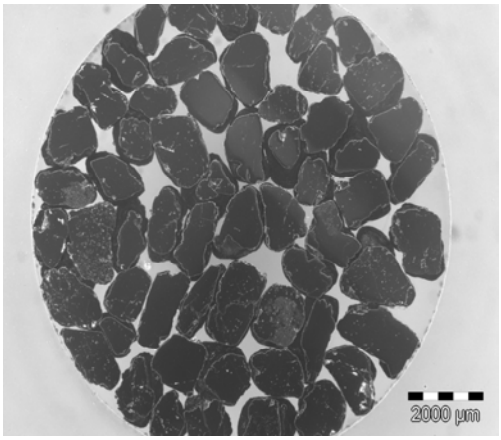

Fig. 2: Be pebbles produced by Bochvar Institute with grain sizes exceeding 100 μm.

It is notable that Be pebbles from all three batches of Be pebbles produced by Bochvar Institute have potato-like shapes. Fig. 2 shows the general view of Be pebbles with the grain sizes exceeding 100 μm.

Conclusions

Some preliminary conclusions relevant for the TBM design can be drawn based on the results of the study of pebbles produced by Bochvar Institute:

- Potato-shaped form of Be pebbles produced by mechanical milling of beryllium hot-pressed blocks or ingots (in the case of their application) can influence in a great extent the operation of the breeding module.
- Large-scale fabrication of Be pebbles depends on the availability of initial Be blocks or ingots.
- Be pebbles with the grain sizes ranging 10-30 μm have smaller inner porosity compared to other two batches.
- The batch of Be pebbles with the grain sizes ranging 30-60 μm has the smallest iron content (highly-activated element).

KIT Staff:

A. Abou-Sena
V. Chakin
P. Kurinskiy
A. Möslang
H.-C. Schneider
R. Rolli
P. Vladimirov

List of External Contributors:

E. Alves (ITN)

Acknowledgement

This work was supported by Fusion for Energy under the grant contract No. F4E-2009-GRT-030(PNS-TBM) - Action 2 - with collaboration by ITN Portugal. The views and opinions expressed herein reflect only the author's views. Fusion for Energy is not liable for any use that may be made of the information contained therein.

Post Irradiation Examination of Be Materials Irradiated in HIDOBE-01 Campaign (F4E-2009-GRT-030 (PNS-TBM) - Action 3)

After two years of irradiation at the HFR, the HIDOBE-01 experiment reached its target of 3000 appm helium production. This irradiation experiment was performed by an international cooperation of EU, Japan and the Russian Federation (RF). Small beryllium pebbles of different sizes and advanced beryllium alloy such as titanium beryllide were included to the experiment to study the state of beryllium materials after high neutron dose exposure at temperatures of 425, 525, 650 and 750 °C. These irradiation parameters are relevant to the Helium Cooled Pebble Bed (HCPB) blanket of DEMO and also for the Test Blanket Module (TBM) of ITER where beryllium will be used as a neutron multiplier material to increase the tritium breeding ratio (TBR) performance. Within the contract GRT-030 A3 with Fusion for Energy (F4E) a series of Post Irradiation Examinations (PIE) is foreseen on a selection of beryllium grades with maximal resistance to the radiation damage. The different PIE will be performed by the four following institutes in the contract: Nuclear Research and consultancy Group (NRG), Karlsruhe Institute of Technology (KIT), Instituto Technologico e Nuclear (ITN), and University of Latvia (UL). Within the contract, several PIE are planned on the irradiated beryllium materials: helium pycnometry by NRG, tritium release measurements by NRG, KIT and UL, microscopy (OM and SEM) by NRG and KIT, TEM and creep measurements by KIT, oxidation and chemical analysis by ITN. From KIT site IMF I and FML IMF II are widely involved to the contract GRT-030 A3 performance.

The first report within the contract with the detailed PIE HIDOBE-01 plan was delivered to F4E by NRG as the leading institute of this activity at 14 October 2010. This report was prepared by participation of KIT and others involved institutes. In the frame of the report content KIT has received from NRG 1.876 g of irradiated beryllium samples including unconstrained pebbles with diameters of 0.5, 1.0 (2001), 1.0 (2003), 2.0 mm and pellet fragments of Be electrode, Be-5%Ti and Be-7%Ti.

At present visual inspections of all received irradiated beryllium samples were performed. Fig. 1 shows typical views of beryllium pebbles with diameter of 1 mm irradiated at temperature of 750 °C having a helium production of 3000 appm in HIDOBE-01 experiment.

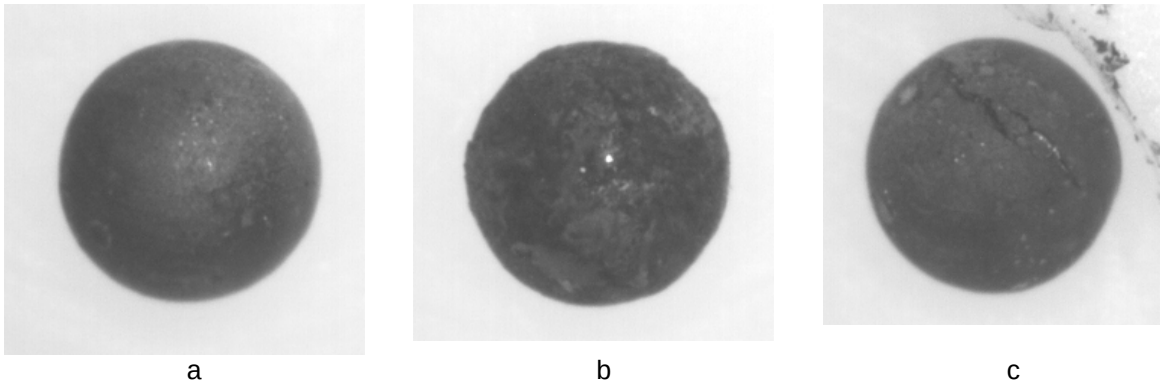

a b c

Fig. 1: General views of beryllium pebbles with diameter of 1 mm (2003) irradiated at T_{irr} = 750 °C to a helium concentration of 3000 appm in HIDOBE-01 experiment:
a) the pebble with smooth surface; b) the pebble with rough surface; b) the pebble with cracks.

The first preliminary conclusion after the visual inspections is that the state of irradiated beryllium samples from HIDOBE-01 is quite satisfactory but separate irradiated pebbles have surface changes such as rough relief or sometimes cracks.

Future activities:

The main part of the PIE HIDOBE-01 will be performed in 2011. Continuation of measurements as referred to above:

- tritium release tests using the new mass-spectrometer from MKS which will be installed in the tritium desorption device at the Fusion material laboratory (FML) on first half of 2011;
- microscopy investigations by OM, SEM and TEM (with the new 200 kV high resolution transmission electron microscope for investigation of radioactive materials down to atomic scale);
- creep tests of individual pebbles at temperatures equal to irradiation temperatures.

Staff:

P. Barié
V. Chakin
J. Ehrmann
A. Erbe
M. Gilpert
M. Holzer
H. Jackisch
M. Klimenkov
P. Kurinskiy
S. Lautensack
G. Mangei
A. Moeslang
H. Ries
M. Rietschel
G. Rösch
R. Rolli
I. Sacksteder
R. Schmidt
H.-C. Schneider
H. Steinle

Literature:

[1] V. Chakin, A. Moeslang, P. Kurinskiy, R. Rolli, H.-C. Schneider, E. Alves, and L.C. Alves, Tritium permeation, retention and release properties of beryllium pebbles, Proceedings of 26th Symposium on Fusion Technology, 27 September-1 October 2010, Porto, Portugal, to be published in Fusion Engineering and Design, 2011.

[2] P. Kurinskiy, A. Moeslang, V. Chakin, R. Rolli, E. Alves, L.C. Alves, Ch. Dorn, and A.A. Goraieb, Comparative study of fusion relevant properties of $Be_{12}V$ and $Be_{12}Ti$, Proceedings of 26th Symposium on Fusion Technology, 27 September-1 October 2010, Porto, Portugal, to be published in Fusion Engineering and Design, 2011.

Acknowledgement

This work was supported by Fusion for Energy under the grant contract No. F4E-2009-GRT-030(PNS-TBM) - Action 3 - with collaboration by NRG Petten, The Netherlands; ITN Sacavém, Portugal and ISSPI, Riga, Lativa. The views and opinions expressed herein reflect only the author's views. Fusion for Energy is not liable for any use that may be made of the information contained therein.

Study of the Impact Caused by the Implementation of Mitigation Means for ITER TF TBM-induced Ripple on TBMs Design (F4E-2009-GRT-037 (PNS-TBM))

EUROFER, the selected structural material for both the EU TBMs (the Helium Cooled Lithium Lead, HCLL, and the Helium Cooled Pebble Bed, HCPB), is a Ferritic Martensitic (FM) steel that shows “soft” magnetic properties with a residual magnetisation of about 3.5 A·m2/kg at the TBM operational temperatures. This material has an effect on the surrounding magnetic field producing local distortions of the magnetic lines. Recent preliminary studies have envisaged that the present configuration of the TBMs in an ITER equatorial port could cause Toroidal Feld ripples incompatible to the plasma operation objectives. The dimensions of the ripples increase with the EUROFER mass in the port and decrease with the distance of this mass from the plasma surface. Also if at the present the correlation between ripple dimensions and effect on plasma performances is not known well, mitigation actions have been proposed by ITER based on a drastic reduction of the EUROFER mass per TBM (down to 650 kg from the present 1.3-1.4 t) and simultaneously a TBM recession to 350mm (from the present 50mm).

The Contract for the Grant F4E-2009-GRT-037 was signed 12 February 2010 and started on 1st March 2010 for a foreseen duration of 4 months. The objective of this F4E Grant was to evaluate in the EU TBM Project (and in the other TBMs of the international Test Blanket Programme in ITER) the impact of these proposed counter measurements on the design feasibility and on the testing programme of the ongoing design of the TBM.

In the first part of the work, the HCLL (CEA) and HCPB (KIT) design group prepared jointly a proposal of TBM configurations (at conceptual level) that comply with the Grant objectives. The proposal was discussed and agreed with F4E during a dedicated meeting. In the second part the identified configurations were assessed by TBM-CA experts according to: ITER integration, design functionality (change in cooling, breeding performances, etc.), achievement of test objectives, and manufacturing issues. A presentation detailing the main outcome of the study was prepared on the basis of the agreed proposal for TBM configurations for both concepts. After acceptance of F4E the beneficiaries attended the workshop organised by ITER (“Workshop on TBM Impact on ITER plasma physics and potential countermeasures”, Cadarache 13-15 April 2010); in this meeting a presentation with the title “Assessment on effect of “reduction” and “recession” in the EU TBM design “ was presented by L.V. Boccaccini.

So for this Grant an assessment has been carried out examining the impact of the proposed counter measurements proposed by ITER in term of reduction of FM steel amount and increasing of the recession on a selected number of possible configurations. The main result of this assessment shows that the full acceptance of the ITER proposal makes the present EU strategy of TBM testing questionable in term of reduction of the objectives. In particular the proposed recession produce in the analysed configurations a large reduction of the operational parameters (i.e. heat and T production). It has been shown that to preserve the main important objectives of the test in the Breeding Zone key elements are to keep a large test volume and the relevance of the main operational parameters (e.g. level of temperatures). If in the future these counter measurements will be unavoidable, it means that a deep revision of the present strategy should be performed.

Also if the scope of the report was not to fix an alternative strategy, some points of it have been already identified: in particular it is suggested to look at a combination of different modules in order to cover separately the items of the testing programme. Together with “reduced” full FM module, it seems unavoidable to introduce also partial or full austenitic module with the scope to save test volume and relevance of test parameters. In this case the related technology for austenitic steel in TBM application has to be developed.

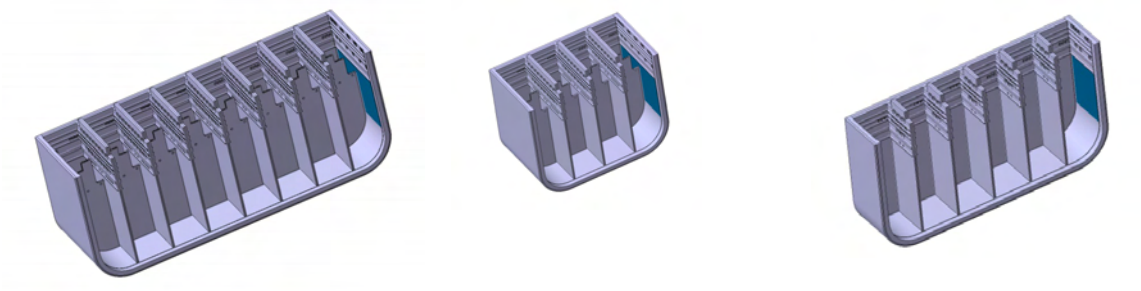

TBM (8x2), full scale. TBM (4x2), reduced TBM (6x1), reduced

Fig. 1: Different TBM configurations considered in the assessment.

Staff:

L.V. Boccaccini
F. Cismondi
U. Fischer
E. Magnani
I. Maione
C. Mistrangelo
J. Rey
A. Simakov

List of CEA Contributors:

G. Aiello
F. Gabriel
L. Forest
G. Rampal
J-F. Salavy

Acknowledgement

This work was supported by Fusion for Energy under the grant contract No. F4E-2009-GRT-037 (PNS-TBM).with collaboration by CEA, France. The views and opinions expressed herein reflect only the author's views. Fusion for Energy is not liable for any use that may be made of the information contained therein.

Goal Oriented Training Programme “Breeding Blanket Developments for Fusion Reactors” (WP08-GOT-EUROBREED (FU07-CT-2008-00047))

The EUROBREED network is integrating almost all of the important aspects of the breeder blanket programme including development of breeder materials, characterisation and modelling of properties (e.g. thermo-mechanics and tritium release), test of these materials in out-of-pile and in-pile experiments, integration of them in ITER, and also some aspects for the integration in the future DEMO reactor. Thus, the broad range of competences required in the European breeder development in the future is addressed, and the proposed project will provide a significant and necessary improvement in the expert basis required.

EUROBREED, jointly conducted by KIT, AEUL, CEA, CIEMAT, ENEA, FOM-NRG, HAS-University of Budapest, and CCFE, consists of eight work packages (WP). Two of them are hosted at KIT (WP1 and WP2): WP1 is entitled “Design, procurement and test of solid breeder units” and WP2 “Pebble bed development and testing for the EU solid breeder blanket”. Furthermore KÍT is in charge of the Coordination of this network.

In 2010 the activities related to EUROBREED network continued regularly for the second year. Progress meeting were held in Riga (May) and Budapest (November) with presentation of the work by all the trainees, presentation and visit of the host laboratory and Meeting of the Coordination Board. In particular a coordinated participation to the SOFT-2010 of EUROBREED has been organised successfully. Each trainee presented a poster under the logos of EUROBREED in the normal poster sessions of SOFT and an additional poster was prepared by the management to present the entire network, the same posters were presented during a special poster session dedicated to the EFDA Goal Oriented Programme (Monday, 27th September) and a presentation on the network was held by the EUROBREED coordinator [1] to a satellite meeting on 29th September also in the EFDA GOTP framework.

In **work package No. 1**, the technical programme of the trainee consists of three parts: (1) the design and analyses of a TBM Breeder Unit (BU), (2) fabrication, procurement and assembly of a BU mock-up and (3) testing of the BU mock-up. The three years long training period started on the 24th of August 2009.

Within part 1 the trainee started working on the BU reference design given in [2], [3], [4]. The first task of the trainee consisted in improving the helium coolant mass flow distribution in the BU’s Cooling Plates. This has been done by means of detailed CFD analyses. As the mass flow of the He coolant through the cooling channels of the Cooling Plates was not homogeneous the trainee proposed an optimization of the distributor’s back plate geometry. Several geometrical configurations have been proposed, resulting in a final considerable improvement of the mass flow distribution in the BU’s Cooling Plates. Final results of the fluid dynamic studies have been obtained early in 2010 and have been used as input for the thermal analyses of the BU. The second task within part (1) consisted in the determination of the temperature field in the BU Eurofer structure (finite element analyses by means of Ansys 12.0). The FE element computations have been carried on in collaboration with the Budapest University of Technology: the trainee was supported by a CFD model realised in Budapest providing the boundary conditions to be used for the thermal analyses. The temperature field on the BU’s Cooling Plates and radial manifold plates is shown in Figure 1: a hot spot (at 560,9°C) is present in the bottom corner of the U-bended lateral wrap. Taking into account the conservative approach adopted, the results of the thermal analyses are satisfying and the design proposed is considered as basis for the structural design assessment. Fluid dynamic and thermal analyses of the have been presented by the trainee at the SOFT Conference 2010 in Porto [5].

The final results of the thermal analyses have been obtained in September 2010: the trainee has then started structural analyses of the BU, calculating Primary and Secondary stresses fields under steady state conditions. The assessment of the structural design with respect the

Codes and Standard (done in November 2010) has shown a good overall behaviour of the BU, although some design optimization must be implemented in order to solve some local issues (high peak stresses are observed in a few junctions and transition regions in the geometry).

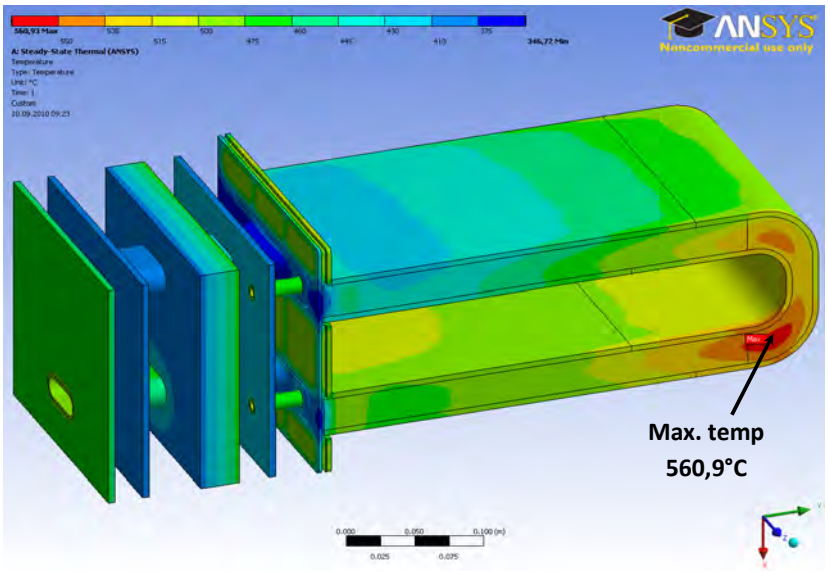

Fig. 1: Temperature field on the BU Eurofer structure.

Within part (2), build to print drawings of the BU CPs have been compiled. The trainee has been involved in the activity of the fabrication team for the preparation of the mock-ups aimed at qualifying the manufacturing process.

A short mobility of 2 weeks took place in November 2010 in NRG facilities in Petten. The goal of this mobility was to introduce and teach the trainee to in-pile testing technologies and instrumentation techniques and to consolidate the trainee knowledge on the Breeder Blanket development Programs for DEMO.

The trainee attended courses on CFD and CAD tools (Ansys CFX, ICEM-CFD and CATIA), as well as in Fusion Technologies (Lectures at the KIT Campus Süd on Fusion Technologies).

In **work package No. 2**, the technical programme of the trainee consists of three parts: the fabrication and characterization (1) of lithium orthosilicate pebbles as ceramic breeder and (2) of beryllium/beryllium alloy pebbles as neutron multiplier, and (3) the experimental testing of TBM Breeder Unit (BU) mock-ups in collaboration with WP 1.

Within part 1 the trainee for WP 2 was responsible for selected tasks of the development of ceramic breeders. He supervised the investigations aiming at a modified melt-based process for lithium orthosilicate pebbles and was in charge for the quality control of the produced pebbles. The influence of several process parameters such as pressure, cooling conditions and drop height on the pebble properties was investigated. While short drop heights were realized by a rapid quenching of the droplets/pebbles in a cooling media, the pebbles were cooled in air for extended drop heights up to 14 m. It was found that a rapid quenching in a cooling media increases the tendency to crack formation in the pebbles. On the other hand, extended drop heights and a moderate cooling of the pebbles seem to give rise to smaller grains or dendrites (Figure 2). With increasing drop heights an increasing crush load of the pebbles were achieved [6]. As unexpected corrosion phenomena inside the Pt-alloy crucible hampered the feasibility study and a systematic investigation of the process parameters, the activities were extended to corrosion studies of alternative crucible materials [7]. This part of the technical programme was finished in September 2010.

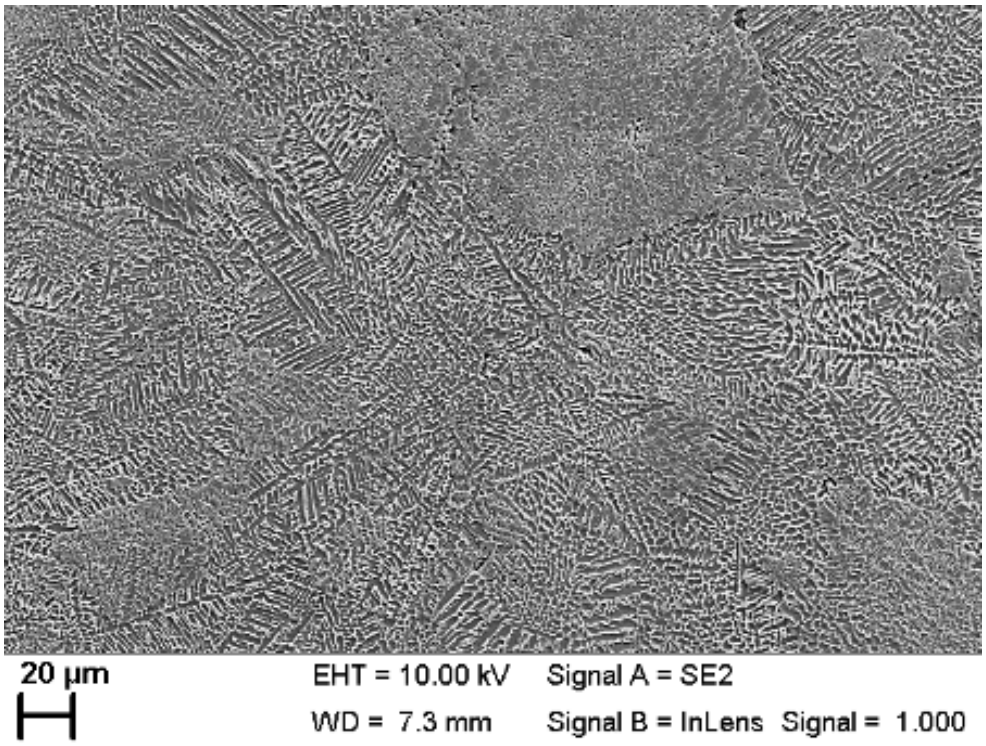

Fig. 2: Characteristic microstructure of a pebble with small dendrites, fabricated with a drop height of 14 m (etched cross-section, SEM).

During a two-month research visit at NRG, Petten, the work of the trainee was focused on post-irradiation examinations and tritium release investigations of ceramic breeder pebbles [8]. In part 2 of the technical programme, the trainee started to work on the fabrication and characterisation of neutron multipliers. As intended in the training programme, the trainee also attended various training courses, which covered technical and management issues, as well as topics to further improve the soft skills of the trainee.

Staff:

L.V. Boccaccini
F. Cismondi
U. Fischer
M. Henn
F.A. Hernández González (trainee, WP 1)
R. Knitter
M. Kolb (trainee, WP 2)
A. Möslang
D. Radloff

Literature:

[1] L.V. Boccaccini and the EUROBREED Team, Status of the EFDA Goal Oriented Training Programme EUROBREED, presentation to the EFDA GOTPs Satellite Meeting at the SOFT-2010 in Porto (September 2010)

[2] F. Cismondi, S. Kecskés, M. Ilic, G. Légrádi, B. Kiss, O. Bitz, B. Dolensky, H. Neuberger, L.V. Boccaccini, T. Ihli, Design update, thermal and fluid dynamic analyses of the EU-HCPB TBM in vertical arrangement Fusion Engineering and Design 84, 607-612 (2009).

[3] F. Cismondi, J. Rey, A. von der Weth, S. Kecskés, H. Neuberger, M. Ilic, O. Bitz, L. V. Boccaccini, T. Ihli, Design update and mock-up test strategy for the validation of the EU-HCPB-TBM concept, Fusion science and technology (2009), vol. 56, no 1 (551 p.).

[4] F. Cismondi, S. Kecskés, P. Pereslavtsev, E. Magnani, U. Fischer Preliminary thermal design and related DEMO relevancy of the EU-HCPB TBM in vertical arrangement Fusion Engineering and Design 85 (2010) 2040–2044

[5] F. Hernandez et al., Fluid dynamic and thermal analyses of a HCPB TBM Breeder Unit mock-up, SOFT 2010, to be published in Fusion Engineering and Design

[6] M. Kolb, R. Knitter, U, Kaufmann, D. Mundt, Enhanced fabrication process for lithium orthosilicate pebbles as breeding material. 26th Symp. on Fusion Technology (SOFT 2010), Porto, P, September 27 - October 1, 2010, to be published in Fus. Eng. Des.

[7] U. Kaufmann, M. Kolb, R. Knitter, Die chemisch-thermische Beanspruchung von Platinwerkstoffen durch lithiumreiche Silikatschmelzen. In: Kneissl, A. [Ed.] Fortschritte in der Metallographie : Berichte der 13. Internat.Metallographie-Tagung, Leoben, A, Sept. 29 – Oct. 1, 2010; Frankfurt: MAT-INFO, Werkstoff-Informationsges., Praktische Metallographie: Sonderbd. 42 (2010) 43-48.

[8] S. Van Til, M. Kolb, A.J. Magielsen, R. Knitter, Irradiation of lithium orthosilicate in the high flux reactor in Petten for the fusion fuel cycle. 1st Internat. Conf. on Materials for Energy, Karlsruhe, Jul. 4-8, 2010

Acknowledgement

This work, supported by the European Communities under the contract of Association between EURATOM and Karlsruhe Institute of Technology, was carried out within the framework of the European Fusion Development Agreement. The views and opinions expressed herein do not necessarily reflect those of the European Commission.

Goal Oriented Training Programme “Power Supply Engineering” (WP08-GOT-PSE (FU07-CT-2009-00084))

The Power Supply Engineering plays an important role in the design, operation and exploitation of the fusion experimental devices and relevant test facilities. The role of the power supply engineers in this sense is a key role, as the power supplies are active devices which can be designed, optimized and upgraded to satisfy the requirement. These are the power supply engineers needed for ITER and to form them in this sense is the main objective of this training program.

The training activities are divided into two main areas:

- General engineering training and experience including personal development.
- Training and experience in specific technical areas to conclude with involvement in and/or management of one or more significant technical projects.

The general training consists mainly of a collaborative training program in coorporation with the participating associations, based on comprehensive set courses and shadowing activities on the operation of the facilities present in each laboratory. In 2010 this encompassed two-week-courses at ENEA Frascati, Consorzio RFX in Padova and Tore Supra in Cadarache where the respective fusion reactors and power supplies have been studied. Besides this, basic knowledge about fusion technologies has been gathered at the 4th Karlsruhe International School on Fusion Technologies.

The specific training consists of practical work experience at the HELOKA-HP (Helium Loop Karlsruhe – High Pressure” experimental facility). The object of HELOKA-HP is to test the HCPB-blanket concept and to gain experience in operating such kind of helium facilities. In this sense it also acts as a prototype for the ITER helium cooling system.

At the moment the working activities of the training are mainly focussed on the Data Acquisition and Control System (DACS) of HELOKA-HP since most of the power supplies are already in place and operational (see Fig. 1 for an overview of the power supply system). Following the build-up of HELOKA-HP, the DACS is being realized in three stages. A short description of each stage and the contributed work done in the frame of this programme is outlined below:

- Stage I went in operation in 2009; it is dedicated to the control of the basic water cooling system. A revision of the alarms and the FSM control approach was done in preparation for the next stage; the completion of this work will be achieved in 2011.
- Stage II is currently under construction (contract with Siemens started in October 2010) and will integrate the helium loop with all its subsystems (loop instrumentation, turbo circulator, helium supply and heating, vacuum system, mass spectrometer, central interlock and safety system). A lot of design work has been done and at the moment the main activities are the procurement and installation of this stage in collaboration with Siemens AG Karlsruhe; this work is planned to be finished in May/June 2011. In October/November 2010 the following up of the commissioning of the turbo circulator was accomplished in the framework of stage II,
- Stage III will cover the implementation of the TBM test section. Hence, first a suitable heating device for the test object has to be selected. Conceptual design has already started and some work will be done in this respect at the beginning of 2011. Design and integration of Stage III will then cover most of the second half of 2011.

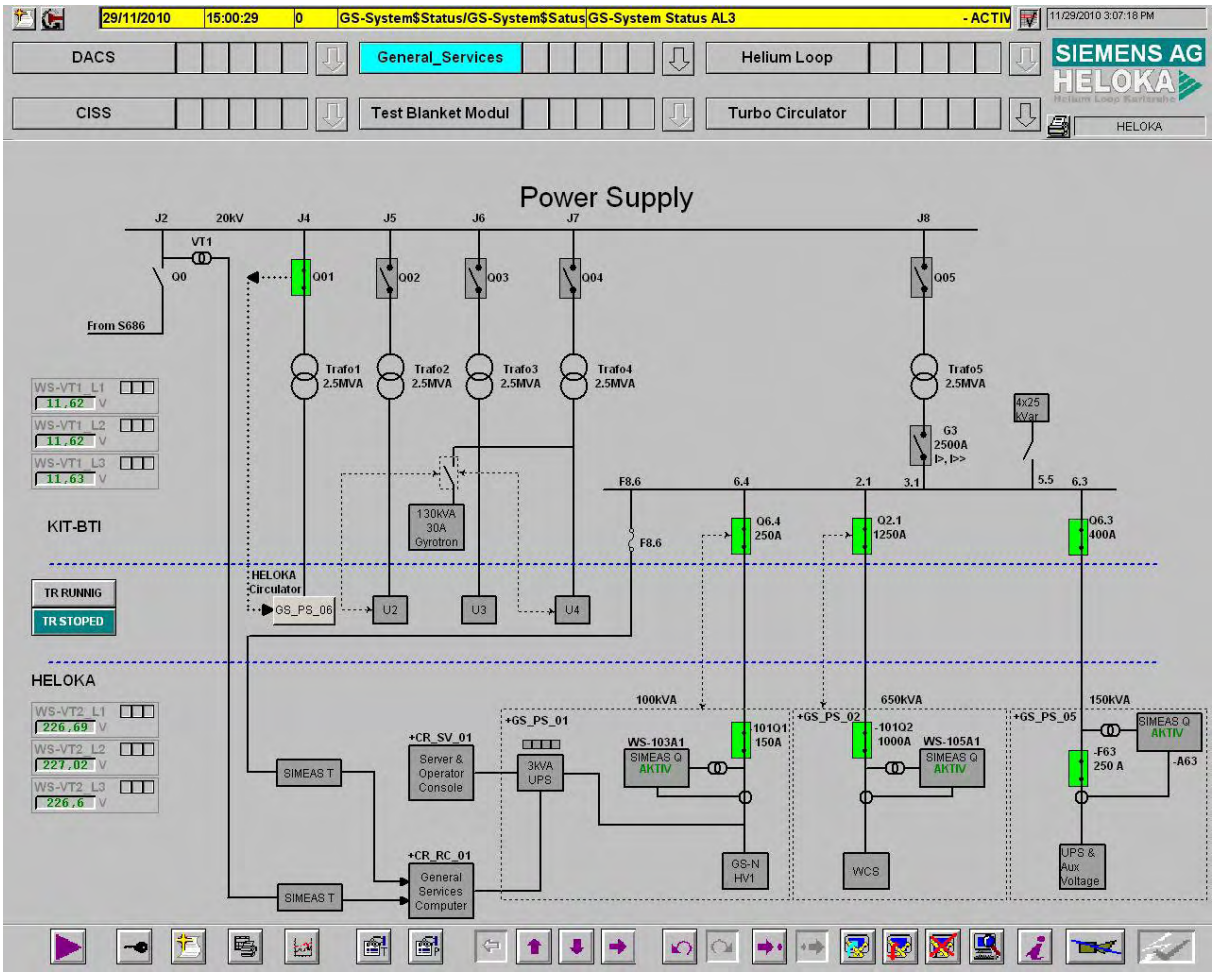

Fig. 1: The HELOKA-HP power supply from the control system view.

Staff:

A. Kunze
V. Marchese
M. Schmid

Acknowledgement

This work, supported by the European Communities under the contract of Association between EURATOM and Karlsruhe Institute of Technology, was carried out within the framework of the European Fusion Development Agreement. The views and opinions expressed herein do not necessarily reflect those of the European Commission.

Modelling of Pebbles and Pebble Beds (CoA)

The crush load distribution of Li_4SiO_4 pebbles has been obtained from experiments. The crush load probability of pebbles and pebble bed are studied using discrete element simulations. A semi-analytical tool has been developed to estimate the probability of crush strength of pebbles based on a critical energy approach.

Crush Tests

Crush tests have been performed on *Li_4SiO_4 pebbles with a custom built expe*rimental set-up. The crush load distribution for a single Li_4SiO_4 pebble for different plates (stiff WC and Compliant Al used for applying the compressive stress) have been obtained as shown in Fig. 1 where the size variation of pebbles is ignored. The geometry investigation of the samples shows that most of the pebbles are spherical and hence the spherical geometry was used through out this study.

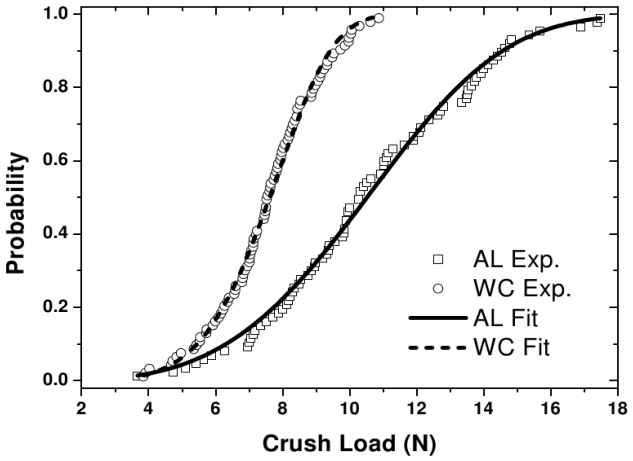

Fig. 2: Crush load distribution for single Li_4SiO_4 pebbles in air.

Stress in Pebbles

An analytical solution for the stresses in an elastic sphere subjected to various loads is developed. The results from the analytical solution for Hertz pressure distribution agrees very well with the FEM simulation where a sphere is compressed by two parallel elastic plates. The analytical solution can also make use of other pressure distributions in a more realistic situation. The numerical evaluation of the solution (see Fig. 2) also shows the influence of coordination number (or number of contact points) N_c on the stress inside the sphere.

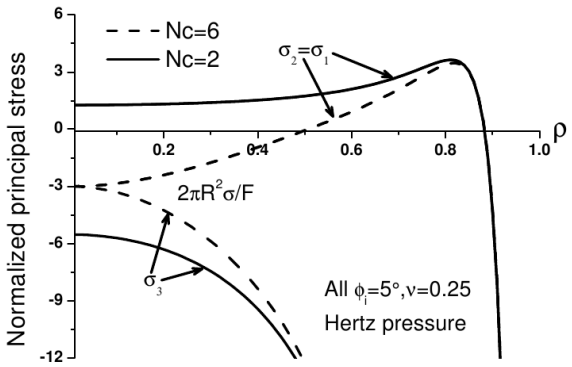

Fig. 3: Normalized stress along the loading axis calculated from the analytical solution for N_c=6 with Hertz pressure.

Pebble strength characterization

A Weibull distribution model in terms of absorbed energy is used to characterize the pebble-pebble contact strength. This model has the advantage of incorporating the influence of coordination number on the pebble strength. The strength distribution of pebbles in a pebble bed is derived using the crush load distribution from fusion materials laboratory (FML) at KIT. This strength will be used as a material constant in DEM simulations for investigating the pebble failure.

Pebble failure

The macroscopic stress-strain response of the pebble bed assembly is investigated while the pebbles in the assembly are assigned with specific critical failure energy. The DEM code developed[1] at KIT was used for the simulations. It is assumed that the pebbles have a spherical shape with an equal radius of 0.25 mm and only elastic deformation of pebbles is taken into account. A periodic boundary condition is used for the assembly of 5000 pebbles. A

pebble is considered to be failed when the absorbed energy (strain energy) is more than its critical failure energy. In the simulation, simply the size of the failed pebble was reduced by a factor *r_* (see Fig. 3) to represent the failure. As a result the failed pebble looses its contact resulting in stress relaxation in the system. Figure 4 shows the stress-strain response of the assembly for different reduction ratios employed for failure characterization. A considerable stress hardening regime can be observed after first pebble failure and with further failure propagation. A reduction ratio of up to 0.85 has significant influence on the stress-strain response while a further decrease in reduction ratio does not show any influence on the behaviour of the system. The simulation is carried out for a packing factor of 63.728% with a coefficient of friction of 0.1 as shown in the figure.

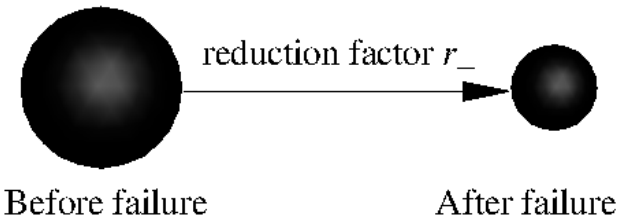

Fig. 4: Schematic showing pebble size reduction during failure.

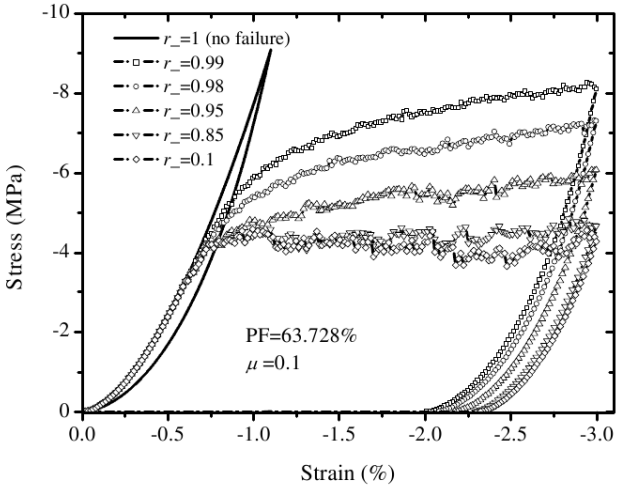

Fig. 5: Influence of reduction ratio on the stress-strain response of pebble bed assembly.

A semi-analytical approach has been developed to find the crush load probability. The probability of absorbed strain energy is found to be

$$P_{\mathrm{e}} = 1 - \exp\left[- (0.340(E_{\mathrm{a}} + 0.809))^{1.61}\right]$$

for uniaxial loading and

$$P_{\mathrm{e}} = 1 - \exp\left[- (0.406(E_{\mathrm{a}} + 0.398))^{1.08}\right]$$

for triaxial loading, where E_a is the absorbed strain energy. The advantage of the analytical solution over the simulations is that it allows us to estimate the failure probability without the need for time consuming simulations for different parameters.

Staff:

M. Kamlah
Y. Gan
S. Zhao
R. K. Annabattula

Literature:

[1] Gan, Y. & Kamlah, M. Discrete element modelling of pebble beds : With application to uniaxial compression tests of ceramic breeder pebble beds. *Journal of the Mechanics and Physics of Solids* **58**, 129-144(2010).

Development of Materials Sciences and Advanced Materials for DEMO (CoA)

Procurement and Quality Control of Lithium Orthosilicate Pebbles – OSi 10

In collaboration with Schott AG, Mainz, the Karlsruhe Institute of Technology is developing and investigating slightly hyperstoichiometric lithium orthosilicate pebbles to be used in the HCPB blanket. The pebbles with a surplus of 2.5 wt% SiO_2 are produced by melting a mixture of $LiOH \cdot H_2O$ and SiO_2 powders and then spraying the liquid material in air. The characteristics of the final product are influenced by the batch wise melt-spraying process, which is rather difficult to control in the small facility. Consequently, the reproducibility from one production run to the other is not very high, and it is therefore necessary to control the quality of each batch of pebbles received from the industrial producer, in order to provide a well-defined standard material in all experimental activities with pebbles or pebbles beds.

In 2010 6.25 kg Li_4SiO_4 (OSi) pebbles were delivered in four batches (OSi 10/1). The pebbles with diameters ranging from 250 to 630 µm were characterised in the initial state according the standard test program for quality control. These four batches feature some differences concerning their properties, especially in the morphology, the SiO_2 excess and the crush loads (Table 1). A survey of the pebble morphology, the microstructure at surfaces and at etched cross-sections for two of the batches OSi 10/1 is given in figure 1. In all batches, but particularly in batch 1, 3 and 4, several pebbles are blistered. At cross-sections the pebbles reveal quite a lot of micro cracks that give rise to differences in the mechanical properties.

Table 1: Physical properties of lithium orthosilicate pebbles OSi 10/1.

Batch	**OSi 10/1-1**	**OSi 10/1-2**	**OSi 10/1-3**	**OSi 10/1-4**
Principal Constituents / wt% (Schott)				
Li_2O	48.48	48.41	48.26	48.42
SiO_2	51.22	51.33	51.40	51.18
excess SiO_2	*2.48*	*2.66*	*2.88*	*2.50*
Size Distribution				
d_{50} / µm	330	320	325	330
He-Pycnometry				
closed porosity (calc.) / %	0.8 ± 0.0	0.8 ± 0.0	0.7 ± 0.0	0.8 ± 0.0
Hg-Porosimetry				
density / g cm^{-3}	2.30 ± 0.02	2.30 ± 0.02	2.30 ± 0.01	2.30 ± 0.03
density / % TD*	95.9 ± 0.8	95.8 ± 0.7	96.0 ± 0.6	95.9 ± 1.0
open porosity / %	3.9 ± 0.2	4.4 ± 0.8	3.9 ± 0.2	3.8 ± 0.2
Pebble Bed Density				
tap density / g cm^{-3}	1.47 ± 0.00	1.47 ± 0.01	1.47 ± 0.01	1.47 ± 0.00
Crush Load Tests				
mean crush load / N (IMF II)	5.8 ± 1.2	6.8 ± 1.6	6.0 ± 1.7	6.3 ± 1.5

* A theoretical density of 2.4 g/cm^3 was assumed for the OSi material.

To investigate the differences in the mechanical stability, for each batch crush load measurements were performed on 40 pebbles. Mean values of 5.8-6.8 N were determined with standard deviations of 1.2-1.7 N. The average crush loads of all samples are consistent with the values determined for former batches, like OSi 07 and OSi 08.

Two types of pebbles - opaque and translucent - are clearly apparent in optical microscopy for all batches, which is exemplary shown for OSi 10/1-1 in fig. 2. The delivered pebbles were screened to a diameter range of 250-630 µm, resulting in fractions with a mean pebble diameter (d_{50}) between 320 and 330 µm for all four pebble batches OSi 10/1 (fig. 3). The maximum of the distribution in each case is asymmetrically shifted to smaller diameters and agrees with the results of OSi 07 and OSi 08.

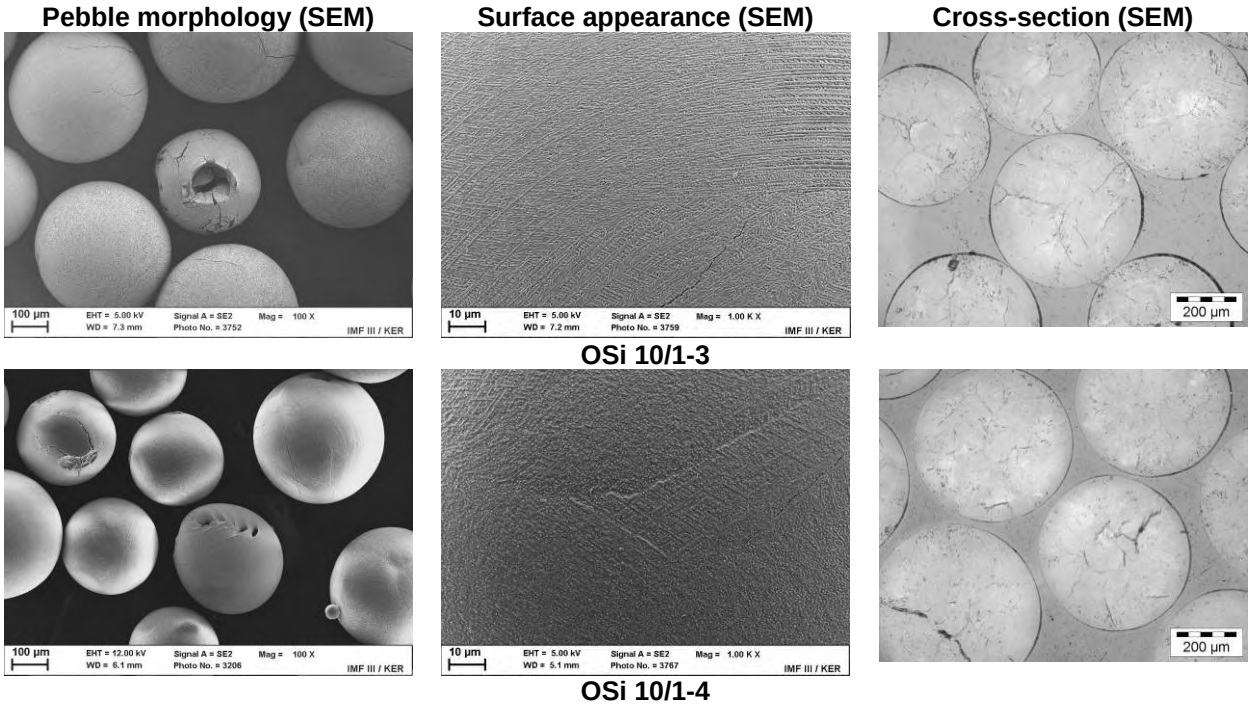

Fig. 1: Morphology and microstructure of lithium orthosilicate pebbles in the initial state.

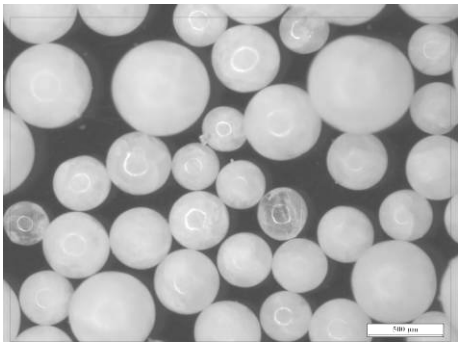

Fig. 2: Pebble morphology of OSi 10/1-1 (OM).

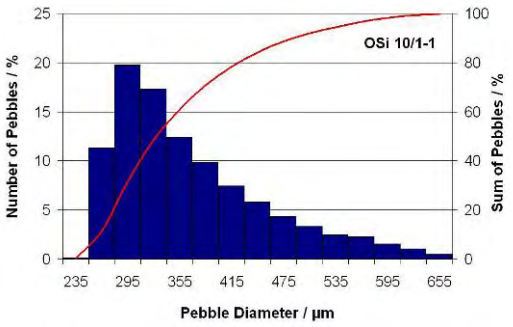

Fig. 3: Diameter distribution of pebbles, exemplary shown for OSi 10/1-1.

Small samples of the lithium orthosilicate pebbles were annealed at 950°C for 1 week under air to obtain the thermodynamically stable phases, lithium ortho- and metasilicate and a homogeneous microstructure in all pebbles. The results obtained for the conditioned pebble batches are summarised in table 2. By thermal annealing, the crush load of the pebbles slightly decreased to 5.2-6.0 N with standard deviations of 0.8-1.2 N. Only batch OSi10/1-2 shows an increased value of 7.7 ± 1.7 N. All pebbles of the examined batches exhibit a homogeneous microstructure after annealing, which is exemplarily shown for the batches 1 and 2 in figure 4. The inferior pebble morphology is still apparent. The expected grains of lithium metasilicate are visible at the pebble surface.

Table 2: Physical properties of lithium orthosilicate pebbles OSi 10/1 cond.

Batch	**OSi 10/1-1-c**	**OSi 10/1-2-c**	**OSi 10/1-3-c**	**OSi 10/1-4-c**
Pebble Bed Density				
tap density / g cm^{-3}	1.45 ± 0.00	1.46 ± 0.01	1.46 ± 0.00	1.45 ± 0.01
Crush Load Tests				
mean crush load / N (IMF II)	5.2 ± 1.0	7.7 ± 1.7	5.6 ± 0.8	6.0 ± 1.2

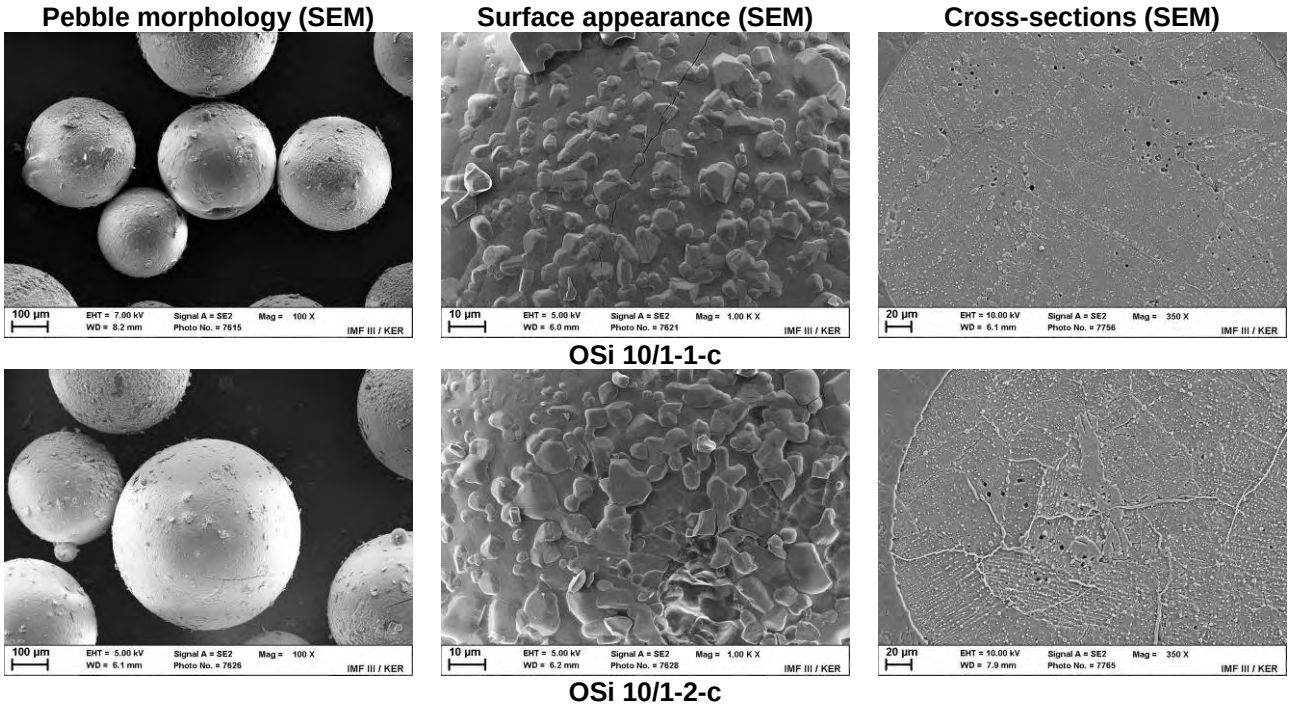

Fig. 4: Morphology and microstructure of lithium orthosilicate pebbles after conditioning.

Production of advanced breeder pebbles by a modified process

As part of the BA DEMO activities a facility was assembled to investigate a modified fabrication process for lithium orthosilicate pebbles [1]. Several batches were fabricated to study the influence of process parameters such as pressure, cooling conditions and drop height on the pebble properties. Figure 5 shows a schematic drawing of the test facility, a view of the triple nozzle experiment, and the resulting pebble spread in an experiment with a drop height of 14 m. The modified process is designed to provide high process control resulting in a narrow size distribution. Yet, it has to be stated that a narrow size distribution cannot be obtained at present, as shown by a typical example in figure 6. The mean pebble size is considerably larger than the mean diameter of lithium orthosilicate produced by SCHOTT (fig. 7). However, the pebbles produced with the modified process show fewer defects than the pebbles produced with the standard process. The investigation of the porosity of the pebbles reveals that they are virtually dense and large pores cannot be observed anymore. The closed porosity is almost 0 % and thus reduced compared to the value of 0.5-1 % of pebbles produced with the standard process [2].

Fig. 5: Experimental setup – test facility (drawing), triple nozzle experiment, and test with a drop height of 14 m.

It was shown that the impurities introduced via the modified process are not significantly higher than the ones introduced in the established process. Nevertheless, corrosion phenomena with the platinum alloy crucible were observed [3], which have to be sorted out during future investigations to achieve a high yield and a narrow pebble size distribution together with high pebble purity.

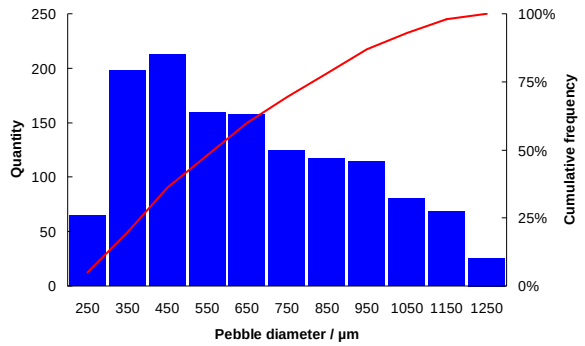

Fig. 6: Size distribution of pebbles, produced by the modified process.

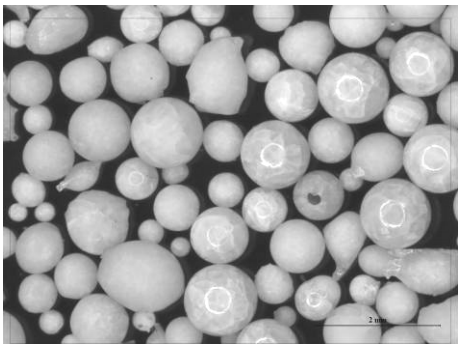

Fig. 7: Morphology of pebbles fabricated with a drop height of 14 m.

The microstructure of the pebbles was observed to be influenced by a variation of the drop height. The typical microstructure of lithium orthosilicate pebbles as known from the standard process was also detected at pebbles made by the modified process with short drop heights, i.e. the pebbles feature large domains of dendritically grown crystals made of lithium orthosilicate, Li_4SiO_4, with lithium orthodisilicate, $Li_6Si_2O_7$, at the grain boundaries (fig. 8). By increasing of the drop height to 3 m and more, it was possible to generate pebbles with much smaller dendritic domains (fig. 9) [2]. These two types of pebbles with small and large dendrites appear in optical microscopy as opaque and translucent, resp. (fig. 7).

Figure 10 shows the influence of drop height on the crush load of 500 µm pebbles. The tendency of crack formation is increased with decreased cooling time. It was found that a rapid quenching of the droplets in a cooling media, i.e. short drop heights, increases the tendency to crack formation in the pebbles. An increasing amount of pebbles without cracks were observed in batches fabricated with extended drop heights and a moderate cooling of the pebbles. A larger drop height leads to higher crush loads in total. An average crush load of 8 N was achieved with a drop height of 14 m (500 µm pebbles). A close connection between crush load and microstructure of lithium orthosilicate pebbles was found, opaque pebbles showed much higher crush loads than translucent ones. However, the reason for the different crystallization behaviour is not yet clear, and a qualified statement of the influence of process parameters on pebble quality is not yet possible.

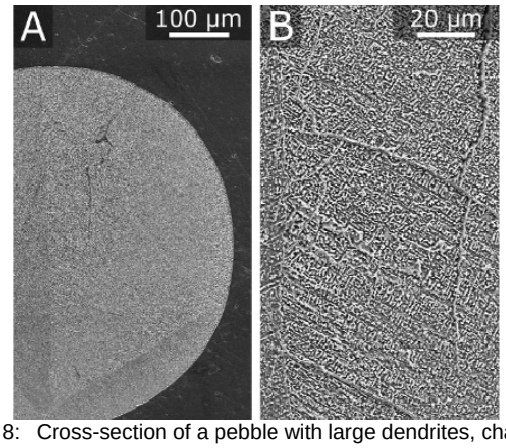

Fig. 8: Cross-section of a pebble with large dendrites, characteristic for small drop heights.

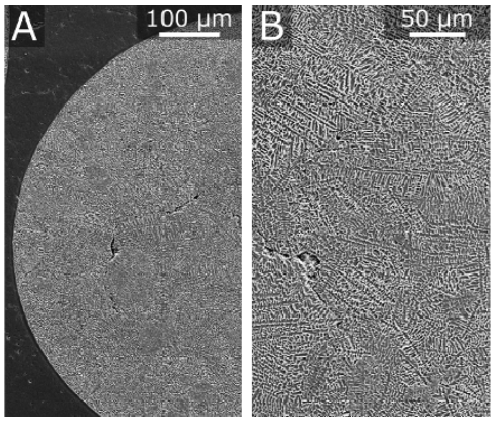

Fig. 9: Cross-section of a pebble with small dendrites, observed with larger drop heights.

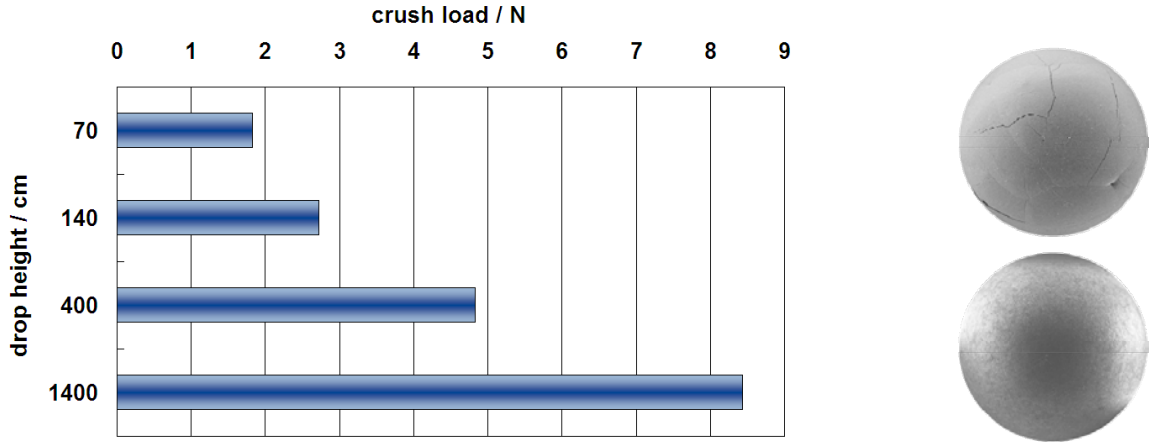

Fig. 10: Influence of drop height on the crush load of 500 µm pebbles. The tendency of crack formation is increased with decreased cooling time.

Staff:

<u>C. Adelhelm</u>
B. Dörzapf
B. Ehlert
U. Kaufmann
<u>R. Knitter</u>
M. Kolb
B. Löbbecke
C. Odemer
M. Offermann
R. Rolli

Literature:

[1] Hayashi, K.; Araki, M.; Baluc, N.; Yamanishi, T.; Nishitani, T.; Hernandez, T.; Morono, A.; Moriani, A.; Tosti, S.; Nozawa, T.; Lindau, R.; Spätig, P.; Tanigawa, H.; Kurinskiy, P.; Nakamichi, M.; Knitter, R.; Hoshino, T., Progress in DEMO R&D activities within the BA-IFERC project. 8th Joint Conf. on Fusion Energy, Takayama, J, Jun. 10-11, 2010.

[2] Kolb, M.; Knitter, R.; Kaufmann, U.; Mundt, D.: Enhanced fabrication process for lithium orthosilicate pebbles as breeding material. 26th Symp. on Fusion Technology (SOFT 2010), Porto, P, September 27 - October 1, 2010, to be published in: Fus. Eng. Des.

[3] Kaufmann, U.; Kolb, M.; Knitter, R., Die chemisch-thermische Beanspruchung von Platinwerkstoffen durch lithiumreiche Silikatschmelzen. In: Kneissl, A. [Ed.] Fortschritte in der Metallographie : Berichte der 13. Internat.Metallographie-Tagung, Leoben, A, Sept. 29 – Oct. 1, 2010; Frankfurt: MAT-INFO, Werkstoff-Informationsges., Praktische Metallographie: Sonderbd. 42 (2010) 43-48.

[4] Abou-Sena, A.; Löbbecke, B.; von der Weth, A.; Knitter, R., Effect of post welding heat treatment of the HCPB TBM on the Eurofer and lithium orthosilicate pebbles. 26th Symp. on Fusion Technology (SOFT 2010), Porto, P, Sept. 27 – Oct. 1, 2010, to be published in: Fus. Eng. Des.

[5] Knitter, R.; Odemer, C., Synthesis of lithium ceramics as tritium breeder materials. 11th Internat. Conf. on Ceramic Processing Science (ICCPS-11), Zürich, CH, Aug. 29 – Sept. 1, 2010.

[6] Van Til, S.; Kolb, M.; Magielsen, A.J.; Knitter, R., Irradiation of lithium orthosilicate in the high flux reactor in Petten for the fusion fuel cycle. 1st Internat. Conf. on Materials for Energy, Karlsruhe, Jul. 4-8, 2010

[7] Zarins, A.; Kizane, G.; Supe, A.; Baumane, L.; Tilika, V.; Pajuste, E.; Knitter, R., Influence of pretreatment of lithium orthosilicate pebbles on radiation stability. 26th Annual Institute of Solid State Physics Scientific Conf., University of Latvia, Riga, LV, February 17-19, 2010.

[8] Knitter, R., Status of lithium orthosilicate pebbles fabricated by melt-spraying. In: H. Tanigawa and M. Enoeda [Eds.], Proc. CBBI-15, JAEA, 2010, 82-100

Support of the EU/RF Collaborative Task on Fabrication of Be Pebbles for Fusion Application and Beryllium Recycling (EFDA/06-1394 - TW6-TTB-RFMON2)

Introduction

Within the frame of the EFDA/05-994 contract with EFREMOV, a collaborative Task on “Fabrication of Be pebbles for fusion application and Beryllium recycling” has been performed. The objective of this activity was the exploration of the possibilities to identify the properties of Be pebbles defined as a base material for application in Solid Breeder Blanket. The different aspects of the fabrication and utilization of the beryllium pebbles with different morphology were investigated. In addition, the particular features of beryllium recycling after operation has been considered and analyzed. The complete Task description is reported in the final EFDA Report. In detail the scope was

- to prepare, check and present input technical information,
- to perform the technical monitoring of a collaborative Task, including participation in the progress meeting(s), analysis of progress reports, orientation of technical activities with regard to the HCPB Project needs,
- to assess the intermediate and final technical reports.

Several progress meetings have been performed, both at KIT and Moscow (Bochvar Institute). The technical part was mainly focused on analysis of capabilities and features of beryllium reprocessing/recycling after operation under neutron irradiation.

Technical achievements

The issues of handling of radioactive beryllium wastes after their use in ITER and DEMO have been disclosed. Different strategies of the disposal/recycling of neutron-irradiated beryllium were proposed and included:

- use of high-purity beryllium
- storage without reprocessing
- partial reprocessing to remote on level
- purification of material to hands on level
- "combined method"

Also, the current status of fabrication and characterization of beryllium pebbles was shown.

<u>Production of Be pebbles</u>

Three batches of beryllium pebbles differing from each other by the sizes of grains (10-30 µm, 30-60 µm and >100 µm) were fabricated and shipped to KIT (former FZK). The weight of each batch was approximately 200 g. Fig. 1 depicts the general view of beryllium pebbles having the grain sizes between 10 and 30 µm.

Due to a final stage of fabrication which includes fragmentation and attritioning or ball milling of beryllium blocks/ingots, all three batches of beryllium pebbles have potato-shaped form with sizes ranging from 0,8 mm up to 1,2 mm. Schematically, the process of fabrication of Be pebbles can be summarized as follows:

- Preparation of Be billets by Vacuum Hot Pressing (grain 10-30 µm and 30-60 µm) and Be ingots by melting (>100 µm), followed by
- Fragmentation by press equipment, followed by

- Disk attritioning or ball milling, followed by
- Sieving (+0,8 -1,2 mm).

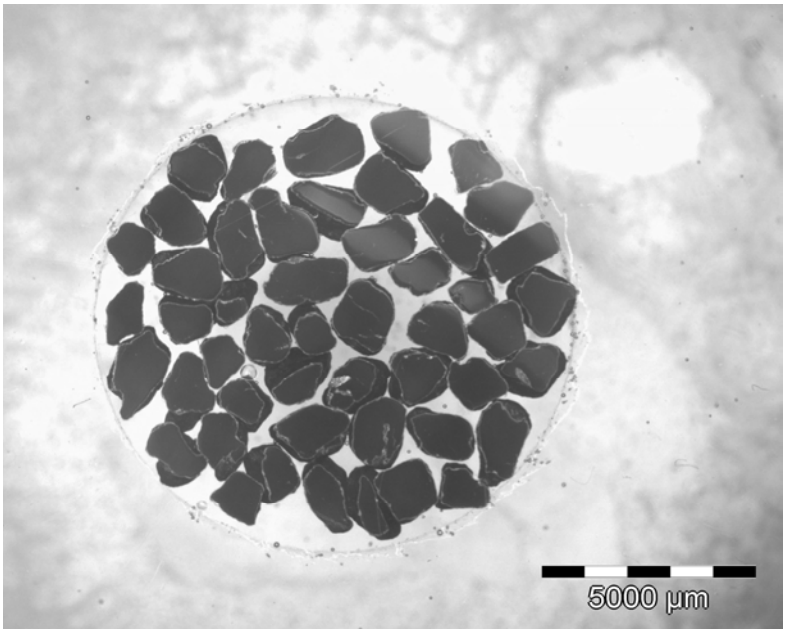

Fig. 1: Be pebbles with grain size of 10-30 µm.

The typical view of the pebbles' shapes (grain sizes 10-30 µm) caused by the attritioning is shown in Fig. 2.

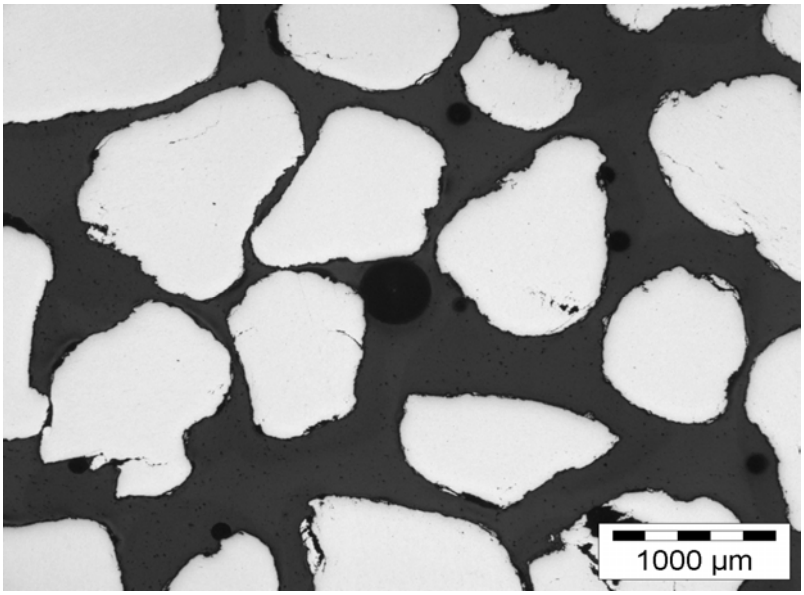

Fig. 2: Optical microscopy (reflected light) of Be pebbles.

Beryllium billets or ingots were used as initial materials for the fabrication off all three batches of beryllium pebbles. The microstructure of hot-pressed beryllium billet which was used as an initial material for the production of beryllium pebbles with the grain sizes of 30-60 µm is shown in Fig. 3.

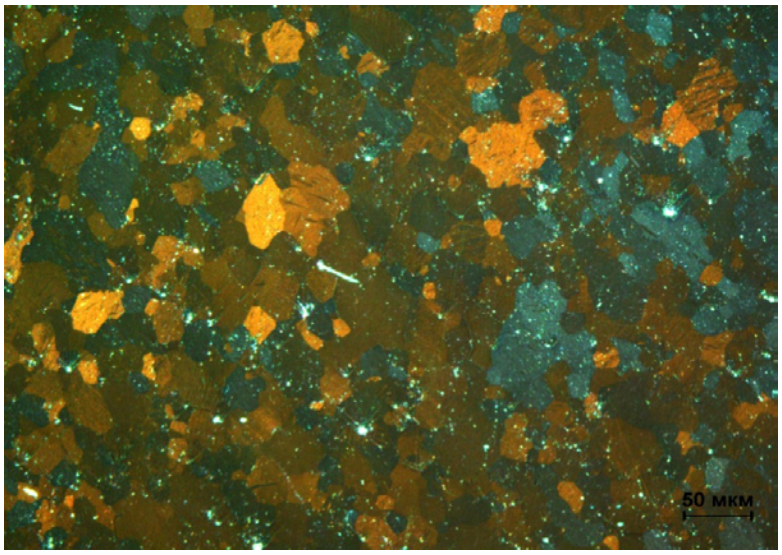

Fig. 3: Microstructure of hot-pressed beryllium billet (grain sizes 30-60 µm).

Investigations of microstructure and chemical composition of Be pebbles

A preliminary characterization of the fabricated beryllium pebbles was performed by means of optical microscopy. Fig. 4 shows the microstructure of Be pebbles having the grain sizes of 10-30 µm. The information relating to weight contents of highly-activated elements (e.g., iron) is an important factor which influences further use and disposal of beryllium products in ITER and DEMO. Therefore, the impurity content of beryllium pebbles was measured for the batches with the grain sizes of 10-30 µm and more than 100 µm (Table 1).

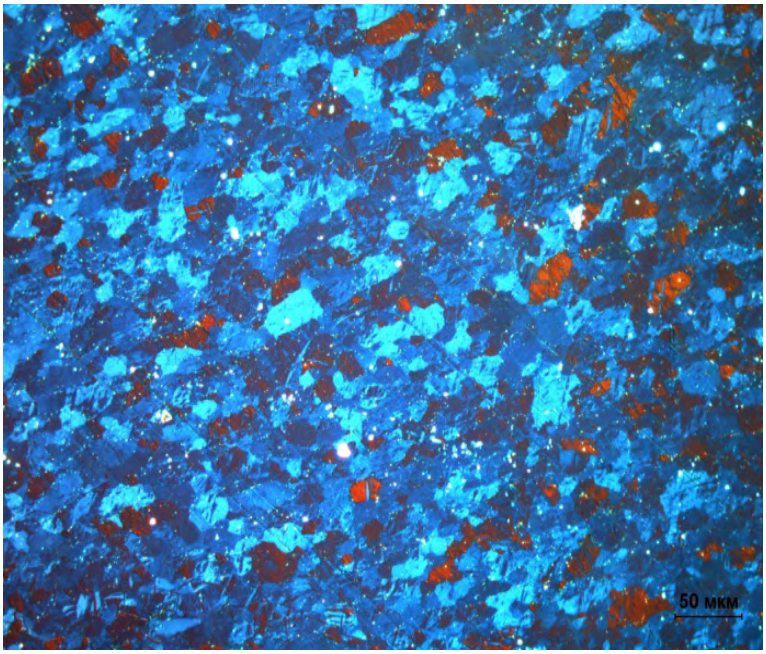

Fig. 4: Microstructure of Be pebbles with grain sizes of 10-30 µm.

Table 1: Impurity content of Be pebbles with grain sizes of 10-30 µm and >100 µm.

Grain size of pebbles	Fe	Si	Al	Cr	Cu	Ni	Ti	Pb	Mn	Mg	Ca
>100 µm	0.044	0.028	0.0096	0.015	0.0038	0.034	0.0019	<0.001	0.0017	0.0011	0.008
10-30 µm	0.056	0.023	0.017	0.022	0.038	0.005	0.0073	<0.001	0.0022	0.0031	0.005

Measurements of packing density and pebble size distribution

The value of the packing density of beryllium pebbles is needed for the design of tritium breeding module (TBM). The estimated packing density of beryllium pebbles after vibration was equaled to 1,12 g/cm^3 and 1,16 g/cm^3 for the batches with grain sizes of 10-30 µm and more than 100 µm, respectively. The batch Be pebbles with grain sizes exceeding 100 µm have following dimensions:

- 80% of pebbles are in the range between 0,8 and 1,2 mm
- 13% of pebbles are bigger than 1,2 mm
- 7% of pebbles are smaller than 0,8 mm.

For 85% of total amount of Be pebbles (grain size >100 µm) the maximum size/minimum size ratio corresponding to a single pebble is less than 1,5.

Beryllium recycling/reprocessing after operation under neutron irradiation

Presently, beryllium is considered as a base material for neutron multiplier of breeding blanket of future commercial power thermonuclear reactors, similar to the DEMO reactors. Beryllium becomes radioactive when interacting with the neutrons formed in the cores of nuclear and thermonuclear reactors. Due to swelling and/or cracking caused by accumulation of helium in beryllium during irradiation, beryllium components need to be regularly replaced during operation and after decommissioning of a reactor. Used/spent beryllium is to be recycled or disposed. This poses an environmental hazard, especially in the case of future thermonuclear power industry dealing with rather high amount of beryllium used (12.5 tons in the first wall of the ITER reactor and more than 300 tons in a ceramic blanket of the DEMO reactor).

Therefore, the minimization of radiotoxicity and amount of the waste sent for geological disposal requires development of effective methods for reprocessing and recycling of spent beryllium in the nuclear fuel cycle. The reprocessing and recycling of beryllium in the nuclear fuel cycle will permit to reduce accumulation of radioactive and toxic waste, decrease costs of the waste management and reduce scope of primary reprocessing of scarce resources in the course of production of new materials.

In spite of the fact that traditionally beryllium is referred to the class of weakly activated materials, however, impurities available in commercial beryllium create a considerable radioactivity in it. Issues of reprocessing of irradiated beryllium were not seriously considered in the past due to several reasons:

- its insignificant radiation danger, compared to fuel or other structural materials, used in nuclear reactors,
- sufficiently limited amount of beryllium wastes due to a comparatively high operational resource of beryllium components.

Immediately after irradiation in a thermonuclear reactor, beryllium would be referred to the class of highly active wastes (**HLW – High Level Waste**), the cost of which burial is high. The reason for this are the impurities in the Beryllium. For transition of beryllium wastes into the status of a usual substance (**Hands on level**) 70 to 100 years are required after their use in ITER and more than 10000 years after the use in DEMO. However, the **Low Level Waste (LLW)** criterion that is needed for recycling would be achieved already after short time of dismantling, depending on the impurities.

Fabrication of three batches of Be pebbles with different grain sizes

Beryllium pebbles with three different grain sizes were fabricated using beryllium billets or ingots as initial materials. It is notable that the initial beryllium blocks (ingots or billets) already have known grain sizes which will not be changed during further cold-working of material. Fragmentation by the press equipment and further attritioning by the ball mill or disk attritor lead to potato-shaped form of the obtained pebbles. Also, possible surface contamination of Be pebbles during their grinding should be taken into account.

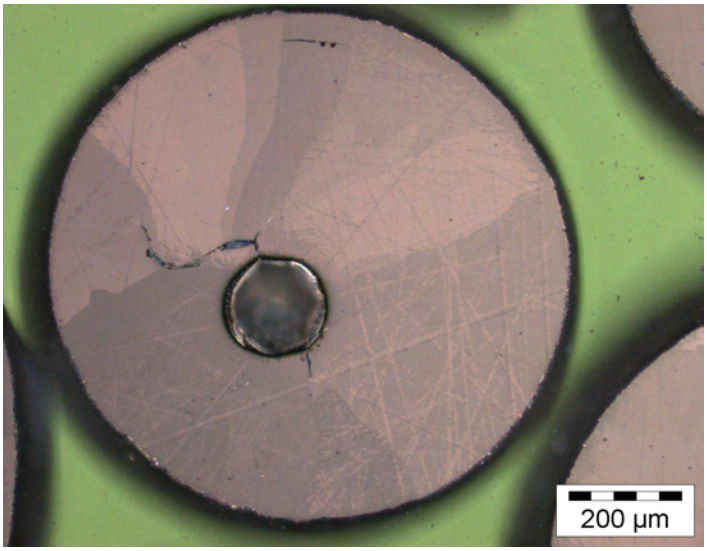

Fig. 5: Microstructure of 1 mm pebble produced by NGK, Japan.

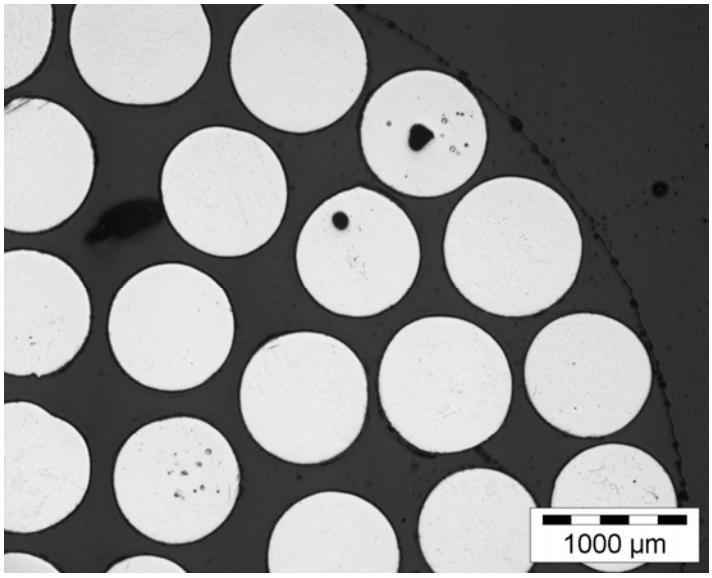

Fig. 6: Several Be pebbles produced by NGK in reflected light (optical microscope).

Presently, 1 mm beryllium pebbles produced by Rotating Electrode Method (REM) at Company NGK are considered to be the main candidate materials for the neutron multiplier in Helium Cooled Pebble Bed in ITER. The optical micrograph of 1 mm beryllium pebble in polarized light is shown in Fig. 5. The pebble consists of only few grains which are oriented from central zone to periphery what is determined by the direction of a rapid solidification from Be melt. Fig. 6 depicts several polished Be pebbles (in reflected light). It is obvious that some of the pebbles have pores in the central part. This factor can have some negative influence on the further use of these pebbles in the thermonuclear reactor: pores in the central zone of pebbles can initiate the material failure under neutron irradiation at blanket-relevant temperatures.

The characteristics of tritium retention and release of materials of TBM depend on the properties of microstructure and, in particular, on the sizes of grains. One can conclude that this method of fabrication of beryllium pebbles with the "controlled" sizes of grains in the material bulk is of a great interest. The disadvantage of Be pebbles fabricated by attritioning/ball mil-

ling is their non-spherical shapes what should be taken into account. However, the fabrication of Be pebbles with the grain sizes ranging 10-30 µm and 30-60 µm excludes the use of the high-cost melting process of material which needs the implementation of additional safety requirements. Therefore, further investigation of fusion-relevant properties of obtained Be pebbles is suggested.

Evaluation of the fabrication of the three batches of Be pebbles with different grain sizes

Three batches of Be pebbles with different grain sizes (10-30 µm, 30-60 µm and >100 µm) fabricated by means of attritioning/ball milling of Be billets or ingots were shipped to KIT. The weight of each batch equaled to approximately 200 g. The characterization of the Be pebbles included:

- Optical microscopy of produced Be pebbles (grain sizes 10-30 µm and 30-60 µm)
- Measurement of chemical composition of Be pebbles (grain sizes 10-30 µm and >100 µm)
- Preliminary evaluation of the packing density of Be pebbles (grain sizes 10-30 µm and 30-60 µm)
- Measurement of the size distribution of Be pebbles and evaluation of maximum/minimum size ratio corresponding to a single pebble were performed (grain sizes >100 µm)

Despite of the irregular shape, quite high packing densities have been achieved after vibration: 1.12 g/cm^3 and 1.16 g/cm^3 for the batches with grain sized of 10-30 µm and >100 µm, respectively. This is already in the range of packing densities from spherical pebbles produced by REM. However, it is not obvious that the production method of the irregular Beryllium fragments is cost effective and technically scalable to huge quantities.

Conclusions

The Deliverable D4 of the task TW6-TBB-RFMON2 contained:

I. Progress reports and presentations issued by Efremov

II. Minutes of the progress meeting

III. Summary of the main technical results obtained within Efremov contract 05-994/Task 2

IV. Technical assessment of obtained results and consistency with TBM Project objectives

V. Major results:
The results on hot pressed beryllium followed by fragmentation and attritioring have shown among others (i) a confirmation of the nominal grain sizes (10-30µm, 30-60 µm, and >100 µm, (ii) no significant variation of impurity contamination with varying grain size, (iii) and, as expected, a strong influence of impurity content on the decay time of neutron irradiated beryllium. Even the Russian Beryllium with the smallest grain size was much purer than the typical Beryllium quality from other sources. Despite of the irregular shape, the packing density was quite good, namely between 1.12 -1.16 g/cm^3 for the different qualities.

Staff:

V. Chakin
P. Kurinskiy
A. Möslang
P. Vladimirov

Acknowledgement

This work, supported by the European Communities under the contract of Association between EURATOM and Karlsruhe Institute of Technology, was carried out within the framework of the European Fusion Development Agreement. The views and opinions expressed herein do not necessarily reflect those of the European Commission.

Magneto-hydrodynamic Flows in a HCLL Blanket Mock-up (CoA)

Experimental investigations for liquid-metal magnetohydrodynamic (MHD) flows in a scaled mock-up of a helium cooled lead lithium (HCLL) blanket concept have been complemented by additional experiments performed in a spatially varying magnetic field in order to assess to which extent radial variations of the magnetic field, will influence the flow behavior. The results are important because the test blanket module (TBM) will be located in ITER at a position at which the magnetic field is high and non-uniform as shown in Fig. 1.

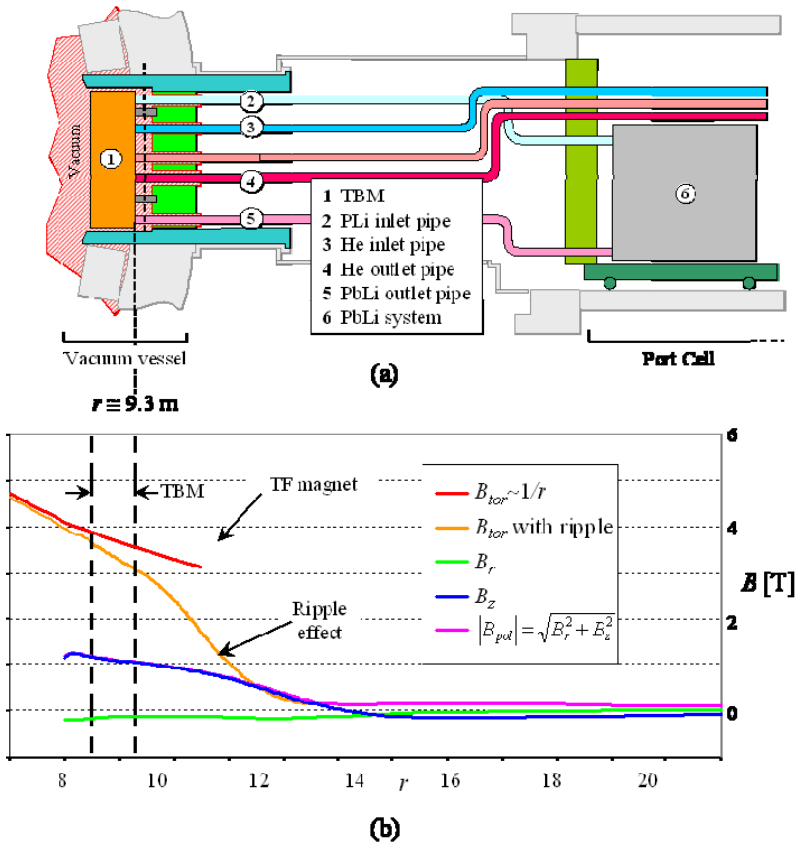

Fig. 1: Position of TBM in ITER. The magnetic field within the TBM varies essentially with radial position.

In previous experiments performed in uniform magnetic fields, typical contributions for the total MHD pressure drop Δp have been identified [1]. It was found that the major ones arise from flows in poloidal manifolds Δp_M and when the fluid passes through narrow gaps at the back plate (BP) Δp_{BP} and at the first wall (FW) Δp_{FW}. In these last experiments these contributions have been recorded together with the local strength of the magnetic flux density B when the mock-up was placed at different axial positions ξ in the dipole magnet of the MEKKA laboratory (see Fig. 2).

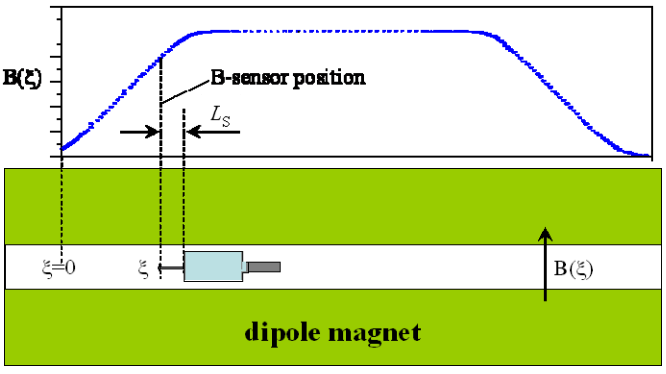

Fig. 2: Position of mock up in the dipole magnet of the MEKKA laboratory. The distribution of the magnetic field is measured by a Hall sensor attached at a distance L_S ahead of the first wall and measured along ξ.

As a result it is found that the major contributions to the pressure drop depend essentially on the local magnetic field strength at the manifold and at the BP. When the test section is

moved along the axis ξ of the magnet, the pressure drops $\Delta p_M(\xi)$ and $\Delta p_{BP}(\xi)$ scale as the square of the magnetic field, taken at the location of the manifold and BP. This is a clear indication for a balance between pressure forces and the electromagnetic Lorentz force, and field gradients seem unimportant. The reason for this behavior is that the radial extent of the manifold and the BP is small so that the field does not vary too much across these elements.

At the gap near the FW the situation appears different. Here a similarly close correlation between $\Delta p_{FW}(\xi)$ and B^2 at the same position cannot be established. Instead one can locate the origin for Δp_{FW} to a position inside the breeder unit, indicating that this fraction of pressure drop is created by large-scale 3D current loops involving some part of the breeder units. Although very interesting from a physical point of view, Δp_{FW} remains small in comparison with pressure drops at pipes, manifolds or BP. First results have been published in [2].

Additional information on MHD flows related to HCLL blankets have been published by the MHD group at IKET in references [3]-[9].

Further development of a numerical code for MHD flow simulations

In the framework of the study of a European helium cooled lead lithium (HCLL) blanket concept for ITER, numerical tools are developed to complement experimental activities. Full capability to simulate numerically the global magnetohydrodynamic flow and pressure distributions resulting from the interaction of the liquid metal with the strong plasma confining magnetic field is not achieved yet. Calculations should support the selection and validation of physical models for 3D coupled phenomena, like magneto-convection, as well as for corrosion and tritium permeation processes. Moreover, simulations help to interpret measurement data and to enhance the development of extrapolation procedures from small-scale experiments to a DEMO reactor.

The description of MHD flows involves the equations of fluid dynamics, the Navier-Stokes equations, stating conservation of momentum and mass, and those of electrodynamics, describing charge conservation, where the current density is given by Ohm's law for moving electrical conductors. These equations have been implemented in the open source code OpenFOAM [10]. A cell-centered (collocated) finite volume method is used to discretize the equations. In these first studies we are mainly concerned with the spatial accuracy of the employed schemes. The spatial discretization is second order accurate [11].

A segregated solver is employed, i.e. the equations are solved one after the other, and for the coupling between pressure and velocity the Pressure-Implicit with Splitting of Operators (PISO) algorithm is used. The electromagnetic force is treated explicitly and defined at cell-centers. The required centroid currents are obtained by interpolation from the face current fluxes using the vector identity $\mathbf{j} = \nabla\cdot(\mathbf{jr})$, where $\mathbf{j}$ is the current density and $\mathbf{r}$ is the distance vector. This current conservative interpolation procedure is crucial for accurate numerical predictions of MHD flows when strong magnetic fields are applied [12].

Simulations of MHD flows in channels with walls of arbitrary electric conductivity can be performed by using two different approaches. One consists of solving the equations for electric potential and electric current both in a fluid and in a solid domain. The solutions are then coupled by implementing suitable boundary conditions to ensure the continuity of wall normal current and electric potential at the fluid-wall interface. The other method is the implementation of the so called thin wall condition [13], which allows determining the wall electric potential distribution from the normal current exchanged between fluid and solid. This approximation assumes that the wall is so thin compared to the characteristic size of the considered geometry that the potential does not vary across it and the current entering the solid domain distributes only in tangential direction. The current entering the fluid is taken from the balance of this tangential current in the wall. The advantage of using the thin wall condition is that the

computational domain extends only up to the fluid-solid interface and therefore no nodes are required outside the fluid region to resolve the wall. This reduces the computational time.

Both these solution procedures have been implemented in OpenFOAM and verified by comparing the numerical results with analytical solutions. As an example let us consider the fully developed MHD flow in a square duct with insulating side walls, parallel to the magnetic field, and Hartmann walls, perpendicular to **B**, of finite electric conductivity for Hartmann number $Ha = 10^4$. This characteristic non-dimensional group gives a dimensionless measure for the applied magnetic field. Numerical results are compared with the analytical solution given in [14]. A particular feature of this flow is the formation of thin high-velocity jets in the boundary layers along the insulating side walls. The proper resolution of these near-wall regions is crucial for the accuracy of the solution. In Figure 3 and Figure 4 the velocity and the electric potential are plotted along the symmetry line on a plane perpendicular to **B**. The symbols indicate the numerical results and the solid line the analytical solution. In the fluid domain the employed mesh is refined near the wall to suitably resolve the boundary layers.

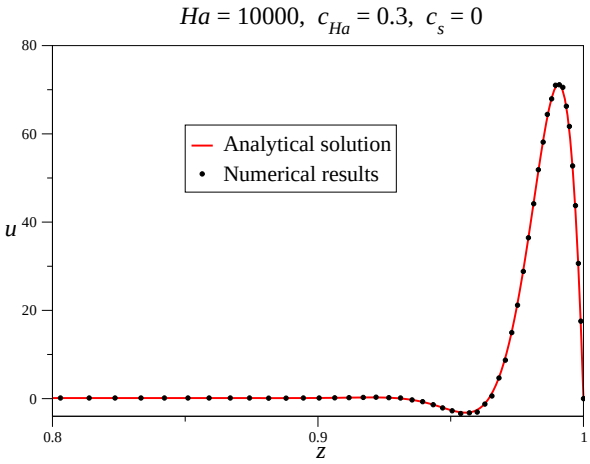

Fig. 3: Comparison between analytical (solid line) and numerical (symbols) solution for axial velocity along the symmetry line perpendicular to B in a duct with insulating side walls and conducting Hartmann walls at $Ha = 10^4$.

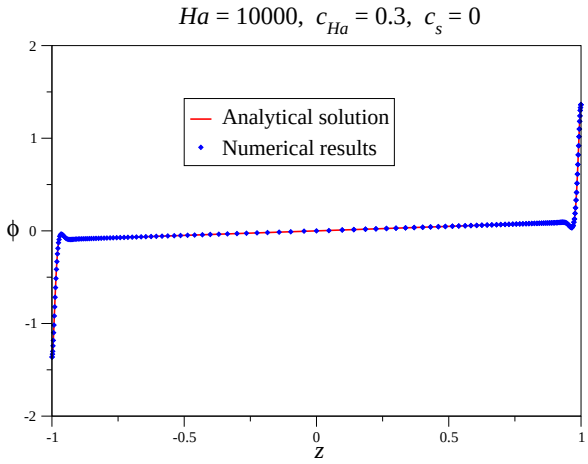

Fig. 4: Electric potential distribution along the symmetry line perpendicular to B in a duct with insulating side walls and conducting Hartmann walls at $Ha = 10^4$. The solid line is the analytical solution, the symbols the numerical data.

Numerical calculations of MHD flows in circular pipes have been also carried out, using non-orthogonal or unstructured grids. The outcomes show the importance of adding a correction term when evaluating the electric potential gradient at cell faces in case of non-orthogonal meshes [15]. Results highlight the need of further analyzing the best form of this correction especially for intense magnetic field applications in weakly conducting geometries.

It should be mentioned that the described solver has been already used to successfully simulate 3D MHD flows in insulating and electrically conducting sudden expansions.

Additional work on modeling of MHD flows has been published by the MHD group at IKET in references [16]-[18].

Staff:

H.-J. Brinkmann
L. Bühler
S. Ehrhard
S. Horanyi
C. Mistrangelo

Literature:

[1] C. Mistrangelo and L. Bühler. Magnetohydrodynamic pressure drops in geometric elements forming a HCLL blanket mock-up. 26th Symposium on Fusion Technology (SOFT), Porto, September 27-October 1, 2010.

[2] L. Bühler and C. Mistrangelo. Effects of radial variation of the magnetic field on the pressure distribution in the European liquid-metal blanket concept. 19th Topical Meeting on the Technology of Fusion Energy, Las Vegas, November 7-11, 2010.

[3] A. Aiello, L. Bühler, Ciampichetti, D. Demange, L. Dörr, J.F. Freibergs, B. Ghidersa, M. Ilic, G. Laffont, G. Messemer, I. Platnieks, G. Rampal, and A. Tincani. Mockup testing facilities and qualification strategy for EU ITER TBMs. Fusion Engineering and Design, page in press, (2010).

[4] L. Bühler and C. Mistrangelo. Determination of flow distribution in a HCLL blanket mock-up through electric potential measurements. In Proceedings of the 26th Symposium on Fusion Technology (SOFT), Porto, September 27-October 1, 2010.

[5] L. Bühler and C. Mistrangelo. Draining of a helium-cooled lead lithium test blanket module by gravity under the influence of a strong magnetic field. IEEE Transactions on Plasma Science, 38(3), pp.328-332, March 2010.

[6] L. Bühler, S. Horanyi, and C. Mistrangelo. Magnetohydrodynamic flow in the helium-cooled lead-lithium test blanket for ITER. International Workshop on Liquid Breeder Blankets Madrid, September 23-24. 2010.

[7] C. Mistrangelo. Helium cooled lead lithium blanket for ITER: Liquid-metal MHD mock-up experiments. Satellite meeting on liquid metal application on Fusion Science, Porto, September 30, 2010.

[8] C. Mistrangelo and L. Bühler. MHD Mock-Up Experiments for Studying Pressure Distribution in a Helium Cooled Liquid-Metal Blanket. IEEE Transactions on Plasma Science, 38(3), pp. 254-258, March 2010.

[9] S. Smolentsev, R. Moreau, L. Bühler, and C. Mistrangelo. MHD thermofluid issues of liquid-metal blankets: Phenomena and advances. Fusion Engineering and Design, 85:1196-1205, 2010.

[10] OpenFOAM Documentation: 2010. Available from: http://www.openfoam.com/docs/.

[11] C. Mistrangelo. Simulation of magneto-hydrodynamic (MHD) flows in OpenFOAM. In Proceedings of the OpenFoam Workshop, Zagreb, September 1-15. 2010.

[12] M.-J. Ni, R. Munipalli, P. Huang, N. B. Morley, and M. A. Abdou, A current density conservative scheme for incompressible MHD flows at a low magnetic Reynolds number. Part II: On an arbitrary collocated mesh, *J. Comp. Phys.*, **227**(1), 205-228 (2007).

[13] Walker, J. S., Magnetohydrodynamic flows in rectangular ducts with thin conducting walls, *Journal de Mécanique*, **20**(1), 79-112 (1981).

[14] J. C. R. Hunt, Magnetohydrodynamic flow in rectangular ducts, *J. Fluid Mech.*, **21**, 577-590 (1965).

[15] C. Mistrangelo and L. Bühler. Development of a numerical tool to simulate magnetohydrodynamic interactions of liquid metals with strong applied magnetic fields. 19th Topical Meeting on the Technology of Fusion Energy, Las Vegas, November 7-11, 2010.

[16] M.-J. Ni, L. Bühler, N. Morley, and M. Abdou. Direct simulations of 3D MHD flows in a sudden expansion using a consistent and conservative scheme. Fusion Engineering and Design, in press, (2010).

[17] D. K. Fidaros, L. Bühler, A. P. Grecos, and N. S. Vlachos. Numerical modelling of rotating tangential layers (jets) in shells under strong uniform magnetic field. International Journal for Numerical Methods in Fluids, 62 (6), pp.660-682, 2010.

[18] C. Mistrangelo and L. Bühler. Perturbing effects of electric potential probes on MHD duct flows. Experiments in Fluids, 48 (1), pp.157-165, 2010.

Proposal for a First Wall Fabrication Route (BMBF Reference No. 03FUS0011)

Overview

All ITER Test Blanket Module (TBM) designs include basically six subcomponents which have to be fabricated and assembled: first wall, caps, stiffening grid, breeding units, back plates/manifolds, and attachment system. Here, one of the most important technologies needed for blanket fabrication is joining of parts, particularly for the production of plates with internal cooling channels, like the first wall. The joining methods may be divided into two groups: diffusion or solid phase welding, and fusion welding (electron beam, laser beam, tungsten-inert gas, etc.), whereas the first is either performed in a hot isostatic press (HIP) or in an uniaxial hydraulic press, both after different specific preparations. Obviously, for first wall fabrication diffusion welding is the most appropriate and promising process. The candidate structural material will be EUROFER or some similar reduced activation ferritic-martensitic steel.

Initial Status

For the characterization and evaluation of diffusion welding technologies for the fabrication of first wall components a large number of weld samples and some small mock-ups have been fabricated using different milling tools and parameters. Within this initial program the effect of the surface fabrication process on the diffusion weld quality was studied. It could be seen that basically all industrial standard milling tools are suitable for the surface fabrication. In some cases, however, a specific chip removal leads to porous surfaces and, hence, to remaining cavities in the weld interface which deteriorate the Charpy properties significantly.

Another study concerned the effect of heat treatments on the surface milling process. Here a solution to the chip removal problem was given by hardening the surfaces.

Finally the effect of a second HIP step was tested on defective welds. A rather beneficial effect of such a high pressure cycle could be demonstrated. All cavities vanished and there was no detectable weld line. That is, the second HIP step can be applied, so to say, as repair or back-up solution. In any case, it could and should be performed as a security measure.

Elementary diffusion weld parameters for EUROFER with respect to industrial production processes have been determined. In summary, it was elaborated that diffusion welding is not only sensitive to surface contamination but depends also strongly to the surface structure which results from milling. However, it could be demonstrated that two-step HIP diffusion welding can eliminate unfavorable surface fabrication defects and, therefore, might allow for more efficient milling processes. A fault-tolerant weld process, however, can only be achieved by welding at elevated temperatures like 1150 °C. Some of the results may be applied to the fabrication of parts with inner cooling channels (for example the first wall). This is especially true for surface fabrication, contamination and cleaning aspects.

Progress

The final missing step within this task was to adopt the investigated and optimized fabrication processes to an optimum first wall production cycle, with respect to efficiency, quality, redundancy, fault-tolerance, and operation safety.

Therefore, the envisaged fabrication alternative for the TBM first wall which is based on HIP diffusion bonding of a series of pipes into two half-shells was finally perfomed. Its main advantages over the existing procedures are (1) the inherent fail-safe design due to the application of the double containment principle, (2) the applicability of cost effective standard fabrication processes, and (3) the dimensional stability of the whole component even after maximum pressure and high temperature HIP cycles without pressure plates and encapsulation.

The single production steps were performed as follows:

1. Bending of two plates (see Fig. 1)
2. Milling of surface and grooves into the plates (see Fig. 2)
3. Fabrication of pipes (TIG or Laser welding and bending)
4. Assembling plates and pipes (see Fig. 3)
5. Sealing with EB welds
6. High temperature – high pressure HIP (see Fig. 4)

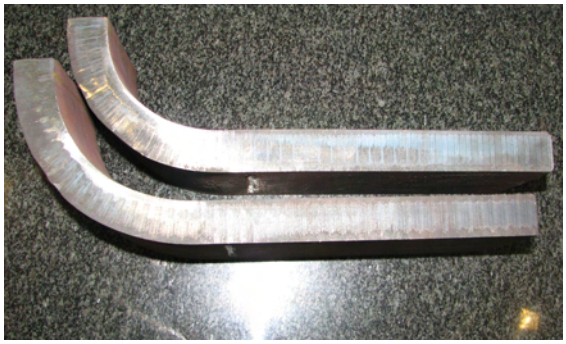

Fig. 1: Plates after cold bending (previously a perlitization heat treatment was applied).

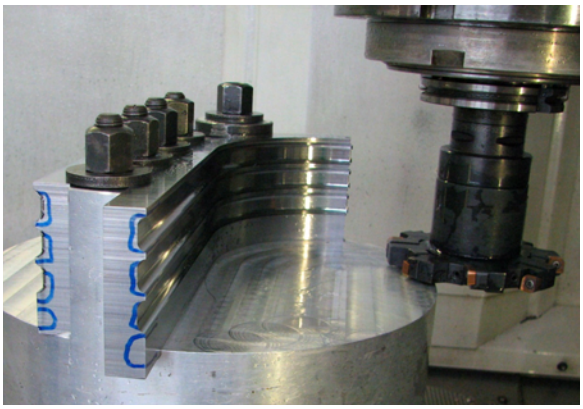

Fig. 2: Parts after surface and groove milling.

Fig. 3: Assembling the single parts (bended pipes and plates).

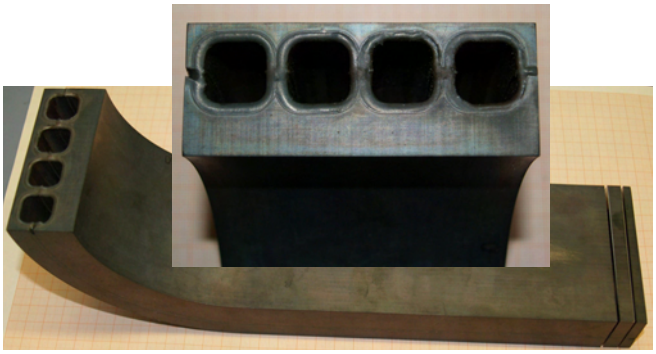

Fig. 4: The final Mockup after sealing and HIP.

The required pipes of step 3 could be commercially manufactured. For such a low number of pipes, however, we had produce them out of massive material in the own workshop. But in principle, all fabrication steps could be performed in an industrial environment and by common standards.

First investigations on the weld quality were also carried out (see Fig. 5). First result of micrograph analysis showed only minor defects.

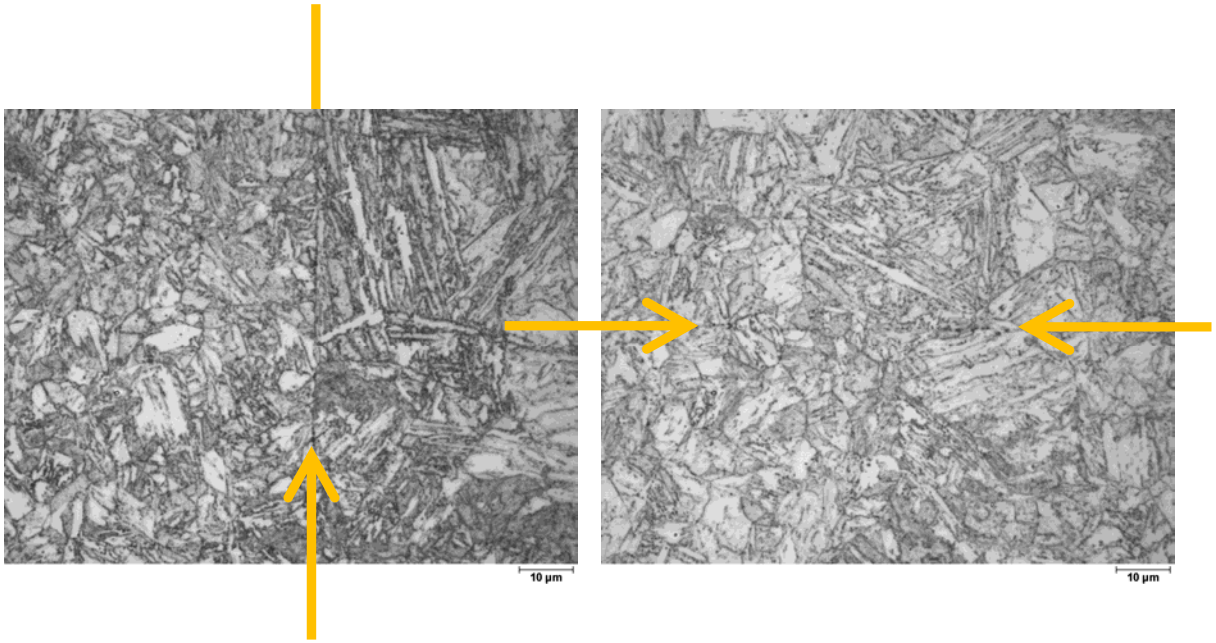

Fig. 5: The analysis of some weld interfaces showed only minor defects.

Conclusions and Outlook

The proposed first wall fabrication route follows the most important requirements for commercial large-scale blanket production. (1) It is compatible with industrial environments, which allows for the use of standard fabrication processes and also shows robustness against environmental influences like corrosion, rough handling, and long-term storage. It is further tolerant against scattering of most process parameters. (2) Efficiency in terms of cost and resource consumption is garanteed. (3) Safety and reliability criteria are fullfilled, since dimensional accuarcy is assured, quality controls can be performed easily, the whole production sequence is reproducible, and finally, it is a inherently fail-safe design.

Staff:

A. Baumgärtner
B. Dafferner
S. Heger
U. Jäntsch
M. Klimenkov
M. Rieth
R. Ziegler
H. Zimmermann

Literature:

[1] Rieth, M., *Specific welds for test blanket modules,* 13th Internat. Conf. on Fusion Reactor Materials (ICFRM-13), Nice, F, December 10-14, 2007.

[2] M. Rieth, B. Dafferner, S. Heger, H. Zimmermann, *Diffusion weld study for Test Blanket Module fabrication*, 25th Symposium on Fusion Technology, SOFT 2008, 15. - 19. September 2008, Rostock, Germany.

[3] M. Rieth, B. Dafferner, U. Jäntsch, H. Zimmermann, *Welding Techniques for Blanket Fabrication*, Annual Meeting on Nuclear Technology, Hamburg, Germany, May 27-29, 2008.

[4] Rieth, M., *Specific welds for test blanket modules*, Journal of Nuclear Materials, 386-388(2009), 471-74.

[5] Rieth, M., *Diffusion weld study for test blanket module fabrication,* Fusion Engineering and Design, 84(2009), 1602-05.

[6] M. Rieth, B. Dafferner, S. Baumgärtner, S. Dichiser, T. Fabry, S. Fischer, W. Hildebrand, O. Palussek, H. Ritz, A. Sponda, R. Ziegler, H. Zimmermann, *Cost effective fabrication of a fail-safe first wall*, 1st Joint ITER-IAEA Technical Meeting on Analysis of ITER Materials and Technologies, 23 – 25 November 2010, Monaco.

Acknowledgement

This work was financially supported by the Ministry of Research and Education (BMBF) under the grant No. 03FUS0011. The views and opinions expressed herein do not reflect necessarily those of the BMBF or the European Commission.

Development and Qualification of Industrial Fabrication Technologies (BMBF Reference: 03FUS0011)

Sub-component manufacturing and assembly concepts for the fabrication of the Helium Cooled Pebble Bed Test Blanket Module have been developed since more than one decade in the KIT. In accordance to the progressing design verification, the fabrication and assembly technology needs to be transferred from experimental scale to industrial application taking into account the requirements for qualification of processes according to the codes and standards applied in ITER.

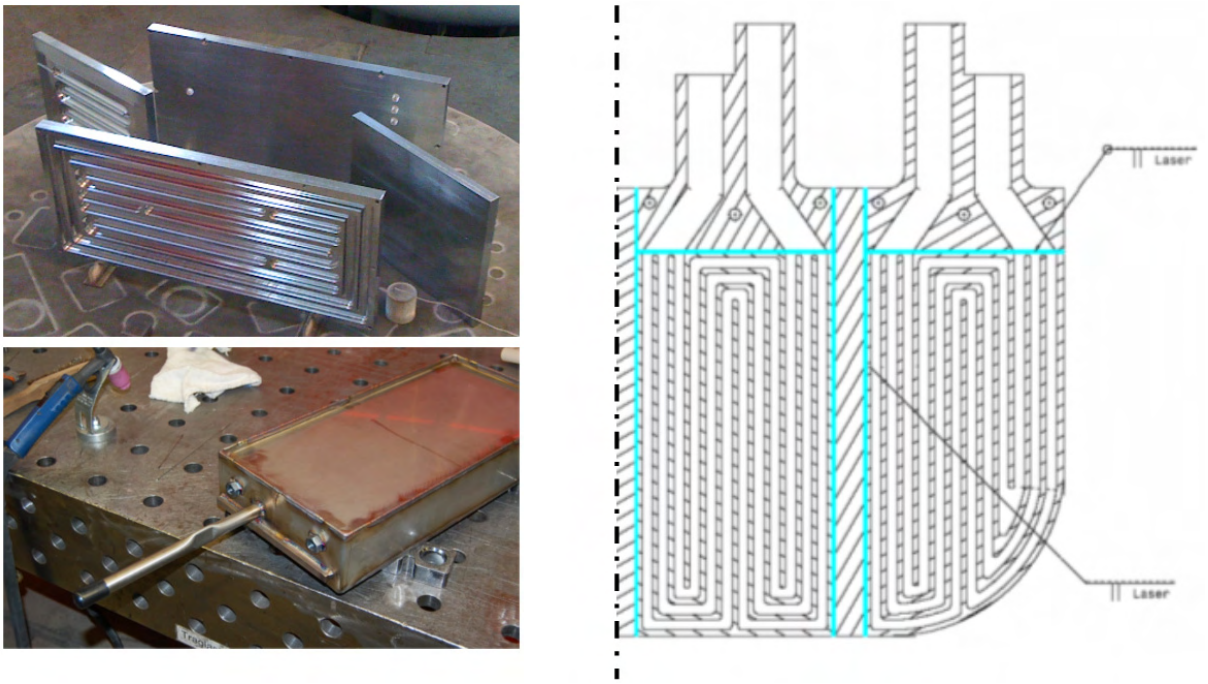

Fig. 1: Medium scale fabrication experiments (left) and recent design modifications of the stiffening plates (right).

The preliminary TBM box fabrication plan has been detailed and progressed in the frame of the F4E grant F4E-2008-GRT-09. The results are reported in the corresponding technical note T22.1-D2 Step 2. The cost estimation has been revised and detailed on level of the TBM sub components fabrication (First Wall, Cap- / Stiffening plates and Breeder Zone Cooling plates). The estimation also takes into account intermediate steps such as Mock Ups in medium scale for transfer of laboratory scale fabrication parameters to relevant dimensions in collaboration with industry. Additionally the present status of development has been recalled for each technology required for TBM sub-component fabrication and the TBM assembly. The fabrication concept for the Stiffening Plates has also been revised into a modular arrangement consisting of diffusion welded parts and transition pieces in between (see Figure 1) [1].

Staff:

P. Freiner
H. Neuberger
J. Rey
A. von der Weth

Literature:

[1] H. Neuberger, A. von der Weth, J. Rey, KIT ACTIVITIES TO SUPPORT FABRICATION, ASSEMBLY AND QUALIFICATION OF TECHNOLOGY FOR THE HCPB-TBM, Poster presented to the SOFT-2010 in Porto (September 2010).

Acknowledgement

This work was financially supported by the Ministry of Research and Education (BMBF) under the grant No. 03FUS0011. The views and opinions expressed herein do not reflect necessarily those of the BMBF or the European Commission.

Development of a Helium-cooled Divertor using Tungsten as Structural Material

Deep Drawing of Thimbles (WP10-MAT-WWALLOY-01-02)

Due to the required large number of cooling finger of about 250,000 in the entire reactor, an economical method for mass production of tungsten parts is being sought [1]. One of the cost-saving methods for function-oriented and load-oriented production of tungsten alloy thimble is the deep drawing. This kind of forming process provides an advantage in that the grains of the material are formed uniformly along the contour, which is favorable for the strength increase in the structure. The deep drawing investigation was started with related press-rolling method [2]. It was first tried on steel and TZM (molybdenum alloy with titanium and zirconium) sheets which were successfully pressed to form a thimble at a temperature of about 400°C (Fig. 1). In a further step cupping was performed on 1 mm W sheets in a newly constructed tool with electric heater (Fig. 2, left). To date, a thimble-profile depth of ~6 mm was reached (Fig. 2, right) at a deep-drawing temperature of about 600°C. In order to deep draw the thimble completely to its end form, further improvements have to be made to the tool e.g. a) remedy against cracking of the work piece by larger transition radius in the tool, b) increasing the deep-drawing temperature to enhance the ductility of tungsten work piece. These activities are ongoing.

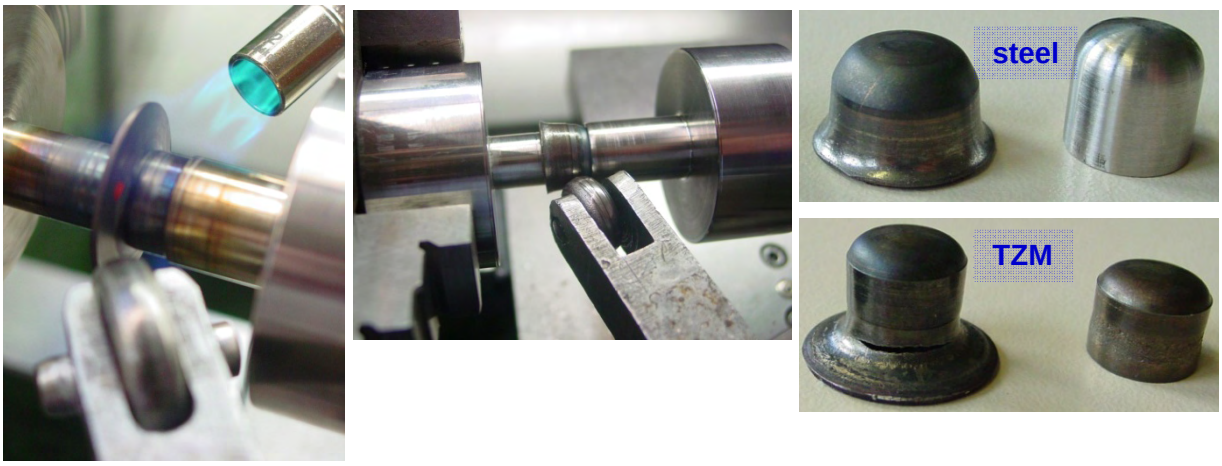

Fig. 1: Roll pressing attempt using butane gas heating (left), thimble cap from 1 mm sheet of steel and TZM (right).

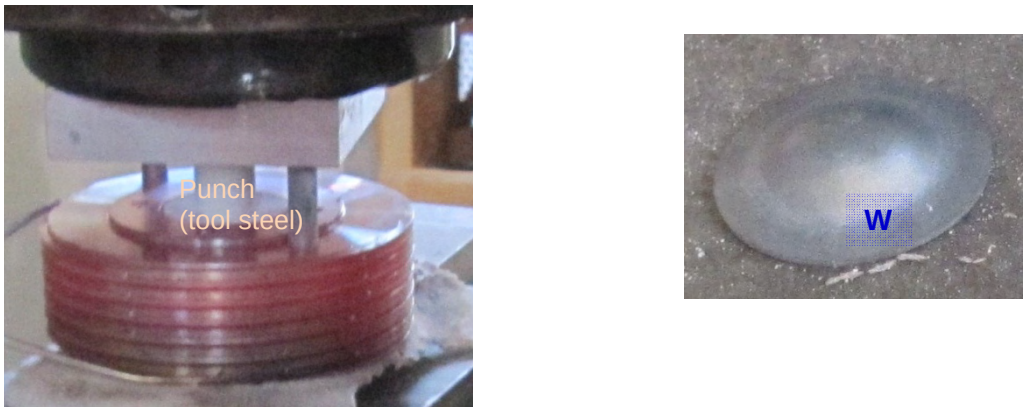

Fig. 2: First W deep draw attempt with a new developed tool (left), thimble cap from 1 mm W sheet (right).

Development of W-Eurofer and W-W Joints by Brazing (WP10-MAT-WWALLOY-01-13)

A type of failure observed in the preceding tests was the detachment of tile and thimble due to an overheating of the brazed joint - top surface melting of the W tile as a consequence - when ramping up the incident heat flux beyond 13 MW/m^2. This failure was assumed to be caused by overheating of the W tile/WL10 thimble joint which was brazed with STEMET®1311. In order to improve the braze joint a study on new brazing technology for high-temperature brazing has been launched at KIT. A new brazing filler 60Pd40Ni (liquidus temperature Tliq = 1238°C) was chosen for the W-WL10 joint (working temperature ~1200°C), taking into account the recrystallization temperature of WL10 material (1300°C). For the brazing of WL10-Steel joint (working temperature ~700°C) 18Pd82Cu filler (Tliq = 1100°C) was found suitable. In both cases W-WL10 joint with PdNi and WL10-steel joint with CuPd good adhesion to the base material of the parts were achieved. Figures 3 and 4 show the EDX scan results of the two successful solder connections. In the EDX spectra (bottom) the EDX signal intensity is plotted as a function of photon energy corresponding to the point-scan data of the elements in the table (top).

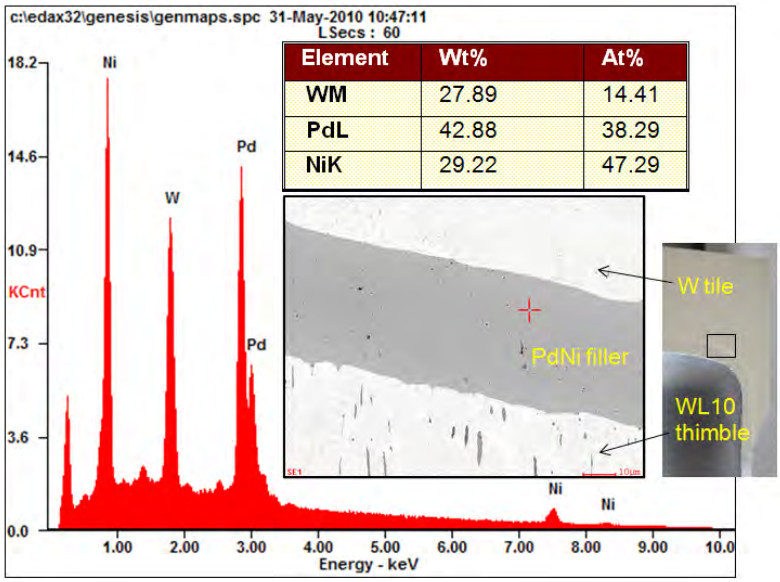

Fig. 3: SEM and EDX scan results of a successful brazed joint W tile - WL10 thimble with PdNi40.

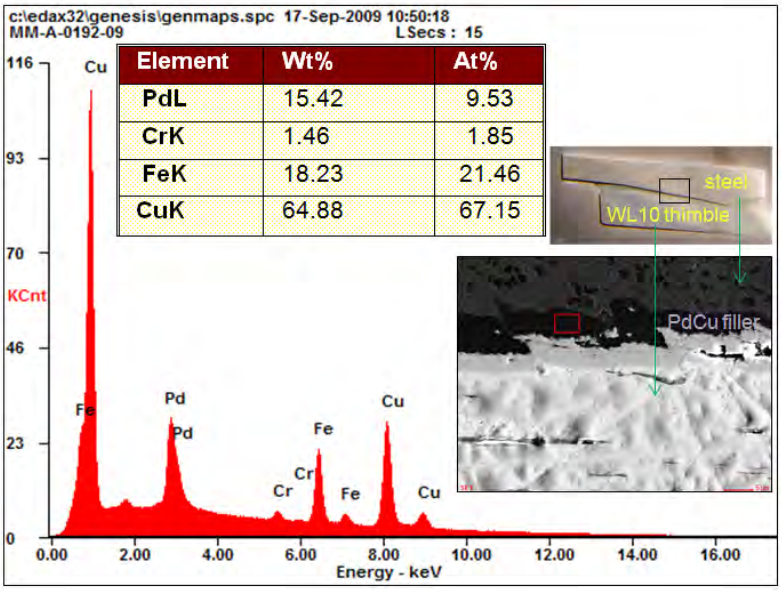

Fig. 4: SEM and EDX scan results of a successful brazed joint WL10 thimble - steel conic sleeve with PdCu.

High Heat Flux Tests on Optimised Finger Module Mock-ups (WP10-MAT-WWALLOY-01-14)

The HHF experiments on the six surviving mock-ups (Fig. 5) were continued at the beginning of 2010 with the new EB gun. The same thermohydraulics test conditions as in the previous test series with the old gun were used and the heat flux was set to 10 MW/m^2. The mock data and the test conditions are summarized in Table 1. Table 2 shows the experimental results with the number of cycles reached by mockups. The tested mockups survived between 180 and 1100 cycles under the maximum heat load of at least 10 MW/m^2 before failure. The best results were obtained with the KIT optimized mockup #18, which survived more than 1000 cycles before going to fail. Two types of failures were identified: (a) damage on top, helium leak (e.g. Mock-up #18, Fig. 6), and (b) damage on the side of tile, overheating, but no leak (Mock-up #25, Fig. 7).

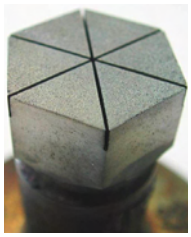

#18
KIT design,
Plansee W rod

Tested twice,
total no. of cycles > 200:
50 @ ~11 MW/m^2 (soft ramp)
50 @ ~11 MW/m^2 (sharp)
12 @ ~12 MW/m^2 (sharp)

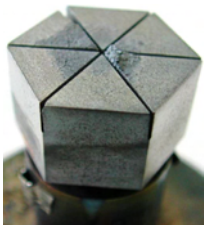

#22
RF design,
Plansee W rod

Tested twice,
total no. of cycles > 200:
54 @ ~10.5 MW/m^2 (soft ramp)
50 @ ~11 MW/m^2 (soft)
10 @ ~11 MW/m^2 (sharp)

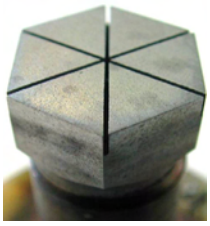

#25
KIT design,
RF W rod

Tested once,
Total no. of cycles > 100:
10 @ ~ 10 MW/m^2 (sharp ramp)
100 @ ~11 MW/m^2 (sharp)
10 @ ~11.5 MW/m^2 (sharp)

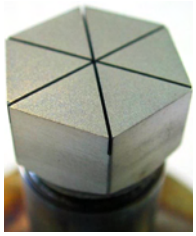

#27
KIT design,
RF W rod

Tested once,
total no. of cycles > 100:
100 @ ~ 11 MW/m^2
15 @ ~11.5 MW/m^2
(all sharp ramp)

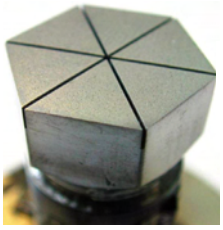

#28
KIT design,
RF W rod

Tested once,
total no. of cycles > 100:
100 @ ~11 MW/m^2
12 @ ~12 MW/m^2
(all sharp ramp)

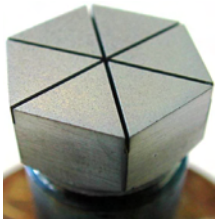

#31
KIT design,
RF W rolled plate

Tested once,
total no. of cycles > 100:
30 @ ~10 MW/m^2
72 @ ~11 MW/m^2
(all soft ramp)

Fig. 5: Six surviving mock-ups from the 3rd series (2008) available for further testing.

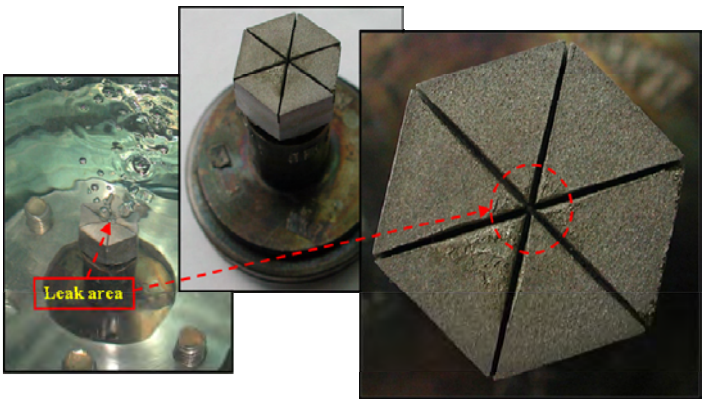

Fig. 6: 2010 HHF tests: leak test of mock-up No. 18 after 1112 cycles at ≥ 10 MW/m^2.

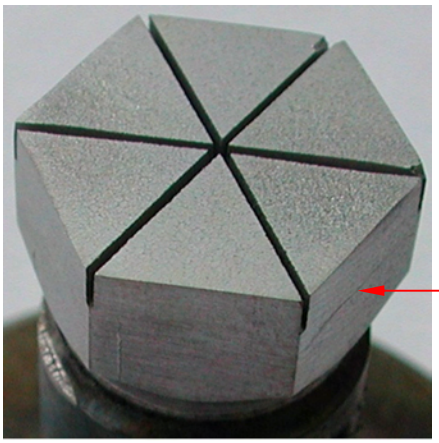

Fig. 7: 2010 HHF tests: image of mock-up No. 25 after 510 cycles at ≥ 10 MW/m^2.

Table 1: The fourth experiment series 2010 with new EB gun. Mockup details.

Mockup parts: castellated W tile, Plansee WL10 thimble, Eurofer structure; Brazing: tile/thimble with STEMET®1311, thimble/steel conic sleeve with 71KHCP, both at 1050°C brazing temperature. Absorbed power ≥10 MW/m^2, Beam on/off, 15/15 s; Helium coolant: mass flow rate 13 g/s, helium inlet temperature 500°C.				
W tile geometry			W tile material / grain orientation	Type of fabrication
Design type	tile height (mm)	castellation depth (mm)		
KIT	12	2.7	Plansee rod/vertical	turning/grinding
RF	12	4	Plansee rod/vertical	EDM
KIT	12	2.7	RF rod/vertical	turning/grinding
KIT	12	2.7	RF rod/vertical	turning/grinding
KIT	12	2.7	RF rod/vertical	turning/grinding
KIT	11.3	2.3	RF rolled plate/horizontal	turning/grinding

Table 2: The fourth experiment series 2010 with new EB gun. HHF test results.

Mock-up no.	Number of cycles		Total number of cycles to failure (summed over all test series)	Failure type
	reached in the previous testseries	reached in thelast tests 2010		
#18	214 (2nd and 3rd)	900	1114	A
#22	214 (2nd and 3rd)	50	264	B
#25	120 (3rd)	300	420	B
#27	115 (3rd)	299	414	B
#28	112 (3rd)	99	211	B
#31	102 (3rd)	74	176	A
A: damage on top, helium leak; B: damage on the side of tile, overheating, no leak.				

Conclusions and outlook

After a one-year break due to an upgrade of the test facility, the HHF test series was continued in early 2010. It began with the continued testing of the six mockups that have survived earlier HHF tests by more than 200 cycles at 10 MW/m^2 without any damage. One of the tested mock-ups survived more than 1000 cycles under 10 MW/m^2 before it failed after a total number of 1112 cycles. The first breakthrough was thus achieved. Future tests mockups will be further improved, e.g. by using suitable high temperature brazing filler metal such as Ti-alloy to avoid overheating.

Staff:

S. Antusch
S. Berberich
P. Norajitra
H.-J. Ritzhaupt-Kleissl
L. Spatafora

Literature:

[1] P. Norajitra, S. Antusch, R. Giniyatulin, V. Kuznetsov, I. Mazul, H.-J. Ritzhaupt-Kleissl, L. Spatafora, Progress of He-cooled Divertor Development for DEMO, 26th SOFT, Porto, Portugal, 27.09.-01.10.2010.

[2] P. Norajitra, J. Reiser, H.-J. Ritzhaupt-Kleissl, S. Dichiser, J. Konrad, G. Ritz, Development of a He-Cooled Divertor: Status of the Fabrication Technology, Fusion Science and Technology, Volume 56, Number 1, July 2009, Pages 80-84.

Intellectual Property Rights (IPR)

In the frame of this work a new element of know-how has been generated.

Acknowledgement

This work, supported by the European Communities under the contract of Association between EURATOM and Karlsruhe Institute of Technology, was carried out within the framework of the European Fusion Development Agreement. The views and opinions expressed herein do not necessarily reflect those of the European Commission.

Structural Materials – Steels

Fatigue and Creep-fatigue Tests and Crack Monitoring on Neutron Irradiated EUROFER (250, 450 °C) and Unirradiated Miniaturized Fatigue Samples (TW2-TTMS-005b D 4)

Introduction

The objectives of this task were:

- Fracture morphology from crack and micro-crack initiation and propagation monitored continuously during mechanical testing of SSTT fatigue specimens in order to prove the transferability of the technique from standard to miniaturized fatigue specimens (micro crack monitoring);
- Comparison of fracture mode between fatigue, creep and creep-fatigue testing using miniaturized SSTT specimens;
- Comparison between unirradiated and neutron irradiated (16 dpa, T_{irr} = 250 and 450°C) miniaturized fatigue specimens, also to validate the suitability of these samples for high dose neutron load at typical blanket relevant temperatures.

Evaluation of micro crack monitoring of SSTT fatigue specimens

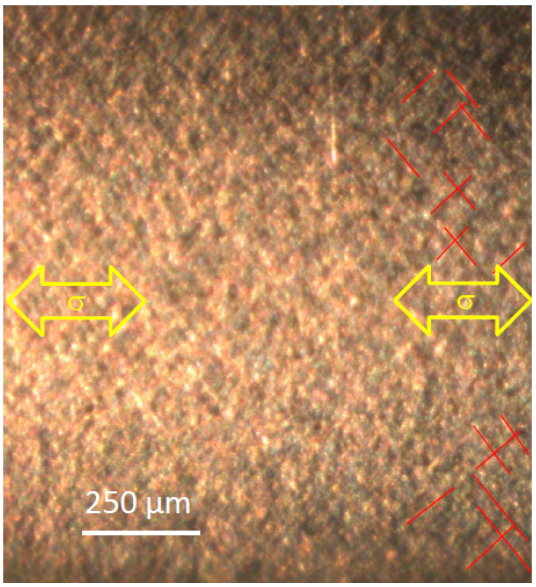

Fig. 1: Polished EUROFER 97 fatigue sample after 1094 cycles at $\Delta\varepsilon$=1.0%.

An initial attempt has been tried to apply the technique based on a high resolution camera to miniaturized SSTT fatigue specimens. For the evaluation of the micro-crack monitoring on surface polished miniaturized fatigue specimens, symmetric push-pull fatigue tests (R = -1) have been performed at room temperature and have been monitored with a long range high resolution mirror microscope (QUESTAR).

The red lines (Fig. 1) indicate the “zig-zag-pattern” of the persistent slip bands. The typical length of the individual segments is in the range of a grain size and therefore in quite good agreement with earlier observations on RAFM steels. Also the angle to the load axis (marked in yellow) of the uni-axial fatigue tests is in the range of 45 degree as expected.

Comparison of fracture mode between fatigue, creep and creep-fatigue testing using miniaturized SSTT specimens

In future nuclear fusion reactors, the combined creep and fatigue loading of structural materials due to pulsed operation and/or maintenance periods and the associated thermal cycling plays a crucial role. Therefore, fatigue, creep and creep-fatigue tests have been conducted on EUROFER 97, the European candidate structural material for DEMO. Contrarily to prior investigations, the creep and fatigue loads were decoupled during the creep-fatigue experiments, in order to get a better and more direct understanding on lifetime limiting loading conditions. This was achieved by interrupting a fatigue test after half of the previously determined specimen’s lifetime and by applying a constant (creep) force afterwards until fracture occurred. Hence, the damage contributions of fatigue and creep were accessible to separate analyses.

All tests were carried out at 550 °C with miniaturized, axisymmetric specimen with a cylindrical gauge length of 7.6 mm at a diameter of 2 mm. The fatigue tests were performed in a strain-controlled manner under symmetric tension/compression conditions (R=-1) at a constant strain rate of 0.1%/s, whereas the creep tests were operated at constant load. The creep-fatigue experiments were performed in the first stage under strain controlled conditions until 50% of the lifetime of only fatigue tested specimens has been achieved, followed by the second stage that was stress controlled creep until fracture of the specimen occurred. The strain was measured in-situ with a strain sensor with ceramic tips. During fatigue testing, a number of stress strain hysteresis loops were collected. Fatigue tests have been performed at strain ranges between $\Delta\varepsilon$=0.45% and $\Delta\varepsilon$=1.0%, pure creep tests at stresses from σ=180 Mpa to 220 Mpa, and finally, creep-fatigue tests at strain ranges from $\Delta\varepsilon$=0.45% to $\Delta\varepsilon$=1.0% and with a subsequent creep stress of σ=180 Mpa. The definition of fatigue life N_f is the cycle number where the largest crack starts propagation perpendicular to the load axis; this is the beginning of the rapid drop of the strain amplitude. Microstructural analysis included scanning electron microscopy of the fracture surfaces and the cylindrical specimen surface as well as microstructural investigations using transmission electron microscopy.

Fig. 2 shows for <u>pure fatigue</u> tested specimens the evolution of the positive stress amplitude σ_a as a function of cycles. Obviously, in the temperature range investigated, a specific feature of this class of steel is the common behaviour of σ_a: despite the wide range of applied strain ranges $\Delta\varepsilon$, all stress amplitudes σ_a are practically similar beyond about 50 cycles. Consequently, large strain amplitudes show more pronounced cycling softening as small strain ranges. That is, the deformation response on individual fatigue loading occurs specifically in the early phase of fatigue testing.

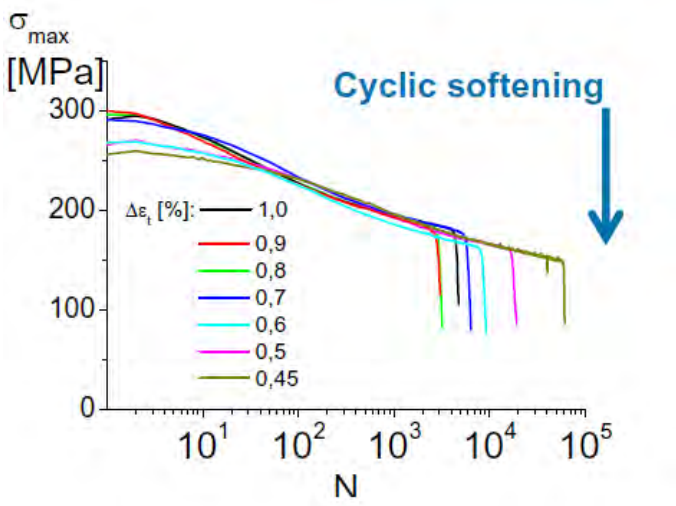

Fig. 2: Evolution of the positive stress amplitudes σ_a as function of cycles N for different strain ranges $\Delta\varepsilon$ at 550 °C of EUROFER 97.

For the <u>combined creep fatigue</u> tests in a first step, the individual specimens have been strain controlled fatigue tested up to 50% of the lifetime at 550°C at strain ranges ranging from $\Delta\varepsilon$ =0.45-1.0%. In a second step these pre-fatigued specimens were assembled in a creep testing device and tested also at 550 °C at a creep stress of 180 Mpa until creep rupture occurred. Fig. 3 shows the corresponding creep rupture times. The lifetime in pure creep at 550°C and σ=180 Mpa load was 135.7 h. That is, the lifetimes in the creep stage of the creep-fatigue tests are strongly reduced and range only from 4-19% of that value. Within the statistical uncertainties, except for the pre-fatigued specimen at $\Delta\varepsilon$=0.45%, the creep rupture time shows no visible dependence of the strain range of prior cycling.

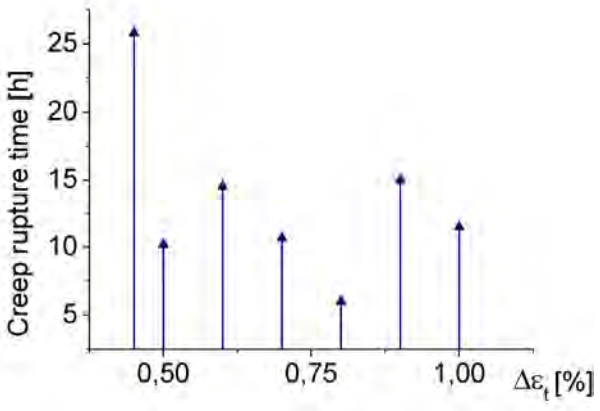

Fig. 3: Combined creep-fatigue tests at 550 °C: After fatigue endurance to 50% N_f, creep tests have been performed. The creep rupture time is shown for different pre-fatigued specimens.

Several images of the lateral (free) surfaces obtained by SEM are shown in Fig. 4. Different surface appearances develop during the three types of load cases: The surfaces show subtle intrusions and extrusions after pure fatigue, a uniform pattern of surface cracks perpendicular to the load direction after pure creep, and a branching network of coagulating cracks after creep-fatigue. Although all specimen surfaces have been carefully polished, the surface cracks of the pure creep tested specimen can be attributed to tiny machining grooves. Specifically damaging is obviously not pure fatigue testing or pure creep testing but a longer applied stress following pre-fatigue cyclic loading.

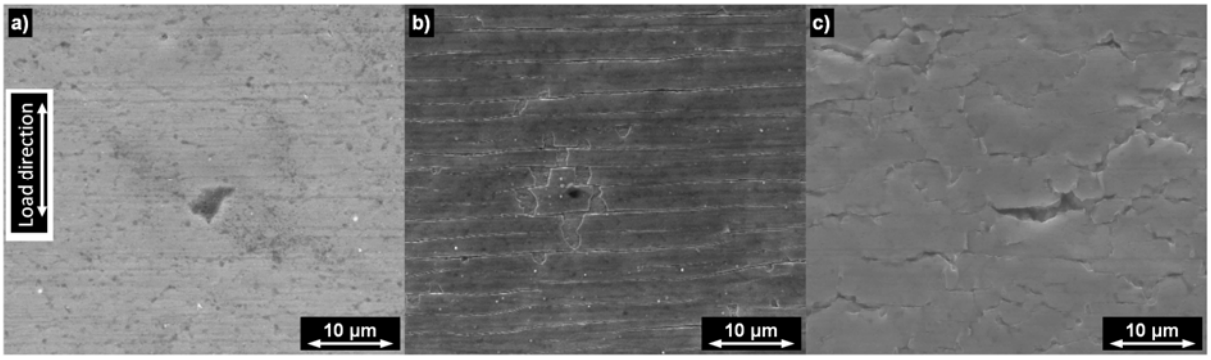

Fig. 4: Lateral surfaces of a specimen after pure fatigue at Δε =0.6% for 9258 cycles (a), after pure creep at σ=180 Mpa for 165 h (b), and after creep-fatigue with Δε =0.6% for 5050 cycles and σ=180 Mpa for 14.56 h (c). The load direction is always vertical.

Fig. 5 reveals ductile dimple structures on the fracture surfaces from SEM analyses after creep-fatigue with Δε = 0.6% for 5050 cycles and σ = 180 MPa for 14.56 h (a) and after pure creep at σ=180 MPa for 165 h (b). Ductile dimple structures are visible as a result of both load cases, which suggests that transgranular crack growth leads to failure and that failure relevant crack initiation occured in the specimen's volume and not on the free surfaces. Compared to pure creep loading (Fig. 5b), much larger dimples are visible after creep fatigue damage (Fig. 5a). This observation can be attributed to the severe reduction of dislocation density and the subsequent sub-cell formation that causes pronounced cyclic softening during pre-fatigue testing. Consequently, the pre-fatigued specimen has a much smaller strength at the beginning of the creep test compared to virgin creep specimens.

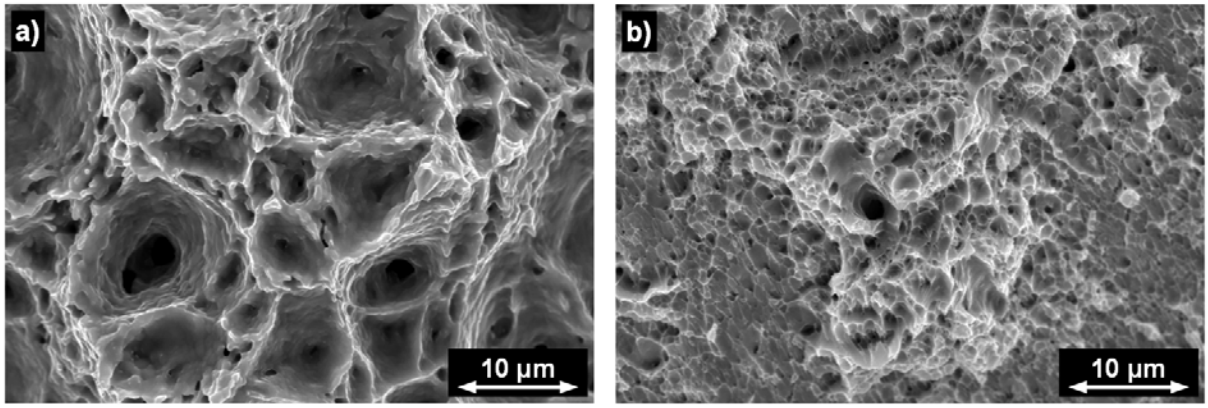

Fig. 5: Ductile dimple structures on the fracture surfaces (SEM) after creep-fatigue with Δε =0.6% for 5050 cycles and σ=180 MPa for 14.56 h (a) and after pure creep at σ=180 MPa for 165 h (b).

Push-pull fatigue on SSTT specimens after neutron irradiation at 250 and 450 °C

The neutron irradiation was performed in the mixed spectrum reactor HFR Petten, The Netherlands in a special wrapper in the central part of the reactor core at irradiation temperatures of T_{irr} = 250 °C and 450 °C. The cumulative neutron fluence E>0.1 MeV m^{-2} was 22.85 x 10^{25}, resulting in a calculated displacement damage dose of 16.3 dpa for stainless steel. After the

irradiation, the specimens were transported to the Hot Cell facility of the Fusion Material Laboratories at the Karlsruhe Institute of Technology to perform isothermal fatigue tests at $T_{test} = T_{irr} = 250$ °C and 450 °C, respectively.

Equally to tensile results, the fatigue tests have shown a pronounced irradiation hardening at the low irradiation temperature of 250 °C. This can be observed during fatigue testing in the stress strain hysteresis loops in figure 6. The total stress amplitude dependence on the fatigue cycles reveals the typical cyclic softening of the martensitic/ferritic steels. As a consequence of the significant irradiation hardening, the plastic strain amplitude of irradiated specimens is much smaller. An important feature of the 250 °C irradiation is the very moderate cyclic softening, indicating a remarkable stability of the irradiation induced interstitial type loops. This indirect conclusion from the mechanical fatigue tests is confirmed directly by the TEM results.

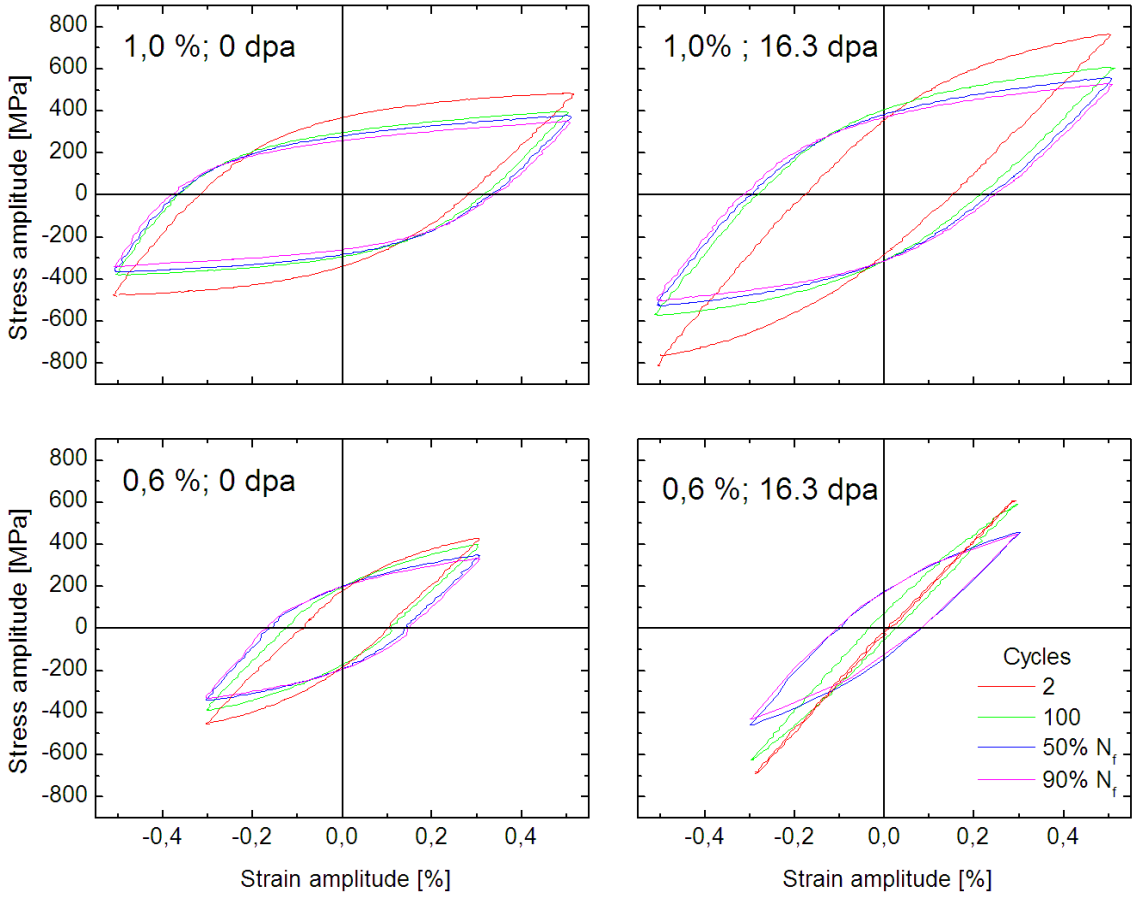

Fig. 6: Comparison of stress-strain hysteresis loops of unirradiated and irradiated EUROFER 97 at $T_{test}=T_{irr}=250$ °C.

It is a novel and major result of this work that specimens irradiated at the low irradiation temperature of 250 °C show a remarkable fatigue life increase that progressively steps up with decreasing strain amplitude, as shown in Fig. 7. At the lowest strain amplitude of $\Delta\varepsilon = 0.5\%$, the N_f increase is about 10 times that one of un-irradiated controls.

In contrast to the 250 °C irradiation, no hardening induced by dislocation loops has been observed after 450 °C irradiation to 16 dpa. For both, the stress amplitude and the plastic elongation as function of cycles the values are for the unirradiated and the irradiated experiments in the entire parameter range of $\Delta\varepsilon$ very similar. Also the lifetime of the unirradiated and the irradiated specimens is therefore very similar within the usual uncertainties.

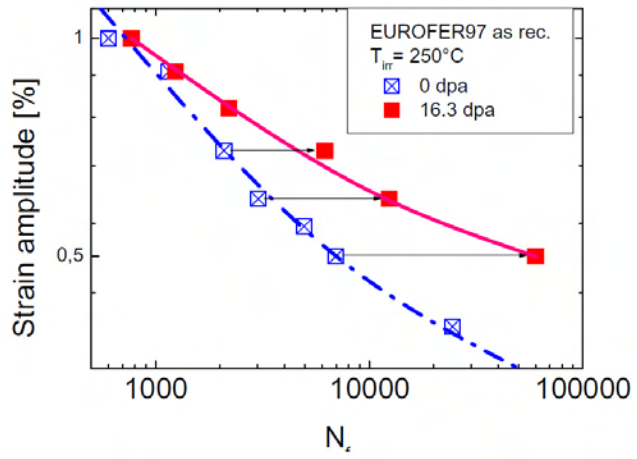

Fig. 7: Effect of low temperature irradiation on fatigue lifetime N_f at $T_{test}=T_{irr}=250$ °C.

Broad based microstructural analyses (Fig. 8) followed after fatigue testing. The fracture initiation was very clear visible in every specimen beginning at the specimen outer face. The further fracture propagation is recognizable by fatigue fracture paths, striations and lines. A detail of every fatigue fracture is shown in the third picture of every column. The width of the fatigue striations increased with larger amplitudes. It is remarkable that the irradiated specimens at higher loads had considerable differences in height between the individual fracture paths. The reason is that more crack initiations at different distances occurred, but during the fracture formation they grew together to the final crack. In the unirradiated state, the final fracture is always observable as a shear fracture with ductile homogenous dimple formations. After irradiation, the final fracture sheared off with much less macroscopic ductility, but a mixture of shear and ductile forced fracture with distinctive dimple formation.

As TEM analysis has shown, the material formed after irradiation at 250 °C a subgrain or cell structure during the fatigue tests. Dislocation free sub-grains aside areas with higher dislocation were observed. Regarding the stability of irradiation induced defects, TEM has indeed confirmed that despite of fatigue testing most dislocations are still pinned on loops and/or α`-precipitates. This explains naturally why the level of strain amplitude remains even after severe fatigue loading significantly above the one of un-irradiated controls. This view is supported by the subgrain formation which is less pronounced in the irradiated specimens. In addition, along with the cyclic motion of dislocations during fatigue testing, a coarsening of precipitates occurred. This is an indication that a transport of alloying elements goes along with the cyclic motion of dislocations during the fatigue tests. The structural stability of the unirradiated and neutron irradiated miniaturized fatigue specimens has been confirmed within the broad loading window tested so far.

Staff:

S. Baumgärtner
U. Jäntsch
M. Klimenkov
R. Lindau
E. Materna-Morris
A. Möslang
R. Rolli
Ch. Vorpahl

Literature:

[1] E. Materna-Morris, A. Möslang, R. Rolli, and H.-C. Schneider; Effect of 16.3 dpa Neutron Irradiation on Fatigue Lifetime of theRAFM-Steel EUROFER 97; SOFT-26; September 26 – October 1, 2010, Porto, submitted for the proceedings

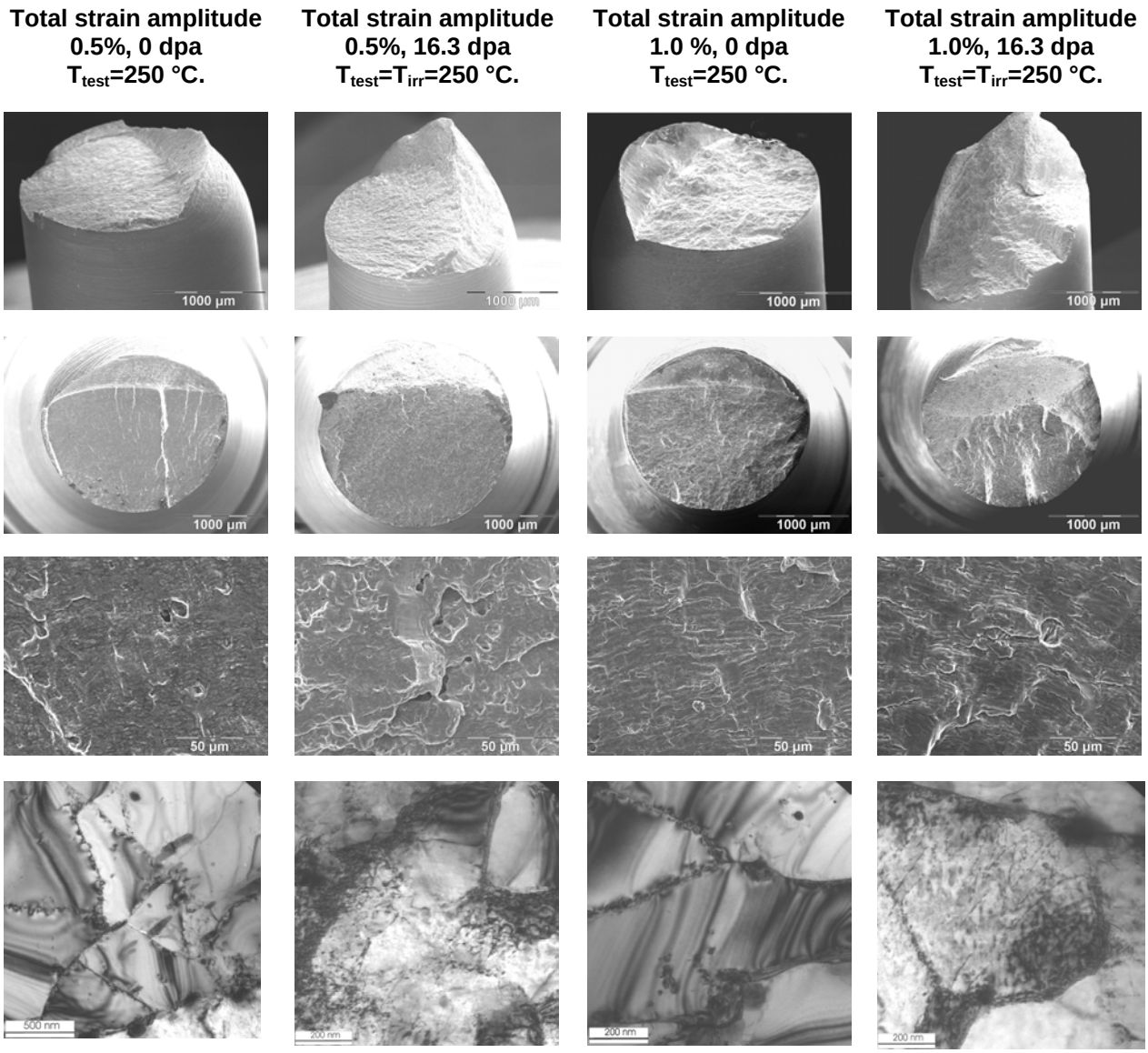

Fig. 8: Fracture surfaces and microstructure before and after 16.3 dpa neutron irradiation; 1a – 4a, 1b – 4b reveal SEM overviews of the fatigue fractures, 1c – 4c details of the fatigue fractures, and 1d – 4d TEM micrographs of the microstructures after fatigue testing.

Acknowledgement

This work, supported by the European Communities under the contract of Association between EURATOM and Karlsruhe Institute of Technology, was carried out within the framework of the European Fusion Development Agreement. The views and opinions expressed herein do not necessarily reflect those of the European Commission.

Fabrication and Irradiation of FE-54 Enriched Samples to Study the Influence of He/dpa Ratio on Materials Degradation up to Medium Dose Level (TW4-TTMS-001 D 1, TW5-TTMS-001 D 2)

Overview

The structure components of future fusion reactors will suffer from specific irradiation damage, i.e. the ratio of helium production (in appm) to displacement rate (in dpa) varies around 10 appm He/dpa. Due to the lack of appropriate high energy neutron sources there seems to be only one promising way to generate such irradiation damages in a RAFM steel with common in-pile fission reactor irradiation experiments: If the content of natural iron would be replaced by the stable isotope Fe-54, helium production would be stimulated by the according (n, alpha) reactions. A significant advantage over the alternative boron-10 helium production technique would be a uniform helium distribution through the whole matrix.

Therefore, the goal of the task is to produce a heat similar to EUROFER using Fe-54 instead of natural iron. Then miniaturized charpy and tensile specimens with cores of Fe-54 substituted EUROFER steel have to be fabricated. Finally, an appropriate irradiation program has to be planned and managed.

Status

All material production steps are developed and qualified. For the further casting of the plates, high quality aluminium-oxide crucibles were purchased and tested successfully. The whole specimen fabrication processes are developed and qualified: Electron beam welding of stripes of EUROFER 97 to core plates of Fe54- EUROFER to spare the valuable isotope material, then heat treatment and specimen fabrication by EDM and turning.

During the final fabrication step the crucible broke and the isotope material was contaminated with carbon. The ongoing decarbonization treatment was performed in boron-nitride crucibles which, unfortunately, increased the boron content in the isotope alloy significantly. However, for the successful continuation of this task, it was absolutely necessary to remove the boron from the contaminated isotope cast materials.

Progress

Boron cannot be easily removed from steel. Therefore, the cleaning procedure has to be performed chemically and not by melting in reducing atmosphere. The first idea was to solve the material in acid, start a boron fall-out reaction, and separate the fallen-out boron compound physically by a centrifuge. But the method failed.

The next idea resulted from a former boron analysis method which made use of the fact that boron forms easily an ester which is rather volatile. The cleaning process that was developed in the following can be summarized as follows:

- The steel is solved in acid sulphur where the boron forms to boric acid (H_3BO_3),
- With acid sulphur as catalyst, boric acid together with methanol forms boric ester and water: $H_3BO_3 + 3\ HOCH_3 \rightarrow B(OCH_3)_3 + 3\ H_2O$,
- Distillation of the mixture. The volatile boric ester evaporates. The remaining iron hydroxide is free of boron and can be neutralized and precipitated by soda lye: $3\ Fe^{3+} + 3\ NH_3 + 3H_20 \rightarrow Fe(OH)_3 + 3\ NH_{4+}$,
- After filtering, the iron hydroxide is oxidized at about 200°C in air: $Fe(OH)_2 \rightarrow FeO + H_2O$ and then $2\ FeO + O_2 \rightarrow Fe_2O_3$,

- Finally, the cleaned iron oxide can then be reduced in a sinter furnace under hydrogen atmosphere.

The foreseeable progress of this task should evolve like follows:

- The chemical cleaning will take another 4 month at least,
- In parallel, reduction tests in the sinter furnace could take place. Therefore, EUROFER 97 material has to be solved in acid and precipitated with the same methods which are applied for cleaning the isotope material. That is, it is also time consuming.
- Hopefully, the cleaned isotope material will not significantly suffer during the reduction process (possible impurities, loss of material due to cinder formation, etc.). This provided, the final Fe54-EUROFER batches could be produced by end of 2011.

However, there is a significant uncertainty factor: The facilities used for casting the Fe54-EUROFER batches are located in and operated by the Max-Planck-Institute for Metal Research (MPI). Due to restructuring plans, the personnel and maybe also the equipment was available only until November 2010.

Conclusions and Outlook

The first aim of this task was to fabricate a heat like EUROFER but where the natural iron is completely replaced by the isotope Fe54. The lowest impurity level is reached by pre-alloying the different elements by arc melting and finally using an induction furnace for casting. In this way, the impurities result mainly from the crucible. It has been experienced that it is better to accept an increased oxygen content using aluminum-oxide crucibles rather than casting with a boron-nitride crucible which increases nitrogen, and even worse, boron contamination.

Moreover, from the presented investigations the following conclusion might be drawn:

- Small-scale EUROFER-like batches in the range of about 100 to 200 grams can be produced by casting. The mechanical properties are still within an acceptable range, even without hot or cold working, like for example, rolling and/or forging.
- The substitution of only core elements in Charpy and tensile specimens by the valuable isotope alloy is feasible. The shown technique of EB welding stripes of standard EUROFER to the Fe54-steel prior to specimen fabrication leads to reproducible and reasonable results.
- If the cleaning of the remaining isotope material succeeds finally, there should be enough specimens available for a comprising irradiation programme. The according test matrix which considers relevant cross-links to other irradiation campaigns has been set up.
- From the neutronics point of view, the irradiation should be performed in the HFIR at Oak Ridge, USA.

Staff:

C. Adelhelm
B. Dafferner
S. Heger
U. Jäntsch
A. Möslang
M. Rieth
P. Vladimirov
H. Zimmermann

Intellectual Property Rights (IPR)

In the frame of this work a new element of know-how has been generated.

Acknowledgement

This work, supported by the European Communities under the contract of Association between EURATOM and Karlsruhe Institute of Technology, was carried out within the framework of the European Fusion Development Agreement. The views and opinions expressed herein do not necessarily reflect those of the European Commission.

Mechanical Post Irradiation Examinations of FZK-Specimens Irradiated in the ARBOR 2 Experiment in the BOR 60 Reactor (TW5-TTMS-001 D 10)

Objectives

In an energy generating fusion reactor structural materials will be exposed to very high levels of irradiation damage of about 100 dpa. In the framework of the ARBOR 2 irradiation programme EUROFER 97, selected RAFM steels (F82H-mod, OPTIFER XI, OPTIFER XII, BS-EUROFER, OPTIMAX), EUROFER ODS HIP, EUROFER based boron doped steels and technological specimens (diffusion welded EUROFER, EB welded EUROFER) have been irradiated in the BOR-60 experimental fast reactor of JSC “SSC RIAR” to reach an irradiation damage dose up to 70 dpa (up to 80 dpa for CEA specimens). Within the ARBOR 2 irradiation programme KIT irradiated 144 mini-tensile/ LCF and 124 Charpy impact specimens for investigation of neutron irradiation induced embrittlement, hardening and changes in the fatigue behaviour.

Status December 2009

The mechanical PIE of ARBOR 2 specimens were performed at the material science laboratory of SSC RIAR. The post irradiation Charpy impact and tensile testing of the specimens from ARBOR 2 was finished in 2008. In addition the influence of the post irradiation annealing on the mechanical properties has been studied. In the course of 2009 the majority of the LCF specimens have been tested in isothermal strain controlled experiments.

Status of PIE of ARBOR 2

In the course of 2010 the remaining irradiated LCF specimens were tested in strain controlled push-pull experiments performed at a constant temperature of 330 °C with total strain ranges ($\Delta\varepsilon_{tot}$) between 0.8 and 1.2% and at a common strain rate of $3x10^{-3}$ s^{-1}. The tests were performed with an electro-mechanical testing machine of INSTRON-DOLI 1362 type equipped with a 100 kN load cell, a three-zone furnace and high-temperature extensometer, installed in the K-12 hot cell of the SSC RIAR. Miniaturized cylindrical specimens of 7.6 mm gauge length and 2 mm diameter were used for the investigation of LCF properties. In addition, inelastic strain amplitudes ($\Delta\varepsilon_{inelastic}$) at $N_f/2$ were determined for given total strain amplitudes from the hysteresis loops.

Fig. 1 shows the LCF properties of boron doped EUROFER 97 based RAFM steels ADS2 (82 wppm natural B), ADS3 (83 wppm 10B) and ADS4 (1120 wppm 10B) in the reference unirradiated state and after neutron irradiation to a damage dose up to 71 dpa at 334-338 °C. Neutron irradiation leads to a strong increase of lifetime in comparison to the unirradiated state which is more pronounced for low total strain ranges. Such a large lifetime increase can be attributed to the neutron irradiation induced hardening and related strong reduction of the inelastic strain amplitude in comparison with unirradiated state for adequate total strain ranges.

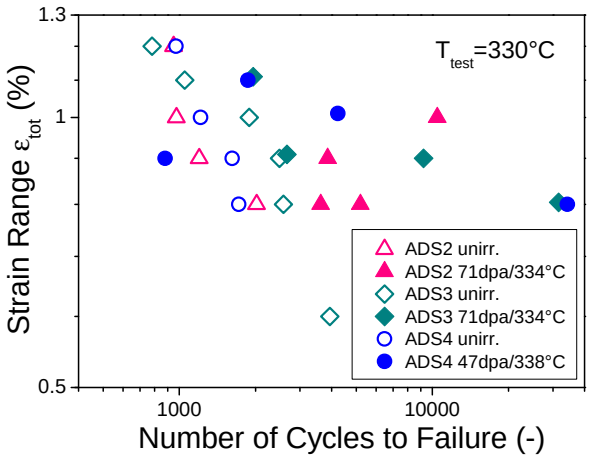

Fig. 1: Fatigue lifetime vs. total strain range of unirradiated and irradiated boron doped EUROFER 97 based RAFM steels.

The LCF properties of EUROFER 97 based ODS steel, EURODShip (containing 0.5 wt% Y_2O_3, HT 980°C, 31 min/air + 760 °C, 90 min/air) are shown in Fig. 2. The neutron irradiation to 46.8 dpa at 337.5 °C leads to a strong

lifetime increase for a total strain range of 1%. For one specimen an endurance behavior is observed. Lifetime increase can be attributed to a strong reduction of the inelastic strain amplitude due to irradiation induced hardening. The post irradiation annealing of the specimen at 550 °C for 3 h leads to a lifetime which is only slightly above the corresponding value in the unirradiated state, indicating considerable recovery of the radiation damage.

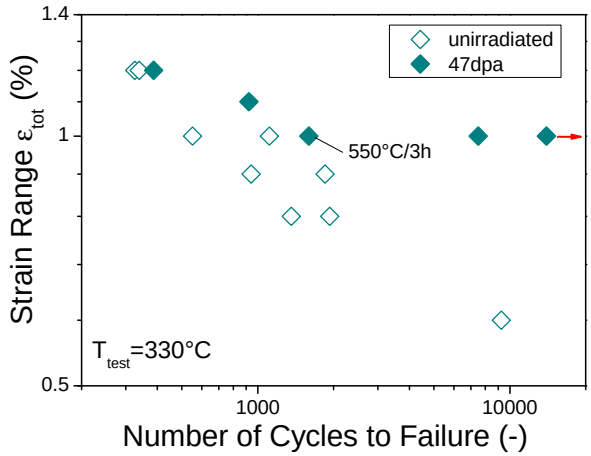

Fig. 2: Fatigue lifetime vs. total strain range of unirradiated and irradiated EUROFER 97 based ODS steel with 0.5 wt% Yttria.

Within ARBOR 2 irradiation Programme KIT contributed to technological studies by diffusion welded EUROFER 97. The impact and miniaturised tensile specimens were machined from the FW and CP component mock-ups produced in diffusion welding experiments by using HIP. The components were produced in one (1xHIP) or two (2xHIP) successive HIP welding steps. Finally, all components have been subjected to PWHT at 750 °C for 120 min. In the course of 2010 irradiated miniaturized double-T shaped specimens machined from the FW and CP component mock-ups were tested in uniaxial tensile experiments.

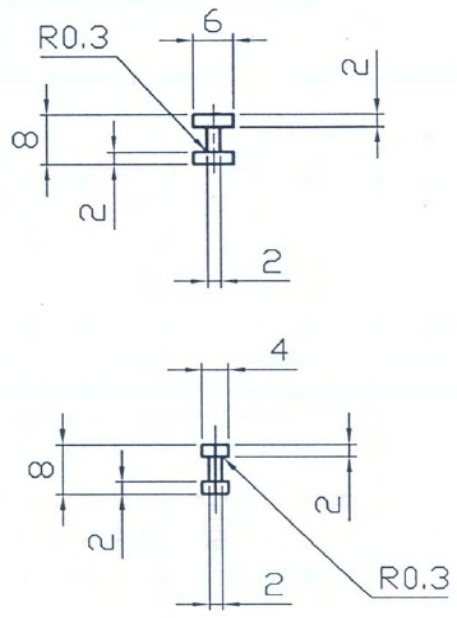

Fig. 3: Double-T shaped specimens for the tensile testing of diffusion welded specimens.

The geometry of the tensile specimens is shown in Fig. 3. The estimated gauge length of the specimens is 3.5 mm. The tensile tests have been performed with an electro-mechanical testing machine of INSTRON-DOLI at two temperatures of 20 and 300 °C and at two crosshead speeds of 0.1 and 1.0 mm/min. Almost all specimens were broken within the gauge length. Fig. 4 shows the Rp0.2 yield stress of 1xHIP and 2xHIP welded specimens in the unirradiated condition and after neutron irradiation to 36.2 dpa at 336.8 °C. For comparison the results obtained with double-T shaped specimens on the unirradiated base EUROFER 97 subjected to a similar HIPping process are also included. The yield stress values of unirradiated and 1 and 2 times HIPped base EUROFER 97 are comparable to those of as delivered ERUOFER 97. The Rp0.2 yield stress of HIP welded specimens shows scatter in the unirradiated condition in Fig. 4. Furthermore, in the unirradiated condition 2xHIP welded specimens show Rp0.2 values well above the yield stress values for base material. The neutron irradiation leads to a strong hardening of welds. Exact assessment of the hardening is not possible due to scattering of the tensile results. The post irradiation annealing at 550 °C for 3 h lead to substantial recovery of the tensile properties both for 1xHIP and 2xHIP welded specimens.

Fig. 5 shows the yield stress as a function of crosshead speed at two different test temperatures. Due to a large data scatter no clear effect of the crosshead speed on the yield stress can be identified both in the unirradiated and irradiated conditions. Also for the base material no strong effect of the deformation rate on the yield stress is observable.

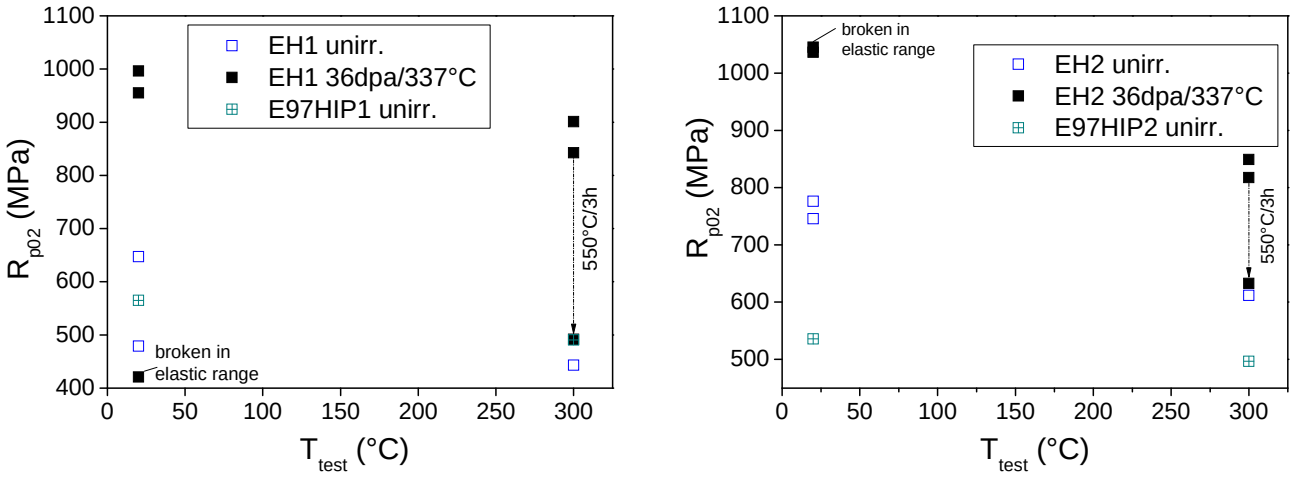

Fig. 4: Yield stress vs. test temperature for 1xHIP (EH1) and 2xHIP (EH2) welded specimens in the unirradiated condition and after neutron irradiation to 36.2 dpa at 336.8 °C. The results on 1x HIPped (E97HIP1) and 2x HIPped (E97HIP2) base EUROFER 97 in the unirradiated condition are also included. Crosshead speed 1.0 mm/min corresponds to 4.8x10-3 1/s strain rate. Dashed arrows indicate recovery of the Rp0.2 in post irradiation annealing at 550 °C for 3 h.

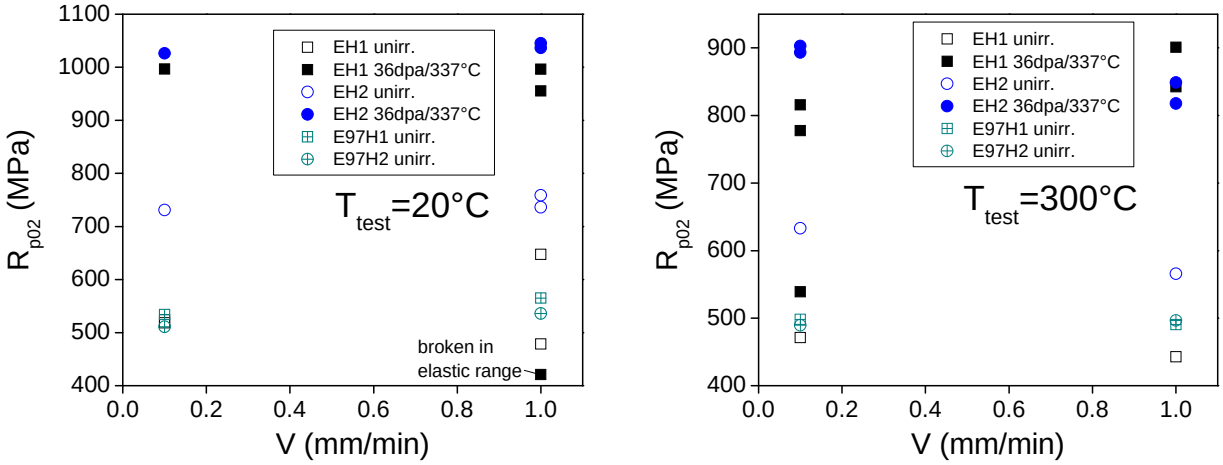

Fig. 5: Yield stress vs. crosshead speed for 1xHIP (EH1) and 2xHIP (EH2) welded specimens in the unirradiated condition and after neutron irradiation to 36.2 dpa at 336.8 °C. The results on 1x HIPped (E97HIP1) and 2x HIPped (E97HIP2) base EUROFER 97 in the unirradiated condition are included.

Uniform elongation values obtained with miniaturized double-T shaped specimens are shown in Fig. 6. Neutron irradiation leads to a strong reduction of the uniform elongation in comparison to the reference unirradiated state both for 1xHIP and 2xHIP welded specimens. An outliner was one 2xHIP welded specimen which yielded a uniform elongation comparable to that of unirradiated state at a test temperature of 300 °C. Post irradiation annealing at 550 °C for 3 h yielded recovery of the uniform elongation at a test temperature of 300 °C. The total elongation values quantified with miniaturized double-T shaped specimens were well above the corresponding values quantified with mini-tensile specimens indicating non optimized geometry of double-T shaped specimens.

Summary and Outlook

The influence of the neutron irradiation on fatigue behaviour was determined for boron doped EUROFER 97 based ADS steels, ODS EUROFER steel and other RAFM steels. The comparison with the corresponding results in the reference unirradiated state has been performed. The limited number of available irradiated specimens does not allow detailed statis-

tical analysis. In the most case the neutron irradiation leads to a lifetime enhancement which is more pronounced for the low total strain ranges. Such behaviour can be attributed to the reduction of the inelastic strain range due to neutron irradiation induced hardening.

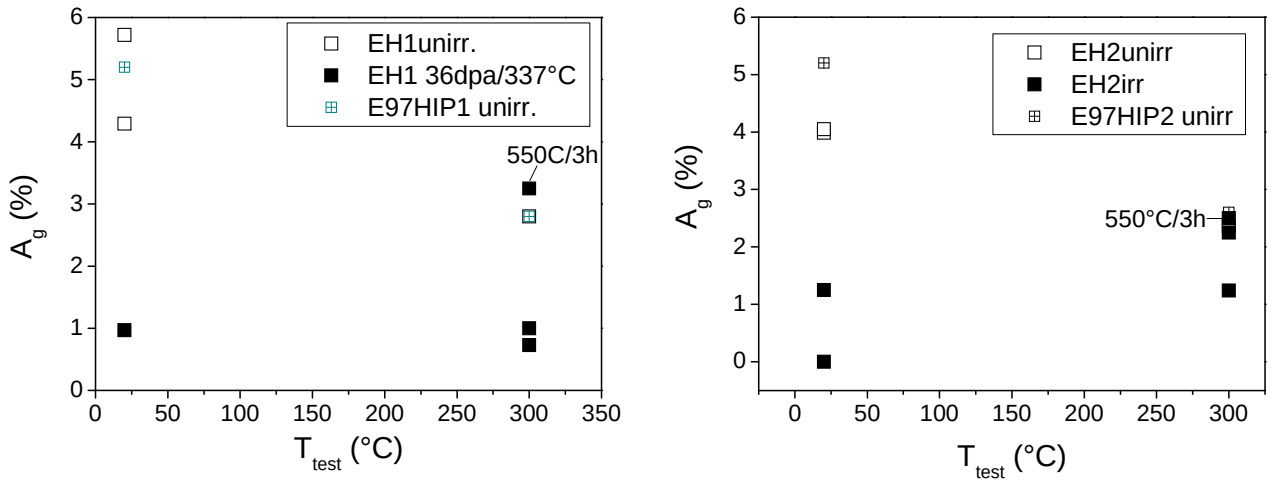

Fig. 6: Uniform elongation vs. test temperature for 1xHIP (EH1) and 2xHIP (EH2) welded specimens in the unirradiated condition and after neutron irradiation to 36.2 dpa at 336.8 °C. The results on 1x HIPped (E97HIP1) and 2x HIPped (E97HIP2) base EUROFER 97 in the unirradiated condition are included. Crosshead speed was 1mm/min.

Tensile testing of the miniaturized double-T shaped specimens machined from the diffusion welded EUROFER mock-up with cooling channels has been performed. The results can be used for a qualitative assessment of the irradiation resistance of the welds. The scattering of the data obtained with miniaturized double-T shaped specimens, however does not allow quantitative assessment of the irradiation induced hardening. The post irradiation annealing of irradiated specimens leads to a substantial recovery of the tensile properties.

Post Irradiation Mechanical Examination of the irradiated specimens at SSC RIAR has been successfully finished. Irradiated specimens will be transported to the FML of IMF II for microstructural and fractographic investigations.

Staff:

U. Bürkle
E. Gaganidze
M. Klotz
C. Petersen

Literature:

[1] E. Gaganidze, C. Petersen, J. Aktaa, A. Povstyanko, V. Prokhorov, E. Diegele, R. Lässer, Low Cycle Fatigue Properties of Reduced Activation Ferritic/Martensitic Steels after High Dose Neutron Irradiation, Proc. of 23rd IAEA Fusion Energy Conference, 11-16 October 2010, Daejeon, Korea; Paper FTP/3-4Rb.

Acknowledgement

This work, supported by the European Communities under the contract of Association between EURATOM and Karlsruhe Institute of Technology, was carried out within the framework of the European Fusion Development Agreement. The views and opinions expressed herein do not necessarily reflect those of the European Commission.

Studies of the Effect of Implanted He on EUROFER on Mechanical Properties (eg Tensile) in the T-range 300-500 °C (TW6-TTMS-001 D 5)

Introduction

Reduced activation ferritic/martensitic steels with nanoscaled oxide dispersion strengthened (ODS) particles like EUROFER-ODS appear to be promising candidates for structural materials of fusion reactors because of their high temperature mechanical properties and their potential radiation resistance. Helium can considerably contribute to the low temperature irradiation embrittlement (below ~400 °C) and dislocation channelling in bcc steels. On the other hand, ODS steels have shown recently very favourable tensile properties with significant work hardening capability even after substantial neutron irradiation (30 dpa). In addition it is expected that another favourable behaviour of RAFM-ODS steels is the capability of ODS particles to act as very effective trapping centres for migrating helium, thus suppressing substantially helium bubbles formation at lath and grain boundaries or the surface of larger $M_{23}C_6$ precipitates. As a consequence, nano-dispersed ODS particles are expected to retard the helium embrittlement.

Tensile samples made of EUROFER and EUROFER-ODS were irradiated with 30 MeV alpha particles up to the fluence 10^{18} α/cm^2, thus implanting ~1000 appm helium very homogenously in the deformation volume. The irradiation temperature will vary between 300 and 550 °C covering the most relevant temperature range for DEMO fusion reactor blanket, where EUROFER-ODS will be used as structural material. The post irradiation examinations include instrumented tensile tests at room temperature and detailed microstructural analyses with TEM to study helium and defect morphology as well as their interaction with ODS particles. The results also provide a major input for the validation of modelling of the kinetics of atomic helium and He_nVac_m-clusters and their interaction with dislocations and with nanodispersed ODS particles.

For this purpose, a cyclotron accelerator adopted for high energy helium implantation in the Kurchatov Institute, Moscow has been equipped with various additional devices. This cyclotron is the only accelerator still available to our knowledge in Europe that allows not only surface implantation like JANNUS or others with subsequent microstructural investigations in the micrometer range, but the homogeneous implantation of sufficiently thick steel samples for subsequent mechanical testing.

The experimental results of microstructure investigations and changes of mechanical properties of nano-structured EUROFER alloy irradiated at 300°C and 500°C have been analysed.

Experimental

A characteristic feature of ion irradiation is a strong inhomogeneity of spatial damage distribution. Usually a well defined damage peak is produced near the ion end of range. Such inhomogeneity is not desirable for the samples which will be mechanically tested after irradiation as far as they can not be compared with samples homogeneously irradiated with neutrons. To avoid this effect and to ensure uniform damage distribution a rotating degrader wheel with aluminium foils of different thickness situated between the beam entrance window and the target was used. Ions went through the foil, lose part of their energy and produce a damage peak at another depth (see Fig. 1). The degrader has 24 windows from which 23 were covered with aluminium foils (0.01-0.23 mm) and one was left empty providing the ion energy variation from 0 to 30 MeV.

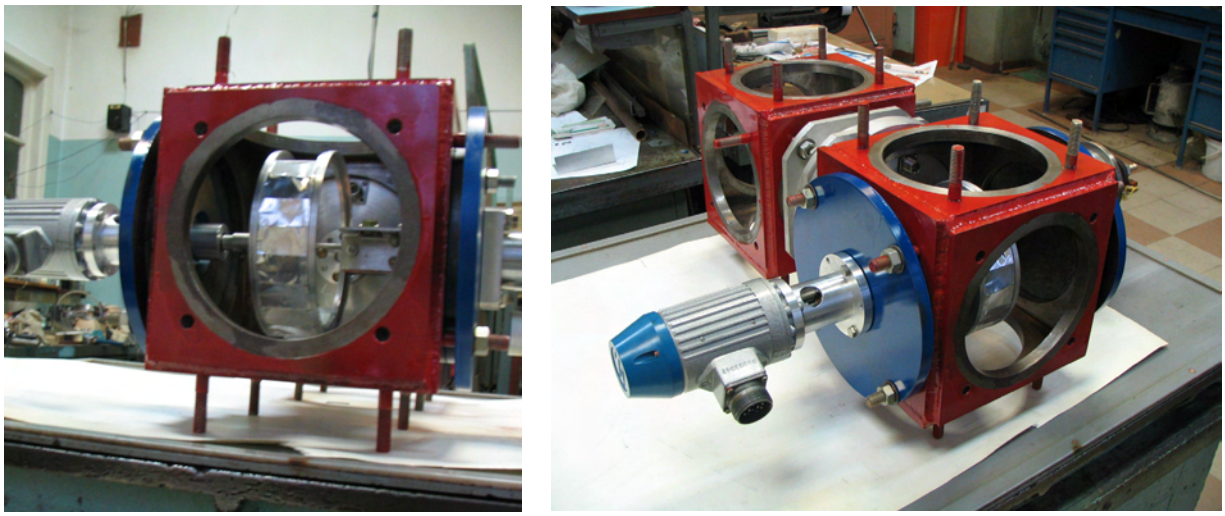

Fig. 1: Target chamber with degrader wheel and step motor.

The tensile tests were performed at room temperature using a universal testing machine Inspekt 50.

Irradiated samples have shown significantly lower stress to rupture i.e. demonstrated softening. Unfortunately, the first two irradiated samples were fixed from both sides during irradiation. Beam induced heating resulted in buckling of the samples, which lost the contact with the thermocouples. The temperature of these samples was supposed to be higher than that measured by the temperature control system, namely approximately 500 °C at the center and 300 °C near the edges.

TEM analysis of non-irradiated and implanted specimens

The microstructural changes of EUROFER-ODS samples were investigated before and after helium ion irradiations using transmission electron microscopy (TEM). The obtained TEM results of the microstructural investigations are shown in Fig.2- Fig.6.

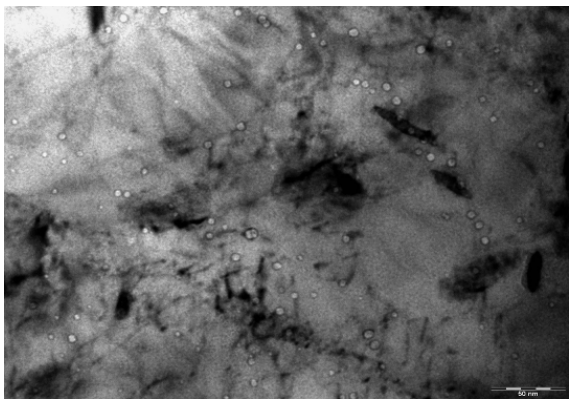

Fig. 2: Microstructure of irradiated ODS materials at 500 ºC with the system of helium bubbles in matrix (scale 50 nm).

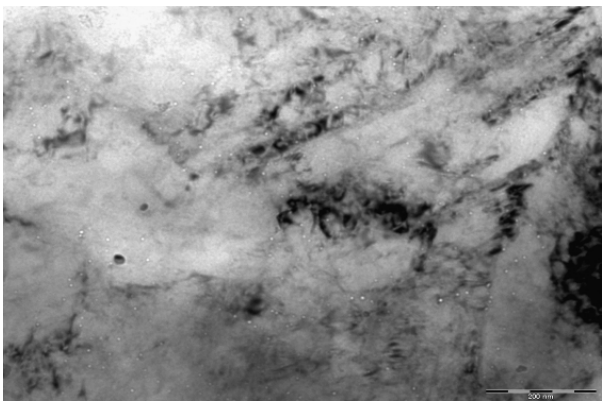

Fig. 3: Microstructure of irradiated ODS materials at 500 ºC with the system of helium bubbles in matrix (scale 200 nm)

Very small helium bubbles can be detected even after irradiation at 300 °C. Sometimes they are found near the surface of large ODS particles. The size of the bubbles is of the order of several nm and is difficult to estimate more precisely due to the stress contrast around the bubbles.

At 500 °C the helium bubbles are much larger (up to 10 nm) and can be observed already at low magnification. Large bubbles have facetted form. Some bubbles are associated with ODS particles. It is clearly seen in, e.g., Figures 5 and 6 that ODS particles pin dislocations thus contribute to the high temperature creep resistance of ODS steels.

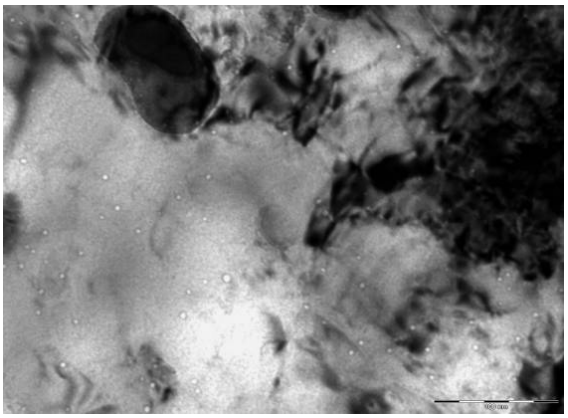

Fig. 4: Microstructure of irradiated ODS materials at 500 ºC with the system of helium bubbles in matrix (scale 100 nm).

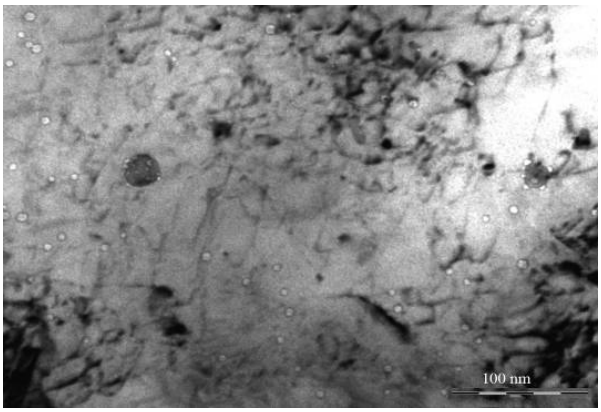

Fig. 5: Microstructure of irradiated ODS materials at 500 ºC with the system of helium bubbles in matrix (scale 100 nm).

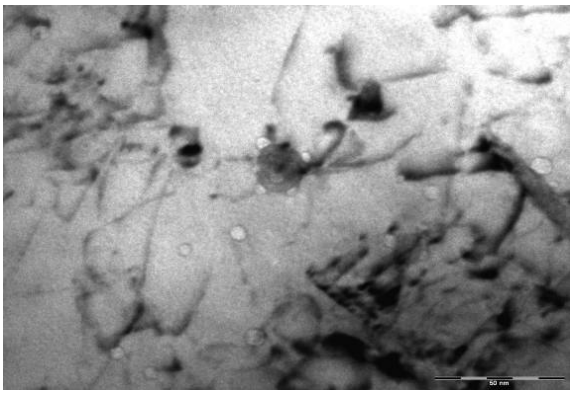

Fig. 6: Microstructure of irradiated at 500 ºC EUROFER ODS with dislocation pinned by Y_2O_3 particle and helium bubbles attached to the particle surface (scale 50 nm).

Conclusions

The helium implantation facility based on the RRC KI cyclotron with maximum helium beam energy of 30 MeV allows the investigation of the effect of helium atom implantation in ODS EUROFER samples on microstructure changes and mechanical properties in the temperature interval 300-500 °C.

- The experimental method for uniform saturation of EUROFER ODS materials by He atoms at different temperatures has been developed and realized using RRC KI cyclotron based on:
  - Numerical calculations of stopped helium ions and radiation damage profiles with helium ion degrader,
  - Design and manufacturing of degrader system for decreasing energy of fast helium ions and uniform saturation of EUROFER ODS materials by helium atoms.
- Mechanical tests of irradiated and unirradiated EUROFER ODS material have been performed. Helium embrittlement (decreasing of elongation to rapture) in irradiated ODS material at T=300 °C and T=500 °C has been observed.

- Microstructure investigations (TEM) of EUROFER ODS materials before and after irradiation have been performed.
- Helium bubble formation in irradiated EUROFER ODS materials at two temperatures: 300 °C and 500 °C has been observed. At both temperatures ODS particles act as effective trapping centers for helium bubbles. With increasing irradiation temperature the number and size of trapped bubbles increase. Large bubbles observed in the bulk of the material are presumably located on dislocation lines providing additional obstacles for dislocation motion.

Staff:

A. Möslang
P.V. Vladimirov
A.I. Ryazanov (Russian Research Center “Kurchatov Institute”, Moscow, Russia)
S.T. Latushkin (Russian Research Center “Kurchatov Institute”, Moscow, Russia)

Acknowledgement

This work, supported by the European Communities under the contract of Association between EURATOM and Karlsruhe Institute of Technology, was carried out within the framework of the European Fusion Development Agreement. The views and opinions expressed herein do not necessarily reflect those of the European Commission.

SANS and TEM Measurements on Irradiated and B-alloyed EUROFER (SPICE Irradiation Campaigns) to Determinate the Effect of He on the Microstructure (TW6-TTMS-001 D 3)

Introduction

Material research for innovative fission and fusion nuclear systems has become a field of growing relevance worldwide. While primary international goals of innovative fission reactors include besides proliferation resistance the minimization of waste and natural resource utilization, future fusion power reactors are expected to use systematically “reduced activation materials” that decay orders of magnitude faster compared to conventional alloys.

Reduced activation ferritic martensitic steels (RAFM) with 8-10%Cr-WTaV are leading candidates for the application in fusion reactors. The EUROFER 97 with 9% Cr has become the European reference RAFM steel for fabrication of blanket material for the future fusion reactor. It is expected that structural materials in a fusion reactor will be exposed to very high levels of irradiation induced displacement damage of more than 100 displacements per atom (dpa) and relatively high He concentrations of up to 10 appm He/dpa, the latter due to inelastic transmutation reactions of energetic fusion neutrons. While displacement damage can lead to a significant strength increase of several hundred MPa accompanied with loss of ductility below an irradiation temperature of about 400 °C, helium can play an additional and severe role in embrittlement in a wide temperature range. Although ferritic martensitic steels have a high sink density that acts as traps for diffusing He atoms thus being more immune to helium embrittlement as many other steels, high concentrations of helium lead nevertheless to a significant population of He bubbles often trapped at interfaces such as precipitates, lath and grain boundaries, or precipitates. The bubble morphology depends very much on irradiation temperature and local microstructure. Although helium is presently considered worldwide as one of the major lifetime limiting factors defining the lifetime of structural components of fusion reactors, the related micro-structural evolution and its implications on relevant macroscopic properties is still not sufficiently understood.

Method

A special wrapper, with irradiation capsules accommodating the tensile- and further impact and fatigue specimens, was inserted in the central part of the reactor core of HFR. The irradiation was set to 250, 300, 350, 400, and 450 °C. The ambient medium was sodium and the temperatures were controlled by changing the gas mixture (helium and neon) in the gas gaps surrounding the specimens. Just small deviations were determined. The cumulative neutron fluence E>0.1 MeV m^{-2} was 22.85 x 10^{25}. The neutron irradiation was carried out in 771 FPD (full power days) up to nominal dose of 15 dpa. The experimental obtained damage levels for monitor set positions in the specimen holder varied between 13.4 to 18.1 dpa. Neutronic calculations have shown that the volume-average displacement dose of all specimens was 16.3 dpa for stainless steel. Alloys on the basic composition of EUROFER 97 with different B contents were included in this program to investigate the behavior of irradiation induced He.

The microstructural examinations included application of TEM methods: the conventional bright field (BF) imaging. The TEM investigations were performed using a FEI Tecnai 20 F microscope equipped with a Gatan image filter for EELS measurements as well as with an HAADF detector for scanning TEM (STEM). The microscope was operated at 200 kV accelerating voltage with a field emission gun.

Results

Characterisation of ADS 3 specimen

One import aim of this irradiation program was to compare the material properties with alloys which had higher concentrations of boron, e.g. ADS3, Heat 826, with 83 ppm ^{10}B. The calculated irradiation induced He concentration was ~415 appm He. This effect was clearly observable by a high concentration of homogenously distributed He bubbles, but combined with a high concentration of dislocation loops and small α`-precipitates, too, Fig. 1, 2. After the tensile tests at 300 °C, the orientation of dislocation loops and small α`-precipitates were not as distinctive as in EUROFER 97 HT, but the high density of He bubbles was still maintained, Fig. 3. Recovery could be observed after T_{irrad} and T_{test} = 450 °C, too, Fig. 4. Dislocation loops and small α`-precipitates were not developed, but the He bubbles were concentrated along dislocations and grain boundaries, fig. 4. Often was observed that the bubbles form the pattern on the grains boundaries (Fig. 4). The size distribution histogram of the bubbles in the specimen irradiated at 450 °C is shown in the Fig. 5. The average bubbles size was measured to 4-5 nm.

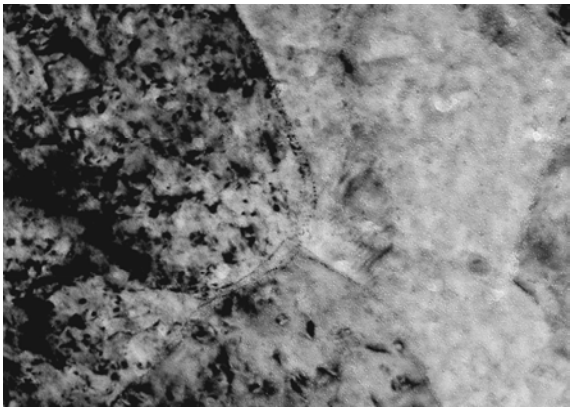

Fig. 1: ADS3, Heat 826, undeformed, 16.3 dpa, Tirr = 250°C.

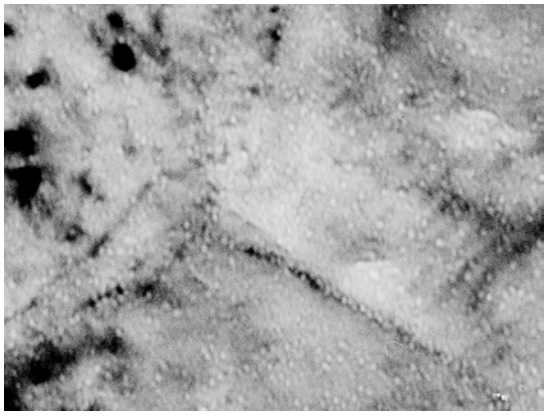

Fig. 2: Detail of fig. 1.

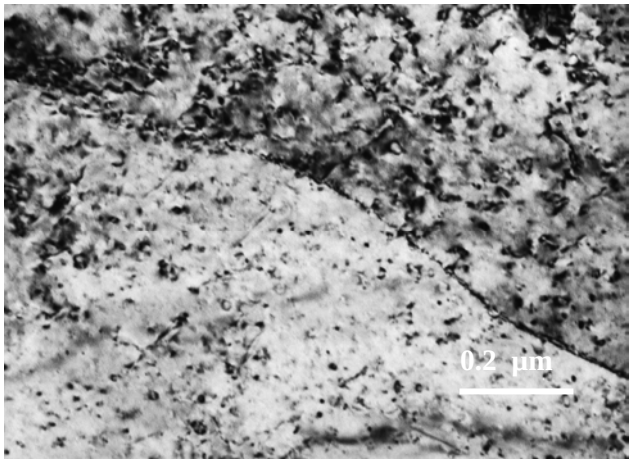

Fig. 3: ADS3, Heat 826, after tensile test 16.3 dpa, Tirr = Ttest = 300 °C.

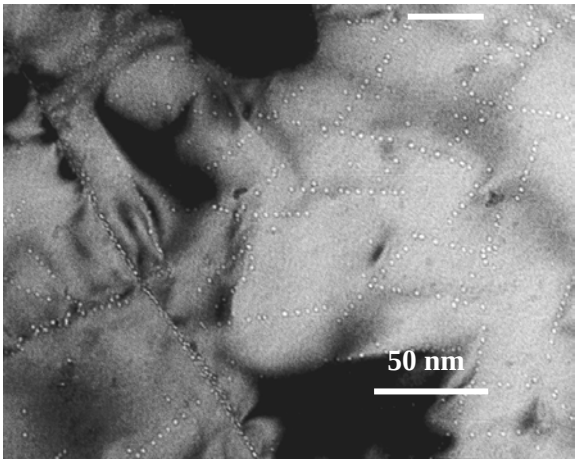

Fig. 4: ADS3, Heat 826, after tensile test, 16.3 dpa, Tirr = Ttest = 450 °C.

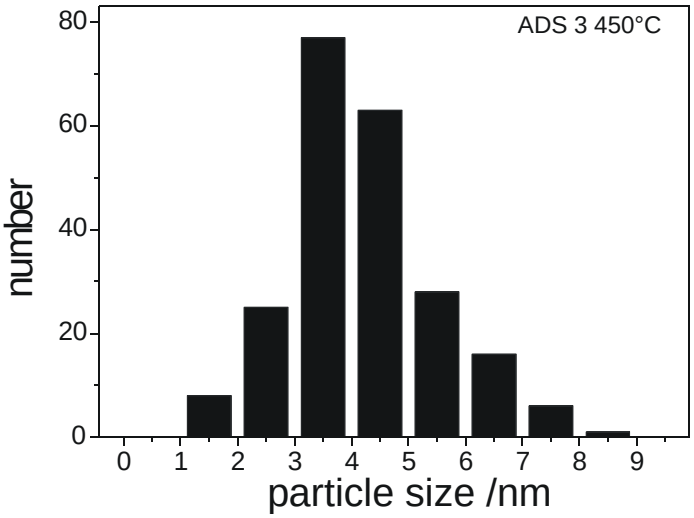

Fig. 5: Size distribution histogram of the bubbles in the ADS3 specimen. Tirr=450°C.

Characterisation of ADS 4 specimen

The ADS4 material contains about 5800 appm helium. The investigation of the specimens after irradiation at 300 °C show the formation of homogenously distributed He bubbles (Fig. 6). The size distribution histogram of the He bubbles is presented in Fig. 7. The bubble size in the specimen varied from 1 to 10 nm. The average size can be estimated to 6 nm. However, decoration of some lath boundaries can be clearly observed.

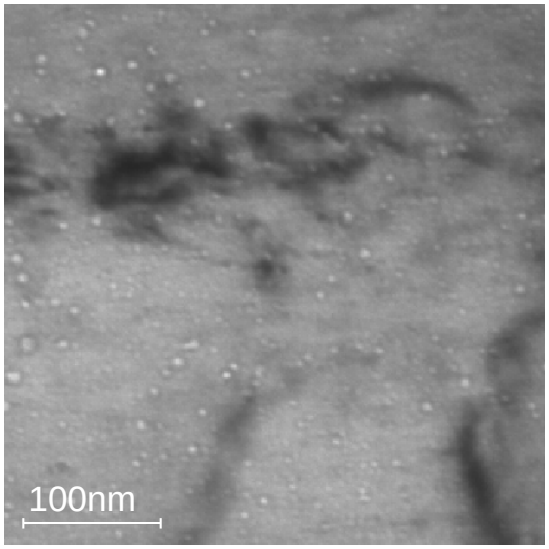

Fig. 6: He bubbles in the ADS4 specimen Tirr = 300 °C.

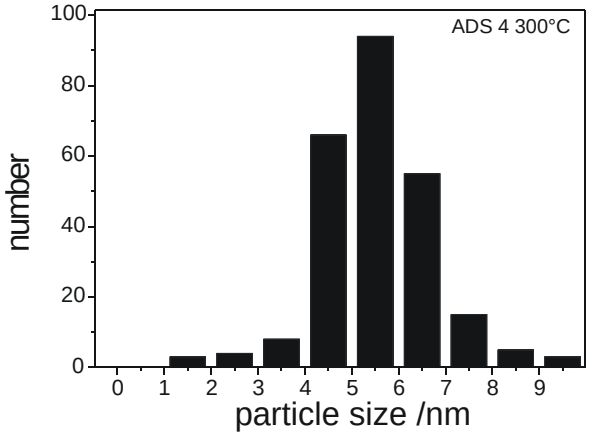

Fig. 7: The size distribution histogram of He bubbles in ADS4 specimen Tirr = 300 °C.

In Fig. 8 are presented the TEM investigations of the specimen irradiated at 400°C. The bubbles with the size of few tens nanometer are clearly visible in the image. The bubbles found were present inside the lath as well as along the grain boundaries. They are statistically distributed in the specimen. The bubble size varied from 5 to 40 nm with an average of 14 nm (Fig. 9).

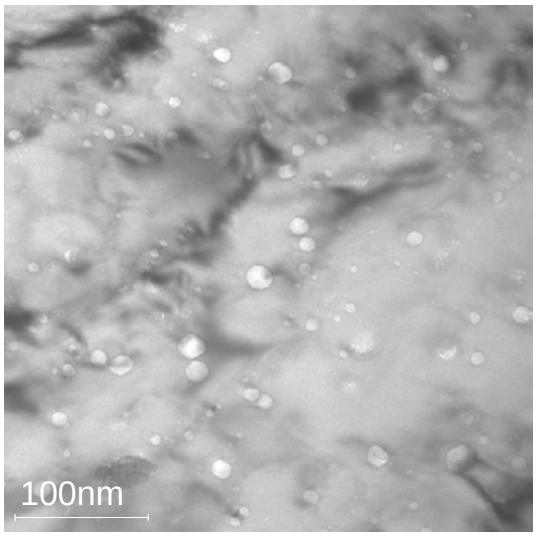

Fig. 8: He bubbles in the ADS4 specimen Tirr = 400 °C.

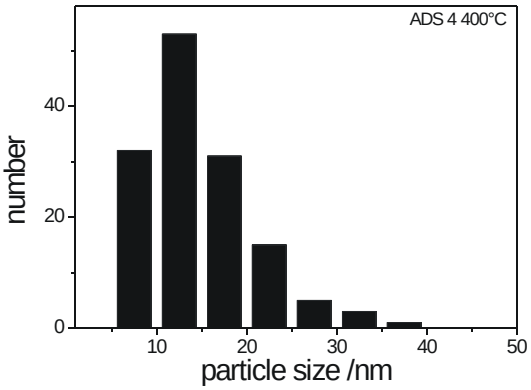

Fig. 9: The size distribution histogram of He bubbles in ADS4 specimen Tirr = 400 °C.

Conclusions

TEM characterizations of boron alloyed specimens, that have been irradiated up to 16 dpa at irradiation temperatures between 250-450 °C were performed. The achieved He concentration by $^{10}B(n,\alpha)^{7}Li$ generation was <10 appm He, ~80 appm He, ~415 appm He, and ~5800 appm He, respectively, resulting in a helium/defect ratio from <<1 to ~350 appm He/dpa.

Helium bubble distribution: However already at ^{10}B-contens of 83 appm (He concentration of 415 appm after irradiation) B segregates at larger precipitates, resulting in a corona of He bubbles around the precipitate. The distance of the He corona corresponds roughly to the calculated range of the 1.6 µm of the 1.7 MeV He-atoms, that are emitted as a result of the ^{10}B decay.

Staff:

M. Klimenkov
R. Lindau
E. Materna-Morris
A. Möslang

Intellectual Property Rights (IPR)

In the frame of this work a new element of know-how has been generated.

Acknowledgement

This work, supported by the European Communities under the contract of Association between EURATOM and Karlsruhe Institute of Technology, was carried out within the framework of the European Fusion Development Agreement. The views and opinions expressed herein do not necessarily reflect those of the European Commission.

TEM Investigations of Neutron Irradiated EUROFER 97 and Boron Doped EUROFER (WP10-MAT-REMEV-08-01)

Introduction

Specimens of EUROFER97 prepared for impact tests have been irradiated up to an average dose of 16.3 dpa at irradiation temperatures of 250°C, 300°C, 350°C, 400°C and 450 °C. The TEM investigations have been performed to study radiation induced changes of the microstructure. The investigations show the temperature dependant formation of small interstitial dislocation loops and He bubbles as well as their statistical analysis. The ½<111> Burgers vector of dislocation loops has been detected.

Method

The neutron irradiation was performed in the HFR (High Flux Reactor, Petten, Netherlands). Neutron flux was 3.99 x10 18 $m^{-2}s^{-1}$ (E>0.1 MeV). The TEM specimens were prepared and analyzed in the FML (Fusion Materials Laboratory) of the Hot Cell facility of Karlsruhe Institute of Technology.

For the preparation by electrochemical etching used the Tenupol-3 jet polisher with a 20% H_2SO_4 + 80% CH_3OH solution as electrolyte. A voltage of 10-12 V was used for etching. The investigations were performed using a FEI Tecnai 20 F microscope suitable for analysing of active specimens. The microscope was operated at 200 kV accelerating voltage with a field emission gunby strong electric field pulses. Some fraction of the evaporated and ionized atoms (usually ~50%) fly to a detector where they are registered and their final position is fixed. Their initial position in the lattice can be recalculated using known electric field distribution. Analysis of the measured time of flight of each atom from the tip of the probe to the detector provides information on the charge to mass ratio, which is usually sufficient to determine uniquely the nature of evaporated chemical specie.

Results

Analysis of dislocation loops

The bright and dark field images of small dislocation loops in a specimen after irradiation at 250 °C is shown in Fig. 1 as an example. Both images were obtained near the [001] zone axis. The diameter of the defects ranged from 2-5 nm to the 15 nm dislocations loops, where the fraction beyond 15 nm is very low. In the case of small (2-5 nm) defects it is sometimes difficult to definitely determine whether they are small dislocation loops or point defects. In the weak beam dark field image g(4g) g={020} numerous small white dots and few loops are visible (Fig. 1b). The concentration of the detected visible defects was estimated to 2±0.5 x 10^{15} cm^{-3}. The dislocation loops have a ½<111> Burgers vector as it can be determined using standard **g**·**b**=0 invisibility criteria. For this measurement the specimen was imaged near the [001] zone axis.

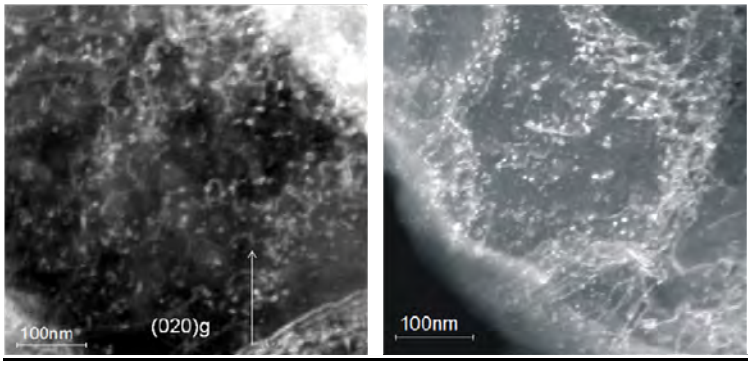

Fig. 1: TEM image of the specimen irradiated at 250 °C using **g**=110 (a) and weak beam image g(4g) g=200 (b).

Fig. 2 shows the ±g analysis of dislocation loops. The weak beam (**g**=4**g**) image shown in the part (a) was obtained using **g**=(01-1). The image shown in the part (b) was obtained using **g**=(0-11). In both images the same dislocation loops are visible; however, they show a different inside-outside contrast. The loops marked by different arrows show the different inside-outside behaviour by changing the **g** vector. The investigations confirm that these loops have an interstitial nature.

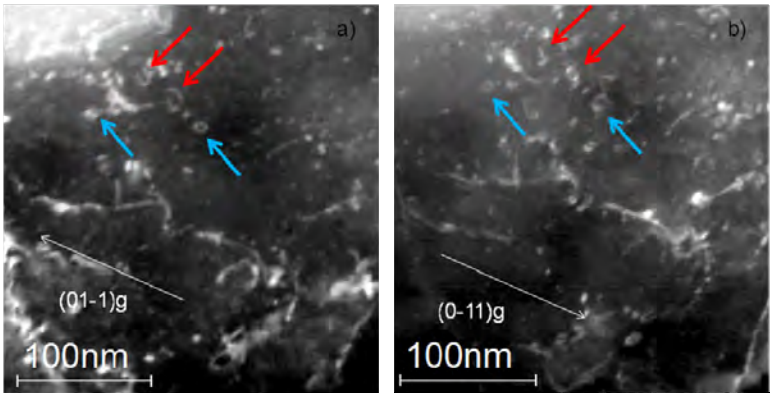

Fig. 2: TEM image of the specimen irradiated at 250 °C (a) +g and (b) using –g.

Analysis of helium bubbles

He embrittlement is investigated in boron alloyed EUROFER 97 based steels. The specimens have been alloyed with different contents of natural boron and the separated ^{10}B-isotope (0.008-0.112 wt.%). The alloyed steels show pronounced embrittlement and reduction of toughness with increasing boron and following helium amount. At T_{irr} =300 °C helium induced embrittlement is most pronounced.

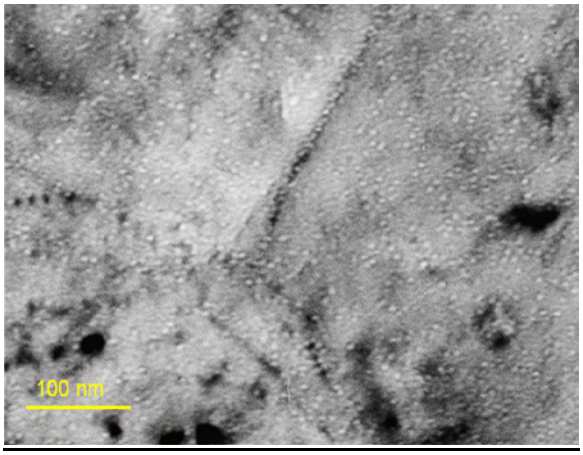

Fig. 3: Images of He bubbles in the specimen with 415 appm He irradiated at 250 °C.

He bubbles with the sizes down to 10 nm have been detected in the specimen with the He irradiated at 250 °C (Fig. 3). The bubbles decorate the grain boundaries and are also homogeneously distributed inside grains or laths. The distribution of the grains and dislocation lines has been detected in the same specimen after irradiation at 450 °C (Fig. 4). In the cut-out presented in Fig.4 the bubbles form a pattern on the lath boundary.

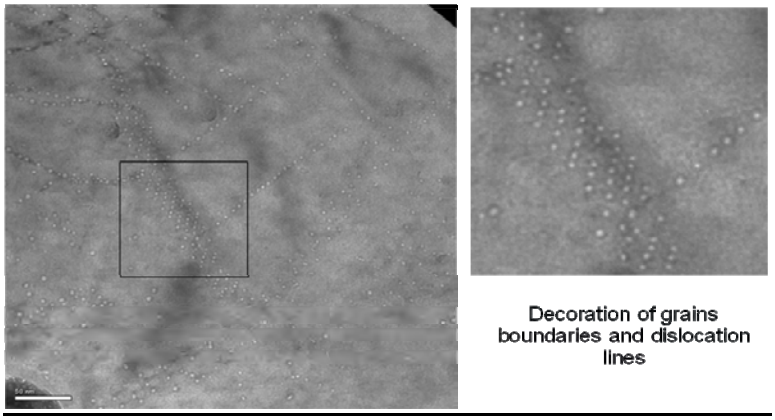

Fig. 4: Images of He bubbles in the specimen with 415 appm He irradiated at 450 °C.

Conclusions

After neutron irradiation of EUROFER 97 between 250 and 450 °C up to 16.3 dpa density, size, orientation and nature of irradiation induced defects have been analyzed by TEM. All loops investigated showed a Burgers vector of ½<111>. The application of **g**, **-g** analysis show that inside-outside contrast changes correspond to the interstitial loops. While the defect density revealed a strong decrease from 300 °C towards 400 °C as expected, an abnormal density decrease from 300 °C to 250 °C has been observed. However, this observation correlates with recent tensile and Charpy results that showed a maximum of irradiation hardening and embrittlement also around 300 °C. Very few and completely non-homogeneously distributed voids or helium bubbles have been found that can be attributed to the production of helium from segregated boron.

Staff:

M. Klimenkov
E. Materna-Morris
A. Möslang
R. Rolli
H.-C. Schneider

Acknowledgement

This work, supported by the European Communities under the contract of Association between EURATOM and Karlsruhe Institute of Technology, was carried out within the framework of the European Fusion Development Agreement. The views and opinions expressed herein do not necessarily reflect those of the European Commission.

TEM & SEM Microstructural Investigations of Irradiated Specimens from WTZ and ARBOR 1 (WP10-MAT-REMEV-08-02)

Objectives

The current task aims at analyzing the neutron irradiation induced evolution of the microstructure in the RAFM steel EUROFER 97 addressing (a) irradiation dose dependence of *sizes* and *volume densities* of radiation defects (e.g. defect clusters, dislocation loops, precipitates); (b) neutron flux dependence of *sizes* and *volume densities* of radiation defects. A long term goal is the correlation of the neutron irradiation induced changes in the microstructure to the changes in the mechanical properties, as well as the development of a phenomenological model describing the evolution of radiation defects in RAFM steels. The specimens to be studied in this task stem from SPICE (15 dpa/300 °C, HFR, NRG, Petten), WTZ (15 dpa/330 °C, Bor-60, JSC "SSC RIAR", Dimitrovgrad) and ARBOR 1 (32 dpa/ 330 °C, Bor-60, JSC "SSC RIAR", Dimitrovgrad) irradiation programs. The neutron fluxes (>0.1 MeV) for Bor-60 and HFR irradiations were 1.8×10^{19} $m^{-2}s^{-1}$ and 4.0×10^{18} $m^{-2}s^{-1}$, respectively.

Task Current Status

The microstructure of EUROFER 97 specimens irradiated in the WTZ and ARBOR 1 irradiation programs was analyzed quantitatively with the high resolution FEI Tecnai G² F20 X-TWIN TEM installed in the hot cells of the FML.

The WBDF technique was used for imaging of radiation induced defects in the 15 and 32 dpa samples. Using 11 different diffraction conditions WBDF micrographs were taken and analyzed in detail, with respect to size distributions and volume densities of the defects. The thicknesses of the analyzed specimen areas necessary for the determination of defect densities were obtained by application of the CBED technique. Exemplarily Fig. 1a) shows a WBDF micrograph of the ARBOR 1 sample (32 dpa) taken with a diffraction vector g={200}, g(4.1g).

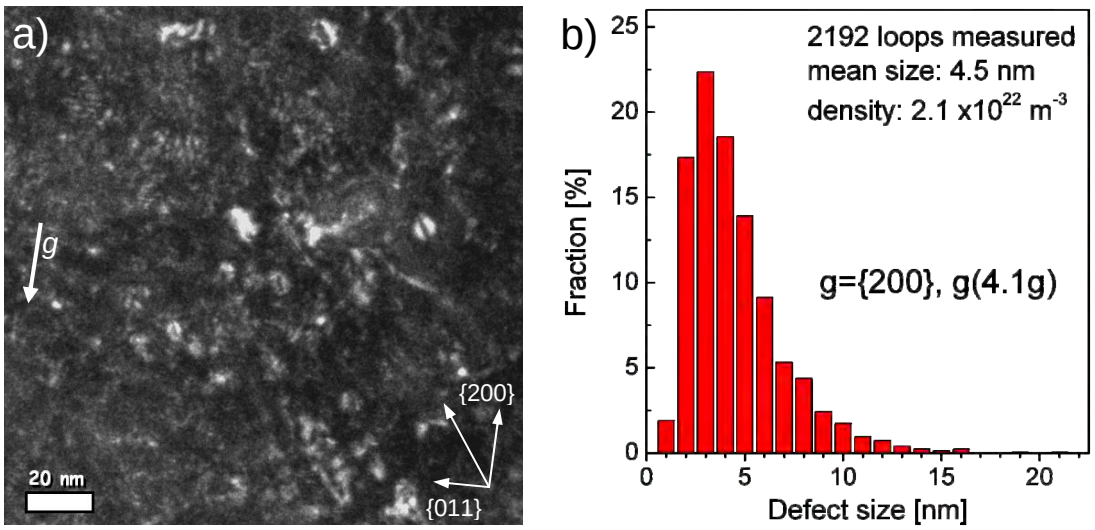

Fig. 1: a) WBDF micrograph of EUROFER97 irradiated to 32 dpa, taken with g={200}, g(4.1g) (ZA=<011>).
b) Size distribution and volume density of radiation induced defects for the corresponding specimen and diffraction condition.

Dislocation loops with diameters of up to 20 nm are visible in Fig. 1 a). Most of the loops appear edge on, with strong double arc contrast and are oriented along {211} directions. The analyzed grain was oriented with the <011> ZA parallel to the electron beam and was 106 nm thick. The corresponding size distribution and density of the defects are given in Fig. 1b). The resulting average sizes (d) of the defects are 3.4 nm & 4.8 nm and the average densities (N) are 1.4×10^{22} m^{-3} & 1.7×10^{22} m^{-3} for the 15 dpa and the 32 dpa specimens, respectively.

The change of N and d is relatively small, which agrees well with the experimentally observed hardening and embrittlement of the material tending to saturate at high damage doses. It is important to notice that due to different orientations with respect to the direction of the electron beam only a fraction of defects is visible in the analyzed micrographs. Furthermore, for the case of EUROFER 97 irradiated to 32 dpa, the nature of the dislocation loops has been analyzed by investigating a certain area of a specimen using different diffraction conditions. By applying the invisibility criterion g•b=0 it was found that most of the dislocation loops have Burgers vectors of the b = ½<111> type.

Analyzing EUROFER 97 specimens irradiated to 15 dpa in the BF image mode small cavities became visible when going off-focus. A systematical through-focus series analysis showed that the contrast of these defects changes from a white dot with a black ring to a black dot with a white ring (Fresnel contrast) when going from underfocus to overfocus, which confirms the presence of voids or bubbles. To check for transmutation helium EELS spectra were measured with a very fine electron beam inside and outside of the voids. A comparison of the spectra revealed no He absorption edge (at around 21.2 eV). Fig. 2 a) shows an underfocused BF micrograph with several voids. As depicted in Fig. 2 b) size distribution and density of voids in the 15 dpa specimens were determined, the average values are 2.6 nm and 3.6 x 10^{20} m^{-3} respectively.

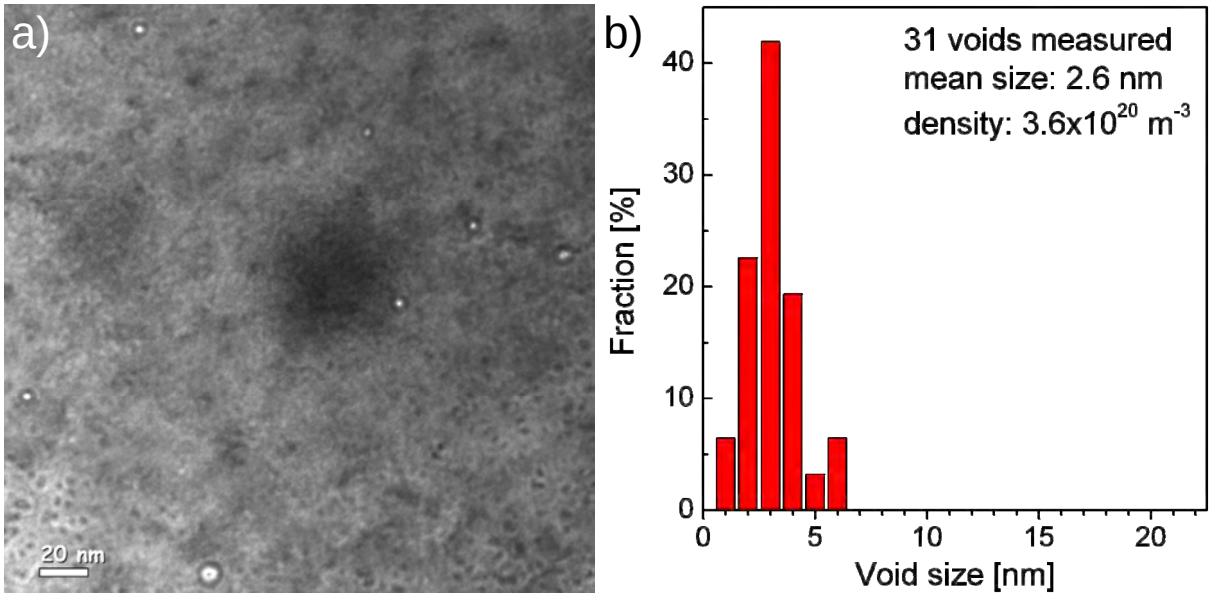

Fig. 2: a) Underfocused (-2 µm) Bright-field (BF) image of EUROFER 97 irradiated to 15 dpa showing irradiation induced voids. b) Density and size distribution of voids for the corresponding specimen.

The results of the quantitative investigations are summarized in Tab. 1.

Tab. 1: Quantitative microstructural data from TEM investigations of neutron-irradiated EUROFER 97

Irrad. program	Dose (dpa)	T_{irr} (°C)	Av. defect size (nm)	Av. defect density (m^{-3})	Av. void size (nm)	Av. void density (m^{-3})
WTZ	15.0	332	3.4	1.4×10^{22}	2.6	3.6×10^{20}
ARBOR 1	31.8	332	4.8	1.7×10^{22}		

Within the HRJRG-13 project a phenomenological model describing helium cluster/bubble growth kinetics under neutron irradiation has been developed. The model is based on kinetic rate equations and is solved by a Fortran code. Simulations were performed for the EUROFER 97 based boron doped alloys ADS2 and ADS3, which differ in the alloyed ^{10}B amount and therefore produce different helium concentrations under irradiation (see Fig. 3). Characteristic irradiation conditions of SPICE and ABROR 1 experiments were taken into account by adapting the parameters like temperature and varying helium generation rates due to different boron transmutation cross sections in the considered irradiation programs.

Fig. 3 shows the final cluster size distributions in ADS2 and ADS3 for SPICE and ABROR 1 experiments. The irradiation times as well as the final helium amounts generated by transmutation of helium producing isotopes are given in the figure legends. Simulation yield peak bubble diameters of 3.8 and 4.6 nm for SPICE and 8.4 and 9.5 nm for ARBOR 1. Increased helium diffusivity at higher temperatures is mainly responsible for larger bubbles in ARBOR 1, while higher helium generation rates in SPICE yield higher cluster densities.

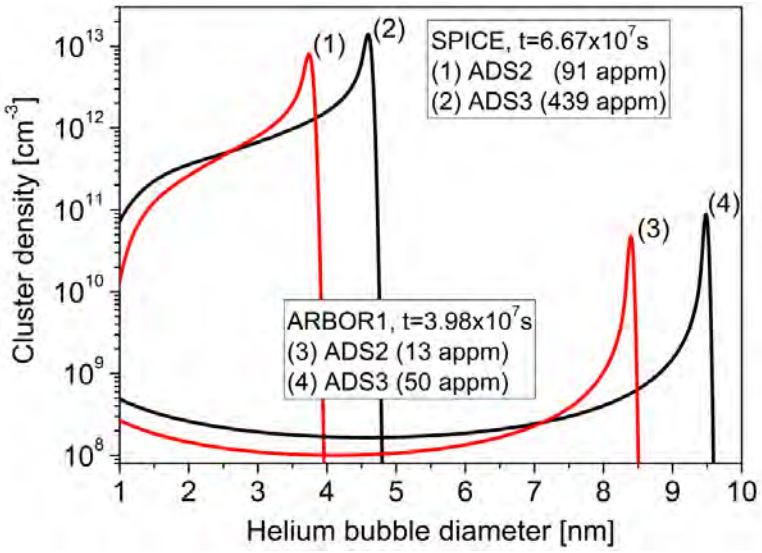

Fig. 3: Simulations of the final cluster size distributions in SPICE and ARBOR 1 irradiation experiments for the given irradiation times.

Model validation will be done by the comparison of simulation results with bubble size distributions to be investigated by a quantitative TEM analysis. Future work will consider helium clustering at sinks. Finally, simulations will predict helium bubble distributions as they are expected in the First Wall of a future fusion reactor.

Conclusion and Outlook

The volume densities and size distributions of the dislocation loops have been quantified for EUROFER 97 samples irradiated to 15 and 31.8 dpa at 330-332 °C. In addition size distribution of voids has been studied in a 15 dpa irradiated specimen. The average size and average volume density of dislocation loops show only slight increases from 15 to 32 dpa in a good accordance with the experimentally observed hardening and embrittlement tending towards saturation at high damage doses.

Further TEM investigations of irradiated EUROFER97 specimens will be conducted, with respect to quantification of sizes and volume densities of radiation induced defects (e.g. defect clusters, dislocation loops, voids/bubbles precipitates). The activities will particularly include analysis of voids and Cr-rich alpha-prime precipitation in EUROFER 97 (WTZ, ARBOR 1) as well as investigation of helium bubble distribution in high dose irradiated boron containing steels (ARBOR 1). Investigation of 70 dpa irradiated steels will be performed depending on availability of ARBOR 2 specimens. The results of quantitative microstructure analysis will be used for verification of models for evolution of the radiation defects in RAFM steels.

Staff:

C. Dethloff
E. Gaganidze
O. Weiß

Literature:

[1] O. J. Weiß, E. Gaganidze, J. Aktaa, Quantitative TEM investigations on EUROFER 97 irradiated up to 32 dpa, Advances in Science and Technology Vol. 73 (2010) pp 118-123.

[2] O. Weiß, E. Gaganidze, Quantitative TEM investigation of neutron irradiated EUROFER97 from ARBOR 1, EFDA Monitoring Meeting: Radiation Effects Modelling and Experimental Validation, July 1-2, 2010, San Sebastian, Spain

[3] O. Weiß, E. Gaganidze, Quantitative TEM investigation of neutron irradiated EUROFER97 from WTZ and ARBOR 1, EFDA Monitoring Meeting: Radiation Effects Modelling and Experimental Validation, November 22 - 23, 2010, Paris, France

[4] C. Dethloff, E. Gaganidze, V. Svetukhin, M. Tikhonchev, O. Weiß, J. Aktaa, Modeling of helium bubble formation and growth in RAFM steels under neutron irradiation, Proceedings of the 1st International Conference on Materials for Energy, July 4-8, 2010, Karlsruhe, Germany

[5] C. Dethloff, E. Gaganidze, V. Svetukhin, M. Tikhonchev, O. Weiß, J. Aktaa, Modeling of helium bubble growth in neutron irradiated boron doped RAFM steels, Proceedings of the 5th International Conference on Multiscale Materials Modeling, October 4-8, 2010, Freiburg, Germany

Acknowledgement

This work, supported by the European Communities under the contract of Association between EURATOM and Karlsruhe Institute of Technology, was carried out within the framework of the European Fusion Development Agreement. The views and opinions expressed herein do not necessarily reflect those of the European Commission.

Operation of the Fusion Materials Laboratory (Underlying Technology) (CoA)

The Fusion Materials Laboratory provides the infrastructure for the performance of tasks defined in the EFDA and F4E work programmes related to the characterisation and testing of irradiated and non-irradiated materials. Methods such as optical and electron microscopy, tritium adsorption and desorption, He pycnometry and Hg porosimetry, crush load, micro hardness, creep, charpy impact, tensile, LCF and instrumented indentation tests as well as long-time annealing tests are applied. The work includes Post Irradiation Examinations (PIE) of Reduced Activation Ferritic Martensitic (RAFM) steels (reference material for DEMO and ITER-TBMs) and tungsten as well as investigations on materials relevant for the HCPB blanket (ceramic breeder materials, beryllium).

PIE on selected samples from the HFR IIB and BOR 60 experiments were performed. For this purpose, charpy impact tests, tensile tests, and LCF tests were performed and density of irradiated and unirradiated materials was compared. Tested specimens' small cuts were prepared for light optical, scanning and transmission electron microscopy and examined. Broken halves of charpy specimens were prepared for instrumented indentation and served for identifying material parameters and Vickers hardness. The aim of the investigations was to study the irradiation effects on the mechanical and structural properties of these materials and to investigate the possibilities of a post-irradiation heat-treatment in order to reduce irradiation defects.

The investigation of blanket materials was continued. Lithium orthosilicate pebbles were investigated by light optical microscopy and their porosity and deformation hardness were determined. Different batches of materials were characterised with respect to the influence of parameters of the fabrication process on the mechanical and structural properties. Tritium adsorption/desorption tests and creep tests were done on beryllium, beryllium vanadium, and beryllium titanium alloys and on BeO-doped beryllium, both on single pebbles and on pebble beds.

Adsorption and desorption experiments were also done with unirradiated beryllium titanium pebbles. Furthermore different beryllium titanium alloys were characterized by light optical and scanning electron microscopy. Porosity measurements and creep tests were performed. Activated beryllium from the HIDOBE irradiation was investigated by light optical and scanning electron microscopy, by densiometry, and specimens were prepared for SANS experiments.

Detailed results and consecutive analysis of the measurements are reported in the respective chapters of this report.

For the PIE the following equipment was used:

- Charpy impact, LCF and tensile testing devices
- Indentation device for instrumented ball-indentation and Vickers hardness-test
- Light optical, scanning electron and transmission electron microscopes with analysis of chemical elements
- Desorption device with high temperature furnace for tritium and helium release measurements
- He-pycnometer and Hg-porosimeter
- Sphere crush and creep testing apparatus.

Regular operation of the new 200 kV high resolution transmission electron microscope for investigation of radioactive material down to atomic scale started. Various results, identifying the damage mechanisms in highly irradiated steel, could be published. A new glove-box for

safe electrochemical preparation and plasma-cleaning of transmission electron microscope specimens was installed.

The purchase of a new mass spectrometer, able to identify the tritium release and retention of fusion-relevant materials, and preparing of its installation was effectuated in the reporting period.

Furthermore, a new shielded transfer cell was built, allowing connecting with various casks for receiving transports of highly active specimens.

Fig. 1: Newly installed shielded transfer cell with positioning and docking system for various transport casks.

Future activities:

Continuation of measurements as referred to above:

- PIE of the HFR II B irradiation phase, 15 dpa
- PIE of the BOR 60 irradiation campaign, 15 – 30 dpa
- PIE of the OSIRIS FURIOSO high temperature irradiation, WL10-tungsten, 5 dpa
- PIE of the HIDOBE irradiations
- Installation of the new mass spectrometer
- Installation of a device for instrumented indentation at elevated temperatures
- Characterization of new batches of ceramic breeder materials and beryllium
- Operation of a gamma-ray spectrometer to study the activation of RAFM steels

Staff:

B. Albinski
P. Barié
J. Ehrmann
A. Erbe
M. Gilpert
M. Holzer
W. Ibbe
S. Lautensack
G. Mangei
H. Ries
M. Rietschel
R. Rolli
I. Sacksteder
M. Scherwitz
R. Schmidt
H.-C. Schneider
H. Steinle
M. Weber

Literature:

[1] Chakin, V., Rolli, R., Vladimirov, P., Kurinskiy, P., Klimenkov, M., Möslang, A., Ryczek, L., Dorn, C., Markovsky, A.: Temperature-programmed desorption of tritium loaded into beryllium. Physica Scripta, T138(2009) S.14035/1-4 DOI:10.1088/0031-8949/2009/T138/014035

[2] Chakin, V., Rolli, R., Möslang, A., Kurinskiy, P.: Thermodesorption examination of beryllium pebbles with loaded tritium. Proc.of the 9th IAE Internat.Workshop on Beryllium Technology (BeWS-9), Almaty, KZ, September 15-17, 2009, P. 76-84

[3] Gaganidze, E., Petersen, C., Materna-Morris, E., Dethloff, C., Weiß, O.J., Aktaa, J.; Povstyanko, A.; Fedoseev, A.; Makarov, O.; Prokhorov, V.: Mechanical properties and TEM examination of RAFM steels irradiated up to 70 dpa in BOR-60. 14th Internat. Conf. on Fusion Reactor Materials (ICFRM-14), Sapporo, J, September 7-12, 2009, paper to be published in proceedings

[4] Klimenkov, M., Materna-Morris, E., Möslang, A.: Characterization of radiation induced defects in EUROFER after neutron irradiation. 14th Internat.Conf.on Fusion Reactor Materials (ICFRM-14), Sapporo, J, September 7-12, 2009, paper to be published in proceedings

[5] Kurinskiy, P., Chakin, V., Möslang, A., Rolli, R., Goraieb, A.A., Harsch, H., Dorn, C.; Haws, W.: Mechanical performance of titanium beryllides. Proc.of the 9th IAE Internat.Workshop on Beryllium Technology (BeWS-9), Almaty, KZ, September 15-17, 2009 Kazatomprom, 2009 P. 52-55

[6] Sacksteder, I., Schneider, H.-C.: Further characterization of irradiated steels by indentation at high temperature. 26th Symp.on Fusion Technology (SOFT 2010), Porto, P, September 27 - October 1, 2010, paper to be published in proceedings.

[7] Schneider, H.-C., Rolli, R., Nägele, W.: Experimental facilities in the Karlsruhe Fusion Materials Laboratory. 46th Annual Meeting of the Hot Laboratories and Remote Handling Working Group, Praha, CZ, September 20-23, 2009, Proceedings

Define and Perform Accompanying Experiments to D5 (e.g. creep crack growth at 550°C) (TW5-TTMS-005 D 6)

Background and Objectives Task

For TBM's licensing, in order to establish design rules for the materials, joints and specific sub-components, a broad set of R&D activities have been launched within the WP 2002. These activities will continue with emphasis on implementation in DSCD (Demo structural design code) and verification and validation experiments. Additional rules for HT (high temperature) fatigue-creep interaction need to be formulated, in particular for fracture mechanics.

The low ductility of EUROFER (in particular after irradiation) gives very conservative limits for design against fast fracture and local flow localization. Some experiments are required in support of special design code activities that could lower very conservative assumptions in existing frameworks.

In addition, development of small scale test techniques in fracture mechanics will continue including transferability of the small size specimen tests to the behaviour of the TBM's sub-components.

The objective of this subtask is to perform long time creep crack growth experiments on EUROFER to determine the da/dt (crack velocity) - C* (C*-integral)-behaviour at the temperatures 500 °C and 550 °C. The results are needed for the determination of material parameters in HT fracture mechanical rules.

Status January 2010

The assembling of the experimental set-up was finished. Preliminary tests with the set-up for the DC potential method were done in order to determine the correct correlation between voltage and crack length in the relevant temperature range. Special clip gauges were developed and fabricated to measure the crack opening during the main experiments. The rods of two creep testing machines were modified to implement the specimens and the measurement devices, respectively, within the test facilities.

Actual Status

Upon completion of the test set-up, which is shown in Fig. 1, the functionality of all electronic measurement devices was checked in pre-tests under different load conditions at 550 °C.

Afterwards, the time-consuming tests to determine the suitable load cases for the long term experiments at both 500 °C and 550 °C were started. For that purpose, starting with initial weights, the

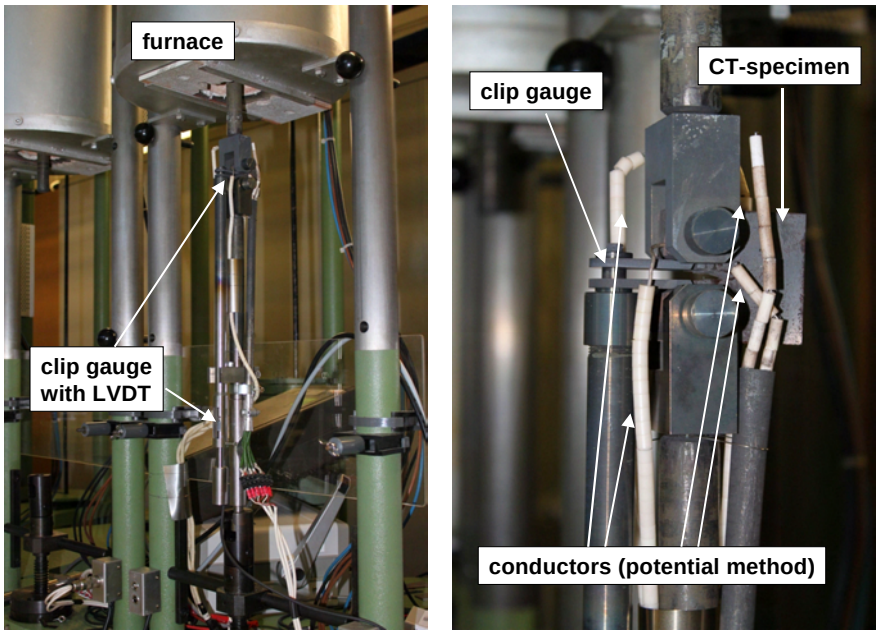

Fig. 1: Complete test set-up for the long time creep crack growth experiments.

loads were reduced stepwise as far as the crack growth rates reached the desired values (compare example shown in Fig. 2). Within these tests it was found, that the crack propagation of a creep crack in EUROFER is not comparable with the fatigue crack growth in this material as one can see in Fig. 3. This has to be taken into account when calculating the current crack length from the corresponding potential change value during the test. Currently the main experiments are running.

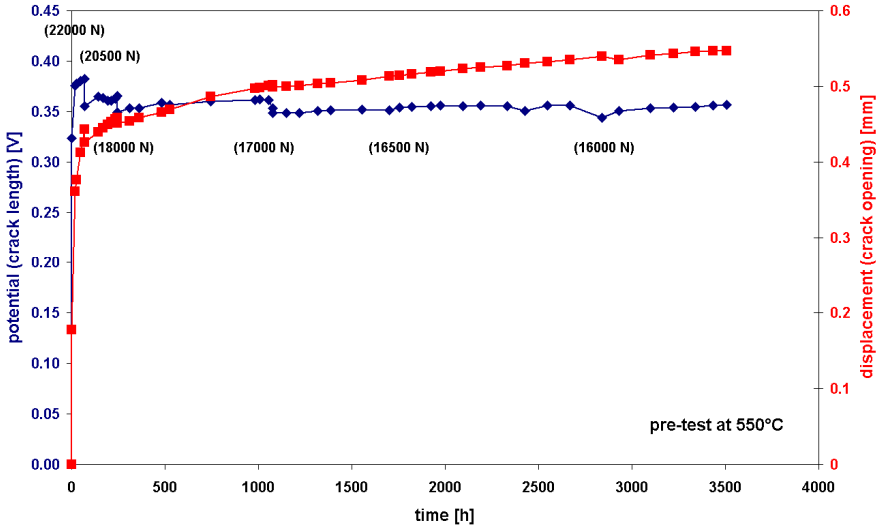

Fig. 2: Result of a pre-test in order to determine the necessary load for the long term tests

Conclusion and Outlook

The experimental set-up for the long time creep crack growth tests was configured and the tests to determine the suitable load cases for the long term experiments were finished. Currently, the main experiments are running.

Staff:

M. Klotz
St. Knaak
M. Walter

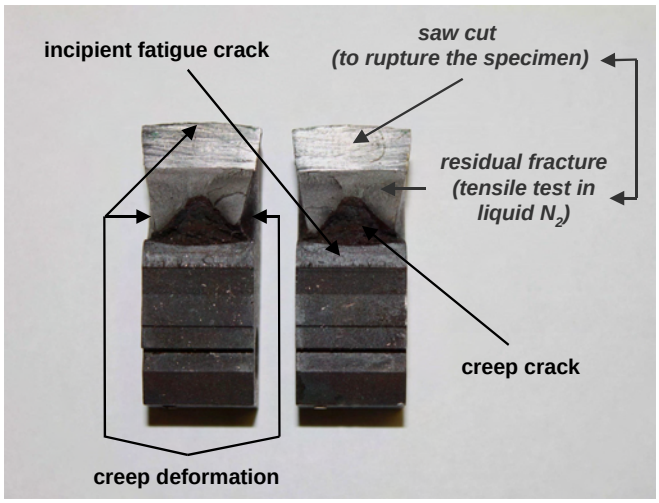

Fig. 3: Deformation as well as damage formation of a CT-specimen from EUROFER 97, tested under long term creep loading.

Acknowledgement

This work, supported by the European Communities under the contract of Association between EURATOM and Karlsruhe Institute of Technology, was carried out within the framework of the European Fusion Development Agreement. The views and opinions expressed herein do not necessarily reflect those of the European Commission.

Characterisation of Reference EU ODS-EUROFER Batch (Tensile, Creep and Charpy) (TW5-TTMS-006 D 6)

Introduction

The efficiency of future fusion reactors will strongly depend on the operating temperature allowed by selected structural materials. With this respect, ODS steels are attractive candidates since they would allow to increase the operating temperature by approximately 100 °C. The reduced activation martensitic steel EUROFER-97 (8.9 Cr, 1.1 W, 0.2 Ta, 0.42 Mn 0.11 C wt%), which is currently considered as a European reference for structural application, has been selected as a base material. Based on the experience with a precursor a 50 kg EU-ODS-EUROFER batch has been specified and produced (TW3-TTMS-006 D1a). Within this task the mechanical properties of the material should be determined. This work is strongly intertwined with Task TW5-TTMS-006 D10 which investigated the influence of heat treatments on the microstructure.

The improvement of the mechanical behaviour, especially the high temperature tensile ductility and impact properties should be achieved by different heat treatment (HT) procedures. The principal heat treatment conditions were derived from the outcome of TW5-TTMS-006 D10. Nevertheless additional HTs were applied after the mechanical tests to improve the performance of the material.

Heat treatments

The heat treatment experiments were performed under vacuum using an evacuated quartz tube which was heated up in a tubular 3-zone furnace. The holding time at each temperature was two hours. The cooling down was performed by withdrawal of the furnace. Due to the low mass of the samples, the cooling rate is close to air-cooling conditions. On the other hand, a water quenching cannot be performed after heating in such a vacuum furnace. The results of hardness measurements after the heat treatment are shown in Figure 1.

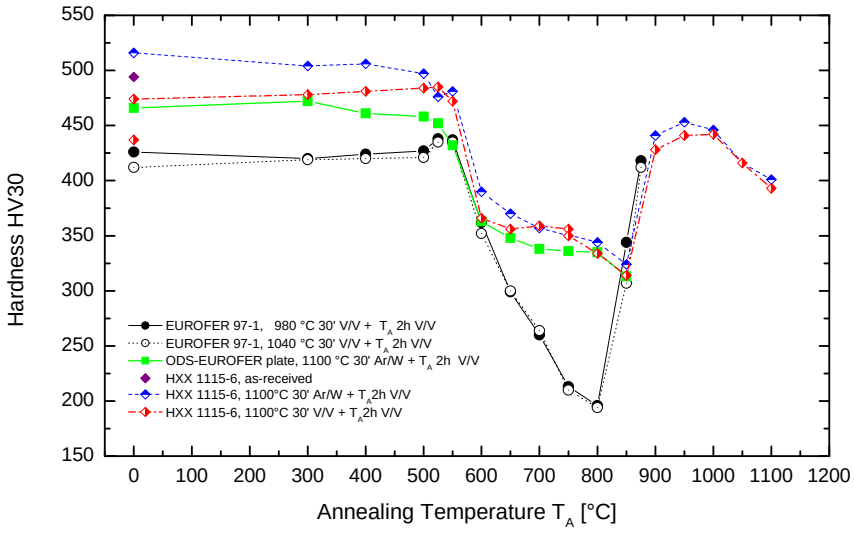

Fig. 1: Vickers hardness HV30 in dependence of the annealing temperature.

Applying this method, the so-called FZK-batch did not form martensite when cooled down from the normalisation temperature because the achievable cooling rate is not high enough. The reason for this behaviour is the lower carbon (0.08 wt.%) content of the FZK-batch, while of the EU batch has a sufficiently high C-content (0.1 wt.%). Water quenching gives higher

hardness values until 550 °C tempering temperature. Above this value there is nearly no difference between the water quenched and air-cooled samples. The hardness decreases continuously until 850 °C.

At 900 °C tempering temperature a strong increase of the hardness values close to the values of the vacuum cooled specimens (red diamonds) without annealing on the upper left side (at 0 °C) of the diagram can be observed for the EU batch. Above 900 °C the red and blue diamonds show similar hardness values. This behaviour is also clear, because the normalisation heat treatment and cooling down is being performed under vacuum conditions.

Two heat treatments were derived from the described annealing behaviour; 1100 °C 30 min + 750 °C (std. HT) and 1100 °C 30 min + 850 °C. The latter one should decrease the hardness and thus increase the ductility of the material.

A third three step heat treatment was also performed with the goal to get as much carbon into solution at a high normalisation temperature of 1100 °C and to form smaller grains at a second step normalisation at 950 °C. The following tempering was performed at 850 °C to get a good ductility.

Mechanical testing

Miniaturised test specimens for the mechanical testing according to Figure 2 were fabricated by spark erosion of blanks which were then, after a heat treatment, milled and turned to the final shape.

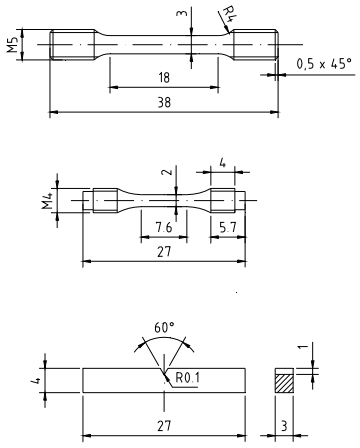

Creep

Tensile
LCF

Charpy

Fig. 2: Test specimen geometries.

Figures 3 to 5 give the results of the tensile tests of specimens of ODS-EUROFER batches with different heat treatments in comparison with standard EUROFER.

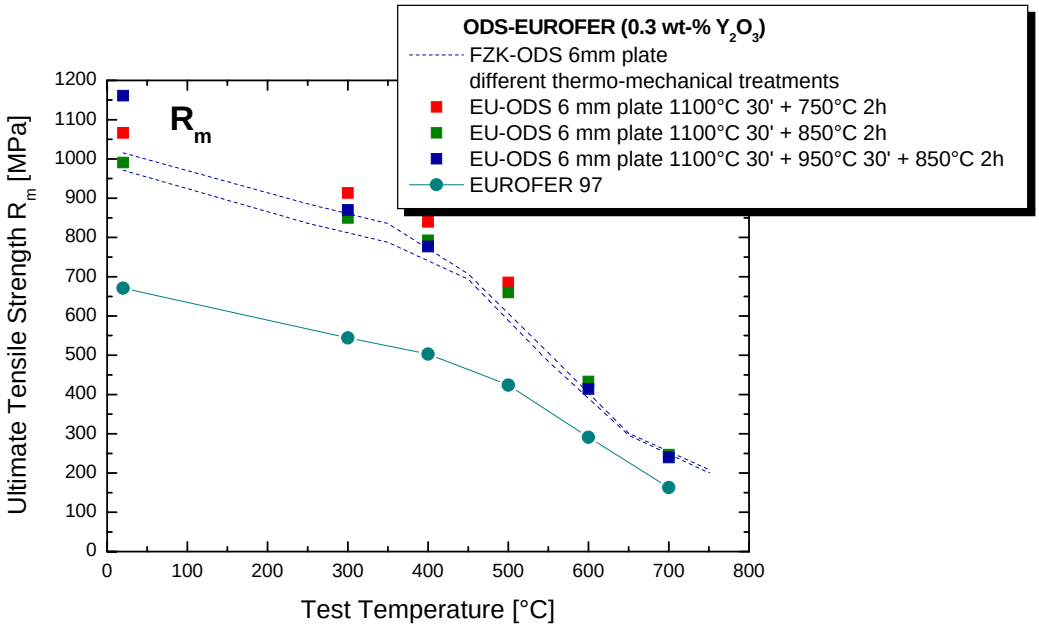

Fig. 3: Ultimate tensile strength R_m of ODS-EUROFER compared to EUROFER 97.

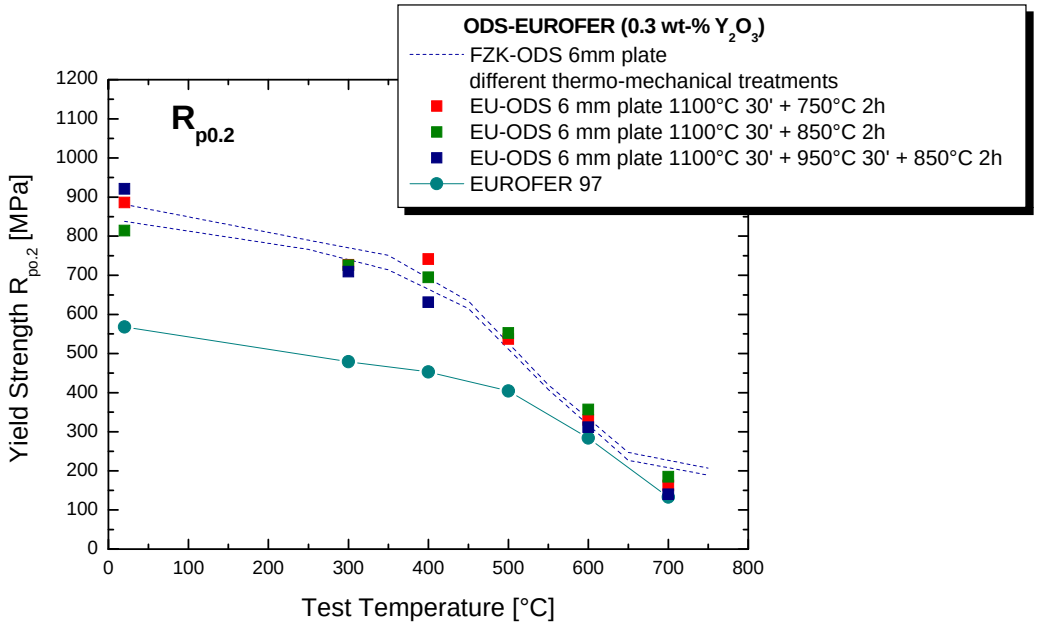

Fig. 4: Yield strength $R_{p0.2}$ of ODS-EUROFER compared to EUROFER 97.

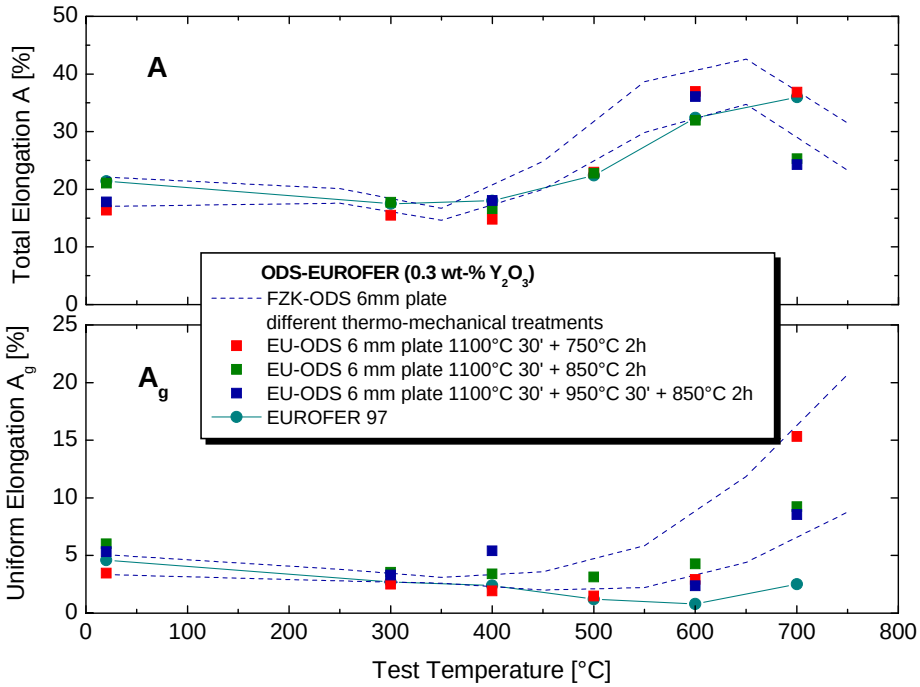

Fig. 5: Uniform A_g and Total Elongation A of ODS-EUROFER compared to EUROFER 97.

The tensile strength R_m and $R_{p0.2}$ of the “standard” heat treated specimens (1100 °C 30’ + 750 °C 2h) have a higher strength up to about 500°C test temperature. These strength values are also higher than those of the FZK batch. The specimens with the higher annealing temperature and the 3-step heat treatment have no advantage also compared to the FZK batch. Only at RT the latter heat treatment is higher. The ductility values of the EU specimens are in the scatter band of the FZK batch values.

While the tensile properties don’t show a significant influence of the different heat treatments, the impact behaviour is much more sensitive to changes in heat treatment. Figures 6 and 7 show the impact behaviour of different ODS- EUROFER batches which were differently heat treated in comparison to the standard EUROFER steel.

The upper shelf energy (USE), i.e. the maximum absorbed energy of the EU ODS- EUROFER alloy, reaches values of about 5.6 J. This is 15 to 18% lower than scatter band of the FZK-batch data. The ductile-to-brittle-transition-temperature (DBTT) of the EU-batch material, which is the temperature at half the upper shelf energy, lies at about -40, which is worse than that of the FZK-batch, where DBTT ranges between -53 and -80 °C. The latter values were taken from the upper and lower boundary of the scatter band of the FZK-batch data. Nevertheless, none of the ODS steels does reach the good properties of standard EUROFER 97 (blue-green hatched area), which reach, depending on the heat treatment, USE values between 8.5 and 9.8 J and DBTT values between -60 and -100 °C.

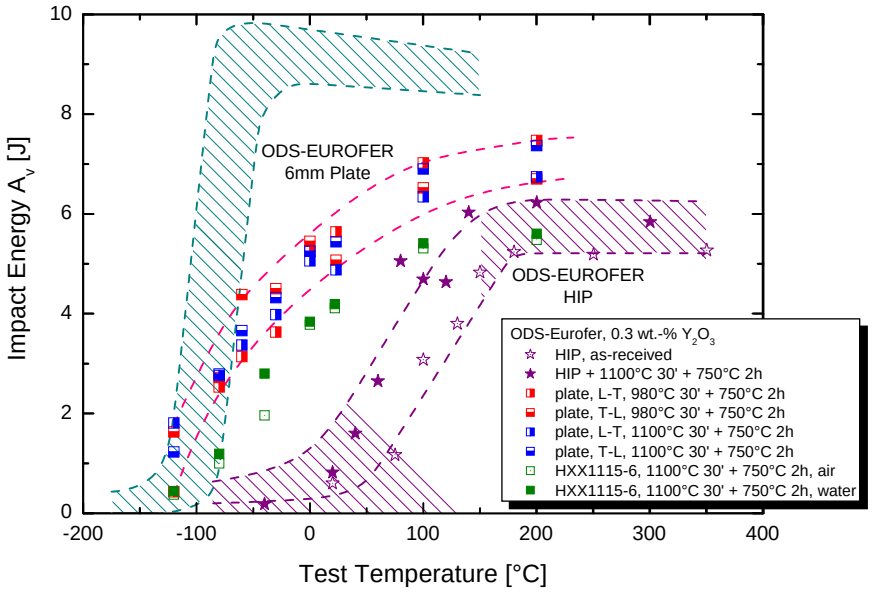

Fig. 6: Comparison of the Impact Energy Av of EU ODS-EUROFER normalised and tempered at 1100 °C 30 min and 750 °C 2h compared to the FZK-batch and standard EUROFER 97.

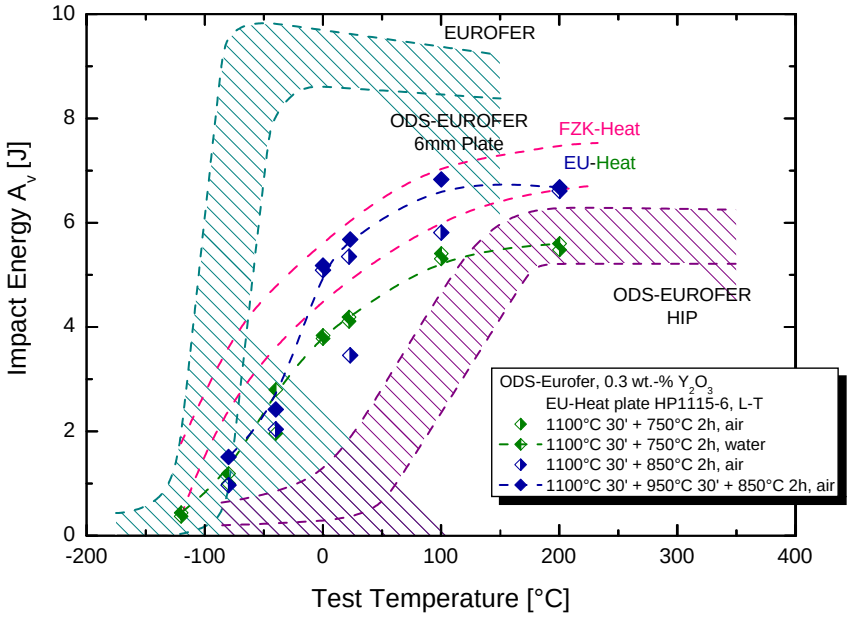

Fig. 7: Comparison of the Impact Energy Av of EU ODS-EUROFER normalised and tempered at 1100 °C 30 min and 750 °C 2h (green) and alternative heat treatments (blue) compared to the FZK-batch and standard EUROFER 97.

Figure 7 shows the results of improvement trials. In one case the tempering was increased to 850 °C to make the material softer and thus increase the ductility. In fact, above 0 °C the upper shelf energy was increased (half filled blue diamonds) compared to the “standard” heat treatment described above (green diamonds). Below -40 °C the impact energy was comparable to the air-cooled data. Introducing a double normalization (blue full diamonds, dashed line) the upper shelf energy could be increased above 0 °C to higher values than that of the specimens with the standard normalization treatment (half filled blue diamonds). Since there

is always some scatter and the number of one or two samples per temperature is relatively low, it is hard to state that the improvement in ductility is mainly due to the double normalization. It is clear, that a higher tempering temperature makes the material softer but on the other hand the carbide precipitates could perhaps get larger and thus negatively influence the crack initiation.

Summary and Conclusions

Different heat treatments have been applied on tensile and impact specimens made of the so-called EU ODS-EUROFER batch of a 9 Cr 1.1 W 0.2 V 0.04 Ta 0.3 Y2O3 RAFM ODS steel. Tensile and impact tests were performed. It was shown, that a double normalisation treatment followed by a tempering treatment could improve the impact properties with respect to upper shelf energy and ductile to brittle transition temperature. Nevertheless, the impact properties were worse than those of a similar ODS steel called FZK-Heat.

Staff:

S. Baumgärtner
B. Dafferner
S. Heger
U. Jäntsch
M.Klimenkov
R. Lindau
A. Möslang
M. Rieth
H. Zimmermann

Acknowledgement

This work, supported by the European Communities under the contract of Association between EURATOM and Karlsruhe Institute of Technology, was carried out within the framework of the European Fusion Development Agreement. The views and opinions expressed herein do not necessarily reflect those of the European Commission.

Optimisation of the Processes and Techniques for the Production of EUROFER ODS with Respect to DBTT and their Transferability from Laboratory to Industrial Scale (TW6-TTMS-006 D 1)

Introduction

Fe9Cr ODS steels are candidate structural materials for different highly loaded components in future advanced nuclear fusion power reactors beyond ITER. The reduced activation ferritic martensitic steel EUROFER 97 (8.9Cr, 1.1W, 0.2 Ta, 0.42 Mn 0.11 C wt%), which is currently considered as a European reference for structural application, has been selected as a base material. In the past, different batches of such EUROFER-ODS have been produced in laboratory scale as well as semi-industrial batches in close cooperation with a commercial producer (PLANSEE). The last production was the so-called EU EUROFER-ODS batch in different product forms, amounting to about 50 kg.

Since PLANSEE gave up the industrial production of ODS steels, and no commercial producer is available in Europe, it was tried to analyse the production route and to optimise each step in laboratory scale with the goal to transfer the results to industrial fabrication.

With the results of this analysis it should be possible to produce a larger batch of ODS- EUROFER in industrial scale by sub-contracting different companies for the different production steps.

Optimisation trials, results and discussion

The principle of the ODS production route is shown schematically in Figure 1. Since Fe9Cr-ODS steels are foreseen as plating of the First Wall in the so-called Dual-Coolant breeding blanket, extrusion was not considered in this analysis. Nevertheless it could be interesting if tubes e.g. for the He-cooled divertor are needed.

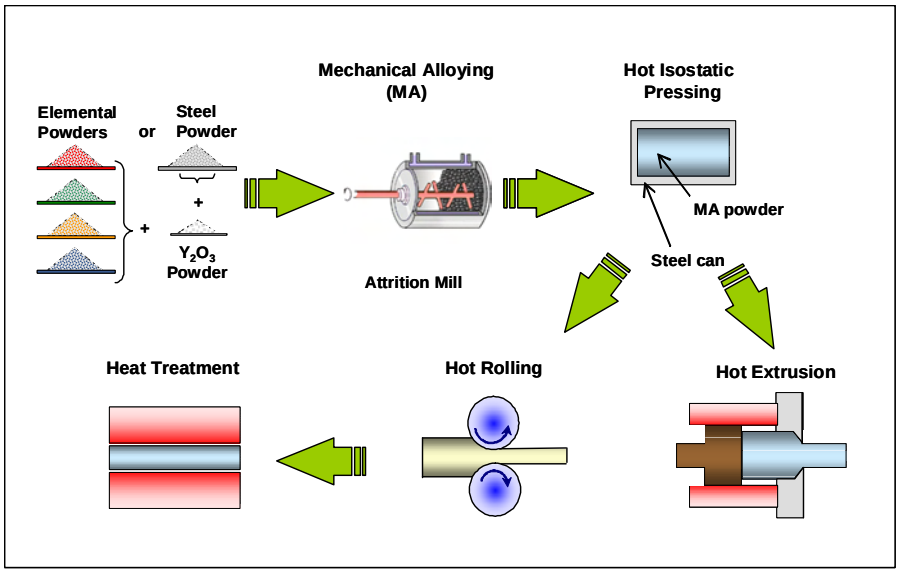

Fig. 1: Schematic draw of the fabrication route for ODS-steels.

It was tried to optimise the different fabrication steps which then should be transferred to larger scale production to be performed by subcontractors.

Since it is believed that the oxygen content in the material should be controlled very carefully, the whole handling of the different powders before and after mechanical alloying was performed under protective atmosphere.

The initial steel powder was produced by gas atomisation in highly pure argon gas after melting the basic steel under vacuum in a crucible. This process can be performed in industrial scale by experienced manufacturers. Mechanical alloying (MA) was made in a laboratory high energy horizontal attritor ZOZ CM 01. The milling parameters were optimised with respect to low contamination of e.g. carbon, oxygen and nitrogen and various protective gases like Ar and H_2 were used. Since the energy input, which is important for the MA process, can be controlled in this type of high energy attritors, the process can be scaled up for higher capacity machines of the same type. The further handling of the MA powder is done in a dedicated glove box containing highly pure argon gas. The protective gas atmosphere can be controlled with a gas purification system to guarantee low oxygen levels in the ppm range. Filling of the capsules for hot isostatic pressing (HIP) and welding of the closure cap with suction pipe for degassing is also done in the glove box. After degassing the HIP capsules the suction pipe is crimped and seal welded by EB or TIG welding.

The hot isostatic pressing is a common process for densification and can be done by several industrial companies.

After HIP miniaturised specimens for tensile and impact testing were manufactured and tested. Figures 2 and 3 exemplarily show the results of tensile tests. Fig. 2 gives the ultimate tensile strength R_m of Fe9Cr ODS steel with 0.3 wt.-% Yttria content with varying MA conditions in comparison to the data for EUROFER-ODS with different heat treatments indicated by the blue dashed lines. The basic steels EUROFER (dark cyan bullets) and the hipped Fe9Cr steel (royal blue squares) are for comparison.

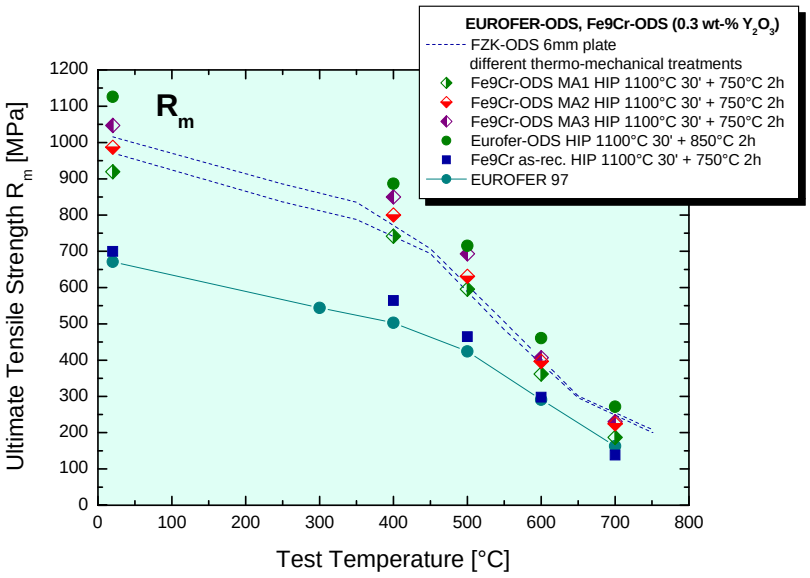

Fig. 2: Temperature dependence of ultimate tensile strength for a 9%Cr ODS steel with varying MA conditions compared to 9%Cr EUROFER-ODS steel and the basic steels.

The diagram shows, that the milling conditions have an impact on the ultimate tensile strength which is most pronounced at lower temperatures.

Figure 3 gives the temperature dependence of the uniform and total elongation of the same alloys and conditions as in Fig. 2. The uniform and total elongation values for the Fe9Cr steel made from powder by hot isostatic pressing has in both cases a better ductility than standard EUROFER 97. While the varying MA conditions had a significant impact on tensile strength, the influence on total elongation is visible but less pronounced. At temperatures above 400 °C the total elongation is clearly below that of the thermo-mechanically treated EUROFER-ODS. It could be expected that such treatment has a similar effect for the Fe9Cr ODS steels. Like for EUROFER-ODS the total elongation at 700 °C does not show a similar in-

crease as for the basic steels. The hipped and heat treated EUROFER-ODS samples which had the highest tensile strength revealed on the other hand the lowest total elongation of all alloys investigated. The uniform elongation of the Fe9Cr ODS steels and the hipped EUROFER-ODS steel are in the vicinity of the lower boundary values of the thermo-mechanically treated EUROFER-ODS.

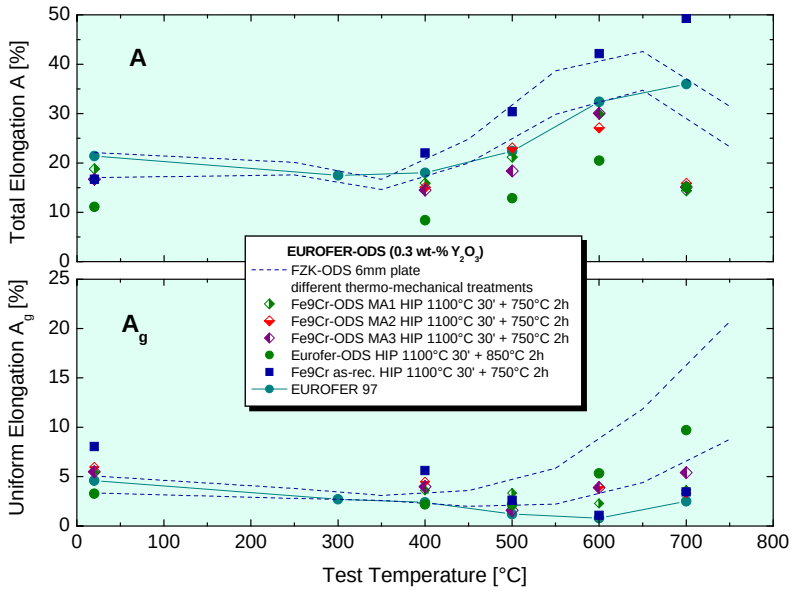

Fig. 3: Temperature dependence of uniform and total elongation for a 9%Cr ODS steel with varying MA conditions compared to 9%Cr EUROFER-ODS steel and the basic steels.

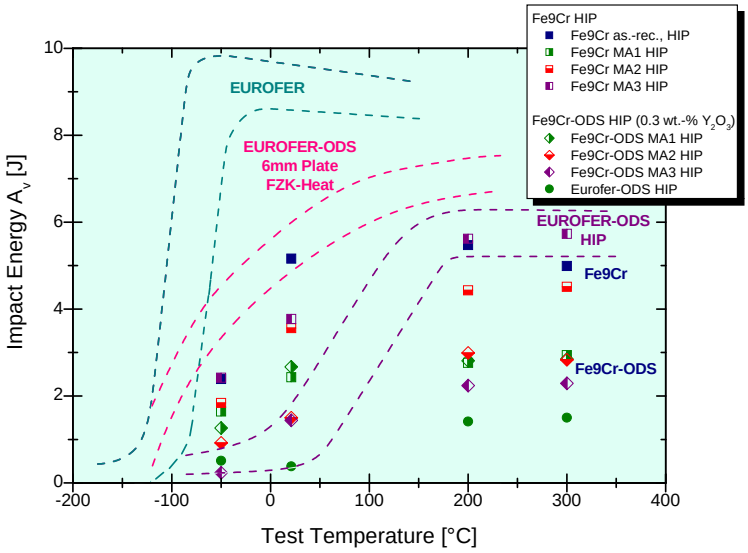

Fig. 4: Impact properties for a 9%Cr ODS steel with varying MA conditions compared to 9%Cr EUROFER-ODS steel and the basic steels.

Figure 4 shows the impact properties of Fe9Cr ODS steel containing 0.3 wt.-% Yttria with varying MA conditions in comparison to the data for EUROFER-ODS after HIP and different heat treatments (purple dashed lines) different thermo-mechanical treatments (FZK-Heat, magenta dashed lines) and EUROFER97 (dark cyan dashed lines).

It is remarkable that only the Fe9Cr alloys without Yttria addition reached roughly the values of hipped EUROFER-ODS. The Fe9Cr-ODS steels containing 0.3wt.-% Y_2O_3 revealed upper shelf energies between 2 and 2.5 J which is only little higher than the values measured for 13.5Cr ferritic ODS steels. The reason for the drop in ductility compared to the hipped EU-

ROFER-ODS can be the higher carbon content and thus a higher density of $M_{23}C_6$ and MC carbides which reduce the strength of the grain boundaries and/or can act as crack initiators.

This adverse effect could be reduced by an optimisation of the heat treatment, but the strongest effect is achieved if the material is thermo-mechanically treated as it was done with EUROFER-ODS (FZK-Heat).

Summary and conclusions

Within this task the production process for Fe9%Cr ODS steels like EUROFER-ODS was analysed in order to understand this process and to transfer the results from laboratory to industrial scale. In this report the optimisation trials with respect to the mechanical alloying process, the powder handling, and their impact on the mechanical behaviour is shown. The milling parameters were optimised but to improve also the ductility, a thermo-mechanical treatment must be applied.

Staff:

C. Adelhelm
S. Baumgärtner
B. Dafferner
U. Jäntsch
T. Kaiser
M. Klimenkov
R. Lindau
A. Möslang
R. Ziegler
H. Zimmermann

Acknowledgement

This work, supported by the European Communities under the contract of Association between EURATOM and Karlsruhe Institute of Technology, was carried out within the framework of the European Fusion Development Agreement. The views and opinions expressed herein do not necessarily reflect those of the European Commission.

Investigate Joining Technologies for ODS/ODS and ODS/Conventional EUROFER (TW6-TTMS-006 D 6)

Introduction

For specific blanket and divertor applications in future fusion power reactors a replacement of presently considered reduced activation ferritic martensitic (RAFM) steels as structural material by suitable oxide dispersion strengthened (ODS) ferritic martensitic or ferritic steels would allow a substantial increase of the operating temperature from ~550 °C to about 650 °C. In all cases appropriate joining technologies have to be developed. Diffusion welding techniques to perform similar and dissimilar joints have been studied successfully.

The microstructure of the weld and heat affected zone as well as the fracture surface of the samples were examined using optical and scanning electron microscopy (SEM), Dual-Beam SEM/FIB, low magnification and analytical transmission electron microscopy (TEM). The changes of the mechanical properties can be well correlated with the detected changes of micro- and nanostructure. SEM and low magnification TEM analyses show significant changes of the microstructure in the welded area. In all specimens a grain coarsening and changes of the distribution and morphology of the carbide precipitates and ODS particles has been observed. The formerly nano-sized ODS particles agglomerate to complex structured yttrium containing larger particles.

Method

The material used in these investigations, is a reduced activation ferritic martensitic ODS steel with a basic composition of 8.9 wt.-% Cr, 1.1 wt.-%W, 0.42 wt.-%Mn, 0.2 wt.-% V, 0.14 wt.-% Ta, 0.07 wt.-% C, and Fe for the balance. Oxide dispersion strengthening was achieved by addition of 0.3 wt.-%Y_2O_3 in the mechanical alloying process of the argon gas-atomised EUROFER basic powder.

Two different post-weld heat treatments (PWHT) were applied to investigate their influence on the mechanical and microstructural properties of the welded joints. One consisted of a full heat treatment of normalisation at 1100 and 980 °C for 30 minutes followed by a tempering treatment at 750 °C for 2 hours. The second was only a tempering treatment of 750 °C for 2 hours. Miniaturised tensile specimens were used to determine the tensile behaviour in the temperature range between RT and 500 °C. KLST specimens were used for Charpy impact tests.

The microstructural characterization of the welding and heat-affected zone after different post-weld heat treatments was performed using optical microscopy (OM), scanning (SEM) and transmission electron microscopy (TEM) methods. The TEM investigations have been performed using a FEI Tecnai 20 FEG microscope with an accelerating voltage of 200 kV, scanning unit for performing scanning TEM (STEM) with high angle annular dark field (HAADF) detector and an EDX detector for elemental analysis. Beam sizes varied from 1.5 to 3 nm have been used for the EDX measurements and mapping. TEM specimens have been prepared by standard electropolishing method in a TENUPOL 5 device using H_2SO_4 + 80% CH_3OH as electrolyte at 12 V working voltage. The determination of the grain structure was performed in a Dual-Beam-SEM FIB FEI Nova applying the ion beam for the imaging.

Results

Mechanical Testing

Tensile and Charpy impact tests were performed to determine the mechanical properties of the welded and heat-treated samples. For both tests Small Specimen Test Technology (SSTT) samples were machined from the welded strips such that the welding seam was in the centre of the samples. The tensile tests were performed on SSTT tensile samples with

Ø2 mm x 7.6 mm gauge length and 27 mm total length using a ZWICK Z030 universal testing machine under vacuum of 8x10-7 mbar. The applied strain rate was 2.38x10-4 s-1 and the elongation was measured with remote-controlled extensometers. Figure 1 gives the ultimate tensile strength Rm (acc. to DIN EN 10 002) of the EB-welded and heat-treated specimens (open circle and squares) in comparison to the ODS-EUROFER base material (full stars) and EUROFER 97 (full dots) at RT and elevated temperatures (400,500°C). It is clearly visible that the tensile strength of the EB-welded ODS-Eurofer samples is significantly decreased to values close to those of the non-ODS EUROFER 97 steel. The total elongation, not shown here is strongly reduced to values below 5%. The Reduction of Area Z amounts to 56%, which is about the value for ODS-EUROFER but lower than for EUROFER 97. The reason for the described behaviour becomes clear in the fractographic and the microstructural examinations.

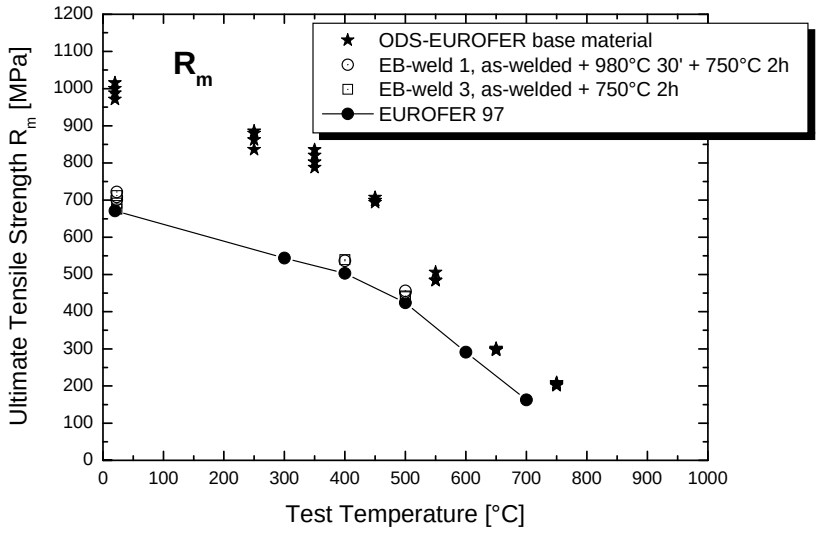

Fig. 1: Ultimate tensile strength R_m of EB-welded samples as a function of test temperature in comparison with ODS-EUROFER and EUROFER 97.

In Figure 2b can be seen, that the deformation is concentrated on the welding seam and the rest of the specimen remains only little deformed. The fracture surface in Fig. 2a to 2e shows a cup and cone fracture with ductile dimple formation. Also the appearance of welding pores can be observed. But more important is the fact that numerous yttria containing particles of 0.2 to 5 µm size can be found inside the dimples. This fact can be assumed to be the reason for the loss of strength of the welded seam. ODS- EUROFER, contains nano-dispersed Yttria particles of 2-10 nm in size, with an average size of 4 nm and a volume fraction of (1.5 ± 0.5) cm-22 which are responsible for the superior tensile and creep strength of this type of materials.

Due to the melting of the material in the EB-welding process, the finely dispersed nanoparticles are floating around and agglomerate to larger yttria-containing particles which are frozen into the material in the fast solidification phase. Due the agglomeration, the strengthening effect of the ODS particles, caused by the impeding of the dislocation movement during the deformation is lost and the strength drops down to values of the non-ODS steel. The deformation in the tensile test thus concentrates on the “weak” welding zone and the ODS parts of the tensile specimens are only somewhat deformed. Subsized Charpy specimens of KLST type measuring 4x4x27 mm, 1mm notch depth and 0.1 mm notch root radius and 60° notch angle (acc. to DIN 50115) were used to determine the impact behaviour of the welded and heat treated material.

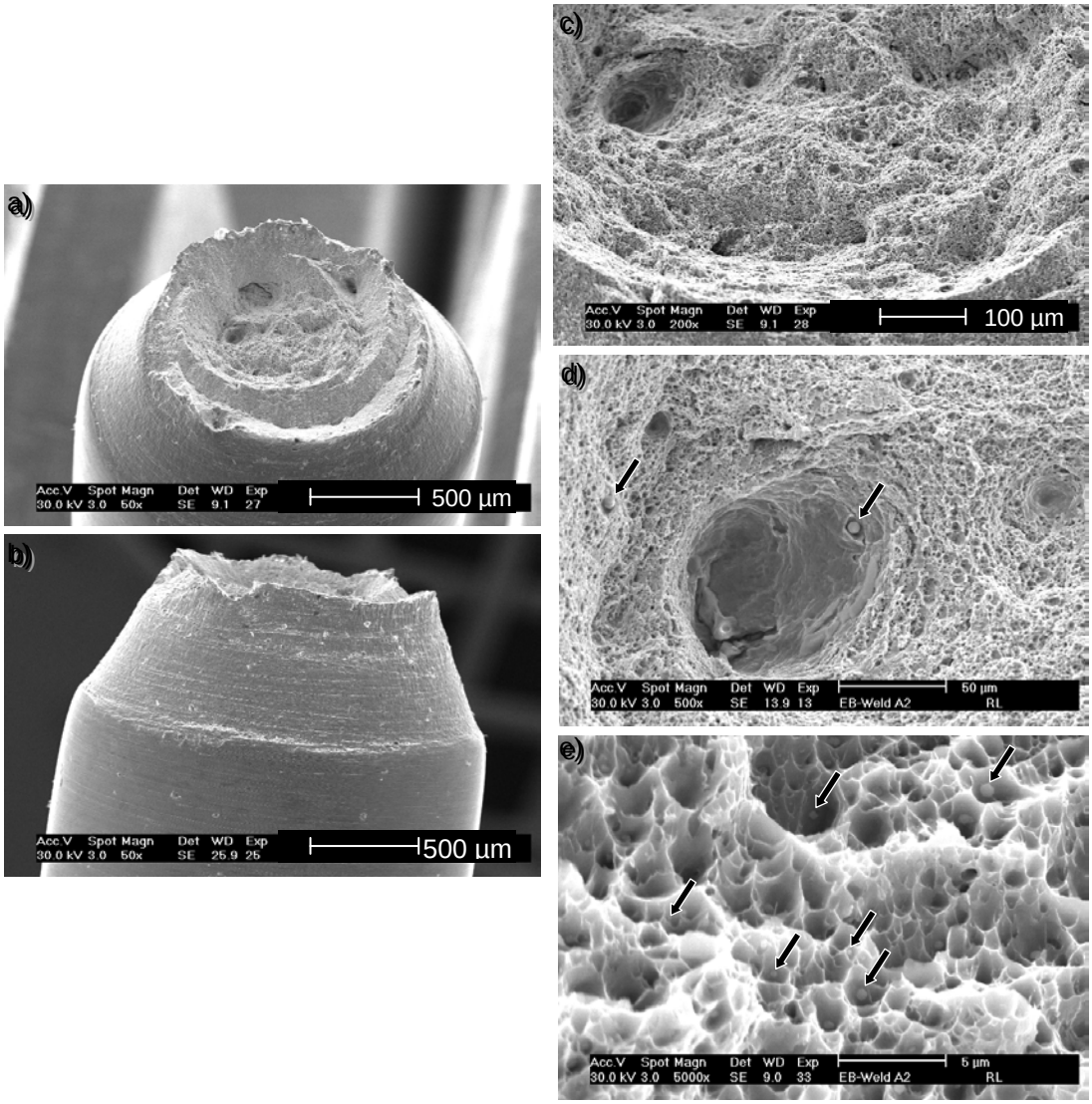

Fig. 2: Fractographic examination of an EB-welded sample tested at room temperature. Ductile fracture with yttrium containing particles (0.2 – 5 µm) in dimples indicated by arrows.

Microstructural investigations

Additionally to the PWHT applied on the samples for the mechanical tests two other heat treatments were investigated for comparison. One consisting of 1100 °C 30' Ar/W + 750 °C 2h air and also the unaffected rolled base material were examined. To show the difference in carbide precipitation between thermo-mechanically treated and only hipped ODS-EUROFER material, samples of the latter are also presented. A Dual-Beam-SEM FIB FEI Nova applying the ion beam for the imaging was used to demonstrate the changes of the microstructure in the heat-treated welding zone (PWHT 3, 750 °C 2h) compared to the base

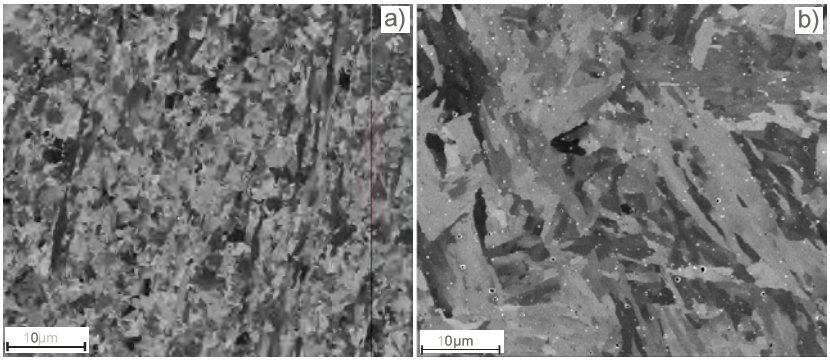

Fig. 3: Ion beam images from the thermally unaffected area (a) and welding zone (b) (PWHT 3).

material. Fig. 3a presents the image of the material taken 3 cm apart from the welding zone, i.e. the unaffected base material, and in Fig. 3b taken directly from the welding zone. The changes in grain size are clearly visible. Due to the welding process a grain coarsening occurs in the welding zone, which cannot be fully recovered by the applied post weld heat treatment.

The histogram in Fig. 4 shows that the average grains size in the welding zone (black bars, foreground) has been significantly increased compared to the base material (wide grey bars, background). In the base material most of the grains, i.e. 80%, have sizes less than 1.1 µm. After the welding procedure the fraction of grains smaller than 1 µm is reduced to about 15%. The distribution maximum rose from approximately 0.6 µm to 1.4µm. Additionally larger yttrium containing particles which are not present in the thermally unaffected zone were found in the welding zone. These particles with sizes varying from 0.2 µm to 0.5 µm are clearly visible as bright spots in the image (Fig. 5b). The same changes of the grain structure were observed in two other specimens, which received a full heat treatment of normalizing and tempering (1100 °C 30' + 750 °C 2h and 980 °C 30' + 750 °C 2h). The changes of the microstructure caused by the additional thermal treatment are less pronounced.

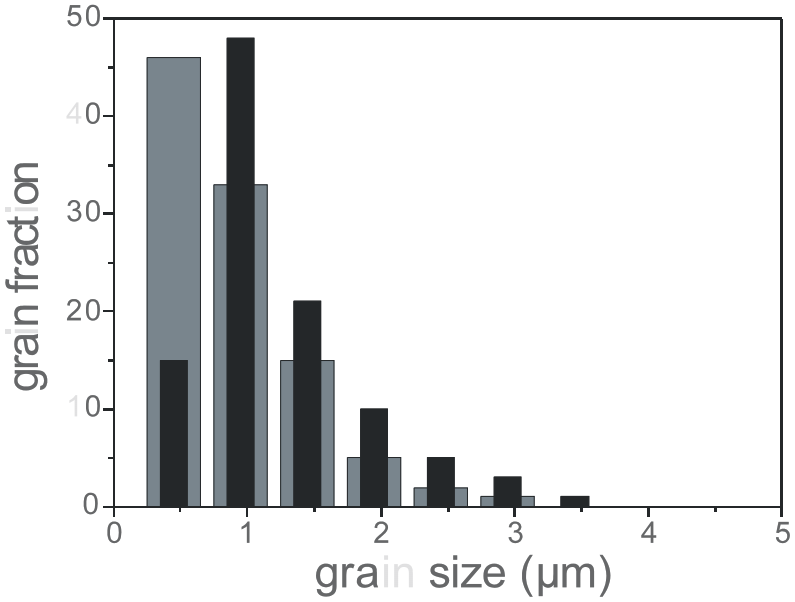

Fig. 4: Histogram of the grain size distribution. The grey wide bars show the grain size in the thermally unaffected area (base material) and the black bars in the welding zone (PWHT 3).

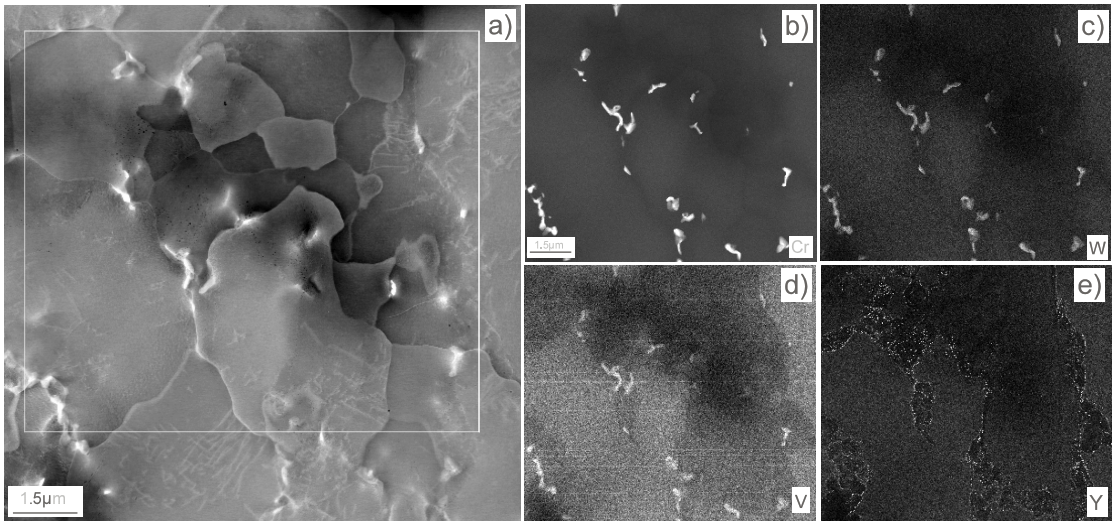

Fig. 5: Analytical investigation of the ODS-Eurofer specimen in the as-hipped state. Part a shows the HAADF image of the investigated area. Parts b, c, d and e show the spatial elemental distribution of Cr, W, V and Y.

The investigation of the distribution of inclusions and precipitates in the welding zone compared to the ODS-EUROFER base material was performed using spectroscopic imaging. In Fig. 5 the results of the investigation of ODS material without any thermo-mechanical treatment procedure i.e. only HIP after mechanical alloying are presented. The $M_{23}C_6$ carbides

with Fe,Cr,W and V composition show an elongated form and are mainly located along the grain boundaries. The precipitates of this type are clearly visible in the Cr (b) and W (c) EDX maps. These precipitates are also visible with poor contrast in the V (d) map. The investigations do not show the presence of V and Ta rich precipitates as it is reported for EUROFER 97. Most of Ta and V are presumably homogeneously dissolved in the matrix. Recent investigations show the formation of V shell around ODS particles. The V signal from ODS particles is too weak to be visible in this investigation. The distribution of Y is shown in the Fig. 9e. The size of these ODS particles was found to be about 30-35 nm. The spatial distribution is not homogenous. In some grains the ODS particles were clearly detected. Especially higher concentration and larger particle size was detected inside several grains and on the grain boundaries. On the other hand closely located grains are without any ODS particles. Recent investigations show the presence of areas in the specimen with different distribution and morphology of ODS particles. Nano-sized ODS particles, with a size of less than 10 nm, cannot be made visible in this large area scan which has only a lateral resolution of about 15-20 nm. Linear arrangements showing a higher concentration of larger ODS particles do not always correlate with the grain boundaries. These lines presumably reflect the surface of steel powder flakes where the Yttria was not perfectly mechanically alloyed.

Conclusions

EB-welding was investigated as potential process to join divertor structures made of ODS-EUROFER. Similar ODS/ODS joints were fabricated and the tensile and impact properties were investigated in dependency of different post-weld heat treatments. Dissimilar ODS-EUROFER / EUROFER 97 joints were fabricated and tested for comparison. The microstructure of the different welds was investigated to explain the mechanical behaviour.

EB-welding of similar ODS-EUROFER joints leads to weak weld seams. The tensile and impact properties are nearly independent from the applied PWHT. The deterioration of the mechanical properties can be related to the change in microstructure in the welding zone. The strengthening nano-dispersoids agglomerate to larger particles thus weakening the weld seam.

Although EB-welding of ODS/ODS is not a suitable joining technique for highly loaded applications, it could be well applied in regions with lower mechanical loads or in the back part where a transition from the high-strength ODS to e.g. EUROFER steel is needed.

Staff:

S. Baumgärtner
B. Dafferner
U. Jäntsch
M. Klimenkov
R. Lindau
H. Zimmermann

Intellectual Property Rights (IPR)

In the frame of this work a new element of know-how has been generated.

Acknowledgement

This work, supported by the European Communities under the contract of Association between EURATOM and Karlsruhe Institute of Technology, was carried out within the framework of the European Fusion Development Agreement. The views and opinions expressed herein do not necessarily reflect those of the European Commission.

Industrial Fabrication of the Present Generation of Nano-structured ODSFS (WP10-MAT-ODSFS-02-01)

Introduction

The developmental work on nano-structured ODS steels in Europe is carried out in laboratories at universities and research centres at laboratory scale, i.e. small batches of a few grams to about 200 grams. The presently identified applications in future nuclear fusion reactors require instead amounts of material that are orders of magnitude larger and need therefore an industrial-scale fabrication. Among others, the transferability of the results gained in lab-scale to industrial scale production has also to be proven. A cooperation of a research centre with a single industrial partner as it was the case in the ODS-EUROFER development performed by KIT (formerly FZK) with PLANSEE is no longer possible due to the decision of PLANSEE to give up the ODS production.

This very fruitful cooperation lead in several developmental steps to a reduced activation ferritic martensitic 9Cr ODS-steel with acceptable mechanical properties that allow to increase the operational temperature compared to the non-ODS EUROFER 97 steel by about 100 °C to 650-700 °C making the material suitable for application in the blanket and divertor of a DEMO-type reactor.

Due to the α-γ phase transformation in these steels, the application temperature of this ODS-steel is limited to temperatures of about 800 °C. To avoid this drawback the development of ODS ferritic steels (ODSFS) which do not show such a phase transformation is pursued. In a preceding study (WP08-09-MAT-ODSFS, Activity 2) it was analysed how to circumvent the lack of an industrial manufacturer for ODS alloys in Europe. It was concluded to divide the fabrication process into single steps and to find industrial partners for each production steps.

This task is strongly interwoven with other tasks in which the influences of composition and production parameters on the properties of ODSFS are investigated. Taking account of the results achieved in the development of ODSFS at KIT and CRPP a common specification should be decided for the ordering of a batch of about 10 kg. As stated in the monitoring meeting in San Sebastián in July 2010, the knowledge at that time was not sufficient to decide such a specification. Due to the progress made in 2010 at both associations, a specification can be discussed and finalised.

Materials, screening, results and discussion

In continuation of the work performed in WP08-09-MAT-ODSFS Activity 2, several batches of a 14 Cr ferritic ODS alloy with various compositions were produced and characterised with respect to microstructure and mechanical properties in order to finalise a European specification for a 10 kg batch. Five 200 g batches of Fe-13.5Cr-2W-(0-0.2-0.3-0.4)Ti-0.3Y_2O_3 were produced in the usual powder metallurgical route. These small batches were tested and characterised in the hipped state. Except for a homogenisation treatment no further thermo-mechanical treatment was performed. This approach was regarded to be sufficient to judge the

Fig. 1: Different types of HIP capsules after hot isostatic pressing (HIP).

influence of Ti on the microstructural and mechanical properties.

Batches of 1 kg size from the most promising compositions were also produced to examine the influence of a thermo-mechanical treatment, i.e. rolling plus heat treatment, on microstructure and mechanical properties.

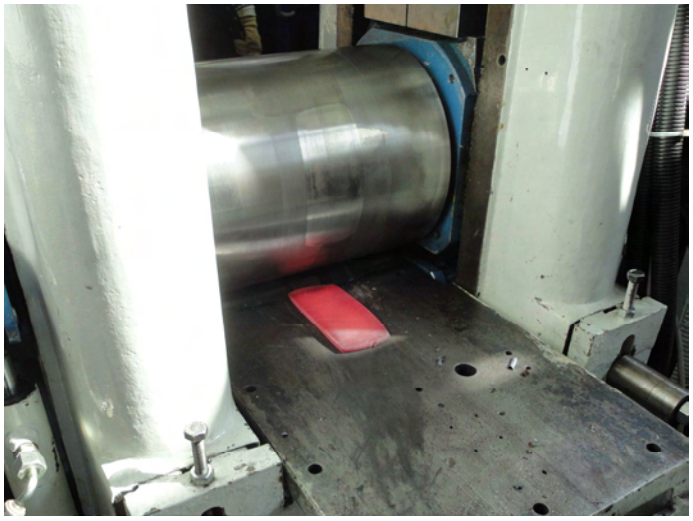

Fig. 2: Rolling of the 1 kg slabs in a 1.800 kN 12 inch Duo Mill.

The whole powder handling during the powder-metallurgical production route was performed under protective gas atmosphere to keep the oxygen content a slow as possible. Fig. 1 shows cylindrical (200 g) and prismatic (1000 g) types of capsules after hot isostatic pressing (HIP). Fig. 2 gives an impression of the rolling of the slabs in a 12 inch Duo Mill.

For the different Ti-contents, the correlation between microstructure and mechanical properties was analyzed by means of scanning electron microscope (SEM) and transmission electron microscope (TEM) equipped with energy- dispersive X-ray spectrometer (EDX) and electron energy loss spectrometer (EELS). A bimodal grain size distribution was observed in all as-hipped Ti-containing ODS alloys as it was seen earlier [1]. These alloys consisted of coarse grains typical ranging from 1 µm to 8 µm and fine grains well below 1 µm in diameter. The addition of Ti resulted in the formation of spherical Ti oxides rather than Cr oxides owing to the stronger affinity of Ti. The influence of Ti on particle size refinement was striking and the optimum effect was obtained when adding 0.3% Ti. Vickers hardness measurements (HV30) increased consistently with increasing in Ti content. The ODS alloying with 0.3% Ti exhibit the highest strength due to the optimum refinement of mean ODS particle size. Detailed results will be given in [2].

The ultimate tensile strength for the experimental 13.5%Cr ODS alloys over the range from RT to 700 °C is shown in Fig. 3 in comparison with data for the 13.5%Cr unmilled base alloy without any yttria and Ti additions, the conventional 9% Cr RAFM steel EUROFER 97, and the 9%Cr EUROFER-ODS steel. Tensile properties for all ODS alloys were remarkably enhanced and a more pronounced strengthening was observed for ODS ferritic steels in comparison with a 9% Cr ODS steel over the test temperature range. At room temperature, the ODS alloy with 0.4% Ti had the highest ultimate tensile strength of 1100 MPa. Up to 500 °C the best tensile strength was observed for the ODS alloy with 0.3% Ti which was in accordance with particle size results. According to the Orowan dislocation by-pass process, the particle strengthening increases approximately with the square root of particle fraction and more strongly with decreasing mean particle size. When increasing the test temperature further, Ti had a minor influence on tensile strength and all Ti-containing ODS alloys exhibited a comparable strength with the 9%Cr ODS steel. In general the ODS alloys with Ti show satisfactory strength up to 500 °C and a steep decrease in strength was clearly visible for these alloys above 500 °C. On the other hand the tensile ductility, i.e. uniform and total elongation of the 13.5%Cr ODS alloys are inferior to that of EUROFER and EUROFER-ODS.

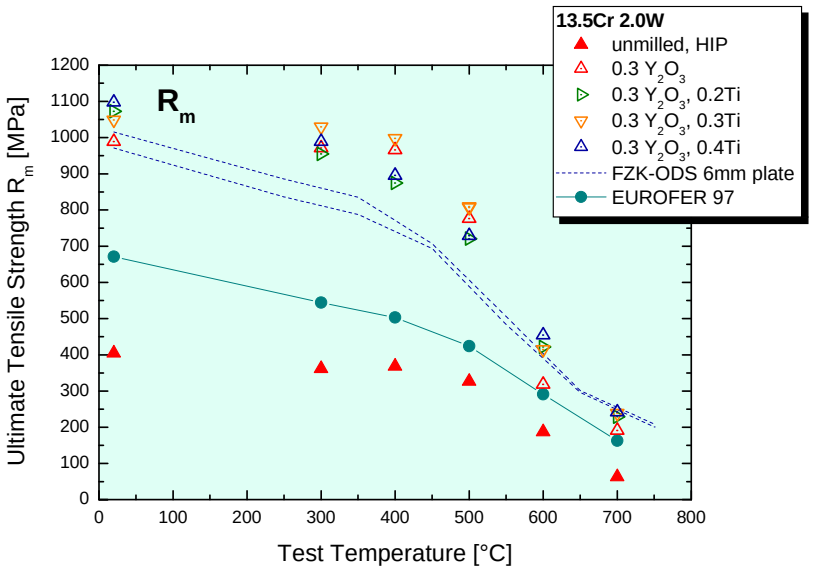

Fig. 3: Temperature dependence of ultimate tensile strength for different 13.5%Cr ODS alloys after annealing compared to 9%Cr EUROFER-ODS steel and the basic steels.

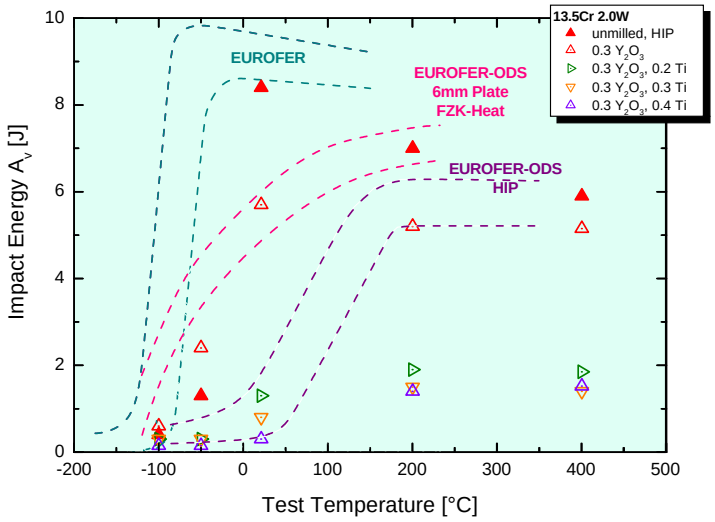

Fig. 4: Temperature dependence of total absorbed energy for different hipped 13.5%Cr ODS alloys after annealing compared to 9%Cr EUROFER-ODS steel and the basic steels.

Figure 4 shows the impact properties of the 13.5%Cr ferritic ODS variations after hipping and homogenisation heat treatment in comparison to the base alloy, EUROFER 97 as well as FZK-Heat of EUROFER-ODS in the thermo-mechanical treated state and the as-hipped condition after different heat treatments. The impact properties for the ODS alloy without Ti is very promising, in terms of a similar USE of 5.8 J and a lower DBTT of about -50 °C in comparison with a hipped EUROFER-ODS steel. This improvement may be attributed to the elimination of elongated Cr carbides by annealing treatment which was observed earlier for EUROFER-ODS [3]. All Ti-containing ODS alloys exhibit a low upper shelf energy (USE) below 2 J which is consistent with the findings of Ch. Eiselt [4]. A further improvement is expected by the application of a thermo-mechanical treatment as it was demonstrated for EUROFER-ODS (FZK-Heat) in Fig. 4.

Summary and conclusions

Several Fe-13.5Cr-2W-(0-0.2-0.3-0.4)Ti-0.3Y_2O_3 ferritic ODS-steels were successfully produced and investigated with respect to microstructure and mechanical properties. While they

show promising tensile strength, the high temperature tensile ductility and impact properties can still be improved.

Staff:

C. Adelhelm
S. Baumgärtner
B. Dafferner
C. Eiselt
P. He
M. Hoffmann
U. Jäntsch
T. Kaiser
M. Klimenkov
R. Lindau
A. Möslang
J. Reiser
R. Ziegler
H. Zimmermann

Literature:

[1] C.C. Eiselt, M. Klimenkov, R. Lindau, A. Möslang, H.R.Z. Sandim, A.F. Padilha, D. Raabe; High-resolution transmission electron microscopy and electron backscatter diffraction in nanoscaled ferritic and ferritic-martensitic oxide dispersion strengthened steels; J. Nucl. Mater., 385 (2009) 231-235.

[2] P. He, M. Klimenkov, R. Lindau, A. Möslang; Characterization of precipitates in nano structured 14% Cr ODS alloys for fusion application; submitted to J. Nucl. Mater.

[3] M. Klimiankou, R. Lindau, A. Möslang; Direct correlation between morphology of (Fe,Cr)23C6 precipitates and impact behavior of ODS steels; J. Nucl. Mater., 367-370 (2007) 173-178.

[4] C.C. Eiselt; Eigenschaftoptimierung der nanoskaligen ferritischen ODS-Legierung 13Cr-1W-0,3Y_2O_3-0,3TiH2, metallkundliche Charakterisierung und Bestimmung von Struktur-Eigenschaftskorrelationen; PhD-Thesis, Scientific Report FZKA 7524 (2010).

Acknowledgement

This work, supported by the European Communities under the contract of Association between EURATOM and Karlsruhe Institute of Technology, was carried out within the framework of the European Fusion Development Agreement. The views and opinions expressed herein do not necessarily reflect those of the European Commission.

Structural Materials - Refractory Alloys

Coordination of the EFDA Fusion Materials Topical Group, and Characterisation of W-alloys by Standard Charpy Tests with KLST Specimens (WP10-MAT-WWALLOY-02-06 and 02-05)

Coordination for EFDA Fusion Materials Topical Group

During the reporting period the EFDA program 2010 on tungsten and tungsten alloys development was compiled and evaluated. The according proposals were assessed. During several working and monitoring meetings the progress was monitored and discussed. The results of the Topical Group were presented. The final activity was the formulation of the next program for 2011 and the assessment of the proposals.

Introduction

Refractory materials, in particular tungsten base materials are considered as primary candidates for structural high heat load applications in future nuclear fusion power plants. Promising helium-cooled divertor design outlines make use of their high heat conductivity and strength. The upper operating temperature limit is mainly defined by the onset of recrystallization but also by loss of creep strength. The lower operating temperature range is restricted by the use of steel parts for the in- and outlets as well as for the back-bone. Therefore, the most critical issue of tungsten materials in connection with structural divertor applications is the ductile-to-brittle transition. Another problem consists in the fact that especially refractory alloys show a strong correlation between microstructure and their manufacturing history. Since physical and mechanical properties are influenced by the underlying microstructure, refractory alloys can behave quite different, even if their chemical composition is the same.

Fabrication and testing of Charpy specimens has been performed according to the EU standards DIN EN ISO 148-1 and 14556:2006-10. That is, small size specimens – sometimes referred to as KLST type – (27 mm x 3 mm x 4 mm, 1 mm notch depth, 0.1 mm notch root radius, 22 mm span) have been used for the tests. The specimens were fabricated by electrical discharge machining (EDM). The notch orientation was L-R (longitudinal-radial) in the case of all rod materials and L-T (longitudinal-transverse) in the case of the plates (see Fig. 1).

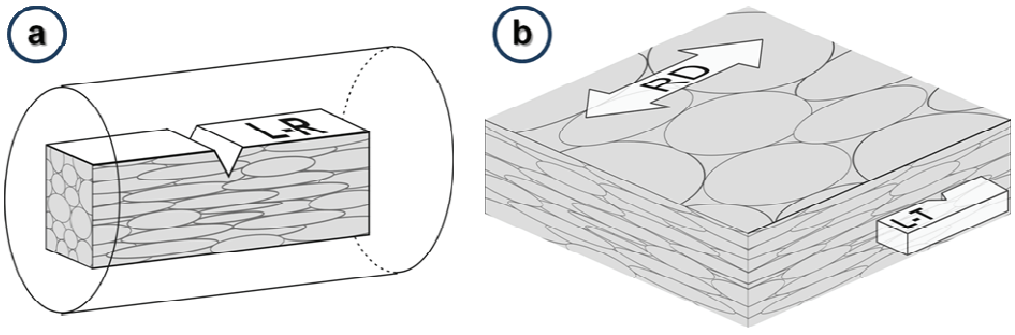

Fig. 1: (a) The only possible orientation for KLST Charpy specimens fabricated from rods with diameters smaller than 27 mm: longitudinal-radial (L-R).
(b) Specimen orientation in the case of plate materials. For the present investigation most specimens were oriented longitudinal-transverse (L-T), that is, with the specimen body parallel to the rolling direction (RD).

Round blanks can be considered either as radially or cross rolled plates. Therefore, the specification of specimen orientation fabricated from round plates is similar (see Fig. 2). Due to the geometry of the materials, the notches had to be fabricated perpendicular to the rolling direction in most cases (for rod materials no other orientation is possible). This is important for the evaluation of the Charpy results, since this orientation produces the most favourable energy and DBTT values.

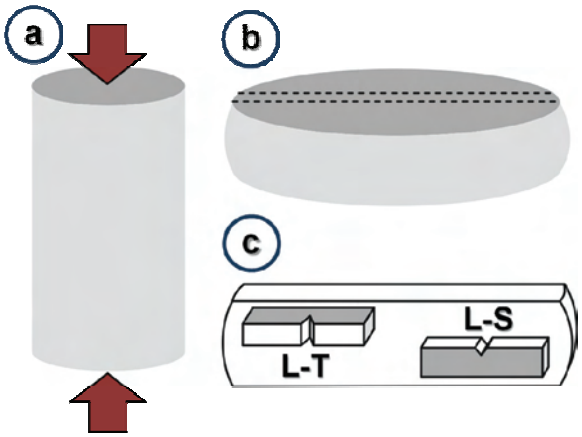

Fig. 2: (a) Round blanks are produced from sintered rods by forging them perpendicular to the axis (indicated by the arrows).

(b) The first step of specimen fabrication consisted in cutting the round blank in halves and then into a slice.

(c) For the present investigations W and WL10 specimens were fabricated in longitudinal-transverse (L-T) orientation. The WTa5 specimens were tested in longitudinal-short transverse (L-S) orientation.

Materials, Study and Results

Different tungsten rod materials were produced by PLANSEE: pure W, WL10 rolled, and WL10 with the highest possible level of deformation by swaging (WL10opt). In addition, Charpy specimens from swaged rods of tungsten (PW) and WL10 (PWL) have also been produced to compare the influence of material production and other details. These two heats are named PW and PWL just to indicate the different production route. Moreover, rolled plates of pure W and WL10 were used for the investigation. Finally, round blanks of tungsten (RW) and of a tungsten-5wt.%-tantalum alloy (WTa5) were also investigated. An overview of the test materials and their fabrication details is given in Table 1. For all materials the content of several interstitial impurity elements was determined: C is less than 30 wt. ppm, S and N are less than 10 wt. ppm, and for the pure tungsten materials O is less than 30 wt. ppm.

All semi-finished products (rods, plates, round blanks) show distinct textures. This can be clearly seen in the according micrographs. Examples for the plate and round blank microstructures are shown in Fig. 3. In rods, the grains are extremely elongated along the axis (needle-shaped). In plates and round blanks, the grains are flattened parallel to their surfaces (pancake-like). These specific microstructures (also indicated in Figs. 1) are closely connected to the fabrication history which included high deformation levels of 80 to 94 % (see Table 1).

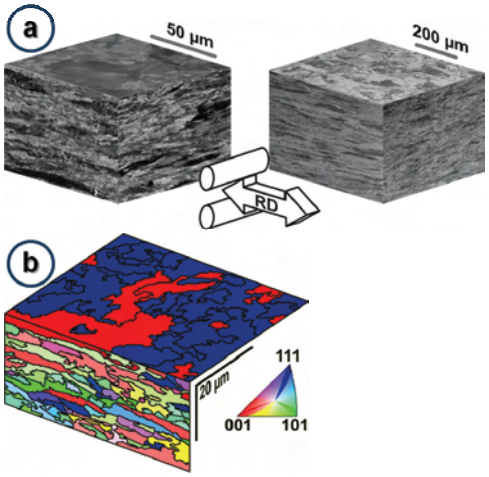

Fig. 3: (a) Microstructure of a tungsten plate in two different resolutions. The rolling direction (RD) is indicated. The images were produced by SEM in electron back scatter mode using the channelling effect of a focused gallium ion beam. The plate has been cross-rolled. Therefore, the pancake-shaped grains are only slightly elongated into rolling direction.

(b) Microstructure of the WTa5 round blank. The images were produced by electron back scatter diffractometry (the crystal orientations are given normal to the surfaces with a reduced number of colours). The pancake-like grain structure seems to be similar to those of the plate materials.

Since high dislocation densities were induced in the materials during the fabrication processes, stress relief heat treatments were applied to all materials. This, finally, led to the typical cell (sub-grain) formation. The thermo-mechanical treatments during production also affect the form and distribution of the oxide particles in the WL10 materials.

Table 1: Materials, size, and fabrication details.

Material	Form	Size	Deformation Degree	Fabrication Process
W	rod	Ø6.9 mm	91%	rolling
WL10	rod	Ø6.9 mm	91%	rolling
WL10opt	rod	Ø16 mm	94%	swaging
W (PW)	rod	Ø20 mm	93%	swaging
WL10 (PWL)	rod	Ø20 mm	93%	swaging
W	plate	thickness 3.6 mm	91%	rolling
WL10	plate	thickness 3.6 mm	91%	rolling
W (RW)	round blank	Ø180 mm, thickness 30 mm	ca. 80%	forging
WTa5	round blank	Ø180 mm, thickness 30 mm	ca. 80%	forging

Hence, the roughly spherically shaped lanthanum-oxide powder particles are elongated along the rolling, swaging, forging, or rolling direction. Since La_2O_3 is not dissolved in tungsten, the oxide particles form needle-like structures in rods. During intermediate annealing the needles break up into strings of smaller oxides which leads to a finer particle distribution. The typical diameter of such lanthanum-oxide needles is about 200-500 nm while the length can be up to 40 µm. Depending on the initial particle size and production parameters, the final oxide form and distribution can be different. They can also be formed flake-like as in the case of WL10opt (see Fig. 4) or they are shorter and thicker like, for example, in a W1Re1La_2O_3 rod used in prior studies.

TEM observations are inappropriate for the analysis of the La_2O_3 particle shape and distribution due to their large size but also due to the rather difficult sample preparation. Presently, the best results are gained by the Slice&View technique (see Fig. 4). The according investigations for the WL10 plate material are still ongoing. Therefore, exact statements about their La_2O_3 particle size and shape cannot be given yet. But it is an obvious assumption that the oxides form elongated platelets or flat strips during the rolling process. This is also confirmed by the very first results from focused ion beam investigations.

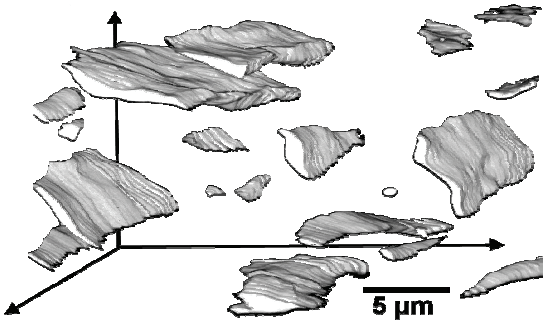

Fig. 4: Three-dimensional reconstruction of lanthanum-oxide particles formed in the WL10opt rod material. The particle shape was imaged by 3D Slice&View techniques [14] using a dual beam FIB (focused ion beam) system (FEI Strata 400). The surface rendering of the oxide particles clearly reveals their flake-like rather than spicular (needle-like) shape.

The results of the dynamic bending tests with specimens of pure tungsten and WL10 rods are shown in Fig. 5. Pure tungsten clearly shows three different regimes in terms of temperature, energy level, and type of fracture. Below about 550-600 °C, it fractures trans-crystalline with Charpy energies lower than 2 J (brittle fast fractures). Above 750-850 °C there are only ductile fractures. This is the upper shelf with Charpy energies between 9 and 12 J. The transition from brittle to ductile fracture takes place in the temperature range of about 600 to 750°C and is accompanied by increased scattering. The reason for that lies in the occurrence of an additional fracture mode: inter-granular delamination fracture. That is, there is no direct transition from brittle to ductile but there are two transitions: (1) from brittle to delamination and (2) from delamination to ductile fracture.

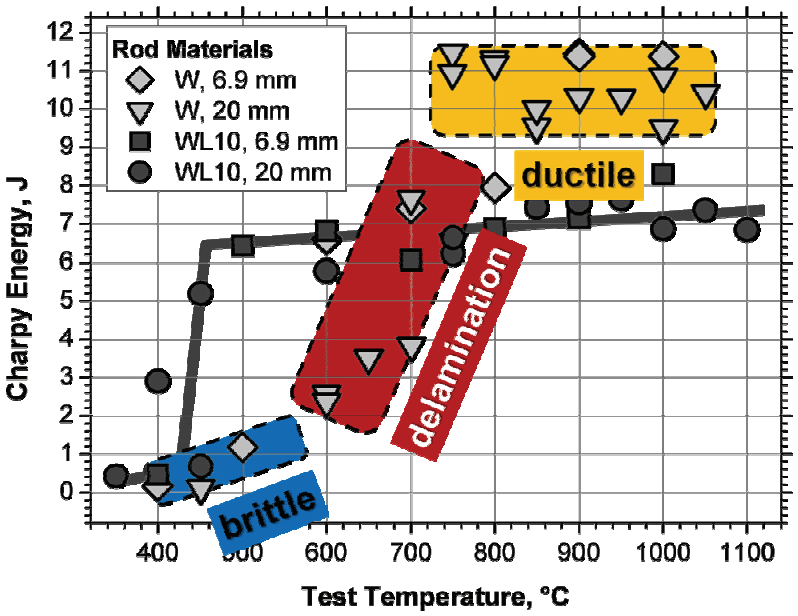

Fig. 5: Charpy test results. The symbols are coloured light grey for pure tungsten and dark grey for WL10 rod materials. Pure tungsten shows distinct temperature ranges for brittle (trans - crystalline) fast fracture and for ductile fracture (upper shelf). The brittle to ductile transition shows broad scattering and is dominat - ed by inter-granular delamination fracture. The WL10 results show a transition from brittle to delami - nation fracture, but no transition to ductile fracture. The delamina - tion regime exceeds even 1100 °C.

In the case of pure tungsten rods, these transitions take obviously place within a relatively narrow temperature range. For WL10, however, this is different (see Fig. 5). Brittle fast frac - ture was observed around 400 °C with a steep transition to inter-crystalline delamination be - tween 400 and 450 °C. The delamination regime extends from about 450 to more than 1100 °C at an energy level of 5-8 J. Up to 1100 °C there was no onset of ductile fracture recogniz - able.

In summary, there are two differences in the Charpy test results of pure tungsten and WL10 rods: (1) WL10 shows only one transition (from brittle to delamination fracture while the de - lamination to ductile transition does not occur up to 1100 °C) and (2) the transition tempera - ture is lower by about 150-200 °C. Both observations may be explained reasonably well by the needle-like rod microstructure as depicted in Fig. 6. Due to the 3-dimensional state of stress, the Charpy specimens are also loaded with stresses in notch direction. At the notch root, local stresses are even increased. Thus, for a certain strain rate and within the right temperature range (between about 600 and 750 °C), the grain boundaries are the weakest link in the microstructure. Therefore, intergranular fracture is most likely to appear. Without a notch, the stress at the grain boundaries would be too low or delamination fractures. This has been verified in [13] with un-notched specimens (cross-section of 3 mm x 3 mm) fabricated of the same pure tungsten rod. They fracture fully ductile above 450 °C without delamination. The addition of lanthanum-oxide – which forms needles or flakes between the tungsten grains (see Fig. 6a) – obviously weakens the grain boundaries. Therefore, above about 450 °C, WL10 shows only delamination fracture.

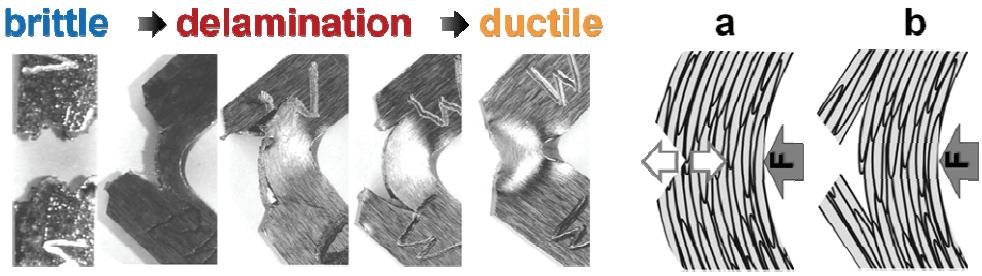

Fig. 6: In specimens of pure tungsten rods, the fracture mode changes with raising temperature from brittle to delamination and, finally, to ductile fracture. (a) During loading, the Charpy specimen is bended which generates tensile stress, but also stresses in notch direction (indicated by the white arrows). (b) If the testing temperature is high enough, the brittle trans-crystalline fracture mode changes to inter-granular fracture. The cracks are initiated slightly below the notch which is the point of maximum stress normal to the grain boundaries.

The Charpy test results for the plate and round blank materials are shown in Fig. 7. Compared to the results of the rod materials, the Charpy energies are significantly lower. In all materials, pure ductile fractures did not occur, even at temperatures up to 1100 °C. Brittle fracture occurs at 400 °C for the tungsten plate and at 700 °C for the round blank material. Furthermore, the delamination fracture regime is decreased in the WL10 tests. Figure 8 shows the specific plate delamination fractures which were observed in all plate materials. It also illustrates a reasonable explanation for the observations. Due to the stress σ, the grains are further elongated and small pores form first near the notch root. These pores propagate then inter-granularly along the tips of the pancake-shaped grains (perpendicular to the notch root). The still conjunct ligaments are further elongated and thin out (Fig. 8, lower left sketch). At lower temperatures (about 500 to 900 °C), the ligaments break by trans-crystalline fracture (Fig. 8, lower middle sketch). Above about 900 °C, the ligaments show distinct necking and finally break ductile (Fig. 8, lower right sketch). In both cases, the typical grooves in the fracture surfaces would be the result of inter-granular cleavage. Obviously, the addition of lanthanum-oxide weakens the grain boundaries and, therefore, promotes the inter-granular cleavage even more which lowers the Charpy energy. A comparable behaviour was observed in the case of the WL10 rod specimens.

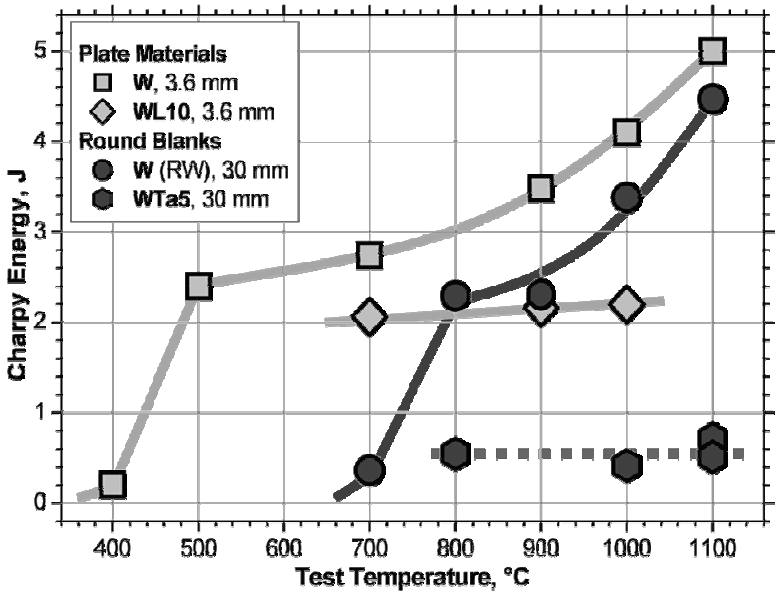

Fig. 7: Charpy test results of plate and round blank materials. The transition to brittle fracture is significantly lower for the tungsten plate than for the round blank. All specimens with Charpy energies higher than 2 J broke in a specific way, that is, by plate delamination. All WTa5 specimens showed mixed brittle-delamination fractures comparable to those of the rods.

The result for the W-5wt.% Ta alloy, however, is disappointing. In the temperature range of 800-1100 °C the specimens fractured in a mixed mode (partly brittle and delamination fractures) but on a very low Charpy energy level (less than 1 J). This result was surprising since the grain size of WTa5 is smaller and first tensile tests showed a higher strength compared to that of pure tungsten (RW). Further investigations have to be carried out to find explanations for the considerable reduction of the dynamic fracture toughness.

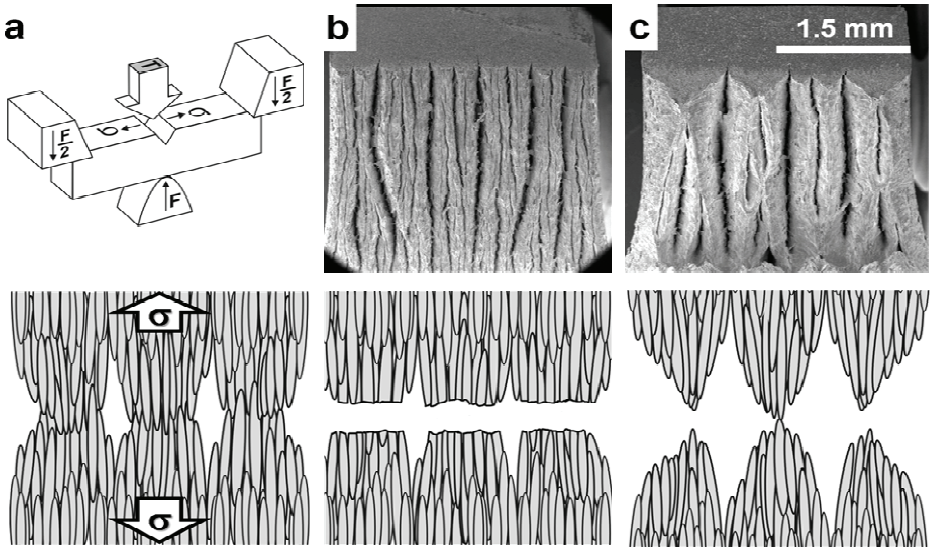

Fig. 8: (a) Charpy test load and top view on the notch (arrow). Fracture surface of a W plate specimen tested at (b) 700 °C and at (c) 1100 °C. The lower row of sketches illustrates the influence of the plate microstructure (see Fig. 2 and 6) on the fracture surface (by top view). Left: The bending stress leads to pores. Middle: Trans-crystalline fracture at 700 °C. Right: Further elongation, necking, and ductile fracture at 1100°C.

Conclusions

Pure tungsten shows lower creep strength compared to WL10. Therefore, it might not fulfil the requirements for structural helium-cooled divertor applications. WL10, on the other hand, shows lower thermal conductivity. But even in the worst case, it is still above 90 $Wm^{-1}K^{-1}$ at 1300 °C which would meet the design criteria. The fracture behaviour of WL10, however, is rather problematic: Even at temperatures up to 1100 °C there is still inter-granular cleavage. Specimens of pure tungsten rods break fully ductile at temperatures higher than 800 °C, at least.

Nevertheless, the specific anisotropic microstructure of the tungsten materials limits their applicability. The Charpy specimens in the present investigations were oriented in the optimum way, that is, they were loaded perpendicular to the elongated grains. In this way, tensile/bending stresses appear parallel to the fibrous or plate-like grains which yield the highest Charpy energies. But in real parts like pipes or thimbles, which play a major role in helium-cooled divertors, the microstructure cannot be easily oriented perpendicular to the maximum bending load.

Therefore, the ongoing investigations should focus on further optimization of the chemical composition (presently, WTa5 looks not promising) for a possibly lower brittle fracture temperature as well as on alternative part fabrication processes to allow for an optimum microstructure alignment.

Staff:

C. Adelhelm
S. Baumgärtner
B. Dafferner
S. Heger
U. Jäntsch
M. Klimiankou
A. Möslang
P. Lukits
M. Rieth
M. Rohde
R. Ziegler
H. Zimmermann

Literature:

[1] M. Rieth, A. Hoffmann, B. Dafferner, S. Heger, *Impact Bending Tests on Selected Tungsten Materials*, 1st International Conference on New Materials for Extreme Environments, June 2-4, 2008, San Sebastián, Spain. Published in: Trans Tech Publ., 2009, S.101-04 (Advanced Materials Research ; 59), ISBN 978-0-87849-344 - 9.

[2] M. Rieth, A. Hoffmann, B. Dafferner, S. Heger, E. Materna-Morris, H. Sandim, H. Zimmermann, *Mechanical properties of different refractory materials for nuclear fusion applications*, Materials Science and Engineering, Sept. 1-4, Nürnberg, Germany.

[3] M. Rieth, A. Hoffmann, *Fracture behavior of tungsten materials depending on microstructure and surface fabrication*, 18th Topical Meeting on the Technology of Fusion Energy (TOFE-18), San Francisco, Calif., Sep - tember 28 - October 2, 2008.

[4] M. Rieth, A. Hoffmann, M. Rohde, *Tungsten as Structural Material for Power Plant High Heat Flux Compo- nents*, Int. High Heat Flux Components Workshop, San Diego, Calif., December 10 - 12, 2008.

[5] M. Rieth, A. Hoffmann, B. Dafferner, S. Heger, U. Jäntsch, M. Klimenkov, P. Lukits, M. Rohde, H. Zimmer - mann, *Tungsten as Structural DEMO Divertor Material*, Jahrestagung Kerntechnik 2009, 12.-14. Mai, Dres - den, Germany.

[6] Raffray, A.R.; Nygren, R.; Whyte, D.G.; Abdel-Khalik, S.; Dörner, R.; Escourbiac, F.; Evans, T.; Goldston, R.J.; Hölzer, D.T.; Konishi, S.; Lorenzetto, P.; Merola, M.; Neu, R.; Norajitra, P.; Pitts, R.A.; Rieth, M.; Rödig, M.; Rognlien, T.; Suzuki, S.; Tillack, M.S.; Wong, C.; *High heat flux components - readiness to proceed from near term fusion systems to power plants*; 36th International Conference on Plasma Science (ICOPS) and 23rd Symposium on Fusion Engineering (SOFE-23), San Diego, Calif., May 31 - June 5, 2009

[7] Rieth, M.; Snead, L.L.; *The challenges of high heat flux components in fusion reactors with respect to mate- rial selection*; 36th International Conference on Plasma Science (ICOPS) and 23rd Symposium on Fusion Engineering (SOFE-23), San Diego, Calif., May 31 - June 5, 2009.

[8] Rieth, M.; Boutard, J.L.; *Review of the EFDA programme on divertor materials technology and science*; 14th Internat.Conf.on Fusion Reactor Materials (ICFRM-14), Sapporo, Japan, September 7-12, 2009.

[9] M. Rieth, A. Hoffmann, *Influence of microstructure and surface fabrication on impact bending properties of tungsten materials*, 17th PLANSEE SEMINAR, 25-29 May 2009, Reutte, Austria.

[10] M. Rieth, P. Norajitra, *Divertor Concepts, Coolants, and Structural Materials*, DEMO Technical Meeting, EFDA-CSU, Garching, 29.-30. Sept. 2009.

[11] M. Rieth, A. Hoffmann: Adv. Mater. Res. 59 (2009), p. 101-104.

[12] M. Rieth, A. Hoffmann: Fus. Sci. Technol. 56 (2009), p. 1018-1022.

[13] Rieth, M.; Armstrong, D.; Dafferner, B.; Heger, S.; Hoffmann, A.; Hoffmann, M.D.; Jäntsch, U.; Kübel, C.; Materna-Morris, E.; Reiser, J.; Rohde, M.; Scherer, T.; Widak, V.; Zimmermann, H.; *Tungsten materials for structural divertor applications*, 1st Internat.Conf.on Materials for Energy, Karlsruhe, July 4-8, 2010.

[14] M. Rieth, *Tungsten as a structural material for nuclear fusion reactors*, University of Oxford, GB, 20.Mai 2010.

[15] Rieth, M.; Armstrong, D.; Dafferner, B.; Heger, S.; Hoffmann, A.; Hoffmann, M.D.; Jäntsch, U.; Kübel, C.; Materna-Morris, E.; Reiser, J.; Rohde, M.; Scherer, T.; Widak, V.; Zimmermann, H.; *Tungsten as a structural divertor material*; 12th Internat.Conf.on Modern Materials and Technologies (CIMTEC 2010), Including the 5th Forum on New Materials, Montecatini Terme, I, June 6-18, 2010.

[16] Rieth, M.; Hoffmann, A.; *Influence of microstructure and notch fabrication on impact bending properties of tungsten materials*; International Journal of Refractory Metals and Hard Materials, 28(2010) S.679-86.

[17] Rieth, M.; Linke, J.; Linsmeier, Ch.; *High heat flux materials: status and perspectives*; 26th Symp.on Fusion Technology (SOFT 2010), Porto, P, September 27 - October 1, 2010.

[18] Raffray, A.R.; Nygren, R.; Whyte, D.G.; Abdel-Khalik, S.; Dörner, R.; Escourbiac, F.; Evans, T.; Goldston, R.J.; Hölzer, D.T.; Konishi, S.; Lorenzetto, P.; Merola, M.; Neu, R.; Norajitra, P.; Pitts, R.A.; Rieth, M.; Rödig, M.; Rognlien, T.; Suzuki, S.; Tillack, M.S.; Wong, C.; *High heat flux components - readiness to proceed from near term fusion systemsto power plants*; Fusion Engineering and Design, 85(2010) s.93-108.

Acknowledgement

This work, supported by the European Communities under the contract of Association between EURATOM and Karlsruhe Institute of Technology, was carried out within the framework of the European Fusion Development Agreement. The views and opinions expressed herein do not necessarily reflect those of the European Commission.

Development of W-PIM Parts (WP10-MAT-WWALLOY-01-01)

Objectives of the task

The He-cooled divertor is one of the most important plasma-facing components of the future DEMO fusion power plant reactor and has to withstand high surface heat loads (up to 10 MW/m²). The main function of the divertor is to remove reactor ash and eroded particles. The KIT divertor design is based on a modular concept of cooling finger units [1]. This design will help to reduce the thermal stresses. Each cooling finger unit (the so-called “1-Finger module”) consists of many single parts e.g. tile and thimble. For the whole divertor system more than 250,000 single parts e.g. of the tile are needed.

The most promising material for the tile to withstand the extreme conditions is tungsten. The advantages of tungsten are the high melting point of 3420 °C, high thermal conductivity, high strength, low thermal expansion and low activation. But the disadvantages are brittleness and hardness and these properties cause major problems in the fabrication of parts by mechanical machining such as milling.

Powder Injection Molding (PIM) is a time and cost effective near-net-shape manufacturing method for ceramic and metal parts and has been adapted and developed at KIT for tungsten. W-PIM pre-tests on basic samples were studied and first promising results achieved. The motivation for this work is to manufacture the tungsten tile by PIM in view of mass production aspects.

State of the art PIM R&D

First successful experiences with W-PIM were made in 2009. A new feedstock with a binary tungsten powder particle system (50% fine and 50% raw powder with a grain size distribution in the range 0.7 to 1.7 µm FSSS) and a 50 vol.-% wax/thermoplastic binder system was successfully developed [2].

The manufactured basic samples reached after debinding and heat-treatment (pre-sintering and HIP) a final density of approximately 97.6 % TD and a Vickers-hardness of 457 HV0.1.

The knowledge gained by the pre-tests on basic parts was transferred to the design of a new PIM tool to produce the divertor part W tile. The PIM process route comprises powder preparation; feedstock (powder and binder) formulation; filling simulation; manufacture of the new PIM tool; injection moulding process; debinding; sintering and HIP. The main results shall be discussed below.

Results

<u>Design and Simulation of a new PIM tool</u>

Fig. 1 shows the filling simulation with the PC software “Moldflow®” of the part “W tile” with complete gating system. This is very helpful to detect air traps, to define the location and numbers of the injection points as well as the gating system and give information about the fill time.

For the new PIM tool W tile a 2-point halve gating system with position in the middle of the part is used. The fill time is nearly 1 sec. The finished new PIM tool is shown in Fig. 2.

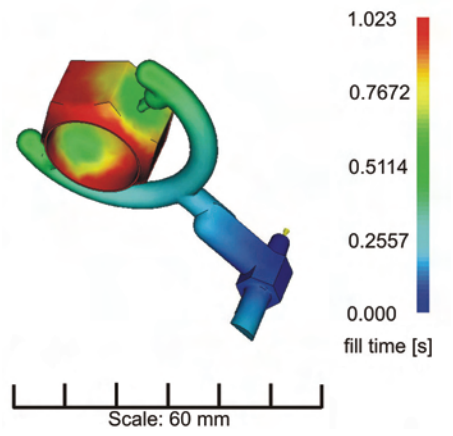

Fig. 1: Filling simulation of W tile with gating system.

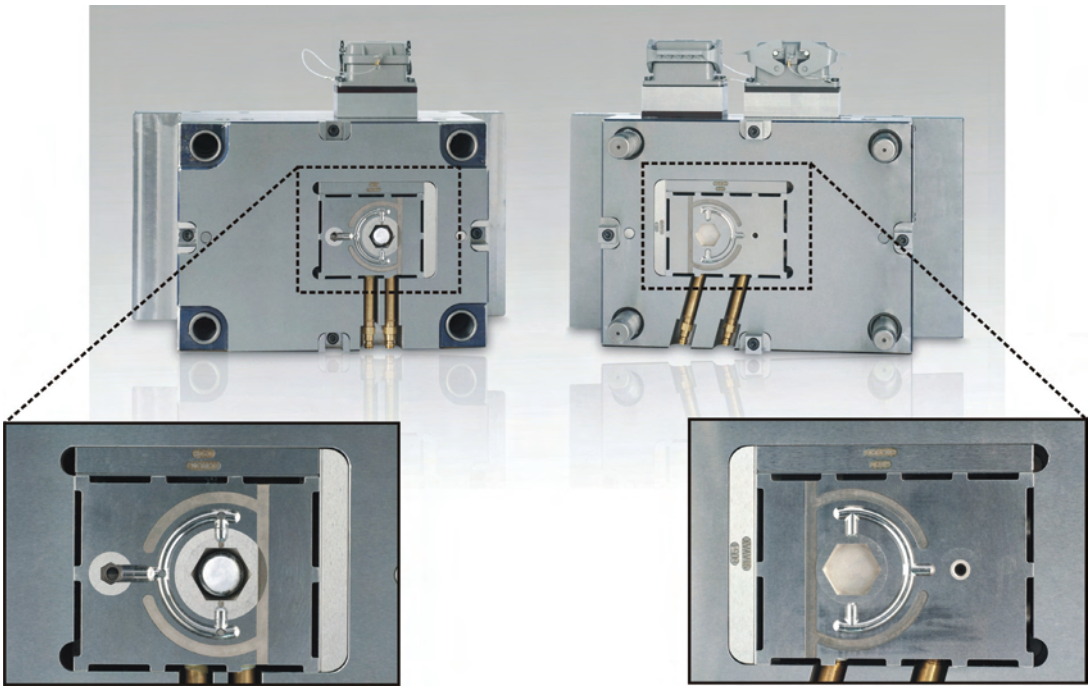

Fig. 2: The new PIM tool, ejection side (left), nozzle side (right).

Properties of the W-PIM divertor part “tile”

The powder injection molding of the parts was performed by an ARBURG injection molding machine, Type “Allrounder 420C”. The composition of the used feedstock with 50 vol.-% solid load includes a binary tungsten powder particle system (50% fine and 50% raw powder). After injection molding, the green parts have been debinded, at first solvent debinding in n-Hexane for 48 hours @ 50 °C followed by thermal debinding for ½ hour @ 550 °C in dry H_2 atmosphere. The heat-treatment is a two step procedure, first pre-sintering in a sinter furnace @ 1650 °C in dry H_2 for 2 hours in order to reach the closed porosity necessary for the HIP treatment. After that, the samples were compacted by use a HIP-cycle @ 1600 °C under 250 MPa for 3 hours and argon atmosphere. Fig. 3 shows the green part and the finished W tile after heat-treatment. The linear shrinkage is nearly 20% [3].

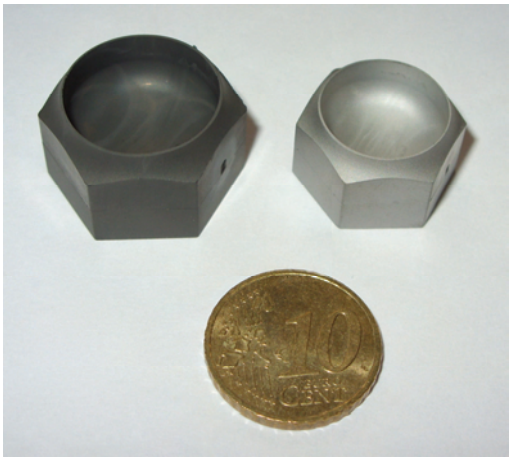

Fig. 3: Green part (left) and finished W tile after pre-sintering and HIP treatment (right).

The final samples were compacted and reached values near the theoretical density (98.6 - 99%TD), a Vickers-hardness of 457 HV0.1 and a grain size of approximately 5 µm. The resulting microstructure is shown in Fig. 4. No porosity or cracks are visible.

Conclusions and outlook

Based on PIM pre-tests a new tungsten feedstock with a binary W powder system was developed. The knowledge gained by the pre-tests on basic parts was transferred to the design of a new PIM tool to produce the divertor part W tile. Also a filling simulation to define the gating system and the position of that and detect possible air traps was performed.

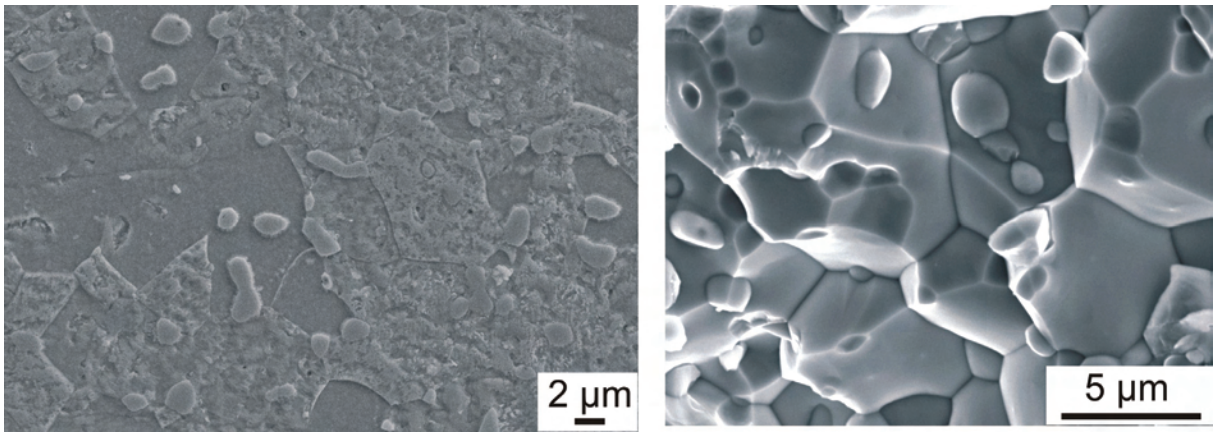

Fig. 4: Microstructure of the finished W tile, metallographic section (left), and fracture surface (right).

Future work will focus on joining methods and tests under “real” conditions. The so produced PIM W tiles will undergo high heat flux tests at the Efremov Institute, St. Petersburg, Russia, after joining by HT-brazing to a divertor finger mock-up. After these tests the PIM tiles will be characterized and compared with mechanically manufactured tiles, tested under the same conditions.

A future step will be to develop new W-alloy feedstock and to design a two-component powder injection molding tool for replicating fusion relevant components such as tile and thimble in one step.

Staff:

S. Antusch
P. Holzer
P. Norajitra
V. Piotter
K. Plewa
H.-J. Ritzhaupt-Kleissl
L. Spatafora
R. Vouriot
H. Walter

Literature:

[1] P. Norajitra, S. I. Abdel-Khalik, L. M. Giancarli, T. Ihli, G. Janeschitz, S. Malang, I. V. Mazul, P. Sardain, Divertor conceptual designs for a fusion power plant, Fusion Engineering and Design 83 (2008) 893–902.

[2] S. Antusch, P. Norajitra, V. Piotter, H.-J. Ritzhaupt-Kleissl, Powder Injection Molding for mass production of He-cooled divertor parts, Journal of Nuclear Materials (2010) submitted.

[3] S. Antusch, P. Norajitra, V. Piotter, H.-J. Ritzhaupt-Kleissl, L. Spatafora, Powder Injection Molding – an innovative manufacturing method for He-cooled DEMO Divertor components, In: Proceedings of 26th SOFT, Porto, Portugal, 27. September – 01. October 2010, to be published in Journal of Fusion Engineering and Design.

Acknowledgement

This work, supported by the European Communities under the contract of Association between EURATOM and Karlsruhe Institute of Technology, was carried out within the framework of the European Fusion Development Agreement. The views and opinions expressed herein do not necessarily reflect those of the European Commission.

Electro Chemical Machining (ECM) of Tungsten and Tungsten Alloys (WP10-MAT-WWALLOY-01-04)

Introduction

As application in a fusion power system, a helium cooled divertor concept is investigated, which is envisaged to remove heat loads of up to 15 MW/m². This divertor design is based on a modular arrangement of cooling fingers, which is to be fabricated from a heat resistant material like tungsten (alloys). But shaping of tungsten, a hard and brittle material, is by the state of the art only possible by applying spark erosion methods (EDM), which systematically introduces microstructural defects into the bulk or by rather cost intensive milling technology which is also not risk-free concerning microcracks. Looking at the divertor structures and symmetries of some parts, it is obvious that only erosive machining methods can be used. EDM can surely produce such structures e.g. in steel, but not in W-alloys with the required quality. Beyond needed excellent surfaces without any damages and microcracks, economical costs are also an important figure which pushes the development of advanced technologies for processing of tungsten [1, 2].

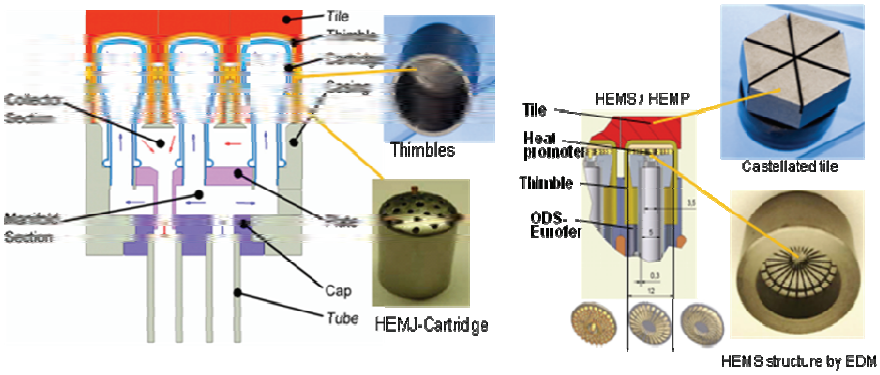

Fig. 1: Design variants HEMJ and HEMS / HEMP of cooling fingers. Especially in the later ones, micro-structurally shaped W-arrays are integrated into the thimble made of WL10 (W1%La2O3) to enhance heat transfer. The shown array structures are: pin, straight slot and curved slot arrays with groove dimensions of approx. 1.5 x 0.3 mm (H x W) and a total diameter of approx. 12 mm.

Innovative ECM (Electro Chemical Machining) technology can produce defect-free surfaces and high precision parts at low costs by an etching process which is controlled by electrochemical dissolution [3] with well defined and controlled parameters as e.g. applied in steel processing. However, such an electrochemical application in W-alloy processing is still missing. Tests of established and well-tried ECM industrial processes working with electrolytes specially adapted to steel shaping showed irreversible passivation effects.

Development of electrolytes and physical aspects for ECM (Electro-Chemical Machining) of tungsten

Tungsten is, given by its pure properties, in theory less stable than iron in acidic etching solutions, but in reality, tungsten forms, after an initial electro-chemical oxidation, completely insulating oxide layers and the tungsten scales are totally insoluble in commercial ECM electrolytes. Standard changeable electrolytes cannot remove those passivating layers from tungsten by dissolution. This is the reason why shaping of W failed in industrial electrolytes. All results shown here were achieved in aqueous two-component systems (TCEE) specially developed for tungsten machining.

The focus for activities in 2010 was set on the further optimization of EDM-machined surfaces of different geometric features, as they are found in the foreseen tungsten fusion-components. Shown in Fig. 1, the required W components have very different shapes and

sometimes also high geometrical complexity e.g. castellation with high aspect ratios, macroscopic curved shapes and different grain orientations.

Developed ECM process variants

The evaluation of the general electro-chemical behaviour of tungsten and the development of specific electrolytes opened the path for the development of ECM processing variant adapted to special needs in W machining. As process variants were identified three different branches in electrochemical machining and called M-ECM, a mask assisted process, C-ECM and S-ECM. The prefixes **C** and **S** are standing for the synonyms “**C**athode” assisted shaping and “**S**urface” for etching by “Surface” treatment processes [4].

S-ECM surface finishing

As generally known tungsten is a hard and brittle material at least at room temperature. Surfaces processed by conventional methods (e.g. EDM, milling) exhibit as a general rule surface defects (microcracks) which will influence dramatically later material and component suitability under real application conditions up to total failure and collapse. The structuring by electrochemical-etching of free, unmasked surfaces was developed to achieve a smoothing effect of the worked surface by ablation of layers in dimensions of micrometers. The main goal of this type of electro-polishing is to remove mechanically introduced microcracks and generate thus higher failure stability.

Deducted from preceding results it is obvious that parts with mixed geometrical surface structures required specially developed parameter sets to obtain a homogeneous material removal at all position e.g. on the flat surface and inside of narrow gaps.

Because of the fact, that the performance of tungsten surfaces revealed as an important aspect, and based on the demand of corresponding suitable manufacturing methods, surface finishing was set in the focus of tungsten ECM in the report period. Therefore ongoing research focused on the surfaces of: a.) Plain surfaces, and b.) gaps with high aspect geometries.

Plain surfaces

The successfully performed development showed that S-ECM can be applied for polishing in the 1 µm range and for removal of surface defects like microcracks with depths of about 100 µm. Two types of raw material – polycrystalline and single crystals – were processed. S-ECM machining with low erosion depth applied on crystals and polycrystalline samples had the aim to produce mirror like surfaces. Results concerning this topic were already presented in the 2009 report. The further development of this process had the goal to demonstrate crack removal of samples (disks, cylinders) cut by EDM from W-rod material of diameter 16 mm. It is well known that EDM produces microcracks which act as defect positions under load [2].

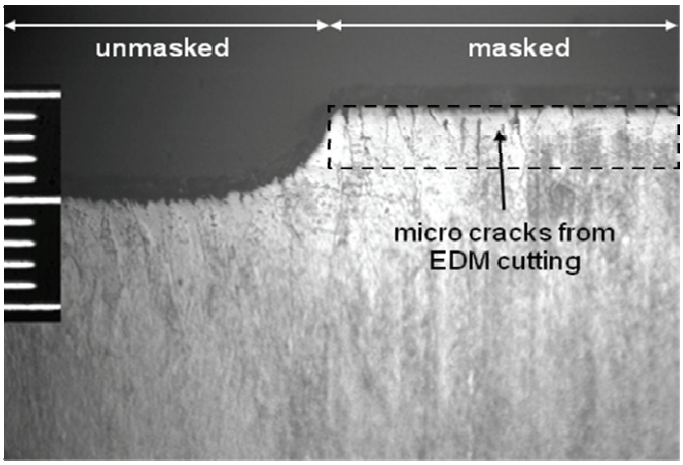

Fig. 2: S-ECM processing of a tungsten disc with half masked surface for comparison purpose. Right side masked and thus unprocessed; left side S-ECM machined with a removal of 60 µm.

Fig. 2 gives the surface structure of the sample (EDM-cut) as delivered with the clearly visible machining defects of microcracks and scratches and after S-ECM processing with slight materials removal by electrochemical dissolution. The electrolyte was of type TCEE [4] and the applied current density was 200 mA/cm². It can be seen, that especially the machined defects as microcracks disappeared. Roughly 60 µm were removed and danageous microcracks disappeared as later cracking centers under stress exposure.

C-ECM structuring

The basics of C-ECM are described in [4, 5]. C-ECM offers fundamental advantages due to working with a not consumable tool which will guarantee replication truth also in manufacturing deep structures in multiple sequenced processes. The C-ECM process works with a water based electrolyte which does not enable redeposition of tungsten on the negatively charged working tool. As showed earlier dissolution can be achieved easily with the developed electrolytes, however, the correct locally dissolution is the challenging task in shaping deep structures. It was shown that several parameters as current density, additionally tool step rate, gap width, convection, current type and mobility of ions have impact on shaping accuracy.

As a decisive parameter for the optimization of tungsten dissolution revealed the current profile. The effect of pulsed currents was demonstrated in a drastic increase of contour accuracy (Fig. 3). The sequence of pictures illustrates clearly the impact of pulsed current application. Dwell and pause times of the current were equal in this test series.

Fig. 3: Effect of pulsed currents. From left to right increasing pulse frequency 0 Hz; 10 Hz; 100 Hz; 500 Hz; 1000 Hz.

Electrochemical dissolution of tungsten is possible only in two consecutive steps, by which the last is a currentless chemical reaction. The need occurred to give this purely chemical reaction enough time for dissolving the complete electrochemical formed tungsten oxide layer.

As result, the current profile is divided in pulses of current intervals (for electrochemical oxidation) and currentless intervals (for chemical dissolution) in millisecond dimensions. The resulting effect is, that the flowing current is not hindered by a passivating layer, and does not evade to positions with lower electric resistance, which would dissolve tungsten metal at undesired positions; at least causing weak accuracy. The cylindrical elevation in the centre of the probes is a perfect reference (Fig. 4). It is the position, were the TCEE leaves the ECM tool and reacts with the tungsten. Only under ideal adjusted conditions this central structure can be formed, and consequently also the further structures at outer positions. The next development steps for further increasing accuracy are seen in application of HF pulses in the megahertz range, variation of dwell to pause ratios, better distance control tool – workpiece and variation of ion mobility. Nevertheless, application of improved electrolytes up to ionic liquids has to be considered for future ECM processes.

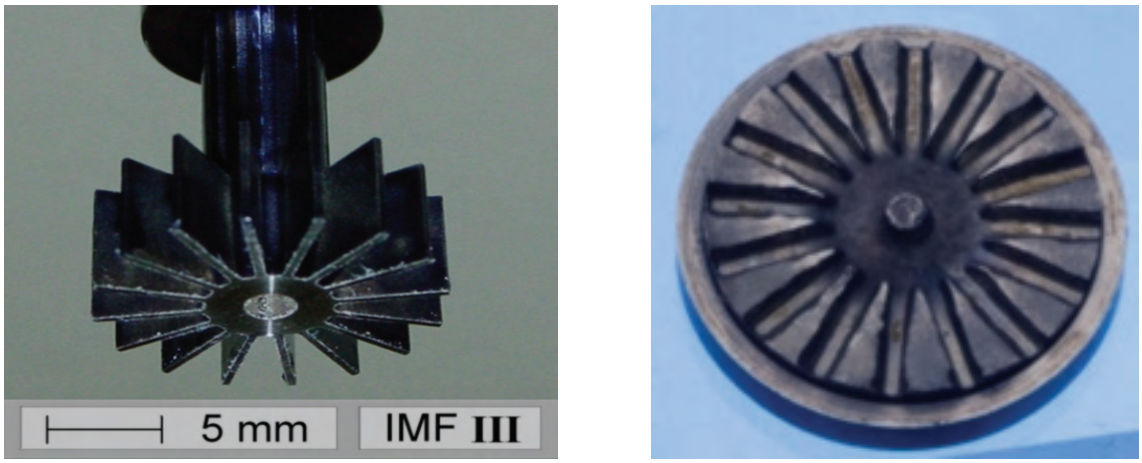

Fig. 4: A complex C-ECM cathode tool (16-fold star with electrolyte channel) and a structured workpiece (at 1 kHz).

Conclusions

The development of the two component electrolyte (TCEE) opened the path for large area processing and shaping of tungsten for the first time. Meanwhile three different branches in ECM processing were selected and developed. Due to the different main application fields (surface finishing by S-ECM, mask assisted surface structuring M-ECM and 3D shaping by cathode tool dissolution C-ECM) the processing parameters have to be adapted to each processing line separately. The development of C-ECM and S-ECM showed that a variation of the electric regime, e.g. pulse sequences will be the right path for process optimization. This is the main (mid-term) objective besides mobility control in the current research program on S-ECM and C-ECM.

The general result of investigations concerning electro-polishing (S-ECM) are, that tungsten surfaces in different geometrical features can be optimized by suitable parameters, which were demonstrated by selection of the concrete structure element. It was additionally shown that surface layers remaining from pre-shaping by EDM or mechanical tooling can be removed in parallel. The essential benefit by soft S-ECM processing was the electro-chemical ablation of microcracks containing surface areas and this also at the ground of deep cuts.

The use of HF pulse currents lead to a clearly visible gain in shaping accuracy and, additionally, to reduction in processing time applying C-ECM. Pulsed current processing have to be further developed to reach also for W-shaping standards known from similar steel working.

The general and future aim is to make ECM technology available for industrial fabrication of all W components as innovative and reliable process. For this purpose, first contacts to ECM manufacturers were realized.

Staff:

N. Holstein
J. Konys
W. Krauss
J. Lorenz

Literature:

[1] P. Norajitra, R. Giniyatulin, T. Ihli, G. Janeschitz, W. Krauss et al., He cooled divertor development for DEMO, Fus. Eng. Design, 82, (2007), 2740-2744.

[2] W. Krauss, N. Holstein, J. Konys, I. Mazul, Investigation of the impact of fabrication methods on the micro - structure features of W-components of a He-cooled divertor, Fus. Eng. Design, Vol. 81, 1-7, (2006),. 259-264.

[3] W. König, F. Klocke, Elektrochemisches Abtragen (ECM), Fertigungsverfahren, Vol. 3, Springer, (1997), pp. 91-121.

[4] N. Holstein, W. Krauss, J. Konys; Structuring of tungsten by pulsed ECM processes for He-cooled divertor application; Fus. Eng. Design, 83, (2008), 1512–1516.

[5] N. Holstein, W. Krauss, J. Konys, Development of a novel tungsten processing technology for electro - chemical machining of plasma facing components, Poster, SOFT-26, Porto/Portugal, 23rd September – 1st October 2010.

[6] N. Holstein, W. Krauss, J. Lorenz, J. Konys, Electro-chemically-based technologies for processing of tungsten components in fusion technology, First International Conference on Materials for Energy 2010, Karlsruhe/Germany, July 4-8, 2010.

[7] N. Holstein, W. Krauss, J. Konys, Development of novel tungsten processing technologies for electro - chemical machining (ECM) of plasma facing components. Fus. Eng. Design (2010), to be published.

Acknowledgement

This work, supported by the European Communities under the contract of Association be - tween EURATOM and Karlsruhe Institute of Technology, was carried out within the frame - work of the European Fusion Development Agreement. The views and opinions expressed herein do not necessarily reflect those of the European Commission.

Microstructure and Micro-mechanics Characterisation of W and W Alloys (WP10-MAT-WWALLOY-05-03)

Objectives

Due to the limited available tungsten material and in view of its characterization in small irradiated volume, there is a strong need to develop characterization methods on a microscopic scale. The intention of the task was to focus on the fracture of tungsten and tungsten alloys by testing small microbeams. Tungsten single crystal was chosen as starting material since there is a comprehensive data base in the literature. This will allow a direct comparison of the microscale experiments with macroscopic fracture experiments.

Performed Work

Usually, specimens for micromechanical tests are produced by using focused ion beam (FIB) machining. However, this preparation method is very time consuming and cost intensive, so that the number and size of specimens is limited. Therefore, an effective and convenient pre-preparation method for such microbeams was developed based on micro-electric discharge machining (µ-EDM) in collaboration with the Institute of Production Science (wbk) at the Karlsruhe institute of technology (KIT). Only in the final preparation step, a FIB workstation is used to introduce the notch into the specimens and do some final finishing of the microbeams.

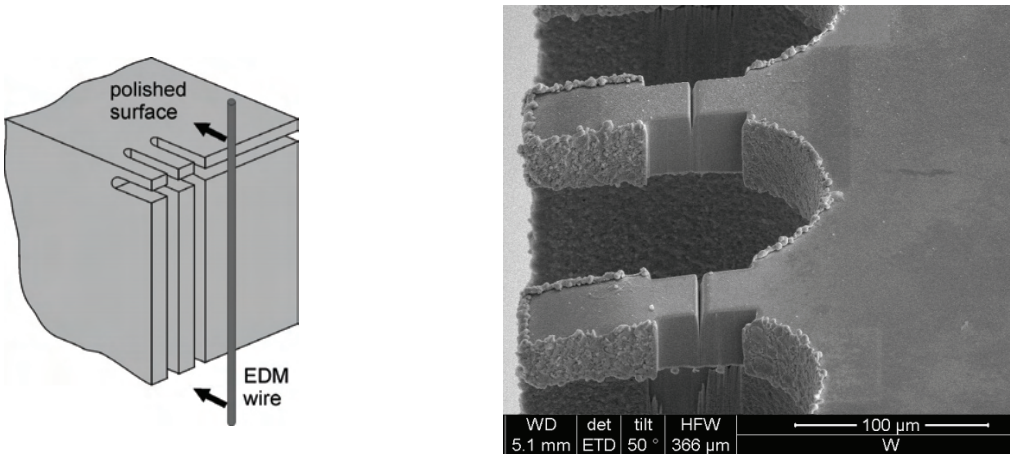

Fig. 1: a) Schematic illustration of the manufacturing of the microbeams using µ-EDM.
b) SEM image of notched microbeams after FIB finishing.

In the first preparation step, tungsten single crystal specimens (3mm x 3mm x 5mm) were mechanically polished and finally electropolished. In the next step, the micro-wire EDM machine (wire diameter 100µm) was used to make a first cut parallel to the polished surface, so that a thin ligament was formed over the whole width of the specimen. Afterwards the specimen was rotated 90° to the EDM wire and multiple cuts were done to produce the final cantilevers (see Fig. 1 a). The investigation of the cantilevers showed that the surface damage layer induced by the EDM process is only several micrometers thick. This surface layer was removed by FIB in the region where the notch was introduced into the cantilevers. Fig. 1 b) shows the final geometry of the notched cantilevers after FIB finishing.

Several microbeams with a $\{110\}\langle 1\bar{1}0\rangle$-crack system (crack plane + crack front) were produced and tested using a nanoindenter with a spherical indenter tip (tip radius 10 µm). The notched cantilevers were loaded at their free end and load and displacement were recorded during the experiments.

As can be seen from the example in Fig. 2, the tested microbeams exhibited a surprisingly ductile behaviour and no crack growth could be observed so far. The examination after the experiment showed a large plastic deformation of the microbeam and a significantly blunting of the notch without signs of brittle cracking (see Fig. 3a) and b)).

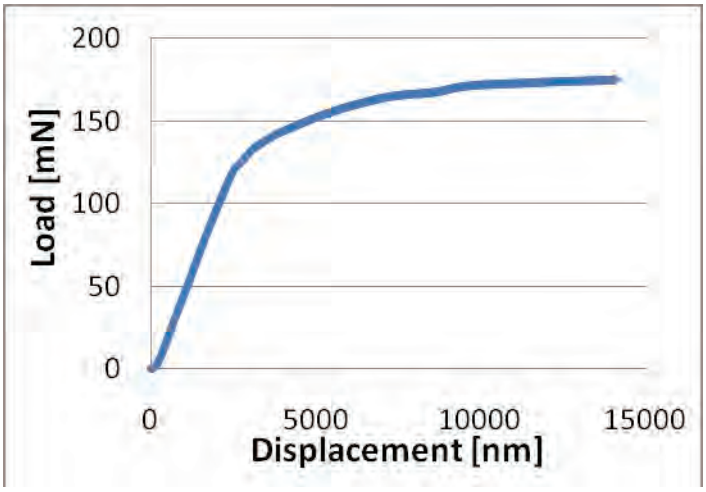

Fig. 2: Load-displacement curve recorded during the experiment. The microbeam was loaded at its free end using a nanoindenter with a spherical indenter tip.

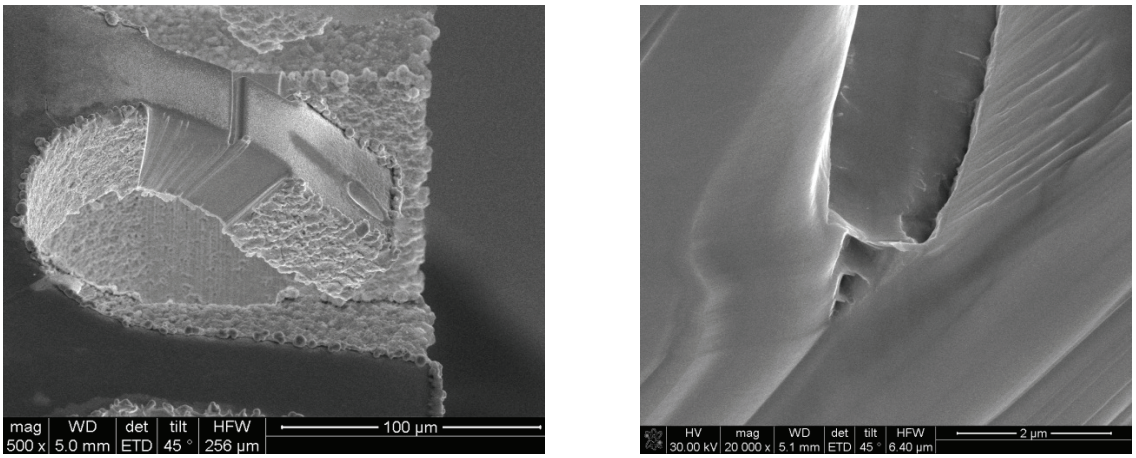

Fig. 3: a) SEM image of a notched microbeam after the experiment showing large plastic deformation.
b) Blunted notch at higher magnification.

Conclusion and Outlook

A novel specimen preparation method has been developed for fracture experiments at the micro scale by combining µ-EDM and FIB milling. The method was successfully applied for the preparation of specimens from tungsten single crystals. First experiments were conducted on specimens with a $\{110\}\{1\bar{1}0\}$-crack system. In contrast to macroscopic fracture experiments, no brittle cracking could be observed for this crack orientation. This may be due to the relatively small notch depths which were selected in the performed experiments. Specimens with deeper notches will be produced to address this effect.

Specimens from tungsten single and polycrystals with different crack orientations will be produced and characterized. The results of the fracture mechanical tests will be compared to those of macroscopic experiments. Furthermore the influence of loading rate and temperature will be investigated.

Staff:

J. Aktaa
D. Rupp

Literature:

[1] D. Rupp, Dissertation, Schriftenreihe Werkstoffwissenschaft und Werkstofftechnik Nr. 61, Shaker Verlag, Aachen, Germany, (2010)

Acknowledgement

This work, supported by the European Communities under the contract of Association between EURATOM and Karlsruhe Institute of Technology, was carried out within the framework of the European Fusion Development Agreement. The views and opinions expressed herein do not necessarily reflect those of the European Commission.

Basic Fracture Mechanical and Microstructural Characterisation of W-Ti, W-V, and W-Ta Alloys (WP10-MAT-WWALLOY-02-04)

Objectives

Inherent low fracture toughness of tungsten combined with the high DBTT are major drawbacks for structural application of tungsten alloys. Furthermore, FM properties are expected to exhibit strong anisotropy due to (i) different grain shape/orientation with respect to the rolling direction and (ii) texture. The current task aims at FM characterization of different laboratory and industry scale W-alloys (W-Ti, W-V, W-Ta) in the interesting temperature window for fusion applications (RT-1300 °C). Emphasis is put on the investigation of microstructure and load rate dependence of the fracture toughness (K_{IC}). The investigations should be accompanied by fractographic and microstructural investigations.

Performed Work

FM investigations have been carried out on tungsten and ODS tungsten alloys manufactured at CRPP-EPFL by MA and HIPping. Formation of Y_2O_3 oxide particles in the HIPping process of mechanically alloyed W-2wt.%Y powder has been reported by the manufacturer. Quasi-static three point bending tests were performed on pre-cracked rectangular SENB specimens with dimensions of 3x4x27 mm and with machined V-shaped notches. Sharp crack starter notches have been introduced by means of a razor blade polishing. This method allowed reduction of the notch radius down to 20 µm. During the experiments, force, displacement and temperature were recorded. The FM experiments have been performed over the temperature range of RT to 1000 °C. Tests above 350 °C were performed in high vacuum to avoid oxidation of the specimens. The mode I fracture toughness K_{IC} has been calculated following the ASTM E399 standard using the overall notch depth as a crack length.

Fig. 1 shows load displacement curves obtained on W-2wt.%Y ODS tungsten alloy. All specimens failed by brittle fracture in the entire test temperature range. The analysis of the fracture surface morphology has not revealed ductile deformation of the tested specimens. Fig. 2 shows SEM images of the fracture surfaces of investigated W-2wt.%Y alloy after testing at RT and at 1000 °C. Large areas with a low degree of the material consolidation observed in SEM images explain brittle behaviour of the material up to 1000 °C. Some isolated areas with higher degree of consolidation found in SEM images, seem to have no significant influence on the overall fracture-mechanical behaviour.

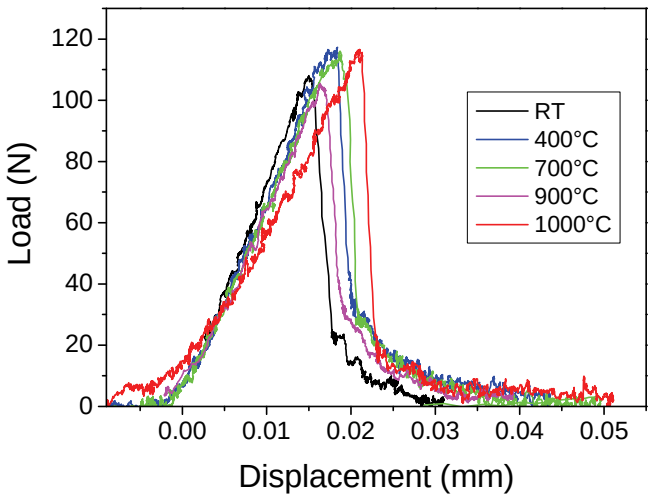

Fig. 1: Load displacement diagrams of mechanically alloyed and HIPped W-2wt.%Y ODS tungsten. dK/dt = 0.5-0.8 $MPam^{1/2}/s$.

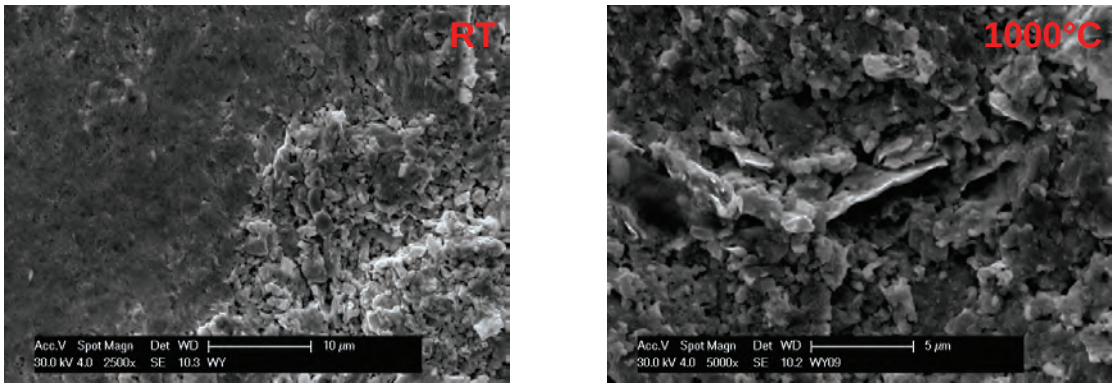

Fig. 2: SEM images of W-2wt.%Y ODS alloy after testing at RT and at 1000 °C.

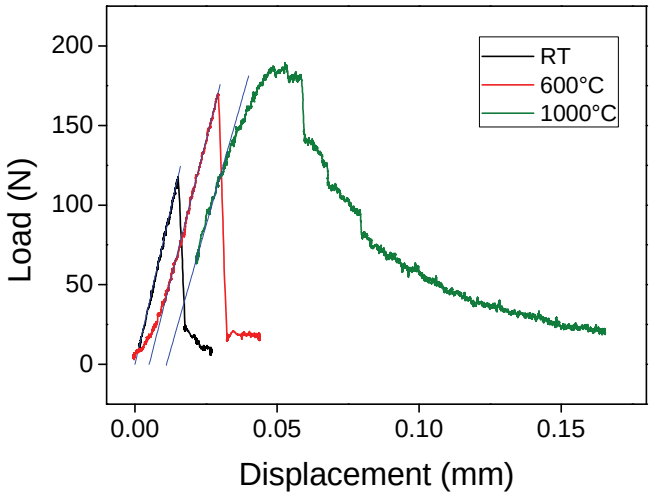

Fig. 3: Load displacement diagrams of mechanically alloyed and HIPped W. dK/dt=0.3 MPam$^{1/2}$/s.

Mechanically alloyed and HIPped tungsten manufactured with parameters identical to those used for W-2wt.%Y has been studied for comparative purposes. The load displacement diagrams are shown in Fig. 3. At test temperatures below 600 °C the curves reveal unstable crack propagation with no sign of ductile behaviour. At a test temperature of 1000 °C, in contrast, a plastic deformation followed by crack emission and arrest events was identified.

Deformation free fracture with no significant changes in fracture surface morphology was found in the entire test temperature range. SEM images of a fracture surface of a specimen tested at RT shown in Fig. 4 are good representative for all tested specimens. Low degree of material consolidation observed is considered to be responsible for predominantly brittle fracture. Locally pronounced grain growth as well as “flower” like microstructural defects was found in addition in all specimens. Different sintering stages characterized by I) necking formation and open porosity, II) neck blunting and channel closure, III) grain coarsening accompanied by pore break down into discrete pores were identified in “flower” like defects.

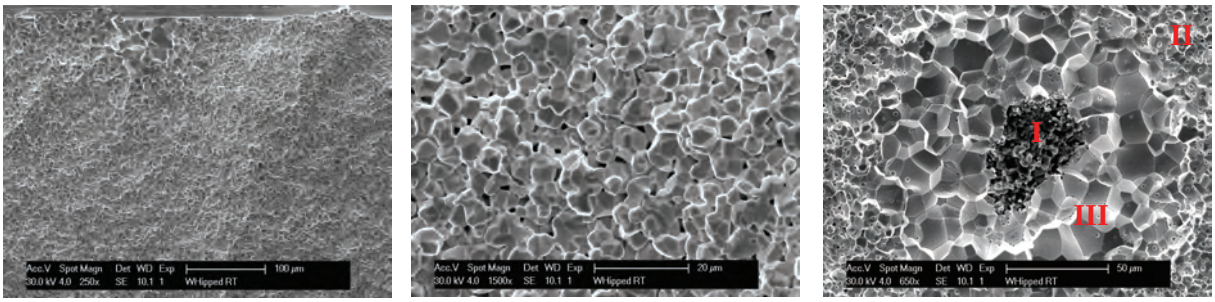

Fig. 4: SEM images of MA and HIPped W alloy after testing at RT. Marked areas correspond to different sintering stages characterized by I) necking between particles and open pore structure; II) neck blunting and channel closure; III) pore break down into discrete pores.

Calculated mode I fracture toughness for MA and HIPped W-2wt.%Y and W alloys is shown in Fig. 5. MA & HIPped W-2%Y shows low, temperature independent fracture toughness which is ascribed to poorly consolidated matrix. HIPped W shows low, weakly temperature dependent fracture toughness which is also attributed to poorly consolidated matrix. The test result at 1000 °C on W-alloy was invalid according to ASTM E399 standard thus giving only a lower bound for mode I fracture toughness.

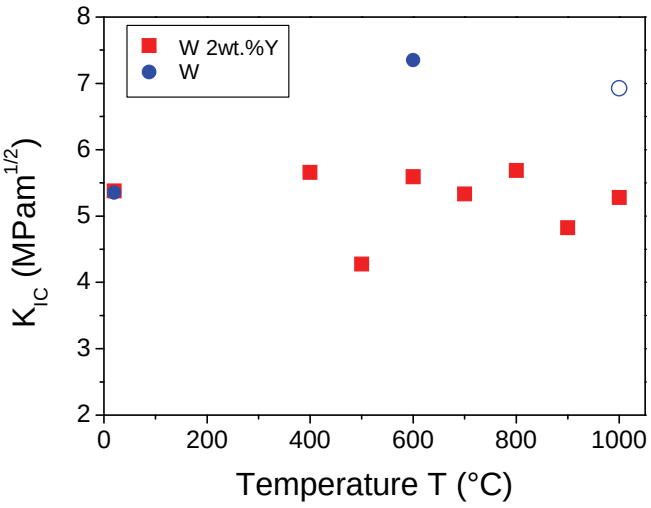

Fig. 5: Fracture toughness vs. test temperature for MA & HIPped W-2%Y and W alloys. The open circle indicates the measurement to be invalid according to ASTM E399 standard thus giving only a lower bound for fracture toughness.

Conclusion and Outlook

Fracture mechanical and microstructural characterization of novel tungsten alloys provided within EFDA "Tungsten and Tungsten Alloys Development" Task Agreement has been performed. The MA and HIPped W-2wt.%Y and W alloys showed low fracture toughness values in the entire test temperature range up to 1000 °C. Brittle fracture with low fracture toughness values are ascribed to a low degree of the material consolidation found by SEM indicating further need of optimization of the process parameter.

FM characterization of tungsten alloy produced by PLANSEE in a powder metallurgical route involving sintering into rods and accompanying forging into round blanks will be performed. Due to specific fabrication route a material revealed an anisotropic microstructure characterized by existence of the platelet shaped grains transverse to the axis of a round blank. Emphasis will be put on the investigation of microstructure and load rate dependence of the fracture toughness (K_{IC}). FM experiments will be accompanied by fractographic and microstructural investigations.

FM characterization of different novel laboratory and industry scale W-based structural materials (W-Ti, W-V, W-Ta) that are being developed under EFDA "Tungsten and Tungsten Alloys Development" Task Agreement will be performed in the interesting temperature window for fusion applications (RT-1300 °C). The J-Integral and/or COD methods will be applied for the investigation of upper shelf fracture toughness. To avoid an expected influence of the loss of the stress concentration at the notched crack tips on the fracture toughness a method for introducing sharp controlled pre-cracks will be developed.

Staff:

U. Bürkle
E. Gaganidze
S. Knaak
D. Rupp

Literature:

[1] D. Rupp, *Bruch und Spröd-duktil-Übergang in polykristallinem Wolfram: Einfluss von Mikrostruktur und Lastrate.* Dissertation, Schriftenreihe Werkstoffwissenschaft und Werkstofftechnik Nr. 61, Shaker Verlag, Aachen, Germany, (2010)

[2] D. Rupp and S. M. Weygand, *Loading rate dependence of the fracture toughness of polycrystalline tungsten.* Journal of Nuclear Materials, accepted (2010)

[3] D. Rupp, R. Mönig, P. Gruber and S. M. Weygand, *Fracture toughness and microstructural characterization of polycrystalline rolled tungsten.* International Journal of Refractory Metals and Hard Materials **28**, 669–673 (2010)

[4] D. Rupp and S. M. Weygand, *Anisotropic fracture behaviour and brittle-to-ductile transition of polycrystalline tungsten.* Philosophical Magazine **90**, 4055–4069, (2010)

Acknowledgement

This work, supported by the European Communities under the contract of Association between EURATOM and Karlsruhe Institute of Technology, was carried out within the framework of the European Fusion Development Agreement. The views and opinions expressed herein do not necessarily reflect those of the European Commission.

Development of Functionally Graded Tungsten/EUROFER97 Joints for Divertor Applications (WP10-MAT-WWALLOY-01-08)

Objectives

Finite element simulations performed so far show that a functionally graded joint between tungsten and EUROFER 97 can drastically decrease the thermal mismatch stresses and strains occurring in divertor components and thus improve their failure behaviour during thermal cycling. However the functionally graded layer shall have a sufficient thickness what has been taken into account in the evaluation of the methods capable for the realization of functionally graded joints. Thereby the magnetron-sputtering (PVD) and the vacuum plasma spraying (VPS) are identified to be eligible and most promising.

Within this work, the fabrication of functionally graded tungsten / EUROFER 97 joints will be investigated considering the PVD and VPS methods. Therefore experiments are foreseen, in which layers with different tunsten/EUROFER 97 compositions will deposited on tungsten substrates. The bonds obtained then are characterized by means of chemical, metallographic and micro-mechanical methods. Their thermal stability at temperatures up to 700°C will be investigated in addition. Based on the results until then first functionally graded layers on tungsten substrates will be produced and analyzed.

Task current status

Homogenous samples at different mixing ratios were fabricated by VPS and PVD. They were analyzed by XRD, nano- and macroindentation, optical and scanning electron microscopy.

Pure tungsten as well as pure EUROFER 97 layers could be sputtered at a thickness of 10 µm on WL10 substrates, showing a good quality with non-detectable porosity. However, layers with mixed ratios could be only fabricated with a thickness of 2 µm. High hardness values and a slight peak broadening in the x-ray diffraction pattern indicate a nanocrystalline structure and a high dislocation density. Tungsten concentrations ranging from 30 at.% to 90% could be achieved along the different samples. The feasibility of a full gradation range was tested with the help of shielding plates. Tests concerning the thermal stability of the coatings have to be postponed until functional graded layers are produced, since thermal mismatch between tungsten substrate and coatings with high steel content is too large for a heat treatment at 760 °C.

The porosity of the plasma sprayed layers could be reduced to a level lower than 4% in a second experimental run. The microscopic images prove the melting of both materials by their arbitrary shape and distribution. The Brinell-Hardness values of the mixed composites were found between those of pure tungsten and EUROFER 97. Heat treatments will follow soon.

Further finite element simulations were performed to access the expected lifetime of an ideal functionally graded joint. Hereby only the EUROFER 97 and tungsten sections of the thimble were considered which was based on the availability of time-to-rupture and fatigue data for both materials. First results showed that functionally graded joints provide a large gain in lifetime compared to brazed or direct joints. Due the conservatism of the rules used the allowable lifetime calculated for functionally graded joints is not fully sufficient. Therefore a more sophisticated analysis shall reveal the real expectable lifetime. The use ODS-EUROFER 97 instead of EUROFER 97 shall be evaluated in addition.

While for the EUROFER 97 section the most likely failure mechanism is creep damage, it is spontaneous brittle fracture at low temperatures for the tungsten section. Therefore a probabilistic approach has been considered which allows the estimation of failure probability for the tungsten section on the base of Weibull parameters of tungsten. These parameters were

determined for WL10 (rolled rod material by Plansee AG) at room temperature performing and evaluating a statistically sufficient number of four point bending tests.

Staff:

J. Aktaa
T. Weber

Literature:

[1] T. Weber, J. Aktaa, S. Ulrich, M. Stüber, Fabrication and Characterization of Magnetron Sputtered Tungsten/EUROFER 97 Coatings, CIMTEC 2010, Montecatini, Italy, 2010

[2] T. Weber, J. Aktaa, Numerical Assessment of Functionally Graded Tungsten/Steel Joints for Divertor Applications, Fusion Engineering and Design, submitted, 2010

Acknowledgement

This work, supported by the European Communities under the contract of Association between EURATOM and Karlsruhe Institute of Technology, was carried out within the framework of the European Fusion Development Agreement. The views and opinions expressed herein do not necessarily reflect those of the European Commission.

Development of Diffusion Bonded Tungsten / EUROFER 97 Joints (WP10-MAT-WWALLOY-01-09)

Objectives

In the helium cooled divertor, which should withstand a heat flux up to 10 MW/m², tungsten shall be used as a shield as well as a structural material. Its use as a structural material however is limited to the high temperature parts which shall be connected by means of solid state diffusion bonding to the low temperature parts built from the reduced activation ferritic/martensitic steel EUROFER 97. The method for realizing such kind of joining is restricted by a lot of problems related to the large differences in their melting temperatures and coefficients of thermal expansion (CTE). The latter causes high thermally induced residual stresses at the interface, while the joined materials are cooled down from the process temperature to the ambient temperature (RT). According to earlier investigations [1], the bonded samples possessed a very high strength. The bonding seams were very brittle and were not able to endure the thermal loading and therefore failed during PBHT (post bonding heat treatment). To solve the problem above, V interlayer with CTE among that of both materials to be joined is introduced.

Task Current Status

Within the time period reported here, diffusion bonding experiments using V interlayer were performed to investigate the feasibility of joining between W and EUROFER 97. The bulk materials used in this work were an 18 mm diameter polycrystalline W rod with a purity of 99.96% manufactured by Plansee Metall GmbH and a 25 mm thick EUROFER 97 plate (2nd batch with a heat number of 993402). The commercial V plate used as interlayer had a thickness of 1 mm with a purity of 99.9%. As bonding specimens, the tungsten-rod was cut by EDM (Electrical Discharge Machining) in a length of 16 mm, the EUROFER 97-plate in a diameter of 18 mm and a length of 22 mm with a bonding surface parallel to the rolling plane. The V interlayer was cut to a disc with a diameter of 18 mm. Before diffusion bonding, the specimens were ground and polished to remove the surface impurities containing carbides and oxides. These impurities were found out especially on the surface of the V plate (about 30 nm thick) by means of AES (Auger electron spectroscopy). To exclude significant influences of the surface parameter on diffusion bonding results, the surfaces of all specimens were polished up to a surface roughness $R_z \leq 1$ µm. After the cleaning procedures, the specimens to be bonded were piled on each other with the interlayer inserted between EUROFER 97 and W, and then diffusion bonded in the vacuum furnace (5×10^{-5} mbar). The diffusion bonding experiments were hold in true stress mode. Subsequently, PBHT was carried out at 760 °C for 90 min.

The first experiment was performed at the maximum bonding temperature allowed for EUROFER 97 (1030 °C) and the stress was calculated to 5% creep deformation on the EUROFER 97 side and for a bonding duration of 1 h. After machining in small specimens, it is evident that the bonding seams were sound and free of cracks as shown in Fig. 1. It seems that the V interlayer can reduce the residual stress caused by the CTE mismatch of tungsten and EUROFER 97 and improve the bonding even when PBHT was performed. At the bonding seam of EUROFER 97/V in Fig. 1a, a narrow dark and discrete region with a thickness of about 5 µm was formed. According to the chemical concentration distribution analysed by AES, this region consisted of vanadium carbides as a result of the decarburization of EUROFER 97 and the diffusion of C in the V interlayer. On the other side, V diffused in the EUROFER 97 up to a thickness of about 100 µm from the interface. This process is believed to induce the formation of ferritic microstructures and grain growth (Fig. 2a). Below this region and up to the next 100 µm depth, the ferritic microstructures and the grain growth were assumed to be caused by the local reduction of C content. On the other side, at the bonding interface of V/W, no reaction region was recognized in Fig. 1b and 2b. Furthermore it was

evident, that the grains of the V interlayer coarsened since the bonding temperature was much higher than its recrystallization temperature, which is about 800 °C.

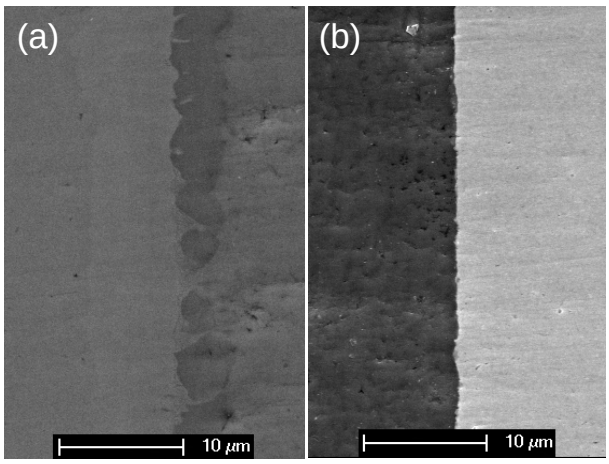

Fig. 1: SEM photomicrographs at bonding interfaces between a) EUROFER 97 and V interlayer, b) V interlayer and W.

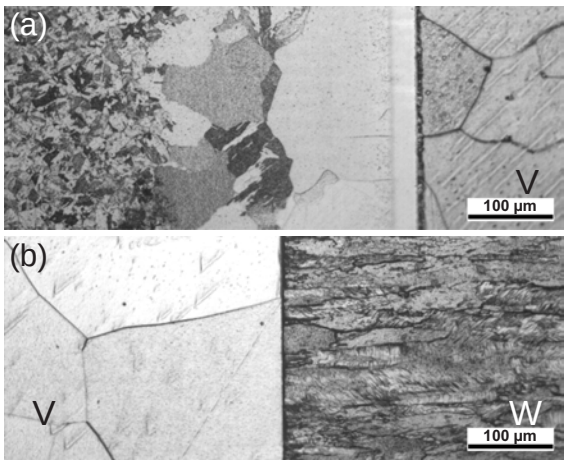

Fig. 2: Microstructure at the interfaces between a) EUROFER 97 and V interlayer, b) V interlayer and W.

For getting information about the mechanical properties, the bonded specimens were investigated by tensile and Charpy impact testing at RT and 550 °C. For the tensile tests cylindrical specimens were used with a diameter of 2 mm and gauge length of 7 mm with V interlayer in the middle of it. For the Chapy impact tests, KLST specimens were used with the notch placed among the cross section of V interlayer. The results as listed in Table 1 showed that the toughness of the bonding seam at RT reached about 73% of that of W and at 550 °C about 21%. The tensile strength σ_{UTS} at RT was about 31% of that of EUROFER 97. At test temperature of 550 °C, it was about 50% of that of EUROFER 97 with a marginal plastic strain of 0.06%. It must be mentioned, that the strain seams to be too low, if it was assumed that at this level of tensile stress, bulk materials did not deform plastically. All specimens failed at the interface between EUROFER 97 and V. The investigation on the fracture surface of tensile specimens showed cracks around the grain boundaries. The XRD analysis on a fractured specimen tested at RT confirmed the existence of vanadium carbides on both sides of fractured surfaces.

Table 1: Mechanical properties of diffusion bonded specimens and the bulk materials in as-obtained condition for comparison.

	RT			**550 °C**		
	joint	W	EUROFER97	joint	W	EUROFER97
α_v (J/cm²)	1.21	1.66	107	1.42	6.70	
σ_{UTS} (MPa)	207.3	1260	663	172.0	428	345
$\sigma_{0.2}$ (MPa)	---	1252	544	---	399	322
A (%)	---	0.41	24.80	0.06	29.08	21.55

For improving the mechanical properties of the bonding specimen, the thermally induced residual stresses at the bonding seam and the thickness of the metal carbide layer must be reduced. This can be realized by decreasing the process temperature. According to this idea, the diffusion bonding was performed for 1 h and at a constant bonding temperature of 800 °C, at which the V interlayer did not recrystallize. The compression stress was chosen to be 60 MPa, such that the creep strain can be kept constant at 5%. The results of microstructural investigations indicated a small reaction zone at the interface of EUROFER 97/V, which was definitely much narrower than that of the specimen bonded at 1030 °C. Tensile tests and Charpy impact tests were also carried out at RT and at 550 °C. The results are presented in Table 2 and Table 3 respectively. For specimens tested at RT, no significant changes can be

found. At a test temperature of 550 °C, the improvement in strength and toughness was noticeable. Compared to specimens bonded at 1030 °C, the bonded specimens showed 22% higher strength. They yielded plastically and experienced necking with a high strain to rupture of about 3.11%. The Charpy impact test showed a high impact toughness, which was more than 50% than that of W. By investigating the surfaces of fractured tensile specimens, no cracks were found at the grain boundaries.

Table 2: Mechanical properties of specimens bonded at 800 °C and tested at RT.

Bonding parameter	α_v (J/cm²)	σ_{UTS} (MPa)	$\sigma_{0.2}$ (MPa)	A (%)
800 °C / 60 MPa / 1 h	1.08	214	---	0.1
800 °C / 60 MPa / 2 h	1.04	215	---	0.1
800 °C / 60 MPa / 4 h	1.17	220	---	0.1

Table 3: Mechanical properties of specimens bonded at 800 °C and tested at 550 °C.

Bonding parameter	α_v (J/cm²)	σ_{UTS} (MPa)	$\sigma_{0.2}$ (MPa)	A (%)
800 °C / 60 MPa / 1 h	3.42	209	159	3.11
800 °C / 60 MPa / 2 h	4.02	192	148	2.21
800 °C / 60 MPa / 4 h	2.58	182	---	0.1

It is also generally known, that the bonding duration has an influence on the mechanical properties of the bonded specimen. By increasing the bonding duration, the closure process of the voids at the bonding interfaces will be enhanced by diffusion mechanisms. On the other hand, if the bonding duration is too long, the interdiffusion across the bonding interfaces will be predominant. In the case of diffusion bonding between EUROFER 97 and V, it means that the metal carbide layer can be much broader and consequently the toughness at the bonding seam is reduced significantly. Therefore diffusion bonding processes were performed for 2 h and 4 h. The other bonding parameters were kept constant (T = 800 °C and σ = 60 MPa). The creep strains were about 6% and 8%, respectively. As presented in tab. 2, the mechanical properties of the bonded specimens tested at RT did not change significantly. At a test temperature of 550 °C, it was found in tab. 3 that the impact toughness was improved from 3.42 J/cm² for bonding duration of 1 h to 4.02 J/cm² for 2 h. It means that about 60% of the impact toughness of W was reached. While tensile tested, the specimen bonded for 2 h deformed plastically and also experienced necking with a relatively high strain to rupture of about 2.21%. By increasing the bonding duration to 4 h, the impact toughness decreased substantially. The tensile strength was reduced and the strain to fracture was negligible.

Staff:

J. Aktaa
W. W. Basuki

Literature:

[1] W.W. Basuki, J. Aktaa, submitted to J. Nucl. Mater. (2009).

Acknowledgement

This work, supported by the European Communities under the contract of Association between EURATOM and Karlsruhe Institute of Technology, was carried out within the framework of the European Fusion Development Agreement. The views and opinions expressed herein do not necessarily reflect those of the European Commission.

Development of W-EUROFER & W-W Brazed Joints. Commercial Joints Deposited by Electro-Chemical Methods: (i) Aqueous Electrolytes and (ii) Organic Electrolytes (WP10-MAT-WWALLOY-01-03)

Introduction

The helium cooled divertor concept, which is projected to remove heat loads of up to 15 MW/m², is based on a modular arrangement of cooling fingers. Designated materials are tungsten-alloys due to e.g. the high melting temperature and the excellent heat conductivity and EUROFER steel. Fig.1 shows a sketch drawing of the finger layout together with the temperature loads in the joining areas between tile – thimble and thimble – steel housing. From the plasma facing material (tile) with the highest temperature (approx. 1700 °C at the surface), the heat is transferred via tungsten alloy e.g. WL10 (acting as structural material) to the cooling gas He. In the lower part the W-alloys are connected to the steel base fabricated from EUROFER or ODS-EUROFER.

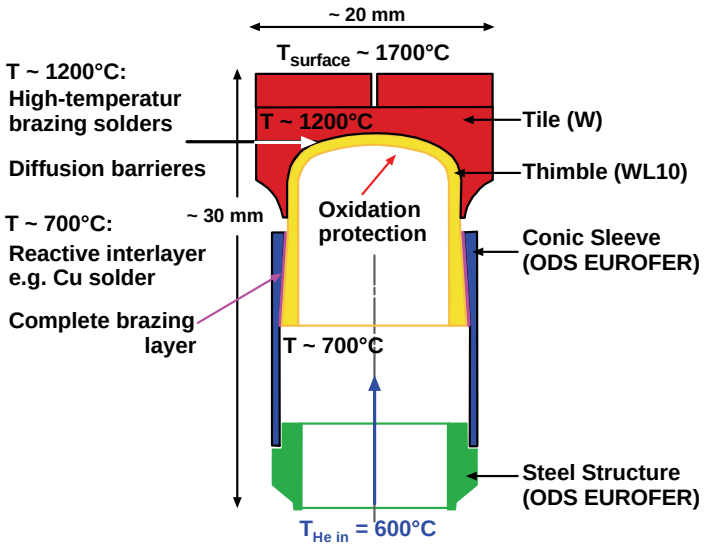

Fig. 1: Positions in the divertor finger layout for brazing layers.

All these components have to be connected precisely, and have to withstand high mechanical and thermal stresses without any danger of failure. This duty shall be done by brazing materials, where the solders besides a force-fit connection guarantee also a certain ability to compensate mechanical stresses coming from the highly different thermal expansion coefficients.

The two indicated joining positions in the divertor have different demands to fillers:

a) The connection between tungsten tile and tungsten/WL10 thimble in the upper part of the finger design. This connection has functional characters and must withstand temperatures of approx. 1250 °C; here exists a high chemical metallurgical similarity of the both metal sides, but the high temperatures reduce drastically the choice of convenient materials for brazing.

b) The connection between tungsten thimble and steel sleeve (ODS-EUROFER) at lower position. The operation temperatures are about 700 °C; but here the connection underlies high pressure forces (80 bar cooling gas pressure). The connection must be gastight, furthermore stable also under cycling conditions with repeated cold-warm changes. Fig. 2 shows such an arrangement with copper casting for tungsten steel connection as demonstrated within the KIT – Efremov cooperation. However, copper acts here as a type of rubber sealing due to no metallurgical bonding to tungsten.

Fig. 2: Assembled cooling finger by copper casting

Here, the differences in thermal expansion coefficients are drastic, and the metals with completely different chemical properties have to be connected by a solder with a contact affinity to both sides. In the illustrated assembling the Cu is casted into the gap but no brazing to

tungsten takes place. If Cu should be used as filler metal a functional scale on top of the tungsten part is required to allow a metallurgical reaction and alloy formation for good adhe - rence. Nickel beyond some other elements may be such a metal which has affinity to both copper and tungsten and will be model metal for first tests.

For the suitable brazing solders materials arises the question to manufacture the layers se - lectively at the desired positions, even with a high degree of uniformity and reproducibility. In the light of the needed numbers of divertor units, which have to be produced in mass - production, also economic aspects are not negligible.

Electrochemical metal deposition

Electro-chemistry allows the deposition of metallic layers on a solid substrate from a liquid system. Galvanic depositions from aqueous systems generally take place in temperature regions of < 100 °C. So far, the electroplating does not affect the substrate by thermal forces. Moreover, because of the fact, that the deposition takes place from a liquid system under normal pressure without any further force (besides the electric voltage), the solid substrate material is not affected by any mechanical stresses; which is important for brittle substrate materials. Electro-chemical deposition is also one of the few techniques, where deposition on the surface all over the substrate can take place simultaneously and scale thicknesses are controllable by the process parameters current density and time.

Liquid media (electrolytes) in electro-chemical technology are mostly based on aqueous sys - tems looking on common metals like copper or gold, however, for more reactive metals liquid organics, aprotic media, have to be used and are under investigation since some time. The first group comprises the transition metals e.g. iron, copper, silver, palladium, nickel and chromium, which are used in electro chemical coating technology and electroforming since long times. Thus, a good knowledge in scale deposition is available e.g. as protective scales. However, application with respect to joining of unconventional metal combinations e.g. braz - ing of tungsten onto EUROFER steel is missing. Additionally, tungsten and its alloys are in electro-chemical coating technique no common materials. All technical electrolytes used in industrial coating technique exhibit mostly acidic pH-values, in which tungsten easily forms passivating oxide layers.

Targets of brazing development

For the task of joining under WP10-MAT-WWALLOY investigations were carried out compris - ing following aspects:

- Development of electro-chemical technologies based on commercially known filler compositions out of the Group VIII and IB elements from aqueous systems for brazing of divertor components. The main goals are here analyzing deposition on tungsten and brazing conditions incl. the metal / filler reactions under load conditions.
- Development of surface conditioning tools for coating of tungsten, multi-layer deposi - tion of e.g. Ni, Pd and Cu, as well as analyzing of inter-diffusion during heat treatment up to 1100 °C.
- Fabrication of demonstrators brazed by electrochemically deposited scales for W - steel and W – W joints.
- The next main step is development of electro-chemical coating technologies for deposi - tion of ‘refractory metals’, suitable for designing advanced brazing metals under fusion aspects. The name ‘refractory metals’ indicate here Group VB and VIB elements like W, Ta to Ti which in difference to other transition metals, cannot be deposited from aqueous electrolytes due to their chemical and electrochemical nature (elementary reaction with water). The technological challenge is to evaluate appropriate aprotic resp. non-aqueous electrolytes of type ionic liquids (IL) and IL-metal combinations in

conjunction with adjusted concentrations and current/voltage parameters for deposition.

Results

Substrate surface characterization and pretreatment

The nature of the tungsten parts, which are commonly machined by EDM or turning, became an important aspect for the deposition. E.g. EDM cuts reveal often a much distorted surface with cracks of about 30-100 µm and reacted surface layers. These surface films have to be removed to guarantee a good wetting by the electro-chemically deposited scales. Thus, a pretreatment process based on (electro) chemical etching technology for the machined tungsten parts was analyzed. The tested variants are listed in Tab. 1. Valuing process stability, availability in industries and environmental aspects an etching media based on $K_3[Fe(CN)_6]$ * KOH was selected, which showed best homogeneous scale removal and only small surface roughing. Electrochemical Ni deposition applied as model substance showed excellent moulding and wetting on these pretreated surfaces and thus confirmed the suitability of the chosen reactant.

Table 1: Surface activation of tungsten by current less etching with respect to scale adherence in joining and environment.

No.	Chemical agent	Valuation
1	$K_3[Fe(CN)_6]$ * KOH	Small roughening, Good adherence
2	$HNO_{3\ (conc.)}$ * HF	High temp. process, HF risk
3	KOH	Polishing, lower adherence
4	NaOH * $KMnO_4$	Multi step process, cleaning
5	HCl * H_3C-COOH	Roughening, inhomogeneous
6	NH3 * $NaNO_3$	Polishing, lower adherence

From aqueous systems deposited scales for tungsten – EUROFER joining

The pretreatment of tungsten parts was done applying an alkaline hexacyanoferrate solution as suitable etchant for the nickel depositon. The electrolyte for nickel deposition consisted of a mixture of 410 ml/l commercial nickelsulphamate (76 g/l Ni^{2+}), 35 g/l Boric acid, 0, 15 g/l fluorinated tensile and a non dimension-stable nickel anode. Further deposition parameters were. T = 52 °C and pH = 3,3 - 3,5. The current density with homogeneous coating behaviour was found to be optimal near i = 10 m A/cm². The scale thickness is adjustable easily by deposition time in the range 5 to 100 µm depending on the requirements of joining. Homogeneous coatings below 5 µm require however surface roughness below 1 µm of machined parts.

The model element nickel was deposited on both joining parts, tungsten and EUROFER, to activate the surface for joining by copper. On the functional nickel layer the filler metal copper was deposited from a sulphuric acid electrolyte. Optimal copper layers were achieved from a mixture of 120 g/l $CuSO_4$ in 120 g/l H_2SO_4, 0.19 ml/l HCl and 10 ml tensile Solution Primus CD KN 438021. A copper anode was applied to keep Cu concentration stable in the electrolyte. A current density of i = 30 mA/cm² was used in a well stirred bath at room temperature.

The coated parts were assembled and heated in an Ar atmosphere for brazing. Brazing time was varied for optimization of the joints. Fig. 3 shows the SEM picture and the line scan of a cut through a W-EUROFER joint. Fig. 3 shows a brazed part consisting of a EUROFER plate and a tungsten disc with roughly 16 mm diameter.

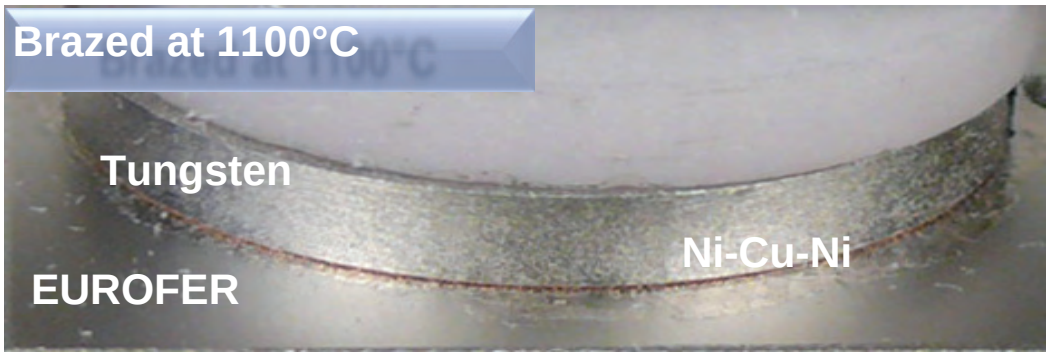

Fig. 3: Tungsten – EUROFER demonstrator joined by electrochemically deposited scales.

Tungsten – tungsten joining by electrochemically deposited scales

Due to the immiscibility of copper and tungsten it is not possible to deposit copper on tungsten direct as a brazing layer. Therefore an interlayer has to be used to overcome this lack if copper is the desired filler metal. The criteria to select such a metal are that at least a limited solubility of tungsten exists in this metal and that at optimal condition a solid solubility with the filler metal occurs. Due to low cost and high knowledge in deposition technology Ni was selected as model substance to study the deposition and brazing processes. Under later fusion conditions Ni has to be replaced by e.g. Pd with similar metallurgical behaviour.

Deposition parameters were similar to the steel – tungsten testing. Fig. 4 shows a brazed demonstrator. On both W-discs an activation layer of about 10 µm was deposited. The scale thickness of the filler metal Cu was roughly 70 µm. The microcut depicted in Fig. 5 shows that a good wetting of the parts is achieved during brazing at 1100C under Ar-atmosphere.

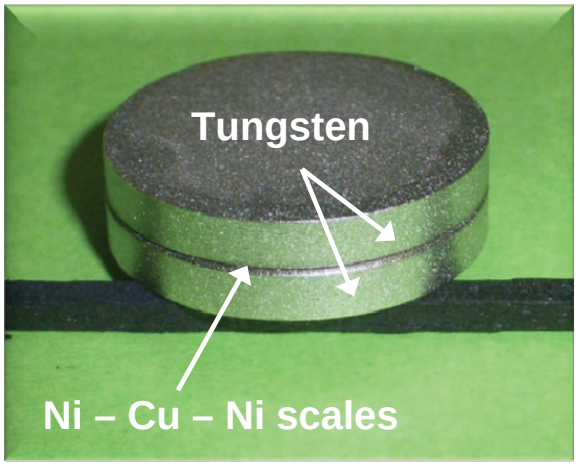

Fig. 4: Tungsten- tungsten brazed demonstrator.

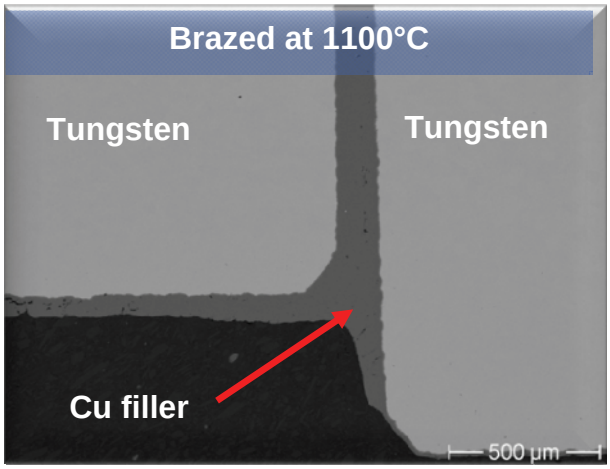

Fig. 5: Microcut through brazed W-W demonstrator.

An increase of application temperature of the brazed components above the melting temperature of the filler metal pure copper (~1083 °C) is possible in binary metal systems with formation of solid solutions if the second component has a higher melting point than copper. The system Cu-Ni is such a representative combination. Successfully was shown that alternating Cu and Ni scales can be deposited to obtain after heat treatment (brazing) due to occurring diffusion Cu-Ni mixtures with higher melting point. The melting point of the solis solution can be roughly estimated by a linear fit of the pure metal melting points weighted with the chemical composition. As an example may be given Cu44Ni with a melting temperature of roughly 1250 °C. The evaluated parameters will be used for future tests with the system Cu-Pd which is of similar nature.

Deposition from non-aqueous electrolytes e.g. W deposition

In comparison to transition metals like Fe, Pd and Ni, tungsten is by its electrochemical standard potentials much more noble, and therefore, should be in theory better applicable in electro-chemical deposition technology. But the standard reaction is bound to a reaction with water and intermediate formation of tungsten hydroxides. As result, the aqueous deposition of tungsten from water is more or less workable, but the deposition of pure tungsten metal not realizable, due to incorporation of a high percentage of oxides.

Here the absence of water during deposition is afforded. Such aprotic electrolytes were mostly molten salt systems in the past with all the disadvantages of high temperature electrolyte systems. Electrolytes of type ionic liquids (IL), which are also molten salt systems, of organic amine cations, as result with drastic reduced melting temperatures, can open new paths in electrochemical deposition if a suitable combination of IL and metal salt, a TCILE, a Two Component IL Electrolyte can be designed / evaluated for deposition of refractory metal e.g. W, Ta or Ti. Due to the good knowledge of tungsten behaviour in ECM processing (Electro Chemical Machining) tungsten was selected as model alloy out of the refractory metals for deposition from the new class of electrolytes.

The used Ionic Liquid was the first commercial available IL, Ethyl-Methyl-Imidazolium Chloride (EMIM-Cl), which revealed already as a suitable electrolyte type for Al-deposition on EUROFER for formation of corrosion and tritium permeation barriers [1, 2].

The investigation of the EMIM-Cl tungsten systems revealed drastic differences to Al systems. The mixed EMIM-Cl and WCl_6 as tungsten carrier does not form a room temperature liquid, but rise the melting point up to 120 °C (pure EMIM-Cl: 80 °C). As consequence, low viscous solutions can not be handled below 150 °C working temperature. Metallic tungsten scales could be successfully deposited with a thickness of roughly 20 µm. This result indicates that the electrolytes of type IL open the path for electro-chemical deposition of refractory metals which can be used as diffusion barriers or as filler metals. It has to be considered in the next steps of the development work that EMIM-Cl has not to be the best IL in coating development and that additional potentiometric measurements are absolutely necessary to determine optimized deposition parameters for improved scales and more reactive metals like Ta.

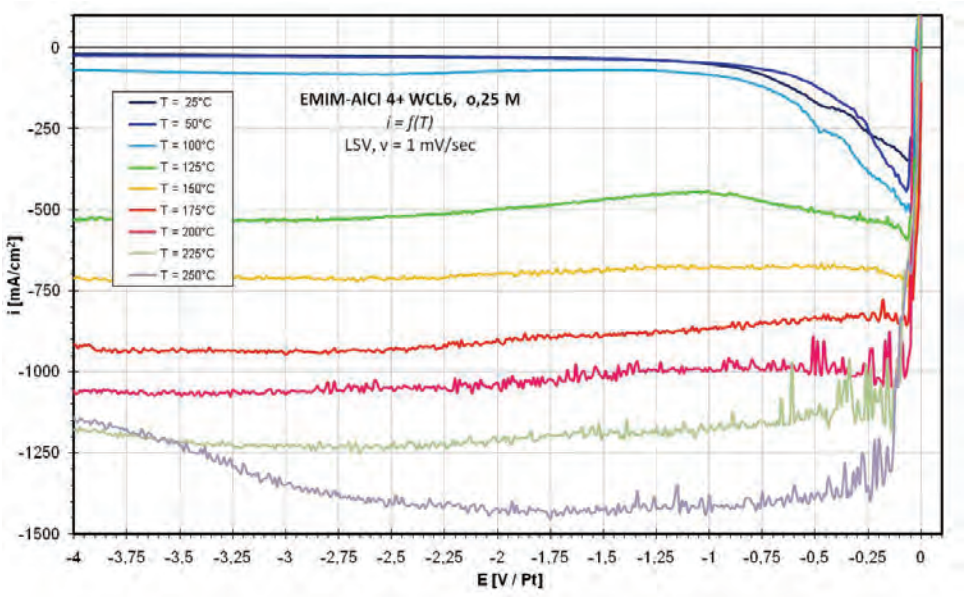

Fig. 6: LSV of a IL-tungsten solution, showing drastic increase of current density at temperatures from RTIL temperatures up to > 200 °C.

For this reason, investigations of advanced tungsten chloride system were carried out with focus on the voltammetric measurements (linear and cyclic) under different physical parameters and different chemical compositions. Fig. 6 shows the curves of linear scanning voltammetry of WCl6 in EMIM-AlCl4 salt mixture, and. indicates a strong rise of the conductivity with rising temperatures. It is visible, that in such systems high currents will be achieved only at significant higher temperatures, because then the typical high viscosity is minimized to sufficient low values.

Conclusion

The development of suitable and long term stable joints for He cooled divertor fingers is essential for the successful operation of this design. Challenging are both required joints, the steel / W alloy combination due to the high expansion mismatch and the strong differences in alloy characteristics and the high temperature brazing of the W alloys between tile and thimble. The general screening has shown the needs for functional interlayer's to allow brazing instead of only casting or to suppress inacceptable diffusion reactions and last not least the homogenous coating and complete wetting of surfaces to be joined.

Driven by this facts and requirements of He cooled finger joining the development of electro chemical coatings was started. In the first step commercially used filler metal combinations were selected for the deposition process. As electrolytes water based systems were investigated. The performed tests showed that especially tungsten has to undergo a surface cleaning and conditioning due to oxide / hydroxide scales before any coating is performed. It was demonstrated that copper brazing instead of only casting of tungsten can be applied if functional scales were deposited on tungsten. Performed heat treatments and pre-brazing studies imply that such scales may be in the dimension of roughly 10 µm. A homogeneous coating of tungsten was successfully achieved by Ni deposition as functional inter layer which was subsequently electro chemically coated by a Cu layer which acts as filler metal in tungsten – EUROFER brazing. The performed analyses indicate a high rate of reproducibility and excellent wetting of the joining parts a condition for defect free brazing. This positive results in application of electro chemical deposition of coatings point out that this technology can be applied in combination with fusion relevant alloys like tungsten and EUROFER steel. Additionally was shown, that multi layer systems can be deposited to form higher melting solid solutions during brazing at moderate temperature. Modification of filler metals and functional scales (e.g. Fe, Pd instead of Ni) will be the focus of next steps in the development of electro chemical brazing tools from aqueous systems.

Diffusion barriers and high temperature fillers require combinations of / or with refractory metals (e.g. W, Ta or Ti type). However these elements can not be deposited from aqueous electrolytes due to e.g. oxide formation. Thus an alternative and innovative development line in electro chemical deposition technology based on the use of novel ionic liquids as electrolytes was started to have access to the unique properties of these elements in high temperature application. For first evaluation of the applicability of IL as electrolytes the aprotic component EMIM-Cl was selected. Basic potentiostatic investigations were performed in combination with metal salts e.g. WCl_6 to demonstrate and verify the applicability and syntheses of electrolytes suitable for metal deposition in general. Based on these successfully performed pretests tungsten deposition from electrolytes liquid near room temperature could be performed for the first time. The deposited tungsten scales had a thickness of roughly 20 µm and good adherence to the base material EUROFER steel. The further development in aprotic systems will include also other IL and refractory metals with focus on high temperature W&W alloy brazing.

Staff:

N. Holstein
J. Konys
W. Krauss
J. Lorenz

Literature:

[1] N. Holstein, W. Krauss, J. Konys: Development of advanced Al coating processes for future application as anti-corrosion and T-permeation barriers, Fus. Eng. Design, 85, (2010), 2141-2145.

[2] W. Krauss, N. Holstein, J. Konys, H. Zimmermann: Al-based anti-corrosion and T-permeation barrier development for future DEMO blankets, Fus. Eng. Design, to be published.

[3] N. Holstein, W. Krauss, J. Lorenz, J. Konys: Electro-chemically-based technologies for processing of tungsten components in fusion technology, First International Conference on Materials for Energy 2010, Karlsruhe/Germany, July 4-8, 2010.

[4] N. Holstein, W. Krauss, J. Konys: Alternative electro-chemically based processing routes for joining of plasma facing components, Poster, SOFT-26, Porto/Portugal, September 23 – October 1, 2010.

[5] N. Holstein, W. Krauss, J. Konys: Development of novel tungsten processing technologies for electro-chemical machining (ECM) of plasma facing components. Fus. Eng. Design, available online December 2010.

[6] W. Krauss, N. Holstein, J. Konys: Advanced electro-chemical processing of tungsten components for He-cooled divertor application, Fus. Eng. Design, 85, (2010), 2257-2262.

Acknowledgement

This work, supported by the European Communities under the contract of Association between EURATOM and Karlsruhe Institute of Technology, was carried out within the framework of the European Fusion Development Agreement. The views and opinions expressed herein do not necessarily reflect those of the European Commission.

Post Irradiation Examination (WP10-MAT-WWALLOY-04-02)

High temperature alloys (such as tungsten) are assumed to be primary materials candidates for structural application in the divertor. Different tungsten materials will be base characterised at RT by instrumented indentation. Registering hardness tests (Vickers, Rockwell, and Berkovich) are performed, in a further step at higher temperatures and in irradiated condition.

The applicability of the indentation method for bulk material and even for porous tungsten coatings could be demonstrated with indents made in a cross-section of a polished W-coating deposited on an Eurofer substrate (plasma-spray, material furnished by IPP Garching).

In preparation for the tests at high temperatures and on irradiated material, the update of an indentation device for unirradiated reference-experiments was done. In combination with a second generation neural network based analysis method, the identification of viscoplastic material parameters from small tungsten specimens was carried out.

For a future investigation of irradiated tungsten, there were made initial tests on unirradiated tungsten samples. These experiments were done to test the general feasibility of indentation tests on a wider range of materials then done so far. The experiment series contained cyclic indentation tests on different tungsten samples, provided by IPP. Due to their size, the samples have to be mounted on a specimen holder. The first task was to identify and compensate the combined holder's and machine's stiffness. For the same indentation depth, the force values differ on polycrystalline and single crystalline bulk material, as seen in Fig. 1. The different crystal orientations (100 and 110) of the latter cannot be seen in the force-displacement data, but in an anisotropic pile-up round the indents (see Fig. 2). For a correct analysis using the neural networks the determination of the pile-up is essential.

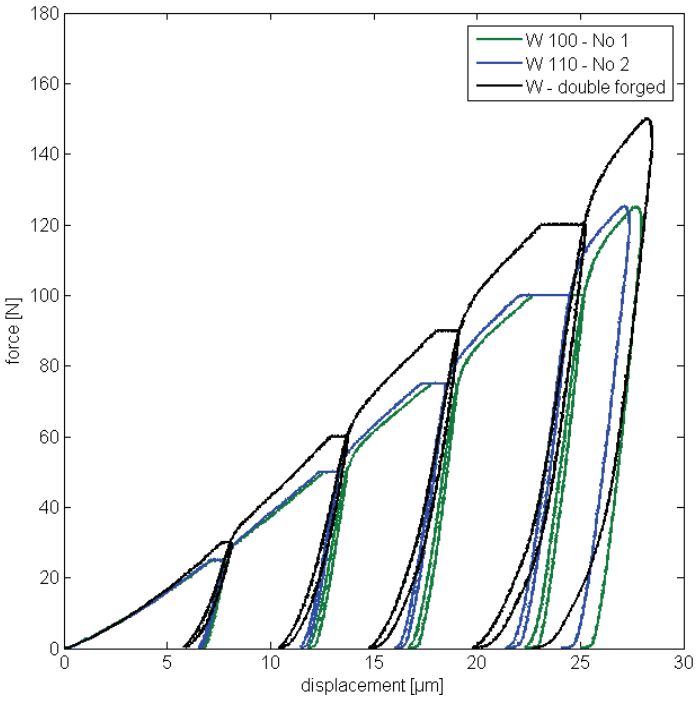

Fig. 1: Load-displacement curves for W-poly- and single crystals of different orientation.

In addition, preparing work for fracture mechanical characterization was done by investigation of cube-corner indents and the crack initiation in the area of highest stress concentration of the tetraedical indent. The development and procurement of the high-temperature indentation devices is still going on.

Future activities:

- Basic Characterisation of different tungsten materials
- Determination of the pile-up-factor
- Investigation on deformation behaviour of single crystalline tungsten
- Characterisation of irradiated tungsten by instrumented indentation
- Installation of two different high temperature indentation devices
- device 1 for temperatures up to 650 °C and forces up to 200 N
- device 2 for temperatures up to 1000 °C and forces up to 2 N

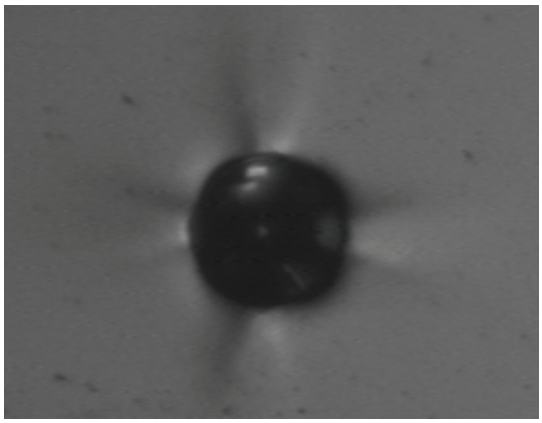

Fig. 2: Anisotropic pile-up around an indent in a W-single crystal

Staff:

B. Albinski
S. Lautensack
I. Sacksteder
H.-C. Schneider

Literature:

[1] Sacksteder, I., Schneider, H.-C.: Further characterization of irradiated steels by indentation at high temperature. 26th Symp.on Fusion Technology (SOFT 2010), Porto, P, September 27 - October 1, 2010, paper to be published in proceedings.

Acknowledgement

This work, supported by the European Communities under the contract of Association between EURATOM and Karlsruhe Institute of Technology, was carried out within the framework of the European Fusion Development Agreement. The views and opinions expressed herein do not necessarily reflect those of the European Commission.

Mechanical Characterisation of W-Armour Materials (WP10-MAT-WWALLOY)

Background and Objectives

Tungsten and tungsten alloys are presently considered for helium cooled divertor and possibly for the protection of the helium cooled first wall in DEMO designs, mainly because of their high temperature strength, good thermal conductivity, and low sputter rates. There are two types of applications for these materials which require quite different properties: one is the use as plasma-facing armour or shield component, the other is for structural purposes. An armour material needs high crack resistance under extreme thermal operation condition while a structural material has to be ductile within the operation temperature range. Both material types have also to be stable with respect to high neutron irradiation doses and helium production rates.

The part protection materials development focussed on an optimisation of armour materials and high heat flux testing. Candidate materials have to be characterised by fatigue and shock tests for an assessment of their possible lifetimes. Additionally, basic mechanical characterisations have to be performed on new developed materials, to support the alloys optimisation processes.

The objective is a mechanical characterization of the selected W-ODS materials, based on tensile tests, LCF tests and TMF tests in the interesting temperature region for fusion applications (up to 1600 °C).

Status January 2010

The first new developed W-ODS material (W-2%Y) was provided by PSI – CRPP (Switzerland) in form of one small mechanically alloyed ingot (d = 26 mm, l = 36 mm).

Actual Status

In addition to the small sintered ingot, some small rods from the same material, but additionally mechanically compacted, were provided also by PSI – CRPP in June 2010. From both the ingot and the rods sub-sized tensile specimens were fabricated by EDM technique and tested. It was found, that the mechanically alloyed W-2%Y material shows a ductile to brittle transition temperature (DBTT) of ca. 1200 °C, whereas the DBTT of the additionally compacted alloy is slightly higher. Compared with the not compacted W-2%Y, the compacted alloy in general is less ductile and has a lower strength as one can see in Fig. 1.

Conclusion and Outlook

The first new developed W-ODS material (W-2%Y), provided by PSI-CRPP was tested. Unexpectedly, the mechanical properties of the not compacted material are clearly better than the properties of the compacted material. It is planned to modify the fabrication process and to perform further tests on the optimised alloy. Additionally, it is planned to investigate the mechanical behaviour of another W-ODS alloy (system W-Cr-Si), which will be produced and provided by CEIT (Spain, San Sebastian).

Staff:

M. Walter

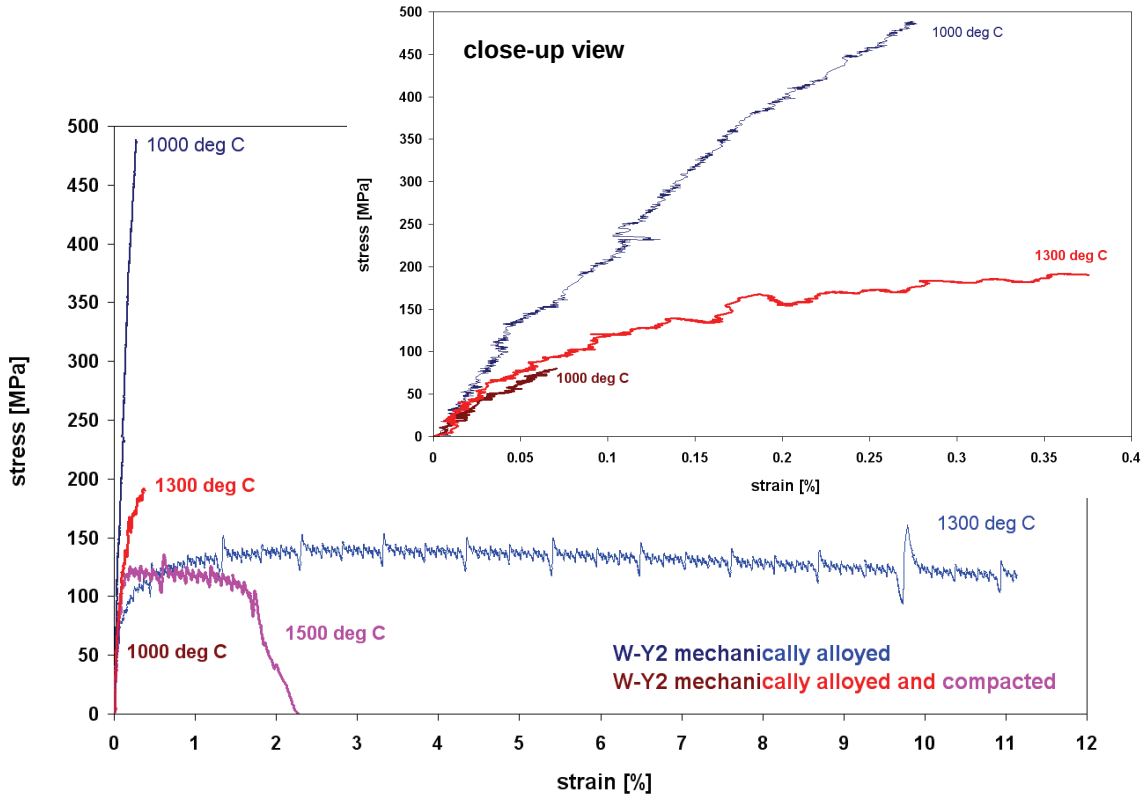

Fig. 1: Results of tensile tests on mechanically alloyed W-2%Y (manufactured at PSI-CRPP).

Acknowledgement

This work, supported by the European Communities under the contract of Association between EURATOM and Karlsruhe Institute of Technology, was carried out within the framework of the European Fusion Development Agreement. The views and opinions expressed herein do not necessarily reflect those of the European Commission.

Nuclear Data

Improvement of Nuclear Data, Development of Tools and Experiments/ Validation in Support of ITER Activities (F4E-2008-GRT-014-01 (ES-AC), Action 1, NUDATA_Files; EFDA HPC-FF MCCov)

Overall objective: The overall objective of the grant agreement was to further contribute to the development of a qualified nuclear data base and validated computational tools for nuclear calculations of fusion reactors. The related tasks of KIT were devoted to the evaluation, processing, application, and benchmarking of required nuclear cross section and uncertainty data as well as the development of computational tools for uncertainty calculations.

Task 3
Finalize updating and testing of the MCsen code and prepare in a format so that it can be used by general users of the MCNP code. Prepare documentation

The objective of this task was to prepare a release version of the Monte Carlo sensitivity code MCsen. MCsen is an extension to the MCNP Monte Carlo code with extended sensitivity capabilities, developed and implemented with support of several EFDA subtasks over the past years. Task 3 of the current F4E-2008-GRT-014-01 nuclear data grant was devoted to the preparation of an installation package of MCSEN as a patch to an existing MCNP installation. The MCsen sensitivity capabilities, added during the preceding development stages, were thoroughly tested, validated and documented in the frame of this task.

MCsen allows the efficient calculation of sensitivities of different types of nuclear responses (tallies in MCNP parlance), based on point-detector and track length estimators, to many (multi-bin) parameters such as reaction cross sections and Legendre moments of angular distributions. The applied algorithms are based on Hall’s differential operator method and have been implemented into the MCNP code, version 4c.

Several MCNP routines have been modified to this end. In addition, some new routines have been added. The MCsen version of MCNP changes also the "common" decks, so that many more routines are (indirectly) affected. The specific additional input to MCsen makes use of the general input tools supplied by MCNP. The specific input is done with the standard MCNP input options "fu" (user tallies) and "idum". In the user-tally, the boundaries of the sensitivity energy bins (groups) are given. In the "idum" input, information about the required sensitivity isotope and reactions is entered.

The present version based on MCNP4c has been tested first on the suite of MCNP test cases, which showed identical results. This indicates that MCsen is not interfering with the standard MCNP routines. Beyond this validation exercises, several test calculations have been repeated which have been conducted in the development of MCsen in the past years. This includes sensitivities to material densities, to Legendre coefficients of angular distributions and to nuclear cross sections both for point-detector as well as track-length estimators. Comparison with available data from the former tests (numerical or graphical) showed that the same results have been obtained with the most recent MCsen version.

The user-package of MCsen was built by assessing the source code differences to the original MCNP4c version to be used for a direct patch routine. This allows any user of MCNP4c having its source code to upgrade it to MCsen. The dispatch contains the source code patches and install scripts which build a serial MCsen version in the directory tree of MCNP.

User instructions have been assembled to assist users of the MCsen code. They contain installation instructions, annotated input and output statements. The full MCsen dispatch including source code patch, installation script and manual has been submitted to the NEA Databank of the OECD, Paris, for dissemination.

Staff:

U. Fischer
D. Leichtle
R. Perel (Hebrew University of Jerusalem)

Task 4
Produce cross-section data evaluations for the ^{50}Cr, ^{53}Cr and ^{54}Cr isotopes interacting with neutrons up to the energy of 150 MeV and prepare general purpose files from these evaluations in ENDF format.

Task 5
Analyze suitable chromium integral benchmark experiments using the MCNP code, test the recent chromium evaluations and provide feedback to improve the evaluations.

The objectives of these tasks were to provide general purpose nuclear data evaluations and files describing the interaction of neutrons with the Cr isotopes 50, 53, and 54 up to 150 MeV neutron energy (Task 4), to test the chromium evaluations, including the one performed for ^{52}Cr in the frame of the previous EFDA Task TW6-TTMN-001, D4, against suitable benchmark experiments and provide feedback to improve the data evaluations (Task 5).

The work performed under tasks 4 and 5 of the F4E-2008-GRT-014-01 nuclear data grand consisted of the following activities:

- Production of cross-section data evaluations of ^{50}Cr, ^{53}Cr and ^{54}Cr for interactions with neutrons with energies up to 200 MeV using the best parameter set and experimental data.
- Comparisons of the results with experimental data to demonstrate the correctness of the evaluations.
- Evaluation of co-variance data based on the Unified Monte Carlo (UMC) approach.
- Production of ENDF formatted data files including co-variance data.

The nuclear data calculations were performed with the nuclear model code TALYS of NRG Petten. The pre-analysis performed for the n + Cr interactions, however, showed severe deficiencies of the nuclear models available in TALYS for the pre-equilibrium emission of complex particles at high energies. To improve the simulation of such processes, the so-called geometry dependent hybrid model (GDH) including a model for the non-equilibrium cluster emission was introduced in the TALYS code as a new option (keyword preeqmode 5).

For the description of the nuclear level densities the phenomenological generalized superfluid model was invoked (keyword ldmodel 3).

The global optical model potentials (OMPs) invoked in TALYS for complex particles are based on the so-called folding approach. Within this approach, the OMP for each complex particles (d, t, He-3, alpha) is folded (built-up) on the basis of the available neutron and proton OMPs in accordance with simple rules. In the case of incident neutron and protons, the use of such OMPs gives satisfactory agreement with experimental data both for excitation functions and particle emission spectra. In the case of incident d, t, He-3 and alpha particles, the total reaction cross section is underestimated significantly with this approach. Therefore global OMPs were taken in this work for complex particles. The incident energy range of each OMP extends up to 200 MeV. Thus the evaluated data become continuous for all neutron incident energies. For deuterons and alpha particles, published OMP parameters were

adopted for the evaluation. For tritons and He-3, we elaborated global OMPs making use of experimental data and available OMPs for some target nuclides.

The nuclear structure data base for TALYS calculations comes from international Reference Input Parameter Library (RIPL). For the present evaluation, a table of experimental nuclear masses was taken. The calculations of the direct reactions were done with the so-called DWBA model.

New resonance parameters for n + ^{50}Cr, ^{53}Cr, ^{54}Cr interactions were separately evaluated by L. Leal, ORNL, using the SAMMY code. This evaluation was based on new measurements performed at ORNL on natural Cr for the capture cross sections (energy range 10 eV- 600 keV) and for the neutron transmission (10 eV- 600 keV). Based on these data new resonance parameters were produced for all stable chromium isotopes. For ^{50}Cr, the resonance region was set from 10-5 eV to 783 keV, for ^{53}Cr from 10-5 eV to 564 keV, and for ^{54}Cr from 10-5 eV to 834 keV.

As described above, the evaluation of the Cr nuclear cross-section data was based on the use of TALYS results with adjusted model parameters and additional post-processing adjustments to experimental data. In spite of its apparent advantage, such an approach could lead to inconsistencies of the whole evaluation resulting, for example, in negative heating values at the data processing step. Therefore we tried to take advantage of the nuclear models applied and focused the adjustment procedure on the nuclear model parameters that provide internal consistency for the whole set of evaluated data.

The adjustment of nuclear model parameters has been made using the BEKED code package and other tools adopted for nuclear data evaluation. Experimental cross-sections for 22 nuclear reactions (n,xnyp) and (p,xnyp) at primary nucleon energies up to 150 MeV were used to get the improved values of parameters of nuclear models implemented in TALYS.

Within the adjustment procedure, co-variances were calculated using the BEKED code package and the TALYS code. The Unified Monte Carlo (UMC) approach proposed earlier by D. Smith has been applied to obtain co-variance matrices for the cross-sections. The generation of co-variances implied the following steps:

- Definition of the “best” set of parameters for the “best” nuclear models used for the cross-section calculation,
- Definition of uncertainties of model parameters,
- Monte Carlo sampling of N number of input data sets for the code implementing selected “best” models,
- Execution of calculations for using the generated input data files,
- Calculation of co-variance matrices for specific reactions.

Uncertainties of optical model parameters, deformation parameters, and nuclear level density parameters were considered as having primary importance.

The uncertainty assigned to nuclear level density parameters of the generalized superfluid model was taken from the available experimental information and from the analysis of the quality of systematics applied to nuclear level parameters. Several thousands of computer runs for each isotope were performed to obtain the information about cross-section correlations. Fig. 1 shows examples of calculated correlation matrices for (n,n’) and (n,2n) nuclear reactions on ^{54}Cr at neutron incident energies up to 200 MeV.

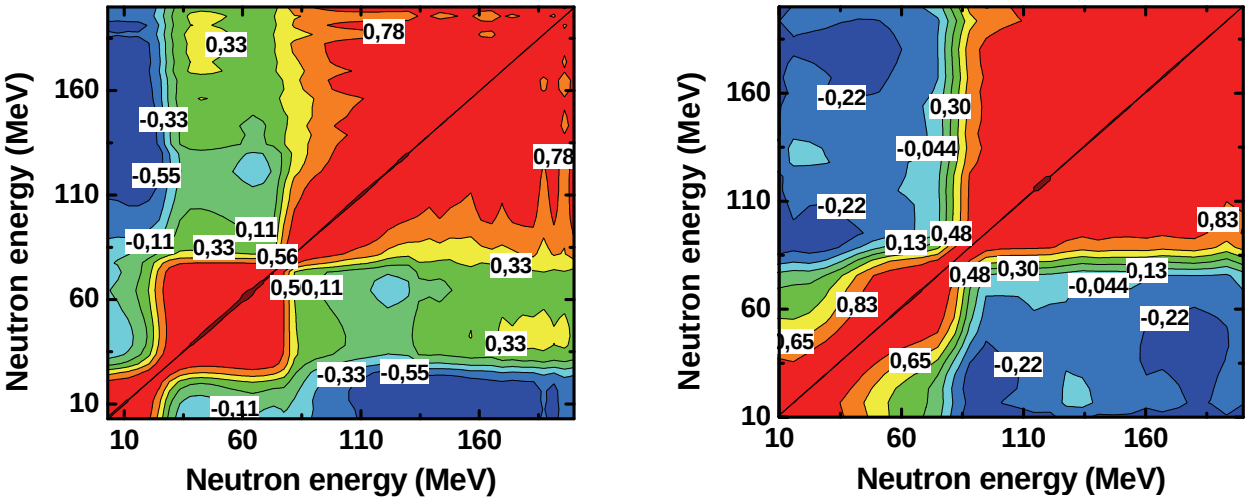

Fig. 1: Correlation matrices for the (n,n') (left) and (n,2n) (right) reaction cross-sections of ^{54}Cr.

Figs. 2 and 3 show examples of cross-sections and their uncertainties obtained from nuclear model calculations before fitting to experimental data and evaluated cross-sections and uncertainties obtained after the application of experimental data through the UMC procedure.

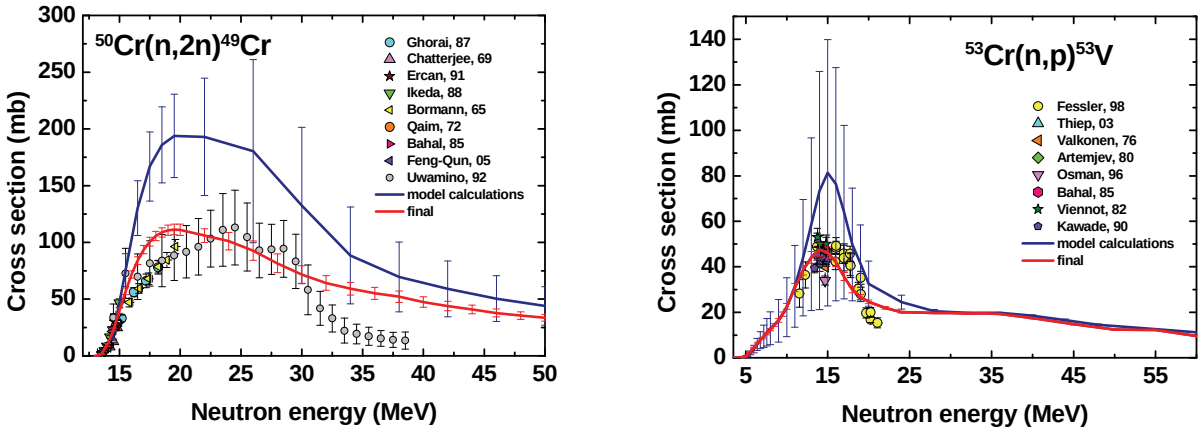

Fig. 2: Calculated (blue lines) and evaluated (red lines) n + Cr cross-sections.

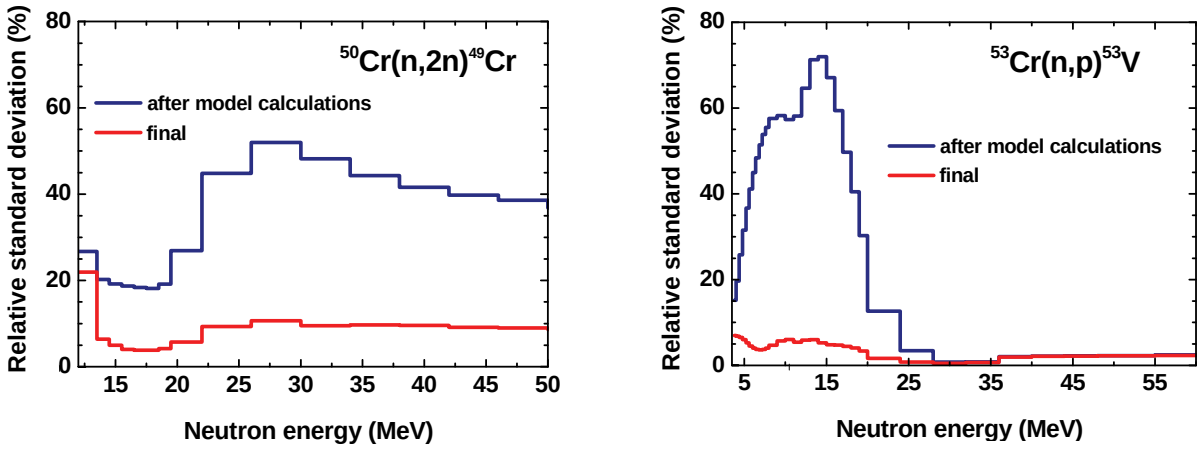

Fig. 3: Evaluated cross-section uncertainties due to nuclear model uncertainties (blue lines) and uncertainties obtained after the evaluation taking into account experimental data (red lines).

General purpose neutron data files were eventually prepared for n+^{50}Cr, n+^{53}Cr, n+^{54}Cr in accordance with ENDF-6 format rules. Special attention was devoted to the consistency of the evaluations. Thus the evaluated data files include all information required for particle transport calculations: resonance parameters, excitation functions, angular distributions of the elastically and inelastically scattered neutrons, particle emission spectra, recoil production cross sections and recoil energy spectra.

The ENDF-6 format provides a good possibility to store high energy data irrespective of the particle incident energy. This is an option of the MT=5 section which is defined as sum of all reactions not given explicitly else. Hence all information can be stored in this section. In this case each particle or nuclide production cross section can be identified and their multiplicities are given on File 6 (MF=6). The production cross section (individual particle or nuclide) can be retrieved by multiplying of the cross section in MT=5 (MF=3) to the yield (or factor) in MF=6, MT=5. In the same way the particle emission spectra or recoil spectra can be retrieved using normalised spectra in File 6, MT=5 and corresponding cross section in File 3, MT=5.

In the present evaluation the advantage of representing data on file 10 (MF=10) is used. Section MT=5 on file MF=10 contains cross sections for all reactions (including) isomers with Z and A designator for each residual nuclide. The related co-variances for all residual nuclide production cross sections are stored on file 40 (MF=40), section MT=5.

The resonance parameters and their co-variances are given in the standard way on the files MF=2 and MF=33, section MT=151. File MF=8 is provided to satisfy the ENDF-6 format rules: The MF=8 MT=5 contains information for the residual nuclides and possible isomers for which the information on file MF=10 is given.

The evaluated neutron data files were successfully processed with the ACER module of the standard NJOY99 code and used with MCNP Monte Carlo benchmark calculations. The co-variance data contained in File MF=40 cannot processed yet with the current version of the NJOY99 code although it is foreseen by the ENDF-6 format. The NJOY99 code needs to be slightly modified to process such kind of data.

The Cr data evaluations were finally submitted to the NEA Data Bank for testing, benchmarking and integration into the Joint Evaluated Fission and Fusion File (JEFF) which represents a complete data library of general purpose data evaluations satisfying both fusion and fission needs.

Staff:

U. Fischer
A. Konobeev
P. Pereslavtsev
S. P. Simakov

Literature:

[1] P. Pereslavstev, A. Yu. Konobeyev, L. Leal, U. Fischer, Evaluation of 50Cr, 52Cr, 53Cr, 54Cr neutron cross section data for energies up to 200 MeV, International Conference International Conference on Nuclear Data for Science and Technology (ND2010), April 26-30, 2010 Korea

[2] A. Yu. Konobeyev, U. Fischer, P.E. Pereslavtsev, “Computational Approach for Evaluation of Nuclear Data Including Covariance Information”, International Conference International Conference on Nuclear Data for Science and Technology (ND2010), April 26-30, 2010 Korea

[3] A. Yu. Konobeyev, U. Fischer, A.J. Koning, P.E. Pereslavtsev, M. Blann, “Implementation of the Geometry Dependent Hybrid Model in TALYS”, International Conference International Conference on Nuclear Data for Science and Technology (ND2010), April 26-30, 2010 Korea

[4] P. Pereslavtsev, A. Konobeyev, U. Fischer, Status of the evaluation and benchmarking of the Cr-50,53,54 neutron cross-section data up to 150 MeV, EFF/EAF Nuclear Data Monitoring Meeting, NEA Data Bank, Paris, November 25 – 27, 2009, EFF-DOC-1083.

Intellectual Property Rights (IPR)

In the frame of this work a new software and a new element of know-how have been generated.

Acknowledgement

This work was supported by Fusion for Energy under the grant contract No. F4E-2008-GRT-014-01 (ES-AC) with collaboration by CCFE, United Kingdom; NRG, Netherlands; IFIN HH, Romania; TU Wien, Austria and JSI, Slowenia. The views and opinions expressed herein reflect only the author’s views. Fusion for Energy is not liable for any use that may be made of the information contained therein.

Nuclear Data Studies/Experiments in Support of TBM Activities (F4E-2008-GRT-014-02 (ES-AC), Action 2, NUDATA_Exper)

Overall objective: The overall objective of the grant agreement was to provide the experimental data base required for the validation of the nuclear data libraries EFF and EAF developed in the frame of the EU Fusion Technology Programme. The focus of the KIT tasks was on experimental validation activities of ITER and TBM design calculations and cross-section validation experiments relevant for IFMIF.

Task 2
Results of tests of measurement techniques for radiation dose deposited in blanket structures in the mixed neutron-photon field and improvement of measurement techniques for tritium production rate measurements

The objective of this task was to perform tests of a measurement technique for dose deposition with a method not applied so far in Test Blanket Module (TBM) mock-up experiments. The method is based on optically stimulated luminescence detectors (OSLD) made of beryllia (BeO). Such detectors could also become candidate measurement techniques for future experiments with the TBMs in ITER if future dedicated assessments are in favour.

In addition, investigations were performed of higher order peaks in the glow curve of LiF thermoluminescense detectors (TLD). The measurement principle has been used before in tritium production rate experiments, however in these measurements only the lower order glow peaks have been used since such neutronics mock-up experiments are conducted at room temperature. LiF-TLD show also luminescence at higher temperatures. These peaks appear at temperatures above 250 °C during read-out of the TLD chips and therefore could become also a candidate measurement technique for TBM experiments provided the TLD chip temperature could be maintained below this temperature during irradiation.

BeO OSLD: Experiment

The HCLL-TBM mock-up

The HCLL-TBM mock-up was the same as in recently performed experiments measuring the tritium production rate. It was built from bricks of lithium-lead with the sizes 3.6 cm x 17 cm x 9 cm. They were arranged in 11 horizontal layers, the layers were separated by EUROFER sheets with a thickness of 9 mm. Two polyethylene sheets were inserted above and below the central LiPb layer. Their purpose was to shape the neutron spectrum making it more similar to the spectrum expected in a breeding blanket. The BeO detectors were placed along the axis of the mock-up in the central LiPb layer. They were evenly spaced with a distance of 4.2 cm between each position and a total of 8 measurement positions and two detectors placed in each. The distance of the first measurement position from the front surface of the mock-up was 1.55 cm. A photograph and a sketch of the assembly are shown in Figure 1. The setting of the BeO OSLD in one of the two bricks of the central channel of the mock-up is presented in Figure 1.

Irradiation conditions

The mock-up was placed in front of the Ti-T target of the neutron generator of Technical University of Dresden (TUD). The distance between the front of the mock-up and the source of DT neutrons in the Ti-T target was (5.7+-0.1) cm. The integral fast neutron flux impinging on the centre of the mock-up surface was monitored with attached niobium activation foils which were read out after irradiation with a high-purity Ge detector. The time-dependent DT neutron source strength was also monitored with a silicon detector located inside the vacuum beam line of the neutron generator which monitors the alpha particle emission associated with the DT reaction in the Ti-T target. Further monitoring was provided by a NE-213 detector located at a distance of approximately 5 meters from the neutron source which was not calibrated but served as a relative neutron monitor.

The neutron generator was operated in cw mode and delivered deuterons with an energy of 320 keV to the Ti-T target. The typical deuterium current for this measurement was approximately 1 mA. The irradiation time was approximately 1.5 hours with a total DT source yield of 1.06E14 neutrons.

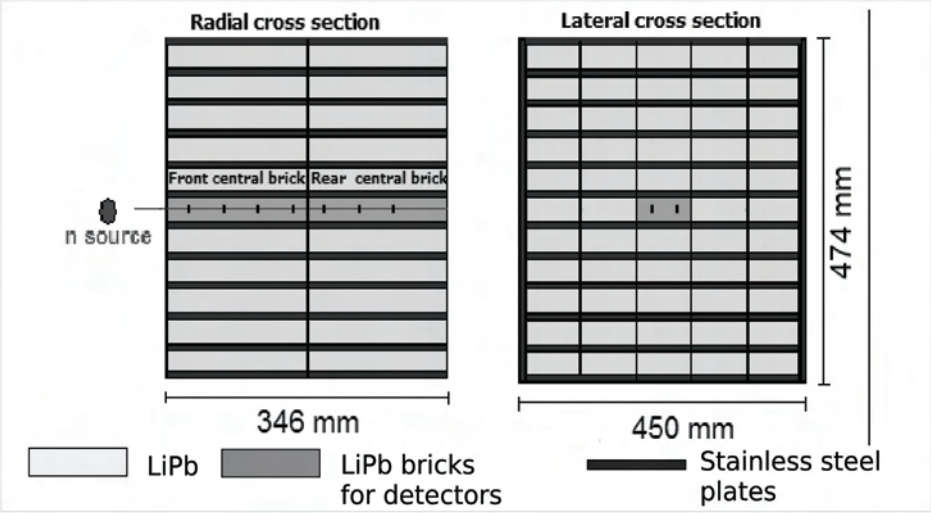

Fig. 1: HCLL neutronics mock-up assembly.

BeO OSLD: Results and Discussion

Measured dose values are shown together with calculated ones in Table 1. In the MCNP calculation, track length estimate tallies with energy deposition were used to compute the dose for both, neutrons and gamma-rays. The calculated gamma doses are approximately one order of magnitude smaller than the doses from neutrons.

Table 1: Experimental and calculated dose values for eight measurement positions in the LiPb mock-up.

Position from front surface (cm)	Calculated dose value [Gy]			Experimental does value [Gy]	C/E
	Neutrons	Photons	Sum		
1.55	4.26E+0	4.76E-1	4.73E+0	2.43E+0	2.0
5.75	1.54E+0	1.93E-1	1.73E+0	8.73E-1	2.0
9.95	7.20E-1	8.60E-2	8.06E-1	3.65E-1	2.2
14.15	3.89E-1	4.27E-2	4.32E-1	1.76E-1	2.5
18.30	2.19E-1	2.56E-2	2.45E-1	8.23E-2	3.0
22.40	1.30E-1	1.30E-2	1.43E-1	5.22E-2	2.7
26.50	7.77E-2	8.79E-3	8.65E-2	3.03E-2	2.9
30.60	4.49E-2	4.56E-3	4.94E-2	1.68E-2	2.9

The signal of the BeO detectors is due to several dose deposition mechanisms: Energy deposition due to Compton electrons following interaction with gamma-rays and from charged particle emitting reactions with fast neutrons. The charged particles in turn generate energetic electrons on their way until losing most of their energy.

One can see from Table 1 that the calculated values are in general higher than the experimental ones and the ratio between calculated and experimental values increases slightly with depth. This could be due to different responses of BeO to the two mechanisms of dose deposition mentioned above.

Application of BeO OSLD could be extended for example to tritium production rate measurements because it is possible to add materials to some extend to the beryllia without losing OSL capabilities. This may open up the option to measure in-situ by means of optical fibres.

Higher order glow peaks in LiF TLD: Experiment

LiF TLD from GC Technology with natural isotopic composition (TLD-100) and enriched in 7Li (99.99%, TLD-700) have been irradiated with fast neutrons from the neutron generator of TUD. The samples have been placed at two distances from the TiT target, one was attached directly to the target with an effective distance to the neutron source of 1.8 cm, the other one at a distance of 7.5 cm. A third set of detectors was attached to polyethylene to increase the tritium production from 6Li with respect to other reactions and placed at a location approximately 90 degrees to the deuterium beam of the neutron generator at a distance of approximately 9 cm. The local fast neutron fluence was monitored with Nb activation foils attached to the TLD. After irradiation, the TLD were read out with a commercial research TLD reader Harshaw 3500.

Higher order glow peaks in LiF TLD: Results and conclusions

As an example, a typical glow curve of the TLD from this experiment is shown in Figure 2. Clearly seen are the glow peaks 4+5 and 6+7. The responses of the corresponding TLD in each irradiation set did not scatter very much, but both types of TLD with natural and ^{7}Li enriched composition have a different response to the neutron field which should be mostly due to the very different ^{6}Li content of TLD-100 and TLD-700.

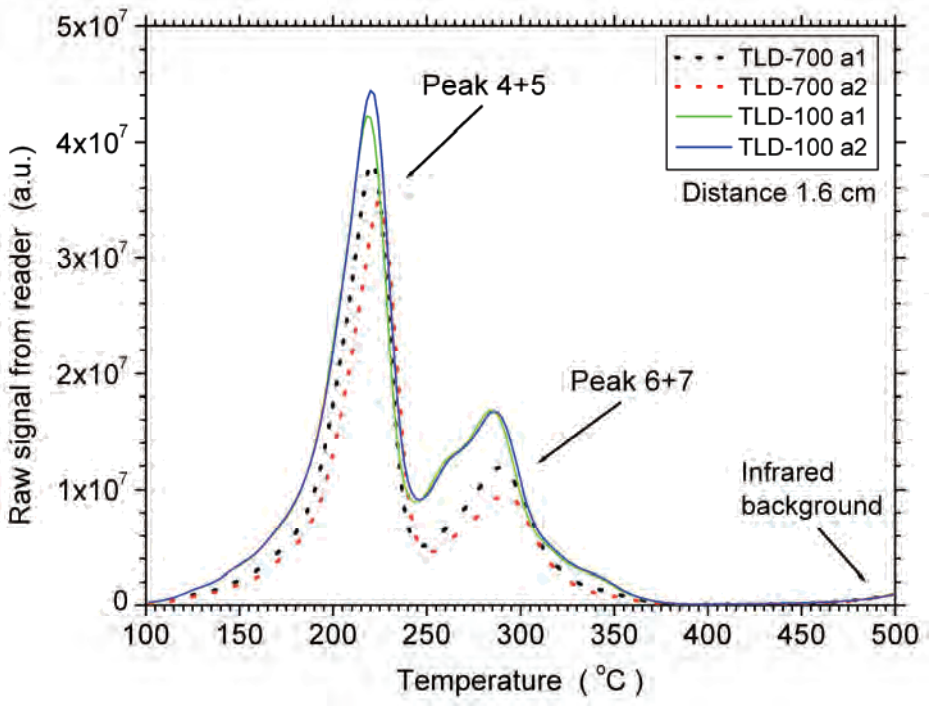

Fig. 2: Glow curves from sample TLD attached to the TiT target of the neutron generator of TU Dresden.

The fast neutron fluence at the location of the samples measured with niobium foils was 1.12 10^{12} n/cm^2, 2.61 10^{11} n/cm^2, and 1.03 10^{10} n/cm^2 for the samples mounted directly to the TiT target, at a distance of 7.5 cm and at the Polyethylene block, respectively.

From the glow curves it appears that peaks 6+7 could be used to obtain a TPR signal in the same way as from peaks 4+5 in previous work. However, similar conditions would apply, i.e., there will be a dependency of the TPR signal on the neutron spectrum and hence care needs to be taken when the detectors are calibrated. Limitations will arise for high doses which could be expected in the TBM. In order to investigate this issue, glow curves from a previous irradiation in the LiPb neutronics mock-up were checked again. This measurement had been done as part of the EFDA task TW6-TTMN-002B-D2. Two measurements had been performed with different neutron yields from the neutron generator (FNG/ENEA). For the present work, the raw glow curves of the TLD were used and the areas of peaks 4+5 and 6+7 were compared to see whether peak 6+7 would be not or not so much affected by the saturation effect and could be used instead of peak 4+5.

To calculate the area of the peaks, the region-of-interest method was used as described above. The results for both peaks, 4+5 and 6+7, are presented in Figure 3. The figure shows also the differences between the signals from TLD-100 and TLD-700. No clear improvement was found for the measurement positions 1 and 2 in the mock-up. Both detectors show nearly the same response which would render this measurement method not suitable at least for TPR measurements in cases where doses of several Gy would have to be expected for the TLD chips. However, at the other measurement positions the ratio between the signals from TLD-100 and TLD-700 seems to be slightly larger which would improve the signal-to-background ratio slightly when used for TPR measurements from ^{6}Li.

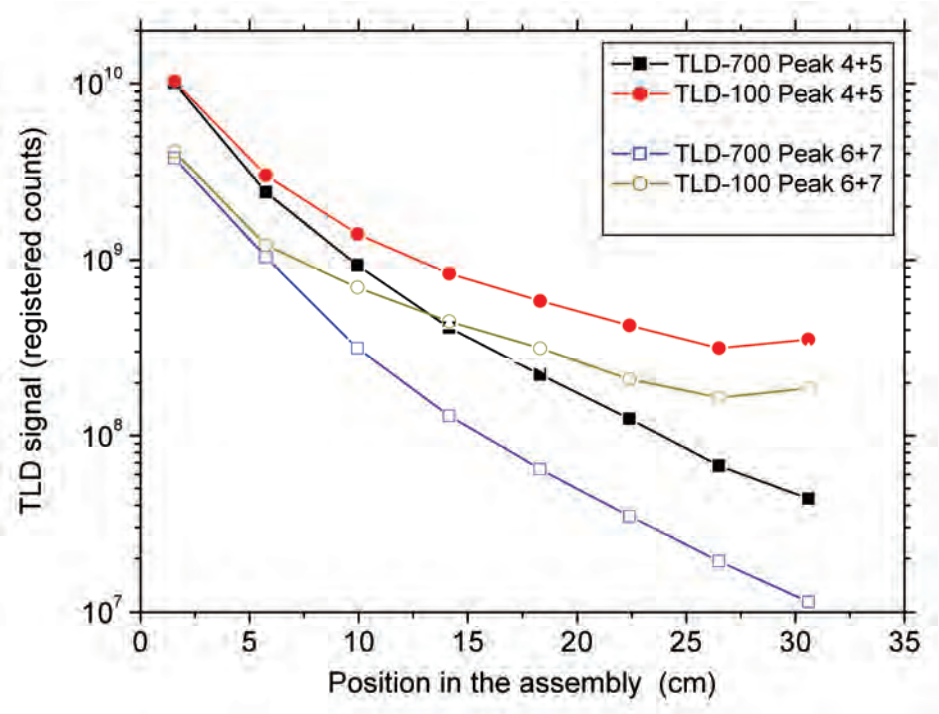

Fig. 3: Comparison of the peak integrals for Peaks 4+5 and 6+7 for the TLD-700 and TLD-100 from the irradiation of these detectors in the LiPb neutronics mock-up irradiated previously at FNG of ENEA Frascati.

Staff:

D. Gehre (TU Dresden)
A. Klix
U. Fischer
D. Sommer (TU Dresden)
M. Sommer (TU Dresden)

Literature:

[1] A. Klix, P. Batistoni, R. Böttger, D. Lebrun-Grandie, U. Fischer, J. Henniger, D. Leichtle, R. Villari, Measurement and Analysis of Neutron Flux Spectra in a Neutronics Mock-up of the HCLL Test Blanket Module, 9th Int. Symp. on Fusion Nuclear Technology, Oct. 11-16, 2009, Dalian, China

Task 4
Monte Carlo based sensitivity/uncertainty analysis of the neutron flux spectra and TPR in the HCLL TBM in ITER for comparison to the TBM mock-up experiment

The objective of Task 4 was the computational analysis of the Helium Cooled Lithium Lead (HCLL) Test Blanket Module (TBM) in ITER using Monte Carlo techniques for transport and sensitivity/uncertainty calculations. The results were compared to the corresponding analyses performed for the HCLL mock-up experiment conducted at the Frascati Neutron Generator in 2009. The MCsen code has been employed for the Monte Carlo sensitivity calculations of neutron fluxes and tritium production on nuclear cross-sections. Available co-variance data were used to obtain nuclear response uncertainties related to nuclear data uncertainties.

The MCNP transport and tritium production calculations were performed with the most recent ITER MCNP model called A-lite. This model represents a 40° torus sector including various dummy ports for the integration of diagnostic tools, test objects, etc. The test blanket port of the A-lite model was modified to allow the integration of a TBM inset. It includes a water-cooled steel frame, the Helium Cooled Pebble Bed (HCPB) TBM in one vertical half of the frame compartment and a HCLL TBM in the other half. The HCPB TBM has been converted into MCNP geometry from a CAD model by the McCad software tool. For the HCLL TBM a simplified model, developed in the frame of the EFDA task TW6-TTMN-002, D3, for benchmark analyses with the previous ITER “Brand” model has been utilized and adapted to the A-lite geometry.

Fig. 4 shows a vertical cut of the A-lite model with the TBM integrated into the test blanket port. The horizontal cuts, at the level of the torus mid-plane, show the test blanket port region at the outboard side of the ITER torus with steel frame and the HCPB and HCLL TBM in place. For comparison with the HCLL mock-up experiment, two representative positions in the front and the rear of the ITER TBM are selected at distances of 3.5-7.1 cm and 27-30.5 cm.

For the MCsen transport and sensitivity calculations typically 2 10^8 histories have been run for each case. Sensitivities to materials from the HCLL TBM itself (like Pb, Li) have been obtained independent from the materials of the ITER tokamak (like Be, O, Ni). For nuclides in both areas, like the steel components Fe and Cr, this can be achieved by using different nuclear data identifiers, since TBM materials use JEFF3.1 data, whereas for ITER components the reference library FENDL-2.1 has been adopted.

The sensitivities obtained for the TPR are generally very small, which could be expected from the HCLL mock-up analysis. However, most of the integrated sensitivities are negative compared to the small positive values in the experiment. Similar to the experiment the sensitivities are slightly decreasing at the deeper position. The TPR is most sensitive to Pb (elastic), H (elastic) and ^{6}Li(n,t) cross-sections. Significant sensitivities are due to ^{6}Li(n,t), ^{9}Be(n,2n), and the ^{56}Fe reactions (elastic, (n,2n) and inelastic). In the case of ^{56}Fe its sensitivity to TPR and neutron flux at the front position differs whether it originates from the EUROFER of the TBM (small positive sensitivity) or from other steels, mainly in the steel frame (small negative sensitivity). Reactions on the other involved nuclides do not contribute largely to the sensitivity, in particular the major alloying elements Cr and Ni.

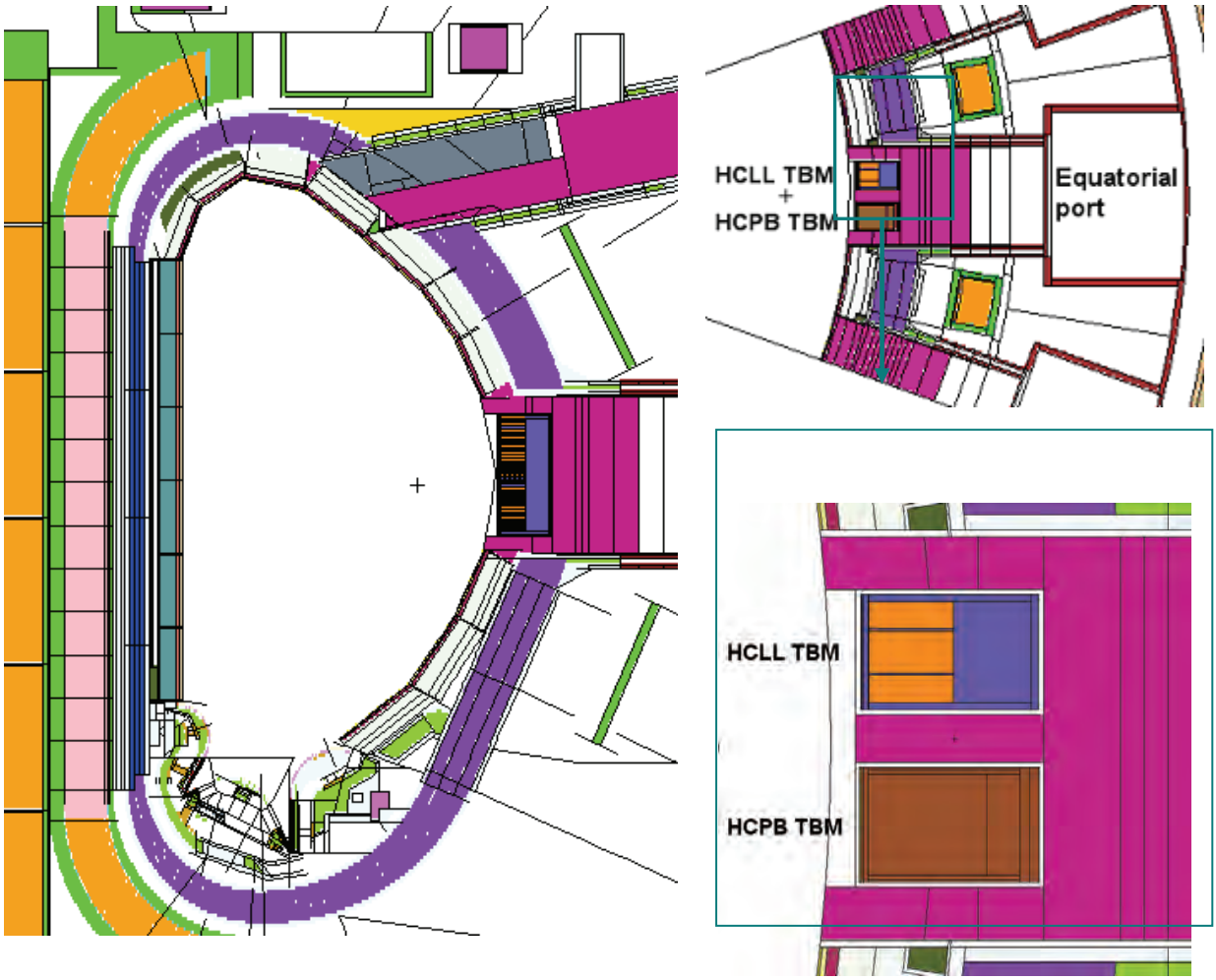

Fig. 4: Vertical (left) and horizontal (right) cuts of the A-lite ITER model with integrated HCPB and HCLL Test Blanket Modules.

For the calculation of uncertainties in the TBM due to uncertainties of the underlying nuclear data the covariance data were taken from different sources, mainly from ENDF/B-VI.8, and the ZZ SCALE-6.0/COVA-44G libraries. For ^{6}Li the data source is EFF-2; the results based on the IRDF-02 dosimetry library yield very similar uncertainties. The data source for ^{7}Li is ENDF/B-VI.8, and for ^{1}H ENDF/B-V. The ^{9}Be and ^{56}Fe covariances are based on EFF-3, the ^{52}Cr covariances were processed from a recent evaluation conducted in the frame of the F4E Nuclear Data Grant GRT-014-01. ^{58}Ni co-variances are JEFF-3.1 based. During the processing and checking of the covariance libraries the quality was found to be relatively poor in some cases, which has been noted in the previous analysis on the mock-up experiment. In particular, the processing of ENDF/B-VI.8 covariances for the inelastic scattering on ^{207}Pb lead to unrealistic large uncertainties and were discarded. In this case the data of SCALE-6.0 has been used.

Generally the uncertainties to individual isotopes are quite low, usually below 2%. The isotopes with the largest contribution to the uncertainty are isotopes that appear in the TBM: ^{6}Li, the Pb isotopes and ^{56}Fe. Isotopes that are part of ITER have generally a smaller influence on the uncertainty. The combined uncertainties due to all presented isotopes are given in Table 2.

The combined uncertainty (one standard deviation) due to all presented isotopes for total TPR is between 2.2% (front) to 4.2% (rear). The combined uncertainty for the total neutron flux is between 1.8% (front) to 3.1% (rear).

Table 2: Combined uncertainties in calculated responses due to cross sections.

Position	Response	TBM materials	ITER materials	All materials
Front	TPR	2.10%	0.62%	2.2%
Rear	TPR	4.14%	0.37%	4.2%
Front	n-flux	1.79%	0.29%	1.8%
Rear	n-flux	3.03%	0.31%	3.1%

Staff:

U. Fischer
D. Leichtle
R. L. Perel (Hebrew University of Jerusalem)
A. Serikov

Literature:

[2] D. Leichtle, U. Fischer, R.P. Perel, A. Serikov, Sensitivity and uncertainty analysis of nuclear responses in the EU HCLL TBM of ITER, Proceedings SOFT-2010, Porto, Sep. 2010, to appear in Fus. Eng. Des.

Acknowledgement

Work under Task 4 was carried out using an adaptation of the Alite MCNP model which was developed as a collaborative effort between the FDS team of ASIPP China, ENEA Frascati, JAEA Naka, and the ITER Organization.

Task 7
Analyses of the validation experiments for Au cross-sections up to 35 MeV

The objective of this subtask was to perform computational pre-analyses for the optimization of the set-up for the Au activation experiments in a quasi-monoenergetic neutron spectrum extending up to 35 MeV and, after completion of the experiment, to perform the computational post-analysis to check the relevant activation cross-section data and, in case of discrepancies, identify the responsible cross-sections.

The pre-calculations had been performed with the MCNPX code and LA-150h cross section data for the Li(p,xn) reaction to predict the intensity and the spectral shape of the quasi mono-energetic neutron source employing a thin lithium target and a carbon proton beam stopper. The comparison of calculations with available experimental data had shown that MCNPX with LA-150h library predicts satisfactorily the energy-angular distributions of the neutrons emitted from the Li/C target.

The activation of Au samples has been performed by the NPI Rez experimental team in the frame of Task of the F4E Contract F4E-GRT-014 (ES-AC). The neutron target consisted of a thin ^{7}Li foil backed by a carbon beam stopper and cooled by flowing water. The measurements have been performed at 15 incident proton energies from 19.8 to 37.5 MeV, which produced neutron spectra having peaks at the energies from 16 to 36 MeV, respectively. The Au foils were located at 4.8 and 8.8 cm distance from the target and were activated during 20 hours. The samples were analysed off-line by the gamma-spectroscopy technique employing two calibrated HPGe detectors with an energy resolution of 1.8 keV at 1.3 MeV. The unstable

decaying isotopes were identified on the basis of the half-lives, the γ-ray energies and the intensities. The measurement period of decaying gammas ranged from minutes to 100 days.

To derive the Au activation cross section from the measured gamma activities we used a modified version of the SAND-II code for the neutron spectrum adjustment. In the present case the usual unfolding procedure was reversed: the neutron spectra in the foil were supposed to be known and fixed, whereas the activation cross section was allowed to vary to get C/E (calculation/experiment) ratios close to unity at all 15 proton energies. In such a way the cross sections for the ^{197}Au(n,xn)$^{197\text{-X-}1}$Au reactions were adjusted to the $^{197\text{-X-}1}$Au specific activities, measured at the distances of 48 and 88 mm. The final cross sections were found by averaging the results at the two distances. The total uncertainties include experimental uncertainties and the deviations between the adjustment results obtained for the two Au samples locations, as well as, additionally, 10% due to the uncertainty of Li(p,n) yield simulation.

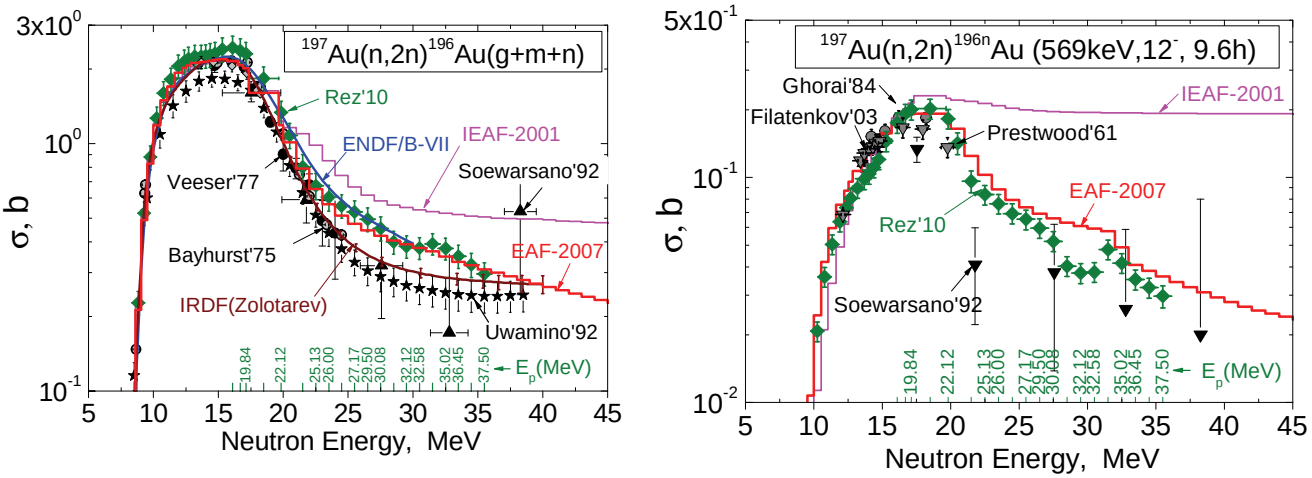

Fig. 5: Activation cross section for the 197Au(n,2n)196(g+m+n)Au (left) and 197Au(n,2n)196nAu (right) reactions derived from the measurements at NPI/Rez (green symbols) in comparison with available experimental and evaluated data.

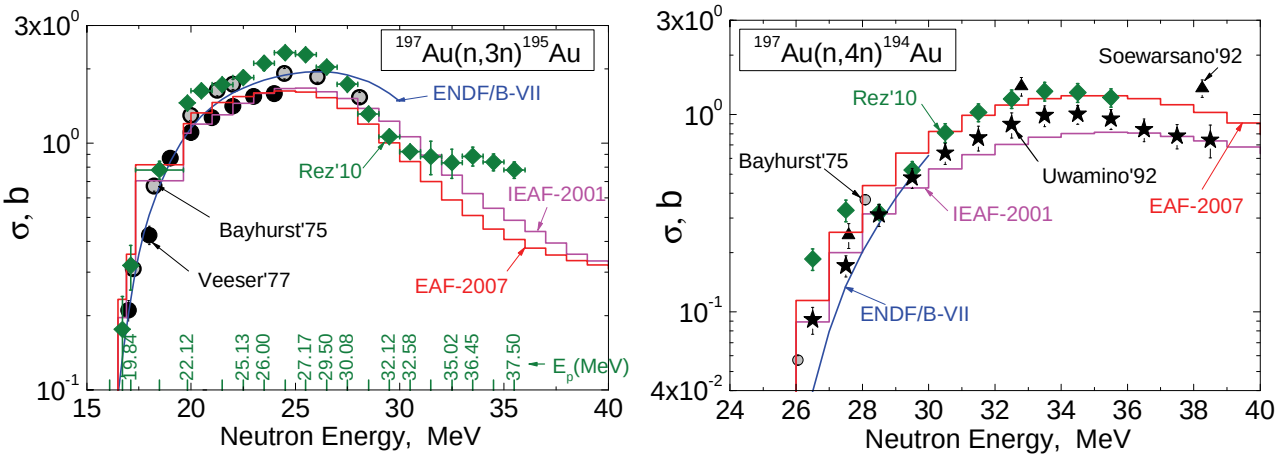

Fig. 6: Activation cross sections for the 197Au(n,3n)195Au (left) and 197Au(n,4 n)194Au (right) reactions derived from the measurements at NPI/Rez (green symbols) in comparison with available experimental and evaluated data.

Figs. 5-6 show the Au activation cross-sections derived from the measured radio-activities in the energy range up to 35 MeV neutron energy by employing the computational approach described above. The cross sections obtained for the ^{197}Au(n,2n)^{196}Au, ^{197}Au(n,2n)^{196n}Au, ^{197}Au(n,3n)^{195}Au and ^{197}Au(n,2n)^{194}Au activations reactions have been compared with available measured and evaluated data. While agreement with the previous experimental results

below 20-25 MeV was found, the presently measured activation cross sections improve the status at higher energies. They confirm the EAF-2007 evaluation for ^{197}Au(n,2n)^{196}Au, indicate a slight overestimation for ^{197}Au(n,2n)^{196n}Au and an underestimation for ^{197}Au(n,3n)^{195}Au, and support it for the ^{197}Au(n,4n)^{194}Au reactions.

Staff:

U. Fischer
S.P. Simakov

Literature:

[3] S.P. Simakov, P. Bém, V. Burjan, U. Fischer, R.A. Forrest, M. Götz, M. Honusek, V. Kroha, J. Novák, E. Šimečková, Determination of neutron spectrum by the dosimetry foil method up to 35 MeV, Proceedings of ISRD-13 (May 2008, Alkmaar); Reactor Dosimetry, State of the Art 2008, World Scientific, 2009, pp. 532-540

[4] S.P. Simakov, P. Bém, V. Burjan, U. Fischer, R. A. Forrest, M. Götz, M. Honusek, V. Kroha, J. Novák, E. Šimečková, Analysis of the dosimetry cross sections measurements up to 35 MeV with the ^{7}Li(p,xn) quasi-monoenergetic neutron source, International Conference International Conference on Nuclear Data for Science and Technology (ND2010), April 26-30, 2010 Korea

Task 8
Validation experiment for gamma activities of Ti / Li_2TiO_3 irradiated in fusion peak neutron spectrum

The objective of this subtask was to provide experimental data for the validation of activation cross-sections for Ti/Li_2TiO_3 irradiated in a fusion peak neutron spectrum. To this end, samples of titanium were irradiated with fusion peak neutrons from a DT neutron generator and the induced gamma activity was determined. The results were compared with calculations with the EASY-2007.

Natural titanium consists of five isotopes which transmute mainly to scandium isotopes by (n,p), (n,d), and (n,np) reactions. The isotopic abundance of natural Ti is as follows: ^{46}Ti 8.2 at%, ^{47}Ti 7.4 %, ^{48}Ti 73.8 %, ^{49}Ti 5.4%, and ^{50}Ti, 5.2 %. A first survey revealed that especially the latter reactions play a significant role for the activation of titanium at neutron energies around the DT fusion neutron peak.

Activation experiments

Two titanium samples were prepared for the irradiation with DT neutrons and consecutive gamma-activity measurements with a high-purity germanium detector. One sample was made of a titanium foil with a purity of 99.99%, a mass of 1.0999 g, and a size of ca. 1 cm squared and 1.2 mm thickness. The other sample was Li_2TiO_3 powder with a mass of 7.8 g sealed in a thin plastic tube so that the shape of the sample was cylindrical with a thickness of 9 mm and a diameter of 26 mm. Both samples were irradiated in the DT fusion peak neutron field of the neutron generator of the Technical University of Dresden (TUD).

The neutron generator was operated with a deuteron energy of 320 keV bombarding a Ti-T target. The sample was arranged at an angle of 0 degrees with respect to the deuteron beam at a distance of approximately 9.8 cm from the neutron source. Nb and Zr foils were sandwiched with the samples for monitoring the local neutron fluence. Nb served as the actual fluence monitor while Zr was used to determine the "effective" neutron energy at the position of the titanium sample. This information is required since some of the cross sections leading to the production of scandium isotopes do contribute significantly but have a threshold around 14~15 MeV.

The time profile of the irradiation was recorded with a silicon detector for the associated alpha particle from the DT reaction in the neutron source and a U-238 fission chamber. This time profile is used in the analysis to correct for decay of the produced isotopes during irradiation in cases of short-living isotopes such as ^{48}Sc but also the Zr foil monitors.

For the EASY calculation, an input neutron spectrum was computed with a detailed calculation of the neutron transport through the tritium target assembly of the neutron generator with the MCNP code. Angle-dependent energy distributions of the neutrons generated in the DT fusion reaction were obtained with the DROSG code. The neutron spectrum at the sample position from the calculation is an asymmetric peak with a maximum at 14.8 MeV and a full-with-at-half-maximum of approximately 0.3 MeV. The calculated spectrum at the sample position was validated by comparing the ratio of produced ^{89}Zr and ^{92m}Nb in the monitor foils with values from the MCNP calculation and activation cross sections from the IRDF-2002 library. An "effective" neutron peak energy of 14.9 MeV was determined, measured and calculated values agreed within 1%.

The neutron fluence at the position of the Ti sample was obtained from the Nb foils using a cross section value of 464 mb with an uncertainty of 4.2% for producing the metastable state of ^{92}Nb. This cross section is nearly flat between 14 and 15 MeV and a fluence of 2.42×10^{11} cm^{-2} was computed. The uncertainty of this value is estimated to be 5.2% taking into account the uncertainty of the activity determination of the niobium foil with 3.1%. The estimate represents the root-mean-square of the uncertainties of the gamma line intensity, the half-life of the sample (decay times during measurement and storage), the efficiency calibration, and gamma counting statistics, and the uncertainty of the ^{93}Nb(n,2n)^{92m}Nb cross section mentioned above. The uncertainty of the measurement of the gamma activity of the titanium sample was for each case approximately 4%.

The uncertainty estimate of the EASY calculation includes the half-life and cross section uncertainties, both from the EASY output.

Discussion of the results

Not all nuclides contributing to the contact dose rate could be investigated in this work partly because irradiation times similar to a fusion reactor cannot be achieved with a neutron generator but also because some of the radio-isotopes produced have only very low gamma line intensities. The measured gamma activities are presented together with their experimental and calculation uncertainties and the production pathways in Table 3.

There is a slight underestimation of the ^{46}Sc production by the EASY calculation as one can see from the calculated-to-experiment ratio (C/E). Approximately 80% of the ^{46}Sc is produced by (n,p) reactions on ^{46}Ti. In most cases this reaction leads directly to the ground state of ^{46}Sc or via the first excited state which has a half-life of 18.7 seconds and decays with a branching ratio of 1.0 into the ground state.

The production of ^{47}Sc is overestimated by the EASY calculation. Most of it is produced by (n,d) and (n,np) reactions on ^{48}Ti which is by far the most abundant Ti isotope. Both reaction cross sections have their threshold around 14~15 MeV and are therefore sensitive to the position of the DT neutron peak. However, the correct position of the peak for the input neutron spectrum for the EASY calculation has been validated by the simultaneous measurement of the Zr foil which applies a well-validated cross section.

The amount of 48Sc in the sample was estimated by the EASY calculation well within the error limits of the calculation and experiment. This isotope is mostly produced by (n,p) reactions on 48Sc and, because of the lower isotopic abundance, to a small amount by (n,d) reactions on 49Sc.

Table 3: C/E (Calculation/Experiment) comparison of measured and calculated (EASY) gamma ray activities. Half-lives, gamma energies and intensities are based on JEFF-3.1.1 data. The reaction contributions and the uncertainty of the calculation DC/C were taken from the EASY output. The experimental uncertainty DE/E is for the activity measurement of the sample. The (n,d) reaction in the reaction contributions column from the EASY output includes (n,np) and (n,d).

Radio-nuclide	Half-life	Eg (keV)/Ig	Reaction contribution (%)		C/E	DC/C (%)	DE/E (%)
^{46}Sc	83.79 d	889.3/1.00 1120.5/1.00	46Ti(n,p)46Sc 46Ti(n,p)46mSc → IT → 46Sc 47Ti(n,d)46Sc 47Ti(n,d)46mSc → IT → 46Sc	64.58 15.67 16.84 2.91	0.93	25.1	3.4
^{47}Sc	3.351 d	159.4 / 0.68	47Ti(n,p)47Sc 48Ti(n,d)47Sc	40.19 59.80	1.13	47.6	4.2
^{48}Sc	1.81958 d	983.5/1.00 1037.5/0.975 1312.1/1.00	48Ti(n,p)48Sc 49Ti(n,d)48Sc	99.01 0.99	0.98	10.0	4.3

Staff:

A. Domula (TU Dresden)
A. Klix
K. Zuber (TU Dresden)

Literature:

[5] A. Klix, A. Domula, R. Forrest, K. Zuber, Measurement and Analysis of Activation Induced in Ti/Li_2TiO_3 with Fusion Peak Neutrons, 14th International Conference on Fusion Reactor Materials, 7-11 September 2009, Sapporo, Japan.

Intellectual Property Rights (IPR)

In the frame of this work a new element of know-how has been generated.

Acknowledgement

This work was supported by Fusion for Energy under the grant contract No. F4E-2008-GRT-014-02 (ES-AC) with collaboration by ENEA, Italy; AGH-UST, Poland; JSI, Slovenia and ASCR-NPI Czech Republic. The views and opinions expressed herein reflect only the author's views. Fusion for Energy is not liable for any use that may be made of the information contained therein.

Neutronics Analysis of the IVVS/GDC (In-Vessel Viewing System/Glow Discharge Cleaning) (F4E-OPE-144-01 (ES-AC)

Objective

The general objective of neutronics analysis was to provide nuclear responses in the IVVS/GDC system as input to the mechanical design strategy concerning its maintenance. Several analyses have been performed assessing nuclear characteristics of the IVVS/GDC system exposed to neutrons emitted from the ITER plasma chamber. The IVVS/GDC design shall be developed to comply with specific limitations at all operation regimes in ITER. Hence, nuclear responses to be addressed for the IVVS/GDC components include both characteristics of the ITER operative conditions, as well as after shutdown of the tokamak. Nuclear heating of the GDC electrode head irradiated by neutrons and promptly emitted secondary particles during ITER operation has been assessed and compared with the heating after shutdown due to the decay of radioactive nuclei and the absorption of decay-photons emitted from the irradiated materials of the IVVS/GDC system and the surrounding structure. This includes some parts of the ITER blanket, vacuum vessel, toroidal and poloidal field coil magnets, intercoil structure, cryostat, and bioshield.

MCNP model and computational approach

A preliminary MCNP5 model of the IVVS/GDC system integrated into the out-dated Alite.004 version of the ITER MCNP model was delivered to KIT with the objective, first, to resolve pertinent geometrical errors in the model, and second, to update the combined model to the reference Alite4.1 model.

Cross-cuts of the IVVS/GDC integrated into Alite4.1 are presented in the following figures. The GDC is the so-called shielding position, with its head 105 cm from the inner side of the vacuum vessel. The ring-shaped gap around the GDC electrode at the blanket has a width of 2.1 cm.

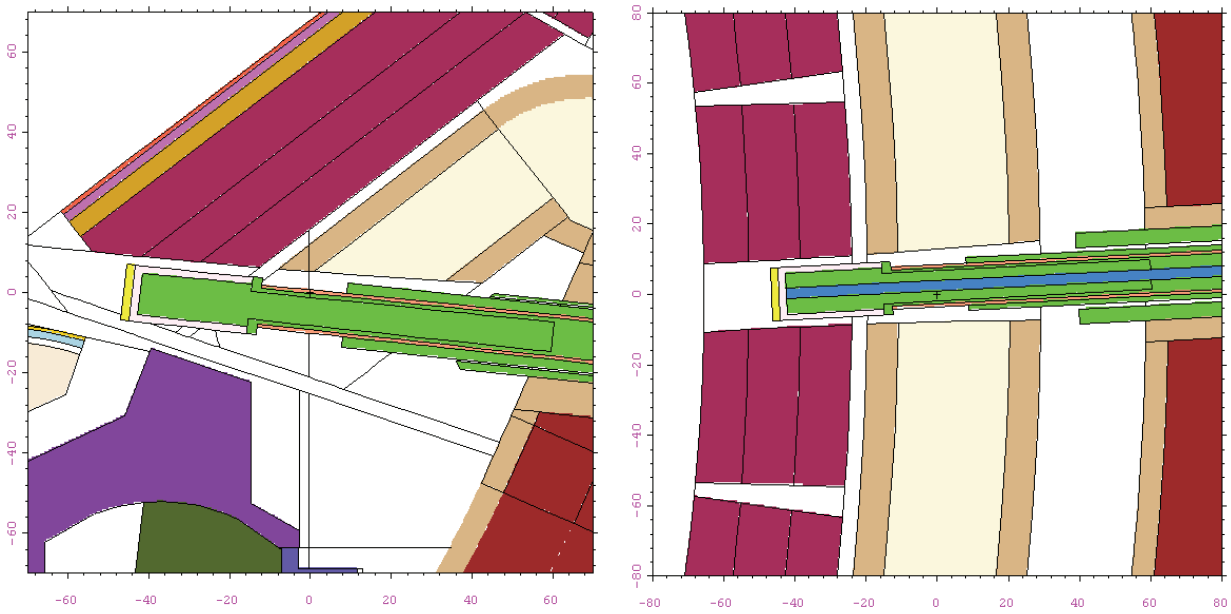

Fig. 1: Vertical and horizontal cuts of the GDC probe head. The cuts are adjusted to the orientation of the GDC probe.

After further segmentation and material assignments in the MCNP model the neutron and gamma transport calculations were performed with a weight window generator on a superimposed mesh. The calculations have been performed in the parallel mode on local clusters at

KIT (CampusGrid and HC3) and at FZ Jülich (HPC-FF/JUROPA) with typically 2E9 particle histories and 6000 CPUh computing time.

The coupled R2S calculation [1] is based on the neutron flux distributions obtained in the IVVS/GDC system and its vicinity. The activation and decay-photon source calculations are performed on the full set of cells according to the so-called SA2 safety scenario for ITER operation as described in the ITER reference document [2]. It is based on a conservative interpretation of the ITER "alternative scenario" for the operational programme (formerly known as "Scenario 1"). The conservatism of the assumptions here is to assure that the irradiation provides the maximum activation in the short, medium and long terms after shutdown. The safety scenario SA2 is based on the most recent understanding of plant availability, maximum pulse rates etc., but retains a reasonable degree of conservatism. According to the request of IVVS/GDC design considerations two irradiation times have been assumed, the first after 4 yr of DT-operation (i.e. 12 yr ITER operation), the second after lifetime irradiation of 12 yr DT (20 yr ITER operation). All FISPACT calculations are initiated by the R2S interface software to provide decay-photon sources for the final shutdown photon transport calculations. A special MCNP source routine is required to sample those photons from the output files of R2S. As the IVVS/GDC system remains in the tokamak after shutdown, the same MCNP geometry model as for the neutron transport run could be used. Decay-photon heat and absorbed dose-rates in the materials of the IVVS/GDC system are then calculated for 5 cooling times (0 s, 1 h, 1 d, 12 d, 100 d) for both irradiation scenarios.

Neutron flux distributions and operational heating in the GDC head

The neutron flux distribution has been obtained from the plasma chamber to the rear part of the IVVS/GDC penetrating the bioshield over a total length of about 11 m. As usual MCNP calculates the neutron flux per source neutron, which has to be normalized to the 500 MW fusion power by the neutron source strength of 1.97×10^{19} n/s in the 40° torus sector. The highest neutron flux values are observed at the level of FW (ca. 10^{14} n/cm^2/s). At the GDC electrode tip the flux is already attenuated to a level of 10^{13} and decreases rapidly further into the IVVS/GDC system due to the appreciable shielding performance of the steel/water mixture in the electrode head, which compensates effectively the blanket module cut out. Over the length of the housing the flux gradient is rather shallow, and the flux level is attenuated by 3 orders of magnitude from the VV exit to the bioshield (10^5 n/cm^2/s).

Table 1: Operational nuclear heating (in W/cm^3) in the MCNP cells of the GDC electrode head.

MCNP cell no.	Material no.	Description	Mass densitiy [g/cm^3]	Cell volume [cm^3]	Nuclear heat [W/cm^3]	Stat. error
9020	210	CuCrZr heat sink	8.81E+00	2.20E+03	5,93E-01	9.90E-03
9021	3	Be layer	1.85E+00	3.53E+02	1,93E-01	1.39E-02
9022	4	SS316 central rod	8.03E+00	6.62E+03	5,28E-01	1.30E-02
9023	4	SS316 jacket	8.03E+00	4.79E+03	3,58E-02	2.26E-02

The operational nuclear heating is imposed by neutrons from the ITER 14 MeV neutron source and by secondary particles emitted promptly upon the nuclear interaction process in the materials of the IVVS/GDC system and its surroundings. The heating was calculated in the same cells of the model as in the neutron flux calculation. Photon heat deposition is dominant for the total heating in heavy materials such as steel and copper. For the light mass element beryllium neutron heating is the main contributor to nuclear heating. The results of total (neutron and photon) heat deposition during ITER DT-operation are presented in Table 1 for the MCNP cells of the GDC electrode head. All results in that region have a statistical

error of less than 10%, which is acceptable for the used MCNP F6 tallies. The maximum operational heating of about 0.6 W/cm^3 is observed for the copper cap (CuCrZr-IG alloy) of the GDC tip. The total nuclear heat in the GDC electrode (Be, CuCrZr, and steel parts) is 3.2 kW.

Activation and inventory

Given the neutron flux distributions in all cells of the IVVS/GDC system and its surrounding the activation of the materials have been calculated using the first step of the R2S code system. Each FISPACT calculation provides not only the decay-photon sources for the shutdown dose calculations (in the following chapter) but also specific activities for both irradiation times and for each cooling time step.

An assessment has been conducted on the activation levels of the IVVS/GDC components and their classification according to French radwaste regulations, adopted by ITER. Accordingly, radioactive waste can be classified depending on specific nuclides' activity, half-life and radio-toxicity. A so-called LMA limit (maximum level of activity) discriminates low active A-type waste from medium active B-type waste; only those types are relevant for ITER tokamak components.

To have a conservative estimate regarding waste treatment and strategy for dismantling of the device the full 20 yr SA2 operation has been considered and also 12 d after shutdown, which is the most convenient cooling period before access to the tokamak. All components, except the Be protective layer of the GDC probe, could be clearly classified as A-type waste. The Be cover will be B-type only due to tritium, whose specific activity is 3.85x10^8 Bq/g (LMA limit: 2x10^5 Bq/g). In the case of the 12 yr irradiation according to the SA2 scenario, the tritium specific activity in Be after 12 d cooling time is 1.37x10^8 Bq/g. This value can be expected from the difference in accumulated neutron wall load between the two irradiation times.

It should be noted, that the mentioned values correspond to accumulated tritium during ITER operation (12 yr or 20 yr) without consideration of release due to ambient temperature. Although it is expected a nearly full release above 900 K due to a complete network of open porosities [3], the tritium concentration might be still considerably above the LMA limit. For maintenance and waste separation considerations it can be concluded based on the activity results, that only the Be layer of the GDC head has to be treated separately from the other parts of the IVVS/GDC plug.

Shutdown dose and absorbed heating

Shutdown decay-photon heating calculations have been performed both for the MCNP5 cells of IVVS/GDC and also on a mesh superimposed over IVVS/GDC and its close surrounding. The methodology applied for these calculations is based on use of well validated and benchmarked Rigorous 2 Step (R2S) approach.

The FISPACT calculations for all cells provided the photon source distributions in each of these cells for both irradiation scenarios at the requested cooling times. Those output files can be read in by a specifically designed MCNP source routine. MCNP5 has been modified with this R2S photon source routine and this tailored version has been used to simulate the decay-photon transport in the activated components. As the photon heating is obtained in MeV/cm^3/s the tally results have to be multiplied by 1.602x10^{-13} for results in units of W/cm^3, which are presented here. For results in units of Gy/s the additional conversion is achieved by dividing by mass density and multiplying by 1000. For this task typically 2x10^8 histories have been simulated for each case, using about 670 CPU*h on 56 CPU at the HC3 Cluster of KIT.

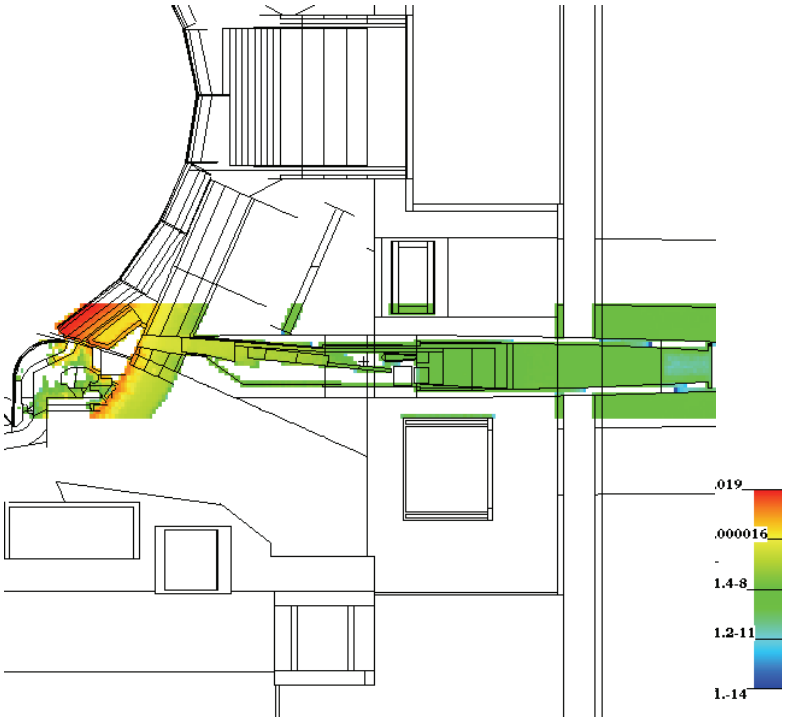

Fig. 2: Map of decay-photon heating distribution after 20 yr operation at cooling time 0 s [W/cm^3].

For the two irradiation times of 12 and 20 yr, a set of dose rate maps have been produced for the requested cooling times. For the full life-time irradiation, it turns out, that even immediately after shutdown the maximum decay-photon heating is only about 4 mW/cm^3 at the Cu heat sink of the GDC probe, which is less than 1% of the respective maximum operational heating. The decay-photon heating decreases rapidly to values of the order of 10^{-8} W/cm^3 at the entrance to the bioshield. As those values refer to the moment of ITER shutdown it can be stated, that the heating due to decay-photons is insignificant compared to the nuclear heating during operation. After 12 d of cooling time the decay-photon heat is reduced by two orders of magnitude in the GDC tip. Those results are listed in Table 2 (in units of Gy/s) in comparison with the respective operational nuclear heat. The absorbed dose values in Gy/s are obtained from W/cm^3 by dividing with mass density times 1000.

Table 2: Decay-photon heating after 20 yr operation (at 0 s and 12 d cooling times) and operational neutron/photon heating (in Gy/s) at the GDC tip.

Cell no.	Material	Oper. dose [Gy/s]	Abs. dose at 0 s [Gy/s]	Abs. dose at 12 d [Gy/s]
9020	CuCrZr heat sink	67.3	0.47	3.9E-3
9021	Be layer	286	1.4	4.1E-3
9022	SS316IG core rod	24.1	0.08	1.2E-3
9023	SS316IG shaft	4.5	0.03	6.4E-4

Conclusion

A neutronics analysis on operational heating in the GDC head and on activation and absorbed dose rates in the IVVS/GDC has been conducted. With regard to the design issues one can conclude that absorbed doses in the system behind the vacuum vessel are of minor concern compared to the operational heating imposed on the GDC head. The GDC head in

shielding position provides an efficient shield assuming rather narrow gaps, as in the present neutronics model. With regard to waste management only the Be layer of the GDC electrode are likely to be disposed as type-B class waste. As the present analysis could only address certain neutronics issues a continuation and extension of the work has been proposed.

Staff:

A. Serikov
D. Leichtle
U. Fischer

Literature:

[1] Y. Chen, U. Fischer, Rigorous MCNP based shutdown dose rate calculations: Computational scheme, verification calculations and applications to ITER, Fus. Eng. Des. 63-64 (2002), pp. 107-114

[2] M. J. Loughlin, N. P. Taylor, Recommended Plasma Scenarios for Activation Calculations, IDM Number: ITER_D_2V3V8G v 1.1, ITER organization, 28 October 2009.

[3] E. Rabaglino et al., “Recent progress in the modelling of helium and tritium behaviour in irradiated beryllium pebbles”, Fusion Eng. Des., 69, (2003) 455-461

Acknowledgement

This work was supported by Fusion for Energy under the service contract No. F4E-OPE-144-01 (ES-AC). The views and opinions expressed herein reflect only the author’s views. Fusion for Energy is not liable for any use that may be made of the information contained therein.

NB Upper Port Shielding Block – Neutronic Analysis (ITER IO/10/4300000148; EFDA HPC-FF MCFUS-2)

Objective

In the framework of this contract a neutronic analysis has been performed for the ITER upper ports in the Neutral Beam (NB) cell. The aim of this work was to assess radiation shielding properties and to provide neutronic service for the designing of the upper port in the NB cell.

Neutronic analysis

The design of the port insertion has been developed at ITER Organization and it featured a diagnostic tube, a cap, and a shielding block. At KIT this design represented in CAD CATIA model has been adapted for neutronic calculations, converted by means of the McCad graphical interface code to the Monte Carlo MCNP5 model, and used for radiation transport calculations. State-of-the-art nuclear data library FENDL-2.1 has been used in radiation transport calculations. Radiation transport provided valuable results of neutron gamma fluxes, as well as energy spectra, and distributions of nuclear heating and other nuclear responses inside the upper port and its surroundings (TFC and PFC superconductive magnets) which are useful for the purposes of farther design development of the upper port in the NB cell. Fast neutron fluence, local and integral nuclear heating, and peak absorption dose in the insulation have been calculated in the parts of the TFC and PFC segments located around the upper port. The results are satisfactory in terms of the radiation design limits for all the nuclear responses in the magnets. For the radiation deep-penetrating calculations, a mesh-based weight-windows generator has been used as the MCNP5 variance reduction technique, demonstrating substantial benefits in gaining of statistical precision and saving of computation time.

Applied computational approach also included activation analysis of the port and the adjacent ITER components (blanket, vacuum vessel, TFC, PFC magnets, cryostat) with the FISPACT-2007 code and the EAF-2007 European Activation File. The activation results produced gamma intensities and energy spectra of decay gamma sources in the irradiated materials after 106 s of cooling time. Neutron irradiation was set according to the ITER SA2 safety scenario. These gamma sources have been supplied using the R2S Rigorous 2-Step method for MCNP5 gamma transport calculations to get gamma flux distributions, which were converted by the ICRP74 fluence-to-dose conversion factors to obtain shutdown dose rates. The distributions of neutron and gamma fluxes, nuclear heating and shutdown dose rates have been calculated using the superimposed MCNP5 fmesh-tallies. Visualization of the mesh-tallies in form of isoline colour maps has been widely applied in this work, making clear presentation of the distributions. Applied in this work R2S mesh-tally capability allowed to extend shutdown dose rate calculation for the non-segmented MCNP models, which use with the mesh-based weight windows is beneficial to speed-up neutronic calculations including assessments after shutdown.

Due to the necessity to provide a fine mesh segmentation for the decay gamma source generation, in view of the computer memory limitation the area of the upper port in the NB Cell was split in two areas of mesh-tallies for decay gamma source calculation: Rear- Mesh-Area-I, and Front-Mesh-Area II. The dose equivalent rate inside the port extension is formed predominantly by decay gamma sources distributed in materials of Rear-Mesh-Area I. The dose in port extension is formed locally. The effect of decay gamma sources originated in Front-Mesh-Area-II in contribution to the dose inside the spherical detectors at front wall of the port extension is estimated on a level of few percents (1%-5%), as maximal values at the entrance to the port. The shutdown dose rate inside the port extension is distributed over a range from 96 microSv/hr to 10 microSv/hr after 106 s of cooling time. This is below the 100 microSv/hr limit giving a possibility for personnel access to the port. No additional shielding is required.

Staff:

U. Fischer
S. Schreck
A. Serikov
P. Spaeh
D. Strauß

Acknowledgement

This work was supported by ITER Organization under the service contract No. ITER IO/10/4300000148. The views and opinions expressed herein reflect only the author's views. The ITER Organization is not liable for any use that may be made of the information contained therein.

Assessment of the Suitability of Neutron and Gamma Detectors in the Future Experiment at JET for the Validation of Shutdown Dose Rate Prediction (JW9-FT-5.31)

Assessment of the Suitability of a CdTe Gamma-ray Detector for Measurements at JET

Deliverable 5 - Irradiation Tests of CdTe Detector with DT Neutron Generator and Mock-up (KIT)

Objective

Local shut-down dose rate assessments for areas near a fusion reactor vessel are necessary input for the design of maintenance schemes and accident scenarios and hence also of importance for the licensing procedure.

A CdTe detector for gamma-ray spectrum measurements as close as possible to the activated JET reactor vessel is tested. Such detectors are very small and light and therefore well-suited for measurements near the JET vessel especially in places with very limited space.

Aim of this work is the preparation of spectra measurements in JET in the vicinity of the vacuum vessel. These spectra will provide information on contributions to the local gamma-ray dose rate and help to identify missing materials in models for shut-down dose rate calculations.

Status of the work

In a first step, a commercially available CdTe detector was characterized with gamma calibration sources. Further work was delayed due to technical reasons. The neutron generator resumed operation in November 2010.

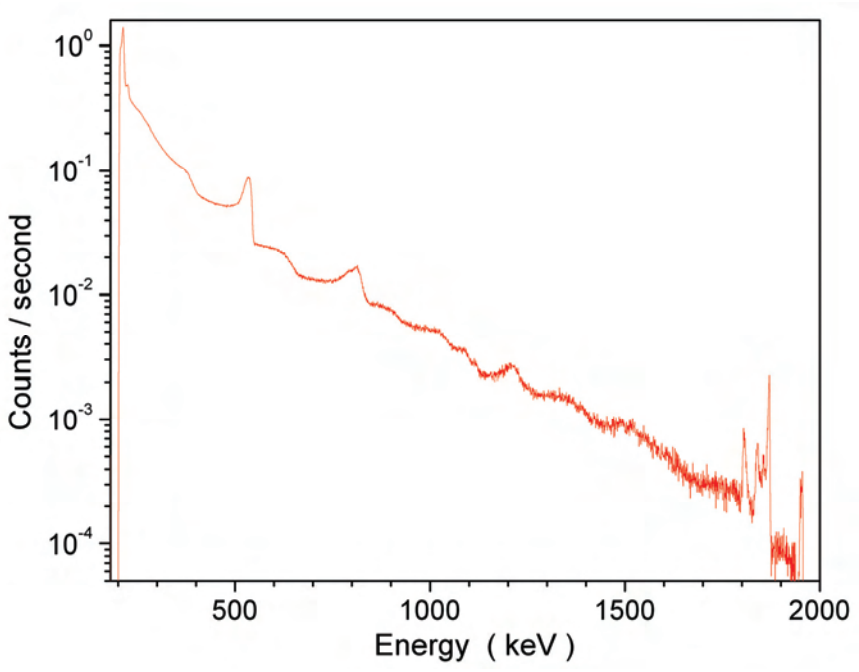

Fig.1: Gamma-ray spectrum of the activated target assembly of the neutron generator recorded with the CdTe detector system.

In order to evaluate the suitability of this detector system for the intended measurements at JET, gamma ray spectra of irradiated steel samples have been recorded. Figure 1 shows such a gamma-ray spectrum of the activated target assembly of the neutron generator of TU Dresden after operation of the generator. The neutron generator was operated with a deuteron current of approximately 1 mA impinging on a TiT target for about 30 minutes. This configuration produces typically about $1...3*10^{11}$ neutrons per second in 4π. The spectrum shown in Figure 1 has been recorded about 15 hours after shut-down of the machine. At this time, the gamma dose rate at the position of the detector was 30 µSv/h measured with a commercial dose rate meter TOL-F (Berthold Technologies). Further analysis is underway.

Staff:

A. Klix
S. Villari (FNG / ENEA Fusion and Nuclear Technologies Department, I-00044 Frascati, Italy)

Acknowledgement

This work, supported by the European Communities under the contract of Association between EURATOM and Karlsruhe Institute of Technology, was carried out within the framework of the European Fusion Development Agreement. The views and opinions expressed herein do not necessarily reflect those of the European Commission.

International Fusion Materials Irradiation Facility (IFMIF)

Broader-Approach Activity:
IFMIF Test Cell and High Flux Test Module (BMBF Reference No. 03FUS0008)

Introduction

In the Engineering Validation and Engineering Design Activities (EVEDA) for the International Fusion Material Irradiation Facility IFMIF, which is an element of the Broader Approach activities launched jointly by several European countries and Japan, the German contribution includes engineering tasks for the IFMIF Test Cell and the IFMIF High Flux Test Module. This report covers tasks performed at the Institute for Neutron Physics and Reactor technology at the KIT attributed to the following procurement arrangements (PA's):

- PA TF-1 EU : Engineering design and Validation of the IFMIF High Flux Test Module.
- PA TF-2: Irradiation in fission reactor (Responsible SCK-CEN, contribution by KIT).
- PA TF-4: Other irradiation modules (Responsible CIEMAT, contribution by KIT).
- PA TF-6: Test Cell, Access Cell, Test Module Handling Cell and Technology Rooms.

According to the planning for EVEDA, these tasks will be performed in the timeframe up to 06/2013.

System Overview

The IFMIF facility is dedicated to fusion-relevant irradiation of structural and functional material specimens, with the objective to create an experimentally validated material properties database suitable for design and licensing of future fusion power plants. The facility is composed of several subsystems, namely the 40MeV 250mA deuteron accelerator facility (AF), the lithium target facility (LF) and the test facilities (TF). The Target- and Test Cell (TTC) is part of the test facilities, containing the lithium target neutron source and the test modules. It has the primary function to shield the environment against the intense radiation generated by the target, and to safely contain all hazardous materials. Inside the TTC, the target and test modules are arranged, as shown in Fig. 1.

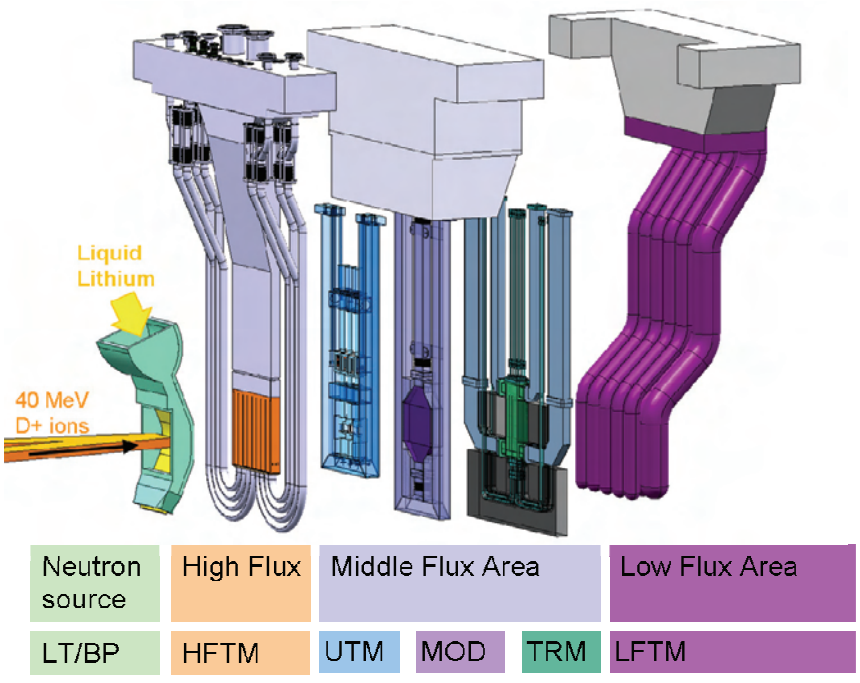

Fig. 1: Overview on the irradiation experiments inside the IFMIF Target- and Test Cell (TTC).

The High Flux Test Module (HFTM) is the irradiation device for miniaturized SSTT samples of structural materials. The HFTM is positioned immediately behind the neutron source inside the TTC. The HFTM contains up to 24 irradiation rigs/capsules with 80 SSTT samples. It is possible to adjust individual temperatures for the specimen in each rig, in the range of 250 – 550°C (A high temperature option 650°C is additionally investigated).

The Tritium Release Test Module (TRM) is filled with specimen of tritium breeding materials, such as Li_2SiO_4, Beryllium, and others. The tritium release can be measured in situ during the irradiation, and the change in specimen structure (porosity etc.) can be examined after the irradiation.

Engineering Design and Validation for the HFTM

HFTM-Assembly engineering design

The overall design of the HFTM-Assembly has been frozen for the engineering analyses at the status of 12/2009. A list of requirements has been proposed and agreed, against which the performance of the design can be compared. Furthermore, the most important boundary conditions for the neighboring components and the associated remote handling procedures and neighboring components have been compiled and distributed.

The focus of the analyses was on the thermal performance of the HFTM. It was proven by CFD analyses, that the system of heaters, insulation gaps and cooling channel can be used to adjust all irradiation temperatures in the required range of 250-550°C. It was furthermore shown in these analyses, that the non-uniformity of the specimen temperature field inside the capsules is limited to the allowed range of 3%. Additionally, the transient behaviour of the HFTM was investigated:

- The time to reach steady state after beam start-up is approx. 5 minutes
- The time to cool the specimen below 200°C after beam shut down is approx. 15 minutes
- Beam-off with continued cooling leads to temperature drop of approx 1K/s
- For loss of cooling, there is an intervention time of (i) 30 seconds for beam-on plus electrical heating, (ii) 50 seconds for only beam-on, and (iii) more than 10 hours for decay heat only, in order to limit the temperature rise to 100°C over the previous irradiation temperature.

The given transient data give valuable input to the design of the test facility control and safety features.

The ability to model the steady state and the transient cases by CFD has been tested against experimental data from the ITHEX experiments. It was shown, that the v2f model of STAR-CD is the most successful to simulate the experimental heat transfer data in the relevant Reynolds number range of $6000 < Re < 9000$. Application of the v2f model to the HFTM geometry has shown however, that the v2f model is very difficult to handle numerically for large models. Further improvements are therefore necessary.

HFTM Irradiation Capsule and Rig

The irradiation capsule, which contains a set of material specimen for irradiation inside the HFTM, was already developed and analyzed to a considerable degree of maturity. Detailed production drawings and instructions were developed for the capsules, including also the necessary quality assurance. The parts for six capsules have been manufactured. They will be assembled and filled with material test specimens, to be delivered to the BR2 reactor for irradiation in 04/2011.

HFTM Mockup experiments

The HFTM single rig experiment aims to investigate the behaviour of a 1:1 rig inside a compartment mockup. The experiment allows to measure pressure drop, flow distribution, capsule and rig temperatures and rig wall deflection for realistic thermal boundary conditions. The compartment mockup has been finalized, and integrated into a test stand adapted for the ITHEX gas loop. The measurement techniques for capacitive displacement measurement and high temperature strain measurements of the rig wall have been experimentally qualified. Manufacturing documents for the dedicated rig parts have been created, and the delivery of the first test rigs is expected in 01/2011.

The HFTM double compartment experiment is the first HFTM container mockup, with a reduced number of compartments (2 instead of 8), but otherwise similar geometry and manufacturing procedures as the HFTM. The experiment therefore represents the first validation of all manufacturing technologies needed for the HFTM, and will also allow relevant measurements of the HFTM container mechanics under operation conditions in the HELOKA-LP helium loop. A CAD model for this experiment has been derived.

Engineering Design of the Target- and Test Cell

The design of the TTC based on the MTC concept has been further developed in the year of 2010 with emphasizes on the following aspects:

- Performing functional analysis on the TTC to identify the detailed technical requirements on the TTC design;
- Optimizing the inner enclosure of the TTC and the attachment means between the vessel and the concrete;
- Performing engineering designs on key elements, including Test Module Interface Heads (TMIHs), the pipe and cable connections [6], the supporting and transferring system for the TMs, in the TTC;
- Introducing additional shielding materials based on neutronic calculations in the TTC [6].

Two modification proposals on the inner enclosure of the MTC have been introduced. To minimize the deformation of the vessel and the supporting structure for the TMs and to guarantee accurate positioning of the TMs against the BP of the target assembly, the cylindrical vessel is directly embedded in the shielding concrete. The intermediate ring and supporting/positioning structure of the TMs keeps untouched. Another proposal, named as MTC-L (MTC-Liner), intends to use liner-on-concrete arrangement instead of using independent TTC vessel in the MTC design. Two permanent concrete walls covered with liner are proposed to hold the TM positioning system instead of using the removable intermediate ring in the MTC design. Both of the proposals fix the vessel or liner on the concrete wall and keep the TMs separating from the shielding materials. The final shape and arrangement of the inner enclosure of the TTC will be decided in the year of 2011.

A summary of the pipes and cables that will penetrate the TTC from the TMs has been outlined. Besides the LFTM whose conceptual design is not available, around 59 pipes and 1000 cables are required to penetrate the TTC. The number of pipe connectors to be handled by RH tools has been reduced by approximately 40%, comparing to the number of pipes that are connected to the TMs. In addition, industrial solutions on quick multi-connector coupling systems for the cables and pipes were being investigated.

Neutronic calculations in the TTC are being performed and the preliminary result suggested that the cable connectors may suffer a high dose rate under which conventional insulation materials, like PEEK, can only survive for a couple days. A shielding plate made of lead is proposed to be installed between the pipe/cable connectors and primary radiation sources to

extend life span of electric insulation materials. With this shielding plate, the conventional shielding materials are expected to reliably function for a complete irradiation campaign. The proposed shielding plate can be seen in Fig. 2.

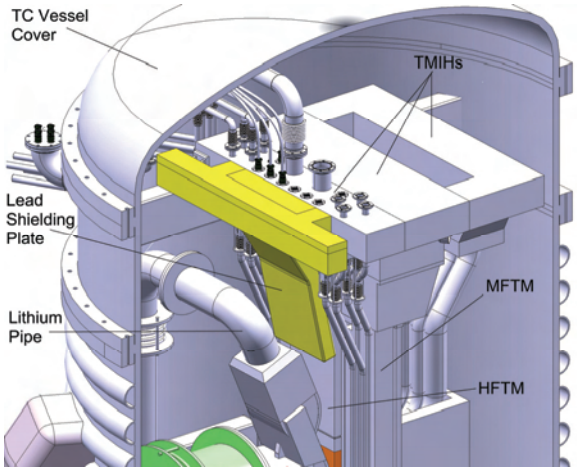

Fig. 2: The lead shielding plate between the TMIH for the HFTM and lithium pipe.

HELOKA-LP test facility

In 2010, the HELOKA-LP test facility has been operated in several campaigns to produce data on the steady-state and transient behaviour, and to optimize the control parameters. The control parameters have been optimized, to enable massflow transients with reduced pressure peaks at the test section inlet, as a means to reduce the cyclic loads on the HFTM. The optimization has reduced the pressure peak from +0.75bars down to +0.08bars.

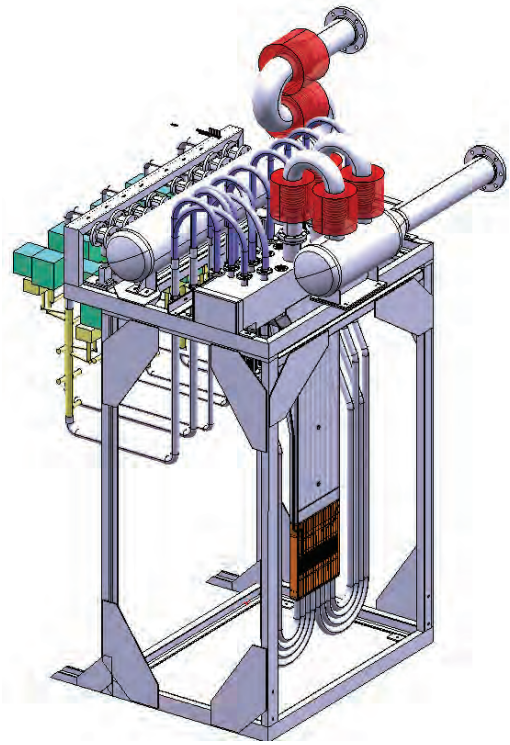

Fig. 3: 3D CAD design of the HELOKA TS-Port integrating the IFMIF High Flux Test Module prototype.

The first HELOKA-LP campaigns were also used to monitor the helium quality. A remarkable result is the low concentration of oxygen, below 5ppm. The absence of oxygen is preliminarily explained by the operation of the activated charcoal filter installed behind the compressor. Generally, the total amount of impurities increases at a rate of approx. 1000ppm/month. The most abundant species is nitrogen, originating from the surrounding atmosphere. These findings stress that a long term operation facility such as the helium cooling system for IFMIF (part of PA TF-6) will need effective helium cleaning devices.

The HFTM Test section port is the device to incorporate the HFTM prototype into the HELOKA-LP facility. This device, with the functions of supporting the HFTM and providing the coolant flow distribution has been designed as a detailed 3D CAD model (Fig. 3). Components (manifolds, valves, instrumentation) have been arranged to fit into the reserved space at the HELOKA-LP facility. A similar mechanical attachment as in the IFMIF Testcell is provided, using the HFTM Interface Head. The loads on the pressure vessel were calculated according to the AD2000 code.

For 2011, more steady state and transient cases will be compiled as a benchmark set for numerical loop models (RELAP, TRACE), which are currently under preparation. The test section port will be built and integrated into the loop to host the double compartment experiments.

Staff:

F. Arbeiter
Y. Chen
B. Dolensky
J. Freund
T. Heupel
Ch. Klein
M. Mitwollen
A.-L. Muche
N. Scheel
G. Schlindwein
P. Schubert
K. Tian
K. Zinn

Literature:

[1] Tian, K., Arbeiter, F., Eilert, D., Heinzel, V., Heupel, T., Mittwollen, M., Concept and engineering design of the IFMIF target and test cell. (2010), Jahrestagung Kerntechnik, Berlin, 4.-6.Mai 2010

[2] Chen, Y., Arbeiter, F., Heinzel, V., Stratmanns, E., Key parameters for controlling the specimen temperature in IFMIF high flux test module. (2010), Jahrestagung Kerntechnik, Berlin, 4.-6.Mai 2010

[3] Arbeiter, F., Heinzel, V., Scheel, N., Heupel, T., Dolensky, B., Chen, Y., Status of design and validation tasks for the IFMIF high flux test module. (2010), Jahrestagung Kerntechnik, Berlin, 4.-6.Mai 2010

[4] Chen, Y., Arbeiter, F., Heinzel, V., Schlindwein, G., Numerical simulations on transient conjugated heat transfer within IFMIF high flux test module. (2010), 8th Internat. Topical Meeting on Nuclear Thermal Hydraulics, Operation and Safety (NUTHOS-8), Shanghai, China, October 10-14, 2010

[5] Tian, K., Arbeiter, F., Eilert, D., Heinzel, V., Heupel, T., Mittwollen, M., New progresses in the IFMIF target and test cell design and a proposal for the specimen flow. (2010), Proc. of the 18th Internat. Conf. on Nuclear Engineering (ICONE-18), Xi'an, China, May 17-21, 2010

Acknowledgement

This work was financially supported by the Ministry of Research and Education (BMBF) under the grant No. 03FUS0008 and is done in the Project IFMIF/EVEDA under the Broader Approach Agreement between Europe and Japan. The views and opinions expressed herein do not reflect necessarily those of the BMBF or the European Commission.

Broader-Approach Activity:
IFMIF EVEDA
Neutronics for IFMIF Creep-Fatigue Test Module
(BMBF Reference No. 03FUS0008)

Introduction

The purpose of the International Fusion Materials Irradiation Facility (IFMIF), which is a deuteron-beam based intense neutron source, is to reproduce as close as possible the irradiation conditions for structural and functional materials in future fusion reactors. In addition to the express irradiation of structural materials to high doses in the high flux test module, the in-situ creep-fatigue and the tritium release test module are foreseen in the medium flux area of the IFMIF.

In this report the irradiation conditions at various parts of the IFMIF Creep-Fatigue Test Module taking into account recent design changes with a focus on the part where electronic and electric part will be installed, were investigated.

Method

The d-Li neutron source and neutron transport were simulated by Monte Carlo code MCDeLicious, which is an extension to MCNP5 with the capability of simulating the generation of neutrons, γ-rays and other d-Li reaction products on the basis of the evaluated Li(d,xn) reaction cross section data.

Comprehensive three dimensional IFMIF test cell geometry model for Monte Carlo calculations developed in the frame of Task TW4-TTMI-003 D5a was used in this study. The model was modified to reflect the latest design modifications of the CFTM.

Since d-Li IFMIF neutron source generates neutron spectrum extending up to 55 MeV, the neutron transport, activation and transmutation calculations require cross sections exceeding the traditional limit of 20 MeV.

CFTM Geometry

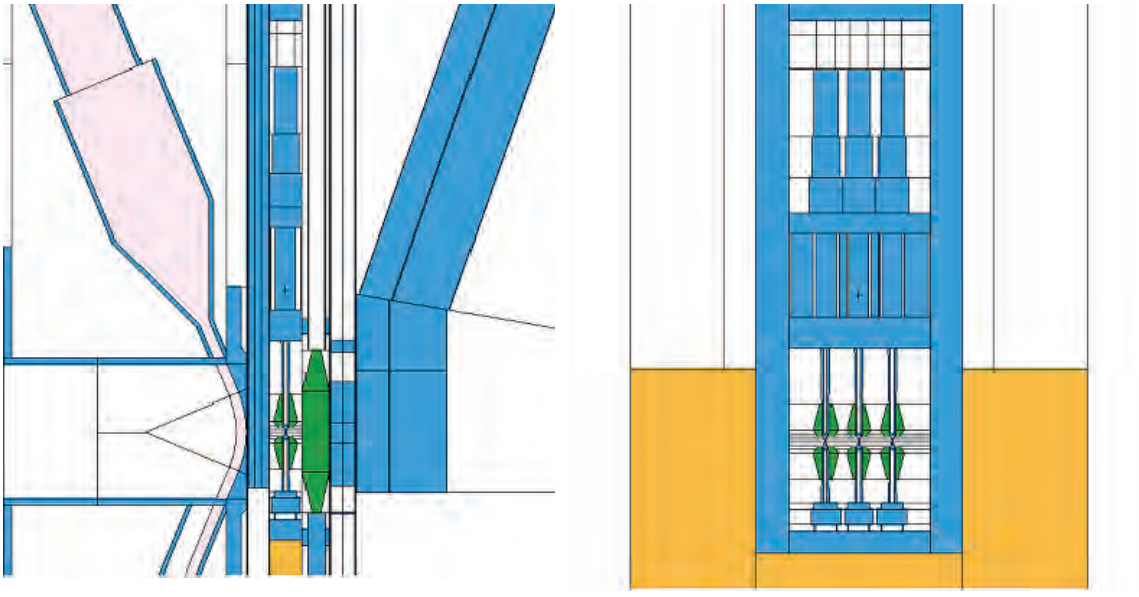

Fig. 1: IFMIF test cell: side (left) and front (right) views.

Side and front views of the IFMIF test cell with respect to the direction of the deuteron beam are shown in Fig. 1. Arrangement of liquid lithium target, high-flux test module (HFTM) and creep-fatigue machine followed by tungsten spectral shifter plate and tritium release module is presented on left part of the figure. Three creep-fatigue specimens, hollow sample holders and tungsten heating bodies as well the frame of creep fatigue machine are shown on the right.

Results

The neutron and gamma induced heating at actuator electric motors situated approximately 70 cm above the creep-fatigue samples were calculated and amount to 1 and 30 Gray/s respectively. This corresponds to the annual dose (with account of 70% availability) about 60 MGray/year. At the same time the radiation induced displacement damage is less than 0.02 dpa/year.

The heating generated at extensometers, which are placed inside the actuator boxes is slightly higher 7 Gray/s for neutrons and practically the same 30 Gray/s for gammas.

Estimated dose near the strain gauges is from 50 to 100 MGray/year.

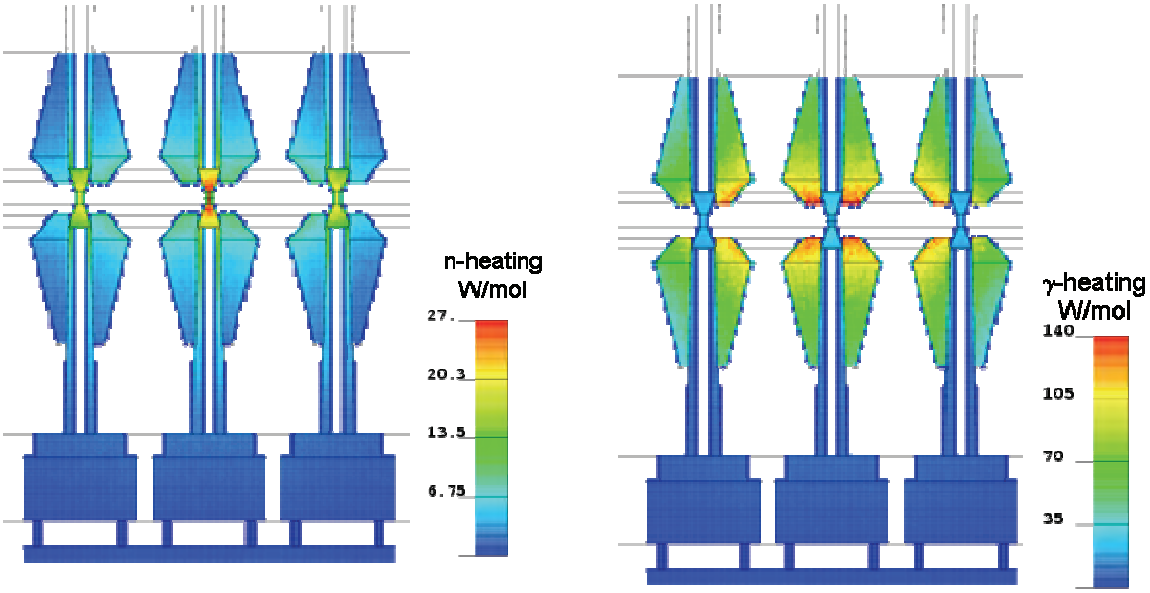

Fig. 2:Neutron (left) and gamma (right) heat depositions in W/mole generated in the middle cross section of the central creep-fatigue specimen (cut along the beam) imposed over the test cell geometry.

Three dimensional heat distributions through the specimens and heating bodies necessary for the thermohydraulic analysis are shown in Fig. 2.

Neither displacement damage nor heat deposition in the samples was affected by the changes of the CFTM design.

Conclusions

The following conclusions relevant for the IFMIF CFTM design can be drawn based on the results of this study.

- Major material responses show only moderate changes against fine details of CFM design.

- In particular, total heat deposition in the c/f samples is ~ 1 W/g in the central and 0.75 W/g in the peripheral samples. Contributions from neutrons and gammas are nearly equal.
- Damage rates remain unchanged: 13 dpa/fpy and 10 dpa/fpy in the central and the peripheral samples respectively.
- Heat deposition in the heating bodies comes mainly due to gammas: 0.3-0.7 W/g in the central and 0.2-0.6 W/g in the peripheral bodies.
- Annual (70% availability) energy deposition at radiation sensitive parts :
    - Motors – 60 MGray
    - Extensometers – 175 MGray
    - Loading cells – 130 MGray
- Materials for wire isolation and isolating substrate for strain gages should be radiation resistant, hence polymer materials should be avoided**.**

Staff:

U. Fischer
A. Möslang
P. Vladimirov

Literature:

[1] P.V. Vladimirov, A. Möslang, *Irradiation Conditions for Breeder Materials in Tritium Release Module of IFMIF*, 14th International Conference on Fusion Reactor Materials, September 6-11, 2009, Sapporo, Japan

[2] P.V. Vladimirov, A. Möslang, *Neutronics for IFMIF Creep-Fatigue Test Module (revisited)*, 3rd IFMIF Workshop, Sept. 20-22, 2010, Madrid, Spain

[3] Arbeiter, F.; Fischer, U.; Heinzel, V.; Klix, A.; Möslang, A.; Simakov, St.; Tian, K.; Vladimirov, P.; Garin, P.; Heidinger, R., *IFMIF test facilities - 3 years of EVEDA*, Jahrestagung Kerntechnik 2010, Berlin, 4-6 Mai 2010, Berlin : INFORUM GmbH, 2010, published on CD-ROM, Paper 810

Acknowledgement

This work was financially supported by the Ministry of Research and Education (BMBF) under the grant No. 03FUS0008 and is done in the Project IFMIF/EVEDA under the Broader Approach Agreement between Europe and Japan. The views and opinions expressed herein do not reflect necessarily those of the BMBF or the European Commission.

Fuel Cycle –
Vacuum Pumping

Final Upgrade of TIMO-Facility (TW5-TTFF-VP 58, F4E-2009-GRT-019-01)

Background and objectives

Following successful completion of the testing of the model pump, a full scale ITER torus pre-production torus cryopump (PPC) is being designed and constructed for testing in the TIMO facility. Certain features of the TIMO infrastructure need to be upgraded to accommodate the larger ITER-scale pump and to operate it according ITER requirements, and the scope of this task was to provide for the supply and installation of these features so as to have a replication of ITER conditions in many aspects for the new pumps. The fully upgraded facility is called TIMO-2. In the reporting period, the enhancement activities towards TIMO-2 were continued and all contractual activities could be completed.

New operation mode for TIMO-2

The KIT TIMO-2 facility is the only available EU facility capable of testing a real size ITER torus cryopump by providing the necessary cryogenic flow rates at different temperature levels between 4.5 K and 470 K. ITER now proposed to operate with lower inlet temperatures of 4.35 K so as to allow for a higher temperature difference across the cryopanels and, consequently, to reduce the needed cryogenic mass flows. In order to accommodate such an inlet temperature reduction, the present TIMO-2 facility, previously used for testing the ITER model cryopump with 4.5 K supercritical helium (ScHe), must be upgraded. This was provided under the F4E Grant F4E-2009-GRT-019.

To reach the lower temperature level inside the ScHe cooling circuit it was necessary to reduce the boiling pressure of the helium bath (which is used to adjust the temperature of the ScHe stream via heat exchange) from 1.3 bar(a) down to close to ambient pressure. To provide this pressure reduction inside the control cryostat a new pressure measurement and control device for the gaseous helium volume was installed. In parallel to this modification in the control cryostat, the available compressor units at the 2 kW LINDE facility were modified such that they can cope with these reduced intake pressures. The signal of the new pressure measurement was integrated to the TIMO-2 PLC (Siemens PCS7) as well as to the PCS7 of the 2 kW LINDE facility and is now used to control the pressure reduction inside the control cryostat by regulation of the compressors of the 2 kW LINDE facility.

Refurbishment of the valve box

In order to achieve the 4.35 K requirement at the inlet of the pump, it was necessary to reduce the thermal losses on the way between the cryostat and the TIMO-2 test vessel to an absolute minimum. The final step of these modification activities was the optimisation of the piping inside the TIMO valve box and the instrumentation for the temperature measurement as well as the pressure measurement.

To have more analytical options, additional temperature sensors were installed inside the TIMO-2 valve box. The piping system inside the valve box was improved in terms of better insulation of the pipes; now, all temperature sensor holders inside the valve box are integrated in the multi-layer thermal radiation insulation (MLI), see Fig. 1. Also the thermal anchoring of the temperature sensors was improved; between the feedthrough and the sensor holder all the electrical cables of the temperature sensors have in the new configuration a connection with the 80 K shield. The aim of these modifications, shown in Fig. 2, was to reduce the heat transfer via radiation between the 80 K shield and the sensor as well as the heat load via the sensor cable from 300 K to the temperature sensors at 4.5 K level.

The final step was a very careful check of all contributions to the data acquisition and measurement chain, in order to have a correct measurement at the requested very high resolution in absolute terms.

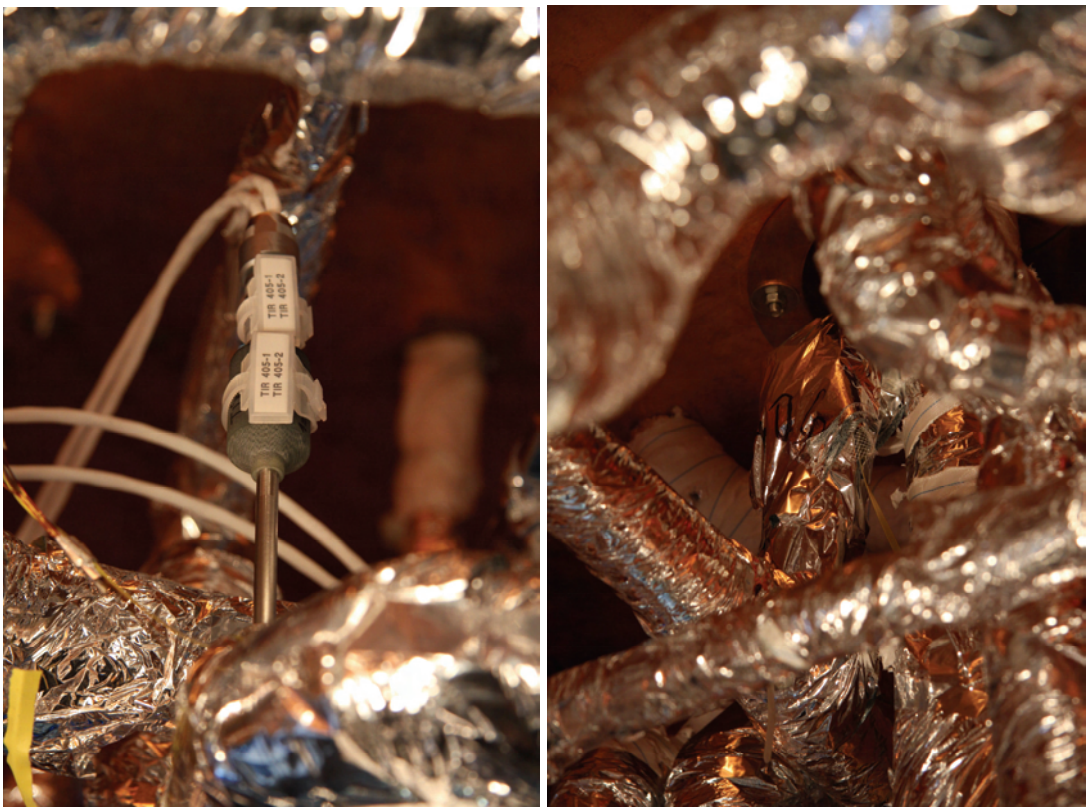

Fig. 1: Installation situation of the temperature sensor holder before and after the revision activities.

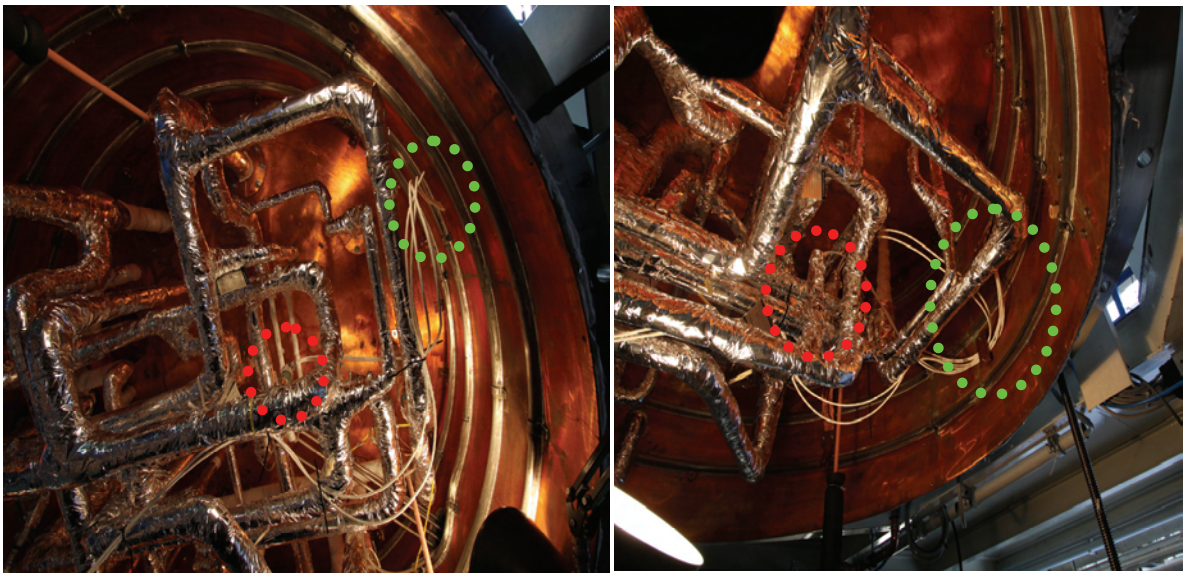

Fig. 2: Original (left) and modified installation situation (right) at the temperature holder (MLI wrap, red circle) and the sensor cabling (thermal anchoring, green circle).

Demonstration test run

Following the F4E Grant F4E-2009-GRT-019 Technical Specification requirements, a demonstration of the new TIMO operation mode was performed on 17th of November 2010. For this purpose, a dummy shortcut between the cryolines was used as test component. During the tests of the cryopanel cooling circuit, the ScHe mass flow was increased stepwise up to 200 g/s. The test objective was to show that the TIMO-2 cryosupply can provide ScHe at 0.4 MPa and 4.35 K (inlet of the test component) at a flow rate of approximately 200 g/s (ITER-relevant range) and ITER-relevant pressure losses.

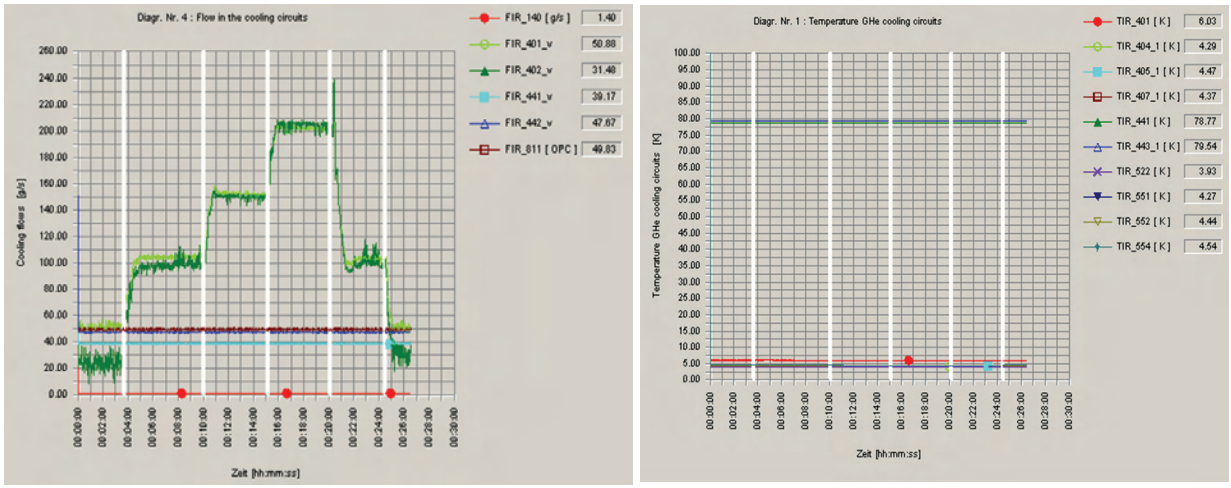

Fig. 3: Online screenshot of the performed demonstration tests for the 4.35 K operation mode which shows the variation of the ScHe mass flow (left side) as well as the corresponding temperature (right side) inside the cooling circuits (cryopanel and thermal shields circuits).

The demonstration tests were very successful, all requirements could be met. The measured pressure drop value at a ScHe mass flow rate of 200 g/s was 120 mbar. In view of the expected pressure drop values of ~45 mbar for the cryopanel circuit of the ITER PPC and the design data of the used Barber Nichols Blower in the TIMO-2 control cryostat with 400 mbar@200 g/s, sufficient safety margins are available for a robust performance of the PPC tests.

New 100 K supply facility for TIMO-2

One key result of the previous experimental campaigns with the ITER model pump was that the standard regeneration of the PPC requires 90 K. Hence, ITER will provide 100 K for this operation mode. In preparation of the planned PPC test programme in TIMO-2, a dedicated facility was built up which provides ScHe at this temperature level. The final action was the integration of a 100 K facility into the TIMO-2 cryogenic supply system.

The order for the 100 K facility was given to the company MESSER GROUP. The concept of their solution is based on a liquid nitrogen bath (~ 640 l), pressurized to the boiling pressure at the requested temperature (100 K corresponds to ~ 7.8 bar). The gaseous helium at that temperature is then provided in a secondary loop via heat exchange against the boiling nitrogen. The order included the facility itself, all the necessary transfer lines and the process control system. The project started at the end of 2009. Following the detailed design phase and the manufacturing, the installation of the new facility into the TIMO-2 infrastructure was performed in May and June 2010. During the first acceptance tests, the need for improvements for some parts became obvious. After these optimization activities the integration of the 100 K facility into TIMO-2 was successfully accomplished in October 2010, see Fig. 4.

Conclusions

The TIMO upgrade project is completed and the TIMO-2 facility is ready for the foreseen experimental campaigns with the PPC.

The EFDA Task TW5-TTFF-VP58 and the F4E Grant F4E-2009-GRT-019 were closed.

Fig. 3: The new 100 K facility integrated in the TIMO-2 cryogenic supply system.

Staff:

Chr. Day
A. Demsoreanu
A. Edinger
H. Haas
Th. Johann
R. Müller
P. Pfeil
M. Scannapiego
H. Strobel
H. Stump
J. Weinhold

Literature:

[1] H. Haas, Chr. Day, TIMO-2 – a versatile cryogenic test bed with supercritical helium supply, 23rd Int. Cryogenic Engng Conf. (ICEC), Wroclaw, Poland, July 2010.

Acknowledgement
Part of this work, supported by the European Communities under the contract of Association between EURATOM and Karlsruhe Institute of Technology, was carried out within the framework of the European Fusion Development Agreement. The views and opinions expressed herein do not necessarily reflect those of the European Commission.

Part of this work was supported by Fusion for Energy under the grant contract No. F4E-2009-GRT-019. The views and opinions expressed herein reflect only the author's views. Fusion for Energy is not liable for any use that may be made of the information contained therein.

Completion of Final Design for the Prototype Torus Cryopump (F4E-2009-GRT-018-01)

Background and objectives

The reference design of the ITER exhaust gas pumping includes 8 cryopumps to pump the torus via 5 ducts. The design of these cryopumps has to consider the different requirements for vacuum pumping, remote handling and safety, and provides strong interfaces to the surrounding environment of the installation port plugs of the ITER machine.

The aim of this task is to provide the build-to-print design of the pre-production cryopump (PPC), including the mechanical analysis and various design supporting activities. This task also includes the test of the main valve seal in 1:1 scale.

Design enhancements

The existing design of the torus cryopump as developed by KIT in 2007 [1] was adapted to the changed ITER requirements on the torus cryopumps (see Fig. 1). It is circular shaped with a maximum outer diameter of 1776 mm and a total length of about 2054 mm. The cryopanel system at 4.5 K with a total pumping surface of 11.2 m² consists of 28 cryopanels in a circular arrangement. The outer thermal shield system at 80 K forms an enclosure around the cryopanel system against the heat radiation from inside and outside the cryopump. The pumping speed can be varied by throttling the main valve, which opens towards the torus with a maximum stroke of 470 mm. The valve inlet diameter is 800 mm. The prototype torus cryopump can be separated into four main subassemblies: the pump housing including the pump plug, the thermal shield system, the cryopanel system and the pump inlet valve.

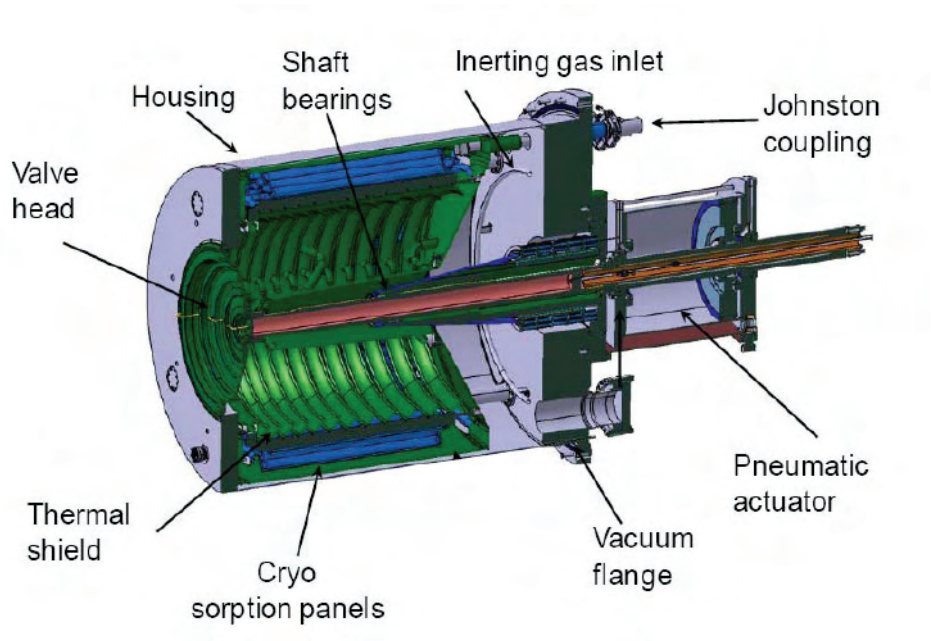

Fig. 1: Basic design of the torus pump as single unit (Axial cut).

In the current detailed design process, the pump has undergone extensive revisions, such as [2]:

- Valve bearings have been moved out of the vacuum space for greater reliability;
- The additional regeneration volume needed for hydrogen safety is now connected to the inner volume of the pump by an external connection (previously, this was done by a connection to the duct volume), allowing effective remote handling;

- The hydrogen safety concept was changed from pure inventory limitation to an active inerting system, thus giving more flexibility.

Any overpressure inside the cryolines is limited by two burst disks (external to the pump). Four Johnston couplings are foreseen as cryo-feedthroughs for the 5 K and 80 K helium supply and return lines.

The pump housing: The KIT design for the housing had to be modified by late design changes coming from IO reflecting new specifications. Now, the IO design of the flanges in the pump plug and the IO design of a lip weld connection between front flange and the cylindrical housing are included in the pump design. The valve seal is now fixed to the housing with a remote handling compatible seal support ring as wished by IO.

The thermal shield system: The design of the thermal shield was finalised in 2009. In 2010 the design was validated by FEM calculations (using ANSYS) which cover the different operation scenarios at ITER, see Fig. 2. The outcome of these results was used also for the FEM calculations of the cryopanel system (see next subsection), because they are coupled e.g. in case of a seismic event.

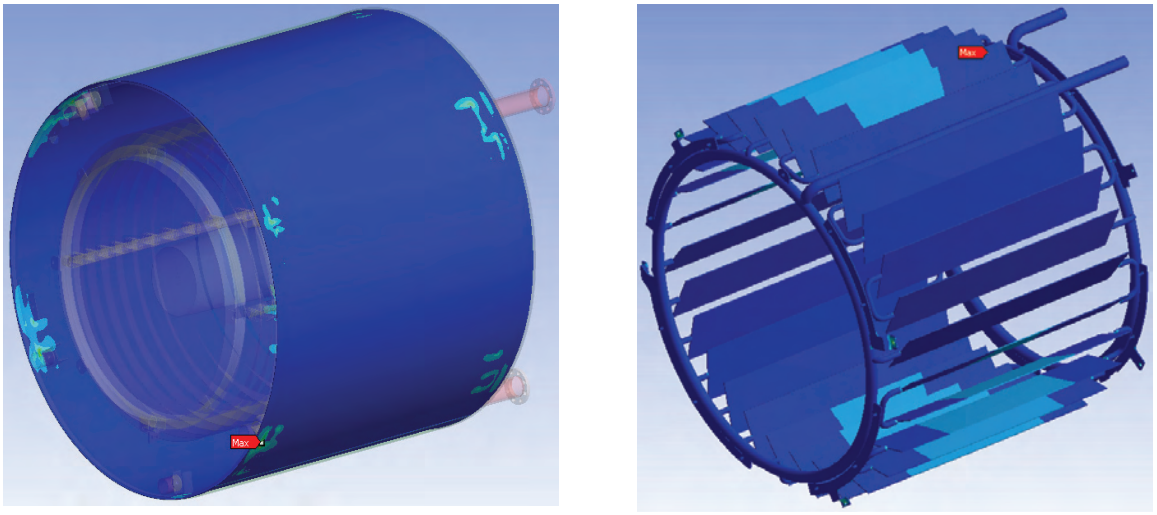

Fig. 2: FEM models for mechanical analysis of the thermal shield system (left) and the cryopanel system (right).

The pressure drops in the PPC thermal shield and cryopanel circuits are critical issues regarding the cryogenic supply. The required mass flows into the cryopump circuits – driven by the heat load on the pump and the required ΔT across the circuits during steady state modes or driven by the allocated time to perform the warming and cooling of the pump during transient regeneration operations – are limited by the pressure loss requirements. Hence, the pressure drops in and the mass flows through the complete thermal shield system at different scenarios were calculated. To support these calculations the front shield of the thermal shield system (see Fig. 3), which is assumed to be the most resistant component, was manufactured in a 1:1 scale and tested in the THEA facility at KIT (please find another specific chapter on thermohydraulic investigations in this annual report) [3, 4]. The internal pressure drops at ITER relevant Reynolds numbers were measured. The calculation results show, that the requirements can be fulfilled with the current design.

The cryopanel system: The design of the cryopanel system was finalised in 2010. The design process was supported by FEM calculations at ITER relevant operation scenarios (see Fig. 2). The results showed that the cryopanel system with advanced supports can withstand all external forces at operation and seismic events.

Fig. 3: Picture of the 1:1 scale hydroformed PPC front shield (external diameter of 1510 mm).

Calculations of the pressure drops for the complete cryopanel system were performed as the required ΔT across the circuits at pumping is very low (0.35 K). The distribution of the coolant (ScHe at 4.35 K) at high mass flows (in total up to 200 g/s) has to be well balanced in all parts to meet this requirement. The most resistant components are the cryopanels which are arranged in 4 groups with seven panels each. One cryopanel was manufactured (Fig. 4) and tested in the THEA facility to support these calculations. The internal pressure drops at high Reynolds numbers (~10^6) were measured in both directions. The calculations showed that the ITER requirements can be fulfilled with the included design, also independent on the installation direction of the panels.

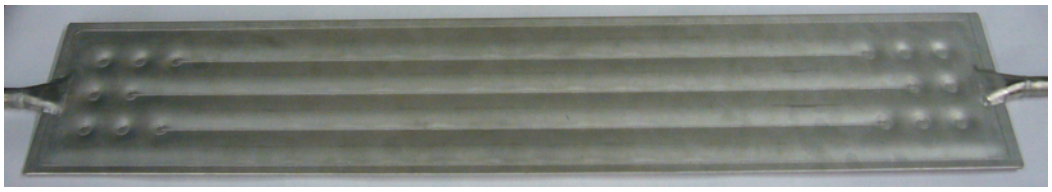

Fig. 4: Picture of one 1:1 scaled hydroformed cryopanel (1m long x 0.2 m wide).

The inlet valve: The inlet valve (see Fig. 5) will be used for throttling of the pumping speed at normal operation as well as to close tight the cryopump at regeneration when the pumped gas is released by heating of the cryopanels. Special emphasis is given to the development of the mechanism of the valve which is the only moving component of the pump (required lifetime of 30,000 open/close cycles).

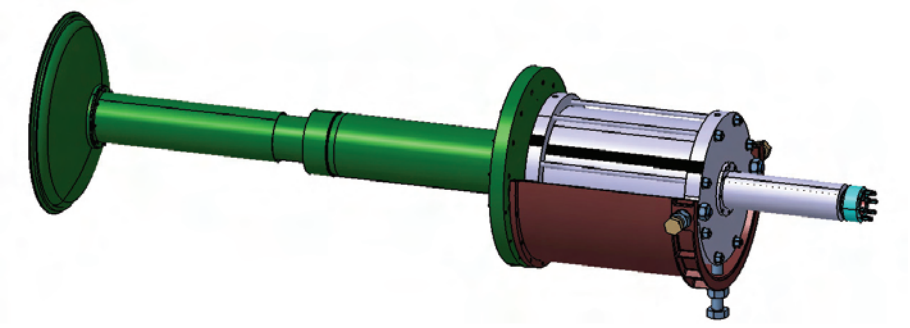

Fig. 5: Inlet valve subassembly of the pre-production cryopump.

To ensure that the required dwell base pressure of $5 \cdot 10^{-4}$ Pa is achieved in the available time, the overall leak rate into the vacuum vessel must be absolutely limited. This defines the leak tightness requirements on the valve seal to be less than 10^{-4} Pam³/s at a differential pressure of 5 kPa and 10^{-3} Pam³/s at a differential pressure of 1 bar. The design solution is an all metal seal, 800 mm in diameter, with a Nimonic spring, a stainless steel jacket, and silver lining. Design supporting tests for three seal variants were performed to characterize the forces needed to ensure the leak rates requested from the inlet valve in its closed position. The forces have to be known accurately, as they directly impact the size and the operating pressure of the actuator which is pneumatically driven, as well as the mechanical design of the valve stem itself. This was the reason to build at KIT a test facility for the seals in 1:1 scale, illustrated in Fig. 6.

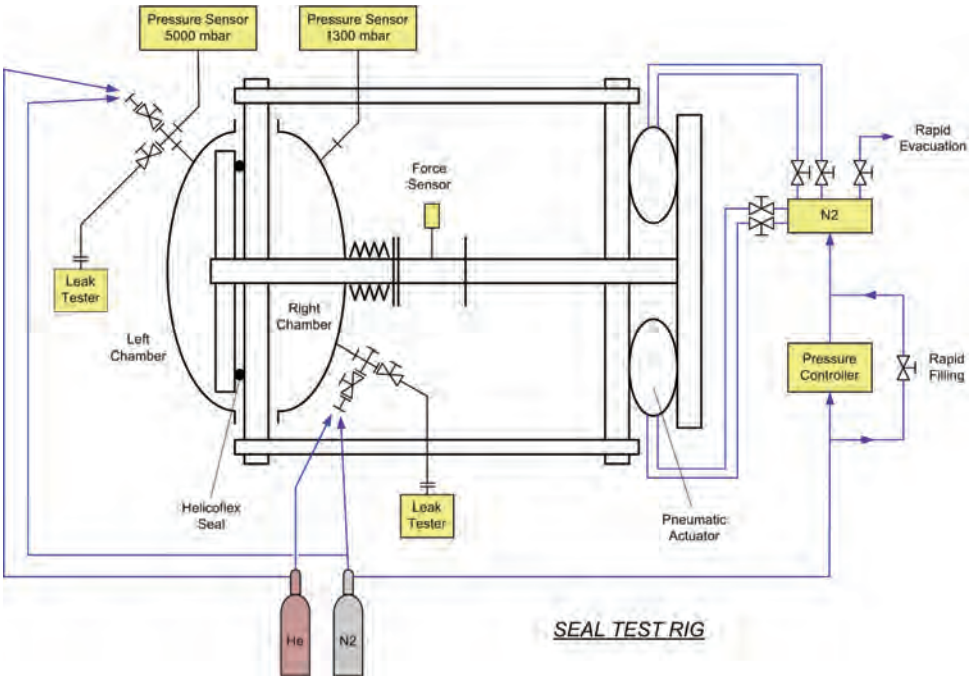

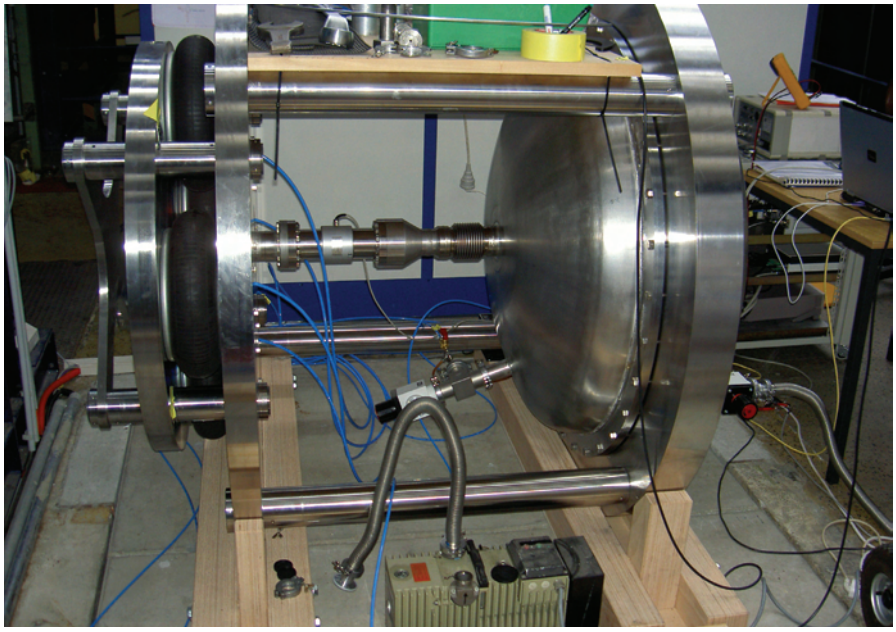

Fig. 6: Metal seal test facility at KIT.

As a result, the best design of the three studied seals could be identified. The actuator design was then modified for the required closing force of 125 kN and an actuator supply pressure of 0.8 MPa.

Another major design change was the change of the double bellow arrangements introduced by IO. The double bellows act as a double seal which separate the inner, tritium containing volume at ITER from the environment. The original design of two circular arranged bellows was replaced by two serial arranged bellows with special welded casing. KIT has included the new design and all changes at pump plug and valve head which are coupled with the new design.

Outlook

The detailed build-to-print design of the PPC design will be fully elaborated, supported by FEM calculations, until mid 2011. After that, the Technical Specification for manufacturing will be written and the manufacturing order will be tendered and placed. When manufactured, the Grant will be resumed and the complete PPC will be tested in the TIMO-2 facility to validate the design.

Staff:

Chr. Day
A. Demsoreanu
H. Haas
V. Hauer
P. Pfeil
M. Scannapiego
R. Simon
H. Strobel
H. Stump
M. Börsch, D. Örtig (Company WEKA, Switzerland, Third Party to KIT)

Literature:

[1] V. Hauer et al., Design of the ITER torus prototype cryopump, Fusion Engineering and Design 82 (2007) 2113–2119.

[2] M. Scannapiego, Chr. Day, St. Hanke, V. Hauer, Thermohydraulic investigation on the ITER torus and neutral beam injector cryopumps, Int. Cryogenic Engng Conf. (ICEC), Wroclaw, Poland, July 2010.

[3] Chr. Day et al., Design progress for the ITER torus and neutral beam cryopumps, SOFT, Porto, Portugal, Sept. 2010.

[4] M. Scannapiego et al., Thermohydraulic investigation on the operation of the ITER torus and neutral beam injector cryopumps, SOFT, Porto, Portugal, Sept. 2010.

Acknowledgement

This work was supported by Fusion for Energy under the grant contract No. F4E-2009-GRT-018-01 with collaboration by SDMS S.A.S. La Chaudronnerie blanche, France and WEKA AG, Switzerland. The views and opinions expressed herein reflect only the author’s views. Fusion for Energy is not liable for any use that may be made of the information contained therein.

Risk Analysis Tool for ITER Operations from Vacuum Leaks (EFDA/07-1704-1568 (TW6-TTFF-LD 71))

Objectives

All large tokamaks suffer downtime due to leaks and the time taken to locate, repair, and recover from these leaks. Generally, the use of water cooled in-vessel components increases the number of leak problems but also other systems introduce significant risks of leakage. ITER requires a strong strategy for leak avoidance, detection, location and repair to ensure adequate machine availability. Leaks will be challenging because of overall complexity, difficult access and the large number of components which could potentially leak. The main purpose of this task was to develop a methodology and a tool for the analysis of risks posed from leakage from different systems so that areas requiring further attention can be readily identified.

The original aim of the task, to identify regions or components requiring further attention to minimize the risk for the cryostat vacuum, was replaced by the development of a tool which offers this analysis. This change was agreed due to the lack of relevant detailed design data and numbers of individual failure rates of components and their consequences.

Analysis of risk for cryostat vacuum system

It was agreed with IO in September 2008 that the issue of the maintenance of the required vacuum conditions in the cryostat shall be used as development case for the risk analysis tool. A good set of input data is needed to perform the proper classification and the arrangement of all components introducing a risk of leaks to the cryostat vacuum. It was agreed that the CATIA model of the entire cryostat shall be used as a basis. Figure 1 shows the model received in April 2009 which, however, was containing only the cryostat without any additional component details. Using only these available input data, no useful classification of components of different type or different arrangement with a certain risk for vacuum was possible. On this basis it was agreed in February 2010 to proceed without available data on components or arrangements relevant for a risk assessment and to develop the tool on a generic basis which enables any future user to perform risk studies on the base of integrated data that will become available in the future.

Description of the software tool

The scheme to be used to collect and analyse the data for all the relevant components was developed as an Excel® tool under MS Excel® version 2003. Due to the fact that currently only insufficient data are available, the entire tool has been checked only with hypothetical data entries to demonstrate the functionality and the options for a later use. In general, the tool is structured in a sequential way to guide the user through the different steps, from the explanation of the used items over the input of several parameters influencing the analysis, the input of the detailed data of all the relevant components and finally to the analysis itself. Figure 2 shows a screenshot of the Excel® sheet, where a (sub)system can be arranged, using components from an integrated database.

The aim of the Excel file was to calculate the impact of the component reliability of a pumping duct on the machine functionality. An arrangement of the components which represent a potential source of leak inside the cryostat is defined by the user, according to the options given by the Excel file. Some areas specific to a particular system (contained pipes, double contained pipes, thermoshield manifolds, feedthroughs, bellows) are pre-defined in the Excel sheet. In these specific areas the user can select in a list the desired components in order to define the system. For example for a double contained pipe, the user has to select in a list a pre-defined pipe, in another list a pre-defined shell (inner shell) and in a third list another pre-defined shell (outer shell). The user can also let pre-defined areas empty, which means that

there is no such system. The specification of all the components given in the list and their risk / probability data to have a leak are tabulated.

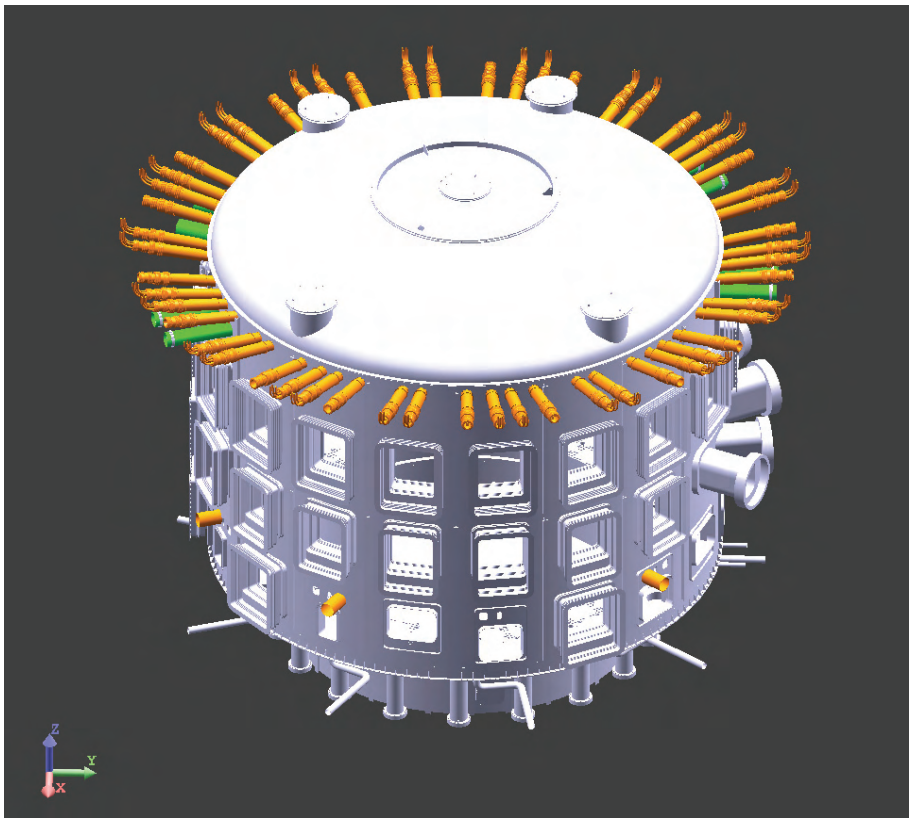

Fig. 1: Model of the cryostat with all the ducts but without any detailed relevant information needed for an in-depth reliability analysis.

5 Definition of the duct components –> Impact on ITER operation and availability

	Duct sub-systems		Components detail information								
	Description	Component type	Name	Material	Diameter / Dimension [mm]	Content	Pressure [bar A]	Temperature [K]	Leak risk/probability [1/y] Detectable	Medium	Major	Ingress
Double contained pipes	Double contained pipe(s) 1	Pipe(s)	P_316L_50_Water_3_300	316L	50	Water	3	300	1.00E-05	1.00E-06	1.00E-07	1.00E-08
			P_316L_50_Water_6_300	316L	50	Water	6	300	1.00E-05	1.00E-06	1.00E-07	1.00E-08
			P_316L_50_Water_12_300	316L	50	Water	12	300	1.00E-05	1.00E-06	1.00E-07	1.00E-08
			--	--	--	--	--	--	--	--	--	--
			--	--	--	--	--	--	--	--	--	--
			--	--	--	--	--	--	--	--	--	--
		Inner shell	S_316L_200_Vac	316L	200	Vac	--	--	1.00E-05	1.00E-06	1.00E-07	1.00E-08
		Outer shell	S_316L_250_Vac	316L	250	Vac	--	--	1.00E-05	1.00E-06	1.00E-07	1.00E-08
	Double contained pipe(s) 2	Pipe(s)	P_316L_50_Water_12_300	316L	50	Water	12	300	1.00E-05	1.00E-06	1.00E-07	1.00E-08
			P_316L_50_Water_3_300	316L	50	Water	3	300	1.00E-05	1.00E-06	1.00E-07	1.00E-08
			--	--	--	--	--	--	--	--	--	--
			--	--	--	--	--	--	--	--	--	--
			--	--	--	--	--	--	--	--	--	--
			--	--	--	--	--	--	--	--	--	--
		Inner shell	S_316L_100_Vac	316L	100	Vac	--	--	1.00E-05	1.00E-06	1.00E-07	1.00E-08
		Outer shell	S_316L_120_Vac	316L	120	Vac	--	--	1.00E-05	1.00E-06	1.00E-07	1.00E-08
	Double contained pipe(s) 3	Pipe(s)	P_316L_80_Water_3_300	316L	80	Water	3	300	1.00E-05	1.00E-06	1.00E-07	1.00E-08
			--	--	--	--	--	--	--	--	--	--
			--	--	--	--	--	--	--	--	--	--
			--	--	--	--	--	--	--	--	--	--
			--	--	--	--	--	--	--	--	--	--
			--	--	--	--	--	--	--	--	--	--
		Inner shell	S_316L_100_Vac	316L	100	Vac	--	--	1.00E-05	1.00E-06	1.00E-07	1.00E-08
		Outer shell	S_316L_120_Vac	316L	120	Vac	--	--	1.00E-05	1.00E-06	1.00E-07	1.00E-08
	Double contained pipe(s) 4	Pipe(s)	--	--	--	--	--	--	--	--	--	--
			--	--	--	--	--	--	--	--	--	--
			--	--	--	--	--	--	--	--	--	--
			--	--	--	--	--	--	--	--	--	--
			--	--	--	--	--	--	--	--	--	--
			--	--	--	--	--	--	--	--	--	--

Fig. 2: The interface of the developed Excel® tool to arrange a dedicated subsystem or arrangement from a database of possible components.

Once the arrangement of the duct is defined by the user, 3 types of impacts are calculated for each system: an impact on the operation of the machine (maintainability), another impact on the localization / repair / replacement time of the component (availability) and a global impact taking into account the two previous impacts with associated coefficients which can be changed by the user according to the importance given by the user to these two different impacts. The impact on the operation of the machine is related to the possibility to run the machine on operation or not in the case of a leak. The impact on the availability is related to the time which is needed to replace a component or a system of components, independently of its impact on the operation.

The file is divided in different sheets:

Sheet 1: *Definition*: Definition of the parameters by the user

Sheet 2: *Calculation summary:* Table summarizing the impact results

Sheet 3: *Impact on operation:* Graphics for the impact on maintainability

Sheet 4: *Impact on availability:* Graphics for the impact on availability

Sheet 5: *Global impact:* Graphics for the global impact

Final results

Based on the analysis of the cryostat vacuum, a tool was developed to collect the required data, to group this input to appropriate subsystems and to calculate risk distributions and several impacts on the machine.

To start the main work using this scheme in the future, additional input data have to be made available. A list of all relevant components contained by the ducts and a detailed model including the arrangement of these components introducing risks to the cryostat vacuum are needed. The tool was fully developed to a ready-to-use level and the use of it with real data will lead to valuable results concerning risky components requiring further attention. Thereby the user has maximum flexibility to represent every possible arrangement of risky components and several possibilities to influence the analysis so as to investigate different approaches of the concept of impact to the operation of the machine. Considering these results the final status was accepted by ITER and EFDA/F4E and the task was closed.

Staff:

St. Hanke
M. Scannapiego

Acknowledgement

This work, supported by the European Communities under the contract of Association between EURATOM and Karlsruhe Institute of Technology, was carried out within the framework of the European Fusion Development Agreement. The views and opinions expressed herein do not necessarily reflect those of the European Commission.

Study of the Effects of ITER Off-normal and Mitigation Events on Torus and Cryostat Cryopumps (EFDA/07-1704-1547 (TW6-TTFF-VP 72))

Background and objectives

The ITER torus and cryostat cryopumps will be sensitive to off-normal events in other components which may affect reliability, maintainability, integrity and safety. This relationship was studied in the present task to determine the effects of postulated safety events. It also provided greater understanding of the operational margins for the pumps.

The ITER safety philosophy

The ITER safety analysis approach comprises any off-normal event with a potential to initiate a sequence leading to some hazardous outcome and differentiates between accidents and incidents. An event is considered to be safety relevant when it relates to mobilization, spreading and release of radioactive materials. These events are to be analysed to demonstrate that these potential consequences are minimised, preferably eliminated but at all times kept below the prescribed limits, by physical processes and by features of the ITER design. Any specific failure consequence which is not associated with a release (so-called non-safety related events), such as operational events with effects on neighbouring systems, had also to be identified for the torus and cryostat cryopumps, because they may still lead to inacceptable long down times.

The categorisation of an event as either an incident or an accident is done mainly according to its likelihood, however both event categories are within design basis, i.e. they have been taken into account and implemented in the ITER design base. Beyond design base accidents are hypothetical events, which have not been taken into account in the design. Nevertheless analysis of these events has been done.

ITER has mainly used two independent methods to identify accident sequences, namely a deterministic approach and the so-called PIT approach (Postulated Impact Tables). The deterministic approach identified 28 ´Reference events´ (and 12 hypothetical events).

The list of 13 bounding events (7 for tokamak, 3 for tritium plant, 1 for hot cell, and 2 during maintenance) originated from a different, non-deterministic analysis approach. The 13 bounding events have been defined on the basis of all in all 93 postulated initiating events (PIEs) that have been treated inside ITER IO according to the PIT approach. These comprise 74 for the ITER tokamak, 14 for the tritium plant and 5 for the hot cells. This means, also in this approach, the cryogenic pumping systems were not (yet) separately considered (whereas the roughing pumps have been, as part of the tritium plant study). With the PIE-PIT approach the deterministically selected reference events could be successfully confirmed. One additional scenario could be identified. All other bounding events are covered by the reference events list.

Safety events affecting torus and cryostat pumping

The next step aimed to identify these events which are of relevance for torus and cryostat pumping. For this exercise, existing FMEA studies were also taken into account. After a detailed study of all relevant events, the cases for the torus cryopump system could be qualitatively grouped as follows (the brackets give the event denominators as used in the ITER safety documentation).

1. Air ingress in the vacuum vessel (VVA2, VNG, hypothetical events 2 and 9),
2. Gas ingress in the vacuum vessel, other than air (service gas nitrogen/helium/neon) (VNG, TVP1/2),

3. Cooling water ingress in the vacuum vessel (all LW, LF, LD, LN cases, hypothetical event 3),
4. Fuelling failure in the vacuum vessel (TPI4),
5. Cryogenic coolant release (break/leak) from the cryopumps (including the case that NB sees torus pumps and vice versa) (VVC, VNC, LPP1),
6. Tritium permeation (TVP6).

And the corresponding cases for the cryostat cryopumps were:

1. Air ingress in the cryostat (VCA),
2. Helium ingress in the cryostat (VCG),
3. Cooling water ingress in the cryostat (LFC1, LWC),
4. Helium and cooling water ingress (hypothetical event 12),
5. Cryogenic coolant release from the cryopumps (MCJ1, VCC, VCH).

After checking the underlying event specifications and including the found non-safety related off-normal events, some key areas of concern were identified, as listed in Table 1. It was then agreed with ITER IO that the first three events shall be treated in full detail.

Table 1: Resulting key areas of concern from this study and suggested approaches for their assessment.

Key area	***Approach for assessment***
Assessment of tritium permeation	An analytic study of the results of tritium permeation under off-normal conditions (470 K regeneration) will be made.
Ability of the cryopumps to handle additional gas loads (inflows as a result to an accident in cryostat or vacuum vessel, within disruption mitigation or from cryogen breaks inside).	Already under nominal pumping conditions, the cryopumps are operated in transitional flow regime. This provides a pumping speed higher than the reference speed according to molecular flow regime. Under increasing gas loads, the cryopump will go further towards viscous operation and, at some point, face a thermal breakdown with consequences to the cryoplant and cryodistribution system (heat loads, pressure drops).
Small gas leaks	In the case of small air leaks, the cryogenic situation may be kept and the leaks therefore be unnoticed for a long time, thereby building up high inventories. From that point of view, it may involve a higher risk than a big leak. The operational boundaries will be assessed and recommendations to manage this risk will be given.
Consequences of severe water ingress conditions on the cryopumps.	The cryosorbent will become saturated with water vapour. The capacity limits will be extrapolated from existing sorption data for the ITER reference charcoal at KIT. In addition, estimates will be given on necessary regeneration conditions to restore full functionality.
Pump drop-out	ITERVAC study of the resulting distribution of gasloads on the remaining pumps.

Tritium permeation

As the cryogenic piping in the torus cryopump is by default single-walled, there is a generic risk to contaminate the cryogen (helium).

It is known that permeation is a mass transfer process which may become dominant at temperatures above ambient. All torus cryopumps know six operational states which are characterised by different cryopanel circuit temperatures. These are nominal pumping (cryopanel circuit at 4.5 K), 40 K operation for leak localisation, 100 K regeneration which releases all hydrogen isotopologues, ambient temperature regeneration to release air-likes, 400 K regeneration to release water (this temperature is under discussion) and 470 K to release any strongly adsorbed substances. Each regeneration step is being performed by pushing gaseous helium at the corresponding temperature through the cryogenic loop. However, an off-

normal condition can result when the 470 K regeneration is conducted without or with incomplete pump-down of the tritium gas in the preceding regeneration step. In this failure mode, a regeneration of the cryopump´s cryopanel circuit would be performed under 470 K at higher tritium partial pressures.

The objective of this analysis was to estimate the potential permeation of the torus cryopump at this failure condition. In case of an issue, one would need to have a separate cryogenic loop for cryopump operation, which would be allowed to be contaminated.

Permeation of gas through a wall is an integral process which combines several sequential steps that follow different laws (e.g. with regard to time and temperature). For tritium permeation, the following steps have to be considered:

1. Adsorption from the gas phase on the outer pipe surface.
2. Dissociation to atomic hydrogen.
3. Migration between surface and bulk.
4. Diffusion through the bulk.
5. Recombination on the inner pipe surface.
6. Desorption into the medium flowing through the pipe.

Within the scope of this study, it was justified to focus on step (4) which is overall rate determining.

The model problem to be solved was to estimate the permeation flux through a pipe or panel wall with a concentration (pressure) jump on one (outer) side of the wall and an initial concentration of zero at the other (inner) side of the wall. This process has first a non-steady state phase, in which the concentration profiles build up, starting on the outer side and propagating through the wall. Finally, a stationary concentration profile will result at which the flux becomes constant.

A very conservative worst case estimation was made which yielded 44 h (accumulated operational hours at 500 K) until the first tritium has permeated through the circuit walls.

The worst-case assumptions for this estimation were:

1. Complete failure in performing regular regeneration at 100 K. Under nominal conditions, an estimated ultimate cross-over pressure to the cryopumps of 10 Pa (given by the forepumping section) is achievable (this increases the permeation flux by factor $\sqrt{1000/10}=10$).
2. High temperature regeneration temperature to be 500 K (rather than 470 K) (this increases the diffusion coefficient by factor 2).
3. Neglected influence coming from the dissociation reaction at the surface which would directly slow down any concentration build-up.
4. Neglected influence coming from the decay of diffusing tritium atoms (this changes the concentration profile at the outgoing surface and thus increases the permeated flux by approx. factor 3 to 4).
5. No influence coming from any potential surface inhibition of the ceramic cement on the cryopanel area.

A less conservative approach of operation at 400 K and without the failure to have no pump-down before the regeneration starts leads to 900 h continuous high temperature operation before one would see the first tritium atom to enter the helium loop, and the resulting steady–

state permeation flow which is achieved after more than 8 years would be of the very low order of 5 Bq/s.

In view of this, the found results did confirm that tritium permeation does not pose a problem for the operation of the ITER torus cryopumps. The same conclusion was found in two companion studies organised by IO [1].

Increased throughputs

It is foreseen to introduce ELM pellet pacing in order to manage the energy dissipation of ELMs. This and other considerations has lead to a proposed increase in the reference fuelling rate for gas puffing and further for pellet injection. Moreover, massive gas injection is the proposed concept to safely terminate a disrupting plasma discharge which would produce additional transient gas loads, the amount of which depending on the type of gas.

The implications of these aspects on the pump operating envelope were analysed [2].

For the ITER type cryopumps, the pumping speed will increase with rising throughput because higher densities and transitional flow regime is resulting. At some point of time, the cryopump performance vanishes because the heat load is above a certain limit. The problem lies in the fact that this qualitative description can not be quantified, as the pumping speed evolution with increased throughput is not a priori known and very difficult to predict. As in the step from the model pump to the 1:1 scale pump, the pumping surface could be almost tripled, whereas the inlet cross-section could only be weakly increased (the ITER pumping port size did not change), the operation point at peak load is given by comparable surface related fluxes as was investigated in TIMO, but significantly higher pump pressures than was the case for the model pump. Hence, the ITER torus cryopump operational point is out of the measured envelope with the model pump, and the scaling law is not known. Moreover, the PTC design is in many aspects different due to a rigorous system optimization so that it is essential for ITER to develop a predictive pumping speed tool for the torus cryopumps based on Direct Simulation Monte Carlo.

Small air leaks

In the case of small air leaks, the cryogenic situation may be kept and the leaks therefore be unnoticed for a long time, thereby building up high inventories. From that point of view, it may involve a higher risk than a big leak.

From previous investigations with the ITER model pump in TIMO, it is known that the pumping speed performance of the pump is not very sensitive to accumulated amounts of air-likes. By this way, oxygen can be accumulated and a flammable mixture may result within hydrogen regeneration. However, such an explosion is a design-base event, so no additional safety measures are needed. But it is strongly recommended to monitor the composition of the released gas in a regular manner in order to have an early detection of any deviations from normal operation.

Final conclusions

This task was closed. Within the ongoing work to develop the detailed design of the torus and neutral beam cryopumps, complementary safety analysis is being performed.

<u>Staff:</u>

Chr. Day

Literature:

[1] R. Kersevan et al., Tritium permeation issues for the ITER torus cryopumps, SOFT, Sept. 2010, Porto, Portugal.

[2] Chr. Day, V. Hauer, X. Luo, R. Pearce, M. Wykes, G. Piazza, Implications of increased gas throughputs at ITER on the torus exhaust pumping system, IAEA Fusion Energy Conf, Oct. 2008, Geneva, Switzerland.

Acknowledgement

This work, supported by the European Communities under the contract of Association between EURATOM and Karlsruhe Institute of Technology, was carried out within the framework of the European Fusion Development Agreement. The views and opinions expressed herein do not necessarily reflect those of the European Commission.

Instrumentation for ITER Cryopumps and Cold Valve Boxes (F4E-2009-GRT-020-01)

Background and objectives

Key components of the ITER high vacuum system are its cryopumps and dedicated cold valve boxes (CVBs) to supply the cryogens at the correct mass flows and temperatures for the various operational needs. Measurement of pressures (cryogenic and vacuum), cryogen flows, gas composition, pumped amounts and temperatures operating in harsh environmental conditions (ionising radiation, magnetic fields) which vary from component to component are required. In addition it has to be considered that some pumps provide tritium confinement and therefore special care needs to be taken with regard to the reliability and availability of the hardware, including the instrumentation and electrical feedthroughs.

This task was performed to support ITER IO in the definition of instrumentation for the cryopumps (torus, cryostat, NBI) and the cold valve boxes reflecting the specific ITER requirements and conditions. The work started in 2009 with the definition of the number and location of sensors needed to fulfil the given ITER measurement tasks under normal and off-normal operation conditions.

The scope included measurement information for temperatures (in a very wide range incl. cryogenic, i.e. ~ 4 K to 500 K), pressures in vacuum (~ 10^{-11} mbar as ultimate pressure up to 2 bar design pressure of the housing) as well as above atmospheric for the pressurized cryogen (up to 18 bar operation pressure and 25 bar set pressure of the burst disk), cryogenic mass flows (up to ~400 g/s helium), gas composition, and pumped amounts.

Cryopumps

The Tables 1 and 2 below summarize the requirements in terms of temperature and vacuum pressure measurement as they result from the operational scenarios foreseen for the various ITER cryopumps.

On top of that, the instrumentation will have to provide data as part of a suite of measures capable to access pumped quantities to identify regeneration requirements. This reflects the new philosophy of ITER to operate the torus cryopumps on a flexible regeneration pattern rather than according to a strict pre-defined scheme.

Table 1: List of torus / cryostat pump operational states.

Operational state	***Temperature***	***Total pressure***
Nominal pumping	Cryopanel circuit: 4.35 K to 4.7 K Thermal shield circuit: 80 K to 90 K	10^{-8} Pa ultimate pressure; ~ 10^{-3} to 10^{-2} Pa during pumping
Mode for leak localisation	Cryopanel circuit : 40-45 K Thermal shield circuit : 80 K (low loads)	Below 10^{-4} Pa
Regular regeneration	Cryopanel circuit : 100 K Thermal shield circuit: 80 to 90 K	kPa range
Ambient regeneration	Cryopanel circuit : 300 K Thermal shield circuit: 300 K	kPa range
High temperature regeneration	Cryopanel circuit : 470 K Thermal shield circuit: passively following or actively warmed (tbd) towards 470 K	kPa range (the pump will have to be backfilled to avoid water condensation during pump-out)
Massive Gas Injection	Pump may evolve from nominal pumping conditions in uncontrolled regeneration	
Ab-normal events (LOVA, water ingress)	No additional demands with regard to the measurement range, but sensor has to survive	Up to 2 bar (g) (= design pressure of the housing)

Table 2: List of NBI cryopump operational states.

Operational state	***Temperature***	***Total pressure***
Nominal pumping	Cryopanel circuit: 4.35 K to 6.7 K Thermal shield circuit: 80 K to 90 K	10^{-8} Pa ultimate pressure; ~ 10^{-3} to 0.2 Pa during pumping
Regular regeneration	Cryopanel circuit : 100 K Thermal shield circuit: 80 to 90 K	Several 100 Pa range
Ambient regeneration	Cryopanel circuit : 300 K Thermal shield circuit: 300 K	Several 100 Pa range
High temperature regeneration	Cryopanel circuit : 470 K Thermal shield circuit: passively following or actively warmed (tbd) towards 470 K	kPa range (the pump will have to be backfilled to avoid water condensation during pump-out)
Ab-normal events (especially water leaks from beamline components)	No additional demands with regard to the measurement range, but sensor has to survive.	Up to 1.5 bar (g) (= design pressure of the vessel)

The performance requirements (wishlist, optimum goals values) were defined by ITER as listed in the following Table 3.

Table 3: List of IO requirements.

Category	***Temp @ cryopanel circuit***	***Temp @ thermal shield circuit***	***Temp at valve head / housing***	***Total pressure***	***Partial pressure***
Range	4-500 K	60-500 K	200-500 K	10^{-9} Pa - 0.2 MPa	10^{-9} Pa to 3000 Pa; 1-50 (100) amu***
Accuracy / Resolution	<20 mK for T<20K <1 K for T< 120 K <5 K full range*	<1 K for T< 120 K <5 K full range*	< 1 K full range	10% reading for p< 10^{-2} Pa 1% reading for p>10^{-2} Pa	1% of reading;
Cycling stability	100,000 for cycles 4 K / 100 K 1000 for cycles 4 K / 300 K** 500 for cycles 4K / 470 K	1500 for cycles 300K/470 K	-	n.a.	n.a.
Response time (full sensor package and support)	< 0.1 s	<0.5 s	<0.5 s	<50 ms	< 0.1 s/ amu

* It would be allowed to shift the full range measurement towards the CVB, if this turns out to be a problem for an in situ cryopump measurement.

** The cryostat cryopump has to provide 3700 cycles.

*** The partial pressure instrument has to be suitable to detect oxygen quantities as monitor for the ozone hazard.

The worst case environmental conditions were taken as 0.5 T magnetic field for the torus/cryostat cryopumps and 0.15 T for the NBI cryopumps, and 10^6 Gy neutrons for all pumps.

A functional analysis was made to categorize the requirements in different importance classes (such as: safety relevant, operationally relevant, nice to have). As a consequence to

this exercise, the goal to have a pressure measurement down to 10^{-9} Pa seemed to be not of real relevance. Also, the requirement to have an absolute measurement accuracy of 20 mK at 4.5 K for the cryopanel circuit (especially for the torus/cryostat cryopump) could be dropped if a reliable measurement is found which provides a repeatability in that few 10 mK range.

Finally, the following recommendations were given:

Temperatures

Table 4 compares the candidate temperature sensors (rating + favourable, 0 neutral, - disadvantageous).

Table 4: Comparison of relevant temperature instrumentation.

Property / Type	***Carbon ceramic (TVO)***	***CERNOX-Resistors***	***Pt-Resistors***	***GaAlAs-Diodes***	***Thermocouple***	***Fibre-Bragg***
Upper temperature	- To be found by selection (permanent damage, shift tbd)	- To be foud by selection (permanent damage, shift tbd)	+	+	+	+
Lower temperature 4K	+	+	- (resolution limited)	+	- (resolution limited)	- (resolution limited)
Lower temperature 80 K	+	+	+	+	+	+
Accuracy	+ (- at 500K)	+ (- at 500K)	+	+ 0 (fibres)	0	0
Magnetic	+	+	+	0	+	+
Radiation	+	+	+	0	0	+

From the Table above, the following conclusions were drawn:

1. There is no single sensor which meets all requirements best.
2. The Pt sensor is the sensor of choice for the thermal shields where the poor resolution at temperatures below 40 K is not relevant.
3. The GaAlAs diode is the only sensor which can be used for read-out in the full temperature range and has no showstopper in any of the other categories, but dependence on radiation and magnetic field is not best.
4. If the TVO and/or CERNOX sensor could be qualified for 500 K, this would provide for a stand-alone solution with one sensor.
5. Otherwise, to cover the full temperature range may imply to have two sensors: One to read out for the upper level (which survives the lower level), and one to read out for the lower level (which survives the upper level). Based on existing instruments, the candidate solution would be Pt for the higher temperatures and GaAlAs for the lower temperatures.

In conclusion, we recommended to try to qualify TVO and CERNOX as a sensor workable (not only surviving, but usable to read out) in the full temperature range until 500 K, but to include the GaAlAs diode in the testing as fallback solution.

Vacuum Pressures

In terms of vacuum pressure instrumentation we recommended:

1. For total pressure measurement to use a combination of MKS Baratron with detached electronics with the commercially available Pfeiffer IKR cold cathode gauge for total pressure measurement.
2. For partial pressure measurement to check the Granville Phillips ART-MS, which is promising, but new on the market and to develop the available MKS HPQ2 with detached electronics as fallback solution.

Pumped amount (torus cryopumps)

The measurement of pumped amount is linked to a safety function and therefore has to provide a very high reliability. This is best met by including two (or more) independent measurement concepts. In view of this, it is suggested to test and validate all concepts in the PPC campaign. We have elaborated five ideas:

- Calculate the operational map (conductance) of the valve characteristic,
- Measure the temperature difference across the panels which scales with pumped amount,
- Measure the rear valve head temperature which scales with the flow,
- Measure the He concentration which scales with the pumped amount,
- Measure the contact resistance of temperature measurement which scales with pressure.

Cryogenic valve boxes

The environmental conditions are less stringent than for the cryopumps. The magnetic field is 0.1 T, the radiation dose to 100 Gy. With regard to temperature instrumentation, no additional requirements are posed, so that the solutions derived for the pumps can be adopted.

With regard to cryogenic pressures, due to strong magnetic environment resistive or piezo measurements have to be applied. These are commercially available.

For flow measurement, reliability, accuracy and size of the sensor have to be checked. For a Coriolis instrument, the pressure loss issue comes on top. No satisfying solution was found. The final conclusion was to cancel this measurement.

R&D needs

Various weaknesses have been identified. This is why an additional R&D programme was proposed to provide a better knowledge and to verify potential solutions:

- Compare and test temperature sensors for thermal cycles up to 500 K;
- Qualify mineral insulated cable package designs for temperature measurement;
- Investigate the long distance transport of tiny level of measurement in noisy electromagnetic environments relevant for ITER;
- Develop feedthroughs;
- Characterise thermometer, pressure gauge and flowmeter in ITER relevant nuclear environment;
- Develop total and partial pressure gauges with separate electronics;
- Benchmark the new Granville-Phillips instrument;
- Develop a flowmeter in supercritical helium flow.

Conclusions and future work

A survey of suitable commercially available instrumentation was elaborated. This included the sensors themselves as well as other parts of the measurement chain. The compilation was organised along criteria and tables which have been defined in the start of this grant. A screening was then done to find matching solutions, and, where this could not be found, a programme for the development and qualification of novel sensors for ITER needs was defined

This grant is closed. ITER IO is evaluating internally how to proceed and which R&D recommendation to follow, if any at all [1].

Staff:

Chr. Day
A. Demsoreanu
H. Haas
V. Hauer
P. Pfeil
H. Stump
J.-L. Marechal (CEA Cadarache, Third Party to KIT)

Literature:

[1] B. Boussier et al., ITER vacuum control system, Int. Vacuum Congress (IVC), Beijing, China, August 2010.

Acknowledgement

This work was supported by Fusion for Energy under the grant contract No. F4E-2009-GRT-020 with collaboration by CEA, France. The views and opinions expressed herein reflect only the author’s views. Fusion for Energy is not liable for any use that may be made of the information contained therein.

PROVAC3D – Development of a Collisional Flow Monte Carlo Code (EFDA HPC-FF SIMVAC)

Background and objectives

ProVac3D, standing for "**3D** density **PRO**file in the **VAC**uum system", is a Monte Carlo simulation program developed by KIT based on the accumulated particle time of flight concept. In previous works, it was successfully cross-checked and used in different applications in the free molecular flow regime, for example it has become the reference code for the NBI vacuum pumping systems. Recently, it has been extended into the transition flow regime by including the collisions between the probe molecule and the gas background. The emphasis of this year's work was to further benchmark the simulation results against experimental data for the transitional gas flow.

Due to the underlying concept, this code offers many promising advantages, such as a comparatively simple description of also very complex geometries and the intrinsic capability to describe transient phenomena. Due to the particle counting approach, it can easily be parallelized for the use on high performance computers, whereas other codes valid in the transitional range (such as DSMC or kinetic equation solvers) are very complicated to be parallelized.

Mathematical procedure

A flow through a tube is considered as illustrated in Fig.1, connecting a dosing dome with gas density n1 and pumping dome with negligible gas density n2<<n1.

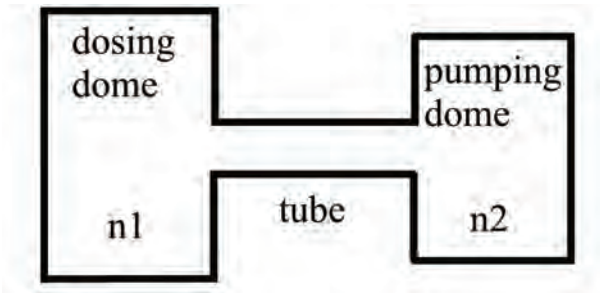

Fig. 1: ProVac3D simulation model.

The gas flow rate is simulated as a function of the gas density n1 in the dosing dome by an iteration process: $n1=n0+k\cdot\Delta n$ ($k=0,1,2,3,\ldots$).

In the simulation n0 is chosen as 10^{18}, corresponding to an initial $P1=3.98\times10^{-3}$ Pa and an initial Knudsen number of Kn=100; this means starting from a free molecular background. Δn is chosen as one order of magnitude smaller than n0, so that the collisions between the probe molecules are always negligible. After k=9990 iteration steps, the final n1 is 10^{21}, which is 1000 times bigger than the initial one, corresponding to a final P1=3.98 Pa and a final Kn=0.1. So the gas flow evolves from the free molecular flow to the beginning of the transitional flow. For each iteration step k, 10^5 test particles are used, which means that one test particle represents about 2.37×10^{10} nitrogen molecules. Cercignani-Lampis boundary conditions have been included to consider the collisions with the wall.

The simulation domain is only the tube itself, we neglect the collisions inside the dosing dome. It is divided into 200 cells by 5 meshes along the radial direction and 40 meshes along the axial direction of the tube. The trajectories of the molecules coming from the source are traced down until they hit a component. By means of the record of the accumulation of the time of flight of every molecules in each cell, we can derive the 3D density distribution by simulation of a high number of molecules based on the hypothesis that the density in one cell is proportional to the accumulation of time of flight of every molecule in this cell and inversely proportional to the cell volume. The average time of flight of all test particles can be easily calculated for each cell and for each k-th iteration step. Even if there are collisions, the density can be calculated because it is still proportional to the time of flight and inversely proportional to the cell volume. The density distribution as obtained in the k-th step is used to de-

termine the new collision time in the (k+1)-th step. In the last step, transmission probabilities are calculated from that and finally the gas flow rate. Other macroscopic parameters, such as bulk velocity and temperature, etc., can be obtained in a similar way.

Simulation results and comparison with experimental data

As an example, the simulation was carried out for a circular tube of length L=0.1570 m and diameter D=0.0161 m. For this circular tube of L/D=9.75, it is not only hard to calculate with kinetic theory because the length-to-diameter ratio is too small, but also hard to calculate with DSMC because the length-to-diameter ratio is too large. The gas simulated is nitrogen at 15°C. The experiment itself was carried out in the TRANSFLOW test rig at KIT [1, 2].

The simulation was finished roughly in 112 hours by a desktop PC with a CPU at 2.67 GHz.

Fig. 2 shows the comparison results [3]. It is seen that the ProVac3D simulation result shows a correct nonlinear increasing of the gas flow which is an excellent proof of principle. The remaining quantitative discrepancy with the experimental data is due to the fact that the pressure in the pumping dome (which introduces a small back streaming) and the entrance effect of the dosing dome have been neglected. The current model is being refined to include these effects.

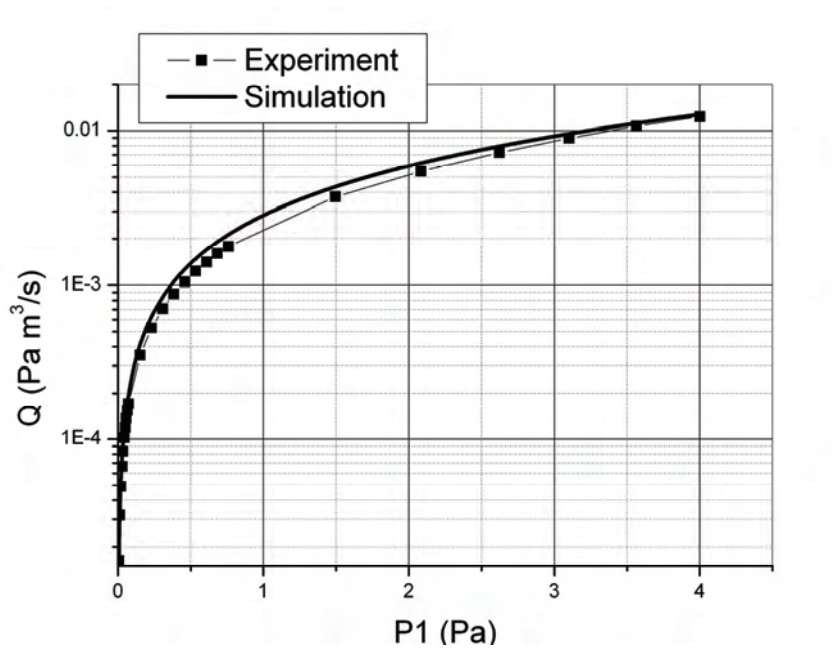

Fig. 2: Comparison of experimental results and ProVac3D simulation for the flow rate.

Graphical user interface

A graphical user interface (GUI) has been developed to provide the user a simulation model development environment, so that the code development and application is separated and the user can concentrate only on the application. In order to be platform independent, the first version of the ProVac3D GUI is developed with Java as shown in Figure 3. Although this GUI is preliminary, it has already been successfully used to optimize a cryogenic baffle geometry.

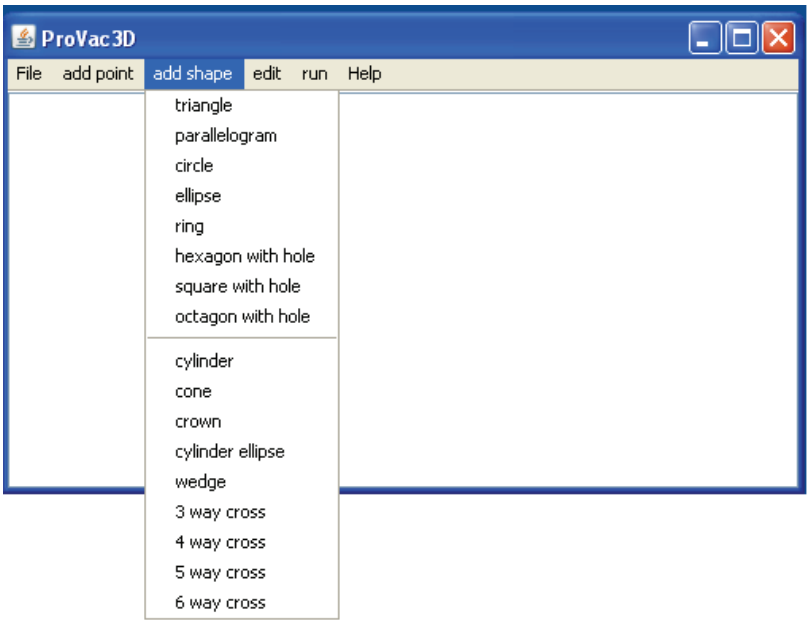

Fig. 3: First version of ProVac3D GUI.

Conclusions

Obviously, this new simulation approach has several advantages. First of all, like usual TPMC, the test particles are simulated one by one. So there is no need for a huge memory like DSMC. This makes the simulation of a complex 3D problem possible. Actually, ProVac3D has already pre-implemented many entities to model a complex 3D vacuum system. This was recently demonstrated by a very detailed modelling of the ITER model pump [4]. The present work shows that the computation is also much faster than DSMC. Secondly, as is well known, DSMC is very hard to parallelize. However, the parallelization of TPMC is straightforward. This work for ProVac3D is in progress. Thirdly, the gas flow is simulated by an iteration process in the suggested normalization scheme. This means that we can even interrupt the simulation process and later on continue the simulation of the further evolution of the gas flow by using the obtained result as the background.

Staff:

X. Luo

Literature:

[1] V. Hauer, Chr. Day, Measurement of the conductance in the Knudsen flow regime, Symp. On Vacuum Science and Technology, Kaiserslautern, Sept. 2010.

[2] S. Varoutis, S. Naris, V. Hauer, Chr. Day and D. Valougeorgis, “Computational and experimental study of gas flows through long channels of various cross sections in the whole range of the Knudsen number”, J. Vac. Sci. Technol. A 27 (2009) 89-100.

[3] X. Luo, Chr. Day, Investigation of a new Monte Carlo method for transitional gas flow, 27th Int. Symp. On Rarefied Gas Dynamics (RGD), Pacific Grove, California, USA, July 2010.

[4] X. Luo, H. Haas, V. Hauer, F. Sharipov, Chr. Day, Systematic vacuum study of the ITER model cryopump by Test Particle Monte Carlo simulation, Int. Vacuum Congress (IVC), Beijing, China, Aug. 2010.

Components and Infrastructures of PRIMA: Cryopumps for MITICA (F4E-2009-GRT-032-PMS-H.CD)

Objectives

The 2010 activities performed at KIT in the area of the cryopumps for Neutral Beams (NB) were focussed on three main aspects of the cryogenic pumping systems. Firstly, the design of the ITER HNB cryopump, finalized in 2008 [1], had to be improved and developed to a BtP design to prepare a call for tender and the manufacturing. Secondly, the critical issue of the thermal hydraulic behaviour of the very complex 80 K shielding system, which can not be predicted on a theoretical basis, was further elaborated; here, an extensive experimental and analytical work was done to characterise the complex behaviour of the shielding. Thirdly, several simulations of gas density profiles and the behaviour of the whole HNB system as well as of individual beamline components were performed. These recalculations, using the KIT vacuum code ProVac3D, are necessary to accompany the design progress by refined simulations to predict the final behaviour of the NBI system.

This work was organised under Grant F4E-2009-GRT-032, which started in spring 2009 and will run until 2011. The grant covers the elaboration of the BtP design of the cryopump for the ITER HNB, while necessary adaptations of this design to special needs of the test facility in Padua are foreseen to be realised in a follow up arrangement.

Design development

For the ITER HNBs the cryopump design was advanced and refined to cover all requirements given by the latest injector design. To achieve this, the following iterative approach of three main areas has been taken:

1. Reduction of bellows:

A basic requirement of the pump design is the reduction of the number of bellows in the cryogenic and shielding circuits. The function of the bellows is to handle the significant thermal expansion of the related pump components (the cryocircuit has to be designed for a temperature range from 4 K to 470 K, the shielding circuit from 80 K to 470 K). But the bellows do also introduce a risk for vacuum leaks so that the ITER design guideline is, wherever possible, to replace bellows by an alternative solution, this has to be implemented in the design.

To fulfil this, several arrangements within the pump had to be redesigned. The basic design solution for this work is to implement a hanging support of the cryo- and shielding panels of the pump, which guarantees the freedom of vertical thermal movement while the resulting mechanical stress is minimized. Fig. 1 illustrates how this has been achieved.

2. Design of supply manifolds:

The supply of the cryo- and shielding panels is a demanding issue due to several reasons. The routing, as a mix of serial and parallel arrangements, is the outcome of the extensive experimental and analytical work using the THEA facility at KIT. This work is summarized separately in another chapter of this annual report. As an example, the following Fig. 2 shows the derived pressure loss of the complete thermal shield system of one of the two halves of the NBI cryopump in nominal pumping cooling conditions (note that the NBI cryopump is divided in two symmetrical pumps supplied in parallel). It was found that the current requirements of a maximum pressure loss of 1 bar can be achieved using a ΔT of 10.7 K, which is just slightly higher than the initial requirements ΔT of 10 K and, thus, fully acceptable.

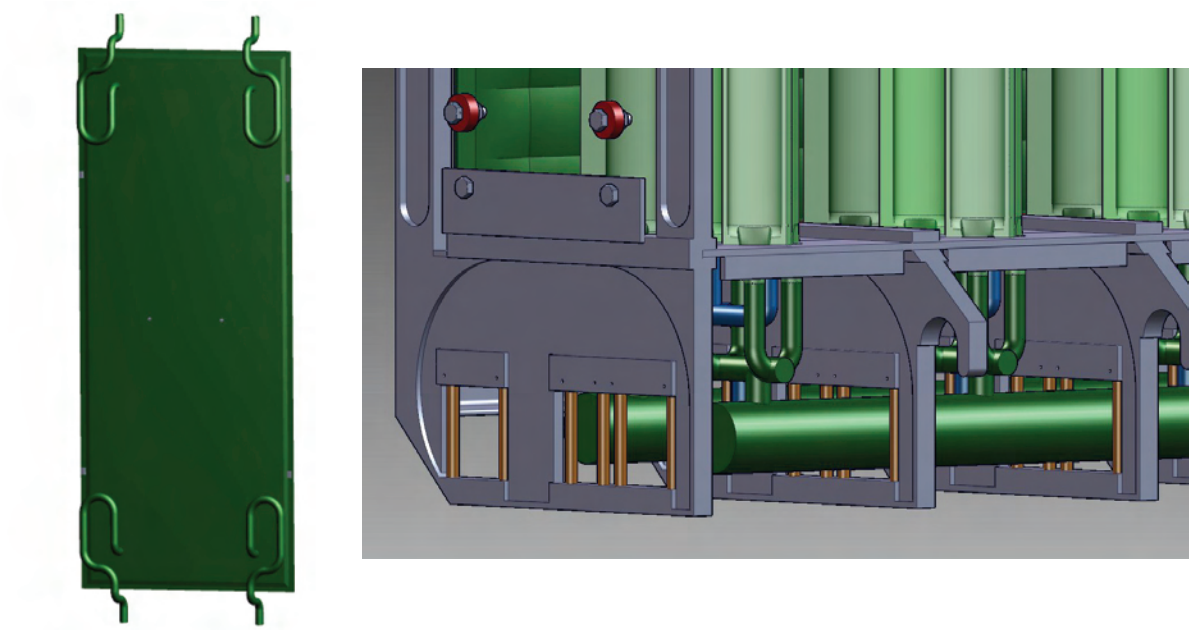

Fig. 1: *Left side*: Radiation back wall with supply pipes which were designed to handle the demanding thermal expansion. *Right side*: Bottom part of the pump showing the hanging support to allow vertical thermal movement while avoiding critical mechanical stresses.

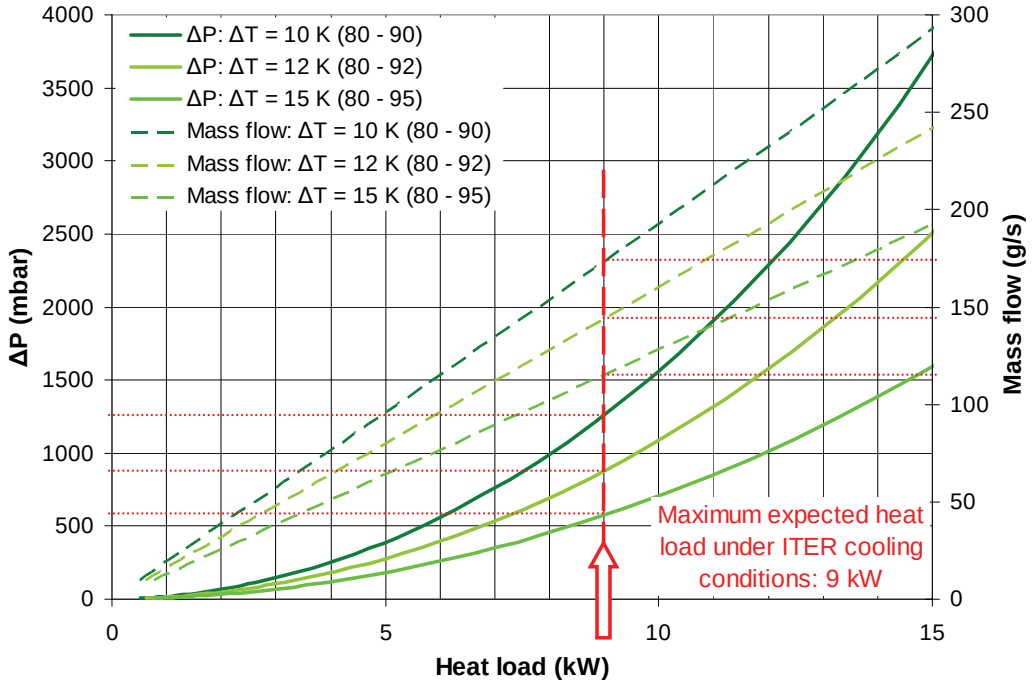

Fig. 2: Pressure drop and mass flow situation in the thermal shield system of one NBI half cryopump during nominal pumping operation depending on the heat load.

Further attention has to be paid on the details of the manifolds to minimize pressure losses and to optimize a balanced mass flow through the different components. Last but not least the whole arrangement has then to be able to withstand all mechanical and thermal stresses and has to fit in the tight space within the cryopump. In addition, during all the design work one has to consider the thermal loads to the circuits caused by thermal conductivity and radiation transport. All these requirements lead to a very demanding design process which can be performed only in a highly iterative way combining design work, FEM analyses, heat load calculations and manufacturing assessments [2]. Figure 3 shows the upper manifold of the cryopump, supplying the cryopanels and the radiation front shielding.

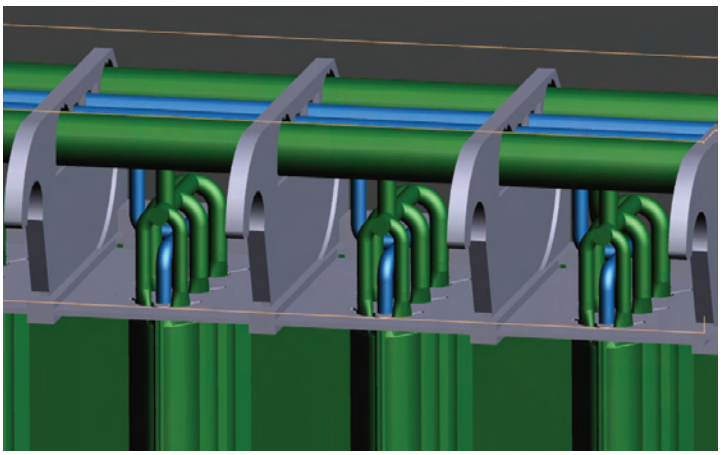

Fig. 3: Upper manifold containing the supply of the cryopanels (blue) and the front shielding panels (green).

3. FEM analyses of all scenarios:

Due to the size of the pump and the demanding temperature range of the pump components during the different operation scenarios, many FEM analyses are needed to check all the individual components, sub arrangements and the whole pump. The thermal loads have to be determined considering that the pump parts are at different temperatures (4 K, 80 K, 300 K). Figure 4 shows a typical result of FEM analyses concerning the estimated bending of the radiation back wall when it is cooled down from 300 K to 80 K.

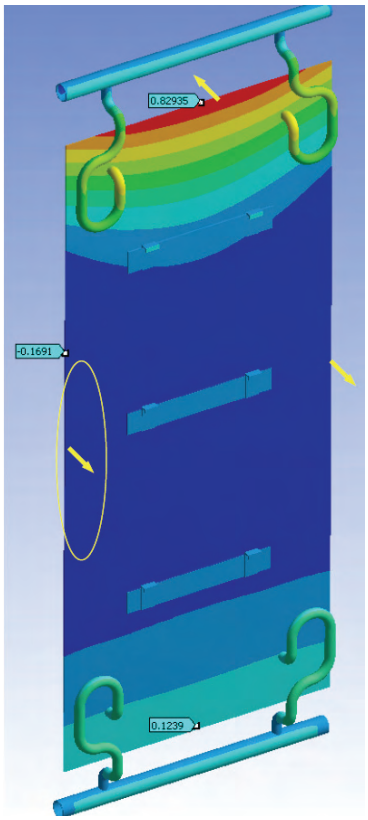

Fig. 4: Example for FEM analyses: curvature of the shielding back wall during bending when cooled down from 300 K to 80 K.

These analyses have to accompany the design process continuously, this means that almost every design step has to be checked and the result is often leading to a redesign and optimisation of the related component.

Gas density simulations of the HNB system

The primary function of the NBI pumping system is to provide a sufficiently low pressure mainly against the high gas flows coming from the neutralizer (43 Pam³/s H_2, 19 Pam³/s D_2). Different to the torus pump, where maximum pumping speed is the design driver, the NBI cryopump must provide a given density profile against three gas sources (ion source, neutralizer, residual ion dump).

Using the KIT vacuum code ProVac3D, the density distribution profiles were calculated in the beam line for different gas baffle designs as well as inside the neutralizer [3]. This work is required to keep the simulations and the resulting predictions up to date, while the design of components in the HNB injector like the gas baffle or the neutralizer is progressing. A refined model of the neutralizer was developed to take into account some unavoidable additional slits and gaps and to assess their consequences to the gas flows and resulting densities. Because the slits allow a certain amount of gas to escape from the neutraliser and this amount of escaped gas has to be pumped properly by the cryopump, such a detail is of a high importance for reliable predictions. Furthermore, several simulations of the gas density profile inside the neutralizer were performed, aiming to describe well the target properties for the beam, which has to be neutralized with a maximum efficiency and homogeneity. Fig. 5 shows these details in the neu-

tralizer design and the result of the two-dimensional gas density simulations inside the neutralizer.

These calculations have been performed at the HPC-FF supercomputer in Jülich.

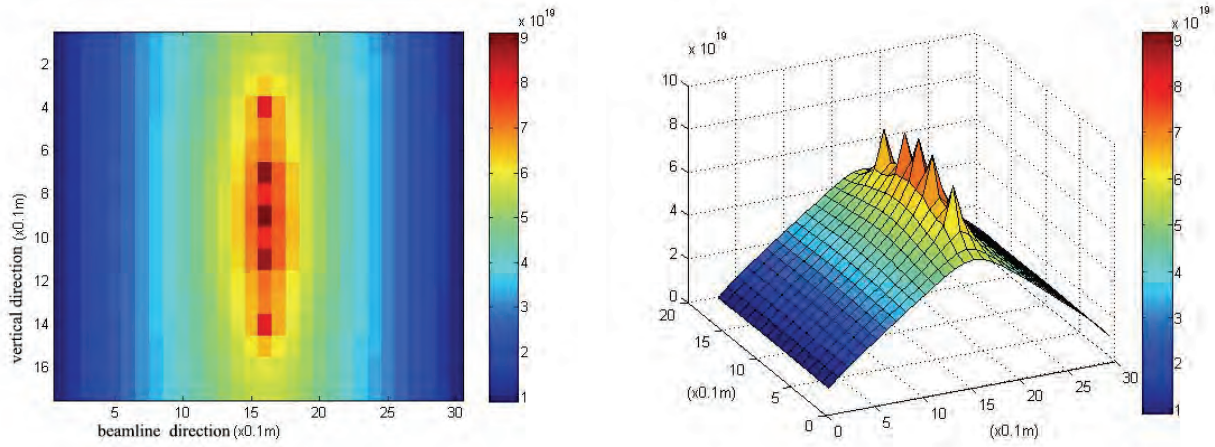

Fig. 5: Refined model of neutralizer for gas simulations and 2 dimensional gas density distribution inside the neutralizer.

Furthermore, the consequences of potential openings in the pump, to realize beam diagnostics in MITICA, were simulated to determine the potential impact on pump operation. These PROVAC3D calculations for the full beamline lead to the conclusion that the implementation of these openings is feasible and will not reduce the pump performance significantly [4]. Nevertheless, the mechanical implementation of the openings will cause an additional design effort which has to be spent in the future. Fig. 6 shows an example of a comparing plot, illustrating the impact of these diagnostic openings in the cryopump on the achievable pressure profile along the beamline.

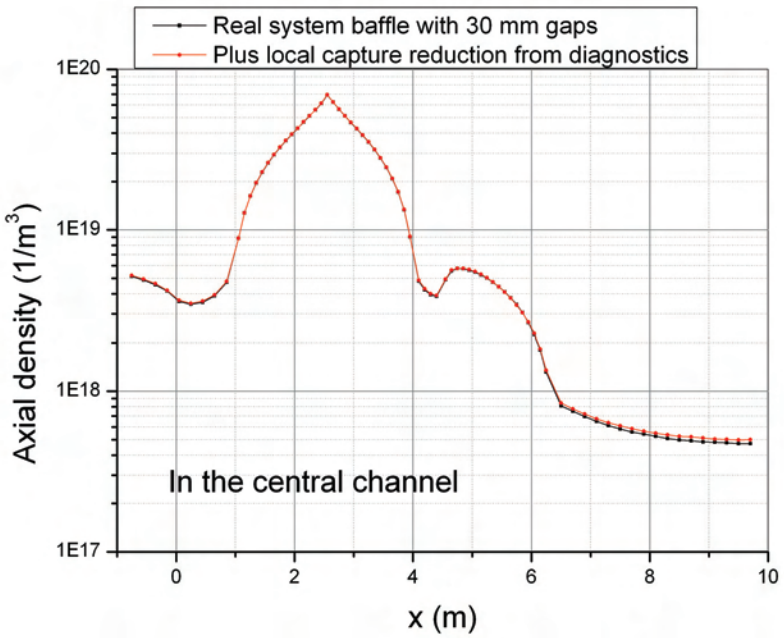

Fig. 6: Gas density simulation with ProVac3D along the beamline. The calculation refers to a beamline with installed gas baffle and compares a cryopump with diagnostic openings and a non affected pump. Obviously the openings reduce the pump performance not significantly.

Conclusions and future work

The design evolution of the HNB cryopump has seen much progress towards the detailed BtP stage. In a follow-up step, the final BtP design of the ITER Heating Neutral Beam cryopump will be adapted to the needs of the PRIMA test bed on site of Consorzio RFX, Italy. The pump for this test bed will be the first NBI pump to be manufactured and the test bed operation also serves the purpose to confirm and validate the design for ITER [5].

The remaining scope of GRT-032 includes the following activities to be performed in 2011:

- Final design of all the passive shieldings, thermal connectors and spacers.
- Recalculation of all pump properties basing on the finalized design.
- FEM analyses of the whole pump for all scenarios.
- Mechanical analyses of the load case caused by ice formation from a water leak.
- Compilation of operating and manufacturing procedures, of the technical specification and all other documents needed for a call for tender.

Staff:

Chr. Day
A. Demsoreanu
St. Hanke
X. Luo
S. Ochoa
M. Scannapiego
R. Simon
H. Strobel

Literature:

[1] M. Dremel, Chr. Day, St. Hanke, X. Luo, Cryopump design development for the ITER neutral beam injectors, Fusion Engineering and Design 84 (2009) 689-693.

[2] Chr. Day, St. Hanke, X. Luo, P. Sonato, The cryosorption pumping system for the neutral beam test facility MITICA, 19th Italian Vacuum Congress, Senigallia, Italy, May 2009.

[3] X. Luo, Chr. Day, A 3D Monte Carlo vacuum modelling of the Neutral Beam Injection system of ITER, Fusion Engineering and Design 85 (2010) 1446-1450.

[4] Chr. Day, H. Haas, St. Hanke, V. Hauer, X. Luo, St. Varoutis, Vacuum engineering of customized cryosorption pumps, 11th European Vacuum Conf, Salamanca, Spain, September 2010.

[5] A. Masiello et al., The European contribution to the developments of the ITER NB injector, SOFT, Porto, Portugal, Sept. 2010.

Acknowledgement

This work was supported by Fusion for Energy under the grant contract No. F4E-2009-GRT-032 with collaboration by RFX, Italy; CNRS, France; IPP, Germany and CCFE, United Kingdom. The views and opinions expressed herein reflect only the author's views. Fusion for Energy is not liable for any use that may be made of the information contained therein.

Investigation of Vacuum Gas Flows for Nuclear Fusion Applications (Fusion Researcher Fellowships – WP08-FRF-FZK/Varoutis)

Background and objectives

Vacuum flows play a central role for several subsidiary systems of fusion reactors. In particular, there are three high vacuum pumping systems for evacuation and maintenance of the needed low pressure levels in the torus, in the cryostat and in the neutral beam injectors (NBI). The achievable pumping speed in all the aforementioned systems is of major importance and therefore a thorough and complete study of the flow conditions is mandatory, so that the optimum values to be achieved.

Each of the vacuum systems consists of networks of various channels with different lengths and cross sections. The flow in such channels varies from the free molecular regime up to the hydrodynamic limit. The aim of this fellowship was to study on numerical and experimental basis overall quantities of practical interest as for instance the mass flow rate and the conductance, for various lengths and cross sections and in the whole range of Knudsen number.

Experimental set-up

To compare with the calculations and to enlarge the existing and still very scarce data base of transitional flows, a large scale test facility has been set up at KIT. The basic principle of the TRANSFLOW test rig (Transitional Flow Range Experiments, see Figure 1) is the measurement of the conductance of different channels in the transitional and near transitional flow regime at isothermal conditions. TRANSFLOW is based on the direct dynamic approach, where a constant flow is adjusted and the pressure difference is measured [1]. The constant flow into the test rig is provided by a dosing unit. The temperature and pressure of the injected gas can be measured in the dosing dome, which is directly connected to the dosing unit. The test channel is following the dosing dome in flow direction. On the downstream end it is connected with the pump dome. The pump dome serves to measure temperatures and pressures at the outlet side of the test channel. It is also equipped with turbomolecular pumps, which are further connected to the forepumps, to maintain the vacuum conditions inside the system. For the experimental work, several short and long channels with various cross sections have been already used [2].

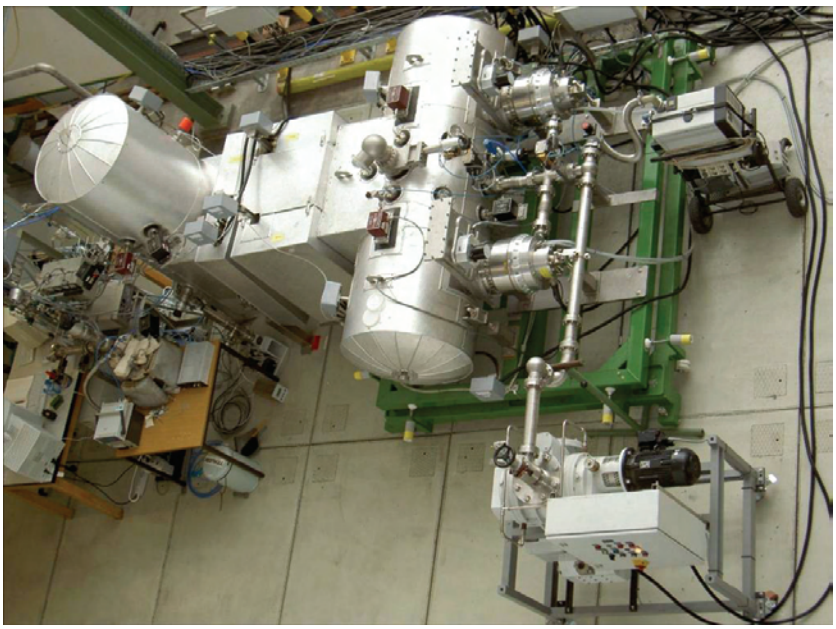

Fig. 1: TRANSFLOW test rig.

Investigation of gas-surface interaction

This investigation was focused on the experimental and numerical simulations concerning the importance of the gas-surface interaction model in the simulation of gas flows through piping elements under low, medium and high vacuum conditions. By implementing the Cercignani-Lampis kernel for the description of the gas-wall interaction in the kinetic equation, the tangential momentum accommodation coefficient (TMAC) a_t could be specified for different gases (in terms of the molecular mass) and for different surfaces (in terms of roughness).

The Fig. 2 exemplifies this work for helium and rough (untreated) surface. By systematic variation of the TMAC and comparison with the experiments, the best fit was found for a_t=1.15. It was also revealed that the TMAC does not much depend on the flow regime. This was not confirmed for all investigated cases, so that further studies will be performed in the future.

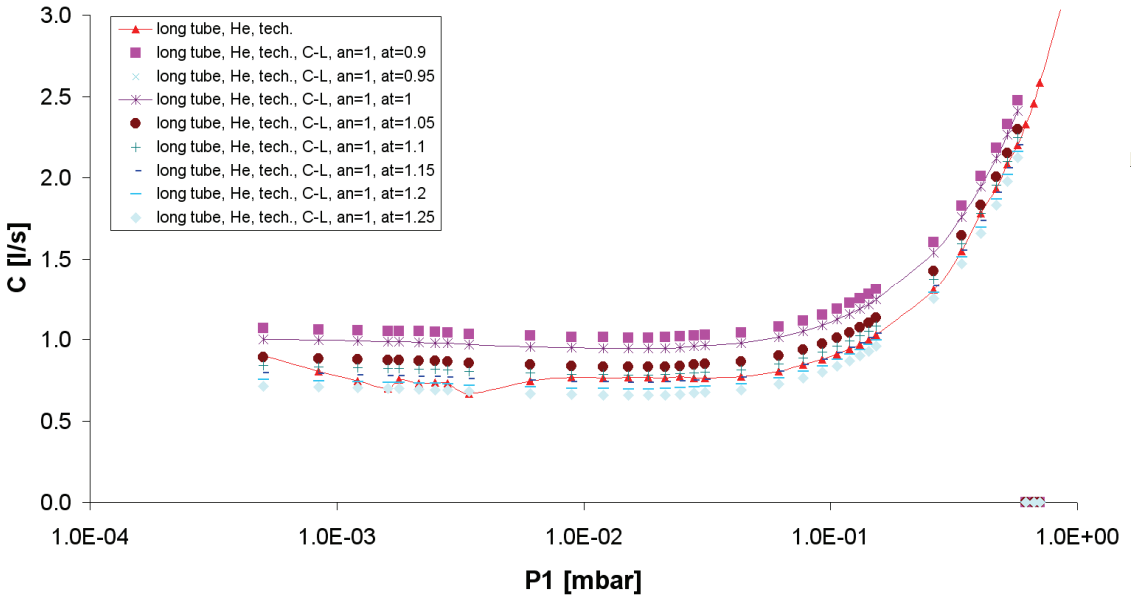

Fig. 2: Experimental and computational conductance in terms of the inlet pressure for a long tube with rough surface and various values of the momentum accommodation coefficient a_t (gas helium, average temperature 296 K).

Rarefied gas flows through short channels

Each vacuum system of the complexity typically found in nuclear fusion devices can be represented by a node network of various channels with different lengths and cross sections. KIT is usually applying the ITERVAC vacuum network code for such systems. The flow in such channels may vary from the free molecular regime, through the transition until the hydrodynamic limit. A typical fusion vacuum system comprises mainly short tubes in which the flow is characterized as developing and end effects may not be ignored. Although an extensive knowledge has been accumulated on transitional flows in orifices and short tubes, there have been few investigations of these geometries from the point of view of vacuum applications [3-5]. Furthermore, comparative studies between computational and experimental results for flows through tubes of finite length are very limited. Thus, to provide a thorough basis for channel flow prediction, and for validation of ITERVAC, a parametric program has been launched at KIT focusing on the experimental and numerical investigation of gas flows through tubes of variable finite lengths. The flow rate and associated pressure difference measurements have been conducted in TRANSFLOW. The flow through such tubes has been computed, both at KIT and at the University of Thessaly, using the direct simulation Monte Carlo method (DSMC) (Fig. 3).

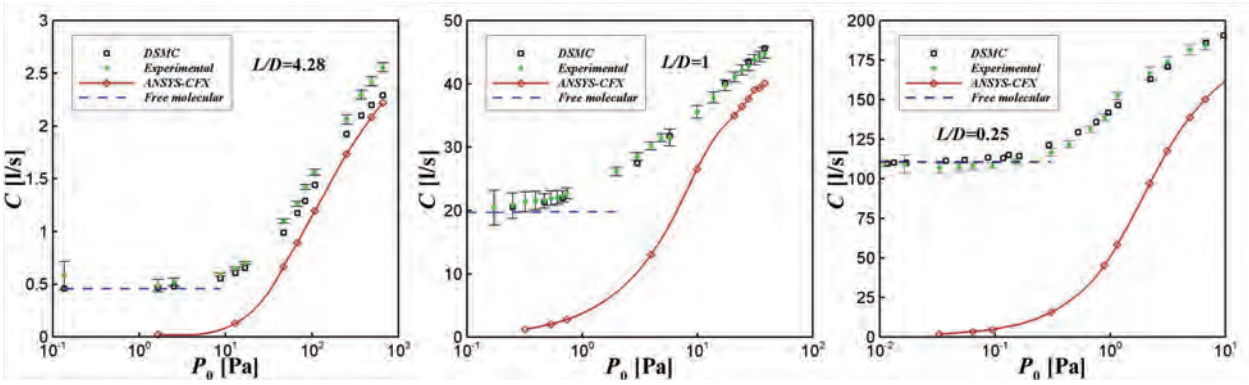

Fig. 3: Comparison between experimental and numerical results for short tubes with L/D=4.28 (left), L/D=4.28 (middle), L/D=0.25 (right), (Gas nitrogen, average temperature 296 K).

It was found that the DSMC method is capable of providing reliable results in the whole range of gas rarefaction and for various configurations [6]. Also, in all presented cases, a very good agreement is observed between corresponding numerical and experimental results for specific range of Knudsen number, while the average relative error is of the order of few percent. Larger discrepancies between experimental and numerical results are only observed at small flows in the free molecular regime, where the measurement uncertainty in the experiments gets higher. However, this regime can be very well described with the TPMC method (these curves are also given in Fig. 3). The corresponding ANSYS-CFX calculations for high values of the Kn number fail to describe accurately the physics of the flow. On the other hand for small values of Kn the corresponding CFX and experimental results are in good agreement.

In addition to the various short circular tubes, rectangular geometries have also been investigated, both experimentally and numerically [7, 8].

Rarefied gas flows through short expanding/contracting tubes

In the last decade, significant progress has been made in modelling flows in long straight tubes where the gas density (or pressure) varies only in the flow direction [2]. The scope of the present work was to study on numerical and experimental basis the flow through two circular tubes with different diameters joined together in the whole range of Knudsen number. The flow is due to a pressure gradient moving from the small towards the large diameter pipe or from the large towards the small diameter pipe. It may be considered as flow through a tube with a sudden expansion or contraction, respectively, and this is a typical set-up in vacuum gas networks.

The computational work was based on the Direct Simulation Monte Carlo method (DSMC), while all experiments (Fig. 4) have been performed at the TRANSFLOW test facility at KIT. The figure shows that the numerical results for ANSYS-CFX based on the Navier-Stokes equation cannot describe the real flow conditions since the Kn number is not low enough in order the continuum approach to be valid. Furthermore, in the viscous and free molecular regime the conductances for a contraction and expansion tube tend to be the same, while in the transition regime a deviation between both geometries of the order of 15% is observed.

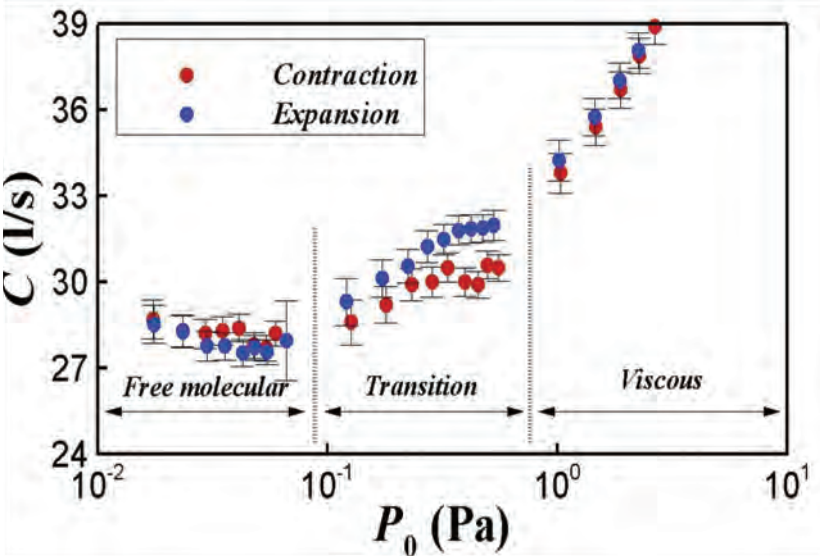

Fig. 4: Experimental conductance curves for contraction and expansion tube (Gas nitrogen, average temperature 296 K).

Numerical modelling of the ITER model cryopump

The main duty and design driver of the vacuum pumping system for the torus of ITER is to pump out a fusion exhaust gas during plasma burn. Such a system must meet many strict requirements. The concept for this cryovacuum system has been developed at the Institute for Technical Physics at KIT. A further development and improvement of the system requires a numerical modelling of the gas flow inside the vacuum chamber and near the cryopanels. When one deals with gas flows in a complicated geometrical configuration, usually, the Direct Simulation Monte Carlo (DSMC) or Test Particle Monte Carlo (TPMC) methods are employed. The first one can be used for arbitrary Knudsen number, but it requires simulating a huge number of model particles simultaneously and is limited in a detailed representation of complex geometries. The second method consists of simulation of individual particle trajectories with less computational effort. This method allows considering three-dimensional flows with many surfaces of complex configuration, but does not hold at lower Kn where intermolecular collisions have to be considered. The aim of the present work was a numerical modelling of the ITER model cryopump combining both DSMC and TPMC methods, namely, the flow between the cryopanels is simulated by the TPMC method and then these results are used as input data for the DSMC method.

Due to the experiments with the ITER model pump which were performed at KIT several years ago, a broad experimental data base is available which could be used to validate the calculations. The detailed comparison demonstrated the reliability of the computational tool [9]. The numerical results provide detailed information about the gas flow field (see Fig. 5) such as pressure distribution, number of particles and energy flux absorbed by each cryopanel, etc. These quantities can be used to optimize the pumping system in order to improve its performance.

It must be noted that this challenging activity was only possible because access to the HPC-FF supercomputer in Jülich was granted via an EFDA task. The massive computational work was done in 2010 under the SIMVAC project and it is aimed to continue the use of HPC-FF for further cryopump design optimisation.

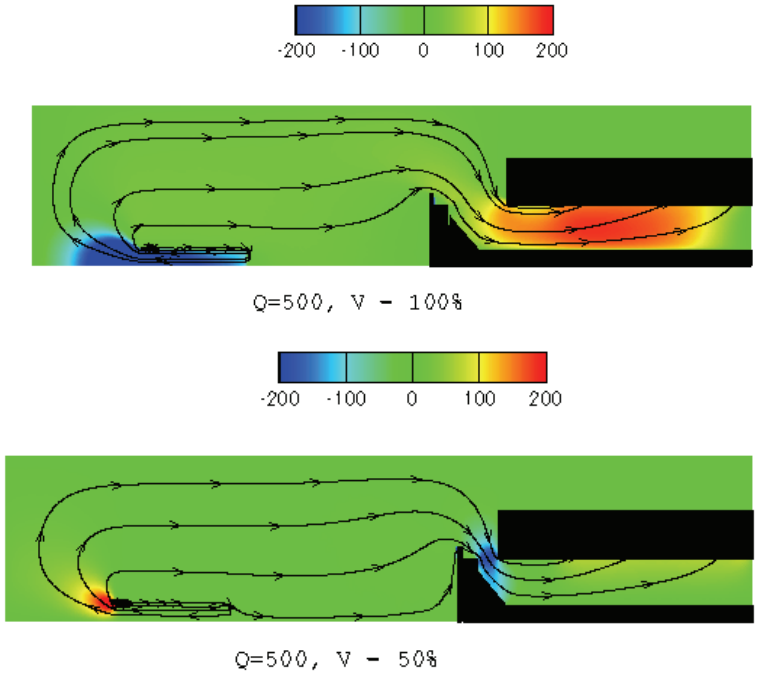

Fig. 5: Axial velocity contour and streamlines for gas helium with throughput 500 sccm and 100% (top) and 50% (bottom) opening of the valve. Shown is the installation situation of the pump in the TIMO test vessel, with a gas flow injected from a tube, passing the inlet valve and being pumped in the pump interior volume.

Conclusions

The scope of this fellowship programme was threefold. Firstly, the experimental facility TRANSFLOW should be largely exploited, all measurements should be fully evaluated and interpreted in a consistent way. Secondly, the ITERVAC code, which was the basis for the design of the ITER divertor pumping system, should be further benchmarked. Thirdly, complementary code development and independent theoretical calculations should be performed.

All three objectives were perfectly met. The facility was under continuous operation except for some (regular and unforeseen) maintenance intervals. By interpretation of the results, the applicability limits of the existing ITERVAC code were assessed and it was found that the description becomes poor for very short channels. Hence, the code will now be upgraded based on the experimental results provided under this fellowship. On top of that, a variety of numerical codes, especially by DSMC, has been developed for several geometries and by comparison with the experimental results it was learnt under what conditions they provide reliable results [10]. Finally, the behaviour of an ITER-type cryopump with its full complexity was successfully described in a two-staged theoretical approach combining TPMC and DSMC. This represents a major milestone in the R&D of fusion vacuum pumping and it is expected that the developed procedure will be further used for ITER as well as for the vacuum systems of a future power plant.

The post-doc researcher has accepted a new working contract by KIT and will further continue his studies in the area of fusion vacuum systems. In the future, additional channels will be calculated and measured in TRANSFLOW including tubes with L/D=40 and 60, slits, bellows and bends, which are important components in vacuum technology.

Staff:

Chr. Day
Th. Giegerich
V. Hauer
X. Luo
P. Pfeil
H. Stump
St. Varoutis
S. Misdanitis, S. Pantazis (Guest scientists, University Thessaly, Volos, Greece)
F. Sharipov (Guest professor, University Curitiba, Brasil)

Literature:

[1] V. Hauer, Chr. Day, Measurement of the conductance in the Knudsen flow regime, Symp. On Vacuum Science and Technology, Kaiserslautern, Sept. 2010.

[2] S. Varoutis, S. Naris, V. Hauer, Chr. Day, D. Valougeorgis, Computational and experimental study of gas flows through long channels of various cross sections in the whole range of the Knudsen number, J. Vac. Sci. Technol. A 27 (2009) 89-100.

[3] S. Varoutis, D. Valougeorgis, O. Shazhin and F. Sharipov, Rarefied gas flow through tubes into vacuum, J. Vac. Sci. Technol. A 26 (2008) 228-238.

[4] S. Varoutis, D. Valougeorgis and F. Sharipov, Simulation of gas flow through tubes of finite length over the whole range of rarefaction for various pressure drop ratios, J. Vac. Sci. Technol. A 27 (2009) 1377-1391.

[5] S. Varoutis, V. Hauer, Chr. Day, S. Pantazis and D. Valougeorgis, Experimental and numerical investigation in flow configurations related to the vacuum systems of fusion reactors, Fusion Engineering and Design, 85 (2010) 1798-1802.

[6] St. Varoutis et al., Experimental and numerical investigation of vacuum gas flows in fusion vacuum systems, SOFT, Porto, Portugal, Sept. 2010.

[7] S. Pantazis, St. Varoutis, Chr. Day, D. Valougeorgis, Gas-surface scattering effect on vacuum gas flows through rectangular channels, European Vacuum Conference (EVC), Salamanca, Spain, Sept. 2010.

[8] St. Varoutis, F. Sharipov, Rarefied gas flows through channels of finite length due to arbitrary pressure ratio, Int. Symp. On Rarefied Gas Dynamics (RGD), Pacific Grove, CA, USA, July 2010.

[9] F. Sharipov, St. Varoutis, Chr. Day, X. Luo, H. Haas, Numerical modelling of the ITER model cryopump, Int. Vacuum Congress (IVC), Beijing, China, Aug. 2010.

[10] Chr. Day et al., Recent developments in vacuum flow modelling, Int. Vacuum Congress (IVC), Beijing, China, Aug. 2010.

Acknowledgement

This work, supported by the European Communities under the contract of Association between EURATOM and Karlsruhe Institute of Technology, was carried out within the framework of the European Fusion Development Agreement. The views and opinions expressed herein do not necessarily reflect those of the European Commission.

Thermohydraulic Investigations on Hydroformed Components (CoA)

Background and objectives

The PPC and NBI cryopumps are composed of a cryopanel system cooled by supercritical helium (ScHe) at about 4.5 K and 0.4 MPa and a thermal shield system supplied by gaseous helium at about 80 K and 1.8 MPa in nominal pumping operation. The cryopumps must operate under a certain ΔT and have to follow a cycle of stagewise regeneration at different temperature levels (100 K, 300 K and 470 K). Thus, the pressure drops across the cryopump systems are critical issues regarding the helium supply. The internal structures of the cryopumps are mainly composed of several hydroformed components used for an optimized cooling of the cryogenic circuits (see Fig. 1). The hydroformed components are made of two stainless steel plates welded one over the other and inflated by high pressure water, resulting in quilted panels of various geometries. Due to the complexity of the internal structure of the hydroformed components it is neither feasible to predict the thermohydraulic behaviour using empirical laws, nor it is possible to fully rely on results obtained with CFD analysis. For this purpose, the experimental facility THEA (Thermohydraulic Experimental Arrangement) is under operation at KIT, in order to measure pressure losses directly at 1:1 scale components and, thus, to build up a most reliable data base for thermohydraulic design of the pumps.

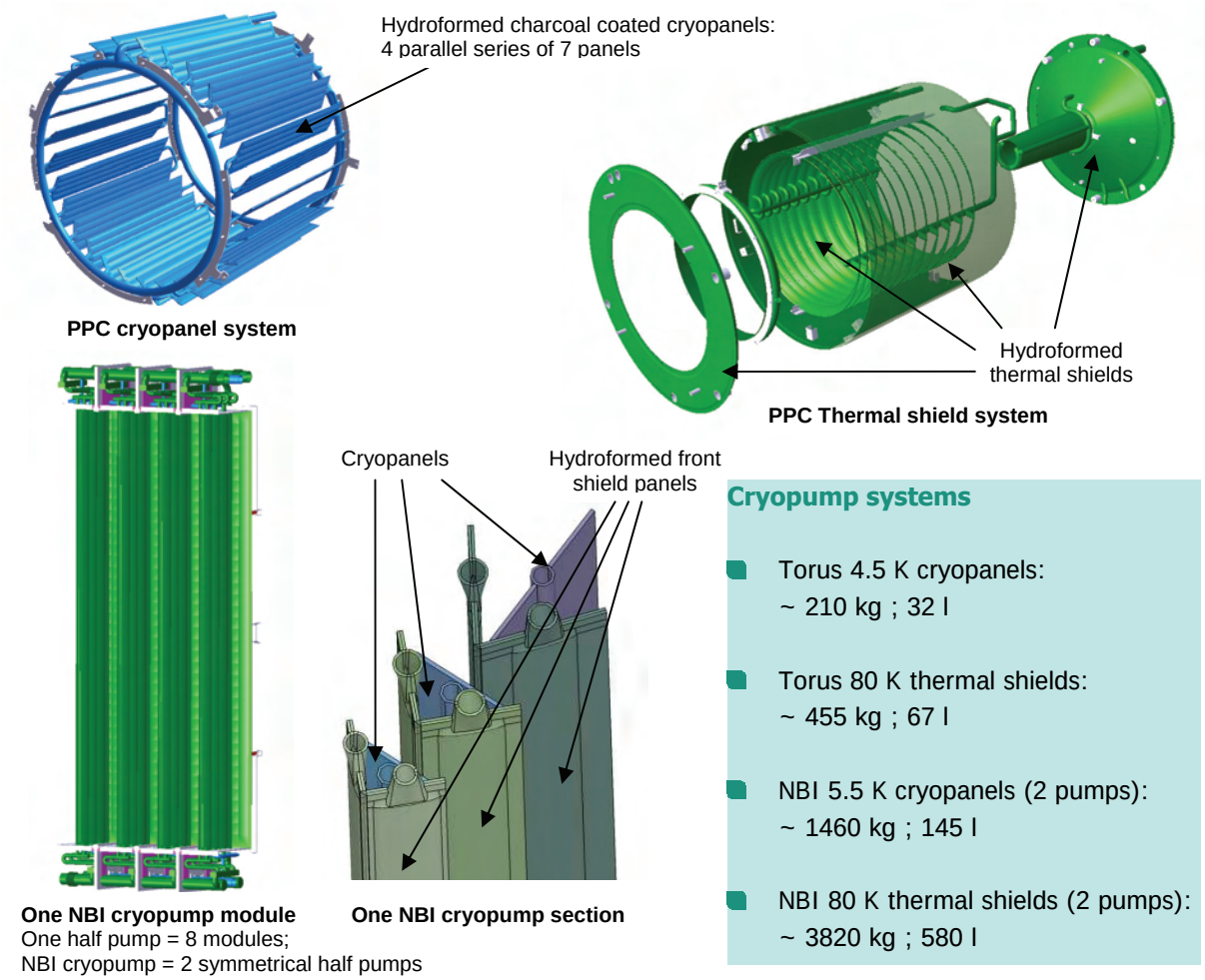

Fig. 1: The PPC and NBI cryopanel systems (in blue) and thermal shield systems (in green) are made of various hydroformed components.

Experimental results: hydraulic resistance coefficients of the hydroformed components

A descriptive approach based on the coefficients of hydraulic resistance – assessed with both experimental results and literature correlation – has been used in order to characterise the pressure drop behaviour of the complete cryopump circuits as precisely as possible. The pressure drop coefficients combine many complex phenomena under a single factor and are therefore well adapted to create models of large and complex systems such as the cryopumps.

For this purpose, some representative hydroformed components have been procured and measured (pressure drop measurements) at KIT using the THEA facility, which is a circulating water loop equipped with sensors (Figure 2). Using the collected data, the hydraulic resistance coefficients can be determined as a function of the Reynolds number. According to the Re analogy, the only criterion to be satisfied if flow conditions – and so hydraulic resistance coefficient – are to be the same in two similar components is that the Reynolds number is the same.

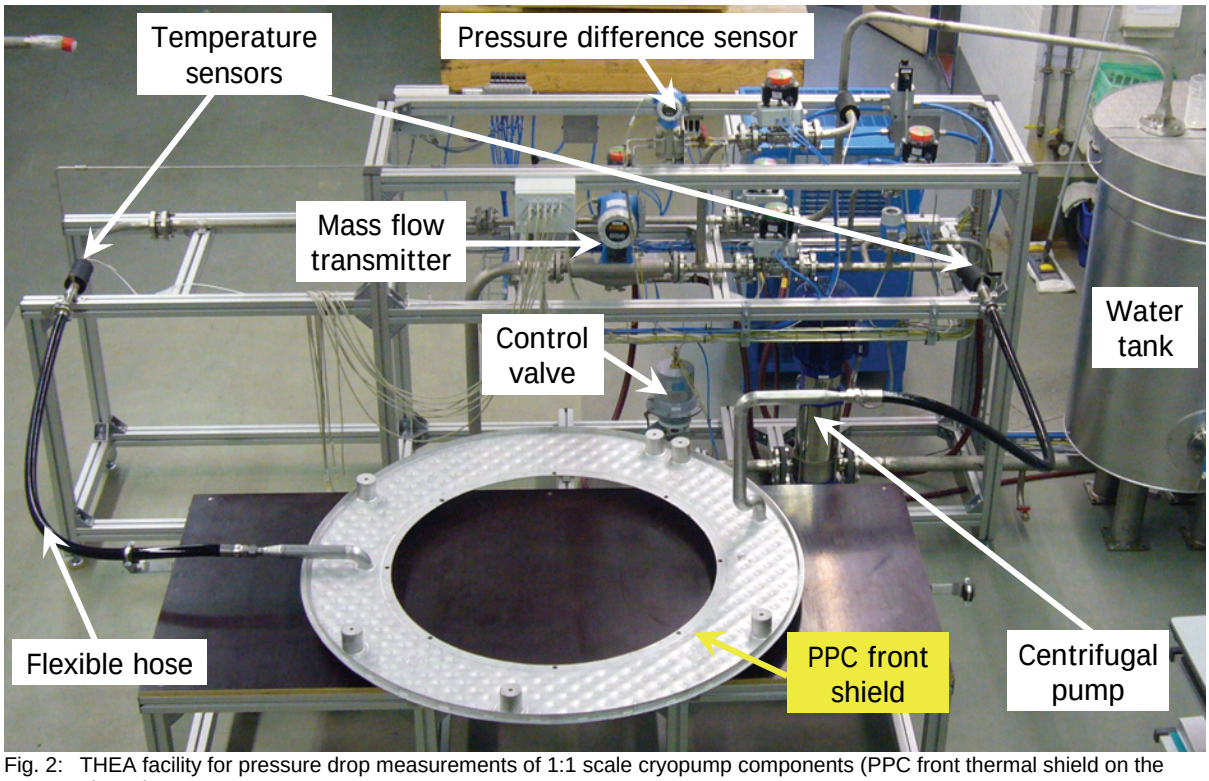

Fig. 2: THEA facility for pressure drop measurements of 1:1 scale cryopump components (PPC front thermal shield on the picture).

Figure 3 illustrates the hydraulic resistance coefficients depending on the Reynolds number for several test components, which will be used in the PPC or the ITER NBI/MITICA cryopump, respectively.

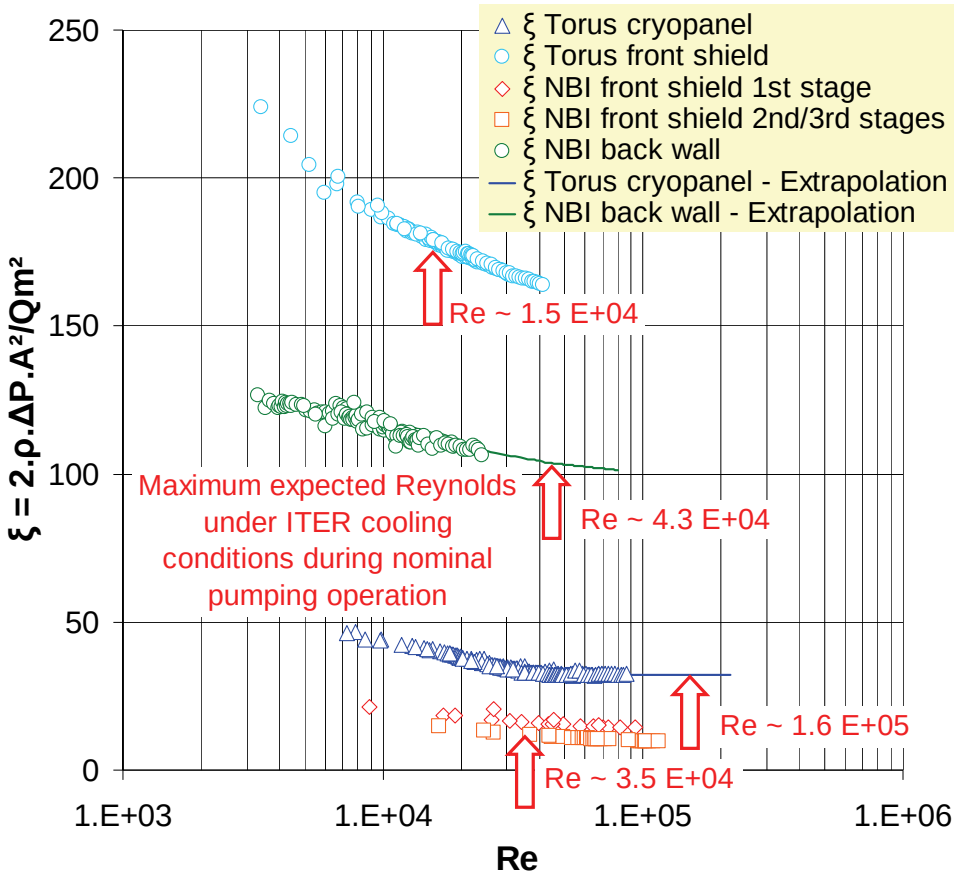

Fig. 3: Hydraulic resistance coefficient ξ depending on the Reynolds number *Re* of several cryopump hydroformed components. ξ combines the pressure drop Δp, the density ρ, the flow cross-section A and the masss flow Q_m.

Pressure drop in the PPC and NBI cryopumps

The various hydroformed components of the cryopump are connected together by assemblies of tubes, bends, diverging and converging tees. The pressure drop coefficients of the latter components have been assessed using empirical laws taken from text books. Then, all the hydraulic resistance coefficients are integrated according to the flow schemes to complete models of the cryopanel and thermal shield circuits which allow calculating the pressure drops in the various part of the circuits, and the corresponding heat load for any steady state flow condition.

The thermohydraulic models of a complete circuit consist of several subsystems seen as black boxes corresponding to one component or a set of components where a specific resistance coefficient and a specific heat load is applied. The helium properties (pressure, enthalpy, temperature, density and viscosity) are recalculated at the outlet of each black box and used as input parameters for the calculations performed in the following box. The distribution of the flow between parallel paths has been assessed. Thus the non uniformity of the heat load and its influence on the temperature distribution and the pressure drops can be investigated. Especially for the NBI cryopump, the unbalanced heat load along the beam line vessel leads to a unequal heat load deposition on the pump and has to be taken into account for a reliable prediction of the behaviour concerning pressure loss, temperature and flow distribution inside the shielding system.

As an example, the following Fig. 4 shows the determined pressure loss of the entire PPC cryopanel and thermal shield systems in nominal pumping cooling conditions. Several cryopanel ΔT corresponding to various inlet temperatures have been investigated, as the inlet temperature of the PPC pump is expected to vary in ITER. The graphic clearly shows the

influence of the variation of the inlet temperature on the helium consumption of the pump (and so the ΔP).

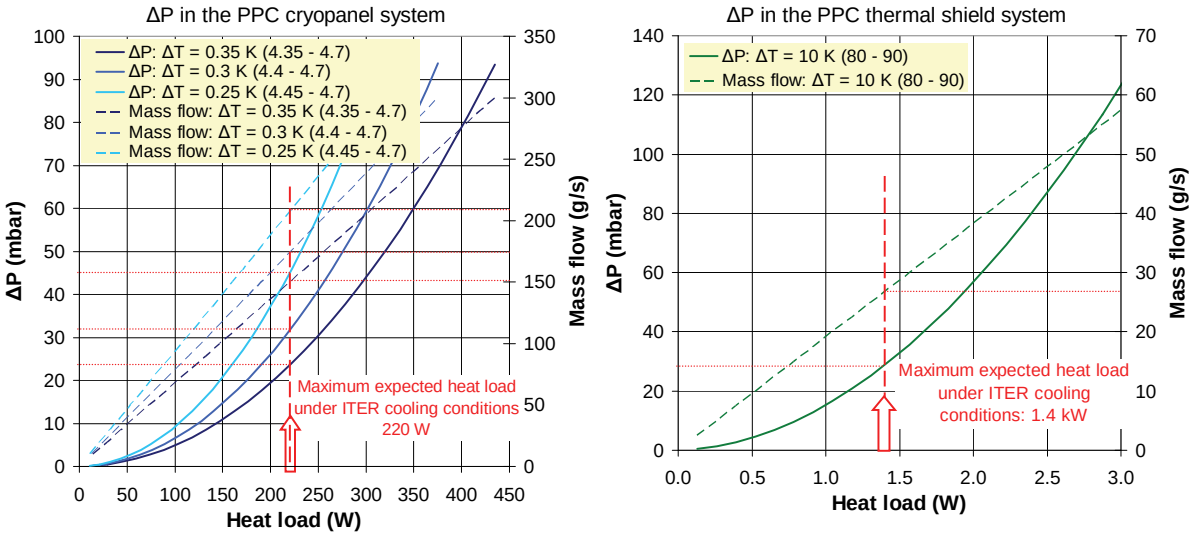

Fig. 4: Pressure drop and mass flow in the cryopanel and thermal shield systems during nominal pumping operation of the PPC depending on the heat load. The current requirements of 0.35 K ΔT (cryopanel system) and 10 K (thermal shield system) and a maximum ΔP of 350 mbar (cryopanel system) and 1 bar (thermal shield system) are achieved.

Additional steady state calculations at regeneration temperatures (around 100 K, 300 K and 470 K) have been performed in the perspective of the cryopump regeneration operation modes study.

Status and future work

The thermohydraulic investigations on the PPC cryopump, partly done under F4E grant F4E-2009-GRT-018, have been fully achieved and no additional work related to the cryogenic cooling of the pump is foreseen [1]. The design work on the NBI cryopumps (ITER-HNB and MITICA) is still ongoing [2,3] and there are a series of open issues which remain to be tackled in order to have a fully consistent modelling of the thermohydraulic behaviour of these pumps.

As mid-term goal for the next years, starting from the steady-state description of the cryogenic circuits, it is intended to elaborate a transient description of the regeneration process [3].

Staff:

Chr. Day
St. Hanke
V. Hauer
T. Johann
M. Scannapiego
R. Simon
J. Weinhold

Literature:

[1] M. Scannapiego, Chr. Day, St. Hanke, V. Hauer, Thermohydraulic investigation on the ITER torus and neutral beam injector cryopumps, 23rd Int. Cryogenic Engng Conf. (ICEC), Wroclaw, Poland, July 2010.

[2] Chr. Day et al., Design progress for the ITER torus and neutral beam cryopumps, SOFT, Porto, Portugal, Sept. 2010.

[3] M. Scannapiego et al., Thermohydraulic investigation on the operation of the ITER torus and neutral beam injector cryopumps, SOFT, Porto, Portugal, Sept. 2010.

Acknowledgement

Part of this work was supported by Fusion for Energy under the grant contracts No. F4E-2009-GRT-019 and F4E-2009-GRT-032. The views and opinions expressed herein reflect only the author's views. Fusion for Energy is not liable for any use that may be made of the information contained therein.

Fuelling & Pumping Studies under the EFDA Heating & Current Drive, Fuelling and Pumping Topical Group (WP10-HCD-01-07, WP10-HCD-02-03)

Background

In 2009, EFDA initiated a new Coordinating Committee on Fuelling and Pumping (CCFP) and KIT is currently providing the acting Chair. The CCFP was formally set up as sub-group within the Topical Group Heating & Current Drive (TG H&CD). The first official step for CCFP was the kick-off meeting held at 10 February 2010 during the TG H&CD week in Cadarache.

The CCFP Chair oversees the execution of the EFDA work programme in the area fuelling and pumping. The main tasks are to develop mid- and long-term strategies towards a power plant device and to advise EFDA in launching new R&D activities.

The CCFP actions in 2010 have been organised in two separate parts, a physics part (monitored by CEA) and a technology part (monitored by KIT).

Assessment of the divertor pumping system for control

The simulation of the ITER torus vacuum system with the ITERVAC network code was already started in 2004/2005 based on a simplified half size model and updated a few times after that. Since the last update in 2007, the design of the vacuum system was under continuous development, especially in the divertor region. It was therefore decided to significantly extend and revise the existing model to simulate the gas flows inside the ITER divertor pumping system and to include new gas sources, paths and sinks. Altogether, the number of channels was increased from 888 (in year 2007) to 1428. The obtained model is shown in Figure 1. It is considered by ITER to still be representative for the situation in 2010.

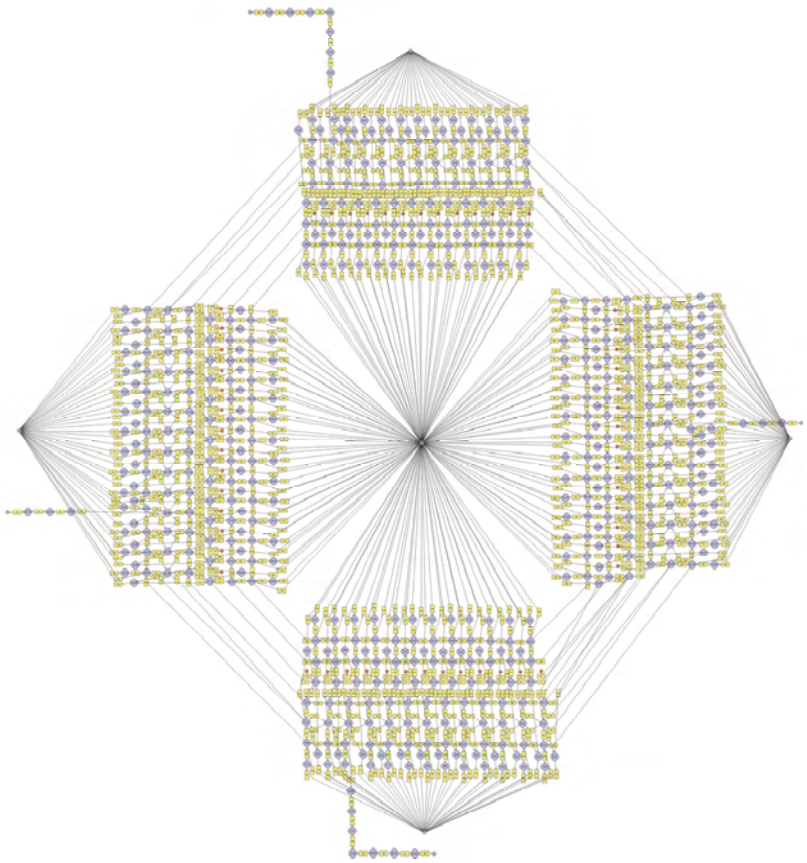

Fig. 1: ITERVAC model of the full ITER torus vacuum system (the plasma (centre) and four active pumps are modelled as sinks; the divertor dome is modelled as source).

The main influence was found to come from the inclusion of the various different diagnostic cassettes and the new design of the outer cassettes support. This helped to reduce the conductance towards the plasma. It became obvious that the recycle flows towards the plasma are in all cases higher than the ones which are pumped by the attached cryopumps. The high backflow of gas to the plasma will reduce the gas throughput into the torus cryopumps and will thus have an influence on plasma edge control. In relative terms, the performance of the divertor pumping system in terms of neutral gas exhaust has not improved compared to the former design of 2007: Still, the conductance towards the plasma side is higher than towards the pump side. But at least the absolute value of system conductance could be increased significantly. The molecular conductance value is now ~ 100 m^3/s (for D_2) and thus approximately three times higher than the limited conductance of the original three-finger configuration has been.

It was confirmed that the ITER project requirements can be met, but it is important to emphasize that the throughput which can be handled is much reduced at the low pressure end. For DT it is a factor 3 smaller than what can be processed at higher pressures; for He, it is even a factor 6.5 smaller. In this respect, the contribution of the divertor pumping system on particle control cannot be employed. It is expected that in most cases, the maximum pumping speed will be required and the inlet valve will always be 100% open. This is an important result, especially in view of the fact that the project requirements given above for helium, are considered to be absolute minimum by the plasma physicists. It is clear now that even to fulfil these, the pump system has to work at 100% of its performance.

For future devices, such as DEMO, it should be aimed to have a more flexible pumping system which is able to cope with significantly higher throughputs than nominal, and is equipped with a control mechanism to throttle the available pumping speed. The much increased pumping speed could be provided by a distributed pumping system rather than a port-located one. The throttling mechanism should be fast (msec scale rather than sec scale (current ITER time constant)).

Fuelling and pumping systems review in view of DEMO

The fuelling and pumping systems of a fusion device are the pacemaker of all torus and plasma operation under nominal and off-normal conditions [1]. The technology for ITER is very much customized and a direct scale-up towards the power plant level is problematic.

A suitable pumping & fuelling system for a fusion power plant also has to include an embedded control function for gas throughputs (fuel gas and He ash recycle flows) to assist the plasma control system and has to be compatible to the disruption mitigation techniques used at the power device (today still unknown). An additional functionality which will be asked from the torus exhaust pumping system (or an additional, dedicated pumping system) is to provide improved density control for the specific magnetic configuration the power plant device will have (divertor concept, plasma shape etc.). The fuelling systems of ITER take over functions of fuel supply and plasma control (disruption mitigation and ELM pacing), but also there remains the issue of proper scale-up. The plasma control function needs further R&D work and is of key importance for a power plant in view of the requested availability.

First step: Check existing technology with regard to its potential for scale-up

The fuelling systems of ITER take over functions of fuel supply and plasma control (disruption mitigation and ELM pacing). Fuelling in ITER relies on pellets at relatively low velocities, injected from the high field side, and on the ∇B-drift to increase core fuelling efficiency. The design of ITER does not allow high speed pellet injection, which is considered to be needed for a power plant.

Concerning pumping systems, cryosorption pumping at 5 K is the reference primary pumping concept for DT reactors to ensure highest pumping speeds and lowest ultimate pressures for

the large fuel throughputs and recycling needs. Expertise in the design of customized cryopumps is available, and any power plant requirements for more pumping speed is more or less a question of giving more cross-section to pump out.

The situation is more critical for the backing pumps, because tritium-compatible mechanical pumping is still an issue. Dedicated R&D had been started in Europe to develop a tritium-compatible screw or roots pump, but the programme was stopped because the ITER fore-pumping procurement package was given to US. Hence, ITER is now using a customized cryogenic forevacuum compressor (JET-style) - which is clearly not an option for a fusion power plant – and combines this with a dry piston pump, which needs further development to reduce the high maintenance requirements.

In summary, it was revealed that one cannot learn from ITER in the areas of blanket tritium extraction technology at the level needed for a power plant, in the area of deep pellet injection, and in the area of rough pumping technology. The lessons ITER will teach are useful for the areas of cryogenic pumping at 5 K and tritium plant systems. However, these two areas are just the ones expected to change for a power plant, see below.

Second step: Development programme of technology for DEMO

For primary pumping purposes, a viable alternative to the 5 K cryopump for burn operation with reduced operating costs and equivalent availability should be demonstrated. Recommended technology to investigate in further detail is the cold turbopump and the superpermeable membrane pump. Complementary to that is the development of a multi-stage tritium-compatible mechanical pump with reduced ultimate pressures. For dwell operation, a cryopump is obligatory, but a sorbent must be identified and validated which works at the expected temperatures of high temperature superconductors.

An integral modelling approach which interlinks fuelling and pumping systems with tritium systems and plasma physics must be developed. The elaboration of predictive tools for neutral gas flows including recent computational algorithms for vacuum gas dynamics is mandatory to end up with a sound design for all sub-systems impacting the plasma operation (pumped divertor, gas injection (incl. gas puffing for ICRF coupling, disruption mitigation and ELM pacing) etc.). This would reduce the needs for future large scale validation experiments in this area.

For fuelling pellet injectors, experiments on present day tokamaks are mandatory because the design of ITER does not allow high speed pellet injection. Points to investigate are – among others - the maximum acceptable pellet particle content, the optimum deposition radius and the possible triggering of NTMs. From an operational point of view, the plasma control function is of key importance in view of the requested availability for a commercial power plant. For massive gas injection for disruption mitigation there results a direct interlink to the torus exhaust vacuum system, which has to be properly considered. On the long term, the possibility of fuelling through the injection of compact toroids will have to be discussed.

Finally, possibilities to simplify the ITER style inner fuel cycle were discussed.

On a mid-term perspective, once the science-based predictive modelling capability is available, it may be possible to develop a novel, much better interlinked pumping and tritium system as is the case for ITER; for example based on direct internal recycling (DIR concept) of the unburnt fuel fractions upstream of the torus vacuum pumps, thus resulting in significantly reduced throughputs for the tritium plant and vacuum pumping systems. Consequently, this would reduce the necessary size/pumping speed of the transfer vacuum pumps towards the tritium plant.

Additional CCFP tasks in 2010

On top of the above two KIT tasks described in detail, CCFP was responsible for the following activities:

1. Constitution of a pellet fuelling and trajectory database (CEA and HAS).
2. Further work on the HPI2 code to model pellet physics (CEA).
3. Analysis of the Kruskal-Schwarzschild instability of a pellet ablation cloud (HAS).
4. Pellet fuelling experiments at MAST (CCFE).
5. Pellet injector technology considerations for deep fuelling purposes (CEA).
6. Studies on cold turbomolecular pumps (CEA).

The technology issues will be continued in 2011 as part of the new Power Plant Physics and Technology activity at EFDA.

Staff:

Chr. Day
Th. Giegerich
V. Hauer

Literature:

[1] Chr. Day, I. Cristescu, B. Pégourié, B. Weyssow, Considerations towards the fuel cycle of a steady-state fusion device, IAEA Fusion Energy Conference, Daejon, Korea, Oct. 2010.

Acknowledgement

This work, supported by the European Communities under the contract of Association between EURATOM and Karlsruhe Institute of Technology, was carried out within the framework of the European Fusion Development Agreement. The views and opinions expressed herein do not necessarily reflect those of the European Commission.

Fuel Cycle –
Tritium Processing

Functional and Performance Evaluation of Sulzer CY Packing in View of ITER ISS (F4E-2009-GRT-023-01)

The hydrogen isotope separation system (ISS) of ITER utilises cryogenic distillation (CD) for enrichment and separation processes. The ISS (European in-kind procurement package) comprises a CD column cascade composed of four inter-linked columns and process piping. The feeds consisting of tritiated protium/deuterium gas streams are coming from various subsystems, like WDS (water detritiation system) or TEP (tokamak exhaust processing).

In order to validate key aspects of the ITER ISS design, a single CD column system with a condensing power of about 250 W at 16 K has been constructed at Tritium Laboratory Karlsruhe (TLK) and linked to a WDS in what constitutes the TRENTA facility. A broad test programme involving the CD system alone and in combination with the WDS is planned at the TRENTA facility, in order to collect data to be used for design optimisation of both tritium plant systems.

In the frame of grant F4E-2009-GRT-023 an ISS stand-alone test programme has been carried out with the main goal of determining liquid hold-up inventories and other key performance data for the **Sulzer CY** CD packing, in order to optimise the design with respect to lower hydrogen inventory and high separation performance. The measured data shall be compared with other packing materials, like Sulzer EX and HeliPak-C, tested in previous experimental campaigns.

Since the first test measurements with Sulzer CY in a 2.7 m long CD column, divided by liquid redistributors in three parts of 0.9 m each, showed unexpected high liquid hold-ups, it was proposed to test the Sulzer CY packing in a new CD column design. This design should avoid any internal installations like redistributors. Thus a single column of 1.2 m length and with a diameter of 50 mm was filled with the Sulzer CY packing. At the top it was connected to an injector unit and in the bottom to a reboiler. In figure 1 all relevant components of the CD system are presented.

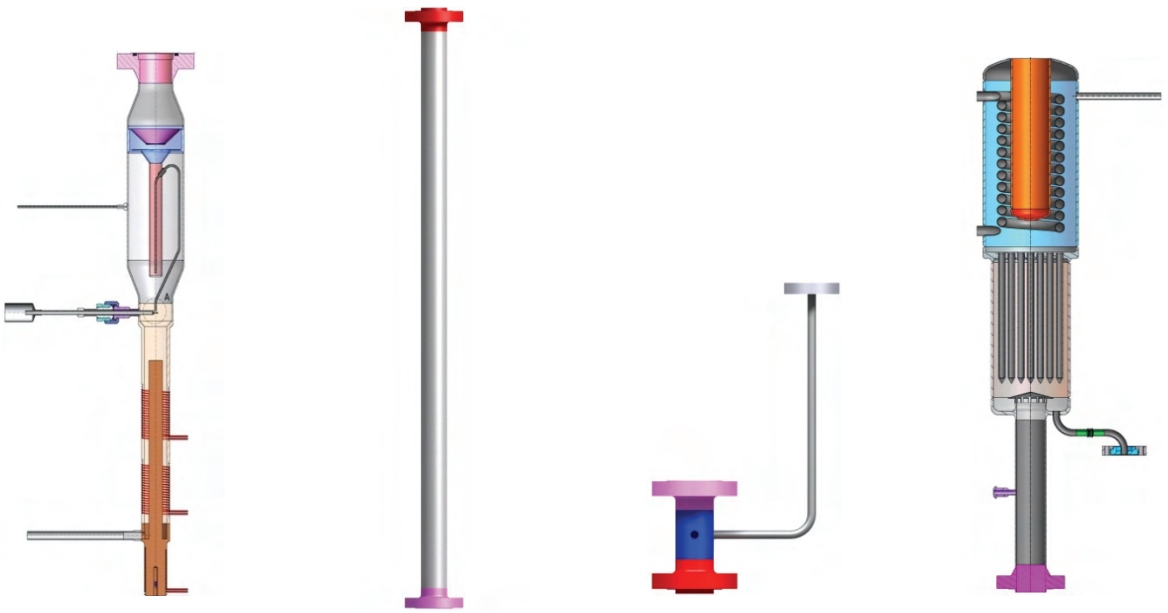

Fig. 1: Components of the CD system at TRENTA: The reboiler (a) is connected to the bottom of the CD column (b). At the top of the column the injectors (c) is located, and on top of that the condenser is installed.

The 1.2 m CD column was filled with Sulzer CY packing (figure 2) up to a height of 1.18 m. This column was tested under different operating conditions to determine the separation performance, indicated by the HETP (Height Equivalent to a Theoretical Plate) value, and the liquid hold-up. The various experimental campaigns are presented in table 1. This list includes the experiments with the old 2.7 m CD column, the 1.2 m CD column and the modified 2.7 m CD column. The modified 2.7 m column was prepared after the successful runs with the 1.2 m column. Those experiments had indicated that without any internal installations acceptable results were obtained.

The experimental data of the 1.2 m and 2.7 m modified CD columns provided reasonable results concerning the HETP and the liquid hold-up. Nevertheless, the results are still higher than the ITER reference values obtained with small CD columns (length and diameter) filled with packing HeliPak-C.

Fig. 2: he Sulzer CY packing is a structured metal wire gauze packing with a surface of about 700 m^2m^{-3}.

Table 1: The experimental campaigns with the three different CD column designs (2.7 m, 1.2 m and the afterwards modified 2.7 m column) are presented. All columns have been packed with Sulzer CY. The experiments were performed at a pressure of about 1.3 bar absolute.

Experimental run No.	**Composition D_2/H_2 (%)**	**CD column design**
08	10/90	2.7 m
09	0/100	2.7 m
10	0/100	2.7 m
11	100/0	2.7 m
12	90/10	2.7 m
13	80/20	2.7 m
14	70/30	2.7 m
23	70/30	1.2 m
24	70/30	1.2 m
25	70/30	2.7 m
26	50/50	1.2 m
27	50/50	1.2 m
28	50/50	1.2 m
29	50/50	2.7 m modified
30	50/50	2.7 m modified

Staff:

N. Bekris
E. Cilbir
I. Cristescu
C. Plusczyk
R. Michling
S. Welte
W. Wurster

Acknowledgement

This work was supported by Fusion for Energy under the grant contract No. F4E-2009-GRT-023-01. The views and opinions expressed herein reflect only the author’s views. Fusion for Energy is not liable for any use that may be made of the information contained therein.

Testing of Isotope Separation System (ISS) with the WDS (TW6-TTFD-TR 63)

In view of mitigation the concern over tritium release into the environment during pulsed operation of the Torus, the Water Detritiation System (WDS) and Isotope Separation System (ISS), based on cryogenic distillation (CD), will operate in such a way that WDS will be a final barrier of tritium for the processed protium waste gas stream discharged from ISS. To investigate the capability of the WDS to achieve this goal, the influence of the additional basically hydrogen stream from ISS and its feeding location into the WDS, the separation performances of Liquid Phase Catalytic Exchange (LPCE) process has to be investigated and accurately mathematically modeled.

In order to develop the experimental data base needed for design of ITER WDS and ISS, the following modes of operation have been considered during the design of the combination WDS-ISS:

- Operation of the LPCE column with composition fluctuation in the stream returned from the CD column,
- Operating of the CD column with composition and flow rate fluctuations in the feeding stream,
- Operation in different dynamic modes in order to validate and bench mark the TRIMO code.

To support the research activities an experimental facility, called TRENTA, has been constructed and is in operation at TLK. The design of the facility was developed in view of the experimental program mainly dedicated to investigate the combination WDS-ISS processes during isotopic and thermal transitory regimes. Therefore, a detailed investigation of the control system and separation performances of the CECE process when working as a final barrier of the top product of the CD column to be discharged into the environment is under investigation.

In support of the above program the following activities have been carried out in 2010:

- Test of the heat exchanger regarding pressure drop and flow rate capability,
- Modification of the heat exchanger for the integration into the cryogenic distillation system; welding of the fittings for the pipe connections (Fig.1a)
- Completion of the hardware set-up of the glove box and valve box installations (Fig.1b+c); both boxes are required as interface systems for the combined operation of the WDS and the cryogenic distillation system,
- Completion of the electrical cabling of the interface components, housed in the glove and valve boxes
- Installation of a ventilated caisson, housing the 0.6 m^3 expansion vessel of the cryogenic distillation system, the 0.1 m^3 vessel for the hydrogen of the condenser unit and the 0.3 m^3 vessel for intermediate storage of tritiated water (WDS).

Staff:

N. Bekris
E. Cilbir
I. Cristescu
C. Plusczyk
R. Michling
S. Welte
W. Wurster

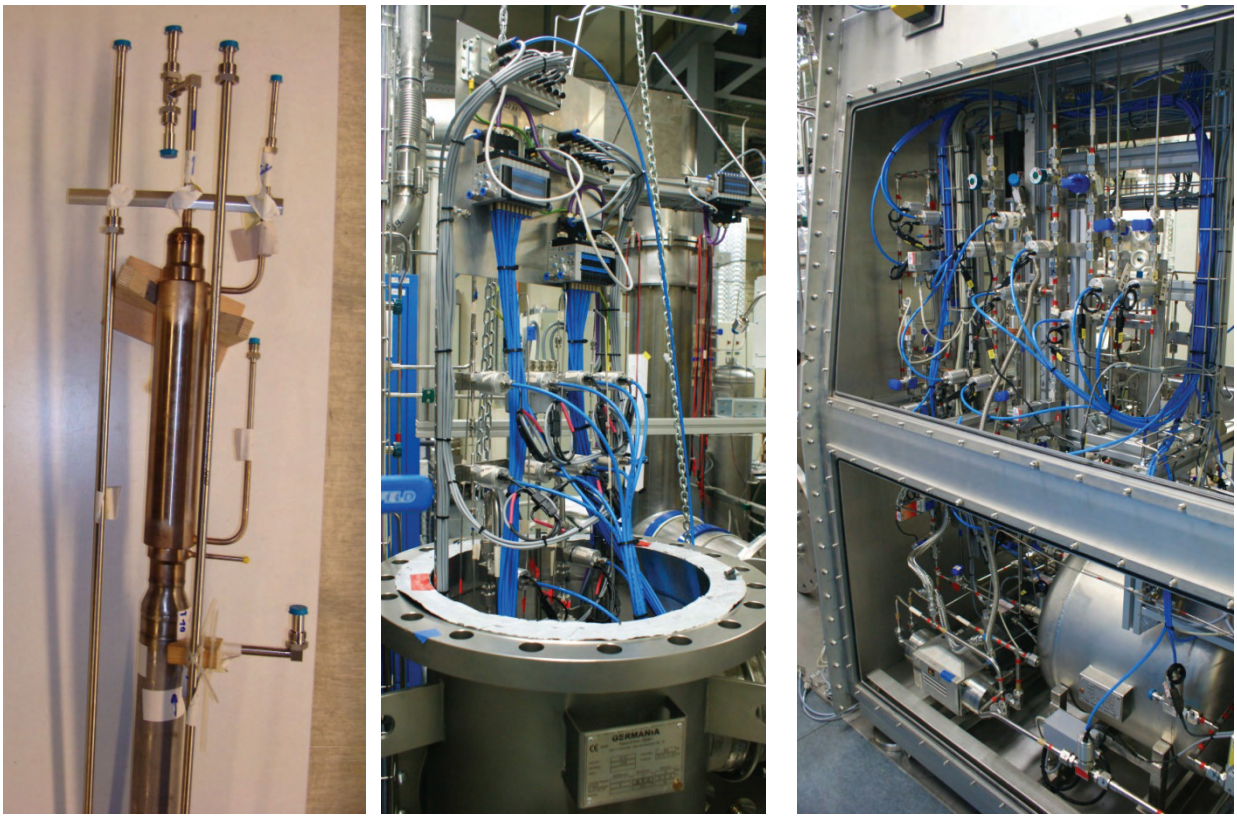

a) b) c)

Fig. 1: Modified heat exchanger a) with the welded fitting connections to be installed inside the cold box of the cryogenic distillation system. Valve box b) and glove box c) with all finished connections of piping and controlling systems.

Acknowledgement

This work, supported by the European Communities under the contract of Association between EURATOM and Karlsruhe Institute of Technology, was carried out within the framework of the European Fusion Development Agreement. The views and opinions expressed herein do not necessarily reflect those of the European Commission.

Assessment of Hydrogen Isotope Separation System 2001 Baseline Design (F4E-2009-GRT-046-01)

The Isotope Separation System (ISS) in ITER is required to process the various mixtures of hydrogen isotopes resulting from torus operation scenarios, wall conditioning, and tritiated gas/water processing. Protium, deuterium and tritium have concentrations that either have to be adjusted to fulfill the system requirements on isotope concentration in product streams or, to be at very low tritium content in order to allow a safe discharge of these gases into the environment. The ISS consists of a cascade of cryogenic distillation columns with feeding locations appropriately defined according to the hydrogen isotope concentrations in the stream to be processed.

However, recently the ITER-IO did propose a revision of the feed and product streams. In order to evaluate these changes and their impact on the current design, it has been required to perform some simulation tests using a programme code that has been proven in the past to be suitable for such an application.

Several tasks have been carried out for the assessment of suitability of the ISS 2001 base-line design for the new ITER operation requirements.

Comparison between the simulation results provided by using the TRIMO code and the FLOSHEET code according to the ISS configuration and operation parameters as specified in the DDD's 2001

From the TRIMO code, the portion related to the ITER ISS cascade has been separated and modified to allow reaching steady state conditions. This change was necessary to allow comparison with the FLOSHEET runs since the FLOSHEET is a steady state code.

The very small differences identified between the FLOSHEET and TRIMO code are due to the following reasons:

- The thermodynamically data concerning the molecular species have been updated in TRIMO software based on recent published data. Detailed investigations on the thermodynamically properties of hydrogen isotopes have been carried out at TLK in 2004 in support of the EFDA task TW4 – TTFD- TR 37.1.

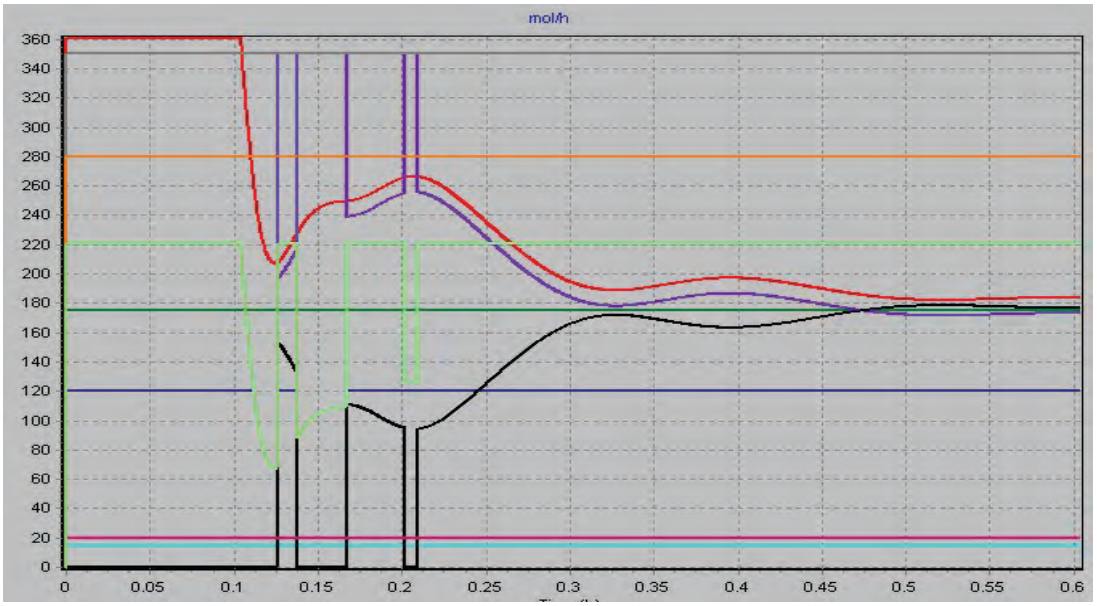

Fig. 1: The control of various streams as implemented in TRIMO.

- In the TRIMO software the control system adjusts the operation in order to maximize the amount of tritium to be extracted, to increase the purity of deuterium to be delivered to NBI and to minimize the tritium in the hydrogen released from the top of the CD1 as shown in figure 1.

Simulation of the performance of ISS column cascade maintaining the same internal parameters as in DDD 2001 but without 50% D-50% T product stream

The simulation of the ISS under the same internal parameters as in DDD 2001 WBS 3.2B has been performed with two different scenarios, first in the original configuration with the 50% T-50% D product stream withdrawn at the lower part of CD4 and secondly without this side product stream. The results show an increase of 15% of the tritium inventory at the temporary peak values (260 g, 300 g) without the 50%T-50% D product stream, whereas there is no increase for the inter-shots basis inventory (105 g). The internal DT concentration of CD4 column is slightly raised for the case that no side product is withdrawn and the tritium flow is brought from 73 mol/h to 77 mol/h. The simulation of ISS without the 50% T-50% D stream during a 3000 s burn scenario yield in a slight increase of the tritium inventory of the CD4 column, but the prevention of the side product stream allows a more simpler and stable controlling strategy of the ISS. Only one tritium product stream has to be processed for subsequent requirements (e.g. fuelling, storage) afterwards.

Simulation of the performance of ISS column cascade maintaining the same internal parameters as in DDD 2001 but with various compositions in the feeding stream from WDS

As far as the various options for feeding the ISS with gas from WDS is concerned, the investigation has clearly shown that only for the case of 280 mol/h with >99%H , < 1%D and 200 ppm of tritium the 2001 ISS configuration can provide the required composition in the withdrawn streams if the location of the deuterium product for NBI will be changed at the stages in the range of #140 - #150.

For the other two cases investigated, both FLOSHEET and TRIMO based software failed during runs or did not provide the expected figures. For the case of 280 mol/s and <50% H, >50% D and 200 ppm of tritium the TRIMO software provides the operation conditions that allows reaching the required composition in the withdrawn streams but the operation parameters are not of use based on the actual operation strategy.

Evaluation of a 3CD Column Configuration for ITER ISS

The analyses lead to the following conclusions:

For a feed from WDS having the composition 50% H2, 50% D2, & 200 ppm T2, in comparison with the case where the feed composition is > 99% H2, < 1% D2 & 200 ppm T2, a larger ISS system is required, or as measured in terms of refrigeration power it requires between 500 and 1000 W more power, which represents a size increase by approximately 50%. However, increasing the ISS size will not have a tremendous impact on the tritium concentration of the WDS return stream as it will be of the level of 20 ppm.

Understandably, the selection between the 3- and 4-column system is not easy and should not be done just on the basis of the refrigeration power and tritium concentration of the WDS return stream. Nevertheless, when deciding between the two configurations, there are also other parameters that have to be taken into account.

Indeed, the 3-column system is perceived as being simpler (at least 25% less complex than the corresponding 4-column system) which implies correspondingly, much lower maintenance requirements. This tends to imply also a much simpler operation.

Staff:

N. Bekris
I. Cristescu
R. Michling

Acknowledgement

This work was supported by Fusion for Energy under the grant contract No. F4E-2009-GRT-046-01. The views and opinions expressed herein reflect only the author's views. Fusion for Energy is not liable for any use that may be made of the information contained therein.

Finalization of the System Capacity, Enhancements Studies and Detailed Design of WDS Components including HAZOP Studies (F4E-2010-GRT-045 (PNS-VTP))

The assignment of WDS (Water Detritiation System) is to recover tritium from tritiated water and to discharge decontaminated hydrogen, which is oxidized to water before released to the atmosphere. The recovered tritium is available in the gas phase (tritiated hydrogen) and partially transferred to ISS for final enrichment and separation. The CECE (Combined Electrolysis Catalytic Exchange) process is applied for WDS, which consists mainly of two processing steps. First tritiated water is converted to gaseous hydrogen by electrolyser units, and secondly along an isotopic exchange column (LPCE) one part of the generated hydrogen stream is decontaminated for discharge whereas the other part is fed to the ISS for final enrichment and separation of the required hydrogen isotopologues.

To control the process in an efficient manner, all tritiated water will be intermediately stored in the holding tanks of WDS, from where the water is constantly fed to the exchange columns or to the electrolyser units, depending on the tritium content and the operation modes of WDS. The main sources of tritiated water are the scrubber columns (SC) and the molecular sieve drier (MS) from the Detritiation System (DS).

The water input to WDS is cleaned over a purification stage prior to be sent to the different holding tanks regarding the tritium content. Tritiated water emerged from accidents/incidents is collected in emergency tanks, which are capable to receive larger amounts of tritiated water.

The basic functions of the WDS can be summarized as follows:

- Temporary storage of tritiated water in holding tanks coming from the scrubber columns and molecular sieve drier of DS during normal operation and maintenance duties,
- Temporary storage of tritiated water in emergency tanks generated by DS or fire fighting during accidents/incidents,
- Processing of tritiated water for tritium recovery,
- Enrichment of tritium from processed water into the gaseous phase to be fed to ISS for further enrichment and separation,
- Decontamination of ISS off-gas by processing through the catalytic exchange column in WDS prior to discharge to atmosphere,
- Discharge of decontaminated hydrogen stream generated from the tritiated water by electrolysis.

In view of the Conceptual Design Review (CDR) that shall be as the basis for the Procurement Arrangement (PA) the following activities have been carried out:

1. The interfaces list to other systems containing the main requirements has been established;
2. The Process Flow Diagrams (PFDs) of the entire WDS have been developed;
3. Expected flows and compositions on critical points of the PFDs have been established;
4. In agreement with ITER IO the number and sizes of the large tritiated water holding tanks to be installed for WDS have been established;

5. The method for tritium containment/confinement of components within the WDS following the guidelines provided by ITER in the tritium manual and in other documents has been implemented;
6. A HAZOP (hazard and operability) study of the conceptual design of ITER WDS has been conducted based on the PFDs.

Staff:

G. Ana – ICIT Romania
N. Bekris
I. Cristescu
R. Michling

Acknowledgement

This work was supported by Fusion for Energy under the grant contract No. F4E-2010-GRT-045 (PNS-VTP).with collaboration by ENEA Frascati, Italy; ICIT, Rm. Vâlcea, Romania and CEA Saclay, France. The views and opinions expressed herein reflect only the author's views. Fusion for Energy is not liable for any use that may be made of the information contained therein.

Goal Oriented Training Programme “Tritium Technologies for the Fusion Fuel Cycle” (WP08-GOT-TRI-TOFFY (FU07-CT-2008-00047))

Background

The overall objective of the project is to support EU activities in the Deuterium-Tritium Fuel Cycle area for ITER by the training of six Early-Stage Researchers. The training program is developed along existing projects in the framework of the European procurement package for the ITER Fuel Cycle with the main focus on water detritiation (WDS) and isotope separation (ISS) systems, detritiation processes, gas analytics and tritium measurements (see overview table: List of Work Packages). The participating Associations are: KIT, CEA, ENEA, HAS/MTA ATOMKI, MEdC/ICIT and CCFE.

No.	Title	Partners involved
1	Combined operation of WDS and ISS	KIT (ICIT, CCFE)
2	Detritiation of waste	CEA (KIT, CCFE)
3	Technologies for tritium recovery and trapping	ENEA (KIT, CCFE)
4	Calorimeter with large sample volume	MTA ATOMKI (KIT, CCFE)
5	Experimental Pilot Plant for Tritium and Deuterium Separation	ICIT (KIT, CCFE)
6	Participation in JET operation	CCFE (KIT)

The project was started in late 2008. It was planned to finalize the process of recruitment of trainees until 3rd quarter of 2009, so that all trainees should have started their employment in 2009.

Status of project

The last 2 recruitments were done in the first part of 2010 and all trainees started their traineeship. The Personal Training Schemes of all trainees were fixed and 4 trainees finished their home based introductionary training and have started with their education at the Tritium Laboratory Karlsruhe (TLK).

All trainees are now fully involved in R&D work and part of them (those who started earlier) have already submitted papers. Four of the trainees have joined the Tritium 2010 conference in Nara and one the SOFT conference in Porto.

In parallel, the coordinator of this network gave a talk in the EFDA GOT PROGRAMS satellite meeting at the SOFT conference. The aim of this meeting was to learn about the different training programs under EFDA, to present each program (their main lines of research), to identify possible common issues and if possible to establish some collaboration.

Outlook

In the next reporting period all trainees shall join a dedicated JET training programme as well as the courses and conferences as foreseen in their career development plans.

<u>Programme Coordinator:</u>

B. Bornschein

Acknowledgement

This work, supported by the European Communities under the contract of Association between EURATOM and Karlsruhe Institute of Technology, was carried out within the framework of the European Fusion Development Agreement. The views and opinions expressed herein do not necessarily reflect those of the European Commission.

Safety

Combined Hydrogen and Dust Explosion and Mitigation Experiments and Model Development. Validation and Application to ITER and New Analysis of Explosion Reference Events (F4E-2008-GRT-01-01 (ES-SF))

For the ITER construction and operating license, safety assessments related to dry and wet bypass, loss of vacuum scenarios have to be provided. In these potential accidents, hydrogen will be desorbed from initially cold surfaces, and in the wet bypass case, additional hydrogen will be generated by steam reacting with beryllium, graphite and tungsten dust. There has been very limited data available for the validation of the state-of-the-art tools applied for consequence analysis, in particular considering the hybrid, hydrogen-dust reactions, the large scale and specific geometry of the ITER vacuum vessel and the thermodynamic initial and boundary conditions. However, the sparse existing data was revised, benchmarks were initiated and new experimental data with more relevance were produced in the course of this project.

Hypothetical hydrogen combustions in the ITER vacuum vessel under accident scenarios were simulated with the CREBCOM model implemented in the CFD combustion / detonation codes COM3D and DET3D. The analyses were dedicated to conservatively estimate the pressure and thermal loads on the ITER structure due to the combustion. The results show that the nitrogen injection system is an efficient mitigation measure. However, the conservative results show short termed and very localized pressure peaks exceeded at least slightly the design pressure of the vacuum vessel.

The precursor phenomena, in particular jet induced gas mixing and dust mobilization, are massively influenced by turbulence. While the currently established turbulence models seem to be applicable, still there is a lack of experience and relevant data for reliable and efficient dust re-suspension modelling. However, in combination with the explosion simulations, it might be derived that the injection close to the location of strongest hydrogen production will give highest potential for an effective mitigation by dilution and oxygen starvation.

The investigations of an early ignition via igniters positioned also close to the maximum hydrogen production zones showed a potential for further mitigation by including this technology in the vacuum vessel design. According to the first results of the sub-atmospheric ignition test program, these igniters can be positioned at locations convenient for the design. This is supported by the result that under the accidental conditions - coined by the early low pressure, limited oxygen, and rich fuel – the resulting combustion will induce only benign pressure loads, in particular if ignition occurs at the edge of the flammable cloud.

Dust Mobilization Modelling

The computer models need further validation. The suggested facilities and associated test programs could help to provide further insights into the potential accidental sequences, and to establish confidence for the application of these tools in regulatory processes.

Explosion Modelling

In general, the validation database needs completion. Also the explosion modelling needs more relevant basic data for the reactivity of the materials involved under the relevant conditions. The reactivity of beryllium dust and mixtures of dusts has to be determined. A suitable substitute for beryllium shall be identified to allow for large scale experiments with non-toxic material.

In particular the process of flame acceleration and the related σ-criterion should be checked against the actual conditions and geometrical configuration.

Wall effects and the influence of radiation, even the feedback of the structural response on the transitional phenomena are not fully addressed yet.

The scale effect of the combustion is accounted for with the suggested large scale integral test. This would be the first test to address all relevant phenomena fully coupled in a relevant size.

The suggested long term project, embedding this test in the final phase after the initial small/medium sized tests, addresses the most urgent topics identified above. It will build on an improved data basis provided with the current project. However, the complexity of the task suggests another pan-European approach via a new F4E project including at least the contributors of the current project.

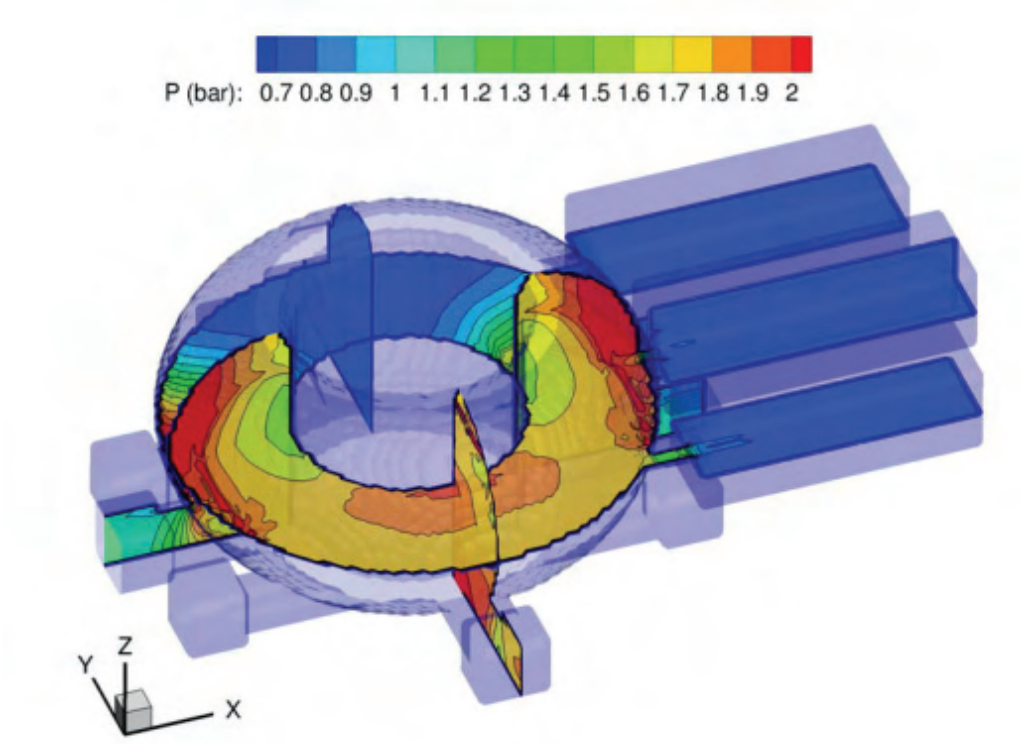

Fig. 1: Pressure distribution at the instant with maximum local pressure of the reference case with nitrogen injection.

Staff:

A. Denkevits
T. Jordan
M. Kuznetsov
B. Oechsler
Z. Xu
J. Xiao
J. Yanez
J. Travis, Dubois-Pitzer-Travis, Offenbach, Germany
A. Veser, ProScience GmbH, Ettlingen, Germany

Literature:

[1] Le Guern, F.; Gulden, W.; Ciattaglia, S.; Counsell, G.; Bengaouer, A.; Brinster, J.; Dabbene, F.; Denkevitz, A.; Jordan, T.; Kuznetzov, M.; Porfiri, M.; Redlinger, R.; Roth, J.; Segre, J.; Sugiyama, K.; Tkatschenko, I.; Xu, Z.: “F4E R&D Programme and Results on In-vessel Dust and Tritium”; 26th Symposium on Fusion Technology (SOFT 2010), Porto/Portugal

Acknowledgement

This work was supported by Fusion for Energy under the grant contract No. F4E-2008-GRT-01-01 (ES-SF) with collaboration by CEA, France and ENEA, Italy. The views and opinions expressed herein reflect only the author's views. Fusion for Energy is not liable for any use that may be made of the information contained therein.

Appendix I: KIT Departments Contributing to the Fusion Programme

KIT Department	KIT Institut/Abteilung	Director	Ext.
Institute for Applied Materials - Applied Materials Physics	Institut für Angewandte Materialien – Angewandte Werkstoffphysik (IAM-AWP)	Prof. Dr. H.J. Seifert Dr. A. Möslang (Acting Head)	23895 24029
Institute for Applied Materials - Materials and Biomechanics	Institut für Angewandte Materialien - Werkstoff- und Biomechanik (IAM-WBM)	Prof. Dr. O. Kraft	24815
Institute for Applied Materials - Material Processing Technology	Institut für Angewandte Materialien - Werkstoffprozesstechnik (IAM-WPT)	Prof. Dr. J. Haußelt	22518
Institute for Pulsed Power and Microwave Technology	Institut für Hochleistungsimpuls- und Mikrowellentechnik (IHM)	Prof. Dr. M. Thumm	22440
Institute for Nuclear and Energy Technology	Institut für Kern- und Energietechnik (IKET)	Prof. Dr. T. Schulenberg	23450
Institute for Neutron Physics and Reactor Technology	Institut für Neutronenphysik und Reaktortechnik (INR)	Dr. R. Stieglitz	22550
Institute for Technical Physics	Institut für Technische Physik (ITeP)	Prof. Dr. M. Noe	23500
- Tritium Laboratory Karlsruhe	- Tritiumlabor Karlsruhe (TLK)	Dr. B. Bornschein	23239
Institute for Data Processing and Electronics	Institut für Prozessdatenverarbeitung und Elektronik (IPE)	Prof. Dr. M. Weber	25612

Appendix II: Fusion Programme Management Staff

Head of the Research Unit	Dr. K. Hesch	ext. 25460 e-mail: klaus.hesch@kit.edu
Secretariat:	Mrs. A. Knoll	ext. 25461 e-mail: anja.knoll@kit.edu
	Mrs. M.-E. Tuzia	ext. 22435 e-mail: maria-elena.tuzia@kit.edu
Program Budget, Administration, Reports, EU-Affairs	BW. M. Henn	ext. 25547 e-mail: michael.henn@kit.edu
	Mrs. I. Pleli	ext. 28292 e-mail: ingrid.pleli@kit.edu
Blanket and Divertor Development, HELOKA, IFMIF, Public Relations	Dr. D. Radloff	ext. 28750 e-mail: dirk.radloff@kit.edu
Fuel Cycle, Structural Materials, Superconducting Magnets, CAD-Office	DI. S. Gross	ext. 25468 e-mail: sigurd.gross@kit.edu
Plasma Heating Technology, Safety Studies, Neutronics, Physics	Dr. K. Hesch	ext. 25460 e-mail: klaus.hesch@kit.edu
Quality Management, Resource Loaded Planning, Document Management	Dr. J. Gafert	ext. 22923 e-mail: juergen.gafert@kit.edu
	Dr. I. Ignatiadis	ext. 85465 e-mail: Ioannis.ignatiadis@kit.edu
	Dr. M. Ionescu-Bujor	ext. 28325 e-mail: mihaela.ionescu-bujor@kit.edu
	Mrs. DI. B. Keim	ext. 24194 e-mail: birgit.keim@kit.edu
	Mrs. DI. Ch. Schweier	ext. 28325 e-mail: christine.schweier@kit.edu

Address: **Karlsruhe Institute of Technology**
Nuclear Fusion Programme Management

Post Office Box 3640, D - 76021 Karlsruhe / Germany

Telephone No: **0721-608-Extensions .....**

Telefax No: **0721-608-25467**

world wide web: **http://www.fusion.kit.edu/**

Appendix III: Publications

Plasma Wall Interaction

[1] Arnoux, G.; Bazylev, B.; Lehnen, M.; Loarte, A.; Riccardo, V.; Bozhenkov, S.; Devaux, S.; Eich, T.; Fundamenski, W.; Jachmich, S.; Thomsen, H.; JET EFDA Contributors
Heat load measurement on the JET first wall during disruptions.
19th Internat.Symp.on Plasma Surface Interactions in Controlled Fusion Devices (PSI-19), San Diego, Calif., May 24-28, 2010; Book of Abstracts S.95

[2] Bazylev, B.; Arnoux, G.; Fundamenski, W.; Lehnen, M.; JET EFDA Contributors.
Modeling of runaway electron beams for JET and ITER.
19th Internat.Symp.on Plasma Surface Interactions in Controlled Fusion Devices (PSI-19), San Diego, Calif., May 24-28, 2010; Book of Abstracts S.198

[3] Bazylev, B.; Landman, I.; Pestchanyi, S.; Igitkhanov, Yu.; Loarte, A.; Pitts, R.; Lehnen, M.; Safronov, V.; Podkovyrov, V.; Klimov, N.; Garkusha, I.; Makhlay, W.
Simulations of material damage and high energy fluxes to ITER divertor and first wall during transients and runaway electron loads.
23rd IAEA Fusion Energy Conference, Daejeon, Korea, October 11-16, 2010

[4] Coenen, J.W.; Bazylev, B.; Brezinsek, S.; Philipps, V.; Hirai, T.; Kreter, A.; Sergienko, G.; Pospieszczyk, A.; Tanabe, T.; Ueda, Y.; Samm, U.; TEXTOR-Team.
Tungsten melt layer motion and splashing on castellated surfaces at the Tokamak TEXTOR.
19th Internat.Symp.on Plasma Surface Interactions in Controlled Fusion Devices (PSI-19), San Diego, Calif., May 24-28, 2010; Book of Abstracts S.65

[5] Coenen, J.W.; Philipps, V.; Brezinsek, S.; Bazylev, B.; Kreter, A.; Hirai, T.; Laengner, M.; Tananbe, T.; Ueda, Y.; Samm, U.; TEXTOR Team
Analysis of tungsten melt layer motion and splashing under Tokamak conditions at TEXTOR.
23rd IAEA Fusion Energy Conference, Daejeon, Korea, October 11-16, 2010

[6] D'Andrea, D.; Munz, C.D.; Schneider, R.
Modeling of long-range intra- and inter-species charged particle collisions for PIC simulations.
Communications in Computational Physics, 7(2010) S.877-903, DOI:10.4208/cicp.2009.09.094

[7] Garkusha, I.E.; Arkhipov, N.I.; Klimov, N.S.; Makhlaj, V.A.; Safronov, V.M.; Landman, I.; Tereshin, V.I.
The latest results from ELM-simulation experiments in plasma accelerators.
Physica Scripta, T138(2009) S.014054/1-6; DOI:10.1088/0031-8949/2009/T138/014054

[8] Garkusha, I.E.; Landman, I.; Linke, J.; Makhlaj, V.A.; Medvedev, A.V.; Malykhin, S.V.; Pestchanyi, S.; Pugachev, A.T.; Sadowski, M.J.; Skladnik-Sadowska, E.; Tereshin, V.I.
Experimental simulation of ITER ELMs impacts to the tungsten surfaces with QSPA Kh-50;
23rd IAEA Fusion Energy Conference, Daejeon, Korea, October 11-16, 2010

[9] Igitkhanov, Yu.; Bazylev, B.
Electric field and hot spots formation.
26th Symp.on Fusion Technology (SOFT 2010), Porto, P, September 27 - October 1, 2010

[10] Igitkhanov, Yu.; Bazylev, B.; Landman, I.
Calculation of runaway electron stopping power in ITER.
19th Internat.Symp.on Plasma Surface Interactions in Controlled Fusion Devices (PSI-19), San Diego, Calif., May 24-28, 2010; Book of Abstracts S.199

[11] Klimov, N.; Podkovyrov, V.; Zhitlukhin, A.; Kovalenko, D.; Landman, I.; Pestchanyi, S.; Bazylev, B.; Janeschitz, G.; Loarte, A.; Merola, M.; Hirai, T.; Linke, J.; Compan, J.; Federici, G.; Riccardi, B.;
Mazul, I.; Giniyatulin, R.; Khimchenko, L.
Experimental study of PFCs erosion and eroded material deposition under ITER-like transient loads at plasma gun facility QSPA.
19th Internat.Symp.on Plasma Surface Interactions in Controlled Fusion Devices (PSI-19), San Diego, Calif., May 24-28, 2010; Book of Abstracts S.51

[12] Landman, I.S.
Tokamak code TOKES. Models and implementation.
4th Alushta Internat.Conf.on Plasma Physics, Alushta, UA, September 13-19, 2010

[13] Landman, I.S.; Pestchanyi, S.E.; Igitkhanov, Y.; Pitts, R.
Two-dimensional modelling of disruption mitigation by massive gas injection.
26th Symp.on Fusion Technology (SOFT 2010), Porto, P, September 27 - October 1, 2010

[14] Landman, I.S.; Pestchanyi, S.E.; Igitkhanov, Y.; Pitts, R.
Modelling of wall and SOL processes and contamination of ITER plasma after impurity injection with the Tokamak code TOKES.
Fusion Engineering and Design, 85(2010) S.1366-70, DOI:10.1016/j.fusengdes.2010.03.044

[15] Lehnen, M.; Alonso, A.; Arnoux, G.; Baumgarten, N.; Bozhenkov, S.A.; Brezinsek, S.; Brix, M.; Eich, T.; Huber, A.; Jachmich, S.; Kruezi, U.; Morgan, P.D.; Plyusnin, V.V.; Reux, C.; Riccardo, V.; Sergienko, G.; Stamp, M.F.; Thornton, A.; Koltunov, M.; Tokar, M.; Bazylev, B.; Landman, I.; Pestchanyi, S. ; JET EFDA Contributers
Disruption mitigation by massive gas injection in JET.
23rd IAEA Fusion Energy Conference, Daejeon, Korea, October 11-16, 2010

[16] Litnovsky, A.; Philipps, V.; Wienhold, P.; Kreter, A.; Kirschner, A.; Matveev, D.; Brezinsek, S.; Sergienko, G.; Pospieszczyk, A.; Schweer, B.; Schulz, C.; Schmitz, O.; Coennen, J.W.; Samm, U.; Krieger, K.; Hirai, T.; Emmoth, B.; Rubel, M.; Bazylev, B.; Breuer, U.; Stärk, A.; Richter, S.; Komm, M.; TEXTOR Team
Overview of material migration and mixing, melting, fuel retention and cleaning of ITER-like castellated structures in TEXTOR.
19th Internat.Symp.on Plasma Surface Interactions in Controlled Fusion Devices (PSI-19), San Diego, Calif., May 24-28, 2010; Book of Abstracts S.73

[17] Loarte, A.; Campbell, D.; Gribov, Y.; Pitts, R.A.; Klimov, N.; Podkovyrov, V.; Zhitlukhin, A.; Landman, I.; Pestchanyi, S.; Bazylev, B.; Linke, J.; Loewenhoff, T.; Pintsuk, G.; Schmitz, O.; Liang, Y.; Evans, T.E.; Schaffer, M.; Fenstermacher, M.E.; Becoulet, M.; Huysmans, G.; Nardon, E.; Baylor, L.; Canik, J.; Maingi, R.; Ahn, J.W.; Riccardi, B.; Saibene, G.; Sartori, R.; Cavinato, M.; Eich, T.; Jakubowski, M.; Lang, P.T.; Thomsen, H.; Suttrop, W.; Da la Luna, E.; Wilson, H.; Kirk, A.
ITER ELM control requirements, ELM control schemes and required R&D.
23rd IAEA Fusion Energy Conference, Daejeon, Korea, October 11-16, 2010

[18] Neudorfer, J.; Stindl, T.; Stock, A.; Schneider, R.; Petkow, D.; Roller, S.; Munz, C.D.; Auweter-Kurtz, M.
Three-dimensional simulation of rarefied plasma flows using a high order particle in cell method.
13th Results and Review Workshop of the HLRS, Stuttgart, October 4-5, 2010

[19] Pestchanyi, S.
Modeling of brittle destruction of W surfaces under repetitive loads.
ITPA Technical Group Meeting, Seoul, Korea, October 16-21, 2010

[20] Pestchanyi, S.; Garkusha, I.; Landman, I.
Simulation of residual thermostress in tungsten after repetitive.
26th Symp.on Fusion Technology (SOFT 2010), Porto, P, September 27 - October 1, 2010

[21] Pestchanyi, S.; Garkusha, I.; Landman, I.
Simulation of tungsten armour cracking due to small ELMs in ITER.
Fusion Engineering and Design, 85(2010) S.1697-1701, DOI:10.1016/j.fusengdes.2010.05.005

Physics: Heating and Current Drive – ECRH

[1] Albajar, F.; Alberti, S.; Avramides, K.A.; Benin, P.; Bonicelli, T.; Cirant, S.; Darbos, C.; Gantenbein, G.; Gassmann, T.; Goodman, T.P.; Henderson, M.; Illy, S.; Ioannidis, Z.; Hogge, J.P.; Jin, J.; Kern, S.; Latsas, G.; Lievin, C.; Pagonakis, I.G.; Piosczyk, B.; Rzesnicki, T.; Thumm, M.; Tigelis, I.; Tran, M.Q; Vomvoridis, J.
The European 2 MW gyrotron for ITER
16th Joint Workshop on Electron Cyclotron Emission and Electron Cyclotron Resonance Heating, Sanya, China, April 12-15, 2010; Book of Abstracts

[2] Avramides, K.A.; Dumbrajs, O.; Vomvoridis, J.L.; Kern, S.
Gyrotron interaction simulations with tapered magnetostatic field.
35th Internat.Conf.on Infrared, Millimeter and Terahertz Waves (IRMMW-THz 2010), Roma, I, September 5-10, 2010; Proc.on USB-Stick

[3] Beringer, M.H.; Illy, S.; Jin, J.; Kern, S.; Lievin, C.; Thumm, M.
Design of major components for a 4 MW 170 GHz coaxial-cavity gyrotron.
11th Internat.Vacuum Electronics Conf.(IVEC 2010), Monterey, Calif., May 18-20, 2010; Proc.S.35-36; Piscataway, N.J. : IEEE, 2010; ISBN 978-1-4244-7099-0

[4] Beringer, M.H.; Illy, S.; Jin, J.; Kern, S.; Thumm, M.
Physical component designs and thermo-mechanical studies towards a 4 MW 170 GHz coaxial-cavity gyrotron.
ITG Vacuum Electronics Workshop, Bad Honnef, November 15-16, 2010

[5] Beringer, M.H.; Illy, S.; Jin, J.; Kern, S.; Thumm, M.; Lievin, C.
A 4 MW 170 GHz coaxial-cavity gyrotron - design of the major components.
22nd Joint Russian-German Meeting on ECRH and Gyrotrons, Nizhny Novgorod, Russia, June 29 - July 5, 2010; Folien auf CD-ROM

[6] Bongers, W.A.; Graswinckel, M.F.; Goede, A.P.H.; Kasparek, W.; Danilov, I.; Fernandez Curto, A.; de Baar, M.R.; van den Berg, M.A.; Donne, A.J.H.; Elzendoorn, B.S.Q.; Heidinger, R.; Ivanov, P.; Kruijt, O.G.; Lamers, B.; Meier, A.; Piosczyk, B.; Plaum, B.; Ronden, D.M.S.; Thoen, D.J.; Schmid, M.; Verhoeven, A.G.A.
A remotely steered millimetre wave launcher for electron cyclotron heating and current drive on ITER.
Fusion Engineering and Design, 85(2010) S.69-86; OI:10.1016/j.fusengdes.2009.07.001

[7] Braune, H.; Erckmann, V.; Illy, S.; Michel, G.; Noke, F.; Purps, F. ; W7-X ECRH-teams at IPP, IPF and KIT
Collector loading during high frequency power modulation.
35th Internat.Conf.on Infrared, Millimeter and Terahertz Waves (IRMMW-THz 2010), Roma, I, September 5-10, 2010; Proc.on USB-Stick

[8] Bruschi, A.; Bin, W.; Cirant, S.; Dell'Era, F.; Gantenbein, G.; Leonhardt, W.; Muzzini, V.; Samartsev, A.; Schmid, M.
Progress and test of the spherical matched load designed for 2 MW-CW.
Workshop on RF Heating Technology of Fusion Plasmas, Como, I, September 13-15, 2010; Folien auf CD-ROM

[9] Bruschi, A.; Erckmann, V.; Kasparek, W.; Petelin, M.I.; Thumm, M.; Bin, W.; Cirant, S.; D'Arcangelo, O.; Hollmann, F.; Lubyako, L.; Noke, F.; Plaum, B.; Purps, F.; Zohm, H. ; ECRH Team at IPP Greifswald
Diplexers for power combination and switching in high power ECRH systems.
IEEE Transactions on Plasma Science, 38(2010) S.1427-38, DOI:10.1109/TPS.2010.2047658

[10] Dammertz, G.; Erckmann, V.; Schmid, M.
Method and apparatus for collector sweeping control of an electron beam.
JP-OS 2010 526 417 (2010.07.29)

[11] Damyanova, M.; Kern, S.; Illy, S.; Thumm, M.; Sabchevski, S.; Zhelyazkov, I.; Vasileva, E.
Modelling and simulation of gyrotrons for ITER.
Internat.Workshop and Summer School on Plasma Physics, Kiten, BG, July 5-10, 2010

[12] . Darbos, C. ; ITER EC International Design Team
Status of the ITER electron cyclotron H&CD system.
35th Internat.Conf.on Infrared, Millimeter and Terahertz Waves (IRMMW-THz 2010),
Roma, I, September 5-10, 2010; Proc.on USB-Stick

[13] Flamm, J.
Analysis of cylindrical waveguides with specifically perturbed inner wall using an FFTF based spectral method.
KIT PhD Symp., Karlsruhe, 30.September 2010

[14] Flamm, J.; Jin, J.; Neudorfer, J.; Roller, S.; Thumm, M.
Investigations on wave propagation in launchers of advanced gyrotron output couplers.
35th Internat.Conf.on Infrared, Millimeter and Terahertz Waves (IRMMW-THz 2010),
Roma, I, September 5-10, 2010; Proc.on USB-Stick

[15] Flamm, J.; Jin, J.; Thumm, M.
An FFT based spectral method for analysis of launchers in advanced gyrotron output couplers.
ITG Vacuum Electronics Workshop, Bad Honnef, November 15-16, 2010

[16] Gantenbein, G.; Dammertz, G.; Erckmann, V.; Kasparek, W.; Kern, S.; Latsas, G.; Lechte, C.; Piosczyk, B.; Rzesnicki, T.; Samartsev, A.; Schlaich, A.; Thumm, M.; Tigelis, I.; Vaccaro, A.
Progress in stable operation of high power gyrotrons for ECRH.
22nd Joint Russian-German Meeting on ECRH and Gyrotrons, Nizhny Novgorod, Russia,
June 29 - July 5, 2010; Folien auf CD-ROM

[17] Gantenbein, G.; Dammertz, G.; Flamm, J.; Illy, S.; Kern, S.; Latsas, G.; Piosczyk, B.; Rzesnicki, T.; Samartsev, A.; Schlaich, A.; Thumm, M.
Experimental investigations and analysis of parasitic RF oscillations in high-power gyrotrons.
IEEE Transactions on Plasma Science, 38(2010) S.1168-77, DOI:10.1109/TPS.2010.2041366

[18] Gantenbein, G.; Dammertz, G.; Kern, S.; Latsas, G.; Piosczyk, B.; Rzesnicki, T.; Samartsev, A.; Schlaich, A.; Thumm, M.; Tigelis, I.
Progress in stable operation of high power gyrotrons.
16th Joint Workshop on Electron Cyclotron Emission and Electron Cyclotron
Resonance Heating, Sanya, China, April 12-15, 2010; Book of Abstracts

[19] Gantenbein, G.; Erckmann, V.; Illy, S.; Kern, S.; Kasparek, W.; Lechte, C.; Leonhardt, W.; Lievin, C.; Samartsev, A.; Schlaich, A.; Schmid, M.; Thumm, M.
140 GHz, 1 MW CW gyrotron development for the ECH system of the stellarator W7-X.
35th Internat.Conf.on Infrared, Millimeter and Terahertz Waves (IRMMW-THz 2010), Roma, I,
September 5-10, 2010, Proc.on USB-Stick

[20] Gantenbein, G.; Erckmann, V.; Illy, S.; Kern, S.; Kasparek, W.; Lechte, C.; Leonhardt, W.; Lievin, C.; Samartsev, A.; Schlaich, A.; Schmid, M.; Thumm, M.
Status and recent results of the 140 GHz, 1 MW CW gyrotron development for the stellarator W7-X.
Workshop on RF Heating Technology of Fusion Plasmas, Como, I, September 13-15, 2010;
Folien auf CD-ROM

[21] Gantenbein, G.; Rzesnicki, T.; Piosczyk, B.; Kern, S.; Illy, S.; Jin, J.; Samartsev, A.; Schlaich, A.; Thumm, M.
2.2 MW operation of the European coaxial-cavity pre-prototype gyrotron for ITER.
23rd IAEA Fusion Energy Conference, Daejeon, Korea, October 11-16, 2010

[22] Henderson, M.; Albajar, F.; Alberti, S.; Baruah, U.; Bigelow, T.; Becket, B.; Bertizzolo, R.; Bonicelli, T.; Bruschi, A.; Caughman, J.; Chavan, R.; Cirant, S.; Collazos, A.; Cox, C.; Darbos, C.; deBaar, M.; Denisov, G.; Farina, D.; Gandini, F.; Gassman, T.; Goodman, T.P.; Heidinger, R.; Hogge, J.P.; Illy, S.; Jean, O.; Jin, J.; Kajiwara, K.; Kasparek, W.; Kasugai, A.; Kern, S.; Kobayashi, N.; Kumric, H.; Landis, J.D.; Moro, A.; Nazare, C.; Oda, J.; Omori, T.; Pagonakis, I.; Piosczyk, B.; Platania, P.; Plaum, B.; Poli, E.; Porte, L.; Purohit, D.; Ramponi, G.; Rzesnicki, T.; Rao, S.L.; Rasmussen, D.; Ronden, D.; Saibene, G.; Sakamoto, K.; Sanchez, F.; Scherer, T.; Shapiro, M.; Sozzi, C.; Spaeh, P.; Strauss, D.; Sauter, O.; Takahashi, K.; Tanga, A.; Temkin, R.; Thumm, M.; Tran, M.Q.; Udintsev, V.; Zohm, H.; Zucca, C.
An overview of the ITER EC H&CD system and funtional capabilities.
23rd IAEA Fusion Energy Conference, Daejeon, Korea, October 11-16, 2010

[23] Henderson, M.; Albajar, F.; Alberti, S.; Baruah, U.; Bigelow, T.; Becker, B.; Bertizzolo, R.; Bonicelli, T.; Bruschi, A.; Caughman, J.; Chavan, R.; Cirant, S.; Collazos, A.; Cox, C.; Darbos, C.; deBaar, M.; Denisov, G.; Farina, D.; Gandini, F.; Gassman, T.; Goodman, T.P.; Heidinger, R.; Hogge, J.P.; Illy, S.; Jean, O.; Jin, J.; Kajiwara, K.; Kasparek, W.; Kasugai, A.; Kern, S.; Kobayashi, N.; Kumric, H.; Landis, J.D.; Moro, A.; Nazare, C.; Oda, J.; Omori, T.; Pagonakis, I.; Piosczyk, B.; Platania, P.; Plaum, B.; Poli, E.; Porte, L.; Purohit, D.; Ramponi, G.; Rzesnicki, T.; Rao, S.L.; Rasmussen, D.; Ronden, D.; Saibene, G.; Sakamoto, K.; Sanchez, F.; Scherer, T.; Shapiro, M.; Sozzi, C.; Spaeh, P.; Strauss, D.; Sauter, O.; Takahashi, K.; Tanga, A.; Temkin, R.; Thumm, M.; Tran, M.Q.; Udintsev, V.; Zohm, H.; Zucca, C.
EC H&CD system for ITER.
16th Joint Workshop on Electron Cyclotron Emission and Electron Cyclotron Resonance Heating, Sanya, China, April 12-15, 2010; Book of Abstracts

[24] Illy, S.; Beringer, M.; Kern, S.; Thumm, M.
Collector design studies for a 1 MW cylindrical-cavity and a 4 MW coaxial-cavity gyrotron.
35th Internat.Conf.on Infrared, Millimeter and Terahertz Waves (IRMMW-THz 2010), Roma, I, September 5-10, 2010; Proc.on USB-Stick

[25] Illy, S.; Flamm, J.; Gantenbein, G.; Jin, J.; Kern, S.; Piosczyk, B.; Rzesnicki, T.; Samartsev, A.; Schlaich, A.; Thumm, M.
Recent experimental results of the 2 MW, 170 GHz European pre-prototype coaxial-cavity gyrotron for ITER.
37th IEEE Internat.Conf.on Plasma Science (ICOPS 2010), Norfolk, Va., June 20-24, 2010; Book of Abstracts S.234

[26] Ioannidis, Z.C.; Kern, S.; Avramides, K.A.; Latsas, G.P.; Tigelis, I.G.
The contribution of higher-order spatial harmonics in eigenvalues and ohmic losses calculations in coaxial corrugated cavities.
35th Internat.Conf.on Infrared, Millimeter and Terahertz Waves (IRMMW-THz 2010), Roma, I, September 5-10, 2010; Proc.on USB-Stick

[27] Jin, J.; Flamm, J.; Kern, S.; Rzesnicki, T.; Thumm, M.
Design of phase correcting mirror system for coaxial-cavity ITER gyrotron.
11th Internat.Vacuum Electronics Conf.(IVEC 2010), Monterey, Calif., May 18-20, 2010; Proc.S.29-30; Piscataway, N.J. : IEEE, 2010; ISBN 978-1-422-7099-0

[28] Jin, J.; Flamm, J.; Kern, S.; Rzesnicki, T.; Thumm, M.
Theoretical and experimental investigation of a quasi-optical mode converter for a coaxial-cavity gyrotron.
ITG Vacuum Electronics Workshop, Bad Honnef, November 15-16, 2010

[29] Jin, J.; Kern, S.; Rzesnicki, T.; Thumm, M.
Improved design of a quasi-optical mode converter for the coaxial-cavity ITER gyrotron.
16th Joint Workshop on Electron Cyclotron Emission and Electron Cyclotron Resonance Heating, Sanya, China, April 12-15, 2010; Book of Abstracts

[30] Kasparek, W.; Erckmann, V.; Hollmann, F.; Michel, G.; Noke, F.; Purps, F.; Plaum, B.; Brand, P.; Lechte, C.; Filipovic, E.; Saliba, M.; Doelman, N.; van den Braber, R.; Bongers, W.; Krijger, B.; Petelin, M.; Koposova, E.; Lubyako, L. ; Bruschi, A.; Stober, J.; Wagner, D.; Groups at IPF Stuttgart, IPP Greifswald, IAP N.Novgorod, IFP Milano, KIT Karlsruhe, TNO Delft, and FOM Rijnhuisen
Compact resonant diplexers for advanced ECRH: design, low- and high-power tests, and plans;
Workshop on RF Heating Technology of Fusion Plasmas, Como, I, September 13-15, 2010; Folien auf CD-ROM

[31] Kasparek, W.; Erckmann, V.; Hollmann, F.; Michel, G.; Noke, F.; Purps, F.; Plaum, B.; Brand, P.; Lechte, C.; Filipovic, E.; Saliba, M.; Wang, Y.; Petelin, M.; Koposova, E.; Lubyako, L.; Doelman, N.; van den Braber, R.; Bruschi, A.; Bongers, W.; Krijger, B.; Stober, J.; Wagner, D. ; Groups at IPF Stuttgart, IPP Greifswald, IAP N.Novgorod, IFP Milano, KIT Karlsruhe, TNO Delft, FOM Rijnhuizen
Recent results in the development of compact resonant diplexers.
22nd Joint Russian-German Meeting on ECRH and Gyrotrons, Nizhny Novgorod, Russia, June 29 - July 5, 2010; Folien auf CD-ROM

[32] Kasparek, W.; Erckmann, V.; Petelin, M.; Bruschi, A. ; Research Groups at IPF, IPP, IAP, IFP, KIT, TNO and FOM
High-power diplexers for plasma heating and diagnostic systems: developments, experiments, and prospects.
3rd Internat.Workshop on Far-Infrared Technologies (IW-FIRT 2010), Fukui, J, March 15-17, 2010; Abstracts S.20-21; Proc.on CD-ROM; University of Fukui

[33] Kasparek, W.; Lechte, C.; Plaum, B.; Erckmann, V.; Laqua, H.; Michel, G.; Gantenbein, G.; Thumm, M.
Transmission system for ECRH on Wendelstein 7-X.
Institut für Plasmaforschung Universität Stuttgart, Annual Report 2010 S.40-41

[34] Kasparek, W.; Plaum, B.; Lechte, C.; Erckmann, V.; Michel, G.; Zohm, H.; Petelin, M.; Bruschi, A.; Thumm, M.; Bongers, W.; Doelman, N.
A diplexer for power combination and fast switching.
Institut für Plasmaforschung Universität Stuttgart, Annual Report 2010 S.44

[35] Kern, S.; Avramides, K.A.; Roy Choudhury, A.; Borie, E.; Gantenbein, G.; Illy, S.; Samartsev, A.; Schlaich, A.; Thumm, M.
Different types of after cavity interaction in gyrotrons.
Workshop on RF Heating Technology of Fusion Plasmas, Como, I, September 13-15, 2010; Folien auf CD-ROM

[36] Kern, S.; Avramides, K.A.; Roy Choudhury, A.; Dumbrajs, O.; Gantenbein, G.; Illy, S.; Samartsev, A.; Schlaich, A.; Thumm, M.
Simulation and experimental investigations on dynamic after cacity interaction (ACI).
35th Internat.Conf.on Infrared, Millimeter and Terahertz Waves (IRMMW-THz 2010), Roma, I, September 5-10, 2010; Proc.on USB-Stick

[37] Latsas, G.P.; Tigelis, I.G.; Moraitou, M.D.; Kern, S.; Vomvoridis, J.L.; Ioannidis, Z.C.
Parametric study on the effect of the dielectric and geometric properties on the parasitics in gyrotron beam tunnels.
35th Internat.Conf.on Infrared, Millimeter and Terahertz Waves (IRMMW-THz 2010), Roma, I, September 5-10, 2010; Proc.on USB-Stick

[38] Li, G.; Jin, J.; Rzesnicki, T.; Kern, S.; Thumm, M.
Analysis of a quasi-optical launcher toward a step-tunable 2-MW coaxial-cavity gyrotron.
IEEE Transactions on Plasma Science, 38(2010) S.1361-68; DOI:10.1109/TPS.2010.2043267

[39] Omori, T.; Albajar, F.; Alberti, S.; Baruah, U.; Beckett, B.; Bigelow, T.; Bonicelli, T.; Bruschi, A.; Caughman, J.; Chavan, R.; Cox, D.; Darbos, C.; deBaar, M.; Denisov, G.; Gandini, F.; Gassman, T.; Goodman, T.P.; Henderson, M.; Hogge, J.P.; Jean, O.; Kajiwara, K.; Kasparek, W.; Kasugai, A.; Kern, S.; Kobayashi, N.; Kushwah, M.; Moro, A.; Nazare, C.; Oda, J.; Purohit, D.; Ramponi, G.; Rao, S.L.; Rasmussen, D.; Ronden, D.; Saibene, G.; Sakamoto, K.; Scherer, T.; Shapiro, M.; Singh, N.P.; Strauss, D.; Takahashi, K.; Temkin, R.
Status of the ITER EC H&CD system.
Workshop on RF Heating Technology of Fusion Plasmas, Como, I, September 13-15, 2010; Folien auf CD-ROM

[40] Omori, T.; Henderson, M.A.; Albajar, F.; Alberti, S.; Baruah, U.; Bigelow, T.; Beckett, B.; Bertizzolo, R.; Bonicelli, T.; Bruschi, A.; Caughman, J.; Chavan, R.; Cirant, S.; Collazos, A.; Cox, D.; Darbos, C.; de Baar, M.R.; Denisov, G.; Farina, D.; Gandini, F.; Gassmann, T.; Goodman, T.P.; Heidinger, R.; Hogge, J.P.; Illy, S.; Jean, O.; Jin, J.; Kajiwara, K.; Kasparek, W.; Kasugai, A.; Kern, S.; Kobayashi, N.; Kumric, H.; Landis, J.D.; Moro, A.; Nazare, C.; Oda, Y.; Pagonakis, I.; Piosczyk, B.; Platania, P.; Plaum, B.; Poli, E.; Porte, L.; Purohit, D.; Ramponi, G.; Rao, S.L.; Rasmussen, D.A.; Ronden, D.M.S.; Rzesnicki, T.; Saibene, G.; Sakamoto, K.; Sanchez, F.; Scherer, T.; Shapiro, M.; Sozzi, C.; Spaeh, P.; Strauss, D.; Sauter, O.; Takahashi, K.; Temkin, R.; Thumm, M.; Tran, M.Q.; Udintsev, V.; Zohm, H.
Overview of the ITER EC H&CD system and its capabilities.
26th Symp.on Fusion Technology (SOFT 2010), Porto, P, September 27 - October 1, 2010

[41] Pagonakis, I.G.; Hogge, J.P.; Alberti, S.; Piosczyk, B.; Illy, S.; Kern, S.; Lievin, C.
An additional criterion for gyrotron gun design.
37th IEEE Internat.Conf.on Plasma Science (ICOPS 2010), Norfolk, Va., June 20-24, 2010; Book of Abstracts S.236

[42] Pagonakis, I.G.; Hogge, J.P.; Alberti, S.; Illy, S.; Piosczyk, B.; Kern, S.; Lievin, C.; Tran, M.Q.
Status of the EU 170 GHz/2 MW/CW coaxial cavity gyrotron for ITER: the dummy gun experiment.
35th Internat.Conf.on Infrared, Millimeter and Terahertz Waves (IRMMW-THz 2010), Roma, I, September 5-10, 2010; Proc.on USB-Stick

[43] Rzesnicki, T.; Piosczyk, B.; Kern, S.; Illy, S.; Jin, J.; Samartsev, A.; Schlaich, A.; Thumm, M.
2.2-MW record power of the 170-GHz European preprototype coaxial-cavity gyrotron for ITER.
IEEE Transactions on Plasma Science, 38(2010) S.1141-49, DOI:10.1109/TPS.2010.2040842

[44] Rzesnicki, T.; Piosczyk, B.; Kern, S.; Illy, S.; Jin, J.; Samartsev, A.; Schlaich, A.; Thumm, M.
Experiments with the European 2 MW coaxial-cavity pre-prototype gyrotron for ITER.
11th Internat.Vacuum Electronics Conf.(IVEC 2010), Monterey, Calif., May 18-20, 2010; Proc.S.27-28; Piscataway, N.J. : IEEE, 2010; ISBN 978-1-422-7099-0

[45] Rzesnicki, T.; Piosczyk, B.; Roy Choudhury, A.; Illy, S.; Jin, J.; Kern, S.; Samartsev, A.; Schlaich, A.; Thumm, M.
Recent improvements on the 2 MW, 170 GHz coaxial-cavity pre-prototype gyrotron.
ITG Vacuum Electronics Workshop, Bad Honnef, November 15-16, 2010

[46] Rzesnicki, T.; Piosczyk, B.; Roy Choudhury, A.; Illy, S.; Jin, J.; Kern, S.; Samartsev, A.; Schlaich, A.; Thumm, M.
Recent results with the European 2 MW coaxial-cavity pre-prototype gyrotron for ITER.
35th Internat.Conf.on Infrared, Millimeter and Terahertz Waves (IRMMW-THz 2010), Roma, I, September 5-10, 2010; Proc.on USB-Stick

[47] Scherer, T.; Strauss, D.; Meier, A.; Mathis, Y.L.; Judin, V.; Müller-Sebert, W.; Smirnov, W.; Nebel, C.
Investigation of microwave and THz radiation losses in CVD diamond and chemically modified diamond.
Materials Research Society Fall Meeting 2010, Boston, Mass., November 29 - December 3, 2010

[48] Scherer, T.; Strauß, D.; Schreck, S.; Gantenbein, G.; Kleefeldt, K.; Leonhardt, W.; Meier, A.; Mellein, D.; Serikov, A.; Späh, P.; Vaccaro, A.; Aiello, G.
Design validation of the structural components and CVD diamond torus windows in the ITER ECH upper launcher.
Workshop on RF Heating Technology of Fusion Plasmas, Como, I, September 13-15, 2010; Folien auf CD-ROM

[49] Scherer, T.A.; Scheuring, A.; Probst, P.; Stockhausen, A.; Illin, K.; Siegel, M.; Meier, A.; Strauss, D.
Dielectric properties of CVD diamond disks from sub-mm wave to THz frequencies.
35th Internat.Conf.on Infrared, Millimeter and Terahertz Waves (IRMMW-THz 2010), Roma, I, September 5-10, 2010

[50] Scherer, T.A.; Strauss, D.; Meier, A.; Scheuring, A.; Siegel, M.
Sub-mm-wave and THz-applications in material science for nuclear fusion reactors.
2nd Karlsruhe Detector Workshop, Karlsruhe, March 2-3, 2010

[51] Scherer, T.A.; Strauss, D.; Schreck, S.; Meier, A.; Aiello, G.; Vaccaro, A.; Späh, P.; Nebel, C.
Diamond window design for ITER and investigation of surface losses of chemically modified diamond.
22nd Joint Russian-German Meeting on ECRH and Gyrotrons, Nizhny Novgorod, Russia, June 29 - July 5, 2010

[52] Scherer, T.A.; Strauss, D.; Vaccaro, A.; Aiello, G.; Schreck, S.; Meier, A.; Späh, P.
Recent upgrades of the ITER ECRH CVD torus diamond window design and investigation of dielectric diamond properties.
16th Joint Workshop on Electron Cyclotron Emission and Electron Cyclotron Resonance Heating, Sanya, China, April 12-15, 2010; Book of Abstracts

[53] Schlaich, A.
Aufbau und Anwendung eines Systems zur Spektralanalyse von Gyrotronpulsen im Millimeterwellenbereich.
Diplomarbeit, Karlsruher Institut für Technologie 2009
KIT Scientific Reports, KIT-SR 7541 (Juli 2010)

[54] Schlaich, A.
Investigations on parasitic oscillations in megawatt gyrotrons.
KIT PhD Symp., Karlsruhe, 30.September 2010

[55] Schlaich, A.; Flamm, J.; Gantenbein, G.; Kern, S.; Latsas, G.; Rzesnicki, T.; Samartsev, A.; Thumm, M.; Tigelis, I.; Zwick, T.
Erweiterung der Gyrotron-Frequenzmesstechnik.
Treffen des Kompetenzbereichs Systeme und Prozess, KIT, Karlsruhe, 24.-25. März 2010

[56] Schlaich, A.; Flamm, J.; Gantenbein, G.; Kern, S.; Latsas, G.; Rzesnicki, T.; Samartsev, A.; Thumm, M.; Tigelis, I.
Investigations on parasitic oscillations in megawatt gyrotrons.
11th Internat.Vacuum Electronics Conf.(IVEC 2010), Monterey, Calif., May 18-20, 2010
Proc.S.33-34, Piscataway, N.J. : IEEE, 2010; ISBN 978-1-422-7099-0

[57] Schlaich, A.; Flamm, J.; Gantenbein, G.; Kern, S.; Samartsev, A.; Thumm, M.
Characterization of undesired RF oscillations in megawatt gyrotrons.
ITG Vacuum Electronics Workshop, Bad Honnef, November 15-16, 2010

[58] Schmid, M.; Erckmann, V.; Gantenbein, G.; Illy, S.; Kern, S.; Lievin, Ch.; Samartsev, A.; Schlaich, A.; Rzesnicki, T.; Thumm, M.
Technical developments at the KIT gyrotron test facility.
26th Symp.on Fusion Technology (SOFT 2010), Porto, P, September 27 - October 1, 2010

[59] Schreck, S.; Aiello, G.; Gantenbein, G.; Meier, A.; scherer, T.A.; Spaeh, P.; Strauss, D.; Vaccaro, A.
Prototype manufacturing and testing of components of the ECH upper launcher for ITER.
23rd IAEA Fusion Energy Conference, Daejeon, Korea, October 11-16, 2010

[60] Serikov, A.; Fischer, U.; Grosse, D.; Heidinger, R.; Kleefeldt, K.; Spaeh, P.; Strauss, D.; Vaccaro, A.
Overview of recent nuclear analyses for the upper ECH launcher in ITER.
Fusion Engineering and Design, 85(2010) S.1885-1895, DOI:10.1016/j.fusengdes.2010.06.016

[61] Serikov, A.; Fischer, U.; Große, D.; Heidinger, R.; Späh, P.; Strauß, D.
Nuclear-safety-related and shielding analyses of the ITER quasi-optical ECH launcher.
IEEE Transactions on Plasma Science, 38(2010) S.224-31
DOI:10.1109/TPS.2009.2032261

[62] Serikov, A.; Fischer, U.; Grosse, D.; Spaeh, P.; Strauss, D.
Evolution of shielding computations for the ITER upper ECH launcher.
Nevada Section of the American Nuclear Society 2010 Topical Meeting, Las Vegas, Nev., April 18-23, 2010

[63] Spaeh, P.; Heidinger, R.; Kleefeldt, K.; Leher, F.; Meier, A.; Obermeier, C.; Scherer, T.; Serikov, A.; Strauss, D.; Vaccaro, A.
Manufacturing studies of structural components for the ITER EC upper launcher.
Fusion Engineering and Design, 85(2010) S.1406-1409, DOI:10.1016/j.fusengdes.2010.03.058

[64] Stober, J.; Wagner, D.; Gianone, L.; Leuterer, F.; Monaco, F.; Maraschek, M.; Mlynek, A.; Mszanowski, U.; Münich, M.; Poli, E.; Reich, M.; Schmid-Lorch, D.; Schütz, H.; Schweinzer, J.; Treutterer, W.; Zohm, H.; ASDEX Upgrade Team; Meier, A.; Scherer, T.; Flamm, J.; Thumm, M.; Höhnle, H.; Kasparek, W.; Stroth, U.; Litvak, A.; Denisov, G.G.; Chirkov, A.V.; Tai, E.M.; Popov, L.G.; Nichiporenko, V.O.; Myasnikov, V.E.; Soluyanova, E.A.; Malygin, S.A.
ECRH on ASDEX upgrade. System extension, new modes of operation, plasma physics results.
16th Joint Workshop on Electron Cyclotron Emission and Electron Cyclotron Resonance Heating, Sanya, China, April 12-15, 2010; Book of Abstracts

[65] Strauss, D.; Scherer, T.; Aiello, G.; Meier, A.; Schreck, S.; Späh, P.; Vaccaro, A.
Deflections and vibrations of the ITER ECRH upper launcher.
16th Joint Workshop on Electron Cyclotron Emission and Electron Cyclotron Resonance Heating, Sanya, China, April 12-15, 2010; Book of Abstracts

[66] Thumm, M.
Progress on gyrotrons for ITER and future thermonuclear fusion reactors.
37th IEEE Internat.Conf.on Plasma Science (ICOPS 2010), Norfolk, Va., June 20-24, 2010; Book of Abstracts S.333

[67] Thumm, M.
State-of-the-art of high power gyro-devices and free electron masers. Update 2009.
KIT Scientific Reports KIT-SR 7540 (April 2010)

[68] Thumm, M.; Brand, P.; Braune, H.; Dammertz, G.; Erckmann, V.; Gantenbein, G.; Illy, S.; Kasparek, W.; Kern, S.; Laqua, H.P.; Lechte, C.; Leonhardt, W.; Marushchenko, N.B.; Michel, G.; Piosczyk, B.; Schmid, M.; Turkin, Y.; Weissgerber, M.
Status and high power performance of the 10-MW 140-GHz ECH system for the stellarator Wendelstein 7-X.
Plasma and Fusion Research, 5(2010) S.1006/1-8

[69] Thumm, M.; Rzesnicki, T.; Piosczyk, B.; Flamm, J.; Gantenbein, G.; Illy, S.; Jin, J.; Kern, S.; Samartsev, A.; Schlaich, A.
2.2 MW record power of the 0.17 THz European pre-prototype coaxial-cavity gyrotron for ITER.
Terahertz Science and Technology, 3(2010) Nr.1, S.1-20

[70] Thumm, M.; Rzesnicki, T.; Piosczyk, B.; Flamm, J.; Gantenbein, G.; Illy, S.; Jin, J.; Kern, S.; Samartsev, A.; Schlaich, A.
Recent results of the 2 MW-0.17 THz European pre-prototype coaxial-cavity gyrotron for ITER.
3rd Internat.Workshop on Far-Infrared Technologies (IW-FIRT 2010), Fukui, J,
March 15-17, 2010; Abstracts S.12-13; Proc.on CD-ROM; University of Fukui

[71] Thumm, M.; Rzesnicki, T.; Piosczyk, B.; Flamm, J.; Gantenbein, G.; Illy, S.; Jin, J.; Kern, S.; Samartsev, A.; Schlaich, A.
Status of the 2 MW, 170 GHz pre-prototype coaxial-cavity gyrotron for ITER.
22nd Joint Russian-German Meeting on ECRH and Gyrotrons, Nizhny Novgorod, Russia,
June 29 - July 5, 2010

[72] Thumm, M.; Rzesnicki, T.; Piosczyk, B.; Flamm, J.; Gantenbein, G.; Illy, S.; Jin, J.; Kern, S.; Samartsev, A.; Schlaich, A.
Status of the European 2 MW, 170 GHz pre-prototype coaxial-cavity gyrotron for ITER.
Workshop on RF Heating Technology of Fusion Plasmas, Como, I, September 13-15, 2010

[73] Vaccaro, A.; Aiello, G.; Meier, A.; Scherer, T.; Schreck, S.; Spaeh, P.; Strauss, D.; Gantenbein, G.
Silicon oil DC200(R)5CST as an alternative coolant for CVD diamond windows.
16th Joint Workshop on Electron Cyclotron Emission and Electron Cyclotron
Resonance Heating, Sanya, China, April 12-15, 2010; Book of Abstracts

[74] Wagner, D.; Stober, J.; Franke, T.; Leuterer, F.; Monaco, F.; Münich, M.; Reich, M.; Schütz, H.; Zohm, H.; Thumm, M.; Scherer, T.; Meier, A.; Gantenbein, A.; Flamm, G.; Kasparek, W.; Lechte, C.; Litvak, A.G.; Denisov, G.G.; Chirkov, A.V.; Popov, L.G.; Nichiporenko, V.O.; Myasnikov, V.E.; Tai, E.M.; Solyanova, E.A.; Malygin, S.A.
Multi-frequency ECRH system at ASDEX upgrade.
22nd Joint Russian-German Meeting on ECRH and Gyrotrons, Nizhny Novgorod, Russia,
June 29 - July 5, 2010

[75] Wagner, D.; Stober, J.; Leuterer, F.; Monaco, F.; Münich, M.; Reich, M.; Schmid-Lorch, D.; Schütz, H.; Zohm, H.; Thumm, M.; Scherer, T.; Meier, A.; Gantenbein, G.; Flamm, J.; Kasparek, W.; Höhnle, H.; Lechte, C.; Litvak, A.G.; Denisov, G.G.; Chirkov, A.; Popov, L.G.; Nichiporenko, V.O.; Myasnikov, V.E.; Tai, E.M.; Solyanova, E.A.; Malygin, S.A.
Status of the multi-frequency ECRH system at ASDEX upgrade.
Workshop on RF Heating Technology of Fusion Plasmas, Como, I, September 13-15, 2010

[76] Wagner, D.; Stober, J.; Leuterer, F.; Monaco, F.; Münich, M.; Schmid-Lorch, D.; Schütz, H.; Zohm, H.; Thumm, M.; Scherer, T.; Meier, A.; Gantenbein, G.; Flamm, J.; Kasparek, W.; Höhnle, H.; Lechte, C.; Litvak, A.G.; Denisov, G.G.; Chirkov, A.; Popov, L.G.; Nichiporenko, V.O.; Myasnikov, V.E.; Tai, E.M.; Solyanova, E.A.; Malygin, S.A.
Multi-frequency ECRH at ASDEX upgrade, status and plans.
35th Internat.Conf.on Infrared, Millimeter and Terahertz Waves (IRMMW-THz 2010),
Roma, I, September 5-10, 2010; Proc.on USB-Stick

[77] Zaginaylov, G.I.; Kern, S.
Simplified analytic model for improved field calculation inside the coaxial gyrotron cavity.
European Microwave Week, Paris, F, September 26 - October 1, 2010
Piscataway, N.J. : IEEE, 2010 S.240-243; ISBN 978-1-424-47232-1
Also publ.online

Magnets and Affiliated Components

[1] Barth, C.; Weiss, K.P.
Influence of shear strain on current carrying capabilities of HTSC tapes.
3rd Dresden-Karlsruhe Seminar on Materials and Applications of Applied Superconductivity, Bad Liebenzell, June 9-10, 2010

[2] Fietz, W.H.; Fink, S.; Heiduk, M.; Heller, R.; Lange, C.; Lietzow, R.; Möhring, T.; Rohr, P.; Süßer, M.; Rummel, T.
Test arrangement for the W7-X HTS-current lead prototype testing.
Applied Superconductivity Conf., Washington, D.C., August 1-6, 2010

[3] Fietz, W.H.; Heller, R.; Schlachter, S.I.; Goldacker, W.
Application of high temperature superconductors for Fusion.
26th Symp.on Fusion Technology (SOFT 2010), Porto, P, September 27 - October 1, 2010

[4] Heller, R.; Class, A.; Batta, A.; Lietzow, R.; Neumann, H.; Tischmacher, M.
Modeling of the fin type heat exchanger for the HTS current leads of W7-X and JT60-SA.
Cryogenics, 50(2010) S.222-30; DOI:10.1016/j.cryogenics.2009.08.006

[5] Heller, R.; Fietz, W.H.; Fink, S.; Heiduk, M.; Kienzler, A.; Lange, C.; Lietzow, R.; Rohr, P.; Möhring, T.; Rummel, T.; Mönnich, T.; Buscher, K.P.
Test results of the high temperature superconductor prototype current leads for Wendelstein 7-X.
Applied Superconductivity Conf., Washington, D.C., August 1-6, 2010

[6] Heller, R.; Fietz, W.H.; Kienzler, A.; Lietzow, R.
High temperature superconductor current leads for fusion.
26th Symp.on Fusion Technology (SOFT 2010), Porto, P, September 27 - October 1, 2010

[7] Neumann, H.
Cryogenics.
4th Karlsruhe Internat.School on Fusion Technology, Karlsruhe, September 6-17, 2010

[8] Rizzo, E.; Heller, R.; Savoldi Richard, L.; Zanino, R.
Heat exchanger CFD analysis for the W7-X high temperature superconductor current lead prototype.
26th Symp.on Fusion Technology (SOFT 2010), Porto, P, September 27 - October 1, 2010

[9] Savoldi Richard, L.; Class, A.; Fietz, W.H.; Heller, R.; Rizzo, E.; Zanino, R.
CtFD analysis of HTS current lead fin-type heat exchanger for fusion applications.
IEEE Transactions on Applied Superconductivity, 20(2010) S.1733-1736
DOI:10.1109/TASC.2010.2041546

[10] Schlachter, S.I.
Energie der Zukunft - Fusion 2050.
Tag der offenen Tür, KIT, Karlsruhe, 25.September 2010

[11] Schlachter, S.I.
High temperature superconductivity.
4th Karlsruhe Internat.School on Fusion Technology, Karlsruhe, September 6-17, 2010

[12] Schlachter, S.I.; Fietz, W.H.; Goldacker, W.; Grilli, F.; Heller, R.; Kudymow, A.
High-current HTS cables for fusion magnets.
26th Symp.on Fusion Technology (SOFT 2010), Porto, P, September 27 - October 1, 2010

[13] Schwarz, M.; Schacherer, C.; Ehrlich, A.; Weiss, K.P.
Thermal conducitivity of High Temperature Superconductor coated conductors.
Balachandran, U. [Hrsg.]
Advances in Cryogenic Engineering : Transactions of the Internat.Cryogenic Materials Conf., Tucson, Ariz., June 28 - July 2, 2009; Melville, N.Y. : AIP, 2010 S.388-93; incl.CD-ROM: (AIP Conference Proceedings ; 1219); (Advances in Cryogenic Engineering ; 56)
ISBN 978-0-7354-0761-9

[14] Weiss, K.P.
Cryogenic material test Karlsruhe - CryoMaK at the Karlsruhe Institute of Technology.
E.S.E. - Efficiency, Speed, Environment, (2010) Nr.16, S.36-39

[15] Weiss, K.P.; Ehrlich, A.; della Corte, A.; Vostner, A.
Tensile test results on compacted and annealed 316LN material.
Balachandran, U. [Hrsg.]
Advances in Cryogenic Engineering : Transactions of the Internat.Cryogenic Materials Conf., Tucson, Ariz., June 28 - July 2, 2009; Melville, N.Y. : AIP, 2010 S.3-8 incl.CD-ROM; (AIP Conference Proceedings ; 1219); (Advances in Cryogenic Engineering ; 56), ISBN 978-0-7354-0761-9

[16] Weiss, K.P.; Goldacker, W.; Nannini, M.
Finite element analysis of torsion experiments on HTSC tapes.
Applied Superconductivity Conf., Washington, D.C., August 1-6, 2010

[17] Winkler, A.
Transient behaviour of ITER PF coils.
3rd Dresden-Karlsruhe Seminar on Materials and Applications of Applied Superconductivity, Bad Liebenzell, June 9-10, 2010

[18] Winkler, A.; Fietz, W.H.; Fink, S.; Noe, M.
Calculation of transient voltages of ITER poloidal field coils.
IEEE Transactions on Applied Superconductivity, 20(2010) S.419-422
DOI:10.1109/TASC.2010.2041913

Breeding Blanket and Divertor

[1] Abou-Sena, A.; Löbbecke, B.; von der Weth, A.; Knitter, R.
Effect of post welding heat treatment of the HCPB TBM on the Eurofer and lithium orthosilicate pebbles.
26th Symp.on Fusion Technology (SOFT 2010), Porto, P, September 27 - October 1, 2010

[2] Aiello, A.; Bühler, L.; Ciampichetti, A.; Demange, D.; Dörr, L.; Freibergs, J.F. ; Ghidersa, B.; Ilic, M.; Laffont, G.; Messemer, G.; Platnieks, I.; Rampal, G.
Mockup testing facilities and qualification strategy for EU ITER TBMs.
Fusion Engineering and Design, 85(2010) S.2012-2021, DOI:10.1016/j.fusengdes.2010.07.007

[3] Antusch, S.; Norajitra, P.; Piotter, V.; Ritzhaupt-Kleissl, H.J.; Spatafora, L.
Powder injection molding - an innovative manufacturing method for He-cooled DEMO divertor components.
26th Symp.on Fusion Technology (SOFT 2010), Porto, P, September 27 - October 1, 2010

[4] Boccaccini, L.V.; Aiello, A.; Bede, O.; Ilkei, T.; Cismondi, F.; Kosek, L.; Salavy, J.F.; Sardain, P.; Sedano, L.
Study on the conceptual design of the EU test blanket systems.
26th Symp.on Fusion Technology (SOFT 2010), Porto, P, September 27 - October 1, 2010

[5] Boccaccini, L.V.; Radloff, d.; Henn, M.; Gonzalez, s.M.; Commin, L.; Fausser, C.; Hernandez, F.; Rovni, I.; Kolb, M.; Martinez, P.; Pajuste, E.; van Til, S.; Cismondi, F.; Gabriel, F.; Kizane, G.; Knitter, R.; Madeleine, s.; Magielsen, A.J.; Sedano, L.; Szieberth, M.; Coad, J.P.; Fischer, U.; Hegeman, J.B.J.W.; Möslang, A.; Villari, R.
The EFDA goal oriented training programme EUROBREED.
26th Symp.on Fusion Technology (SOFT 2010), Porto, P, September 27 - October 1, 2010

[6] Bühler, L.
Asymptotic methods for modeling of liquid-metal flows in strong magnetic fields
9th School and Workshop on Fusion Physics and Technology, Volos, GR, April 19-23, 2010

[7] Bühler, L.; Horanyi, S.; Mistrangelo, C.
Magnetohydrodynamic flow in the helium-cooled lead-lithium test blanket for ITER.
Internat.Workshop on Liquid Metal Breeder Blankets, Madrid, E, September 23-24, 2010

[8] Bühler, L.; Köhly, C.; Mistrangelo, C.
Liquid metal magnetohydrodynamic investigations at KIT. Design of a new GaInSn loop.
26th Symp.on Fusion Technology (SOFT 2010), Satellite Meeting on Liquid Metal Applications in Fusion Science, Porto, P, September 27 - October 1, 2010

[9] Bühler, L.; Mistrangelo, C.
Determination of flow distribution in a HCLL blanket mock-up through electric potential measurements.
26th Symp.on Fusion Technology (SOFT 2010), Porto, P, September 27 - October 1, 2010

[10] Bühler, L.; Mistrangelo, C.
Draining of a helium-cooled lead lithium test blanket module by gravity under the influence of a strong magnetic field.
IEEE Transactions on Plasma Science, 38(2010) S.328-32; DOI:10.1109/TPS.2009.2037887

[11] Bühler, L.; Mistrangelo, C.
Effects of radial variation of the magnetic field on the pressure distribution in the European liquid-metal blanket concept
19th Topical Meeting on the Technology of Fusion Energy (TOFE), Las Vegas, Nev., November 7-11, 2010

[12] Bühler, L.; Mistrangelo, C.
Magnetohydrodynamic flows in fusion blankets: experiments and simulations
9th School and Workshop on Fusion Physics and Technology, Volos, GR, April 19-23, 2010

[13] Bühler, L.; Mistrangelo, C.; Horanyi, S.
MHD experiments for fusion engineering and code validation.
Workshop on numerical Simulation of MHD Flows, Karlsruhe, October 18-20, 2010

[14] Chakin, V.; Rolli, R.; Schneider, H.C.; Möslang, A.; Kurinskiy, P.; Van Renterghem, W.
Pores and cracks in highly neutron irradiated beryllium.
European Materials Research Society Spring Meeting, Strasbourg, F, June 7-11, 2010

[15] Ciampichetti, A.; Aiello, A.; Nitti, S.; Ricapito, I.; Liger, K.; Demange, D.; Moreno, C.
Design of coolant purification system for the European test blanket modules.
26th Symp.on Fusion Technology (SOFT 2010), Porto, P, September 27 - October 1, 2010

[16] Demange, D.; Stämmler, S.; Kind, M.
Membranes and catalytic membrane reactors in breeder blanket for improved tritium management and facilitated accountancy.
26th Symp.on Fusion Technology (SOFT 2010), Porto, P, September 27 - October 1, 2010

[17] Fidaros, D.K.; Bühler, L.; Grecos, A.P.; Vlachos, N.S.
Numerical modelling of rotating tangential layers (jets) in shells under strong uniform magnetic field.
International Journal for Numerical Methods in Fluids, 62(2010) S.660-82; DOI:10.1002/fld.2036

[18] Gan, Y.; Kamlah, M.
Thermo-mechanical modelling of pebble bed-wall interfaces.
Fusion Engineering and Design, 85(2010) S.24-32, OI:10.1016/j.fusengdes.2009.05.003

[19] Ghirelli, N.; Demange, D.; Gastaldi, O.
Calculations of tritium mass transfer in HCPB TBM concept and impact on systems for DEMO scale up.
9th Internat.Conf.on Tritium Science and Technology (TRITIUM 2010), Nara, J, October 24-29, 2010

[20] Hayashi, K.; Araki, M.; Baluc, N.; Yamanishi, T.; Nishitani, T.; Hernandez, T.; Morono, A.; Moriani, A.; Tosti, S.; Nozawa, T.; Lindau, R.; Spätig, P.; Tanigawa, H.; Kurinskiy, P.; Nakamichi, M.; Knitter, R.; Hoshino, T.
Progress in DEMO R&D activities within the BA-IFERC project.
8th Joint Conf.on Fusion Energy, Takayama, J, June 10-11, 2010

[21] Jin, X.; Ghidersa, B.E.
Thermal-hydraulic system study of a high pressure, high temperature helium loop using RELAP5-3D code.
8th Internat.Topical Meeting on Nuclear Thermal Hydraulics, Operation and Safety (NUTHOS-8), Shanghai, China, October 10-14, 2010

[22] Kaufmann, U.; Kolb, M.; Knitter, R.
Die chemisch-thermische Beanspruchung von Platinwerkstoffen durch Lithiumreiche Silikatschmelzen.
Kneissl, A. [Hrsg.]
Fortschritte in der Metallographie : Berichte der 13.Internat.Metallographie-Tagung, Leoben, A, September 29 - October 1, 2010
Frankfurt : MAT-INFO, Werkstoff-Informationsges., 2010 S.43-48
(Praktische Metallographie : Sonderbd. ; 42)

[23] Knitter, R.; Odemer, C.
Synthesis of lithium ceramics as tritium breeder materials.
11th Internat.Conf.on Ceramic Processing Science (ICCPS-11), Zürich, CH, August 29 - September 1, 2010

[24] Kolb, M.; Knitter, R.; Kaufmann, U.; Mundt, D.
Enhanced fabrication process for lithium orthosilicate pebbles as breeding material.
26th Symp.on Fusion Technology (SOFT 2010), Porto, P, September 27 - October 1, 2010

[25] Koncar, B.; Norajitra, P.; Oblak, K.
Effect of nozzle sizes on jet impingement heat transfer in He-cooled divertor.
Applied Thermal Engineering, 30(2010) S.697-705; DOI:j.applthermaleng.2009.11.018

[26] Koncar, B.; Simonovski, I.; Draksler, M.; Norajitra, P.
Thermal stress prediction in divertor cooling finger using the local heat transfer distribution.
26th Symp.on Fusion Technology (SOFT 2010), Porto, P, September 27 - October 1, 2010

[27] Leichtle, D.; Fischer, U.; Kodeli, I.; Perel, R.L.; Klix, A.; Batistoni, P.; Villari, R.
Sensitivity and uncertainty analyses of the HCLL mock-up experiment.
Fusion Engineering and Design, 85(2010) S.1724-1727; DOI:10.1016/j.fusengdes.2010.05.023

[28] Liger, K.; Ciampichetti, A.; Demange, D.
HCLL and HCPB coolant purification system: preliminary measurement and instrumentation plan.
9th Internat.Conf.on Tritium Science and Technology (TRITIUM 2010), Nara, J, October 24-29, 2010

[29] Magnani, E.; Gabriel, F.; Boccaccini, L.V.; Li-Puma, A.
DEMO relevance of the test blanket modules in ITER-application to the European test blanket modules.
Fusion Engineering and Design, 85(2010) S.1271-1278; DOI:10.1016/j.fusengdes.2010.03.022

[30] Mistrangelo, C.
Implementation of models for wall currents to simulate MHD flows.
Numerical Modelling of Coupled Problems in Applied Physics with OpenFOAM (NUMAP-FOAM), Zagreb, HR, September 1-15, 2010

[31] Mistrangelo, C.
Simulation of MHD flows in OpenFOAM: capabilities and new features.
Workshop on Numerical Simulation of MHD Flows, Karlsruhe, October 18-20, 2010

[32] Mistrangelo, C.; Bühler, L.
Development of a numerical tool to simulate magnetohydrodynamic interactions of liquid metals with strong applied magnetic fields.
19th Topical Meeting on the Technology of Fusion Energy (TOFE), Las Vegas, Nev., November 7-11, 2010

[33] Mistrangelo, C.; Bühler, L.
HCLL blanket for ITER: Liquid-metal MHD mock-up experiments.
26th Symp.on Fusion Technology (SOFT 2010), Satellite Meeting on Liquid Metal Applications in Fusion Science, Porto, P, September 27 - October 1, 2010

[34] Mistrangelo, C.; Bühler, L.
Magnetohydrodynamic pressure drops in geometric elements forming a HCLL blanket mock-up.
26th Symp.on Fusion Technology (SOFT 2010), Porto, P, September 27 - October 1, 2010

[35] Mistrangelo, C.; Bühler, L.
MHD mock-up experiments for studying pressure distribution in a helium-cooled liquid-metal blanket.
IEEE Transactions on Plasma Science, 38(2010) S.254-258; DOI:10.1109/TPS.2009.2036261

[36] Mistrangelo, C.; Bühler, L.
Perturbing effects of electric potential probes on MHD duct flows.
Experiments in Fluids, 48(2010) S.157-65; DOI:10.1007/s00348-009-0710-x

[37] Mistrangelo, C.; Widlund, O.
Simulation of magneto-hydrodynamic (MHD) flows: electric potential formulation.
5th OpenFOAM Workshop, Göteborg, S, June 21-24, 2010

[38] Mochizuki, K.; Munakata, K.; Wajima, T.; Hara, K.; Wada, K.; Shinozaki, T.; Takeishi, T.; Knitter, R.; Bekris, N.; Okuno, K.
Study of isotope exchange reactions on ceramic breeder materials deposited with noble metal.
Fusion Engineering and Design, 85(2010) S.1185-89; DOI:10.1016/j.fusengdes.2010.02.035

[39] Norajitra, P.
Divertors.
4th Karlsruhe Internat.School on Fusion Technology, Karlsruhe, September 6-17, 2010

[40] Norajitra, P.; Antusch, s.; Giniyatulin, R.; Kuznetsov, V.; Mazul, I.; Ritzhaupt-Kleissl, H.J.; Spatafora, L.
Progress of He-cooled divertor development for DEMO.
26th Symp.on Fusion Technology (SOFT 2010), Porto, P, September 27 - October 1, 2010

[41] Norajitra, P.; Giniyatulin, R.; Kuznetsov, V.; Mazul, I.; Ritz, G.
He-cooled divertor for DEMO: Status of development and HHF tests.
Fusion Engineering and Design, 85(2010) S.2251-56; DOI:10.1016/j.fusengdes.2010.09.006

[42] Raffray, A.R.; Nygren, R.; Whyte, D.G.; Abdel-Khalik, S.; Dörner, R.; Escourbiac, F.; Evans, T.; Goldston, R.J.; Hölzer, D.T.; Konishi, S.; Lorenzetto, P.; Merola, M.; Neu, R.; Norajitra, P.; Pitts, R.A.; Rieth, M.; Rödig, M.; Rognlien, T.; Suzuki, S.; Tillack, M.S.; Wong, C.
High heat flux components - readiness to proceed from near term fusion systems to power plants.
Fusion Engineering and Design, 85(2010) S.93-108; DOI:10.1016/j.fusengdes.2009.08.002

[43] Reimann, J.; Benes, O.; Colle, J.Y.; Dorn, C.; Harsch, H.; Kurinskiy, P.
Vapor pressure of beryllides.
19th Topical Meeting on the Technology of Fusion Energy (TOFE), Las Vegas, Nev., November 7-11, 2010

[44] Smolentsev, S.; Moreau, R.; Bühler, L.; Mistrangelo, C.
MHD thermofluid issues of liquid metal blankets: phenomena and advances.
Fusion Engineering and Design, 85(2010) S.1196-1205; DOI:10.1016/j.fusengdes.2010.02.038

[45] Stämmler, S.; Demange, D.; Kind, M.
Potential use of zeolite membranes for separation and recovery of tritium produced in the breeder blanket of fusion machines.
5th Internat.Zeolite Membrane Meeting, Loutraki, GR, May 23-26, 2010

[46] Van Til, S.; Kolb, M.; Magielsen, A.J.; Knitter, R.
Irradiation of lithium orthosilicate in the high flux reactor in Petten for the fusion fuel cycle.
1st Internat.Conf.on Materials for Energy, Karlsruhe, July 4-8, 2010

[47] von der Weth, A.
Genetische Algorithmen und Optimierung von Mikroinductoren.
Vortr.: IHM, KIT, Karlsruhe, 21.Januar 2010

[48] Zarins, A.; Kizane, G.; Supe, A.; Baumane, L.; Tilika, V.; Pajuste, E.; Knitter, R.
Influence of pretreatment of lithium orthosilicate pebbles on radiation stability.
26th Annual Institute of Solid State Physics Scientific Conf., University of Latvia, Riga, LV, February 17-19, 2010

Structural Materials

[1] Aktaa, J.
Nonlinear material and structure modelling for highly loaded components.
Habilitationsschrift, Karlsruher Institut für Technologie 2010

[2] Aktaa, J.; Siska, F.
Assessment of defects in EUROFER 97 first wall/blanket structures taking into account its viscoplastic behavior.
Fusion Engineering and Design, 85(2010) S. 2065-2069; DOI:10.1016/j.fusengdes.2010.07.023

[3] Basuki, W.W.; Aktaa, J.
Diffusion bonding of tungsten / EUROFER97 using vanadium interlayer.
MAT-W&Walloys Monitoring Meeting, San Sebastian, E, June 28-29, 2010

[4] Basuki, W.W.; Aktaa, J.
Investigation of tungsten/EUROFER97 diffusion bonding using Nb interlayer.
26th Symp.on Fusion Technology (SOFT 2010), Porto, P, September 27 - October 1, 2010

[5] Bhanumurthy, K.; Krauss, W.; Konys, J.
Interfacial microstructure of diffusion bonded Fe-Al diffusion couples.
Internat.Conf.on Advances in Electron Microscopy and Related Techniques, Mumbai, IND, March 8-10, 2010

[6] Dethloff, C.
Modeling of helium bubble growth. Recent developments.
4th Meeting of the Helmholtz-Russian-Joint-Research- Group (HRJRG), Karlsruhe, April 13, 2010

[7] Dethloff, C.; Gaganidze, E.; Svetukhin, V.; Tikhonchev, M.; Weiß, O.; Aktaa, J.
Modeling of helium bubble formation and growth in RAFM steels under neutron irradiation.
1st Internat.Conf.on Materials for Energy, Karlsruhe, July 4-8, 2010
Extended Abstracts Book A S.196-9; Frankfurt a.M. : Dechema, 2010; ISBN 978-3-89746-117-8

[8] Dethloff, C.; Gaganidze, E.; Svetukhin, V.; Tikhonchev, M.; Weiß, O.; Aktaa, J.
Modeling of helium bubble growth in neutron irradiated boron doped RAFM steels.
5th Internat.Conf.on Multiscale Materials Modelling (MMM 2010), Freiburg, October 4-8, 2010; Proc.S.675-78

[9] Eiselt, C.C.
Eigenschaftsoptimierung der nanoskaligen ferritischen ODS-Legierung 13Cr-1W-0, $3Y_2O_3$-$0,3TiH_2$, metallkundliche Charakterisierung und Bestimmung von Struktur-Eigenschaftskorrelationen.
Wissenschaftliche Berichte, FZKA-7524 (Januar 2010); Dissertation, Universität Karlsruhe 2010

[10] Eiselt, C.C.; Klimenkov, M.; Lindau, R.; Möslang, A.
Characterization of microstructural and mechanical properties of the 13Cr-1W-0.3Ti-$0.3Y_2O_3$-ODS-steel.
European Materials Research Society Spring Meeting, Strasbourg, F, June 7-11, 2010; Abstract on USB-Stick

[11] Gaganidze, E.; Aktaa, J.; Kraft, O.; Dethloff, C.; Weiss, O.; Svetukhin, V.; Kozlov, D.; Kadochkin, A.; Lvov, P.; Vostretsov, D.; Risovany, V.; Tikhonchev, M.; Sidorenko, O.; Muraleva, E.; Ilina, T.
High dose irradiation damage of RAFM steels.
Helmholtz Russian Joint Research Group Seminar, Moskva, Russia, March 1, 2010

[12] Gaganidze, E.; Petersen, C.; Aktaa, J.; Povstyanko, A.; Prokhorov, V.; Diegele, E.; Lässer, R.
Low cycle fatigue properties of reduced activation ferritic/martensitic steels after high dose neutron irradiation.
23rd IAEA Fusion Energy Conference, Daejeon, Korea, October 11-16, 2010
Book of Abstracts S.401

[13] Gaganidze, E.; Petersen, C.; Aktaa, J.; Schneider, H.C.; Dethloff, C.; Weiß, O.; Povstyanko, A.; Prokhorov, V.; Fedoseev, A.; Makarov, O.; Materna-Morris, E.
Review of mechanical properties of irradiated RAFM steels.
4th Meeting of the Helmholtz Russian Joint Research Group, Karlsruhe, April 13, 2010

[14] Gaganidze, E.; Rupp, D.; Bürkle, U.
Fracture-mechanical and microstructural characterisation of W-alloys.
MAT-W&Walloys Monitoring Meeting, Garching, February 3-4, 2010

[15] Gaganidze, E.; Rupp, D.; Bürkle, U.
Fracture-mechanical and microstructural characterization of W-alloys.
MAT-W&Walloys Monitoring Meeting, San Sebastian, E, June 28-29, 2010

[16] Holstein, N.; Konys, J.; Krauss, W.; Lorenz, J.
Electro-chemically-based technologies for processing of tungsten components in fusion technology.
1st Internat.Conf.on Materials for Energy, Karlsruhe, July 4-8, 2010
Extended Abstracts Book Paper 1334; Frankfurt a.M.: Dechema, 2010; ISBN 978-3-89746-117-8

[17] Holstein, N.; Krauss, W.; Lorenz, J.; Konys, J.
Development of a novel tungsten processing technology for electro-chemical machining of plasma facing components.
26th Symp.on Fusion Technology (SOFT 2010), Porto, P, September 27 - October 1, 2010

[18] Klimenkov, M.; Jäntsch, U.; Lindau, R.; Möslang, A.
Microstructural characterization of electron beam welded RAFM ODS-Eurofer.
European Materials Research Society Spring Meeting, Strasbourg, F, June 7-11, 2010; Abstract on USB-Stick

[19] Klimenkov, M.; Lindau, R.; Möslang, A.
Analytical TEM characterization of 9%Cr ferritic steel.
Solorzano, G. [Hrsg.]
Proc.of the 17th Internat.Microscopy Congress (IMC 17), Rio de Janeiro, BR, September 19-24, 2010
Sociedade Brasileira de Microscopia e Microanalise, 2010; CD-ROM M8.19

[20] Klimenkov, M.; Lindau, R.; Möslang, A.
Transmission electron microscopy study of Ar-filled bubbles in steel.
Journal of Microscopy, 237(2010) S.497-500; DOI:10.1111/j.1365-2818.2009.03307.x

[21] Klimenkov, M.; Materna-Morris, E.
Analytical TEM investigation on boron containing precipitates in ferritic steel.
Solorzano, G. [Hrsg.]
Proc.of the 17th Internat.Microscopy Congress (IMC 17), Rio de Janeiro, BR, September 19-24, 2010
Sociedade Brasileira de Microscopia e Microanalise, 2010; CD-ROM I5.29

[22] Konys, J.; Krauss, W.; Holstein, N.
Development of advanced Al coating processes for future applications as anti-corrosion and T-permeation barriers.
Fusion Engineering and Design, 85(2010) S.2141-45; DOI:10.1016/j.fusengdes.2010.08.018

[23] Konys, J.; Krauss, W.; Holstein, N.
Insulating coating development for anti-corrosion and T-permeation barriers.
Internat.Workshop on Liquid Metal Breeder Blankets, Madrid, E, September 23-24, 2010

[24] Krauss, W.; Holstein, N.; Konys, J.
Advanced electro-chemical processing of tungsten components for He-cooled divertor application.
Fusion Engineering and Design, 85(2010) S.2257-62; DOI:10.1016/j.fusengdes.2010.09.005

[25] Krauss, W.; Lorenz, J.; Holstein, N.; Konys, J.
Alternative electro-chemically based processing routes for joining of plasma facing components.
26th Symp.on Fusion Technology (SOFT 2010), Porto, P, September 27 - October 1, 2010

[26] Lindau, R.; Jäntsch, U.; Klimenkov, M.; Norajitra, P.
Mechanical and microstructural properties of EB welded RAFM ODS-Eurofer steel for applications in helium cooled modular divertor concepts.
European Materials Research Society Spring Meeting, Strasbourg, F, June 7-11, 2010; Abstract on USB-Stick

[27] Martin, T.; Knaak, S.; Aktaa, J.
Immersion ultrasonic testing on EUROFER welded joints for the determination of the minimum detectable flaw size.
Jahrestagung der Deutschen Gesellschaft für zerstörungsfreie Prüfung, Erfurt, 10.-12.Mai 2010

[28] Martin, T.; Knaak, S.; Zhong, Y.; Aktaa, J.
Ultrasonic testing on EUROFER welded joints for determination of the minimum detectable flaw size.
KIT Scientific Reports, KIT-SR 7543 (Juli 2010)

[29] Möslang, A.
RAFM steels for DEMO: properties after irradiation.
12th Internat.Conf.on Modern Materials and Technologies (CIMTEC 2010), Montecatini Terme, I, June 6-18, 2010

[30] Petersen, C.
Post irradiation examination of RAF/M steels after fast reactor irradiation up to 33 dpa and < 340^0C (ARBOR 1).
Wissenschaftliche Berichte, FZKA-7517 (November 2010)

[31] Rieth, M.
Tungsten as a structural material for nuclear fusion reactors.
Vortr.: University of Oxford, GB, 20.Mai 2010

[32] Rieth, M.; Armstrong, D.; Dafferner, B.; Heger, S.; Hoffmann, A.; Hoffmann, M.D.; Jäntsch, U.; Kübel, C.; Materna-Morris, E.; Reiser, J.; Rohde, M.; Scherer, T.; Widak, V.; Zimmermann, H.
Tungsten as a structural divertor material.
12th Internat.Conf.on Modern Materials and Technologies (CIMTEC 2010),
Including the 5th Forum on New Materials, Montecatini Terme, I, June 6-18, 2010

[33] Rieth, M.; Armstrong, D.; Dafferner, B.; Heger, S.; Hoffmann, A.; Hoffmann, M.D.; Jäntsch, U.; Kübel, C.; Materna-Morris, E.; Reiser, J.; Rohde, M.; Scherer, T.; Widak, V.; Zimmermann, H.
Tungsten materials for structural divertor applications.
1st Internat.Conf.on Materials for Energy, Karlsruhe, July 4-8, 2010

[34] Rieth, M.; Dafferner, B.; Baumgärtner, S.; Dichiser, S.; Fabry, T.; Fischer, S.; Hildebrand, W.; Palussek, O.; Ritz, H.; Sponda, A.; Ziegler, R.; Zimmermann, H.
Cost effective fabrication of a fail-safe first wall.
1st Joint ITER-IAEA Technical Meeting on Analysis of ITER Materials and Technologies,
Monaco, MC, November 23-25, 2010

[35] Rieth, M.; Hoffmann, A.
Influence of microstructure and notch fabrication on impact bending properties
of tungsten materials.
International Journal of Refractory Metals and Hard Materials, 28(2010) S.679-86
DOI:10.1016/j.ijrmhm.2010.04.010

[36] Rieth, M.; Hoffmann, A.; Reiser, J.; Armstrong, D.E.J.
Fracture behavior of tungsten materials and the impact on the divertor design in nuclear fusion power plants.
Materials Research Society Fall Meeting, Boston, Mass., November 29 - December 3, 2010

[37] Rieth, M.; Linke, J.; Linsmeier, Ch.
High heat flux materials: status and perspectives.
26th Symp.on Fusion Technology (SOFT 2010), Porto, P, September 27 - October 1, 2010

[38] Rupp, D.; Gaganidze, E.
Microstructure and micro-mechanics characterisation of W and W alloys.
MAT-W&Walloys Monitoring Meeting, San Sebastian, E, June 28-29, 2010

[39] Rupp, D.; Gaganidze, E.; Weygand, S.; Mönig, R.; Walter, M.; Bürkle, U.
Fracture mechanical properties of tungsten alloys.
Vortr.: Centre de Recherches en Physique des Plasmas, Fusion Technology, Materials Group,
Villigen, CH, 22.März 2010

[40] Rupp, D.; Mönig, R.; Gruber, P.; Weygand, S.M.
Fracture toughness and microstructural characterization of polycrystalline rolled tungsten.
International Journal of Refractory Metals and Hard Materials, 28(2010) S.669-673
DOI:10.1016/j.ijrmhm.2010.05.006

[41] Rupp, D.; Weygand, S.M.
Anisotropic fracture behaviour and brittel-to-ductile transition of polycrystalline tungsten.
Philosophical Magazine, 90(2010) S.4055-4069; DOI:10.1080/14786435.2010.504198

[42] Sacksteder, I.; Schneider, H.C.; Albinski, B.M.
Further characterization of irradiated steels by indentation at high temperature.
26th Symp.on Fusion Technology (SOFT 2010), Porto, P, September 27 - October 1, 2010

[43] Sandim, H.R.Z.; Renzetti, R.A.; Padilha, A.F.; Raabe, D.; Klimenkov, M.; Lindau, R.; Möslang, A.
Annealing behavior of ferritic-martensitic 9%Cr-ODS-Eurofer steel.
Materials Science and Engineering A, 527(2010) S.3602-3608; DOI:10.1016/j.msea.2010.02.051

[44] Siska, F.; Aktaa, J.
Validation of R5 assessment procedure for ITER test blanket module by finite element analysis.
Fusion Engineering and Design, 85(2010) S.215-21; DOI:10.1016/j.fusengdes.2010.01.015

[45] Stoller, R.; Odette, G.R.; Kurtz, R.; Sokolov, M.; Katoh, Y.; Byun, T.S.; Möslang, A.
Small specimen and in situ mechanical test methods in the US fusion reactor materials program.
139th Annual Meeting and Exhibition of the Minerals, Metals and Materials Society (TMS 2010), Seattle, Wash., February 14-18, 2010

[46] Svetukhin, V.V.; Gaganidze, E.; L'vov, P.E.; Tikhonchev, M.Yu.; Dethloff, C.
Thermodynamic and kinetic model of chromium nanoclusters formation in Fe-Cr system.
The Nuclear Materials Conf. (NuMat 2010), Karlsruhe, October 4-7, 2010

[47] Tikhonchev, M.; Svetukhin, V.; Kadochkin, A.; Gaganidze, E.
MD modelling of ceramic displacement cascades for Fe-9%Cr-0.1%C.
Irradiation Damage of Materials, Obninsk, Russia April 20-22, 2010

[48] Weber, T.; Aktaa, J.
Functionally graded tungsten / EUROFER 97 joints for divertor applications.
MAT-W&Walloys Monitoring Meeting, San Sebastian, E, June 28-29, 2010

[49] Weber, T.; Stüber, M.; Ulrich, S.; Aktaa, J.
Fabrication and characterization of magnetron sputtered tungsten/EUROFER 97 coatings.
12th Internat.Conf.on Modern Materials and Technologies (CIMTEC 2010),
Montecatini Terme, I, June 6-18, 2010; Book of Abstracts S.58

[50] Weiß, O.
Characterization of defects in neutron irradiated Eurofer97.
4th Meeting of the Helmholtz-Russian-Joint-Research-Group (HRJRG), Karlsruhe, April 13, 2010

[51] Weiß, O.J.; Gaganidze, E.
Quantitative TEM investigation of neutron irradiated EUROFER97 from ARBOR 1.
MAT-W&Walloys Monitoring Meeting, San Sebastian, E, June 28-29, 2010

[52] Weiß, O.J.; Gaganidze, E.
Quantitative TEM investigation of neutron irradiated EUROFER97 from WTZ and ARBOR 1.
Radiation Effects Modelling and Experimental Validation : Monitoring Meeting, Paris, F,
November 22-23, 2010

[53] Weiß, O.J.; Gaganidze, E.; Aktaa, J.
Quantitative microstructural investigation of neutron-irradiated RAFM steel for fusion applications.
2nd Internat.Workshop for Young Materials Scientists, Berlin, August 31 - September 3, 2010

Nuclear Data

[1] Domula, A.; Gehre, D.; Klix, A.; Zuber, K.
Neutron activations at the neutron facility of TU-Dresden.
Frühjahrstagung DPG, Fachverband Physik der Hadronen und Kerne, Bonn, 15.-19. März 2010
Verhandlungen der Deutschen Physikalischen Gesellschaft, R.6, B.45(2010) HK 55.4

[2] Fischer, U.; Batistoni, P.; Dupont, E.; Forrest, R.; Henriksson, H.; Izquierdo,
J.; Sublet, J.C.
The European effort on the evaluation and validation of nuclear data for fusion technology applications.
Internat.Conf.on Nuclear Data for Science and Technology (ND2010), Jeju Island, Korea,
April 26-30, 2010

[3] Fischer, U.; Klix, A.; Serikov, A.; Simakov, S.
Testing of FENDL-3/SLIB neutron cross-section data for applications to the IFMIF neutron source facility.
Internat.Conf.on Nuclear Data for Science and Technology (ND2010), Jeju Island, Korea, April 26-30, 2010

[4] Klix, A.; Batistoni, P.; Boettger, R.; Fischer, U.; Fleischer, K.; Henniger, J.; Lebrun-Grandie, D.; Sommer, M.; Villar, S.
Integral neutronics experiment with a mock-up of the European HCLL-TBM for ITER.
Internat.Conf.on Nuclear Data for Science and Technology (ND2010), Jeju Island, Korea, April 26-30, 2010

[5] Klix, A.; Domula, A.; Fischer, U.; Gehre, D.; Lebrun-Grandie, D.; Leichtle, D.; Sommer, M.
Neutronics experiments for validation of activation and neutron transport data for fusion application at the DT neutron generator of TU Dresden.
Frühjahrstagung DPG, Arbeitskreis Energie, Bonn, 15.-19.März 2010
Verhandlungen der Deutschen Physikalischen Gesellschaft, R.6, B.45(2010) AKE 3.4

[6] Lebrun-Grandie, D.; Klix, A.; Fischer, U.
Measurement and analysis of fast neutron and gamma-ray flux spectra in a neutronics mock-up of the European helium-cooled lithium-lead test blanket module for ITER.
Jahrestagung Kerntechnik 2010, Berlin, 4.-6.Mai 2010; Berlin : INFORUM GmbH, 2010
CD-ROM Paper 814

[7] Majerle, M.; Simakov, S.P.
Modelling d-BE and d-C neutron sources for SPIRAL-2.
Jahrestagung Kerntechnik 2010, Berlin, 4.-6.Mai 2010
Berlin : INFORUM GmbH, 2010; CD-ROM Paper 812

[8] Pereslavtsev, P.; Cismondi, F.; Fischer, U.; Grosse, D.; Weber, V.
Neutronic analysis of the HCPB TBM in ITER utilizing an advanced integral approach.
Fusion Engineering and Design, 85(2010) S.1653-1658, DOI:10.1016/j.fusengdes.2010.05.008

[9] Pereslavtsev, P.; Konobeyev, A.; Leal, L.; Fischer, U.
Evaluation of n+Cr-52 cross section data up to 150 MeV neutron energy.
Internat.Conf.on Nuclear Data for Science and Technology (ND2010), Jeju Island, Korea, April 26-30, 2010

[10] Serikov, A.; Fischer, U.; Grosse, D.; Spaeh, P.; Strauss, D.
MCNP5 parallel computations on JURPA/HPC-FF supercomputer for ITER applications.
Jahrestagung Kerntechnik 2010, Berlin, 4.-6.Mai 2010
Berlin : INFORUM GmbH, 2010; CD-ROM Paper 813

[11] Simakov, S.P.; Pereslavtsev, P.; Fischer, U.
Comparative study of the tungsten irradiation conditions in IFMIF and DEMO.
Jahrestagung Kerntechnik 2010, Berlin, 4.-6.Mai 2010
Berlin : INFORUM GmbH, 2010; CD-ROM Paper 811

International Fusion Materials Irradiation Facility (IFMIF)

[1] Arbeiter, F.; Fischer, U.; Heinzel, V.; Klix, A.; Möslang, A.; Simakov, St.; Tian, K.; Vladimirov, P.; Garin, P.; Heidinger, R.
IFMIF test facilities - 3 years of EVEDA.
Jahrestagung Kerntechnik 2010, Berlin, 4.-6.Mai 2010; Berlin : INFORUM GmbH, 2010
CD-ROM Paper 810

[2] Arbeiter, F.; Heinzel, V.; Scheel, N.; Heupel, T.; Dolensky, B.; Chen, Y.; Klein, Ch.; Stratmanns, E.
Status of design and validation tasks for the IFMIF high flux test module.
Jahrestagung Kerntechnik 2010, Berlin, 4.-6.Mai 2010; Berlin : INFORUM GmbH, 2010
CD-ROM Paper 805

[3] Chen, Y.; Arbeiter, F.; Heinzel, V.; Ihli, Th.; Möslang, A.; Slobodchuk, V.; Stratmanns, E.
Design optimization of IFMIF high flux test module towards uniform specimen temperature distribution. Fusion Engineering and Design, 85(2010) S.1952-1956
DOI:10.1016/j.fusengdes.2010.06.028

[4] Chen, Y.; Arbeiter, F.; Heinzel, V.; Schlindwein, G.
Numerical simulations on transient conjugated heat transfer within IFMIF high flux test module.
8th Internat.Topical Meeting on Nuclear Thermal Hydraulics, Operation and Safety (NUTHOS-8), Shanghai, China, October 10-14, 2010

[5] Chen, Y.; Arbeiter, F.; Heinzel, V.; Stratmanns, E.
Key parameters for controlling the specimen temperature in IFMIF high flux test module.
Jahrestagung Kerntechnik 2010, Berlin, 4.-6.Mai 2010; Berlin : INFORUM GmbH, 2010
CD-ROM Paper 804

[6] Gopejenko, A.; Zhukovskii, Y.F.; Vladimirov, P.V.; Kotomin, E.A.; Möslang, A.
Ab initio simulation of yttrium oxide nanocluster formation on fcc Fe lattice.
Journal of Nuclear Materials, 406(2010) S.345-350; DOI:10.1016/j.jnucmat.2010.09.005

[7] Klix, A.; Fischer, U.; Simakov, S.P.
Assessment of the tritium production in the HFTM specimen cells of IFMIF.
IEEE Transactions on Plasma Science, 38(2010) S.259-64, DOI:10.1109/TPS.2009.203685

[8] Mittwollen, M.; Eilert, D.; Huber, C.; Tian, K.; Heupel, T.; Scheel, N.
Key aspects of remote handling and logistics inside IFMIF test facilities.
Jahrestagung Kerntechnik 2010, Berlin, 4.-6.Mai 2010
Berlin : INFORUM GmbH, 2010; CD-ROM Paper 806

[9] Serikov, A.; Arbeiter, F.; Fischer, U.; Heinzel, V.; Klix, A.; Simakov, S.P.
Shutdown dose rate analyses for the HFTM.
3rd IFMIF Workshop, Madrid, E, September 20-22, 2010

[10] Tian, K.; Arbeiter, F.; Eilert, D.; Heinzel, V.; Heupel, T.; Mittwollen, M.; Möslang, A.; Scheel, N.; Stratmanns, E.
New progresses in the IFMIF target and test cell design and a proposal for the specimen flow.
Proc.of the 18th Internat.Conf.on Nuclear Engineering (ICONE-18), Xi'an, China,
May 17-21, 2010; CD-ROM Paper ICONE18-29427; New York, N.Y.: ASME, 2010

[11] Tian, K.; Arbeiter, F.; Heinzel, V.; Heupel, T.; Scheel, N.; Stratmanns, E.; Eilert, D.; Mittwollen, M.
Concept and engineering design of the IFMIF target and test cell.
Jahrestagung Kerntechnik 2010, Berlin, 4.-6.Mai 2010
Berlin : INFORUM GmbH, 2010; CD-ROM Paper 803

Fuel Cycle – Vacuum Pumping

[1] Antipenkov, A.; Bersier, J.L.; Boussier, B.; Day, Chr.; Dremel, M.; Hauer, V.; Meitner, S.; Pearce, R.; Worth, L.
Overview of the tritium handling within the ITER vaccum pumping system.
9th Internat.Conf.on Tritium Science and Technology (TRITIUM 2010), Nara, J, October 24-29, 2010

[2] Antipenkov, A.; Day, C.; Amoskov, V.; Belov, A.; Belyakov, V.; Gapionok, E.; Kukhtin, V.; Lamzin, E.; Shatil, D.; Sytchevsky, S.
Numerical simulations of electro-magnetic transients in ITER cryopumps with the use of TY-PHOON code.
Bulletin of the Peoples' Friendship University of Russia, Series Mathematics, Information Sciences, Physics, 2(2010) Nr.3, S.81-86

[3] Boussier, B.; Pearce, R.; Mayaux, Chr.; Evrard, B.; Journeaux, J.Y.; Day, Chr.; Marechal, J.L.
ITER vacuum control system. Current status overview and technical challenges.
18th Internat.Vacuum Congress (IVC-18), Internat.Conf.on Nanoscience and Technology (ICN+T 2010), 14th Internat.Conf.on Surfaces Science (ICSS-14),
Vacuum and Surface Sciences Conf.of Asia and Australia (VASSCAA-5), Beijing,
China, August 23-27, 2010

[4] Day, C.
Contributions of rarefied gas dynamics to state-of-the-art vacuum science and technology.
27th Internat.Symp.on Rarefied Gas Dynamics (RGD 2010), Pacific Grove, Calif., July 10-15, 2010

[5] Day, C.
Kryovakuumtechnik und Kryopumpen.
VDI-Wissensforum Kryotechnik, Karlsruhe, 23.-25.Febraur 2010

[6] Day, C.; Cristescu, I.
Technology challenges in the inner fuel cycle of ITER.
1st European Energy Conf., Barcelona, E, April 20-23, 2010

[7] Day, C.; Cristescu, I.; Pegourie, B.; Weyssow, B.
Considerations towards the fuel cycle of a steady-state DT fusion device.
23rd IAEA Fusion Energy Conference, Daejeon, Korea, October 11-16, 2010

[8] Day, Ch.; Hauer, V.
Measurement of the conductance in the Knudsen flow regime.
5th Symp.on Vacuum Based Science and Technology, Kaiserlautern, September 28-30, 2010

[9] Day, Chr.
Cryogenics vacuum technology and cryopumps.
VDI Wissensforum Cryogenics, Karlsruhe, September 15-17, 2010

[10] Day, Chr.; Haas, H.; Hanke, St.; Hauer, V.; Luo, X.; Scannapiego, M.; Simon, R.; Strobel, H.; Fellin, F.; Lässer, R.; Papastergiou, St.; Dremel, M.; Mayaux, Chr.; Pearce, R.
Design progress for the ITER torus and neutral beam cryopumps.
26th Symp.on Fusion Technology (SOFT 2010), Porto, P, September 27 - October 1, 2010

[11] Day, Chr.; Haas, H.; Hanke, St.; Hauer, V.; Luo, X.; Varoutis, St.
Vacuum engineering of customized cryosorption pumps.
11th European Vacuum Conf.(EVC-11), 8th Iberian Vacuum Meeting (IVM-8), 6th European Topical Conf.on Hard Coatings Salamanca, E, September 20-24, 2010

[12] Day, Chr.; Hauer, V.; Luo, X.; Sharipov, F.; Varoutis, S.; Valougeorgis, D.
Recent developments in vacuum flow modelling.
18th Internat.Vacuum Congress (IVC-18), Internat.Conf.on Nanoscience and Technology (ICN+T 2010), 14th Internat.Conf.on Surfaces Science (ICSS-14),
Vacuum and Surface Sciences Conf.of Asia and Australia (VASSCAA-5), Beijing, China, August 23-27, 2010

[13] Dremel, M.; Pearce, R.; Mayaux, C.; Hemsworth, R.; Hanke, S.
ITER neutral beam cryopumps design requirements for the integration.
26th Symp.on Fusion Technology (SOFT 2010), Porto, P, September 27 - October 1, 2010

[14] Haas, H.; Day, Ch.
TIMO-2. A versatile cryogenic test bed with supercritical helium supply.
23rd Internat.Cryogenic Engineering Conf.(ICEC 23) and Internat.Cryogenic Materials Conf. (ICMC 2010), Wroclaw, PL, July 19-23, 2010

[15] Lässer, R.; Papastergiou, S.; Piazza, G.; Day, Ch.; Haas, H.; Hanke, S.; Hauer, V.; Poncet, J.M.; Cirstescu, I.; Michling, R.; Glugla, M.; Pearce, R.; Antipenkov, A.; Dremel, M.; Mayaux, Ch.; Babineau, D.; Kazachenko, O.; Perevenzentsev, A.
Management and status of the European in-kind system of the INTER fuel cycle.
9th Internat.Conf.on Tritium Science and Technology (TRITIUM 2010), Nara, J, October 24-29, 2010

[16] Luo, X.; Day, C.
A 3D Monte Carlo vacuum modeling of the neutral beam injection system of ITER.
Fusion Engineering and Design, 85(2010) S.1446-50; DOI:10.1016/j.fusengdes.2010.04.002

[17] Luo, X.; Day, Chr.
Investigation of a new Monte Carlo method for transitional gas flow.
27th Internat.Symp.on Rarefied Gas Dynamics (RGD 2010), Pacific Grove, Calif., July 10-15, 2010

[18] Luo, X.; Haas, H.; Hauer, V.; Sharipov, F.; Day, Chr.
Systematic vacuum study of the ITER model cryopump by test particle Monte Carlo simulation.
18th Internat.Vacuum Congress (IVC-18), Internat.Conf.on Nanoscience and Technology (ICN+T 2010), 14th Internat.Conf.on Surfaces Science (ICSS-14),
Vacuum and Surface Sciences Conf.of Asia and Australia (VASSCAA-5), Beijing, China, August 23-27, 2010

[19] Maruyama, S.; Yang, Y.; Pitts, R.A.; Sugihara, M.; Putvinski, S.; Li, B.; Li, W.; Baylor, L.R.; Meitner, S.J.; Day, C.; LaBombard, B.; Reinke, M.
ITER fuelling system design and challenges.
23rd IAEA Fusion Energy Conference, Daejeon, Korea, October 11-16, 2010

[20] Masiello, A.; Milnes, J.; Waldon, C.; Alonso, J.; Minea, T.; Boilson, D.; Hemsworth, R.; Franzen, P.; Heinemann, B.; Day, C.; Hanke, St.; Bigi, M.; Chitarin, G.; Luchetta, A.; Marcuzzi, D.; Pomaro, N.; Pasqualotto, R.; Serianni, G.; Sonato, P.; Toigo, V.; Zaccaria, P.
The European contribution to the developments of the ITER NB injector.
26th Symp.on Fusion Technology (SOFT 2010), Porto, P, September 27 - October 1, 2010

[21] Misdanitis, S.; Pantazis, S.; Lihnaropoulos, J.; Valourgeorgis, D.; Varoutis, S.; Hauer, V.; Day, Ch.
Experimental and numerical investigation of vacuum gas flows in fusion vacuum systems.
9th School and Workshop on Fusion Physics and Technology, Volos, GR, April 19-23, 2010

[22] Pantazis, S.; Varoutis, S.; Day, C.; Valougeorgis, D.
Gas-surface scattering effect on vacuum gas flows through rectangular channels.
11th European Vacuum Conf.(EVC-11), 8th Iberian Vacuum Meeting (IVM-8), 6th European Topical Conf.on Hard Coatings Salamanca, E, September 20-24, 2010

[23] Papastergiou, S.; Lässer, R.; Piazza, G.; Day, Chr.; Haas, H.; Hanke, S.; Hauer, V.; Poncet, J.M.; Pearce, R.; Antipenkov, A.; Dremel, M.; Mayaux, Ch.
The European supplied components of the ITER vacuum pumping systems.
9th Internat.Conf.on Tritium Science and Technology (TRITIUM 2010), Nara, J, October 24-29, 2010

[24] Pearce, R.J.H.; Antipenkov, A.; Bersier, J.L.; Boussier, B.; Bryan, S.; Dremel, M.; Hughes, S.; Kersevan, R.; Mayaux, C.; Worth, L.; Wykes, M.; Baylor, L.; Gardner, W.; Meitner, S.; asmussen, D.; Laesser, R.; Piazza, G.; Papastergiou, S.; Day, C.; Haas, H.; Hanke, S.; Hauer, V.; Poncet, J.M.
The realisation of the ITER vacuum systems.
18th Internat.Vacuum Congress (IVC-18), Internat.Conf.on Nanoscience and Technology (ICN+T 2010), 14th Internat.Conf.on Surfaces Science (ICSS-14),
Vacuum and Surface Sciences Conf.of Asia and Australia (VASSCAA-5), Beijing, China, August 23-27, 2010

[25] Scannapiego, M.; Poncet, J.M.; Day, C.; Hanke, S.; Hauer, V.; Papastergiou, S.; Dremel, M.; Mayaux, C.
Thermohydraulic investigation on the operation of the ITER torus and neutral beam cryopumps.
26th Symp.on Fusion Technology (SOFT 2010), Porto, P, September 27 - October 1, 2010

[26] Sharipov, F.
Comment on 'Note on the relation between thermophoresis and slow uniform flow problems for a rarefied gas' [Phys. Fluids 21, 112001 (2009)].
Physics of Fluids, 22(2010) S.049101/1-2; DOI:10.1063/1.3379848

[27] Sharipov, F.
Comments on 'Symmetry of the Linearized Boltzmann Equation' by S. Takata.
Journal of Statistical Physics, 139(2010) S.536-537; DOI:10.1007/s10955-010-9955-2

[28] Sharipov, F.
Numerical simulation of turbomolecular pump over a wide range of gas rarefaction.
Journal of Vacuum Science and Technology A, 28(2010) S.1312-1315; DOI:10.1116/1.3484139

[29] Sharipov, F.
The reciprocal relations between cross phenomena in boundless gaseous systems.
Physica A, 389(2010) S.3743-3760, DOI:10.1016/j.physa.2010.05.019

[30] Sharipov, F.; Graur, I.; Day, Chr.
Leak rate of water into vacuum through microtubes.
Journal of Vacuum Science and Technology A, 28(2010) S.443-48; DOI:10.1116/1.3372839

[31] Sharipov, F.; Graur, I.; Day, Chr.
Modelling of water leak rates through crevices.
26th Symp.on Fusion Technology (SOFT 2010), Porto, P, September 27 - October 1, 2010

[32] Sharipov, F.; Varoutis, S.; Day, Chr.; Luo, X.; Haas, H.
Numerical modeling of the ITER model cryopump.
18th Internat.Vacuum Congress (IVC-18), Internat.Conf.on Nanoscience and Technology (ICN+T 2010), 14th Internat.Conf.on Surfaces Science (ICSS-14),
Vacuum and Surface Sciences Conf.of Asia and Australia (VASSCAA-5), Beijing, China, August 23-27, 2010

[33] Sonato, P.; Bonicelli, T.; Chakraborty, A.K.; Hemsworth, R.; Watanabe, K.; Day, C.; Franzen, P.; Waldon, C.
The ITER neutron beam facility in Padua - Italy: a joint international effort for the development of the ITER heating neutral beam injector prototype.
23rd IAEA Fusion Energy Conference, Daejeon, Korea, October 11-16, 2010

[34] Varoutis, S.; Hauer, V.; Day, Ch.; Pantazis, S.; Valougeorgis, D.
Experimental and numerical investigation in flow configutations related to the vacuum systems of fusion reactors.
Fusion Engineering and Design, 85(2010) S.1798-1802; DOI:10.1016/j.fusengdes.2010.05.041

[35] Varoutis, S.; Misdanitis, S.; Pantazis, S.; Hauer, V.; Giegerich, T.; Day, C.; Valougeorgis, D.
Experimental and numerical investigation of vacuum gas flows in fusion vacuum systems.
26th Symp.on Fusion Technology (SOFT 2010), Porto, P, September 27 - October 1, 2010

[36] Varoutis, S.; Pantazis, S.; Giegerich, T.; Day, C.; Valougeorgis, D.
Experimental and numerical investigation of vacuum gas flows through tubes with sudden expansion of contraction.
11th European Vacuum Conf.(EVC-11), 8th Iberian Vacuum Meeting (IVM-8), 6th European Topical Conf.on Hard Coatings Salamanca, E, September 20-24, 2010

[37] Varoutis, S.; Sharipov, F.
Rarefied gas flow through channels of finite length due to arbitrary pressure ratio.
27th Internat.Symp.on Rarefied Gas Dynamics (RGD 2010), Pacific Grove, Calif., July 10-15, 2010

Fuel Cycle – Tritium Processing

[1] Alecu, C.G.; Köllö, Z.; Kloppe, B.; Bornschein, B.; Besserer, U.; Wendel, J.
Reachable accuracy and precision for tritium measurements by calorimetry at TLK.
9th Internat.Conf.on Tritium Science and Technology (TRITIUM 2010), Nara, J,
October 24-29, 2010

[2] Borgognoni, F.; Demange, D.; Welte, S.; Tosti, S.
Processing test of an upgraded mechanical design for PERMCAT reactor.
9th Internat.Conf.on Tritium Science and Technology (TRITIUM 2010), Nara, J, October 24-29, 2010

[3] Bornschein, B.
Between fusion and cosmology - the future of the Tritium Laboratory Karlsruhe.
9th Internat.Conf.on Tritium Science and Technology (TRITIUM 2010), Nara, J, October 24-29, 2010

[4] Demange, D.; Glugla, M.; Günther, K.; Le, T.L.; Simon, K.H.; Wagner, R.; Welte, S.
Counter-current isotope swamping in a membrane reactor: the PERMCAT process and its applications in fusion technology.
Catalysis Today, 156(2010) S.140-145; DOI:10.1016/j.cattod.2010.02.033

[5] Demange, D.; Le, T.L.; Simon, K.H.; Wagner, R.; Welte, S.
CAPER modifications and first experimental results on highly tritiated water processing with PERMCAT at the Tritium Laboratory Karlsruhe.
9th Internat.Conf.on Tritium Science and Technology (TRITIUM 2010), Nara, J, October 24-29, 2010

[6] Munakata, K.; Demange, D.
Development of numerical simulation code of membrane reactor for detritiation.
26th Symp.on Fusion Technology (SOFT 2010), Porto, P, September 27 - October 1, 2010

[7] Parracho, A.I.R.T.; Brennan, P.D.; Demange, D.; Knipe, S.
Characterisation and optimisation of small Sieve beds in adsorption/desorption process of tritiated water.
9th Internat.Conf.on Tritium Science and Technology (TRITIUM 2010), Nara, J, October 24-29, 2010

[8] Schön, R.
Untersuchung eines BIXS-Detektors zur Messung der Tritiumkonzentration in Wasser.
Frühjahrstagung DPG, Fachverband Physik der Hadronen und Kerne, Bonn, 15.- 19.März 2010
Verhandlungen der Deutschen Physikalischen Gesellschaft, R.6, B.45(2010) HK 18.1

[9] Wagner, R.; Besserer, U.; Demange, D.; Dittrich, H.; Le, T.L.; Simon, K.H.; Guenther, K.
Improvement and characterization of small cross-piece tritium ionization chambers at the Tritium Laboratory Karlsruhe.
9th Internat.Conf.on Tritium Science and Technology (TRITIUM 2010), Nara, J, October 24-29, 2010

Safety

[1] Klimenko, D.; Pasler, V.
Safety of fusion magnets: pressure impact on arcing in model experiments to high-current arcs propagating along the busbars of large fusion magnet coils.
Fusion Engineering and Design, 85(2010) S.1875-1879; DOI:10.1016/j.fusengdes.2010.06.014

[2] Xiao, J.; Travis, J.R.; Breitung, W.; Jordan, T.
Numerical analysis of hydrogen risk mitigation measures for support of ITER licensing.
Fusion Engineering and Design, 85(2010) S.205-14; DOI:10.1016/j.fusengdes.2009.12.008

[3] Xu, Z.; Travis, J.R.; Jordan, T.
Solid particle resuspension model development for the gasflow code.
Proc.of the 18th Internat.Conf.on Nuclear Engineering (ICONE-18), Xi'an, China,
May 17-21, 2010; CD-ROM Paper ICONE18-29681; New York, N.Y. : ASME, 2010

Appendix IV: Glossary

AC	Alternating Current
ACI	After Cavity Interaction
AES	Auger Electron Spectroscopy
AEUL	Association EURATOM – University of Latvia, Riga
AF	Accelerator Facility
Ar	Argon
ARBOR 1	Fast Reactor Irradiation from FZK in BOR 60
ARBOR 2	Fast Reactor Irradiation from FZK and CEA in BOR 60
ASG magnet	Superconducting magnet at CRPP for the ITER gyrotron manufactured by ASG superconductors
ASTM	American Society for Testing and Materials
BA	Broader Approach DEMO
BDT	Brittle-to-Ductile Transition
BEKED	Nuclear Data Evaluation Code System developed by KIT
BF	Bright-Field
BMBF	Bundesministerium für Bildung und Forschung
BN	Boron Nitrite
BOR-60	Fast Reactor at SSC RIAR
BSM	Blanket Shield Module
BtP	Built-to-print
BU	Breeder Unit
C&S	Codes and Standards
CAD	Computer Aided Design
CATIA®	3D CAD software (Dassault Systèmes)
CBED	Convergent Beam Electron Diffraction
CCFE	Culham Centre for Fusion Energy, UK
CCFP	Coordinating Committee on Fuelling and Pumping
CCR	Calabazas Creek Research, Inc., Saratoga, CA 95070 USA
CCRC	Coated Conductor Rutherford Cable
CD	Cryogenic Distillation
CdTe	Cadmium Telluride
CEA	Commissariat à l'Énergie Atomique, Saclay (France)
CECE	Combined Electrolysis Catalytic Exchange
CFC	Carbon Fibre Composite
CFD	Computational Fluid Dynamic

CFTM	Creep Fatigue Test Module
CIEMAT	Centro de Investigaciones Energeticas Medioambientales y Tecnologicas
CNR	Consiglio Nazionale delle Ricerche, Milano, Italy
CoA	Contract of Association
COD	Crack Opening Displacement
CP	Cooling Plate
CPS	Coolant Purification System
CRPP	Centre de Recherces en Physique des Plasmas, Lausanne, Switzerland
CS	Central Solenoïd
CTE	Coefficients of Thermal Expansion
CuLTKa	Current Lead Test Facility Karlsruhe
CVB	Cold Valve Box
CVD	Chemical Vapor Deposition
CW	Continuous Wave
DACS	Data Acquisition and Control System
DAF	Dynamic Amplification Factor
DBTT	Ductile-to-Brittle Transition Temperature
DDD	Design Description Document
DEMO	Demonstration Power Station
DIII-D	Tokamak Name
dpa	Displacement per atom
DROSG	Neutron Source Reaction Simulation Code
DSCD	Demo Structural Design Code
DT	Deuterium Tritium (fusion reaction)
DWBA	Distorted Wave Born Approximation
EAF	European Activation File
EASY	European Activation System
EB	Electron Beam
ECCD	Electron Cyclotron Current Drive
ECM	Electro Chemical Machining
ECH & CD	Electron Cyclotron Heating and Current Drive
ECRF	Electron Cyclotron Range of Frequencies
ECRH	Electron Cyclotron Resonance Heating
ECRH & CD	Electron Cyclotron Resonance Heating and Current Drive
EDM	Electrical Discharge Machining
EDX	Energy Dispersive X-Ray Spectroscopy

EELS	Electron Energy Loss Spectroscopy
EF	Equilibrium Field
EFDA	European Fusion Development Agreement
EFF	European Fusion File
EFTEM	Energy Filtered TEM
EGYC	European Gyrotron Consortium
ELM	Edge Localised Mode
EM	Electromagnetic
ENDF	Evaluated Nuclear Data File (USA)
ENEA	Italian National Agency for New Technologies, Energy and Sustainable Economy Development
EUROFER	European RAF/M Steel
EVEDA	Engineering Validation Engineering Design Activities
F4E	Fusion for Energy
FE	Finite Element
FEM	Finite Element Method
FISPACT	Nuclear Inventory and Activation Code (by CCFE , UK)
FM	Fracture-Mechanical
FMEA	Failure Mode and Effect Analysis
FML	Fusion Material Laboratory
FOM	Institute for Plasma Physics Rijnhuizen
FSM	Finite State Machine
FSSS	Fisher Sub-Sieve Size
FW	First Wall
FZK	Forschungszentrum Karlsruhe
GDC	Glow Discharge Cleaning
GDH	Geometry Dependent Hybrid (nuclear model)
GOT	Goal Oriented Training
H_2	Hydrogen
H&CD	Heating and Current Drive
HAADF	High Angle Annular Dark Field (detector)
HAS	Hungarian Academy of Sciences
HAZ	Heat Affected Zone
HCLL	Helium Cooled Lithium Lead
HCPB	Helium Cooled Pebble Bed
HCS	Helium Cooling System
He	Helium

HEBLO	HElium BLOwer (Helium facility at FZK)
HELLAS	A synonym for the collaborating Greek Institutions National Technical University of Athens, Greece and the National and Kapodistrian University of Athens, Greece
HELOKA	Helium Loop Karlsruhe
HELOKA-HP	Helium Loop Karlsruhe – High Pressure
HETP	Height Equivalent to a Theoretical Plate
HETRA	Heat TRAnsfer Experiment
HFR	High Flux Reactor
HFTM	High Flux Test Module
HGF	Helmholtz-Gemeinschaft Deutscher Forschungszentren e.V.
HIP	Hot Isostatic Pressing
HNB	Heating Neutral Beam Injector
HPGe	High Purity Germanium (detector)
HRJRG-13	Helmholtz Russia Joint Research Group-13
HT	Heat Treatment
HT	High Temperature
HTS	High Temperature Superconductor
HTSCL	High Temperature Superconductor Current Leads
HV	High Voltage
I_c	Critical Current
IAP	Institute of Applied Physics, Nizhny Novgorod, Russia
ICIT	National Institute of Research and Development for Cryogenics and Isotope Technology, Rm. Valcea, Romania
ICRP	International Committee on Radiation Protection
IFMIF	International Fusion Materials Irradiation Facility
IO	ITER International Organisation
INT	Institute of Nuclear Technology, Sacavém, Portugal
IPE	Institute for Data Processing and Electronics
IPF	Institut für Plasmaforschung, Universität Stuttgart, Germany
IPP	Max Planck Institut für Plasmaphysik, Garching, Germany
IRDF	International Radiation Dosimetry File
ISS	Isotope Separation System
ISSP	Institute of Solid State Physics, Riga, Latvia
ITER	International Thermonuclear Experimental Reactor
ITERVAC	Code for Vacuum Gas Flows
IVVS	In-Vessel Viewing System
JAEA	Japan Atomic Energy Agency
JEFF	Joint Evaluated Fission Fusion File

JET	Joint European Torus
JSC “SSC RIAR”	Joint Stock Company “State Scientific Centre Research Institute of Atomic Reactors”
KIT	Karlsruhe Institute of Technology
KLST	Kleinlast Impact Specimen
Kn	Knudsen number
LCF	Low Cycle Fatigue
LF	Lithium Target Facility
LLL	Liquid Lithium Limiter
LOFA	Loss of Flow Accident
LPCE	Liquid Phase Catalytic Exchange
LTS	Low Temperature Superconductor
MA	Mechanical Alloying
McCad	Software for the Conversion of CAD to Monte Carlo Geometry
MCNP	Monte Carlo Code for Neutron and Photon Transport Simulations
MCNPX	Monte Carlo Code for Neutral and Charged Particle Transport Simulations
MCSEN	Monte Carlo Sensitivity Code based on MCNP
MEMOS	Code Name
MGI	Massive Gas Injection
MHD	Magneto Hydrodynamic
MLI	Multi-layer Insulation
MOU	Matching Optics Unit
NB	Neutral Beam
NBI	Neutral Beam Injector
NC	Normal Conducting
NDT	Non-Destructive Testing
NEA	Nuclear Energy Agency, Paris
NJOY	Nuclear Data Processing Codes developed by Los Alamos National Laboratory (LANL, USA)
NPI	Nuclear Physics Institute (Řež)
NRG	Nuclear Research and consultancy Group, national nuclear research institute of the Netherlands, located in Petten
NSTX	Name of Tokamak
OD	Outer Diameter
ODS	Oxygen Dispersion Strengthened
ODSFS	Oxygen Dispersion Strengthened Ferritic Steels
OECD	Organisation for Economic Co-operation and Development
OI magnet	Superconducting magnet at KIT, manufactured by Oxford Instruments
OM	Optical Microscopy

OMP	Optical Model Potential
ORNL	Oak Ridge National Laboratory
OSi	Lithium orthosilicate
PBHT	Post Bonding Heat Treatment
PCB	Printed Circuit Board
PEGASUS	Code Name
PF	Poloïdal Field
PFC	Plasma Facing Components
PIE	Post Irradiation Examination
PIE	Postulated Initiating Event
PIT	Postulated Impact Tables
PIXE	Particle Induced X-ray Emission
PLC	Programmable Logic Control
PPC	ITER Pre-production Torus Cryopump
PPE	Port Plug Engineering
ProVac3D	KIT Code for Vacuum Flow Calculations
PS	Power Distribution System
PSI	Paul-Scherrer-Institute, Switzerland
PWHT	Post Weld Heat Treatment
PWI	Plasma Wall Interaction
QD	Quench Detection
QDU	Quench Detection Unit
QSPA-Kh50	Name of Plasma Gun
QSPA-T	Name of Plasma Gun
R2S	Rigorous 2-Step Method for Shutdown-dose Rate Calculations
RAF	Reduced Activation Ferritic (steel)
RAFM	Reduced Activation Ferritic Martensitic (steel)
RD	Rolling Direction
RF	Radio Frequency
RT	Room Temperature
SA2	Safety Scenario of Irradiation in ITER for Activation Calculations
SAMMY	Resonance Parameter Analysis Code developed by ORNL
SAND-II	Spectrum Unfolding Code
SANS	Small Angel Neutron Scattering
SCK-CEN	Studiecentrum voor Kernenergie, Mol, Belgium
SEM	Scanning Electron Microscopy

SENB	Single Edged Notched Bar
SOL	Scrape-off-Layer
SPICE	Sample Holder for Irradiation of Miniaturized Steel Specimens
SSP	Separatrix Strike Position
SSTT	Small Scale Test Techniques
STEM	Scanning Transmission Electron Microscope
TALYS	Nuclear Model Code (NRG)
TBM	Test Blanket Module
TBS	Test Blanket System
TD	Theoretical Density
TED	Thales Electron Devices at Velizy, France
TEKES	Finnish Funding Agency for Technology and Innovation
TEM	Transmission Electron Microscope
TES	Tritium Extraction System
TF	Test Facility
TF	Toroidal field
THEA	THermohydraulic Experimental Arrangement
TIG	Tungsten Inert Gas
TIMO	Test Facility for ITER Model Pump
TiT target	Titanium-Tritium, solid target used in accelerator-based neutron generations. The tritium is adsorbed in a thin titanium layer on a copper disk.
TLK	Tritium Laboratory Karlsruhe
TMF	Thermo-Mechanical Fatigue
TOKES	Code Name
TOL-F	Name of Measurement Device for the Local Dose Rate
TOSKA	Torusspulen Testanordnung Karlsruhe
TPMC	Test Particle Monte Carlo
TPR	Tritium Production Rate
TQ	Thermal Quench
TRANSFLOW	Test Facility for Vacuum Flows
TRM	Tritium Release Test Module
TTC	Target- and Test Cell
TU Dresden	Technical University Dresden
TZM	Molybdenum, stabilized by small amounts of titanium and zirconium
UMC	Unified Monte Carlo (approach for co-variance data generation)
USE	Upper Shelf Energy
VDE	Vertical Displacement Event

VV	Vacuum Vessel
W	Tungsten
W7-X	The Wendelstein 7-X Stellarator Project in Greifswald, Germany
WBDF	Weak-Beam Dark-Field
WDS	Water Detritiation System
WL10	Tungsten with 10 % of La_2O_3
ZA	Zone Axis

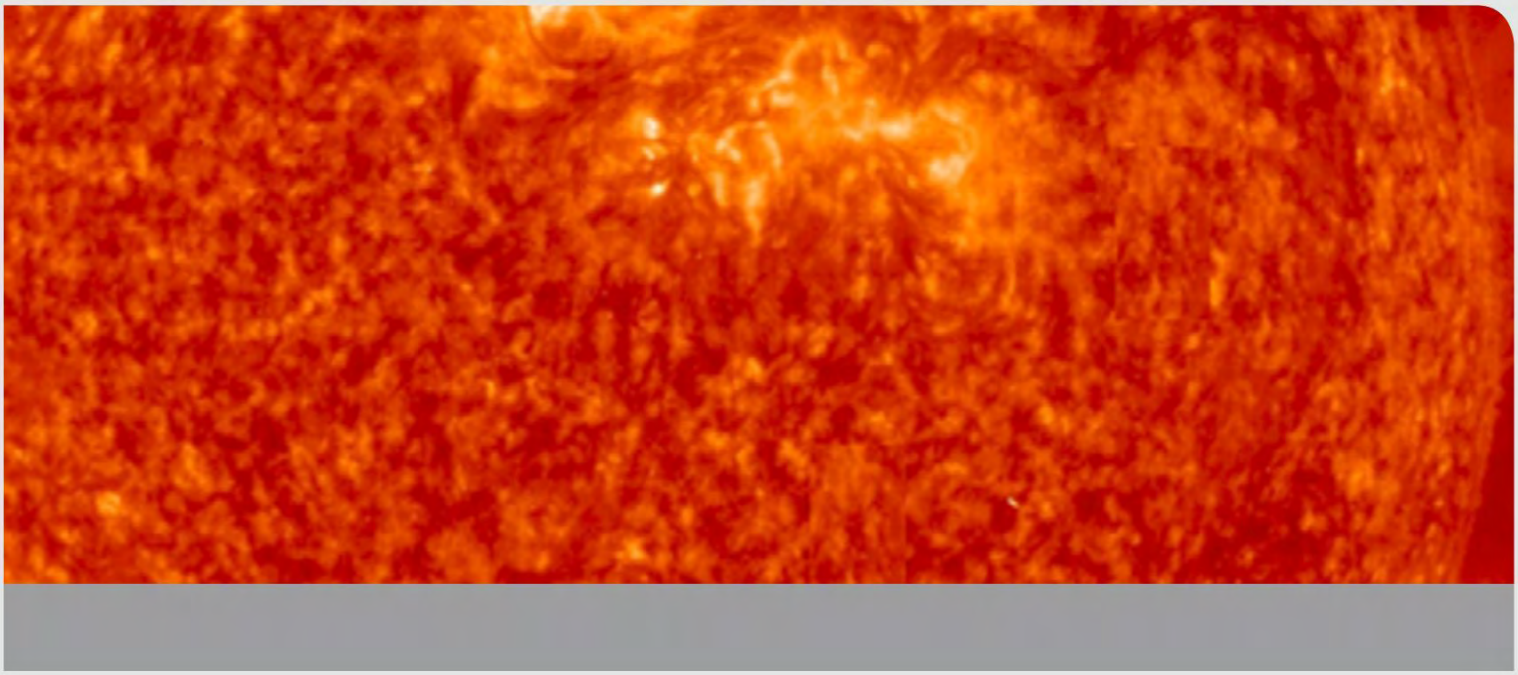

ISSN 1869-9669